Studies on the treatment of the human urine using Electrochemical Advanced Oxidation Process

Thesis

Submitted in partial fulfilment of requirement of the degree of

DOCTOR OF PHILOSOPHY

In

ENVIRONMENTAL SCIENCE & TECHNOLOGY

by:

JAYISHNU SINGLA

(Regd No. 901514005)

School of Energy and Environment

Thapar Institute of Engineering and Technology

Patiala-147004

February, 2020

CANDIDATE'S DECLARATION

I hereby certify that the work which is being presented in the thesis entitled **"STUDIES ON THE TREATMENT OF THE HUMAN URINE USING ELECTROCHEMICAL ADVANCED OXIDATION PROCESS"** in partial fulfillment of the requirements for the award of the degree of Doctor of Philosophy and submitted in the School of Energy and Environment, Thapar Institute of Engineering and Technology, Patiala, India is an authentic record of my own work carried out during a period from July 2015 to July 2019 under the supervision of Dr. AnoopVerma, Associate Professor, School of Energy and Environment, TIET, Patiala and Dr. V. K. Sangal, Associate Professor, Chemical Engineering Department, MNIT, Jaipur. The matter presented in the thesis has not been submitted in part or full to any other institute for the award of any other degree in other University or Institute.

Jayishnu Singla

(Jayishnu Singla)

This is to certify that above statement made by the candidate is correct to the best of our knowledge.

Dr. AnoopVerma

Supervisor

Dr. V. K. Sangal

Supervisor

ACKNOWLEDGEMENT

When I took some tea breaks with friendly squirrels in campus, I used to imagine the moment I write this section, and that moment is now in front of me. Over the last four years of doctoral study in TIET, I feel myself getting solid both in theory and experiments with respect to environmental science. I was sincerely happy and watched my enthusiasm soar as I plowed through these fields. My experience has deeply encouraged me to devote my entire carrier for enhancing science and technology for environments. Words are often less to revels one's deep regards. With an understanding that work like this can never be the outcome of a single person, through this acknowledgment I would like to express my special thanks, gratitude, and regards to a number of people who supported, helped and guided me in completing this Ph.D. program at TIET.

First of all, my heartfelt thanks to the almighty for his abundant blessing showered on me throughout this endeavor to complete this successful work of mine.

I express my foremost gratitude as well as profound regards to my academic advisors, Dr. Anoop Verma and Dr. Vikas K. Sangal for providing me an opportunity to work under their valuable guidance. They have given me a lot of freedom and inspiration to discover my own path of research. Their wide knowledge, valuable suggestions, encouragement, and freedom of independent work provided a platform for learning and performing research. They have been always supportive and encouraged me with excessive compliments which were often more than I deserved. Their enthusiasm and optimism made this experience both rewarding and enjoyable. Their feedback and editorial comments were also valuable for the writing of this thesis. Dr. Anoop Verma allowed me numerous opportunities to teach graduate-level classes and to participate in conferences, which definitely cultivated my academic abilities.

I would also wish to extend my sincere thanks to Dr. Amit Dhir, the present Head of School of Energy and Environment, Dr. N.Tejo Prakash, the former Head of School of Energy and Environment, for providing me an opportunity to join esteemed institution, gave access to research facilities and at all times been very supportive and accommodating. I would like to thank Dr. A.S. Reddy and all other faculty members of School and Energy and Environment for their traffic guidance and support through the duration of this work. I owe a deep sense of gratitude to Dr. Rafat Siddique, the present Dean, Research and Sponsored Projects, and Dr. O.P. Pandey, the former Dean, Research and Sponsored Projects, TIET, Patiala, India, for their valuable guidance and support.

I express my deepest gratitude to my doctoral committee members Dr. Anita Rajor and Dr. Jai Prakash Kushwaha for their constant encouragement, insightful comments and their keen interest in me at every stage of my research work. This research work would not come to successful completion without the help, I received from the entire staff of the SAI Labs, TIET, Patiala. I also wish to thank all the employees of the central workshop for their constant cooperation and kind help throughout my Ph.D. work. I would like to thank all the employees of the School of Energy and Environment for their everlasting support.

It was my great honor, to thank my special labmates, Ms. Palak Bansal, Ms. Himadri Rajput, Mr. Rahil Changotra, Mr. Vagish, Ms. Noorpreet Dhanjal, Mrs. Rachna Panday, Mrs. Parminder Kaur Ms. Ina, Ms. Steffi Talwar, Mr. Pali Rosha, Ms. Priyanka Goyal and others for the stimulating discussions, cooperation, cheerful support and encouragement in carrying out my research smoothly. I was lucky to get helpful advice from Dr. Sumit Jaiswal and Mr. Amanjit Singh whenever required. It is my privilege to thank my special friends, Ms. Ankita Garg, Mr. Devinder Babool, Mr. Jatin Singla, Ms. Jasneet Kaur, Ms. Rajvir Kaur, and others for providing me constant encouragement and sharing some good laughs especially at times of frustration.

Finally, I would like to thank my parents, brother Kamal Singla, and his wife Pratima Singla, who helped me at every stage of my personal and academic life and longed to see this achievement to come true. Words cannot express how grateful I am to my mother Sushma Gupta and father Dinesh Kumar, for all of the sacrifices that you have made on my behalf. Your prayer for me was what sustained me thus far. I would cherish every moment where my family was so keen and curious to know about the details and progress of my work, which boosted my confidence. My acknowledgment would be incomplete without thanking my nephew, Aashish Singla, a little bundle of joy and the biggest source of my happy life who would never let things get dull or boring.

Jayishnu Singla

ABSTRACT

Poor sanitation and lack of effective sustainable approach have become one of the major environmental issues of concern in developing countries like India. Moreover, with continuous discharge of recalcitrant organic pollutants from urinal wastewater into the surroundings has put human health and environment under the potential risk of threat. Therefore, a sustainable yet affordable solution for the safe disposal of urinal wastewater is required. Electro-oxidation (EO) under electrochemical advanced oxidation processes has drawn great attention for the treatment of a wide variety of recalcitrant toxic mixed effluents via generating in-situ strong reactive oxygen species (ROS) such as hydroxyl radical ($OH^{\bullet}$) and reactive chlorine species (RCS). In this study, the treatment performance of the EO process for synthetic urine/actual human urine (SU/AHU) and its metabolites in batch and continuous mode of operation using mixed metal oxide anode (MMO) and doped-mixed metal oxide (doped-MMO) anode was studied. Furthermore, best efforts have been made to integrate two processes i.e. photo-catalysis (PC) and EO within the same treatment unit for enhanced degradation of pollutants.

For systemic studies, the effect of various selected operational parameters such as pH, current density, electrolyte (i.e. NaCl) dose and treatment time has been studied using response surface methodology (RSM). Box-Behnken design (BBD) under RSM has been employed for experimental designing, data analysis, the interaction between EO parameters, their optimization along with evaluation in terms of percentage Degradation (%Degradation) (Y_1) and Energy consumption (Y_2). A quadratic model was suggested by exploiting the sequential F-test and other adequacy measures. Furthermore, experimental data were then analyzed by multiple regression analysis of RSM and simultaneous optimization of various operational parameters for the responses was performed by the desirability function approach. The best appropriate optimized conditions for batch EO treatment of uric acid with MMO anodes was found to be pH= 2, n (NaCl dose) = 0.875 g/L, j (current density)= 7.142 mA/cm^2, t (treatment time) = 6.95 min with Y_1= 91.571% and Y_2= 0.526 kWh/m^3, which showed highest overall desirability, D = 0.899. While for creatinine, the most appropriate optimized conditions were obtained at pH= 2.4, n = 0.75 g/L, j= 12.005 mA/cm^2, t = 85 min, with Y_1= 85.41% and Y_2= 16.826 kWh/m^3 and overall desirability, D = 0.899. The optimal operating conditions for maximum removal of urea were found to be j=18.14 mA/cm^2, n=1.45 g/L, pH= 4 and t= 135 min, with Y_1= 94.78% and Y_2= 20.54 kWh/m^3 which showed combined desirability, D =0.857. The

photo-activity of MMO anode in terms of quantification of generated $OH^{\bullet}$ at MMO was studied under both UV and solar radiations using Fluorescence spectroscopy. The results showed that maximum $OH^{\bullet}$ production was found under UV radiation as compared to solar radiation.

The strength of the present study lies in the demonstration of a significant reduction in treatment time of urine metabolites by incorporating dual effect i.e. photo-electrocatalysis (PEC) under UV radiations. The dual-process with synergistic results prompts its field-scale applications for the wastewater treatment with a significant decrease in treatment time from 7 min to 5 min (uric acid), 85 to 60 min (creatinine) and 135 to 95 min (urea). The quality of treated urine metabolites samples was validated using different analytical techniques. The transformation products of uric acid, creatinine, and urea were identified through LC-MS.

Similar kind of studies was performed for the treatment of urine metabolites with doped MMO. The results depicts the maximum degradation of all urine metabolites at best appropriate optimized conditions were Y_1= 95.35% (uric acid), Y_1 = 90.002% (creatinine) and Y_1 = 91.15% (urea) respectively with minimum Y_2= 2.479 kWh/m^3, Y_2= 25.83 kWh/m^3 and Y_2 = 51.53 kWh/m^3 respectively. The dual-process with synergistic results has shown a significant reduction in treatment time from 43 min to 30 min (uric acid), 140 to 120 min (creatinine) and 195 to 150 min (urea). The quality of treated urine metabolites and the transformation products of uric acid, creatinine, and urea were identified through LC-MS. Based on these identified intermediates a tentative degradation pathway for urine metabolites has been proposed in this study.

The parametric study of EO (batch) treatment of SU was performed using BBD under RSM using four input operational parameters were selected such as pH (Y_1), current density (Y_2), treatment time (Y_3) and N/Cl ratio (Y_4) and %COD removed (Z_1), and specific energy consumption (SEC) (Z_2) as responses. The most appropriate optimized conditions for batch EO treatment of SU with MMO anodes was found to be Y_1= 3.42, Y_2= 30.33 mA/cm^2, Y_3= 8.79 h, Y_4 = 0.42 with Z_1= 85.25% COD removed and Z_2= 11.75 kWh/kg of COD removed, which showed highest overall desirability, D = 0.985. Whereas the most relevant optimized conditions for batch EO treatment of SU with doped-MMO was found to be at Y_1= 4.20, Y_2= 53.91 mA/cm^2, Y_3= 10.05 h, Y_4 = 0.25 with Z_1= 90.55% COD removed and Z_2= 20.851 kWh/kg of COD removed, which showed highest overall desirability, D = 0.941. The photo-activity of MMO and the doped-MMO anode was investigated in terms of synergistic studies by performing treatment of synthetic urine using three different

techniques which include PC, EO, and PEC at optimized conditions. The results showed the increased rate constant values for PEC i.e. 0.2991 h^{-1} (MMO) and 0.3264 h^{-1} (doped-MMO) over the other two processes (i.e. EO and PC). Furthermore, treatment time for SU through PEC was also found to be reduced from 8.8 h to 6 h (MMO) and 10.05 h to 6.5 h (doped-MMO). The results of in-situ chemical analysis, cyclic voltammetry, FT-IR, and LC-MS analysis revealed that most of the organic components got eliminated and transformed into other byproducts which are non-toxic. Besides its efficacy towards oxidation of organic components, the disinfection efficiency of EO was also studied by spiking *E.coli* as (pathogenic microorganism) in SU. The complete elimination of the micro-organisms was achieved within 45 min (MMO) and 75 min (doped-MMO) of the EO treatment process.

To visualize the successful commercialization of the proposed method, treatment technology must provide viable solutions economically and as well as socially over traditional methods. The total operating cost for batch EO treatment of SU with MMO and doped-MMO was estimated as 0.85 $/kg of COD removed and 1.50 $/kg of COD removed at optimized conditions, respectively. However, this cost and overall economy of the studied process depend upon the scale-up version and desirability of electrodes. The results depict a sustainable solution for the on-site treatment of urinal wastewaters in terms of the economic feasibility of the EO process as well as the stability of anodes. Moreover, the overall cost could be reduced further during scale-up studies by modifying the reactor design, operating conditions, recycling the urine as flush water and coupling the decentralized molecular hydrogen production accordingly.

The scale-up trials were executed under continuous recirculation mode for the treatment of SU with a working volume of 2 L in a photovoltaic driven reactor at optimized conditions along with the strong possibility of harnessing the molecular hydrogen (H_2). The results showed 83.43% (MMO) and 74.20% (doped-MMO) reduction in COD within 6 h of electrolysis under continuous recirculation mode. The volumetric fraction of H_2 generated during 6 h of electrolysis in the range of 70.58% -1.7190% (MMO) and 59.142% – 3.340% (doped-MMO). Other by-product gases such as N_2, CO_2, CH_4, and CO has also been generated during electrolysis of SU by both anodes. However, the volumetric molecular fraction of these gaseous byproducts was found increasing with treatment time due to the oxidation of pollutants present in SU into molecular N_2 and CO_2. The total per day cost for the treatment of SU came out to be 0.054 $ (MMO) and 0.055 $ (doped-MMO).

After the successful EO treatment of SU with both types of anodes, the study was further extended for the treatment of AHU with MMO. An almost 68.33% reduction in COD was achieved when the actual effluent was treated under in photo-voltaic driven reactor under continuous recirculation mode. The results also showed the oxidation of nitrogen-based organic compounds i.e. urea (69.09%), uric acid (95.18%) and creatinine 67.95% within 6 h of electrolytic treatment of AHU. The results clearly indicate the oxidation of organic compounds present in AHU was due to the generated RCS and ROS during the treatment process. GC-MS spectra of untreated and EO treated samples of AHU, depicts the elimination of most of the organic components after the treatment process and the identified byproducts present in the treated solution was found non-toxic through toxicity analysis. The volumetric fraction of H_2 and N_2 generated during 6 h of electrolysis were in the range 69.74% – 2.617% and 18.019% – 62.133% respectively. Other byproduct gases such as CO_2, CH_4, and CO were also generated in small fractions during electrolysis.

The durability and stability of the MMO and doped-MMO anodes were checked through various characterized techniques such as EM-EDX, XRD, Raman spectroscopy, XPS and comprehensive characterization studies for both anodes. These characterized techniques confirmed the durability and stability of MMO and doped-MMO even after 400 (1242.5 h) and 500 (1853.166 h) recycles, respectively.

The comprehensive study shows that both electrodes are effectively suitable for actual urine effluent treatment and can be further extended for the commercial-scale applications. To the best of our knowledge, this is one of the few reported studies dealing with EO and PEC using novel MMO and doped-MMO anodes along with the potential of harnessing the commercially useful byproduct i.e. molecular hydrogen gas during scale-up trials for the treatment of urine wastewater. In addition, the proposed study can be boon for underprivileged areas in developing countries like India where either poor sanitation or no sanitation is provided. Thus, the study needs some scale-up executions for further validating the process.

List of Tables

List of Figures

CONTENTS

Chapter-1

INTRODUCTION

From the past several years, India is one of the fastest progressing economies in the developing world, which has made miraculous progress in urbanization and industrialization (Dong et al., 2015). Despite the strong social-economic growth during these years, India has failed to provide a satisfying proportionate pace for sustainable development (Ganesapillai et al., 2016). It is a tragic irony to think that in a country like India where statistics announce the uneven distribution of the fruits of liberalization and globalization in the Indian economy. According to the Joint Monitoring Programme (JMP) for Water Supply and Sanitation conducted by the World Health Organization (WHO) and the United Nations Children's Fund (UNICEF), approximately 2.4 billion people lack access to improved sanitation system and waste disposal facilities due to the acute shortage of clean water (World 2015; Daudey, 2018). Around 66 % of the total population in India still practice open defecation such as roadsides, railway tracks or open fields (Vazhacharickal et al. 2013; Bhatia and Bhatia, 2017). This percentage is much higher than the other developing countries like Pakistan (58%), Indonesia (41%), China (36%), Sri Lanka (33%) and Brazil (19%) (World 2015) (Brocklehurst, 2014; Andres et al., 2017).

According to the small-scale intervention studies, conducted by High Powered Expert Committee for estimating the investment requirements for sanitation in India in 2011 has reported that around half of the total population in rural and urban slum areas do not have even proper sewerage systems. In rural areas and slums, the solid waste generated i.e. human excreta (urine and feces) are not properly managed and widely disposed of in the surrounding environment, mostly at open fields (Katukiza et al., 2012). Moreover, from where it further discharged into areas like agriculture fields, public places, open sewers and water bodies (running water streams, surface water, and groundwater), either by rain or by storm resulting in pounding (Katukiza et al., 2012). Furthermore, due to the continuous discharge of these human waste into the surroundings led to the generation and transmission of harmful pathogens such as viruses, bacteria, protozoans, etc. via human excreta (Mohapatra, 2019). Thus causing non-curable diseases like diarrhea, retarded growth, typhoid, dengue, malaria, malnutrition, anemia, and cholera as well as decreasing the fertility of the

soil, increasing flood risk by blocking water drains, affecting aquatic life, etc. (Srivastava et al., 2015). Every year, more than 1 million population still die due to water and sanitation-related diseases (Majorin et al., 2017; Venkateswarlu, 2019). Approximately 74% of the health burden from intestinal helminths and diarrhoeal disease are experienced by children under the age of 5 to 14 (Tarrass and Benjelloun, 2012) as shown in Figure 1.1 (Google images).

Despite the considerable investment in the water and sanitation sector, the budget allocated to sanitation has been comparatively low (Isunju et al., 2011). Based on the current progress in India, many policies are operated such as Integrated Low-Cost Sanitation Scheme (ILCS), Mega-City Scheme, Integrated Development of Small and Medium Towns (IDSMT), Swachh Bharat Abhiyan (Clean India Campaign), National Urban Sanitation Policy, Accelerated Rural Drinking Water Supply Program (ARWSP) in order to provide basic sanitation facilities to population. Despite this, the problems of sanitation have been looming large. There may be numerous reasons behind the "failure" of sanitation policies such as lack of interest of inhabitant for investing in sanitation and disposal facilities, low priority among stakeholders, inadequate funding, implementation of inappropriate (unsustainable) technologies, etc. (WHO and UNICEF, 2010; Showkat, 2016).

Furthermore, to provide basic sanitation facilities along with sewerage systems to urban slums and rural areas has become big challenge nowadays because of the poor accessibility of the cesspool emptier and solid waste collection trucks to reach in that areas, lack of legal status of these areas and lastly the lack of interest of inhabitant for investing in sanitation and disposal facilities (Katukiza et al., 2012). As a result, a population with lower household income have to suffer by paying much higher prices for water, risk impaired health, and incur significant survival costs. Moreover, due to population growth, resource shortfalls and environmental degradation, further add fuel to the stiff circle of poor sanitation (Cho et al., 2015).

One of the primitive ways is the source separation of urine and fecal. Out of which fecal is handled by traditional solid waste management tools and the reuse of urine for re-flushing is something which can be worked on. The eco-sanitation provides the opportunity for a sustainable yet affordable solution for the safe disposal of human waste. It is an approach to sanitation provision by using human urine as a resource of water. Ecological sanitation demonstrates a closed-loop methodology for reusing as flush waster instead of letting them diffuse into water streams (Simha and Ganesapillai, 2017; Kete et al., 2018). It is a guiding fundamental that favors context-specific

sanitation solutions by understanding that technology is not the adoption of any individual sanitation technology but it is an only end-points or 'means to end' of creating improved sanitation facilities.

Urine is a special type of complex mixer containing both molecular and ionic compounds. It represents a small volume (≈1%) of domestic wastewater, but the major source of water pollution (Spångberg et al., 2014). Urine is difficult to describe as one particular formula because of its high dependence on various factors like climate, age, diet, physical activities. It also contains various micro-pollutants such as synthetic hormones, vitamins, organic acids, pharmaceutical residues which are considered as emerging environmental pollutants (Dbira et al., 2019; Makos et al., 2019). The principal organic fraction of urine is mainly comprised of nitrogen-based components such as urea, creatinine and uric acid. Urine also contains most of the natural nutrients such as potassium, nitrogen, phosphorus, sodium, chlorides, etc. (Dbira et al., 2015). Despite, the presence of such valuable nutrients, the continuous discharge of insufficiently treated urine wastewater to surroundings is harmful to the environment as well as to human health because of their well-known role as endocrine disruptors (Udert et al., 2006; Dixit et al., 2017). Furthermore, Biological oxygen demand from the direct discharge of human waste into water streams is becoming a threat to biodiversity (Cho et al., 2014).

Hence it is necessary to treat this wastewater before its discharge because it has been validating that pathogens present in human urine can remain alive for a longer period of time (Hoglund et al., 2002). The treatment of urine wastewater can prevent the pollution in the environment by treating the harmful micropollutants which are not easily degradable during treatment processes and could be recycled as flush water (Udert et al., 2006). The main principle organic constituents in urine wastewater are urea, creatinine and uric acid. As a residual liquid, their main components may cause detrimental effects on the surrounding environment, in particular, because of their high nitrogen (N) content (Dbira et al., 2015).

The continuous discharge of these organic constituents via urine in the open streams leads to excessive N-loading in surface water and causes algal blooming leaving adverse effects on the ecosystem as well as human well-being. Moreover, its readily automatic conversion to ammonia via enzymatic hydrolyzes by urease leads to the serious environmental and health problems such as an increase in the pH of the soils and release of free ammonia into the atmosphere contributing toxic compounds like ammonium, nitrates, and sulfates (Hernandez et al.,2014). Treatment of such

wastewater becomes a challenge because of its complexity, odor, unstability, and composition which varies every day (Antoniou and Dionysiou, 2007).

During the last few decades, a wide variety of conventional treatment technologies like adsorption, air stripping, aerobic, anaerobic, coagulation, enzymatic decomposition, chemical oxidation, etc. have been used for the treatment of water and wastewater (Adams et al., 2002; Stackelberg et al.,2007; Singh et al., 2017). However, these technologies consume a large amount of water, time and required higher energy to treat wastewater. However, these technologies are proven inappropriate for the treatment of mixed wastewater (urinal) and inefficient for the complete removal of toxic nitrogen-based components (Rajasulochana and Preethy, 2016). In these treatment methods, the polluted water is subjected to successive different process units resulting in the formation of more complex intermediates. Furthermore, it has estimated that only 25% of the total wastewater generated in the country is getting treated and rest is directly discharged into water streams without any biological and chemical treatment (Wu et al., 2016).

The regular/continuous discharge of untreated/ not properly treated wastewater in water streams resulting in the generation of pathogens such as enteric viruses, helminthes (intestinal worms), bacteria, protozoa, *fecal streptococci*, *E. coli*., nutrients, micro-pollutants and traces of toxic organics pollutants. Thus causing potential risk to the environment in terms of polluting groundwater, lowers the pH of the soil, eutrophication in water streams due to excessive discharge of nitrogen-based components, decreasing the potency of agricultural land, etc. Moreover, most of these technologies such as adsorption, air stripping, aerobic, anaerobic, coagulation, enzymatic decomposition, chemical oxidation, etc. requires complex equipment, large economic investments, expertise to operate and consuming enormous amounts of energy and resources along with leaving a lot of emissions in the environments (Hu et al., 2016).

Thus, these traditional treatment technologies are not suitable for a country like India. Hence require effective and strong technologies for the treatment as well as the removal of persistent and recalcitrant compounds from wastewater. The in- capabilities of these treatment technologies have inspired the researchers to work in the field of advanced treatment technologies like ozonation, reverse osmosis, incineration, microfiltration, and advanced oxidation processes (AOPs) and electrochemical advanced oxidation processes (EAOPs). Among all these technologies AOPs and EAOPs have proven better for the degradation and mineralization of recalcitrant compounds.

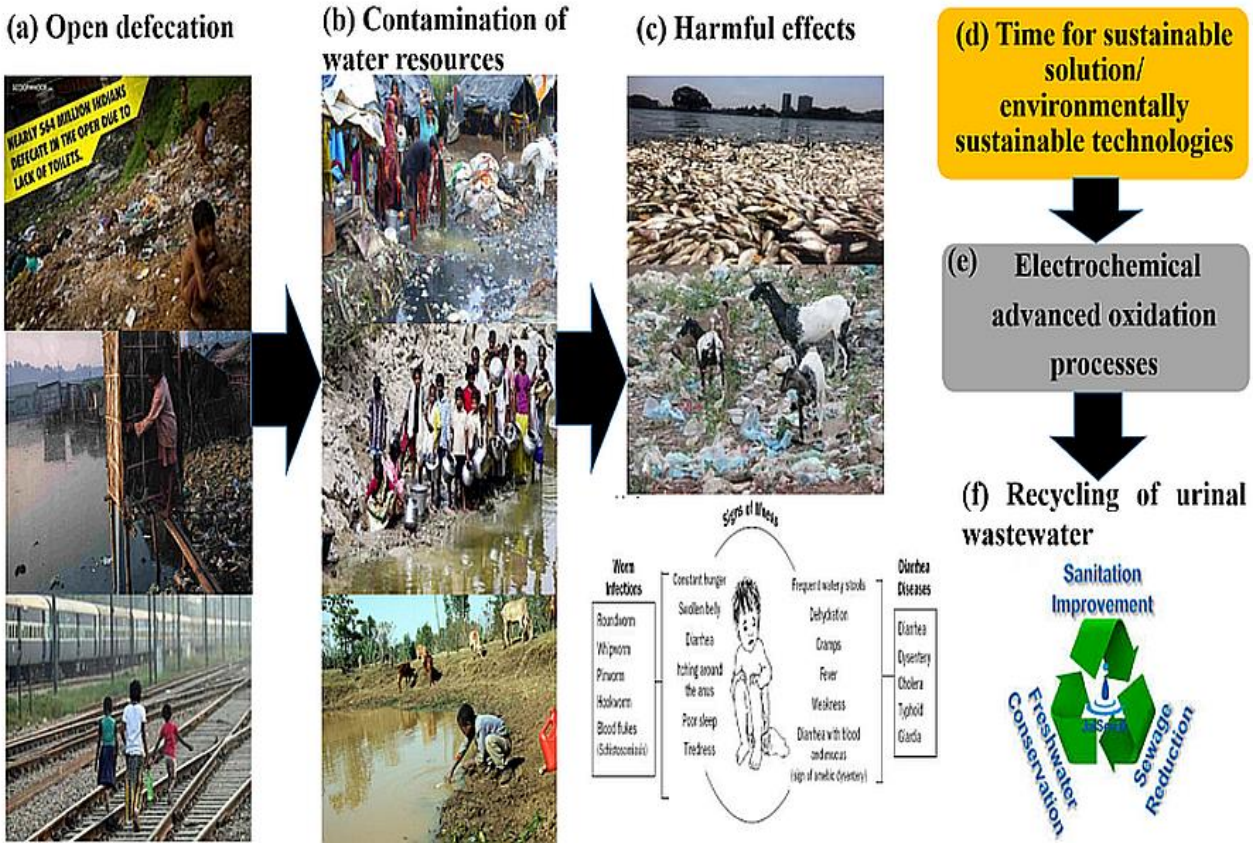

Figure 1.1 Poor sanitation systems and disposal facilities and its sustainable solution.

1.1 Overview of Advanced Oxidation Processes (AOPs) and Electrochemical Advanced Oxidation Processes (EAOPs)

Literature has consolidated the performance of AOPs as promising technologies for the treatment of such complex, toxic and wide variety of bio-recalcitrant pollutants present in water/wastewater (Cernigoj et al., 2007; Lester et al., 2011; Suzuki et al., 2015; Lee et al., 2016; Gagol et al., 2018). AOP's can be classified as photochemical oxidation processes which include various technologies like ozonation, photocatalysis, photolysis, sonophotocatalysis, Fenton, photo-Fenton, cavitation techniques (Kaur and Singh, 2007; Maddikeri et al., 2013; Raut-Jadhav et al., 2013; 2016), etc. as shown in Figure 1.1.1 (Bin and Sobera-Madej, 2012). Studies have been reported in the literature for the treatment of human urine and its metabolites (Liu et al., 2008; Antoniou et al., 2009; Zhang et al., 2015) using heterogeneous photocatalysis. However, AOPs have shown limited effectiveness for target compound oxidation in natural waters because of hydroxyl radical ($OH^{\bullet}$) scavenging by bicarbonate and dissolved organic carbon (DOC). The processes in AOP is

dosage-dependent processes, so the appropriate amounts of $OH^{\bullet}$ molecules are formed to achieve the desired level of treatment. Such complex chemistry will likely need highly skilled engineers to design the system correctly. Furthermore, traditional AOPs suffers from high capital and operating cost due to the continuous requirement of energy source like Ultra Violetrays (UV) and chemical reagents (catalysts and oxidizers) which increases with treatment time, reduced efficiency of titanium dioxide (TiO_2) catalyst in an immobilized state, requires high degree of pre-treatment and operational difficulties as well as a longer period of time for complete disinfection. Hence, it necessitates an immediate requirement for most cost-effective alternative technology (Chaplin, 2014).

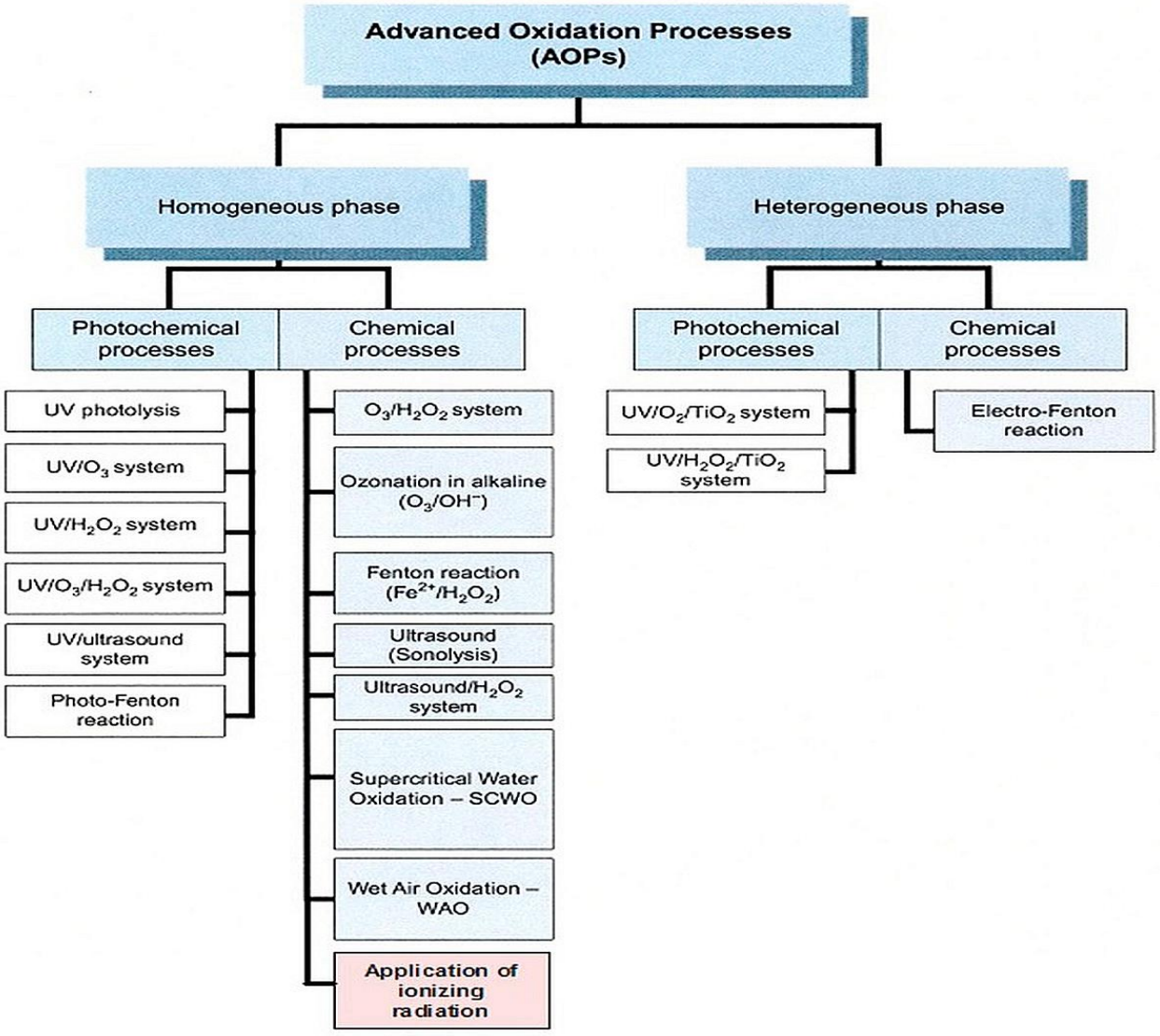

Figure 1.1.1 Classification of AOPs

In recent years, new AOPs based on the electrochemical technology, i.e., EAOPs, have been developed (Fryda et al., 2003; Martínez-Huitle and Ferro, 2006; Brillas et al., 2009) and shown its potential for degrading of a wide variety of pollutants. EAOPs are not a direct replacement for AOPs but have several advantages. A huge number of studies have shown that there is an opportunity for energy recovery from EAOPs by capturing the H_2 that is produced from cathodic reactions during simultaneous oxidation of organic compounds on the anode (Chaplin, 2014). Studies have also shown that the operation of EAOPs is cheaper than traditional AOPs under certain operating conditions (Sahu and Chaudhari, 2015).

EAOP is a technique based on the transfer of electrons (e^-), with the inherent advantage of the compatibility, versatility, and amenability to automation. It offers several promising approaches such as electro-oxidation, electrocoagulation, electro-chlorination, electro-Fenton, photo-electro-Fenton, sonoelectro-Fenton for the prevention and remediation of pollution problems (Brillas et al., 2009; Daghrir et al., 2012; Khandegar et al., 2018) as shown in Figure 1.1.2 (Ganzenko et al., 2014). One of the most attractive and affordable technologies that have come under EAOP's is the electro-oxidation (EO). Studies pertaining to EO have confirmed that the technology is a strong bet for the treatment of toxic and persistent bio-refractive compounds (Canizares et al., 2009; Sires et al., 2014). It is considered as highly efficient, versatile, cost-effective and eco-friendly technology with high oxidation stability and has made considerably huge progress in water/ wastewaters treatment (Zhuo et al., 2011; Sahu and Chaudhari, 2015).

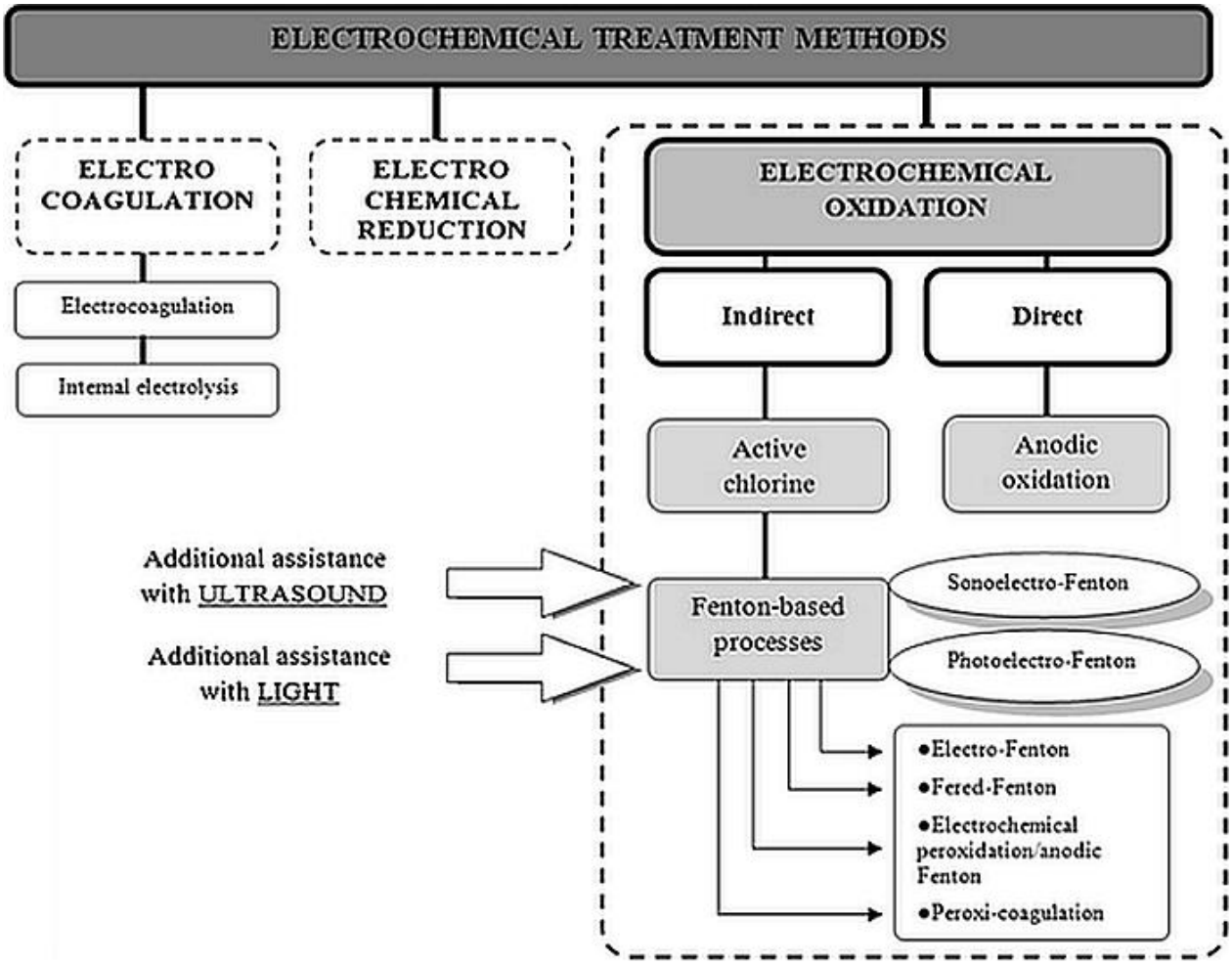

Figure 1.1.2 Classification of EAOP treatment technologies

1.2 Electro-oxidation (EO) Process and Mechanism

EO process involves two mechanisms i.e "direct" (pollutant degrade on electrode surface) and "indirect" (pollutant degrade in the bulk) as shown in Figure 1.2 (Outran et al., 2014). Indirect oxidation, pollutant reaches the anodic surface and degrade on the surface itself through the generation of physically adsorbed "active oxygen" in the oxide lattice as shown in Equations 1.2.1-1.2.2. While in the case of indirect oxidation pollutants degrade by strong oxidants like chlorine, hypochlorite, hypochlorous acid, hydrogen peroxide, ozone, etc produce in bulk during electrolysis as described in Equations 1.2.3-1.2.9 (Panizza et al., 2010; Sarkka et al., 2015).

$$R + H_2O \longrightarrow R(OH^{\bullet}) + H^+ + e^- \quad \textbf{(1.2.1)}$$

$$R(OH^{\bullet}) + P \longrightarrow R + mCO_2 + n\,H_2O + H^+ + e^- \quad \textbf{(1.2.2)}$$

$$2Cl^- \longrightarrow Cl_2 + 2e^- \quad \textbf{(1.2.3)}$$

$Cl_2 + H_2O \longrightarrow HOCl + H^+ + Cl^-$ **(1.2.4)**

$HOCl^- \longrightarrow H^+ + OCl^-$ **(1.2.5)**

$H_2O \longrightarrow OH^\bullet + H^+ + e^-$ **(1.2.6)**

$2OH^\bullet \longrightarrow H_2O_2$ **(1.2.7)**

$H_2O_2 \longrightarrow O_2 + 2H^+ + 2e^-$ **(1.2.8)**

$O_2 + O^\star \longrightarrow O_3$ **(1.2.9)**

EO process does not require any chemical additives like hydrogen peroxide (H_2O_2) for the generation of $OH^\bullet$, moreover, it generates directly from the oxidation of water. These $OH^\bullet$ react with a wide range of recalcitrant pollutants unselectively, generally at diffusion-limited rates. Further, in addition to this, the compounds which are unreactive to $OH^\bullet$ can be degraded through critical rate-limiting step i.e. direct electron transfer (DET) reactions. These types of reactions basically contribute an additional mechanism in the oxidation of the target compound by transferring an electron directly from the pollutant to the electrode. A larger number of studies have shown the involvement of both $OH^\bullet$ reactions and DET reaction in the oxidation pathways of pollutants (Chaplin, 2014). Studies have shown that due to water oxidation an acidic layer was produced at the surface of the anode which prevents the scavenging of $OH^\bullet$ in natural waters by protonating HCO_3^- to H_2CO_3.

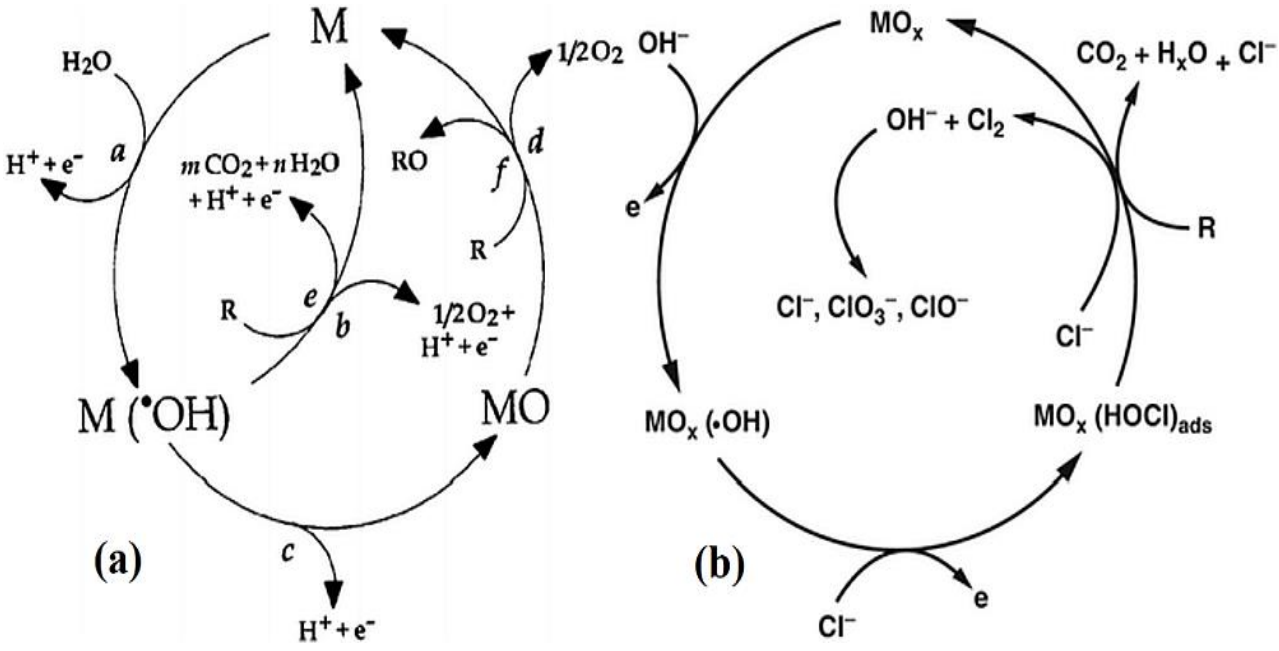

Figure 1.2 Mechanism of EO and Electro-chlorination (Outran et al., 2014)

1.3 Applications of EO for Wastewater Treatment

A large number of studies have shown that EO has come up with as a promising technology for degrading of a wide variety of recalcitrant pollutants such as chlorinated organics, fluorinated organics, phenolic compounds, landfill leachate, human waste, pharmaceuticals and various type of industrial effluents (Anglada et al., 2009; Chaplin, 2014). Studies have also shown that during oxidation of target compounds simultaneously there is an opportunity of recovery energy by capturing gases like hydrogen (H_2) which generate from cathodic reactions (Chaplin, 2014). To gain insight into the use of EO processes, certain conditions likely to be encountered for treating water and wastewater; those are electrode material, operating conditions, the stability of electrodes and configuration of the cell (Urtiaga et al., 2013).

The effectiveness of the process and its feasibility at a commercial level largely depend upon the electrodes material which is capable of generating a lot of strong oxidizing agents such as $OH^{\bullet}$ and various chloro-oxidant species as shown in Equations 1.3.1-1.3.11. Panizza and Cerisola, (2008) divided anodes into two classes i.e. "active" and "non-active" based on the strong and weak interaction of in-situ generated $OH^{\bullet}$ with the electrode surface. Active anodes (IrO_2, RuO_2) exhibit higher electrochemical activity for O_2 potential i.e. has lower oxygen evolution potential (OEP) therefore are unable to perform complete mineralization or do partial oxidation of recalcitrant organic compounds through active chlorine (Cl_2), hypochlorite (OCl^-), hypochlorous acid (HOCl), etc. while non-active anodes (PbO_2, SnO_2) have higher OEP hence are able to do complete mineralization (Martinez-Huitle and Ferro, 2006). Although inactive anodes do complete mineralization due to low conductivity these electrodes are not stable for a longer period of time. To overcome this problem electrodes are doped using common dopants like Sb, B, Bi, etc. to increase their conductivity as well as stability.

$$R(OH^{\bullet}) \longrightarrow RO + H^+ + e^- \quad \textbf{(1.3.1)}$$

$$RO + P \longrightarrow R + PO \quad \textbf{(1.3.2)}$$

$$RO \longrightarrow R + \tfrac{1}{2} O_2 \quad \textbf{(1.3.3)}$$

$$R(OH^{\bullet}) \longrightarrow R + \tfrac{1}{2} O_2 + H^+ + e^- \quad \textbf{(1.3.4)}$$

$$2Cl^- \longrightarrow Cl_2 + 2e^- \quad \textbf{(1.3.5)}$$

$$Cl_2 + H_2O \longrightarrow HOCl + H^+ + Cl^- \quad \textbf{(1.3.6)}$$

$$HOCl \longrightarrow H^+ + OCl^- \quad \textbf{(1.3.7)}$$

$Cl^- + OH^\bullet \longrightarrow ClO^- + H^+ + e^-$ **(1.3.8)**

$ClO^- + OH^\bullet \longrightarrow ClO_2^- + H^+ + e^-$ **(1.3.9)**

$ClO_2^- + OH^\bullet \longrightarrow ClO_3^- + H^+ + e^-$ **(1.3.10)**

$ClO_3^- + OH^\bullet \longrightarrow ClO_4^- + H+ + e^-$ **(1.3.11)**

Where R: electrode; P: pollutant

1.4 Overview of Electrodes

Recently several researchers have presented different groups of novel electrodes for degradation of pollutants are boron doped diamond (BDD), mixed metal oxide anodes (MMO) such as $Ti/TiO_2/RuO_2$-PbO_2, TiO_2-SnO_2, Ti/RuO_2, $Ti/RuO_2/SnO_2$, $Ti/IrO_2/SnO_2$-Sb, Ti/Pt, Ti/Pt-Ir, $Ni/Ni(OH)_2$ as most effective anodes (Szpyrkowicz et al., 2000; Zanta et al., 2003; Panizza and Cerisola, 2009; Wu et al, 2014) while cathodes like graphite or carbon felt, copper, stainless steel etc. are commercially available working electrodes used for in-situ electro-generation of H_2O_2. Nidheesh and Gandhimathi, (2014) and Rosales et al., (2012) have reported that graphite was best cathode material for electro-generation of H_2O_2. These different kinds of electrodes such as lead and lead dioxide, BDD, Graphite electrodes, metal anodes, MMO and doped-MMO have been studied for the degradation of a wide variety of pollutants (Borras et al., 2010; Scialdone, 2009; Aquino et al., 2014).

1.4.1 Lead and Lead dioxide (PbO_2)

EO using lead and lead dioxide has been used efficiently in various lead acid batteries for treatment of various pollutants because of their stability, low cost and oxygen evolution potential which delays the evolution of O_2 over Cl_2. But at the same time, it has also been observed that in presence of acidic electrolyte, an adherent film formed on the surface of anode due to which electrode poisoning occurred along with the dissolution of toxic Pb^{2+} ions. Hence, hinders the use of lead and lead dioxide as anodes (Sarkka et al., 2015).

1.4.2 Boron-doped diamond (BDD)

The other most extensively and promising electrode used for EO is BDD. These electrodes are suitable for wastewater disinfection because of the inertness in tough conditions, high oxygen evolution over potential, electrochemical stability, good current efficiency, high corrosion stability,

and good conductivity (Dbira et al., 2015; Cotillas et al., 2016). It has also been suggested that BDD are not efficient for the treatment of highly saline wastewater because it is less effective in chlorine generation as compared to other electrodes and, due to their high over-potential for oxygen and chlorine evolution, which may generate toxic byproducts like chlorate and perchlorate (Raut et al 2013). Hence require additional treatment for the removal of these toxic products. Moreover, the known high cost of conductive diamonds anodes makes there large-scale industrial application unfeasible.

1.4.3 Mixed Metal Oxide Anodes (MMO)

Recent studies have come up with the use of MMO with market name dimensionally stable anodes (DSA) for the treatment of wastewater containing recalcitrant organics. MMO anodes are one of the effective and electrochemically stable electrodes with better process efficiency, possess high quality for chlorine evolution and competent in the production of the chloro-oxidant species like Cl_2, ClO^-, HOCl, etc. during EO treatment (Chen, 2004; Scialdone,2009) as well as presents longer service life as compared to other electrodes (Chen, 2004; Lacasa et al.,2012). These type of electrodes such as Sn-Sb binary MMO, Ir-Ru binary MMO, Ir-Ta binary MMO, Ti-Ru binary MMO, Ti-Bi binary MMO, Ir-Ru-Sn ternary MMO, Ce-Ru-Sn ternary MMO and Ru-Ir-Sn-Ti quaternary MMO anodes (Wu et al.,2014) have been used for the EO treatment of large variety of wastes such as dyes effluent (Rajkumar and Kim, 2006; Raghu et al., 2009), pesticides and herbicides (Neto and Andrade, 2009; Malpass et al., 2006), phenolic compounds (Wang and Wang, 2008), pharmaceutical waste (Cheng et al.,2013; Fernandes et al., 2014), plasticizers (Wang et al.,2010), chelating agents (Shao et al.,2006) and Microcystin toxins (Shi et al.,2005).

Electrochemical water splitting at MMO generates adsorbed $OH^{\bullet}$ which further evolves towards oxygen evolution reactions and likely to cause complete degradation of organic compounds (Scialdone, 2009). These MMO anodes have established their worth in treating a wide variety of pollutants like paper mill water (Sarkka et al., 2009), reverse osmosis concentrate (Bagastyo et al., 2011), synthetic wastewater (Zhou et al., 2011) and landfill leachate (Panizza and Martinez-Huitle, 2013).

For the past few years, various attempts have been made to develop doped-MMO anodes in order to achieve the better electrocatalytic activity, photoelectrocatalytic activity, corrosion resistance, conductivity, hydrophilic and hydrophobic properties (Singh et al., 2016). Some of the

dopants used in the MMO anodes for corresponding improvements are TiO_2-NTs/SnO_2-Sb, Ti/Ce-PbO_2, Ti/PbO_2-Pr, Ti/Gd-PbO_2, and Ti/ PbO_2-Co-F, etc. (Wu et al., 2014). Several studies have shown that by using this doped-MMO for the degradation for degrading of a wide variety of recalcitrant pollutants with better removal efficiencies.

1.5 Photo-electrocatalysis (PEC)

Another technology which comes under EAOPs is PEC. This technique is a combination of two processes EO and photo-catalysis (PC). Although the photocatalytic process has been extensively studied for degradation of pollutants via using TiO_2 as a photocatalyst under UV illumination. But its practical application on large scale for the oxidation of recalcitrant pollutants has been blocked due to the low photonic efficiency because of the fast recombination of the photo-generated electron/hole (e^-/h^+). Using the electro-catalysis process in combination with PC can prevent the recombination of the e^-/h^+ pair generated during PC (Daghrir et al., 2012). The process increases efficiency, decreases the costs besides increasing the rate of degradation of recalcitrant pollutants (Catanho et al., 2006). PEC oxidation process has received considerable attention in the field of environmental protection and has been applied for the treatment of different effluents like dye (Han et al., 2008; Wang et al., 2010), phenolic compounds (Li et al., 2007; Xu et al., 2012), Humic substances (Selcuk et al., 2003), microbial pollutants (Philippidis et al., 2010), etc. present in wastewater (Daghrir et al., 2012)**.** Hence, the PEC process is considered as a good alternative to conventional PC for improving the degradation rate.

1.6 Pilot Scale Studies with Continuous EO Reactor

The designing of the cell or reactor is an important issue to maintain the high mass transfer rate on the electrode surface in a cell some of the likely methods are used such as gas sparging, use of baffles, incorporation of turbulence promoters. An EO reaction can be operated in batch or continuous (mixed/plug) flow mode with or without recycle. Further division can be made on the basis of parallel or series flow (Sulaymon and Abbar, 2012). The design of electrolytic cells to yield a high conversion of electro-active species, reactor is made while keeping two aspects or in mind, that is electrode geometry and configuration of cell that is two dimensional or three-dimensional construction (based on electrode geometry) and other is undivided or divided cell (based on configuration) (Anglada et al., 2009). To have a successful implementation of electrochemical advanced oxidation processes the role of reactor designing is very important. The reactor

configuration can be modified or redesigned to have a better effect on electrodes and operating conditions. Few studies have shown the effective utilization of large variety of batch and continuous electrochemical reactors at lab scale or field scale for the degradation of recalcitrant pollutants (Raju and Basha, 2005; Brillas et al., 2009; Daghrir et al., 2012; Park et al., 2013; Cho et al., 2014; Menon et al., 2015; Barbosa et al.,2018).

1.7 Aim of the Proposed Study

The goal of this study is to evaluate the efficacy of MMO and doped-MMO electrodes for the EO treatment of synthetic urine/actual human urine (SU/AHU) and its metabolites (urea, creatinine and uric acid). Besides reporting its novelty in terms of first-time use of these types of the anode, efforts have also been done to reduce the treatment time as reported in the literature by incorporating the concept of a dual effect called PEC. The process was executed both at lab scale and at pilot scale with proper optimization of process parameters. The process was validated by executing a lab-scale trial for the EO treatment of actual human urine.

Chapter -2

REVIEW OF LITERATURE

2.1 General

This chapter intended to present a review of the literature related to research work for the treatment of urine metabolites i.e. urea, uric acid and creatinine, SU and AHU by EO and PEC treatment processes. This chapter has been divided into two sections: (i) represents the review of EO and PEC treatment processes along with mechanism and factors which affect the efficiency of these processes and (ii) represents the application of both processes for the treatment urine and its metabolites.

Section I

2.2 Overview

From the past many years, the need for sustainable development in terms of basic sanitation facilities and health has always been neglected or given low priority in developing countries like India. Despite many policies like Mega-City Scheme, Integrated Low-Cost Sanitation Scheme (ILCS), Swachh Bharat Abhiyan (Clean India Campaign), Accelerated Rural Drinking Water Supply Program (ARWSP), etc. India has failed to make proportionate strides in developing its sanitation sector. Till date, 2.4 billion people still living without adequate sanitation facilities and the majority of whom practice open defecation (Langergraber and Muellegger, 2005; WHO/UNICEF, 2015). Freeman et al.,(2017) reported that poor sanitation and a continuous discharge of untreated human excreta (urine and feces) from slums/ rural areas to running streams of water has led to negative impacts on environments and human health. These impacts can cause potential risk of transmission of waterborne pathogens from water to nearby areas which further leads to contamination of soil/ water, generation of non-preventable waterborne diseases such as diarrhea, dengue, malaria, etc. particularly, children less than the age of 5 years (Rautanen and Viskari, 2006; Luthi et al., 2010). Studies have shown that many inhabitants from rural areas and peri-urban slums still lack sewerage and drainage systems results in the accumulation of hazardous toxic waste in-ground/surface water resulting in negative ecological effects.

According to one study, India generates a staggering 1.9 million tons of human waste a day, out of which 75 percent of sewage goes untreated and disposed of in surface water, groundwater, lakes, running streams and coastal areas. This is because of the lack of adequate water supply at the end of the pipeline and less money and manpower to treat all the sewage generated (Centre for Science and Environment and Down To Earth magazine, 2016). A case study has been reported of Malyana, a small town in Shimla had discharged untreated wastewater from Sewage Treatment Plant (STP) into the mainline source of drinking water supplied by the Irrigation and Public Health Department. Due to which an acute jaundice breakout led to the death of seven people and had affected over 1200 people. From the reports, it was found that STP was never in operation due to which sewage was discharged without any biological or chemical treatment (The Indian Express, 2016). Another article in 2017 has reported the sewage pollution in water supply in Indore due to lack of regulation and capacity, more than 20% of untreated sewage waste was dumped into the water supply, while 80% of the sewers were under-utilized or blocked. Due to this, exposure to microbial harmful pathogens and chemicals like nitrogen, phosphorus, and heavy metals have increased in the river resulting in serious health problems (Tahir and Visaria, 2017).

There are still many more case studies were reported in the literature on the direct disposal of untreated sewage in water supply systems which lead to pollution and various non-curable diseases. Due to the in-capabilities of the conventional treatment technologies, this exposure of pathogens and toxic compounds via drinking water to humans and aquatic life has risen the major issues among government, non-governmental water suppliers, water regulators, sewage and wastewater management and public (Luthi et al., 2010). Hence in this developing world, there is a great need for decentralized, effective and sustainable water treatment technologies that drive towards the on-site wastewater treatment in buildings and water reuse technologies with reduced consumption of energy, water, and capital cost. The literature thoroughly reviewed to examine the advancement in the field of sewage and wastewater treatment through EAOP treatment technologies a promising class of AOP. This review clearly addresses the disadvantages and advantages of every aspect of EAOPs (technique, electrode material, parameters, etc.) in context to their practical application at the commercial level. This review considerably aims at the degradation of nitrogenous organic pollutants present in urine wastewater.

2.3 Assets and Liabilities of Electrochemical Advanced Oxidation Processes (EAOPs)

Over the past few years, EAOPs have come up as promising technology for the degradation of recalcitrant and complex mixed wastewater streams. Using electricity (i.e. current/voltage) for the treatment of waters/wastewater was first proposed in 1889 in the UK (Chen, 2004). EAOPs are considered as an alternative class of advanced oxidation processes that rely on the in-situ generation of $OH^{\bullet}$ via the oxidation of water on the surface of the anode as shown in Equation 2.3.1 (Chaplin, 2014). Because of its high oxidation evolution potential, $OH^{\bullet}$ reacts rapidly and unselectively with a wide range of recalcitrant toxic organics pollutants such as phenolic, chlorinated and aromatic compounds (Diaz et al., 2014).

$$H_2O \longrightarrow OH^{\bullet} + H^{+} + e^{-} \qquad \textbf{(2.3.1)}$$

In addition to this, EAOPs offer several advantages in terms of versatility, energy-efficient, environmentally compatible, automation amenable and last but not least cost-effective (Brillas et al., 2009). For these reasons, EAOPs can be considered as a potential alternative inhibitor for the remediation of pollution problems (Sires et al., 2014). The design, development, and application of EAOP's for the treatment of water and wastewater has particularly focused on some effective technologies like electrocoagulation, electrodeposition, electrofloculation, EO, electro-reduction, electro-Fenton, photo electro-Fenton, solo electro-Fenton, electro-chlorination and PEC (Martinez-Hutile and Brillas, 2009; Outran et al.,2009).

2.4 Electro-oxidation (EO)

In recent years, various scientific journals have been thoroughly discussing the applications of EO for the remediation of environmental pollution. The removal mechanism of EO based on two categories i.e. (i) separation technologies in which target pollutant get separated from the aqueous medium without changing its chemical structure (ii) degradation technologies, which cause the breakage in the bonds causing alteration of the complex target compound into simple by-products (Sirés and Brillas, 2012). Usually, in EO recalcitrant pollutant oxidized by two different oxidation mechanisms. Indirect oxidation target compound degrade directly at the surface of anode by transfer of electron or by physisorbed/ chemisorbed $OH^{\bullet}$ generated via oxygen evolution reaction (OER) while in case of indirect oxidation target pollutant destroyed by weakly physisorbed $OH^{\bullet}$ at surface of anode or by other common oxidants such as reactive chlorine species (RCS), persulfates,

percarbonate, O_3, H_2O_2, etc. in the bulk (Moreira et al., 2017). The efficiency of the process is highly dependent on an affiliation between substrate mass transfer and electron transfer from bulk to the anode surface. There are thousands of publication which has been reported on the degradation of pollutants from wastewater via EO. It has been seen that progress and removal efficiency of the process depend upon certain operational parameters such as solution's pH (Kaur et al., 2015), initial concentration of substrate (Rajkumar et al., 2007;), temperature (Schmalz et al., 2009), treatment time (Bansal et al., 2013), applied current (Niu et al., 2013), presence of organic and inorganic content (Chaplin, 2014; Sires et al., 2014), flow rate (Koparal et al., 2007), supporting electrolyte composition (Guzmán-Duque et al., 2014), electrode material (Martı´nez-Huitle and Brillas, 2009) and cell configuration (Brillas et al., 2009).

2.4.1 Effect of pH

The pH of the solution affects the solubility or ionization degree of the organics, adsorption capacity, rate of formation of oxidants during the reaction, surface charge properties, target compound dissociation and valence band oxidation potential (Daghrir et al., 2012). Several researchers have proven that the removal efficiency of pollutants such as dyes, pharmaceuticals, pentachlorophenol, humic acid, etc. was high in acidic solution over the alkaline solution. This might happen because at acidic pH (i) exhibition of the high oxidative potential of the $OH^{\bullet}$ takes place, (ii) inhibition of the OER was there, and (iii) the concentration of bicarbonates and carbonates ions decreases, which are robust scavengers of $OH^{\bullet}$. Some studies have also explained the effect of pH on indirect oxidation with respect to the formation of RCS. At lower values of pH, the chlorine species which dominants is HOCl with high oxidation potential while in case of higher values of pH the species with high concentration is ClO^- having lower oxidation potential (Moreira et al., 2017) as shown in Figure 2.4.1 (Martinez-Huitle and Brillas, 2009).

Some authors have used a point of zero charge (PZC) of TiO_2 whose value lies between (4.5 pH to 7 pH) to study the effect of pH on photo-catalytic oxidation performance. For TiO_2, the PZC has approximately 6 pH and under such case surface charge of TiO_2 becomes neutral due to which the electrostatic interaction between the TiO_2 and organic pollutant is absent. While for (pH values >6) the surface of TiO_2 becomes charged negatively due to which electrostatic repulsion toward pollutant which is anionic dominates. However, in the case of pH lower than PZC, the surface of the catalyst becomes positive (Chong et al., 2010). Selcuk et al., (2003) has explained that the

distribution of TiOH is more than or ≈ 80% when pH value lies (3<pH>10), whereas the distribution of TiO^- and $TiOH_2^+$ were high or ≈ 20% for a pH value (>10 or <3).Thus, organic pollutants better removal efficiency took place at acidic pH values. But some pollutants like dyes remove better at basic pH. This conclude that the pH of the solution highly dependent upon the type of the pollutant, supporting electrolyte as well as the type of electrode material used (Wu et al., 2014).

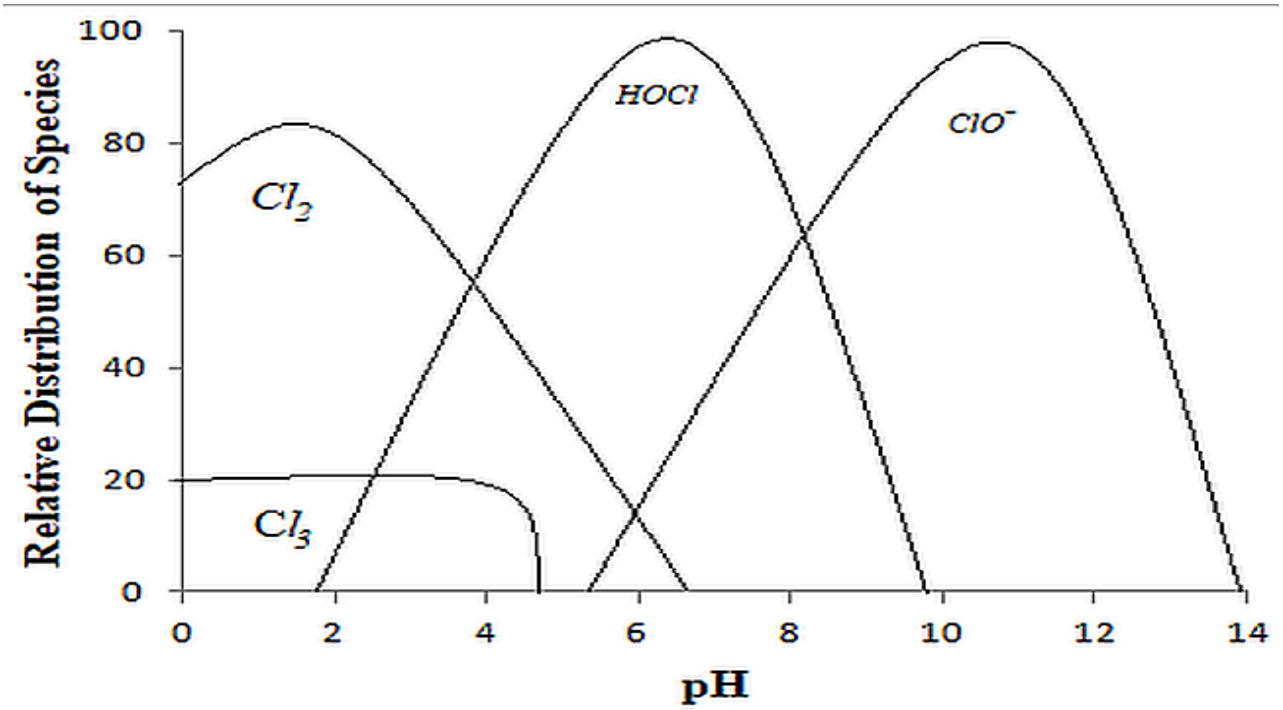

Figure 2.4.1 Generation of Chloro-oxidants species with respect to pH

2.4.2 Effect of temperature

Many studies have been reported in the literature that temperature changes have a significant influence on the rate of reaction of pollutant oxidation, the adsorption capacity of $OH^{\bullet}$ on anode surface and increased electro-generated oxidant species like RCS, peroxodisulfate, etc. (Canizares et al., 2006). Meaney and Omanovic, (2007) and Pan et al., (2012) reported that the rate of reaction of lignin and 4-chlorophenol was increased by 2.5 and 2.7 folds times with the rise in temperature from 20 to 60 ºC at mixed metal oxide (MMO) anode. Several studies have explained the relationship of Arrhenius Equation 2.4.1 with temperature influence on degradation efficiency (Wu et al., 2014).

$$\ln k = -\frac{E_a}{RT} + \ln A \qquad \textbf{(2.4.1)}$$

However, some researchers have reported the negligible influence of temperature on degradation efficiency while others reported the decrease in the concentration of oxidant species such as reactive chlorine species at MMO when temperature increased from 20 to 70 ºC (Borras et al., 2007; Neodo et al., 2012). From reported research, it has been concluded that to have better efficiency and low cost, the EO process was performed at ambient temperature.

2.4.3 Effect of initial pollutant concentration

In general, it was observed that solutions i.e. water/wastewater with higher initial organic pollutant concentration required a longer time to attain a given degree of degradation (Moreira et al., 2017). Moreover, some authors reported that the treatment of pollutants with high initial concentrations in wastewater leads to the high elimination per unit of time, i.e. higher pollutants removal rates. This could be due to the faster oxidation of pollutants with $OH^{\bullet}$ and the inhabitation of parasitic/ side reactions (Da Silva et al., 2014). Niu et al., (2013) reported that rise in concentrations of 2,4 Dichlorophenol (2,4-DCP) from 100 to 200 mg/L led to increase in rate constants (k) values from 0.21 to 0.26 min^{-1} and decrease in half-life ($t_{1/2}$) from 2.8 ± 0.2 to 2.3 ± 0.1 min respectively. On contrary to this some researchers have also reported that pollutant with a high concentration in wastewater decreases the process efficiencies.

Wu et al., (2008) and Liu et al., (2011) in their studies reported that the chemical oxygen demand (COD) removal found a minimum when the initial concentration of pollutants was increased to a higher value. This might happen because of an increase in oxidation load and adsorption rate on the anode surface which further reduces the catalytic ability and adsorption capacity. Thus, increases the treatment time, energy consumption, decreasing process efficiency as well as affecting the service life of anode (Zhang et al., 2013). Moreira et al., (2017) reported that first-order rate constants and $t_{1/2}$ for pollutant removal remained unaffected with a rise in substrate concentration. But when performed experimentally, it was found that the increase in the pollutant concentration in wastewater decreases rate constant values. This happened due to (i) rate-determining step shifting from diffusion process to the charge-transfer process on anode, (ii) mass transfer limitations of oxidative species from/ towards anodes and (iii) comprehensive mechanistic kinetic model limitations.

2.4.4 Effect of supporting electrolyte

The influence of the different types of supporting electrolytes and its concentration on EO efficiency was studied by several authors (Cho et al., 2014; Guzman-Duque et al., 2014; Wu et al., 2014). In general, the electrolyte is used to increase the conductivity of the solution and make them suitable for a particular process. Among various supporting electrolytes (NaCl, Na_2SO_4, $NaNO_3$, $NaSO_3$, $NaNO_2$, and $NaClO_4$) NaCl is highly stable and widely used as a disinfectant (Örmeci et al., 2001; Vanlangendonc et al., 2005; Karuppiah and Raju, 2009). Anglanda et al., (2009) in their study, discussed that increased electrolyte concentration had subsequently lowered the cell voltage for applied current density, thus made the EO treatment process more acceptable and cost-effective. EO with active anodes such as an MMO has greater efficiency in presence of Cl^- as compared to non-active anodes (such as BDD, Ti/SnO_2, etc.) (Guzmán-Duque et al., 2014). However, the contradictory observation was made by (Cui et al., 2012) that the addition of Cl^- in dye wastewater has enhanced the decolorization efficiency but not able to reduce total organic carbon (TOC) to the desired value. The other drawback of employing sodium chloride (NaCl) as supporting electrolyte especially in the case of BDD led to the formation of toxic byproducts such as chlorates (ClO_3^-) or perchlorates(ClO_4^-) (Bergmann et al., 2009). But some studies have also reported the readily consumption of RCS before the process ends, depending upon the type of electrode and concentration of electrolyte used (Wu et al., 2014).

2.4.5 Effect of current density

Among various operational parameters, current density has a strong influence on the oxidation as well as process efficiency. It is also important for the purpose of the mechanistic study as well as a key factor in analyzing the overall cost of the treatment process. Any easy meaning of increasing the current density is the speeding the oxidation process because the ability of electron transfer and generation oxidizing species depends upon the applied current density and type of electrode used. Rajkumar et al., (2007) found that the production of Cl_2/ClO^- was significantly enhanced when current densities increased from 7.22 to 36.10 mA/cm^2. Zhu et al., (2008) reported the maximum percentage removal of phenol was achieved when the applied current density was increased from 10 mA/cm^2 to 50 mA/cm^2. Rapid degradation of crystal violet was observed on IrO_2 at higher current densities while in the case of BDD at lower values of applied current (Guzmán-Duque et al., 2014). In most of the cases, it has been observed that higher values of current densities

always results in maximum destruction of different recalcitrant pollutants. However, it was also observed that the increase in current densities led to maximum energy consumption as well as the cost of the overall process. In industrial applications, the electrochemical treatment of pollutants at high current densities is rarely applied due to the low removal rate at higher values of current, OER occurs which consumed the $OH^{\bullet}$ and produce low potential oxidants and additional energy consumed due to the increase in solution temperature (An et al., 2012). On the basis of the process kinetics, it was observed that pollutant oxidation at higher current values considered as mass transfer limiting reaction and to attain maximum COD removal, a flow rate of supporting electrolyte was increased (Wu et al., 2014).

2.4.6 Effect of stirring rate

Moreira et al., (2017) have reported that in an electrocatalytic reactor the stirring rate of the solution must be monitored to achieve the fast homogenization of the reaction solution by good mixing. This will further avoid the solid deposition on the anode surface, prevent sedimentation and assure the appropriate mass transfer of target pollutants toward the electrode.

2.4.7 Effect of electrolysis time

During the EO treatment process, it was found that time plays an important role in controlling the rate of reaction. Thirugnanasambandham et al., (2015) reported the increase in COD and color removal with increasing time, but after a certain value of the time, it was found that removal became constant. This was due to the passivation of the electrodes and increase in oxygen gas evolution which limits the performance of the EO treatment process (Bansal et al., 2013; Hiwarkar et al., 2017). During electrolysis, it was observed that contaminants bond to the anode surface which grows like a thick film with the passage of time (Kaur et al., 2015). Therefore, due to the resistance of this impermeable film on the surface of the anode has decreases the overall efficiency of the treatment process as well as the increase in energy consumption was also observed.

2.4.8 Effect of the type of electrode

Ideally, the nature and type of electrode have a strong influence on the selectivity, percentage of reduction and efficiency of the treatment process. The electrode used for the abatement of the process should be physically and chemically stable, adequate conductive, resistance to corrosion and highly active, low cost, durable and less active towards side reactions (Zhou et al., 2011). Many

researchers have reported the potential use of the different types of electrodes for the degradation of various types of toxic and recalcitrant organic pollutants along with their comparison and oxidation mechanisms (Barrera-Díaz et al., 2014). There are two classes of electrodes (i) active anodes (IrO_2, RuO_2, Pt) with low O_2-overpotentials, which are characterized by a high electrochemical activity toward oxygen evolution and low chemical reactivity toward oxidation of organics. At these types of anodes, effective oxidation of pollutants occurs at lower values of current while at high current values, the efficiency of the treatment process decreases due to the evolution of side reactions. In contrast (ii) anodes with high O_2 overvoltage known as non-active anodes (BDD, SnO_2, PbO_2), in which M ($OH^{\bullet}$) are weakly physisorbed at the surface of the anode which means anodes has higher chemical reactivity toward pollutant degradation. These types of anodes work at higher current densities with minimum input from OER resulting in complete mineralization (Foti et al., 1999; Martı´nez-Huitle and Ferro, 2006; Anglada et al., 2009; Chaplin, 2014).

Traditionally, the anodes used for the treatment of water and wastewater include lead, lead dioxide, and doped lead dioxide. Cossu et al. (1998) reported that using titanium coated with PbO_2 anode, COD was removed up to a value of 100 mg/dm^3 by the direct oxidation of organics with $OH^{\bullet}$. Zhou and He, (2008) reported the electrochemical degradation of an azo dye, on a novel PbO_2 anode and found that at high current densities and high-temperature values, the degradation was maximum but at the same time the overall cost also increased. Panizza et al., (2010) reported that the organic loading of landfill leachate was efficiently removed using a flow cell equipped with a PbO_2 anode. In particular, the specific energy consumption to reduce the COD below the disposal limit <160 mg/dm^3 or to completely remove the COD was 90 mg/dm^3.

PbO_2 electrodes are inexpensive, superb conductivity and widely used for degradation of pollutants. The only drawback is a generation of highly toxic Pb^{2+} ions in solution from corrosion, leading to serious secondary pollution (Chen, 2004). In order to resolve the issue of release of toxic Pb^{2+} ion, (Kotz et al. 1991; Comninellis, 1992; Grimm et al., 1998; Cossu et al., 1998) were some researchers, evaluated the comparison between PbO_2 anode and antimony doped tin oxide anodes ($Ti/SnO_2–Sb_2O_5$) for the EO treatment of pollutants like phenol, landfill leachate, etc. and found that later anode was much better without any generation of toxic ions in the treated solutions. Despite of immense efficiency for the treatment of organics (Correa-Lozano et al. 1997; Chen et al., 2005) this anode lack sufficient chemical stability as well as found that service life was only up to 12 h at

current density of 1000 A/m^2 in 1M H_2SO_4 solution while at 10,000 A/m^2 and 3M H_2SO_4, this anode last for few seconds only. To increase the life span of the anode, IrO_2 was mixed (Chen et al., 2002) and found that charge storage could be enhanced after polarization in 3M H_2SO_4 solution at 1 A/cm^2 for 1000 h. Unlike (TiO_2, SnO_2, PbO_2), BDD has shown excellent electrochemical stability in strongly acidic media, the extremely wide potential window in aqueous and non- aqueous electrolytes, inert surface with low adsorption properties and have highest oxygen evolution over-potential value (2.7 V). BDD anodes used for the degradation of a wide variety of pollutants completely despite the nature of the pollutants. Besides $OH^{\bullet}$ generation on the electrode surface, it also performs indirect oxidation by electrochemically generated oxidants such as persulfate, perphosphate or hypochlorite depending upon the electrolyte used (Sarkka et al., 2015). Many papers have demonstrated the application of BDD for EO treatment of different organics in synthetic/ real wastewater providing total mineralization (Martínez-Huitle and Brillas, 2009; Panizza and Cerisola, 2008). Despite the numerous advantages, large-scale usage of diamond anodes is not feasible due to its high costs, brittle nature and formation of toxic by-products such as chlorate and perchlorates (Chen, 2004; Martínez-Huitle and Brillas, 2009). Hence, it prompted the scientist to work with cost-effective anodes.

However, before visualizing the commercial-scale applications of EO for the treatment of real wastewater, certain liabilities of the process need to be looked upon carefully as mentioned below:

- Cost and durability of the supported metal oxide electro-catalyst
- Passivation of electrode
- The inertness of the supported electrocatalyst
- Conductivity of electrodes
- Leaching of metals
- Generation of toxic byproducts
- High energy consumption
- The service life of electrodes

To overcome these implications/ disadvantages, MMO anodes have proven their worth for the EO treatment of wastewater (Martı´nez-Huitle and Brillas, 2009; Radjenovic et al., 2012). Several authors have explained the usage of MMO due to its high strength, good anticorrosion

properties, great conductivity, inexpensive, quick repassivation behavior and easy availability (Li et al., 2005; Anglada et al., 2009; Panizza and Cerisola, 2009; Wu et al., 2014).

2.5 Application of MMO in EO

Some of the aforementioned concerns raised in the case of the EO treatment process are being overcome by the widely used anodes i.e. MMO. These anodes represent the important category of solid oxide catalyst which contains more than one metal cations (Martínez-Huitle et al., 2015). Different metal oxides were mixed to make a stable compound having significantly improved catalytic properties. Several studies have been reported on the applications of MMO as a catalyst, sensors, semiconductors, photoconductive thin films and an anode (Wu et al., 2014). MMO as anode material has achieved remarkable progress for EO treatment and complete mineralization of various recalcitrant toxic pollutants such as dyes, phenolics, pesticides, pharmaceuticals, plasticizers, surfactants and microcystin toxins present in water and wastewater (Feng and Li, 2003; Anglada et al., 2009; Panizza and Cerisola, 2008; Martínez-Huitle and Andrade, 2011).

In this review study, a different aspect of MMO anode is discussed particularly its classification, synthesis, characterization and surface modifications. Some of the MMO used for the abatement of the organic pollutants from mixed wastewater based on bulk MMO system are such as Sn-Sb binary, Ir-Ru binary, Ir-Ta binary, Ti-Ru binary, Ti-Bi binary, Ir-Ru-Sn ternary, Ce-Ru-Sn ternary, and Ru-Ir-Sn-Ti quaternary anodes. Various chemical and physical methods of synthesis have been used to fabricate the above-listed electrodes which include thermal decomposition, electrodeposition, anodization, spin coating, magnetron sputtering, physical vapor deposition (PVD), etc. Out of the most widely used method for fabrication of anode is the thermochemical decomposition because of its stability and easy automation. Feng et al., (2010) has described the fabrication of Ti/SnO_2-Sb-Eu at a various temperature from 450 to 850 ºC using thermochemical decomposition method and found that better electrocatalytic properties were achieved i.e. 96.4% phenol was removed when the anode was calcined at 750 ºC temperature. A similar study was also reported by Zanta et al., (2003), in which the service life of Ti/IrO_2/SnO_2-Sb increased when IrO_2 was added along with 95% TOC removal of p-CP was achieved. Although the removal rate was high it was also found that on increasing the temperature above 550ºC cracks were observed in the internal layers which further leads to poor stability.

One of the primitive ways to overcome this pitfall is the use of the electro-deposition method. Wu et al., (2011) reported the fabrication of MMO anode Ti/TiO_2-NTs/SnO_2-Sb by pulse electro-deposition and confirmed that proposed electrode has higher crystallinity, a higher-order degree of the atomic lattice, lower concentration of oxygen vacancies and better electrochemical oxidation ability for the degradation of fluorobenzene and 97.2% TOC reduction in 3 h over the electrode prepared by sol-gel method. The only difference between chemical and physical is that in physical methods the direct use of metal oxides is there instead of metal salt as a precursor and it was found that anodes prepared has better crystalline formation (Lee at al.,2012). However, very few studies in the literature have reported the use of physical methods such as magnetron sputtering and PVD for the fabrication of MMO anodes

In the last few years MMO anodes having nano size-structured, drawn immense attention because of its increased active surface area and enhanced rate of reaction. Several researchers have reported the vertical alignment of the titanium (Ti) substrate to titanium dioxide nanotubes (TiO_2/NTs) through anodic oxidation in order to have a tubular template for implantation of metal oxides to increase the loading capacity of the Ti substrate. Li et al., (2013) has reported the effective electrochemical degradation of phenol by novel TiO_2/NTs/PbO_2 anode. Fabrication of TiO_2/NTs/PbO_2 anode was done by the introduction of electrochemical reduction step and parameters were modified by electro-deposition. It was found that the crystalline structure of β-PbO_2 nanoparticles was successfully deposited into TiO_2/NTs walls without blocking tubes and phenol removal efficiency and COD reduction achieved by this anode were 96.6% and 88.7% respectively.

Similar approaches were applied to deposit other SnO_2 into TiO_2/NTs walls by thermochemical decomposition, pulse electro-deposition, hydrothermal and electro-deposition (Macak et al., 2007). Zhao et al., (2009) has reported the fabrication of 3-D micro structured TiO_2-NTs/SnO_2 as well as evaluated the comparison between electrochemical efficiency of traditional SnO_2 anode and TiO_2-NTs/SnO_2 in context to the degradation of benzoic acid (BA) present in water. From the results, it was observed that service life as well kinetic rate constant for BA with nanostructure doped anode increased 12 times and 3.5 times respectively. In another study, Chai et al., (2011) and Li et al., (2011) have reported the assembling of 2D Mp-SnO_2 electro-catalyst and 1D TiO_2-NTs photocatalyst through a block copolymer soft template method for the degradation of compounds 2,4-dichlorophenoxyacetic acid and p-nitrophenol present in water. The fabricated

anode has shown 3.1 times high photoelectric conversion, larger electrochemical surface absorption volume, smaller surface impedance, and lower electrochemical reaction activation energy. As a result, COD reduction for p-nitrophenol and 2,4-dichlorophenoxyacetic acid 98% and 90% along with the toxicity removal from wastewater.

Recently fabrication of SnO_2-Sb/CA MMO anode by thermochemical decomposition has attracted great attention due to their 3-D network, good electrical conductivity and high surface area. In electrochemical degradation of PFOA, it was found that TOC removal on SnO_2-Sb/CA was 86% which was 17% in the case of SnO_2-Sb/Ti anode (Zhao et al., 2013). Frolova et al., (2012) reported the fabrication of bulk nanostructured Pt/SnO_2–SbO_x–RuO_2 through reversed micelles by adding a surfactant called CTAB for direct alcohol fuel cells. The electrochemical degradation of both methanol and ethanol were maximum at Pt/ATO and Pt/ARTO than those of the Pt/C. These enhanced catalytic properties can be attributed to the effects of SnO_2 adjacent to Pt, such as the bi-functional effect.

Since the last fifteen years, many types of research have made attempts in order to develop doped-MMO anodes with certain improved properties such as electro/photocatalytic activities, better conductivity, anti-corrosion properties, and hydrophobic-hydrophilic properties. In doped-MMO, dopants were inserted into a precursor solution via electro-deposition or by grafting (Wu et al., 2014). Although the performance of MMO anodes enhanced by doping but at the same time it is also important to worth noting that which anode material to be used, level of doping and incorporation of ions either into oxide lattice of MMO or to the anode surface film which is mixture of metal oxides (Liu et al., 2011; Datta et al., 2013). Kong et al., (2007) reported the investigation of doping of rare earth metals with the same concentration (Ce, La, Er, and Gd) into PbO_2 films through XRD. From results, it was found that the crystal structure of all dopants was present in the surface morphology without disturbing the crystal grain of PbO_2 film. Among the four anodes, the Er-PbO_2 has exhibited the best performance by degrading 4-chlorophenol to 100% along with COD removal to 80%.

During the preparation of Ti/PbO_2-Pr_2O_3 anode by chemical vapor deposition and co-electro-deposition (Wang et al., 2013) has found that anode prepared by CVD method had a larger surface area, better stability, excellent electrocatalytic performance, low energy consumption, and longer service life. Thus, concluded that the synthesis methods employed for anode preparation have a great

influence on the surface of crystal phases. He et al., (2011) reported the certainty in the oxidation state of the dopants, while the fabricating the modified Ti/SnO_2-Sb/PbO-Pr anode. From the results, it was concluded that praseodymium (Pr) doping has greatly improved the electrocatalytic activity, improves the stability, enhanced the formation of oxygen vacancies and surface hydroxyl groups. Furthermore, the ionic radius of Pr^{4+} found close to Pb^{4+} but the ionic radius of Pr^{3+} ions was larger and therefore responsible for the enlargement of surface particles. Several studies have reported the wide use of non-metallic dopants in order to have improved conductivity, adhesion, and stability properties of certain anodes such as SnO_2, PbO_2, etc. (Li et al., 2013; Lin et al., 2013). Among them, fluoride and bismuth ions are used by many researches in their studies for the oxidation of nitrophenol, perfluorinated chemicals and pharmaceuticals (Andrade et al., 2008; Liu et al.,2011; Li et al., 2013; Liu et al., 2012; Niu et al., 2012; Park et al., 2012; Cheng et al.,2013; Lin et al., 2013).

Numerous studies have compared the features of un-doped and doped-MMO anodes quantitatively. Xu et al., (2012) has compared the characteristics and electrocatalytic activity of Ti/SnO_2-Sb undoped and Lanthanum (La) and Ruthenium (Ru) doped Ti/SnO_2-Sb anode. Cyclic voltammetry (CV) and electrochemical impedance spectroscopy (EIS) graphs showed an improvement in the peak currents from 0.37 mA/cm^2 (undoped) to 0.52 mA/cm^2 and 0.60 mA/cm^2 (doped) respectively, along with enhanced $OH^{\bullet}$ adsorption capacity and increased active surface area. Also, removal of COD for phenol at both anodes was found much higher i.e. 86.4% and 82.1% than un-doped anode (60.1%). Liu et al., (2011) has investigated the electrochemical efficiency and impedance of Ti/Ce–PbO_2 and Ti/PbO_2 anode. The results showed that incorporation of cerium (Ce) into PbO_2 has enhanced its catalytic activity, stability as well as increased its life span over traditional Ti/PbO_2 anode. Furthermore, it was also observed that doped-MMO over undoped-MMO had shown higher current efficiencies with lower energy consumption at the end of the reaction. The application of MMO anodes in the EO process has nullified the drawback of the high cost of anodes.

Although EO process with MMO has come up with a feasible solution for the treatment of bio-recalcitrant pollutants at the industrial level, certain liabilities are still there which need to be considered for effective economical applications as stated below:

- Increased treatment time
- Less efficient process
- Fewer oxidant formations

- Formation of hazardous species during electrolysis

These disadvantages can be overcome by coupling EO with some other technologies in order to increase the efficiencies obtained by a single process. Many studies in the literature have reported the integration of UV/solar light with EO that is called PEC (Cotillas et al., 2016).

2.6 Photo-electrocatalysis (PEC)

From the previous sections, it has been depicted that the concentration of oxidants generated during the EO treatment process is not very high hence required some sort of activation in order to enhance the production of oxidants during the treatment process. For example transformation of $S_2O_8^{2-}$ into $SO_4^{-\bullet}$ which had increased the performance of the process significantly because of the faster activity of $SO_4^{-\bullet}$ that is 10^3–10^5 times than $S_2O_8^{2-}$ (Wang et al., 2019). There are three different ways by which process performance can be improved. Among them, one is PEC activation by light irradiation in which highly active species generated by light irradiation. This irradiation can be provided artificially (in terms of UV light) or naturally (solar driven). Thus in this way, reactive species are produced by the light decomposition of low oxidant species such as H_2O_2, O_3, peroxosulfates, pyrophosphates, peroxocarbonates, ClO^-, etc. as shown in following Equations 2.6.1- 2.6.5 (Sires et al., 2014).

$$H_2O_2 + h\nu \rightarrow 2OH^{\bullet} \quad \textbf{(2.6.1)}$$

$$H_2O + O_3 + h\nu \rightarrow 2OH^{\bullet} + O_2 \quad \textbf{(2.6.2)}$$

$$S_2O_8^{2-} + h\nu \rightarrow 2(SO_4^{-})^{\bullet} \quad \textbf{(2.6.3)}$$

$$ClO^- + h\nu \rightarrow O^{-\bullet} + Cl^{\bullet} \quad \textbf{(2.6.4)}$$

$$O^{-\bullet} + H_2O \rightarrow OH^- + 2OH^{\bullet} \quad \textbf{(2.6.5)}$$

In recent years, PEC had received the great attention of researchers for remediation undesirable recalcitrant organic compounds present in water/wastewater which are difficult to remove by conventional treatment methods (Li et al., 2002; Leng et al., 2006; Freitas et al., 2011; Li et al., 2011) PEC is a combination of two processes that is electrocatalysis and PC. This technique offers the ability to prevent the recombination of photo-generated e^-/h^+ and possesses better process efficiency particularly and decreased the overall costs of the treatment process.

The results obtained from the coupling of photo and electrolysis technologies led to the synergistic effect which interpreted by two catalytic processes i.e. (i) heterogeneous (external bias

aids in the prevention of electron-hole pair recombination and the UV helps the photons in reaching the electrode surface to form excited radicals) and (ii) homogenous (photoactivation of electrochemically generated reactive species) (Neumann-Spallart, 2007). In literature, it has been reported that the efficiency of the photoelectrocatalytic process depends upon certain parameters. Apart from pH, current density, supporting electrolytes, type anode, few other parameters can affect the efficiency of the PEC process such as light intensity, dissolved oxygen, temperature, type of cathode, etc.

2.6.1 Effect of light intensity

From the reported studies it was depicted that recombination of electron-hole is a rate-limiting step in photo-catalysis. Hence, the rate of the reaction strongly depends on the light intensity irradiated on the surface of the electro-catalyst. On increasing the light intensity, it was observed that excitation of the catalyst along with re-excitation of electrons can be increased which further influence the rate of the photo-catalytic reaction (Wang et al., 2009). Moreover, with an increase in the UV light intensity, degradation of the pollutants or bacteria inactivation rate was found maximum because of the high concentration of generated oxidants on the surface of the TiO_2 anode (Rincon and Pulgarin, 2003; Chen et al., 2010; Kollu and Örmeci, 2012). Chong et al., (2010) has proved that high light intensity always resulted in better degradation as well as proved that the reaction rate is directly proportional to the light intensity.

In contradicting to this, some researchers had proved that the reaction rate is proportional to the light intensity only when light intensities were low, while the reaction rate is proportional to the square root of the light intensity under moderate conditions. Nevertheless, under the high intensity of light, the reaction rate was found as an independent (Yang and Liu, 2007). Pareek et al., (2008) reported the removal efficiency dependence on light intensity distribution within the PEC cell. Hence, it concludes that to have a better rate of reaction and minimum energy consumption, appropriate and sufficient light intensities were required.

2.6.2 Effect of dissolved oxygen

In the PEC, the dissolved oxygen plays important role as it avoids the recombination of photogenerated electron-hole pairs by acting as electron acceptors and participates in the formation of reactive oxygen species such as HO_2^-, $O_2^{\bullet}$, $HO_2^{\bullet}$, H_2O_2, etc. as well as improved the oxidation

efficiency at the semiconductor interface (Zhang, 2003; Leng et al., 2006). Some authors have reported that dissolved oxygen might provide a split mechanism for pollutants like aromatic compounds. A study demonstrated that in PEC on applying high pressure of oxygen by raising the airflow led to a higher photo mineralization rate for pollutants present in water and wastewater (Wang and Hong, 2000).

2.6.3 Effect of temperature

According to the literature survey, the influence of temperature on PEC has not been studied well. However, its effect on photo-catalytic processes has been studied widely. Several studies have reported that when the temperature (T > 80 ºC) enhances the charge recombination due to which adsorption of pollutants on the surface of TiO_2 decreases (Chong et al., 2010). Malato et al., (2009) reported that for optimum photomineralization, the temperature should be in the range (20 – 80 ºC) while in case of photo disinfection, the temperature should be high for the inactivation of microorganisms. Furthermore, it was also found that the collision frequency of molecules in reaction mixture increases on rising the temperature values, thus improves the rate constant for reaction (Rincon and Pulgarin, 2003).

2.6.4 Effect of cathode material

In comparison to conventional photo-catalytic process, PEC has an advantage of the use of cathode material, such as vitreous carbon (VC), graphite, Pt, etc. on which H_2O_2 can be electrochemically generated by cathodic reduction of dissolved oxygen (Xie and Li, 2006). Under UV irradiation, hydrogen peroxide can be decomposed into $OH^{\bullet}$ on the surface of photo-anode and hence, contribute to enhancing pollutant degradation. According to previous studies, such an oxidant agent H_2O_2 is beneficial for photo-catalytic reaction by trapping the conduction band electron in order to generate more $OH^{\bullet}$. Furthermore, the addition of an electron acceptor that is H_2O_2 prevent the electron-hole recombination and increase the photo-catalyst efficiency (Ozer and Ferry, 2001; Xie and Li, 2006; Ding et al., 2010). Several studies in literature have reported the removal of complex pollutants like dyes (Pelegrini et al., 1999; Socha et al., 2005; Frontistis et al., 2011; Rao et al., 2017), pharmaceuticals (Daghrir et al., 2014), tannery waste (Paschoal et al., 2009) and humic acids (Pinhedo et al., 2005) via PEC using MMO anodes.

To explore the field-scale applications of EAOP's, research is now concentrating on the utilization of natural solar radiation. The use of sunlight instead of UV irradiations is an environmentally attractive and economical solution for PEC (Gao et al., 2019). The application of solar-driven PEC process fits well for countries like India which receives immense solar light throughout the year. Till date, few studies have been reported on the use of different novel Ti/TiO_2 photoanodes with and without doping for the degradation of various organic recalcitrant pollutants under direct sunlight (Sires et al., 2014). In this context, Han et al., (2010) reported the photoelectrocatalytic efficiency of undoped Ti/TiO_2 and N-doped TiO_2/Ti photo-anodes for the degradation of Rhodium Blue dye under visible light. An almost 12% increase in the case of doped photo-anode was found in the degradation value over the undoped anode. In addition, the photo-electrochemical efficiency of N-doped TiO_2/Ti photo-electrode was 3% higher than that of undoped TiO_2. Frontistis et al., (2011) reported the solar-driven photoelectrolytic degradation of bisphenol A in a stirred tank reactor over Ti/TiO_2 anode. From the results, it was concluded that at low current values, the rate of degradation of pollutants was maximum and quicker in the case of PEC over individual processes (PC and EO) respectively. Furthermore, it was also observed that the cathodic H_2 production rate was enhanced 4 times and 3 times respectively when compared to photocatalysis and electrolysis alone. However, if natural solar irradiations emitted by the sun are inadequate, can be overcome by combining it with artificial UV lamp for the maximum removal rate of pollutant in minimal time.

Hua et al., (2016) has reported the fabrication of Cu doped TiO_2-NTs and compared its photoelectrocatalytic activity with TiO_2-NTs. From the results, it was observed that the surface sensitization of TiO_2/NTs by Cu has enhanced the absorption of visible light as well as the enhanced the charge separation, transient photocurrent response, and photo-voltage measurements. Furthermore, Cu/TiO_2-NTs electrode showed more effective photo-conversion efficiency and enhanced photoelectrocatalytic activity towards the degradation of diclofenac than pure TiO_2-NTs electrode under simulated solar light irradiation. Wei et al., (2017) investigated the photoelectrocatalytic characteristics of $TiO_2/g\text{-}C_3N_4$ (TCN) under different light sources for the oxidation of phenol-containing coking wastewater. The results showed the complete degradation of phenol in 1.5 h under simulated solar irradiation over the other two light sources along with a 100% TOC removal rate. To the best of our knowledge, PEC has been mostly carried out at the laboratory

scale. Hence, to promote the applicability of PEC at field scale in the near future, it becomes mandatory to execute the scale-up trails of lab-scale results.

2.7 Pilot-scale Applications of EO and PEC

For the successful implementation of large-scale EO and PEC treatment processes, one of the significant factors need to consider is the design of the electrochemical cell. Moreover, it necessitates a multidisciplinary perspective between all the operational parameters which directly or indirectly affects the subsequent utilization of captured photons of light inside a reactor and degradation efficiency. Electrochemical reactors can be grouped as 2D electrochemical systems such as tank cells, plate, frame cells, rotating cells and 3D electrochemical systems such as fluidized bed, packed bed cell, or porous carbon packing cells (Chen, 2004; Cernigoj et al., 2007). These types of 2D electrodes can be operated in batch or continuous mode as well as simple to design, operate, cheap and easy to maintain. Furthermore, it was also observed that in these design mass transfer coefficient can be controlled independently of the residence time and electrolyte flow (Juttner et al., 2000). The 3D electrodes have shown high mass transfer, large specific surface, enhanced specific yield and can even treat diluted solutions. But at the same time, it possesses some drawbacks such as complicated process control, discontinuous process and costly (Zhang et al., 2013).

Electrochemical reactors have really opened new channels where one can visualize the field scale applications with certain design modifications. Numerous studies have reported in the literature about the detailed kinetic studies of reactors employing the basic principles of EO (Walsh et al., 2014) at the lab scale. However, in all these studies, it always remained unclear whether the oxidation of the target compound takes place due to heterogeneous/homogeneous indirect oxidation or direct oxidation. EO has been tested in laboratories using batch reactors for the treatment of a wide variety of toxic pollutants present in wastewater. The electrochemical cells classified into three groups: (i) improved mass transport by placing anodes in motion or by using turbulence promoters thus increasing current density; (ii) efforts were made to accommodate large anodes in a small volume cell-like swiss-role, extended surface electrolysis (ESE) or multiple-cathode cell and (iii) enlarged specific electrode area with improved mass transfer coefficients by the use of electrodes such as rolling tube cell, porous flow-through cell, etc. (Juttner et al., 2000).

The reactors are further categorized in a divided and undivided cell. A large variety of divided electrolytic cells separated by semi-porous membranes such as glass frits, diaphragms,

cationic membranes, etc. containing two separate solutions catholyte and anolyte, worked under potentiostatic or galvanostatic conditions have been utilized for electro-generating H_2O_2 during wastewater treatment. In the undivided cell, both electrodes anode and cathode in one compartment only without any separation membranes worked under galvanostatic conditions. An advantage of using undivided cells over a divided cell is that the lower cell voltage needed for electrolysis because the voltage penalty of the separator of divided cells is avoided. Raju and Basha, (2005) investigated the comparison between divided and undivided electrochemical cell through EO of Ce(III)/Ce(IV) system at MMO anodes and stainless steel cathode. From the results, it was concluded that the total cerium concentration in aqueous methanesulphonic acid makes the electrochemical generation of cerium (IV) was higher in an undivided cell over divided cell as well as the capital and energy costs for undivided cell were also low.

In context to above discussion, there are many factors which have considered while designing of the EO cell, such as flow rate, heat transfer, mass transport, current density, flow rate, and reactions kinetics as they might have a significant effect on the results treatment process when applied at large scale. Moreover, small improvements in the process efficiency could lead to huge money saving during the scale-up of an EO process (Martinez-Huitle et al., 2015). The main points that need to be considered while designing the EO cell from laboratory scale to pilot scale are heat transfer, electrolyte, electrodes, flow patterns, etc. For having the better process efficiency of the EO process, flow pattern plays an important role. Two types of flow patterns are used in the EO process for the oxidation of organic compounds that is plug flow and mixed flow. The main advantage of the flow patterns is to increase the mass transport properties, which further makes the process suitable for the treatment of organic compounds with a lower concentration in wastewater.

Santos et al., (2014) has confirmed that COD removal was found maximum when the flow-pass cell was used over mixed flow. Another important point needs to be considered while designing is the inter-electrode spacing between electrodes because it affects the total resistance in the cell and ohmic loses as electrolyte resistance linearly depends upon the spacing. Furthermore, it also affects the gases formed during the process which has to be removed quickly in order to avoid operating problems. Therefore, the optimum spacing is necessary in order to get better removal efficiency. Several researchers reported that in EO cells the spacing should be between 0.5 and 2.0 cm. From

the experimental works at the bench scale, it was confirmed that electro-oxidation performance was significantly better at optimal lower interspacing between anode and cathode (Scialdone et al., 2011).

In the EO process, when several numbers of electrodes were used in one cell only then it becomes very important to choose connections such as monopolar and bipolar. In the case of monopolar, all anodes and cathodes are connected directly to the direct current (DC) supply while in the case of bipolar, the outermost electrodes were connected to the power supply and current passed through the other electrodes. Unfortunately, very few studies have shown interest in minimizing the energy consumption during the treatment process at pilot scale. Bipolar electrodes considered to be most effective for the removal of pollutants from wastewater, but monopolar entails a lower operating cost due to its operation at lower current densities (Yavuz and Shahbazi, 2012).

In the EO process, another key point that needs to take care while designing of electrolysis cell is temperature because it helps to promote the generation of oxidants during EO. In some literature studies, it has been reported that high temperature always promotes mediated EO, hence enhances the removal rate. But in most of cases, this is not always true because, at high temperatures, the solubility of gases decreases due to which it favors stripping over hypochlorite production thus decreases process efficiency (Canizares et al., 2005). Hence to keep the temperature at the desired set-point, cooling is required. At lab scale, not much consideration was paid for the designing of heat exchangers while at large scale it becomes important.

In context to the above discussion, it was analyzed that certain parameters like inter-electrode spacing, temperature, turbulence promoters, electrode configuration, and flow-pass cells largely depended on the construction details and computational fluid dynamics (CFD) tools. However, the use of these tools by researchers for cell design was rare. Transformation of the discontinuous process into a continuous one was expected to be carried out in the same auxiliary tank, by simply recycling the outlet of treated wastewater (Martinez-Huitle et al., 2015).

From the cited literature studies it has been observed that researchers always concerns about approaching preliminary studies to the scale-up only without much worry about the problems that can be arises during scale-up studies (Dominguez-Ramos and Irabien, 2013; Garcia et al., 2013; Urtiaga et al., 2013). From the above-reported studies, it has been observed that there are two significant points need to be considered while shifting from lab to the pilot scale in electrochemical technologies i.e. (i) raising the area of the electrode for single-cell and (ii) stacking of cells

(management of heat and hydrogen). Lobato et al., (2006) have reported that the studies at the lab scale generate small amounts of hydrogen due to which dangerous situations could be prevented easily while in case of pilot-scale production of hydrogen is large and removal is not as easy. Also, in large-scale plants transfer of heat through wires or into the electrolyte was there due to which ohmic drops and result in a large amount of energy transferred along with a huge amount of heat consumption. Hence to diminish the problem, heat exchangers are to be fitted within the system.

In the electrochemical cell, a large-sized electrode helps in reducing the cost of the cell by minimizing the number of cells included in the stack for a given process (Canizares et al., 2009). Conversely, it was also observed that the larger the electrode area, the more difficult to obtain an even current distribution on the surface of the electrode, thus reduces the overall process efficiency. This point is very important in the case of EO with BDD on a large scale due to its high electric resistance and makes difficult to achieve uniform current distribution during the treatment. Hence to solve the above problems current feeders are provided in order to get good distribution and reduces the overall investment cost of the cell. Therefore, in order to attain maximum process efficiency, optimization of the electrochemical cell is very important along with the optimization of input parameters of the process (Martinez-Huitle et al., 2009; 2015).

In view of the above-discussed studies, it was concluded that operational parameters, electrodes, and reactors used for EO and PEC can open new channels for the effective treatment of mixed and complex wastewater. Furthermore, MMO with doped material incorporates the use of sunlight in these treatment processes which could further present a groundbreaking step in the field of EAOPs by reducing the cost of the overall process.

Section II

2.8 Applications of EO for the Treatment of Urine Metabolites, SU and AHU

In literature, many researchers have put emphasis on the treatment of source-separated urine by developing urine diverting dehydrating toilets. But in a developing country like India, it is not feasible to have this kind of toilets in rural and urban slum areas because of high-density population, space issues, poor financial sustainability, inadequate knowledge, etc. In the past several treatments, technologies were used to treat urine wastewater and reuse as flush water which includes reverse

osmosis, vapor compression distillation, adsorption catalytic, etc. (Li et al., 2015). Though these technologies have proven successful in treating the complex urine wastewater but still they suffer from the high cost of the catalyst, high energy consumption, high water consumption for neutralization, severe membrane fouling and low efficiency. Human urine is mixed wastewater with complex chemical composition and contains most of the nitrogen-based compounds such as urea, uric acid, creatinine, etc. which are toxic, persistent and recalcitrant to conventional treatment technologies, hence require some effective alternative technologies for the on-site treatment of urinal wastewater. As reported earlier EO process has received great attention for the treatment of mixed wastewater because of its effectiveness, environmental compatibility, economical (because of the involvement of the clean reagent i.e. e^-) and provides easy process control. In the literature, several studies have been reported on the use of the EO process for the treatment of urine wastewater but very few on its metabolites. The reason could be the complexity of urinal wastewater, limitations for on-site treatment and process complications.

Ikematsu et al. (2007) have investigated the EO process for the treatment of human urine using PtIr electrodes. From the results, it was concluded that unpleasant odor due to hydrolysis of urea into ammonia by urease has been suppressed well and urine was successfully treated and served as flush water. Moreover, it was also found that the electricity cost still lower than the tap water charges until the treatment cycles reached 64. Amstutz et al., (2012) has demonstrated the effects of carbonate on the electrolytic removal of ammonia and urea from urine with thermally prepared IrO_2 electrodes. From the results, it was observed that fresh urine was efficiently treated on IrO_2 anodes but in the case of stored urine, ammonia was not oxidized on these electrodes due to its lower oxidation potential.

Kim et al., (2013) has demonstrated the production of solar hydrogen during EO treatment of urea/urine through RCS generated in-situ via NaCl present in urine with $BiOx–TiO_2$ as an anode and stainless steel as a cathode and coupled with a solar photovoltaic cell. Another study reported in the literature was EO treatment of human waste coupled with molecular hydrogen production (Cho et al., 2014). In this study, a comprehensive environmental analysis was carried out to investigate the role of various redox reactions mediated by chloride present in human waste. From the results it was observed proteins, color and high-levels of COD were eliminated within 6 h of batch treatment in the water electrolysis cell (WEC). Also, the current efficiency and energy efficiencies for

hydrogen production were estimated to be 90% and 25%, respectively. Formation of chlorinated byproducts during the EO treatment of urine on BDD and thermally decomposed iridium oxide film (TDIROF) anodes was studied (Zollig et al., 2015). It was observed that the formation of short-chained organic chlorination byproducts (OCBPs) on BDD whereas longer chained OCBPs were more frequently found on at higher current densities resulting in complete mineralization of urine components on BDD anode over TDIROF. Some researchers have also worked on the treatment of synthetic/artificial human urine in order to better understand the urine oxidation mechanism on different electrodes. Dbira et al., (2015) were conducted an EO experiment at different current densities (20-100 mA/cm^2) and temperature (25-50 ºC) for the treatment of synthetic urine using conductive-diamond anodes. It was observed that 93.94% COD and 94.94 % TOC were achieved at 20 mA/cm^2 along with the formation of toxic chlorinated by-products. From the results, it was confirmed that the most efficient conditions for total mineralization were low current densities and high temperatures.

Another study conducted by Dbira et al., (2015) in order to overcome the drawback of toxic byproducts by investigating EO treatment of SU using DSA. It was found that oxalic acid, gaseous nitrogen, and oxalic acid were the main byproducts of urine oxidation. There was no effect of temperature was observed on treatment efficiency. COD was completed deleted by DSA anode at low current densities. From the results, it was concluded that for maximum process efficiency and for the prevention of toxic chlorinated by-products, lower current densities are optimum. Li et al., (2015) has investigated the EO treatment mechanism for AHU using BDD and IrO_2 anode. The results concluded that the maximum degradation of organic compounds present in urine was observed at BDD over IrO_2 in 8h of electrolysis. The final breakdown products of inorganic ions on BDD were ClO_4^- and NO_3^- while on IrO_2 anode, the final products generated and left in solution were highly toxic N_2H_4 and NO_2^-. Hence BDD was more effective than IrO_2 for the treatment AHU.

A recent study was reported on the disinfection of synthetic urine by EO with the conductive diamond anode at different current densities (0-100 A/m^2) (Cotillas et al., 2018). It was observed that it is possible to disinfect the urine effluent completely at applied electric charges lower than 2 kAh/m^3, regardless of the applied current density. More than 90% of removal in TOC was achieved. From the results, it was concluded for complete mineralization higher electric charge were required than those needed for disinfection.

A recent study has shown that in India more than 20 million tons of urea which are a potential source of nitrogen was used for agriculture activities (Yadav and Pandey, 2017). Apart from this, many industries like pharmaceuticals, chemical industry, fertilizer companies, etc. are adding woes to the concern of pollution in water due to the continuous discharge of nitrogen-based components during the manufacturing and treatment of wastewater. Combined agriculture and open defecation contribute more than 70% of the total nitrogen nuisance in terms of urea discharge in rivers (Showkat, 2016). Many authors have studied the degradation of urea using a different type of electrodes because urea is the most abundant source of the nitrogen-based compound as well as a principal component of urine wastewater and other mixed wastewater, hence studied widely than other two components that are uric acid and creatinine.

From the literature survey, it was observed that different type of electrodes have shown their worth in detecting the level of uric acid and creatinine in serum and urine but rarely discussed their removal from wastewater (Popa et al., 2000; Aguilar et al., 2004; Radomska et al., 2004; Chen et al., 2006; Lakshmi et al., 2011; Araujo et al., 2012; Zhang and Yin, 2014; Diouf et al., 2017). Till date, there was no study yet on EO treatment of creatinine while in the case of uric acid only one study was reported in the literature on its removal through the EO process.

Dbira et al., (2016) has reported the study on the mechanism and kinetics of EO treatment of uric acid using conductive-diamond anodes. The results confirmed the successful degradation of uric acid into urea and oxalic acid along with the generation of ions NO_3^- and NH_4^+.

Hernlem, (2005) has reported the electrochemical degradation of urea in chloride matrix with DSA electrodes in a batch recirculation mode. EO experiments were performed at different current densities (34–141A/m^2), chloride variations (100 mg/L- 400 mg/L) and at different temperatures (16–34.5 ºC). It was found that urea oxidation was mainly dependent on chloride and temperature and little on applied current density. At higher temperatures and optimized conditions of current and chloride led to complete urea decomposition, leaving behind small traces of residual nitrogen that is nitrates. Also at higher temperature values, elimination of unwanted toxic chlorinated byproducts was suppressed along with the suppression of total available chlorine (TAC) to the lowest level which is not good from the process point of view.

Simka and his coworkers (2007, 2009) have studied the effect of different anodes materials on the degradation of urea using EO. It was observed that out of six electrodes, complete degradation

of urea into N_2 and CO_2 has taken place on these two electrodes Ti/Pt-Ir, Ti/(Ta_2O_5-IrO_2) and Ti/Pt only at a current density of 8 A/dm^2 with chloride concentration 5 gm/dm^3. While on other electrodes urea was degraded into nitrite, nitrate, ammonium ion, etc and was not stable enough. Jara et al., (2008) has investigated the concept of direct and indirect oxidation in terms of urea degradation with platinum titanium electrode. It was observed that urea degraded into nitrates only when direct oxidation takes place in the presence of sulfate ions. While in case of coupling of direct (via $OH^{\bullet}$) and indirect oxidation (via RCS), urea oxidized into molecular nitrogen (N_2) and little amount of NO_3^- at high current densities.

Vedharathinam et al., (2012) has demonstrated the urea degradation mechanism by EO using nickel electrodes in an alkaline medium. It was observed that oxidation of urea mainly occurs after the formation of Ni_3^+ at the electrode surface. Furthermore, it also found that urea oxidation at low concentrations was mainly controlled by diffusion whereas at high concentrations the process was controlled by kinetics. Similar studies were performed on Ni by (Yan et al., 2012) in which Ni-Co bimetallic hydroxide electro-catalyst was evaluated for the EO treatment of urea. From the results, it was noticed that the degradation of urea was much better on Ni-Co bimetallic hydroxide than $Ni(OH)_2$ electrode in alkaline solution due to inhibition of H_2O electrolysis which has ultimately enhanced the urea degradation efficiency.

Abdel-Monem et al., (2013) has reported the EO treatment of urea in human urine using flow by porous graphite electrodes. From the experimental results, it was found that the degradation of urea increased with increasing current densities. However, at higher current densities, it was observed that energy consumption also increased and current efficiency was decreased. Thus, it concludes that for maximum removal of urea from wastewater required optimization of the EO process. Hernandez et al., 2014 has to investigate the different anodes such as Pt, Ti-Ru, BDD, and antimony doped tin oxide for urea degradation. Undoubtedly, it was found that complete removal of urea was achieved only on BDD while on other electrodes partial oxidation takes place with the amount of charge passed is 8 Ah/dm^3. Also when sodium chloride added in the solution it was found that degradation of urea on Pt anode increased by 40%. Thus, sodium chloride plays a very important role as the electrolyte. Cho and Hoffmann, (2014) have investigated the urea degradation by electrochemically generated RCS using bismuth-doped TiO_2 anode. Results of quadruple mass

spectrophotometers have revealed complete degradation of urea into N_2 (91%), NO_3^- (9%) and CO_2 (77%) while chloramines and chloramides were detected as reaction intermediates.

From the literature survey, it was concluded that the EO process for the degradation of urine wastewater and its metabolite is quite efficient. The process parameters for the EO process have an immense impact on pollutant degradation. For maximum removal of the pollutant from wastewater, these process parameters must be optimized. Most of the reported studies in the literature have done optimization of EO process parameters for the treatment of urine metabolites. Therefore, a vast study is required to study the effect of various EO process parameters on the degradation of human/ synthetic urine wastewater which is at the same time is one of the lacunae of the research studies. It was also noticed that most of the studies have reported that the EO process performs better for the degradation of pollutants in the presence of high salt concentration. Human urine contains a huge amount of salt (especially NaCl) which is a vital source for human living and excreted via human urine. Hence, the degradation efficiency of the EO process for urine wastewater must be high. However, a high concentration of salt could affect the electrode material during electrolysis. Therefore, the selection of electrode material must be essential for the EO treatment of urine wastewater.

2.9 Summary

EAOPs have proven their credentials over conventional water/wastewater treatment technologies for the degradation and mineralization of mixed wastewaters such as urinal and sewage wastewater containing recalcitrant nitrogen-based organic toxic pollutants. Yet, field-scale applications of these technologies are still needed to be explored. Even though different technologies under EAOPs, revealed reasonably good degradation efficiency but certain operational implications like strict pH control (pH<3), high dosage of H_2O_2, electrode selective, sludge formation, additional requirement of heterogeneous iron catalysts or complexing agents, passivation of cathode, halogenated by-products formation, etc. limits its large-scale application. EO process nullified most of the problems mentioned above and proven to be effective potential for the treatment of a wide variety of persistent organic pollutants present in wastewater.

EAOPs has proven to be potentially effective and versatile technology for the remediation of a wide variety of mixed waste-waters. Among various EAOPs, EO has provided simple, viable and promising results for the treatment of chloride-free effluents and high saline contained effluents.

Highly stable anode materials such as PbO_2 and BDD electrodes have completely reduced COD and TOC of polluted wastewater because of the direct oxidation mainly with heterogeneous $OH^{\bullet}$ formed during water electrolysis while indirect EO has done by electro-generated RCS and ROS which allows the complete color removal and a high degree of degradation for saline and mixed wastewater. But its application at field scale was limited by the high cost of the anode, production of undesirable toxic by-products such as chlorates and perchlorates, less service life, low conductivity, etc. These pitfalls of the EO process with BDD have been resolved by the use of novel MMO anodes.

MMO anodes have proven to be technically as well as economically remarkably effective for the treatment of mixed wastewater containing recalcitrant organic pollutants by EO. Because of its better electrocatalytic activity, stability, durability and process efficiency, MMO has shown great potential in treating a wide variety of pollutants even in acidic medium and at high temperatures. Moreover, the advantage of coupling electron driven reactions with renewable energy sources i.e. light irradiations called PEC which has already made an interesting option for treating organic pollutants in minimum time with better efficiency as well as helps in reducing the production of toxic halogenated by-products. Also, the doping of MMO with metal/ nonmetals oxides has reduced the complications like an ineffective use of solar light as well as reduced the cost of the overall process by replacing UV lamps with the natural light source.

In literature, few pilot-scale two-dimensional electrodes and three-dimensional electrodes have been employed for the treatment of persistent and toxic pollutants (Juttner et al., 2000). Three-dimensional electrodes have shown its great potential for the destruction of organic pollutants but its higher capital cost, complex structure, and less adsorption and catalytic capacity of electrodes have raised the economic issues of EAOPs. Thus, two-dimensional electrodes have been found to be more economical and feasible for the on-site treatment of mixed wastewater (Anglada et al., 2009). However, few studies have been reported in the literature on the designing kinetics of two-dimensional electrodes under continuous mode as well as the prolonged use of these anodes for the onsite treatment of mixed wastewater. Hence extensive investigation is still required in context to the use of MMO electrodes and continuous reactors for pilot scale designing along with parametric optimization.

Also, very few studies are available in literature related to the scale-up of the dual-process by coupling EO with PC i.e. PEC. The studies have demonstrated a significant improvement in the

process efficiency by overcoming most of the concerns faced by individual processes alone. Hence the EO process could be a well-suited approach for the on-site treatment of urinal wastewater and water recycling coupled with energy production.

2.10 Research Gaps

Based on the literature review some of the scientific gaps have been identified.

- Very few studies have been reported in the literature for the EO treatment of SU/AHU and its metabolites especially creatinine and uric acid.
- Even the reported studies have used costly electrodes such as BDD, Pt, Ir, etc. for EO treatment of SU/AHU
- The stability of electrodes has always been a major concern in all the reported studies.
- Work on the treatment of human urine using PEC (synergetic effects over EO) has not been effectively cited in the literature.

2.11 Objectives of the Study

As a result, efforts have been made in the present research work to suppress the pitfalls by using cheap, economically available novel anodes MMO and doped-MMO for the treatment of synthetic urine and its metabolites through EO. The commercial application of the technique was visualized by executing the EO with a light source that is PEC. The dual-process resulted in a significant reduction in a treatment time of target compounds such as urea, creatinine, uric acid, and synthetic urine. The feasibility of the technique was confirmed by conducting degradation studies of human urine in pilot-scale reactors along with energy production. In this view, the doctoral research work was conducted with the following objectives:

- A parametric study for the optimum operation of electro-oxidation (EO) using different electrodes for the treatment of urine metabolites.
- Treatment of synthetic urine using batch electro-oxidation (EO) and photo-electrocatalysis (PEC) along with the identification of reaction products.
- Performance studies of a continuous reactor for the treatment of urine metabolites.

Chapter 3

MATERIALS AND METHODS

3.1 General

The current chapter includes the depiction of materials used along with the methodologies adopted for performing the EO and PEC experiments, analysis of samples and characterization of the anode during the degradation studies of urine metabolites, synthetic urine, and its metabolites. Furthermore, the experimental setup and electrodes used for the batch and continuous mode of operation have been discussed in detail.

3.2 Target Compounds: Urine Metabolites, Synthetic Urine (SU) and Actual Human Urine (AHU)

Urea, creatinine and uric acid, the three nitrogen-based organic components present in urine wastewater are used as model compounds in present research work. Before actually going for the treatment of SU/AHU, efforts were made to treat its metabolites separately to check the process feasibility.

Urea is also named as carbamide, an organic compound that plays an essential part in the living organisms, as it participates in the biological processes and metabolic pathways such as protein decomposition (Urbanczyk et al., 2016). In our body, urea is being used in various processes, but most importantly during nitrogen excretion (i.e. urine). It is highly soluble in water, odorless, colorless and non-toxic compounds. Despite its low toxicity, it is known to be the most abundant nitrogen carrier from sources like human excreta, production plants and fertilizer waste (Cho et al., 2014). The chemical structure of urea is shown in Figure 3.2.1.

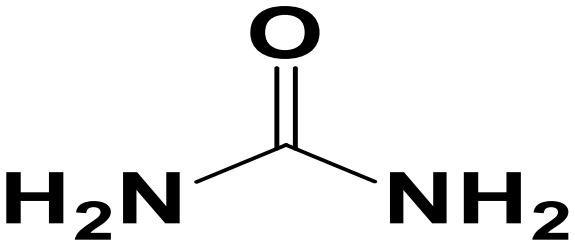

Figure 3.2.1 Chemical structure of Urea

Creatinine with IUPAC name (2-amino-1-methyl-5H-imidazole-4-one) is one among nitrogen-based organic components found in urine wastewater (Atula and Yang, 2014). The chemical structure of creatinine is represented in Figure 3.2.2. The levels of creatinine present in human blood are (0-250 mg/L or 700-1200 mg/L) and excreted via urine (0-500 mg/L or 500-1500 mg/L) in particularly 24 h (Jafari et al., 2015; Diouf et al., 2017). Creatinine is the final byproduct of creatine metabolism in the skeletal muscle during energy production and removed from the body by renal excretion at a relatively constant rate (de Araujo et al., 2012). Creatinine levels in the human body are regarded as advantageous for evaluation of muscular, renal failure, vascular diseases and thyroid dysfunctioning (Chen et al., 2006; Pundir et al., 2013).

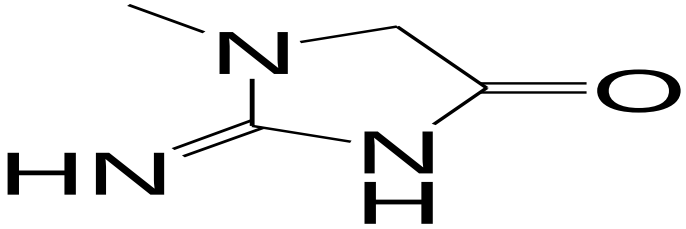

Figure 3.2.2 Chemical structure of Creatinine

Uric acid, (7, 9-Dihydro-1H-purine-2, 6, 8 (3H)-trione) is another principle nitrogen-based compound of urinal wastewater as shown in Figure 3.2.3. It is the primary end product of purine metabolism in the human body which works as an antioxidant and protects against oxidative stress (Ozcan and Sahin, 2010; Molino-Lova et al., 2013; Sautin et al., 2007). It is mainly present in human blood with a normal range of 250 to 750 mg/L with a period of over 24 h (Dbira et al., 2016). In addition, uric acid is excreted via urine (24 mg/L to 70 mg/L) as bio refractory pollutants (Lu et al., 2014). It's a high/abnormal concentration in the body are indicators for the diagnosis of various diseases like gout, leukemia, cardiovascular diseases, pneumonia, kidney diseases and arthritis (Lakshmi et al., 2011).

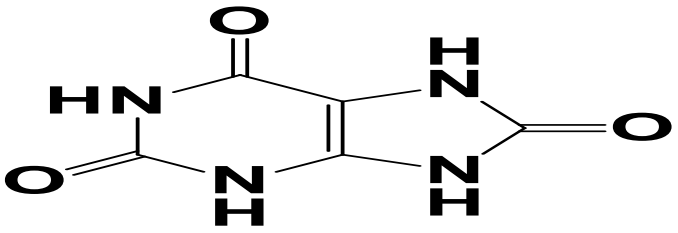

Figure 3.2.3 Chemical structure of Uric Acid

The average adult generates between 1.5–2.0 L of urine per day. The continuous discharge of these excreted metabolites via urine in the open streams leads to excessive N-loading in surface water and causes algal blooming leaving adverse effects on the ecosystem as well as human well-being has been confirmed in various reported studies. Moreover, its readily automatic conversion to ammonia via enzymatic hydrolyzes by urease leads to the serious environmental and health problems such as an increase in the pH of the soils and release of free ammonia into the atmosphere contributing toxic compounds like ammonium, nitrates, and sulfates (Hernandez et al.,2014).

Urine is a multi-component complex fluid excreted via the human body and whose composition is dependent on various factors such as climate, physical activity, individuals, diet, etc. Thus, SU was used for the EO experiments in order to find optimum conditions for EO treatment of AHU. From a literature survey, constituents and their concentrations present in SU were summarized in section 3.4.

3.3 Chemicals and Electrodes

Urea (NH_2CONH_2), creatinine ($C_4H_7NO_3$) and uric acid ($C_5H_4N_4O_3$) with all (>99.0% purity), were of analytical grade (AR) procured from Sigma-Aldrich, Missouri, (U.S.). H_2SO_4 (1N) and NaOH, procured from SD Fine Chemicals Ltd. (India) were used for the initial pH adjustments. Sodium chloride (NaCl) and sodium sulfate (Na_2SO_4) with (>99 % purity) of AR grade were purchased from Loba Chemie Pvt. Ltd. (India) for increasing the conductivity of the aqueous solution. Chemicals used for making SU are all of AR grade with (>98.5-99% purity) were procured from SD Fine Chemicals Ltd. (India).

For COD estimation, silver sulfate ($AgSO_4$), concentrated sulfuric acid (H_2SO_4), potassium dichromate ($K_2Cr_2O_7$), mercuric sulfate ($HgSO_4$) and ferrous ammonium sulfate (FAS) ($FeH_8N_2O_8S_2$) were used. All chemical of AR grade with (>98.0 purity) was purchased from SD Fine Chemicals Ltd. (India).

For spectrophotometric estimation of urea, p-Dimethylaminobenzaldehyde (>99% purity) of AR grade obtained from Sigma-Aldrich, Missouri, (U.S.). Terephthalic acid (TPA) with (>98% purity) of AR grade used for estimation of hydroxyl radical ($OH^{\bullet}$) in photoelectrocatalysis were procured from Merck (U.S.)

Reagents used for the anions analysis (NO_2^-, NO_3^-, chloride, TAC, ammonical nitrogen and total nitrogen) include phosphoric acid, sulfanilamide, NEDA (N-(1 Napthyl) - ethylenediamine dihydrochloride), ethanol, hydrochloric acid (1N), sodium thiosulfate, boric acid, sodium tetraborate, mercuric oxide, NaOH, sodium thiosulfate pentahydrate, potassium sulfate, starch, glacial acetic acid, potassium iodide, potassium chromate, silver nitrate and NaCl. All these chemicals were of AR grade, obtained from Loba Chemie Pvt. Ltd. (India). For the preparation of all aqueous solutions, double distilled water was used.

The anodes used in the study, MMO i.e. Titanium/Iridium oxide/Ruthenium oxide/Platinum ($Ti/IrO_2/RuO_2/Pt$) and doped-MMO i.e. Titanium/Iridium oxide/Tantalum oxide/Tin oxide-Antimony oxide ($Ti/IrO_2/Ta_2O_5/SnO_2\text{-}Sb_2O_5$) were procured from Exotic Elements Private Limited, Mumbai, India. While stainless steel as the cathode was obtained from Bio age Private Limited, Mohali, India. Both anode and cathode electrode has a dimension of 7 cm * 7 cm * 0.5 cm with an active surface area of 42 cm^2. Electrodes were cleaned by dipping it into a solution contains 10% H_2SO_4 (1N) and then dried at room temperature before use for EO treatment.

3.4 SU Composition, AHU and Bacterial Strain

The SU used for EO experiments were prepared by dissolving urea (CH_4N_2O) 12.012 g/L, creatinine ($C_4H_7N_3O$) 0.452 g/L, uric acid ($C_5H_4N_4O_3$) 0.168 g/L, trisodium citrate ($Na_3C_6H_5O_7$) 1.29 g/L, sodium oxalate ($Na_2C_2O_4$) 0.0134 g/L, sodium (Na^+) 1.802 g/L, calcium (Ca_2^+) 0.12 g/L, potassium (K^+) 1.17 g/L, magnesium (Mg_2^+) 0.05 g/L, sulfate (SO_4^{2-}) 1.06 g/L, ammonium ion (NH_4^+) 0.271 g/L, bicarbonate (HCO_3^-) 0.122 g/L, chloride (Cl^-) 3.722 g/L and phosphate (PO_4^{3-}) 0.38 g/L. The synthetic urine was characterized by high organic content with initial total organic carbon ($TOC_o \approx 3.1$ g/L), pH 6.7 and conductivity 4.6 mS/cm.

For the present study, the AHU sample was collected from the house having five members in a family.

The bacterial strain i.e. *E.coli* (MTCC K-12) used in the present study for the disinfection of urinal wastewater was procured from CSIR-Institute of Microbial Technology, Chandigarh, (India).

3.5 Electrodes Fabrication

The MMO and doped-MMO anodes were fabricated from Exotic Elements Private Limited, Mumbai, India. The MMO used in the present study was prepared using ASME grade 1 Ti plates as a substrate. MMO anodes were synthesized by dipping the Ti plate in a mixture of isopropanol/n butanol/hydrochloric acid (HCl) (1:1:1) with a certain amount of water and vibrated ultrasonically. Furthermore, the precursor solutions for different oxide metals such as $TiCl_4$, $RuCl_3.nH_2O$, $H_2IrCl_6.nH_2O$, and $H_2PtCl_6.nH_2O$ were added in the above-prepared mixture in order to articulate 10 consecutive layers at room temperature. For each coating, anodes were dried at 100 °C for 5 min and followed by calcination at 500 °C for 10 min in muffle furnace prior to the next deposition in order to generate phases of different metal oxides. The final annealing was done at 500 ºC for 1 h to finally complete the fabrication process. The $Ti/TiO_2/IrO_2/RuO_2/Pt$ anode prepared by thermal chemical decomposition method having a molar composition ratio of 55:10:30:5 with an average thickness of oxide film was ≈ 2.5 μm. While stainless steel (SS) as the cathode was supplied by Bio age Private Limited, Mohali (India).

The doped-MMO used in the study was also prepared using the same substrate i.e. Ti plate. The quinary oxide film of ($TiO_2/IrO_2/Ta_2O_5/SnO_2$-$Sb_2O_4$) was deposited on Ti mesh by thermal decomposition chemical method. The precursor solution contained salts of $TiCl_4$, $TaCl_5$, $H_2IrCl_6.nH_2O$, $SnCl_4.5H_2O$, and $SbCl_3$ dissolved in an appropriate mixture of ethylene glycol and citric acid. The Ti plate was first sandblasted and then etched with a 20% oxalic acid solution for 1 h in order to clean its surface, thereby rinsed with ultrapure water and lastly dried. The mixture was applied on a substrate with a brush and introduced into the oven at 100 ºC for 5 min. Thereafter, the electrode was calcined at 450 ºC for 10 min in a muffle furnace for thermal decomposition in order to coax the polymerization of the precursor solution. The same procedure was repeated nearly 12 times until the oxide loading of approximately 2.5 mg/cm^2. The final annealing was done at 550 ºC for 1 h in order to complete the fabrication process having molar ratio 34:20:35:10:1 for Ti:Ir:Ta:Sn: Sb. After that, the fabricated anode was cut into small pieces having a dimension (7 cm * 7 cm * 0.5 cm).

3.6 Experimental Setup

The stock solution of each metabolite i.e uric acid (50 mg/L), creatinine (50 mg/L), urea (2000 mg/L) and SU were prepared in double-distilled water. For EO experiments, the working

volume taken was 400 mL. The synthetic solution of all target pollutants was prepared freshly whenever required. EO batch experiments were performed in a single compartment electrochemical flow cell made up of a glass of volume 500 mL as shown in Figure 3.6 with an actual picture of electrodes. For the present study, MMO and doped MMO sheet used as anodes while the stainless steel sheet used as a cathode. In this study, both electrodes were arranged parallelly with an inter-electrode spacing maintained at ~2.0 cm for every experiment. During electrolysis, a current was maintained throughout the experiment run using DC power supply (Model: 0-30V, 0-2A; 0-30V and 0-5A) purchased from DIGITECH, Ambala, (India). For proper homogeneous mixing of the aqueous solution during experimental runs magnetic stirrer was used.

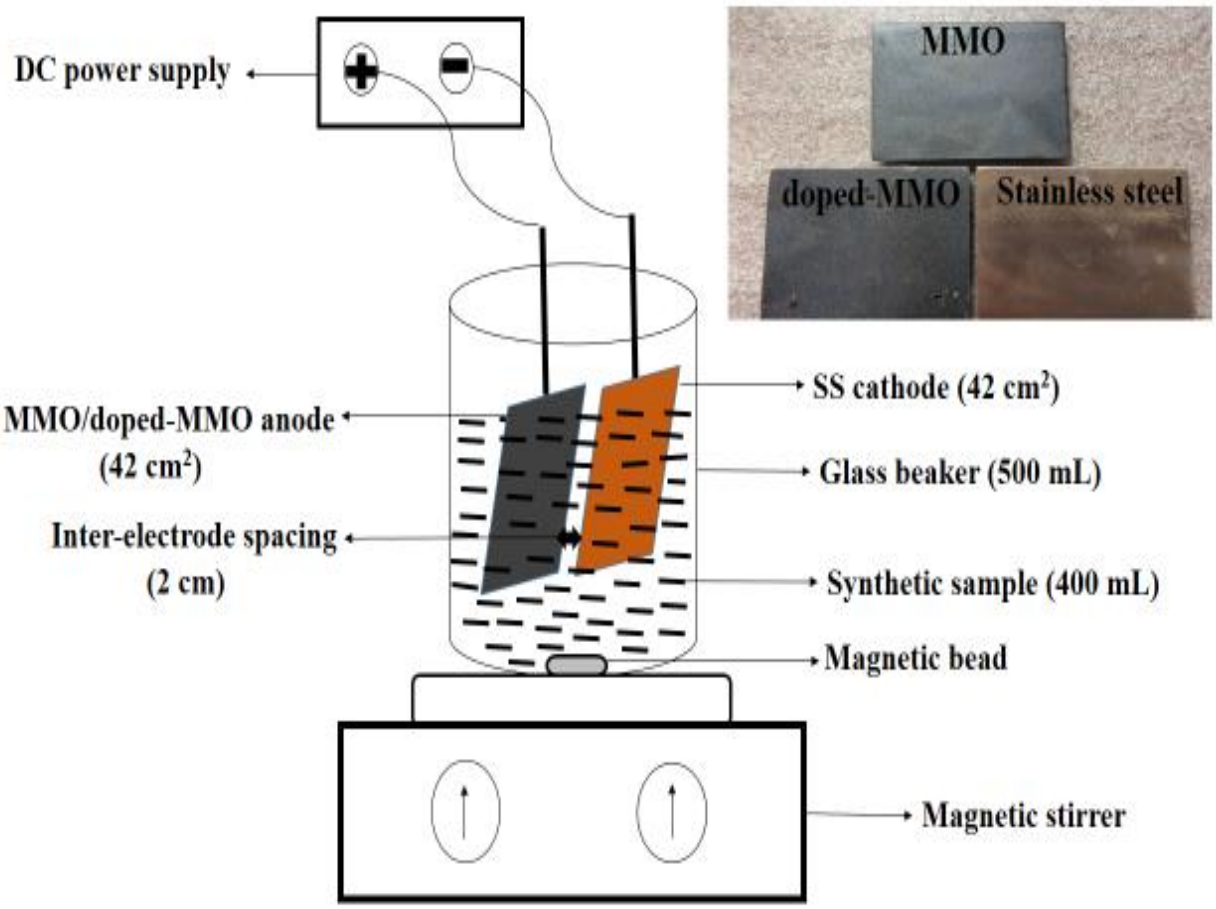

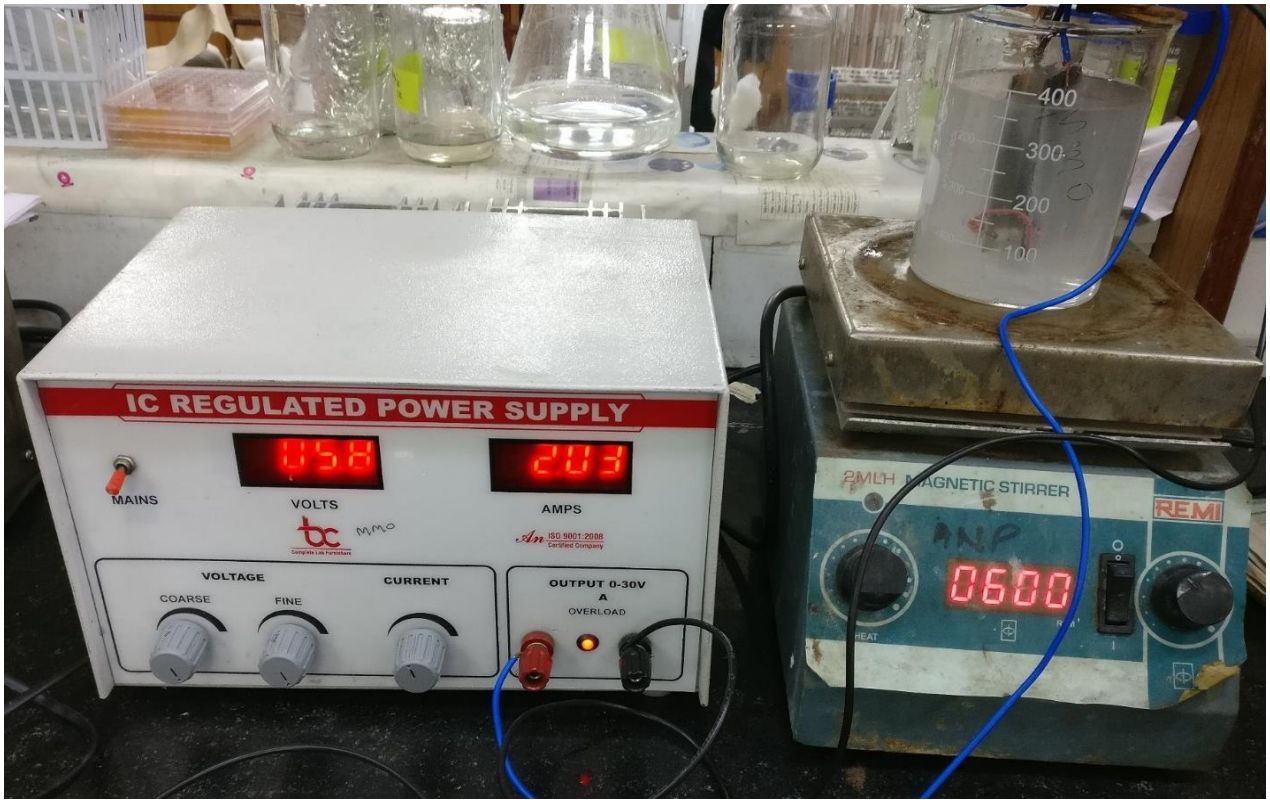

Figure 3.6 Schematic diagram along with an actual picture of the experimental setup for batch EO process.

3.7 Experimental Procedure

EO treatment for synthetic urine and its metabolites (urea, creatinine and uric acid) was performed under galvanostatic conditions. The pH of wastewater was adjusted with NaOH (0.1N) and H_2SO_4 (0.1N) solution as per the requirement for a particular experimental run. For improving the conductivity of the wastewater sample, necessitate an amount of NaCl (electrolyte) was added. The in-situ chemical analysis was carried out periodically by withdrawing a sample volume of 1 mL and pass through millipore filters of size 0.45 µm. The adsorption studies for target compounds on MMO and doped-MMO were performed under dark conditions without applying any voltage with continuous stirring and negligible change in concentration was noticed and thus there was no adsorption. Hence, the efficacy of the treatment process was proven in context to target compounds degradation using EO. All experiments were performed thrice in order to check the reproducibility of results and the average value has been taken. For validation of results, suitable statics was applied.

3.8 Experimental Design and Analysis

For designing the experimental matrix for the EO treatment of each metabolite and SU, response surface methodology (RSM) was employed. RSM is a frequently applied chemometric tool that enables the researchers to simultaneously study the statistical significance of each operational parameter and the development of mathematical models for assessing the optimization problems (Tarley et al., 2009). The main advantage of RSM is to curtail the number of experimental runs and the cost of expensive analysis methods (Bansal et al., 2013; Ranade and Thiagarajan, 2017).

RSM helps in explaining the unknown relationship between the number of associated input parameters and the response of interest by using a low-degree polynomial model. For the model to work effectively, it becomes imperative that responses obtained should fit well to the Equation 3.8.1.

$$y \; or \; z = f(x)\beta + \epsilon \qquad \textbf{(3.8.1)}$$

Where y or z = response; x = x_1, x_2, . . . , x_n (denote the n number of independent natural variables); f is a vector function of p elements; β is a vector of p constant coefficients and ϵ is a random statistical error of zero means. Here, the quantity f(x)β represents the expected mean value of response y or z (Khuri and Mukhopadhyay, 2010). In classical RSM, to predict the maximum and minimum values of response for optimum settings of the control variables, two low degree polynomial models are commonly used that is i^{st} degree model with (d=1) and 2^{nd} degree model with (d=2) as shown in Equations 3.8.2 and 3.8.3 (Khuri and Mukhopadhyay, 2010).

$$y \; or \; z = \beta_0 + \sum_{i=1}^{n} \beta_i x_i + \epsilon \qquad \textbf{(3.8.2)}$$

$$y \; or \; z = \beta_0 + \sum_{i=1}^{n} \beta_i x_i + \sum_{i<j} \sum \beta_{ij} x_i x_j + \sum_{i=1}^{n} \beta_{ii} x_i^2 + \epsilon \qquad \textbf{(3.8.3)}$$

Where β_0, β_i, β_{ii}, β_{ij} are constant regression coefficients; x_i and x_j are coded input factors and £ is an error function. The first order designs are commonly used, 2k factorial, Plackett–Burman, and simplex designs. First-order polynomials are less rotatable designs as well as less stable in the prediction of variance and suffer lack of fit because of interaction between surface curvature and factors (Khuri and Mukhopadhyay, 2010).

Hence, to resolve the drawbacks of first-order design and to improve the optimization process, the second-order polynomial studies are required to construct a quadratic response surface model. The second-order symmetrical designs are Doehlert design, Box–Behnken design, Three-

level factorial design and Central Composite design (Bezerra et al., 2008). Out of them, Box–Behnken design has been selected for the present study.

3.8.1 Box-Behnken design

The Box-Behnken design devised in 1960 by George Box and Donald Behnken. The design provides a three-level factorial arrangement as shown in Figure 3.8 (Ozgen and Yildiz, 2010) and allows the proper evaluation of first and second-order coefficients of the mathematical model. It consists of a distinct subset of factorial combinations taken from 3^k factorial design, hence more efficient and cost-effective, especially when a number of variables are large such as industry research, etc. (Khuri and Mukhopadhyay, 2010).

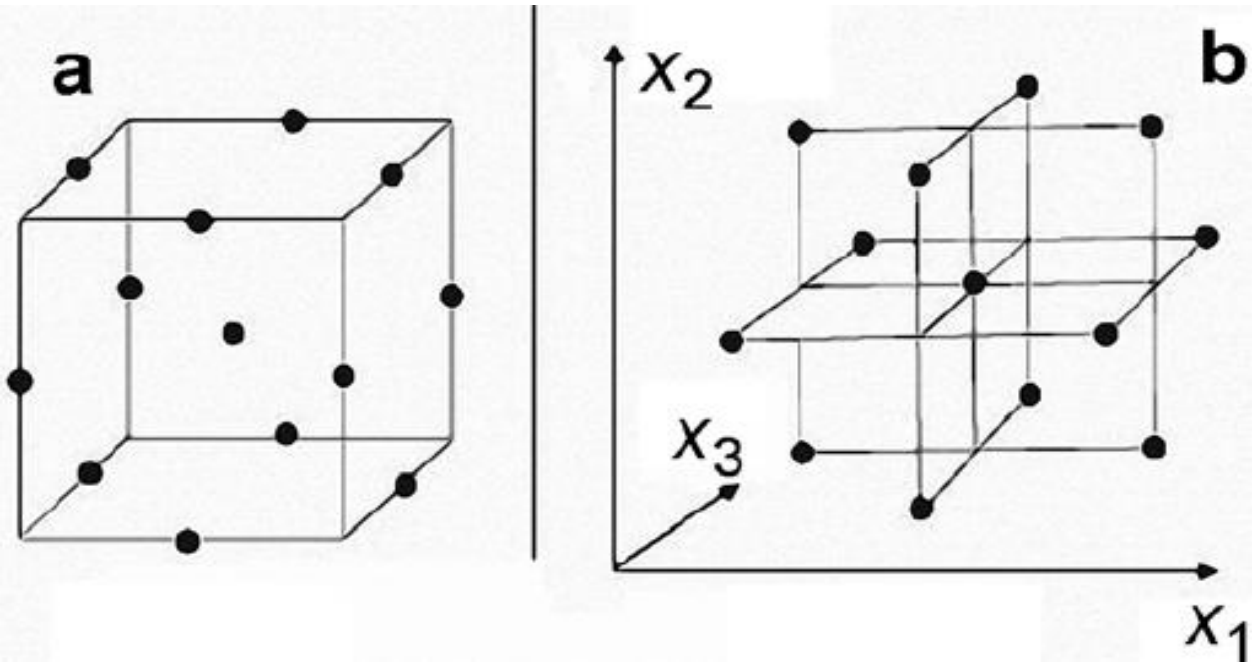

Figure 3.8 Box–Behnken design for a three-factor experiment

Box–Behnken designs (BBD) are a class of rotatable or nearly rotatable designs which based on three-level per factor (-1, 0, +1), but avoids the space of corners and fills it with combinations of center and extreme levels of the cube. Thus, in this way, BBD combines a fractional factorial with incomplete block designs and avoid the extreme vertices to maintain the rotatability of the design (Hanrahan and Lu, 2006). The number of experimental trials (N) required for the optimization of process parameters is designed by using the formula shown in Equation 3.8.4 (Bezerra et al., 2008).

$$N= 2k\,(k-1) + C_0 \qquad \textbf{(3.8.4)}$$

where k is a number of factors and C_0 is the number of replicates for the central points. Thus, Box-Behnken is an overall good and efficient design under response surface methodology because of its applications such as (i) quadratic model parameters estimation; (ii) use of blocks; (iii) sequential designs building and (iv) model fitness (lack of fit) detection (Ferreira et al., 2007).

3.8.2 Statistical analysis with BBD

The present statistical investigation was carried out through Design-Expert software version 6.0.8 (STAT-EASE Inc., Minneapolis, US) in order to minimize the void content and to optimize the experimental data. BBD under RSM was developed by the axial points and additional centers to allow the evaluation of operational variables of a second-order model (Bezerra et al., 2008). The data obtained from the experimental runs designed by BBD was further analyzed to attain the best regression model among other models such as linear, cubic, quadratic, etc. For that experimental data were fitted into second-order polynomial equation (3.3) through non-linear regression analysis

Full and fractional factorial design experimental strategy was applied in which different input parameters are varied together, instead of a single parameter at a time. In the experimental design, the lower and upper ranges of the input parameters are defined and segregated at different levels. Optimization provides the simultaneous effect of all input operational parameters on the selected responses. Experiments consist of a series of runs, the effect of changes in input parameters (x_1, x_2 …., x_n) on the responses (Y or Z) is determined through RSM modeling. In order to examine the interaction between input parameters and responses, ANOVA (Analysis of variance) was studied. ANOVA is a statistical technique that subdivides the total variation into parts i.e. variation related to model and variation related to residual error for the purpose of testing hypotheses on the parameters of the model (Fu et al., 2007).

The interaction of responses (Y or Z) with input parameters (x_1, x_2,..., x_n) can be represented graphically, either in the three-dimensional graphs or as contour plots. To check the adequacy of the model, two different tests were performed i.e. the sequential model sum of a square and model summary statistic (which expressed as R^2, adjusted R^2 and predicted R^2). The statistical significance of the model fitted was checked by values of F and P. The adequate precision ratio illustrates that the model can be used for design space navigation. To check the reliability of chosen developed models for responses, plots of normal % probability versus studentized residuals and studentized residuals versus predicted were examined (Ozer et al., 2009). 3D response graphs developed from

the chosen model were studied in order to see the interactive effect of each operational parameters on responses as well as used to locate the optimal conditions for process parameters

In the present study, more than one responses were there, hence for simultaneous optimization of different responses, multi-response process optimization by desirability function approach was used. The desirability function approach is one of the most widely used methods for the optimization of multiple response processes. One-sided desirability (d) is given in Equation 3.8.5 (Thakur et al., 2018).

$$d = \begin{cases} 0 & if\ Z_i \le Z_{i-min} \\ \left[\frac{Z_i - Z_{i-min}}{Z_{i-max} - Z_{i-min}}\right]^k & if\ Z_{i-min} < Z_i < Z_{i-max} \\ 1 & if\ Z_i \ge Z_{i-max} \end{cases} \quad \textbf{(3.8.5)}$$

Where Zi is the response value, $Z_{i\text{-}min}$ and $Z_{i\text{-}max}$ are the minimum and maximum acceptable values of response i, respectively. Where k is a positive constant weight, used to determine the desirability scale (Mondal et al., 2013; Sangal et al., 2014). The value of desirability function lies between 0 and 1, representing the closeness of response to its ideal value. Desirability function converts each response to corresponding desirability values which further combined to form composite desirability function by changing multi-response into a single response as depicted in Equation 3.8.6 (Costa et al., 2011).

$$Di = (d_1 * d_2 * d_3 \ldots\ldots..)^{1/n} \quad \textbf{(3.8.6)}$$

Where Di is the desirability function; d_1, d_2, d_3, etc. are corresponding desirability's of given responses; n is the number of responses. If given responses reach their ideal values then value Di will be 1. Therefore, overall desirability will also be 1. In any case, if any one response will not reach its ideal value then Di for that particular response will be less than 1 and therefore overall desirability come will also be less than 1 (Hiwarker et al., 2017).

For this research study, BBD under RSM was used to design the experimental runs for EO treatment of metabolites and SU. Moreover, it helps in the analysis of the experimental data along with the optimization of selected input operational parameters such as NaCl dose (n), current density (j), treatment time (t) and pH. The responses selected for EO treatment of metabolites were %Degradation (Y_1) and Energy consumption (Y_2) while in the case of SU, responses chosen were in terms of %COD removal, (Z_1) and specific energy consumption (SEC) (Z_2). For optimization, the

mathematical relationship of the response Y on these significant input factors can be estimated by the second-order polynomial equation. The influence of the operational process parameters on the responses was analyzed from an analysis of variance (ANOVA). In order to simultaneously maximize the %Degradation, %COD removed and for minimization of Energy consumption and SEC, multi-response optimization was employed.

Performance of EO process for the treatment of metabolites and SU was evaluated by analyzing the responses Y_1 (%Degradation), Y_2 (Energy consumption), Z_1 (%COD removed) and Z_2 (SEC). These responses during treatment were calculated using Equations 3.8.7-3.8.10 (Chauhan and Srivastava, 2019).

$$Y_1(\%\text{Degradation}) = \frac{C_0 - C_t}{C_0} X100 \quad \textbf{(3.8.7)}$$

$$Y_2\,(\text{EC}) = \left[\frac{\text{V}*\text{I}*\text{t}}{\text{S}_\text{v}} X10^3\right] \quad \textbf{(3.8.8)}$$

$$Z_1(\%\text{COD removed}) = \frac{COD_0 - COD_t}{COD_0} X100 \quad \textbf{(3.8.9)}$$

$$Z_2\,(\text{SEC}) = \left[\frac{\left(\left(\frac{VIT}{S_v}\right)/10^3\right)}{COD_r/10^6}\right] \quad \textbf{(3.8.10)}$$

Where C_0= Initial pollutant concentration (mg/L); C_t= pollutant concentration at different time intervals (mg/L); COD_0 = Initial COD (mg/L); COD_t = COD at fixed time intervals (mg/L); COD_r = COD removed at different time intervals (mg/L); EC= Energy consumption (kWh/m^3); SEC= specific energy consumption (kWh/ kg of COD removed); I= current (A); V= voltage; t= electrolysis time (h) and Sv = Volume of sample (L).

3.9 Photo-electrocatalysis (PEC)

In order to investigate the photo-activity of MMO and doped-MMO, synergistic studies were performed. After optimization of the input operating parameters through BBD for the EO process, experiments were carried out under UV and solar radiations. These synergistic studies have been done using kinetic rate constant obtained through pseudo-first-order reactions that have been discussed in following section 3.9.1. The degradation experiments of metabolites and SU were performed with both types of anodes in a batch reactor and three different techniques were applied which include PC (interaction of light with anode surface), EO (constant applied current only) and

PEC (constant applied current and light). For PC and PEC, a wooden chamber was fabricated which contains 10 UV tubes. Out of the 10 UV tubes, 7 tubes (Philips) of 36W (365 nm) were attached beneath the top roof while the other 3 UV tubes of 18W (365 nm) attached to the one sidewall of the wooden chamber and aligned horizontally as shown in Figure 3.6. The experiments under UV light were executed at a UV intensity of 23 ± 2 W/m^2 measured by a radiometer (Eppley; model no. 33013). For getting the appropriate intensity of UV light throughout the reaction, the distance of the EO reactor was fixed from the tubes accordingly.

In the case of solar, the EO reactor was placed directly under natural sunlight as shown in Figure 3.9.2. The experiments under solar radiation were performed in the month of April to June from 9.30 am to 4.30 pm at TIET (Thapar Institute of Engineering and Technology), Patiala (30.3398ºN, 76.3869ºE) (Punjab), India. During the experimental study, the average intensity of solar radiation was checked by means of pyrometer which was in the range of 650-750 W/m^2.

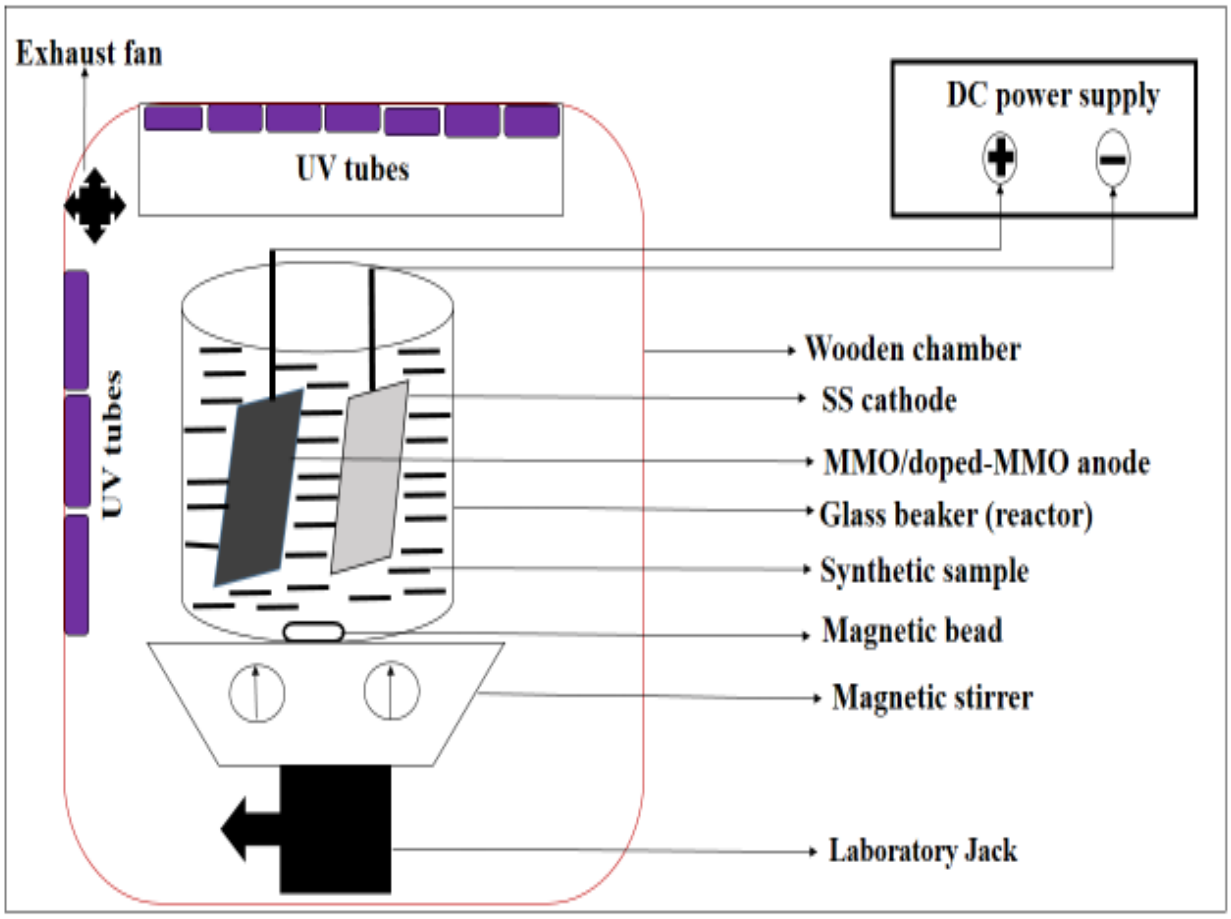

Figure 3.9.1 Schematic diagram of the experimental setup for PEC under UV irradiations.

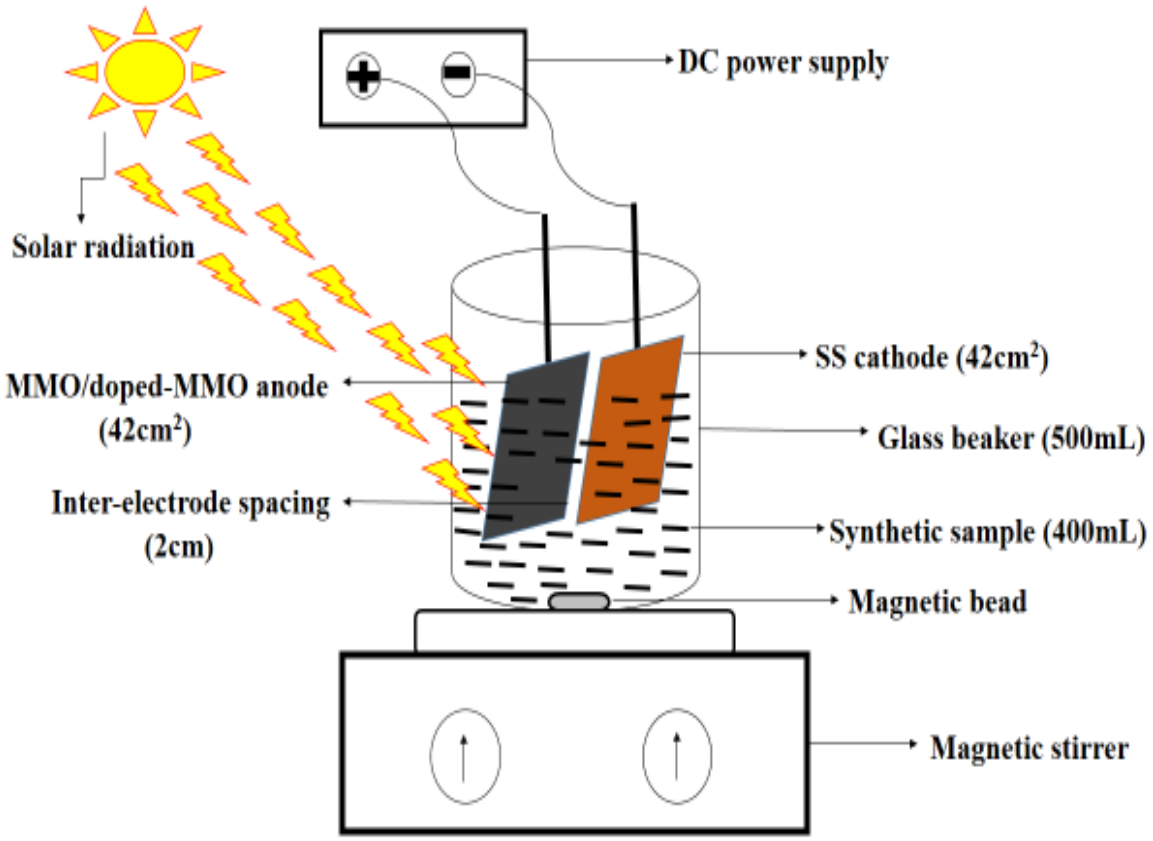

Figure 3.9.2 Schematic diagram of the experimental setup for PEC under solar irradiations.

3.9.1 Synergy calculations

In this present study, the synergy of the dual-process i.e. PEC over individual processes has been calculated using Equations 3.9.1- 3.9.3 (Bansal and Verma, 2018).

Synergy over individual processes [photo-catalysis (PC) or electro-oxidation (EO)]:

$$\%Synergy = 100 \times \left\{\frac{[k_{dual} - (k_{photocatalysis} \text{ or } k_{electroxidation})]}{k_{dual}}\right\} \quad \textbf{(3.9.1)}$$

Overall Synergy:

$$\%Synergy = 100 \times \left\{\frac{[k_{dual} - (k_{photocatalysis} + k_{electroxidation})]}{k_{dual}}\right\} \quad \textbf{(3.9.2)}$$

Where 'k' = pseudo-first-order rate constant (min^{-1}) of each process and calculated from Equations 3.9.3-3.9.4.

$$-ln\frac{C_0}{C_t} = k_1 t \quad \textbf{(3.9.3)}$$

$$-ln\frac{COD_0}{COD_t} = k_1 t \quad \textbf{(3.9.4)}$$

Where C_0 = initial substrate concentration (mg/L); Ct= substrate concentration at any time of treatment (mg/L); COD_0 = Initial COD (mg/L) and COD_t = COD at fixed time intervals (mg/L)

3.10 Pilot-scale Studies for EO Treatment of SU/AHU

In this study, attempts have been made for the EO treatment of AHU coupled with solar energy driven by photovoltaic (PV) panels. EO process study for the treatment of AHU was conducted in a rectangular glass shaped reactor fabricated with a plexiglass sheet having dimensions of 9 cm * 9 cm * 4 cm as shown in Figure 3.10. The reactor was operated in recirculation mode was designed to treat 1-2 L of total sample volume. The reactor was provided with one inlet and one outlet along with one detachable baffle made up of acrylic fiber. In order to capture different gases during EO treatment of AHU, a square glass box made up of acrylic fiber was fabricated equipped with a side-branches sampling port (inlet and outlet) and a gas outlet port on top. The glass square box was placed inversely over the EO reactor. Furthermore, the whole setup was placed on a jack and fixed accordingly with clay so that the infiltration of air was stopped. In order to check the efficiency of the process as well as the efficacy of the novel electrodes for the on-site treatment of urine wastewater, experiments were first performed with SU. An aqueous solution of SU with a working volume of 2 L was used for EO experiments. At certain time intervals, samples of appropriate volume were taken out from the solution and filtered using 0.45 μm filters and underwent various analyses.

As recycle ratio for the current process was taken as infinity as all the water was recycled for the given time. The system behaves as the batch reactor and was designed using batch reactor equations as described in Equations 3.10.1-3.10.6 (Levenspiel, 1999).

$$\frac{dN_A}{dt} = \int r_A \, dV \quad \textbf{(3.10.1)}$$

As reaction mixture was perfectly mixed, r_A becomes independent of position:

$$\frac{dN_A}{dt} = r_A V \quad \textbf{(3.10.2)}$$

Time t, required to reduce the number of moles from N_{A0} to N_{A1} was calculated by the following formula:

$$t = \int_{N_{A1}}^{N_{A0}} \frac{dN_A}{-r_A V} \quad \textbf{(3.10.3)}$$

$$N_A = C_A \, \mathrm{V} \quad \textbf{(3.10.4)}$$

For constant- volume batch reactor this equation can also be represented as:

$$\frac{dC_A}{dt} = r_A \quad \textbf{(3.10.5)}$$

Recycle ratio is defined:

$$R_r = \frac{V_r}{V_o} \quad \textbf{(3.10.6)}$$

In this case: $V_0 = 0$, therefore $R_r = \infty$, hence, the system behaves as a batch reactor

Furthermore, the conversion of substance A is defined by Equation 3.10.7.

$$X = \frac{moles\ of\ A\ reacted}{moles\ of\ A\ fed} \quad \textbf{(3.10.7)}$$

Which further represented by Equation 3.10.8.

$$X_i = \frac{N_{io} - N_i}{N_{io}} = 1 - \frac{C_i V}{C_{A0} V_0} \quad \textbf{(3.10.8)}$$

A number of moles of A in the batch reactor after conversion X has been achieved can be calculated by Equation 3.10.9.

$$N_A = N_{A0}(1 - X) \quad \textbf{(3.10.9)}$$

On differentiating the above equation with respect to t and inserting it into the equation 3.15 for the batch reactor and got Equations 3.10.10- 3.10.11.

$$N_{A0} \frac{dX}{dt} = -r_A V \quad \textbf{(3.10.10)}$$

$$t = N_{A0} \int_0^X \frac{dX}{-r_A V} \quad \textbf{(3.10.11)}$$

Where, N_A= molar concentration of target compound (mol/L), C_A= concentration of compound (mg/L), r_A= reaction rate, R_r= recycle ratio, V_r= volume of reaction mixture returned to the reactor entrance (mL), V_0= volume leaving the system (mL).

To regulate the flow rate (Q) and retention time for a particular run in case of a continuous process, a peristaltic pump (Miclins peristaltic pump PP 20 EX) was used. The space-time or retention time (Ƭ) and a space velocity of the electrochemical reactor were calculated according to the Equation 3.10.12.

$$\tau = \frac{V}{\vartheta_0} \quad \textbf{(3.10.12)}$$

While space velocity (υ) was calculated by Equation 3.10.13.

$$\upsilon = \frac{\vartheta_0}{V} \quad \textbf{(3.10.13)}$$

Where, Ƭ = space-time (min), V = volume of reaction mixture in a reactor (L), v_0 = volumetric flow rate (L min^{-1}), υ = space velocity (min^{-1}). By this dual approach, one can save the cost of electrolytes and electricity consumed for the EO treatment process.

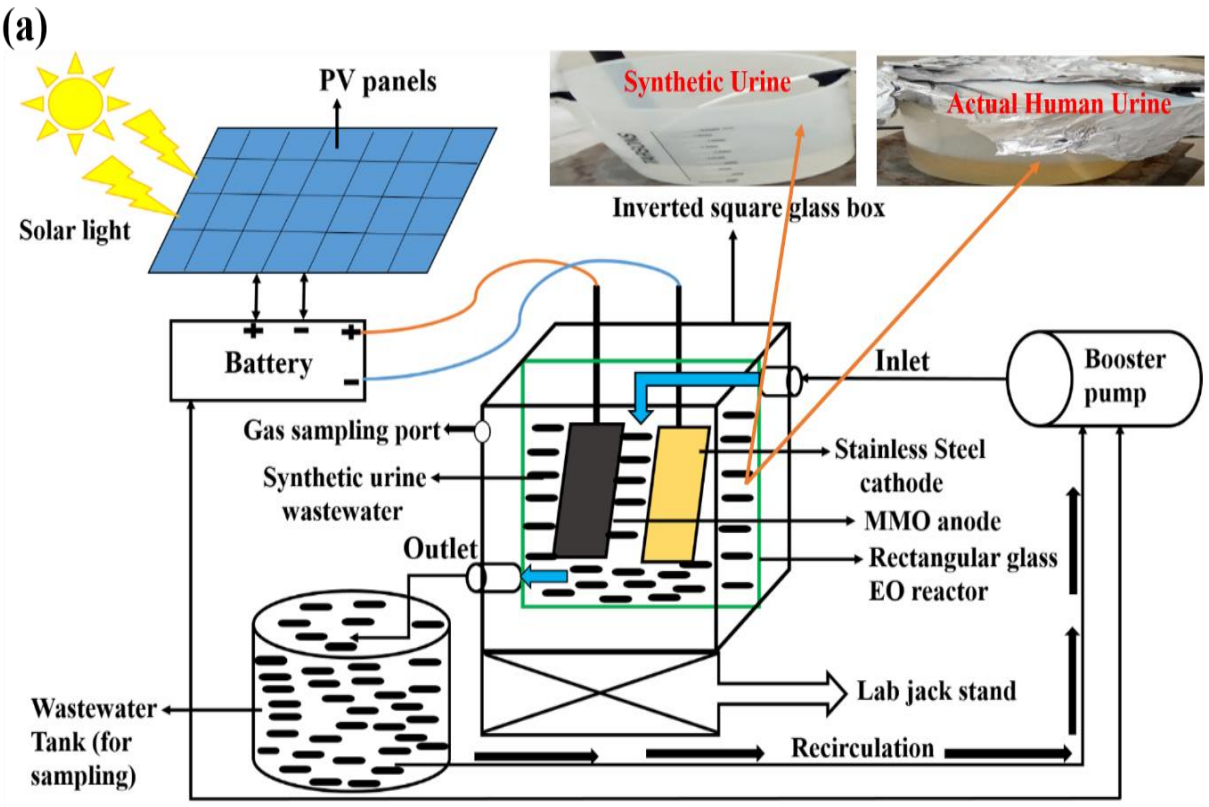

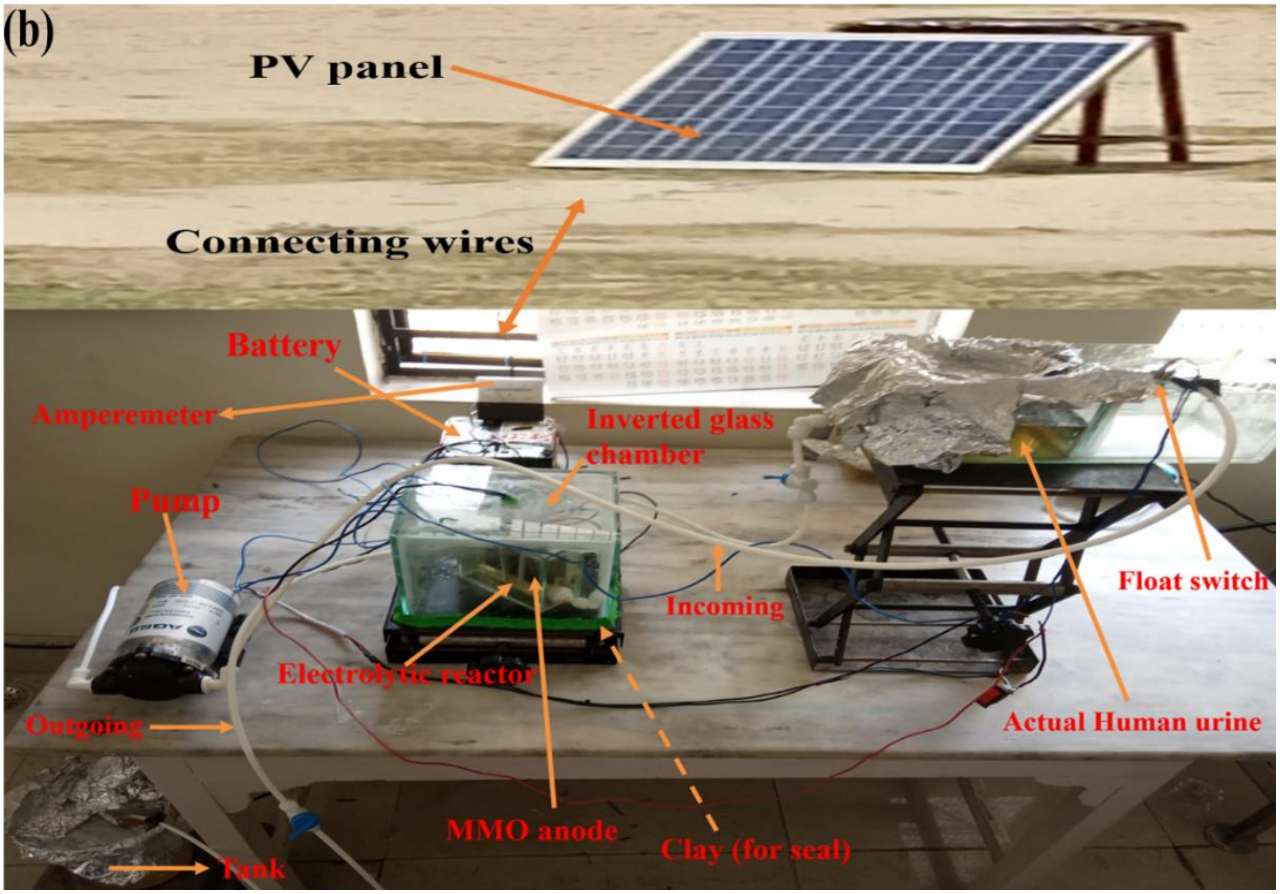

Figure 3.10 (a) Schematic diagram of the experimental setup of PV driven continuous EO reactor for the treatment of SU/AHU and (b) actual photograph of continuous EO reactor for the treatment of AHU.

3.11 Characterization of Anodes

The durability and stability of oxides layers (MMO and doped MMO) on anodes were characterized by various techniques. The anodes were characterized by Scanning electron microscopy [SEM, model- JSM-6510LV, JEOL (Japan)] and Electron dispersive spectroscopy [EDS, model-INCAX-act, Oxford instruments (U.K.)] in order to analyze the surface morphology and elemental composition of metal oxides. The crystalline structure of various metal oxides layers on the anode surface was measured by X-ray diffraction (XRD) [X'Pert pro diffractometer; 2Θ = 10-90º]. Raman spectroscopy was performed at 532 nm on a confocal microspectrophotometer coupled with diode green laser (Model: STR 500), Airix Corporation, Japan. To check the chemical and electronic state of the metal oxide layers, XPS [X-ray photoelectron spectroscopy, Omicron Nanotechnology, Oxford Instrument] was performed. The study of $OH^{\bullet}$ production during EO and

PEC were checked using a fluorescence spectrophotometer (PerkinElmer, LS 45). Terephthalic acid (TPA) was used as a robe which readily reacts with the $OH^{\bullet}$ and produces a fluorescence compound named 2-hydroxyterephthalic acid (TAOH). The intensity of 2-hydroxyterephthalic acid was measured at an excitation wavelength at 315 nm and emission wavelength at 425 nm.

3.12 Analytical Determination

The sample analysis of treated target compounds was carried out at regular intervals of time through UV-vis absorption spectroscopy (LAB INDIA, T60 U) with λ_{max}= 238, 290 and 420 nm for creatinine, uric acid, and urea respectively. A closed reflux method was used for the COD estimation (APHA, 1989: Sec.5220-(C)) of the samples at regular time intervals. COD was measured using the digestive unit (Thermo reactor, model 2025D, Spectra lab). APHA standard methods (1989) were employed for monitoring the generation of ions such as nitrite ions (APHA, 1989: Sec.4500-NO_2 (B)), nitrate ions (APHA, 1989: Sec.4500-NO_3 (E)), COD, Total available chlorine (APHA, 1989: Sec.4500-Cl^{-}(B)), ammonical nitrogen (APHA, 1989: Sec.4500-NH_3- (B&C)), organic nitrogen APHA, 1989: Sec.4500-N) and chloride (APHA, 1989: Sec.4500-Cl^{-} (B)). The TOC content in treated and untreated samples was checked through Multi N/C Model-2100 BU, TOC analyzer, Analytic Jena AG Corporation (Germany). FTIR (Fourier transform infrared spectrum) was measured by the Perkin Elmer spectrometer (range 4000-200 cm^{-1}) using KBr pellets for untreated and treated samples. The redox reactions that occurred during electrolysis of synthetic urine were measured through cyclic voltammetry (Metrohm Autolab; Model- CHI660C) at room temperature. The employed conventional three-electrode assembly consisted of Pt wire as the counter electrode, Ag/AgCl as a reference and commercially available Pt rod with $1cm^2$ area as a working electrode. LC-MS analysis with a mass spectrometer (Q-TOF; Micromass Ltd.), UK was used to identify the degradation products of metabolites and SU generated during the EO treatment process. The injection temperature for ion spray injector was set at 480 °C and de-clustering potential was adjusted to 73 V. Isocratic mode was employed using a mobile phase of solution A: 0.1% formic acid in (50%) acetonitrile and solution B: 0.1% formic acid in (50%) water with Waters XBridge C─18 column (250 mm X 4.65 µm). Data analysis was performed under positive ion mode at a flow rate equal to 200 µL/min. Run time for LC-MS analysis was 20 min The concentration of urea, uric acid, and creatinine in treated and untreated samples of SU/HU was estimated using a semi-auto analyzer (Erba Mannheim, model- Chem 5X). The intermediates formed during the EO treatment of

AHU were identified through gas chromatography-mass spectrometry (GC-MS) analysis. Perkin−Elmer Clarus 500 MS instrument with fused silica capillary columns (25 m × 200 μm internal diameter) coated with a 5% diphenyl/95% dimethyl polysiloxane was used for GC-MS analysis. The m/z was scanned in the range from 25─350. Helium was used as carrier gas with a flow rate of 1 ml/min. The injection temperature was adjusted to 280 °C while the temperature for the GC oven was adjusted to 100─280 °C, with every 25 °C increment in temperature. 1μL of the sample was injected and a 20:01 split ratio was employed for GC. Run time for GC-MS analysis was 24.20 min. The determination of gaseous products like carbon dioxide (CO_2), hydrogen (H_2) and molecular nitrogen (N_2) evolved were analyzed by gas chromatography (GC, CS-5800) with thermal conductivity detector (TCD) and column oven size (260 mm* 280 mm* 155 mm). The packed column was used for TCD with the temperature set at 150 °C. The packed column is split into two solid supports i.e. molecular sieve (5A) and Porapak Q (2 m X 3.175 mm). The column oven temperature was adjusted at 70 °C with every 0.1°C increment in temperature. The temperature for the front injector and front detector were set at 100 °C and 220 °C respectively. 1 mL of sample was injected and run time for GC analysis was 8 min. The carrier gas used for TCD operation is hydrogen. The pH and conductivity of samples were measured using pH meter (HANNA (HI 5221)) and conductivity meter (HANNA (HI 5321)), USA

Chapter-4

RESULTS AND DISCUSSION

4.1 General

In this chapter detailed discussion about degradation studies of synthetic urine and its metabolites by EO with MMO and doped-MMO are done. For analyzing the process efficiency, different parameters are evaluated. Furthermore, the oxidation mechanism of pollutants and their transformation into byproducts after the treatment process has been checked through various analytical techniques. Attempts have been made to study the effect of two processes at the same time in the same system by coupling the light irradiations (under artificial UV light or natural solar radiations) with the EO process i.e. PEC in order to enhance the process efficiency as well to reduce the treatment time.

4.1.1 Overview

For the first time novel combination of different metal oxide at the surface of the single anode was selected for the oxidation urine metabolites such as uric acid, creatinine, and urea through EO. Moreover, an individual drawback of each metal was covered by incorporating these metals into the single anode. The anode selected for a particular study by keeping in mind to have better removal efficiencies even in extreme conditions. This novel combination of different metal oxides was incorporated on titanium anodes in order to have an electro-active surface area (active sites) due to the presence of TiO_2, better stability due to Ir in acidic solutions as well as a high temperature, good resistance properties of Ru, durable enough at high anodic potentials and electrochemically effective even at lower current densities due to presence of Pt.

Similar studies were performed with another anode that is doped-MMO in order to overcome the problem of treating urine metabolites at higher current densities. In this anode, different metal oxides incorporated were a combination of active and non-active metals in order to have more generation of $OH^{\bullet}$ which further led to having better degradation efficiency. In order to get excellent resistance properties and good service life, Ir was incorporated. Ta provides high current densities and enables the anode to work on high values of applied current without causing any damage. The

integration of Sn was done to get more active sites for the generation of ROS. Sb was doped in order to increases the conductivity of anode as well as lowers the oxygen evolution over-potential.

Preliminary EO experiments were carried out with both anodes for the oxidation of urine metabolites in batch mode. For evaluating the performance of the treatment process i.e. EO, various operational parameters such as current density, treatment time, pH and NaCl dose were selected based on a literature survey and preliminary studies performed. Furthermore, a comprehensive study using response surface methodology was carried out in order to investigate/ analyze the influence of these input process parameters on each other as well as their effect on selected responses such as percentage Degradation and Energy consumption. Attempts were made to couple the EO with some other technology in order to study the synergistic effect of dual-process over single processes alone at optimized conditions. Durability studies for both anodes were carried out in order to study the economic feasibility of the employed technique. Mineralization studies were validated through the production of various anions, reduction in TOC and COD and evaluation of gases like CO_2, N_2, H_2, etc. The transformation of target compounds into intermediates was identified through LC-MS analysis. Based on these intermediates, the oxidative degradation pathway for a particular metabolite was proposed in this experimental study.

After knowing the oxidation mechanism of metabolites individually in an aqueous medium, degradation studies for synthetic urine using both anodes were carried out systematically. The process optimization was carried out with MMO by varying the operational parameters that are pH, applied current density, N/Cl ratio and treatment time and subsequently similar performed with doped-MMO. Further PEC with both anodes was carried out under UV light and natural solar radiation at optimized conditions in order to reduce the electrolysis time to some extent and save some energy consumed during the process.

Scale-up studies with novel electrodes were also carried out for the treatment of real human urine wastewater through EO in continuous recirculation mode by incorporation of the PV panels in order to save the energy consumed for a particular process. Successful treatment could lead to the sustainable on-site treatment of urinal wastewater containing these nitrogen-based toxic compounds.

The flow of the experimental research work has been presented in the form of a flow chart (Figure 4.1) to have a clear vision of what and how this study has been done.

Section A (Urine metabolites treatment)

I. Selection of commercially available electrodes (i.e. MMO) was done initially.
II. EO treatment of all metabolites i.e. uric acid, creatinine and urea were done with MMO.
III. Different operational parameters were evaluated using RSM
IV. Synergistic studies were carried out in order to assess in-situ dual process under UV and solar light at optimized conditions.
V. Mineralization studies were performed to check quality of treated effluents.
VI. Selection of another electrode (i.e. doped-MMO) was done so that better wider spectrum of solar light can be used by reducing its band gap as well as to have better process efficiency at extreme conditions.
VII. Similar studies were carried out with doped-MMO and compared with results of MMO.

(Covering objective 1)

Section B (SU treatment)

I. EO treatment of SU was carried out using MMO and doped-MMO based upon results of objective 1.
II. Evaluation of various input operational parameters were done using RSM.
III. Synergistic studies were carried out with both anodes in order to reduce treatment time of study.
IV. Mineralization studies were carried out.
V. Durability studies for both anodes were done in order to check its recyclability for multiple runs of cycles.

(Covering objective 2)

Section C (Scale Up studies)

I. Continuous EO treatment of SU was carried out in PV driven electro-catalytic reactor by both electrodes coupled with molecular hydrogen generation.
II. Mineralization studies were carried out and results has been compared.
III. The actual viability of EO treatment process at field scale was confirmed with the treatment of AHU using MMO anode.
IV. Mineralization studies were performed along with various gas analysis such as H_2, CO_2, N_2, etc.

(Covering objective 3)

Section D (Characterization of electrodes)

I. Durability and stability of both anodes were checked through various characterization techniques such as SEM/EDX, XRD, Raman, XPS and UV-DRS.

Figure 4.1 Framework of results and discussions

4.2 Standard Calibration Curve of Uric acid, Creatinine and Urea

The wavelength scan of urine metabolites i.e. uric acid, creatinine and urea was studied in the range from 200-800 nm. Maximum absorbance i.e. λ_{max} was obtained at 290 nm in case of uric acid, 238 nm in case of creatinine and 420 nm in the case of urea. The standard concentration for uric acid and creatinine were varied from 10-70 mg/L, while for urea it is 200 to 2000 mg/L based on literature studies. The calibration curve was made by plotting a curve between standard concentrations and absorbance. The coefficient of determination, R^2 was found to be 0.998, 0.999 and 0.990 with slope values 0.0552, 0.0513 and 0.0014 respectively as shown in Figure 4.2. The concentration of urine metabolites for the present experimental study has been determined from these calibration curves.

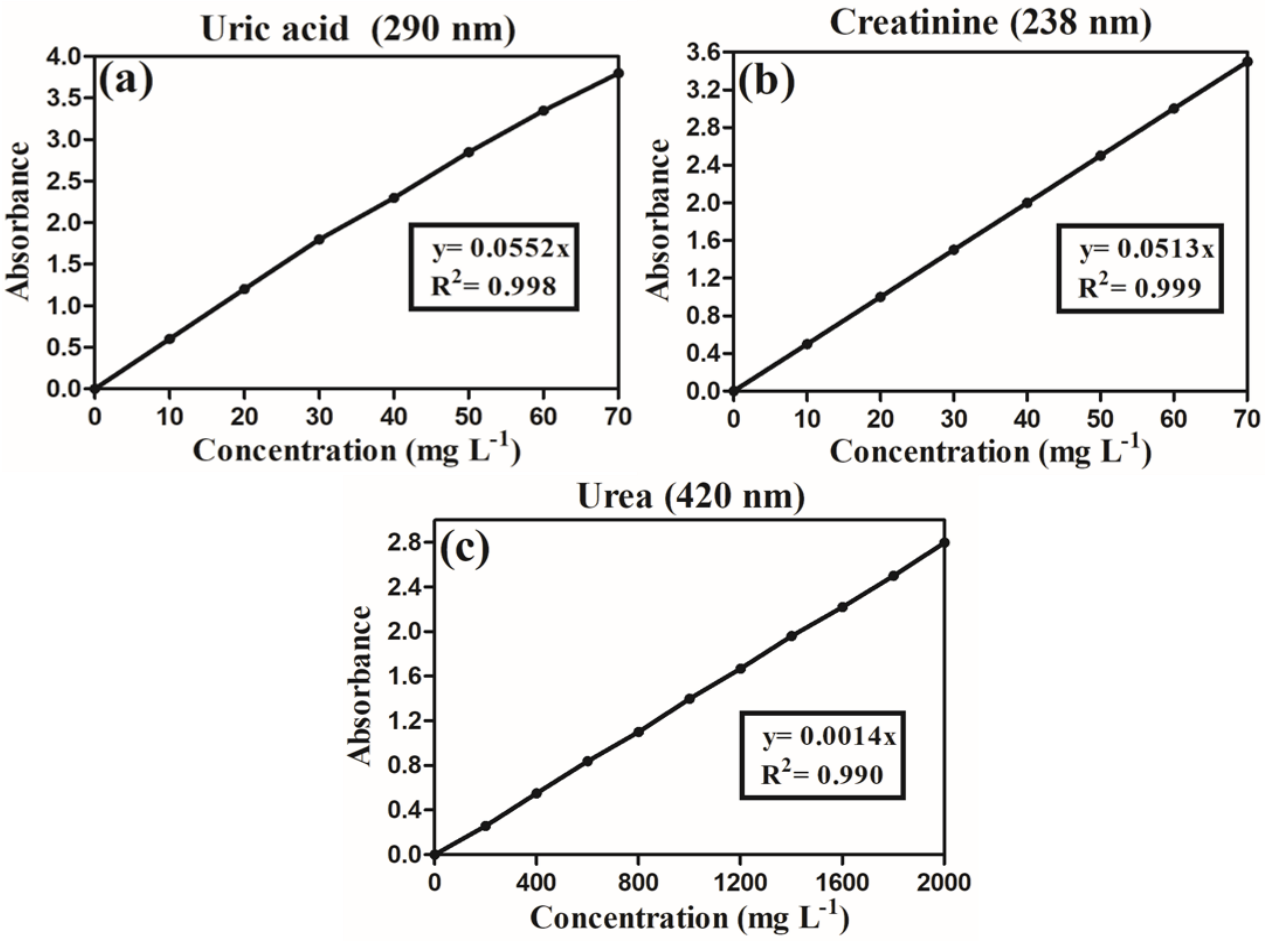

Figure 4.2 Calibration curve of all urine metabolites i.e. (a) Uric acid, (b) Creatinine and (c) Urea.

SECTION-A

4.3 Study on EO Treatment of Urine Metabolites (Uric Acid, Creatinine and Urea) with MMO

4.3.1 Model Fitting and Statistical Analysis

In this study, three-level BBD based RSM has been employed for the designing of EO experiments for urine metabolites using MMO anodes. For establishing the process conditions for the removal of metabolites from aqueous solution, four input operational parameters were selected such as initial pH (X_1), current density (X_2), treatment time (X_3) and NaCl dose (X_4). The actual ranges along with coded values of these listed parameters in Table 4.3.1 were selected on the basis of the reported studies and prior observations. The total number of experimentally designed by BBD for all urine metabolites was 30 with six replication runs at the center. The experimental results of responses like %Degradation (Y_1) and Energy consumption (Y_2) for EO treatment of all urine metabolites (uric acid, creatinine and urea) were calculated by conducting the experimental runs according to the suggested design matrix as shown in Table 4.3.2a,b,c.

Table 4.3.1 Range and coded levels of selected input operational variables for EO treatment of all urine metabolites with MMO

			Range of actual and coded variables		
Compounds	Factors	Variables	-1	0	+1
(a) Uric Acid	X_1	Initial pH	2	5.5	9
	X_2	Current density , j (mA/cm^2)	2.38	7.14	11.90
	X_3	Treatment time, t (min)	2	6	10
	X_4	NaCl dose (n) (g/L)	0.25	0.75	1.25
(b) Creatinine	X_1	Initial pH	2	5.5	9
	X_2	Current density , j (mA/cm^2)	7.14	14.28	21.42
	X_3	Treatment time, t (min)	15	65	115
	X_4	NaCl dose (n) (g/L)	0.25	0.75	1.25
(c) Urea	X_1	Initial pH	3	6	9
	X_2	Current density , j (mA/cm^2)	9.52	19.04	28.57
	X_3	Treatment time, t (min)	60	120	180
	X_4	NaCl dose (n) (g/L)	0.5	1.13	1.75

Table 4.3.2a BBD matrix for EO treatment of uric acid with MMO and their experimental results.

Run	Std	Block	pH	j (mA/cm^2)	t (min)	n (g/L)	%Degradation, Y_1	Energy consumption, Y_2 (kWh/m^3)
1	8	Block1	5.5	7.14	10	1.25	97.28	0.95625
2	4	Block1	9	11.90	6	0.75	79.45	1.29375
3	5	Block1	5.5	7.14	2	0.25	32.7	0.225
4	9	Block1	5.5	7.14	6	0.75	85.5	0.61875
5	7	Block1	5.5	7.14	2	1.25	58.4	0.19125
6	10	Block1	5.5	7.14	6	0.75	85.5	0.61875
7	2	Block1	9	2.38	6	0.75	64.48	0.13875
8	1	Block1	2	2.38	6	0.75	60	0.16875
9	3	Block1	2	11.90	6	0.75	98.4	1.29375
10	6	Block1	5.5	7.14	10	0.25	93.25	1.125
11	18	Block 2	5.5	11.90	10	0.75	96.7	2.15625
12	17	Block 2	5.5	2.38	10	0.75	62.5	0.28125
13	19	Block 2	5.5	7.14	6	0.75	85.5	0.61875
14	15	Block 2	5.5	2.38	2	0.75	9.25	0.05625
15	14	Block 2	9	7.14	6	1.25	86.25	0.57375
16	13	Block 2	2	7.14	6	1.25	74.22	0.13875
17	16	Block 2	5.5	11.90	2	0.75	61.25	0.43125
18	11	Block 2	2	7.14	6	0.25	78.8	0.675
19	12	Block 2	9	7.14	6	0.25	67.23	0.695
20	20	Block 2	5.5	7.14	6	0.75	85.5	0.61875
21	25	Block 3	5.5	2.38	6	0.25	37.2	0.25875
22	27	Block 3	5.5	2.38	6	1.25	55.1	0.13875
23	21	Block 3	2	7.14	2	0.75	51.04	0.20625
24	24	Block 3	9	7.14	10	0.75	93.24	1.03125
25	30	Block 3	5.5	7.14	6	0.75	85.5	0.61875
26	26	Block 3	5.5	11.90	6	0.25	75.89	1.40625
27	23	Block 3	2	7.14	10	0.75	95.05	1.03125
28	29	Block 3	5.5	7.14	6	0.75	85.5	0.61875
29	22	Block 3	9	7.14	2	0.75	41.07	0.21630
30	28	Block 3	5.5	11.90	6	1.25	96.07	1.2

Table 4.3.2b BBD matrix for EO treatment of creatinine with MMO and their experimental results.

Run	Std	Block	pH	j (mA/cm^2)	t (min)	n (g/L)	%Degradation Y_1	Energy consumption Y_2, (kWh/m^3)
1	10	1	5.5	14.28	65	0.75	74	18.1994
2	6	1	5.5	14.28	115	0.25	85.3	42.8226
3	4	1	9	21.42	65	0.75	77.06	47.5298
4	5	1	5.5	14.28	15	0.25	13.5	5.5125
5	8	1	5.5	14.28	115	1.25	87.79	22.4172
6	1	1	2	7.14	65	0.75	60.85	5.11859
7	7	1	5.5	14.28	15	1.25	21.63	2.85
8	3	1	2	21.42	65	0.75	84.63	37.536
9	9	1	5.5	14.28	65	0.75	79.53	18.1994
10	2	1	9	7.14	65	0.75	40.222	5.52483
11	16	2	5.5	21.42	15	0.75	37.36	9.95625
12	19	2	5.5	14.28	65	0.75	78.87	18.1994
13	15	2	5.5	7.14	15	0.75	4.5	1.1625
14	12	2	9	14.28	65	0.25	66.04	24.3743
15	20	2	5.5	14.28	65	0.75	76.47	18.1994
16	17	2	5.5	7.14	115	0.75	81.85	9.1968
17	11	2	2	14.28	65	0.25	76.63	25.593
18	18	2	5.5	21.42	115	0.75	86.6	47.9917
19	14	2	9	14.28	65	1.25	73.84	12.8371
20	13	2	2	14.28	65	1.25	82.74	11.6996
21	25	3	5.5	7.14	65	0.25	50	5.68732
22	23	3	2	14.28	115	0.75	87.94	32.763
23	29	3	5.5	14.28	65	0.75	80.74	18.1994
24	30	3	5.5	14.28	65	0.75	81.89	18.1994
25	24	3	9	14.28	115	0.75	81.11	35.925
26	22	3	9	14.28	15	0.75	15.73	4.575
27	21	3	2	14.28	15	0.75	40.15	4.05
28	27	3	5.5	7.14	65	1.25	42.22	3.81863
29	28	3	5.5	21.42	65	1.25	80.89	25.593
30	26	3	5.5	21.42	65	0.25	74.13	64.8355

Table 4.3.2c BBD matrix for EO treatment of urea with MMO and their experimental results.

Std	Run	Block	j (mA/cm^2)	n (g/L)	t (min)	pH	%Degradation, Y_1	Energy consumption, Y_2 (kWh/m^3)
4	1	1	28.57	1.75	120	6	65	37.2
9	2	1	19.05	1.13	120	6	82	22.4
7	3	1	19.05	1.13	60	9	20	11.86
3	4	1	9.52	1.75	120	6	26	6.76
2	5	1	28.57	0.50	120	6	17	49.92
5	6	1	19.05	1.13	60	3	52	11
8	7	1	19.05	1.13	180	9	46	34.97
10	8	1	19.05	1.13	120	6	82	22.4
1	9	1	9.52	0.50	120	6	15	7.96
6	10	1	19.05	1.13	180	3	98	31.8
15	11	2	19.05	0.50	60	6	19	13.06
13	12	2	9.52	1.13	120	9	23	8.44
18	13	2	19.05	1.75	180	6	76	30
20	14	2	19.05	1.13	120	6	82	22.4
12	15	2	28.57	1.13	120	3	73	43.68
11	16	2	9.52	1.13	120	3	39	6.8
14	17	2	28.57	1.13	120	9	30	46.32
19	18	2	19.05	1.13	120	6	82	22.4
17	19	2	19.05	0.50	180	6	59	37.8
16	20	2	19.05	1.75	60	6	37	10.4
29	21	3	19.05	1.13	120	6	82	22.4
23	22	3	9.52	1.13	180	6	41	10.52
30	23	3	19.05	1.13	120	6	82	22.4
28	24	3	19.05	1.75	120	9	35	21.52
25	25	3	19.05	0.50	120	3	56	25.28
21	26	3	9.52	1.13	60	6	11.5	3.63
24	27	3	28.57	1.13	180	6	62	65.7
22	28	3	28.57	1.13	60	6	22	22.5
26	29	3	19.05	1.75	120	3	88	19.6
27	30	3	19.05	0.50	120	9	28	26.72

The sequential model sum of square and model summary statistic, two different tests were evaluated to obtain the best regression model among various models like linear, 2FI, quadratic and cubic for both responses (Y_1 and Y_2). From the results of the model summary statistic of all urine

metabolites, values of R^2 were found highest for quadratic only, which advocates that the model has explained the experimental data very well and indicates the satisfactory interaction between predicted and observed values of experimental runs. For creatinine, square root for Y_1 and natural log transformation for Y_2, while in the case of urea square root for Y_2 were applied only. However, in the case of uric acid, no transformation was applied to any of the responses. After exploiting sequential F–test and other adequacy measures, the model suggested for all urine metabolites was quadratic as shown in Table 4.3.3.

Table 4.3.3 Various R-squared values for the quadratic model suggested by BBD for responses %Degradation (Y_1) and Energy consumption (Y_2) of all urine metabolites treated with MMO

Compound	Responses	R-Squared	Adj R-Squared	Pred R Squared
(a) Uric acid	Y_1	0.9788	0.9559	0.8384
	Y_2	0.9883	0.9757	0.9069
(b) Creatinine	Y_1	0.9864	0.9718	0.8979
	Y_2	0.9967	0.9931	0.9737
(c) Urea	Y_1	0.9900	0.9793	0.9197
	Y_2	0.9998	0.9995	0.9984

For processing the chosen quadratic model, a manual regression method was applied in which insignificant model terms were evicted automatically and provide compiled results with a reduced quadratic equation. Table 4.3.4a,b,c shows the results of the quadratic model fitting in the form of analysis of variance (ANOVA). ANOVA with higher F values and lower p values ($p<0.0001$) i.e. “Prob>F” for both responses in case of all urine metabolites, supports the quadratic model. Moreover, values of "Prob > F" less than 0.0500 indicate model terms are significant with a 95% confidence level while values greater than 0.1000 indicate that model terms are not significant. The significant and highly significant terms of batch EO process for both responses Y_1 and Y_2 (of all urine metabolites) were observed from the ANOVA tables. The values of adequate precision ratio (signal to noise ratio) in the case of all metabolites have come out above 4, which depicts the goodness of the fitted model and can be used for design space navigation.

An empirical relationship between the responses and the operational parameters in terms of independent coded factors obtained from the design-expert software for all urine metabolites was expressed by the quadratic model equation as shown in Equations 4.3.1-4.3.6.

Uric acid:

$$Y_1 = + 85.50 - 2.15*X_1 + 18.27*X_2 + 23.69*X_3 + 6.85*X_4 - 0.96*X_1^2 - 12.58*X_2^2 - 13.15*X_3^2 - 5.57*X_4^2 - 5.86*X_1*X_2 + 2.04*X_1*X_3 + 5.90*X_1*X_4 - 4.45*X_2*X_3 + 0.57*X_2*X_4 - 5.42*X_3*X_4 \quad \textbf{(4.3.1)}$$

$$Y_2 = + 0.62 + 0.036*X_1 + 0.56*X_2 + 0.44*X_3 - 0.099*X_4 - 0.039*X_1^2 + 0.13*X_2^2 + 0.017*X_3^2 - 0.023*X_4^2 + 7.500E\text{-}003*X_1*X_2 - 2.513E\text{-}003*X_1*X_3 + 0.10*X_1*X_4 + 0.37*X_2*X_3 - 0.022*X_2*X_4 - 0.034*X_3*X_4 \quad \textbf{(4.3.2)}$$

Creatinine:

$$Sqrt(Y_1) = + 8.86 - 0.48*X_1 + 1.01*X_2 + 2.37*X_3 + 0.14*X_4 - 0.012*X_1^2 - 0.70*X_2^2 - 1.66*X_3^2 - 0.35*X_4^2 + 0.26*X_1*X_2 + 0.50*X_1*X_3 + 0.031*X_1*X_4 - 0.93*X_2*X_3 + 0.24*X_2*X_4 - 0.21*X_3*X_4 \quad \textbf{(4.3.3)}$$

$$Ln(Y_2) = + 2.90 + 0.048*X_1 + 1.02*X_2 + 0.99*X_3 - 0.34*X_4 + 0.044*X_1^2 - 0.26*X_2^2 - 0.47*X_3^2 - 0.044*X_4^2 + 0.040*X_1*X_2 - 7.439E\text{-}003*X_1*X_3 + 0.035*X_1*X_4 - 0.12*X_2*X_3 - 0.13*X_2*X_4 + 3.115E\text{-}003*X_3*X_4 \quad \textbf{(4.3.4)}$$

Urea:

$$Y_1 = + 82.00 + 9.46*X_1 + 11.08*X_2 + 18.37*X_3 - 18.67*X_4 - 31.21*X_1^2 - 19.15*X_2^2 - 16.33*X_3^2 - 10.77*X_4^2 + 9.25*X_1*X_2 - 2.62*X_1*X_3 - 6.75*X_1*X_4 - 0.25*X_2*X_3 - 6.25*X_2*X_4 - 5.00*X_3*X_4 \quad \textbf{(4.3.5)}$$

$$Sqrt(Y_2) = + 4.73 + 1.95*X_1 - 0.28*X_2 + 1.19*X_3 + 0.10*X_4 - 0.076*X_1^2 + 0.025*X_2^2 - 0.17*X_3^2 + 0.049*X_4^2 - 0.19*X_1*X_2 + 0.51*X_1*X_3 - 0.025*X_1*X_4 - 0.070*X_2*X_3 + 0.018*X_2*X_4 + 0.037*X_3*X_4 \quad \textbf{(4.3.6)}$$

Table 4.3.4a ANOVA results of uric acid suggested by BBD for responses (Y_1 and Y_2)										
Sources	%Degradation, (Y_1)					Energy Consumption, (Y_2)				
	Sum of square	DF	Mean square	F-value	Prob>F	Sum of square	DF	Mean square	F-value	Prob>F
Block	129.90	2	64.95			0.013	2	6.486E-003		
Model	13924.02	14	994.57	42.80	< 0.0001	6.98	14	0.50	78.47	< 0.0001
X_1	55.43	1	55.43	2.39	0.1465	0.016	1	0.016	2.48	0.1392
X_2	4005.15	1	4005.15	172.34	< 0.0001	3.78	1	3.78	595.43	< 0.0001
X_3	6736.01	1	6736.01	289.85	< 0.0001	2.30	1	2.30	362.08	< 0.0001
X_4	563.76	1	563.76	24.26	0.0003	0.12	1	0.12	18.45	0.0009
X_1^2	6.37	1	6.37	0.27	0.6094	0.010	1	0.010	1.61	0.2272
X_2^2	1085.40	1	1085.40	46.70	< 0.0001	0.12	1	0.12	18.67	0.0008
X_3^2	1185.98	1	1185.98	51.03	< 0.0001	1.990E-003	1	1.990E-003	0.31	0.5853
X_4^2	212.65	1	212.65	9.15	0.0098	3.767E-003	1	3.767E-003	0.59	0.4551
X_1X_2	137.24	1	137.24	5.91	0.0303	2.250E-004	1	2.250E-004	0.035	0.8537
X_1X_3	16.65	1	16.65	0.72	0.4127	2.525E-005	1	2.525E-005	3.973E-003	0.9507
X_1X_4	139.24	1	139.24	5.99	0.0293	0.043	1	0.043	6.77	0.0219
X_2X_3	79.21	1	79.21	3.41	0.0878	0.56	1	0.56	88.51	< 0.0001
X_2X_4	1.30	1	1.30	0.056	0.8167	1.860E-003	1	1.860E-003	0.29	0.5977
X_3X_4	117.40	1	117.40	5.05	0.0426	4.556E-003	1	4.556E-003	0.72	0.4125
Residual	302.12	13	23.24			0.083	13	6.355E-003		
Lack of fit	302.12	10	30.21			0.083	10	8.262E-003		
Pure error	0.000	3	0.000			0.000	3	0.000		
Core total	14356.04	29				7.08	29			

Table 4.3.4b ANOVA results of creatinine suggested by BBD for responses (Y_1 and Y_2)										
Sources	%Degradation, (Y_1)					Energy consumption, (Y_2)				
	Sum of square	DF	Mean square	F-value	Prob>F	Sum of square	DF	Mean square	F-value	Prob>F
Block	0.25	2	0.12			0.015	2	7.699E-003		
Model	109.00	14	7.79	67.53	< 0.0001	27.83	14	1.99	279.98	< 0.0001
X_1	2.76	1	2.76	23.91	0.0003	0.027	1	0.027	3.82	0.0725
X_2	12.24	1	12.24	106.17	< 0.0001	12.57	1	12.57	1770.27	< 0.0001
X_3	67.60	1	67.60	586.28	< 0.0001	11.81	1	11.81	1663.73	< 0.0001
X_4	0.25	1	0.25	2.16	0.1652	1.37	1	1.37	193.38	< 0.0001
X_1^2	1.060E-003	1	1.060E-003	9.193E-003	0.9251	0.013	1	0.013	1.90	0.1914
X_2^2	3.36	1	3.36	29.10	0.0001	0.45	1	0.45	63.55	< 0.0001
X_3^2	18.87	1	18.87	163.70	< 0.0001	1.52	1	1.52	213.58	< 0.0001
X_4^2	0.84	1	0.84	7.30	0.0181	0.013	1	0.013	1.85	0.1964
X_1X_2	0.27	1	0.27	2.33	0.1505	6.375E-003	1	6.375E-003	0.90	0.3606
X_1X_3	1.00	1	1.00	8.66	0.0114	2.214E-004	1	2.214E-004	0.031	0.8626
X_1X_4	3.858E-003	1	3.858E-003	0.033	0.8577	5.011E-003	1	5.011E-003	0.71	0.4160
X_2X_3	3.48	1	3.48	30.20	0.0001	0.061	1	0.061	8.64	0.0115
X_2X_4	0.23	1	0.23	1.99	0.1821	0.071	1	0.071	9.94	0.0076
X_3X_4	0.18	1	0.18	1.54	0.2366	3.882E-005	1	3.882E-005	5.469E-003	0.9422
Residual	1.50	13	0.12			0.092	13	7.099E-003		
Lack of fit	1.44	10	0.14	7.06	0.0673	0.092	10	9.229E-003		
Pure error	0.061	3	0.020			0.000	3	0.000		
Core total	110.74	29				27.93	29			

Table 4.3.4c ANOVA results of urea suggested by BBD for responses (Y_1 and Y_2)										
Sources	%Degradation, (Y_1)					Energy consumption, (Y_2)				
	Sum of square	DF	Mean square	F-value	Prob>F	Sum of square	DF	Mean square	F-value	Prob>F
Block	15.52	2	7.76			0.013	2	6.517E-003		
Model	20575.85	14	1469.70	92.35	< 0.0001	64.95	14	4.64	4058.64	< 0.0001
X_1	1073.52	1	1073.52	67.46	< 0.0001	45.42	1	45.42	39731.68	< 0.0001
X_2	1474.08	1	1474.08	92.63	< 0.0001	0.95	1	0.95	832.04	< 0.0001
X_3	4051.69	1	4051.69	254.60	< 0.0001	16.99	1	16.99	14863.94	< 0.0001
X_4	4181.33	1	4181.33	262.75	< 0.0001	0.13	1	0.13	113.70	< 0.0001
X_1^2	6678.58	1	6678.58	419.67	< 0.0001	0.039	1	0.039	34.19	< 0.0001
X_2^2	2513.57	1	2513.57	157.95	< 0.0001	4.195E-003	1	4.195E-003	3.67	0.0777
X_3^2	1829.33	1	1829.33	114.95	< 0.0001	0.19	1	0.19	168.41	< 0.0001
X_4^2	795.50	1	795.50	49.99	< 0.0001	0.016	1	0.016	14.16	0.0024
X_1X_2	342.25	1	342.25	21.51	0.0005	0.14	1	0.14	121.34	< 0.0001
X_1X_3	27.56	1	27.56	1.73	0.2109	1.02	1	1.02	895.86	< 0.0001
X_1X_4	182.25	1	182.25	11.45	0.0049	2.535E-003	1	2.535E-003	2.22	0.1603
X_2X_3	0.25	1	0.25	0.016	0.9022	0.020	1	0.020	17.39	0.0011
X_2X_4	156.25	1	156.25	9.82	0.0079	1.245E-003	1	1.245E-003	1.09	0.3157
X_3X_4	100.00	1	100.00	6.28	0.0263	5.416E-003	1	5.416E-003	4.74	0.0485
Residual	206.88	13	15.91			0.015	13	1.143E-003		
Lack of fit	206.88	10	20.69			0.015	10	1.486E-003		
Pure error	0.000	3	0.000			0.000	3	0.000		
Core total	20798.24	29				64.98	29			

To check the reliability of developed models for both responses of all urine metabolites, plots of normal % probability versus studentized residuals, studentized residuals versus predicted and

predicted versus actual for the experimental data were examined as shown in Figure 4.3.1 (i, ii, iii). From the plots of normal % probability versus studentized residuals, it was observed that residuals are in the proximity of the straight diagonal line which indicates that the model well satisfies the assumptions of the ANOVA. In the case of studentized residuals versus predicted, the random scatter in the plot indicates that the standard deviation separating the predicted values from actual. Therefore, developed models are considered to be adequate because the residuals for the prediction of each response are minimum. The data points predicted versus the actual plot for all metabolites were found very close to the diagonal line indicating the good correlation between experimental data and predicted data developed by the chosen model.

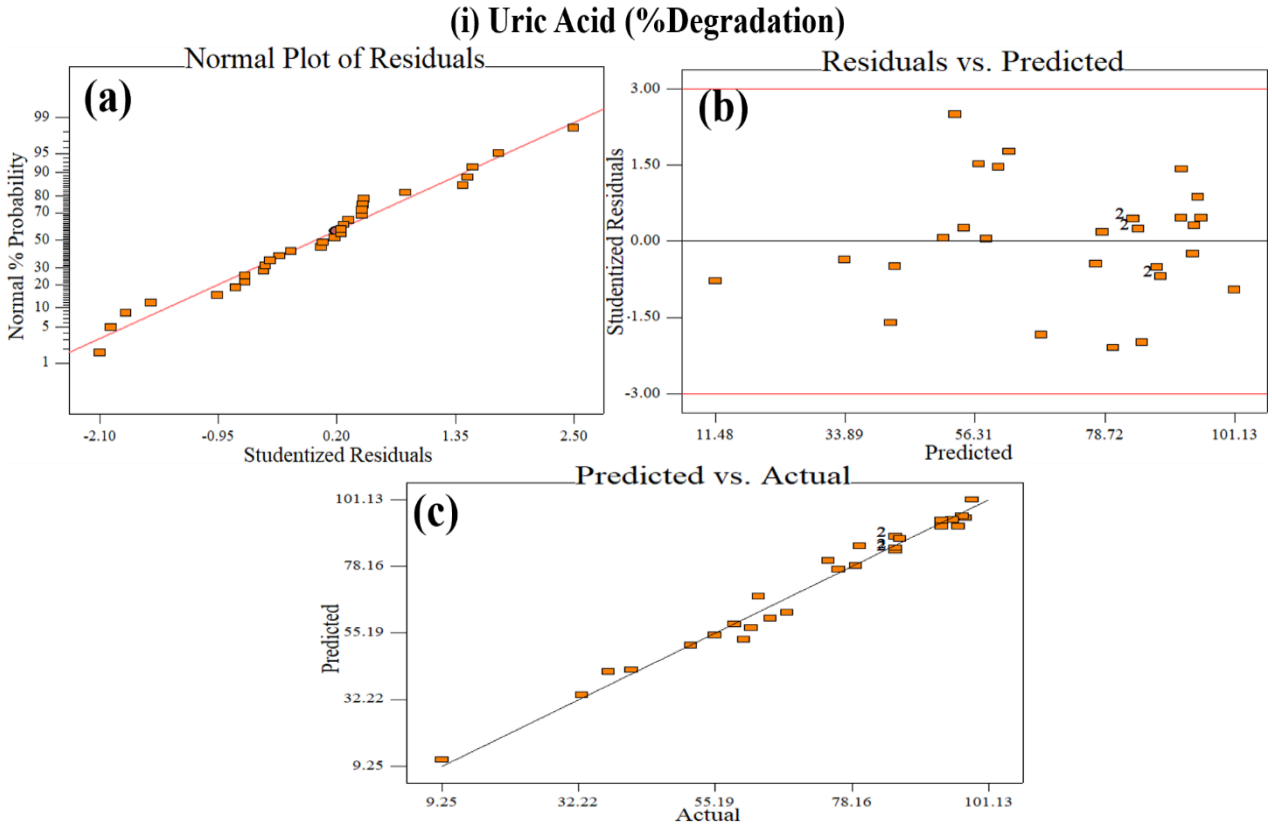

(i) Uric Acid (Energy consumption)

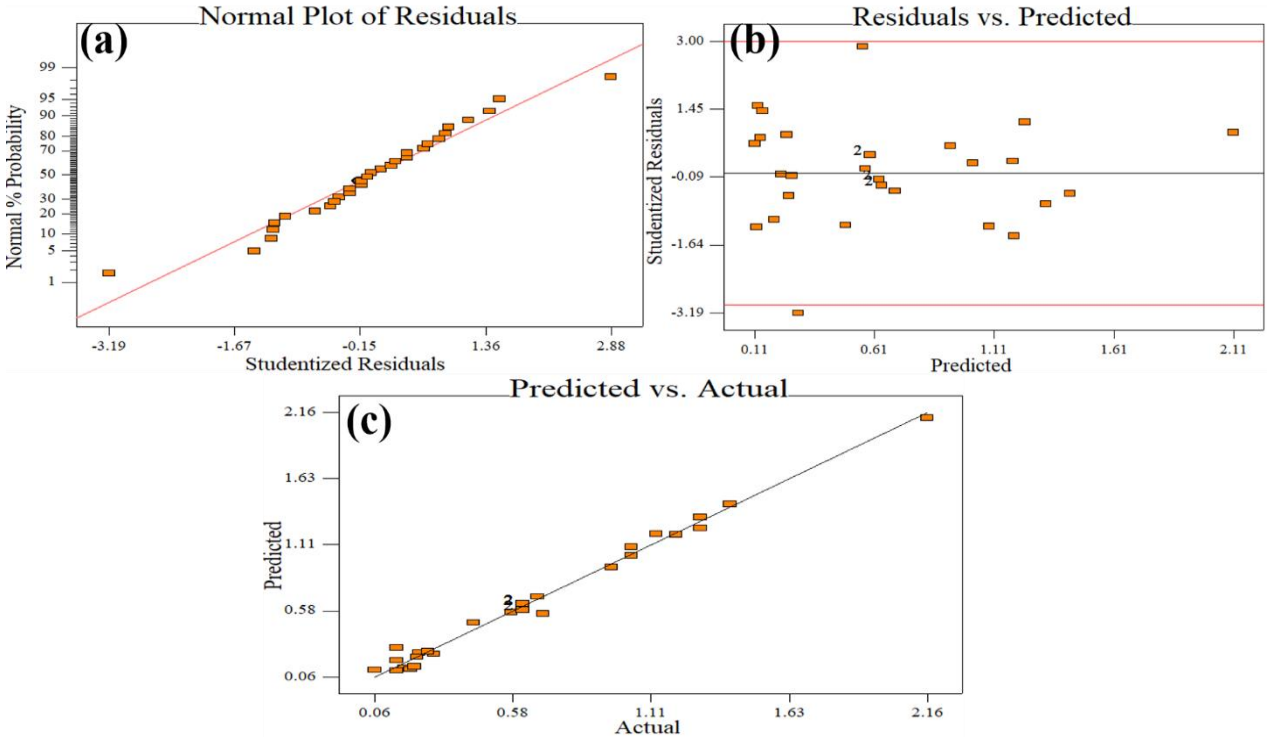

(ii) Creatinine (%Degradation)

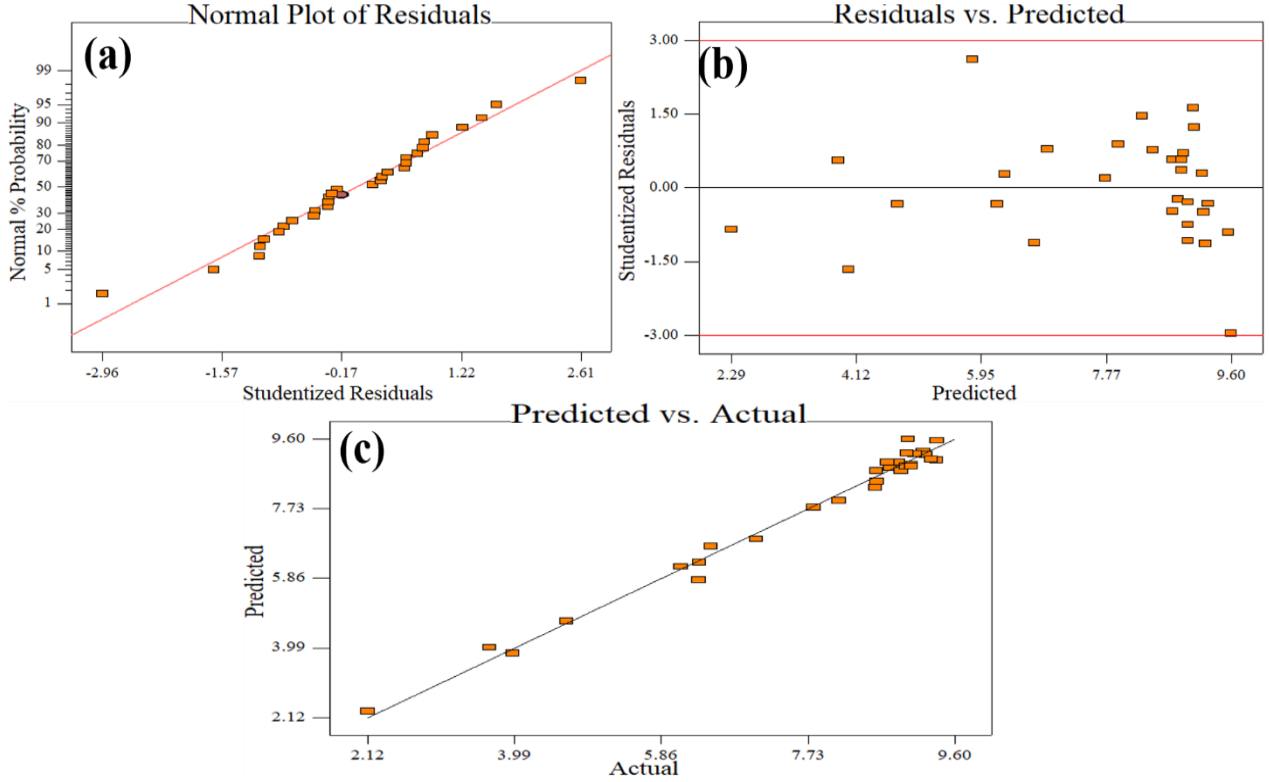

(ii) Creatinine (Energy consumed)

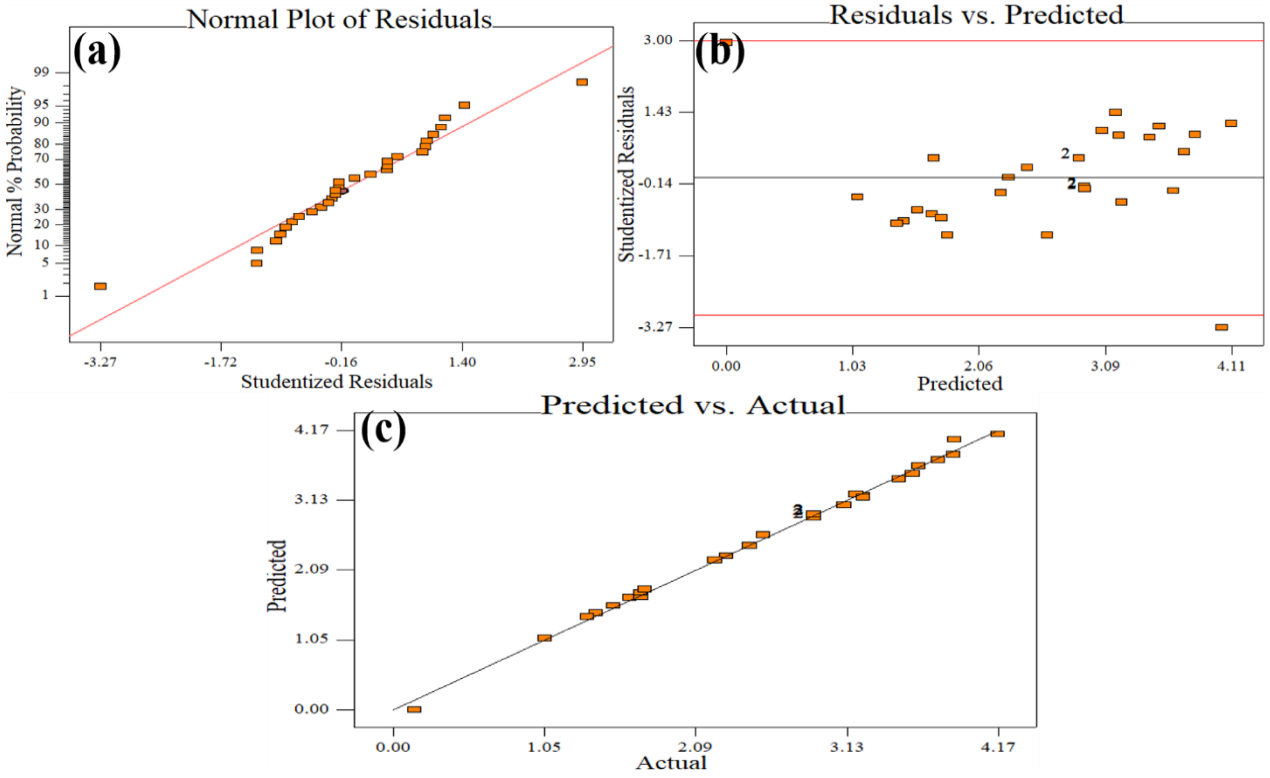

(iii) Urea (%degradation)

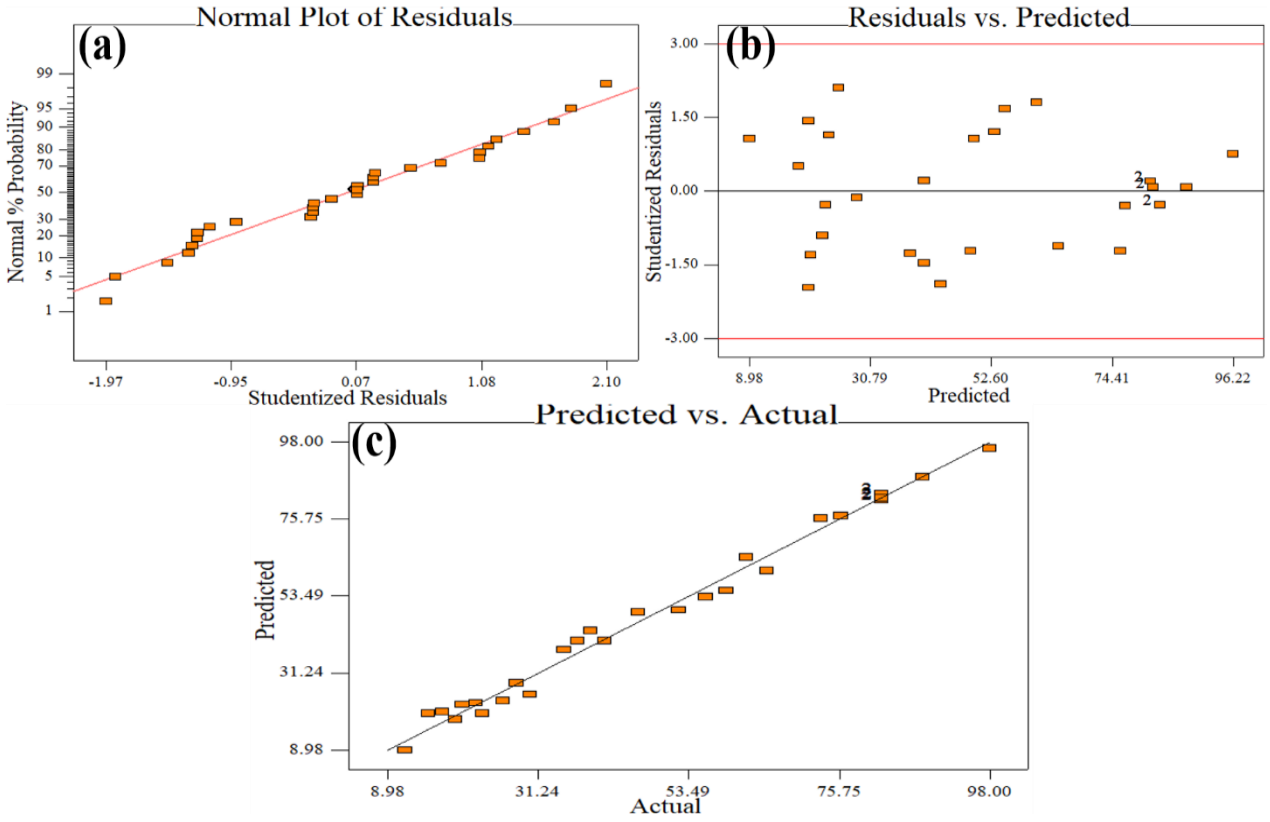

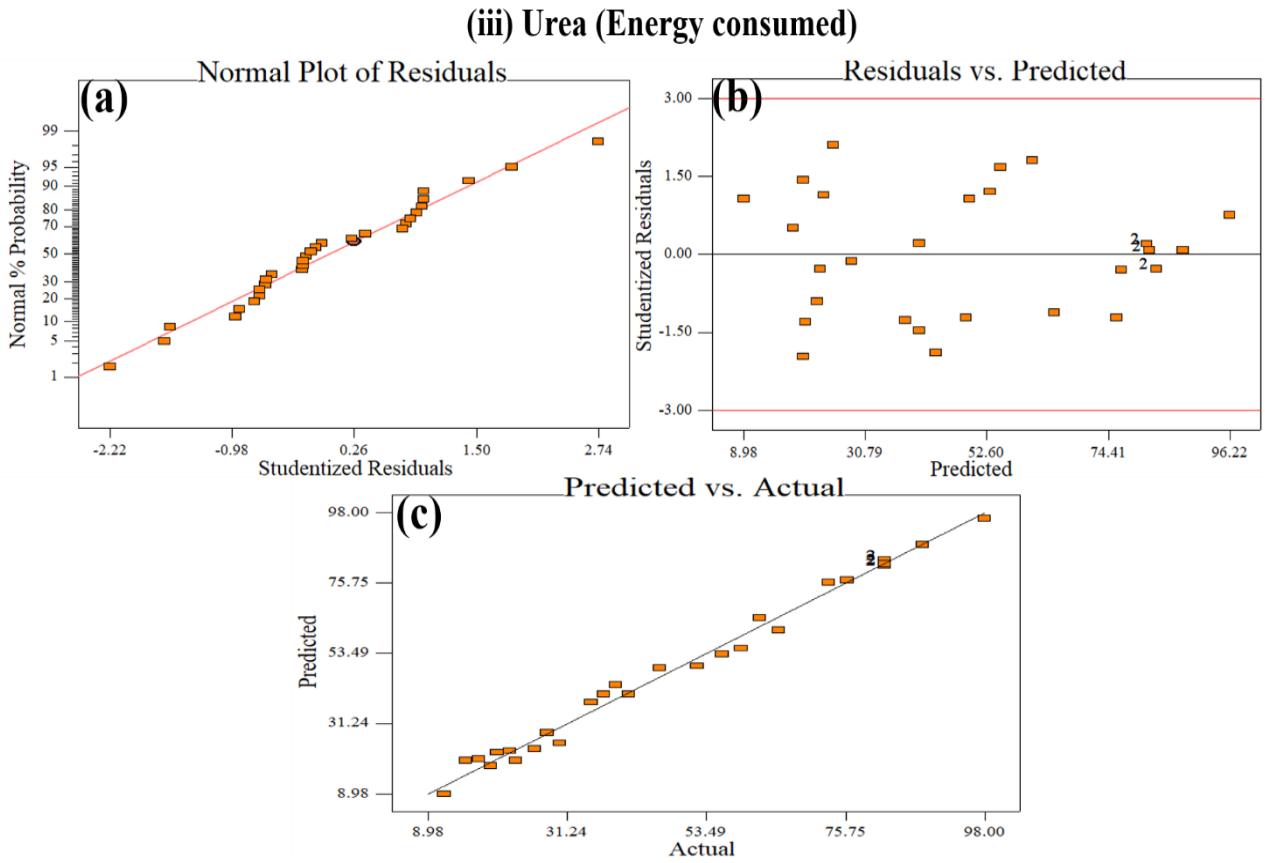

Figure 4.3.1 Plots of (a) normal % probability versus studentized residuals; (b) studentized residuals versus predicted and (c) predicted versus actual for responses (%Degradation and Energy consumed) of all urine metabolites (i) Uric acid, (ii) Creatinine and (iii) Urea treated with MMO.

Three dimensional (3D) response graphs developed from the chosen model were studied in order to see the interactive effect of each operational parameter on responses as well as used to find the best optimal conditions for high process efficiency.

4.3.2 Effect of Process Parameters and Optimization

4.3.2.1 Effect of current density (j) on %Degradation, (Y_1) of uric acid, creatinine and urea

Current density is an important operating parameter in the EO process because of the mechanistic study and cost-effectiveness analysis. Furthermore, the capability of transfer of e^- and generation of oxidant species all depend upon applied current density. Figure 4.3.2a (uric acid) has shown the interaction between j and t as well as their simultaneous effect on Y_1. The graph results showed that Y_1 was found constant at lower values of j up to 4.76 mA/cm^2 for t ≈ 6 min and then it increases gradually with increasing t values. For j values ≈ 9.52 mA/cm^2, Y_1 was increasing

continuously for all values of t. While for j beyond 9.52 mA/cm^2 values, Y_1 was found constantly increasing upto t ≈ 7.5 min and then suddenly become constant for leftover values of i.e. t > 7.5 min.

Figure 4.3.3a (creatinine) showed the effect of j and pH on Y_1. From the graph, it was found that Y_1 was constantly increasing at j ≈ 14.28 mA/cm^2 for all values of pH. Further increase in j values up to 17.85 mA/cm^2, has decreased the Y_1 marginally at pH ≈ 5.5 while an increase in Y_1 was still observed at higher values of pH beyond 5.5. However, at higher values of j> 17.85 mA/cm^2, Y_1 was found the minimum for all values of pH. The maximum value of Y_1 was observed at higher values of j.

In the case of urea, Figure 4.3.4a has shown the effect of j and n on Y_1 and interaction between them. From the results, it was observed that Y_1 first increases gradually with increasing j values up to 19.05 mA/cm^2 and reaches the maximum. But the further increase in j value beyond 19.05 mA/cm^2, Y_1 decreases gradually. This trend was observed at all values of n. From the experimental results it was found that after certain values of j and n, the removal efficiency of urea has become minimum because at higher j values metal dissolution takes place which propagates the growth of the flocs in the solution. As well as increase the temperature of the solution which further interferes with the degradation process and hence decreases the process efficiency.

In the EO process, both mechanisms direct and indirect oxidation takes place simultaneously for the maximum degradation of pollutants. The generation rate of reactive oxidant species like $OH^{\bullet}$, ozone, $HO_2^{\bullet}$ and chloro-oxidant species along with the capability of e^- transfer is highly dependent upon the current density. MMO used is active anode hence some important chemical reactions such as oxidation of water take place at its surface which further led to the formation of adsorbed $OH^{\bullet}$ as shown in Equations 4.3.7- 4.3.8. Both chemical and electrochemical activity of these adsorbed $OH^{\bullet}$ depends upon the nature of anode. Moreover, due to its active nature, it reacts with $OH^{\bullet}$ and could form superoxide or higher metal oxides at the anode surface.

$$MMO + H_2O \longrightarrow MMO(OH^{\bullet}) + H^+ + e^- \quad \textbf{(4.3.7)}$$

$$MMO\ (OH^{\bullet}) \longrightarrow MMO\ (O) + H^+ + e^- \quad \textbf{(4.3.8)}$$

MMO ($OH^{\bullet}$)/ MMO (O), a surface redox couple would act as mediator during the oxidation of urine metabolites as shown in Equation 4.3.9 whereas Equation 4.3.10 competes with side reactions like OER which occurred because of chemical decomposition of superoxide radicals.

$$MMO\ (O) + R \longrightarrow MMO + RO \quad \textbf{(4.3.9)}$$

$$MMO\ (O) \longrightarrow MMO + ½\ O \quad \textbf{(4.3.10)}$$

The oxidation reaction of urine metabolites by redox couple (MMO ($OH^{\bullet}$)/MMO(O)) is seems to be more selective over to the reaction shown in Equation 4.3.11.

$$MMO\ (OH^{\bullet}) + R \longrightarrow MMO + aCO_2 + bH_2O + H^+ + e^- \quad \textbf{(4.3.11)}$$

In literature, it has been reported that at lower values of j, generation of reactive species on MMO anodes was fallen down gradually with time. Due to which rate of pollutant removal decreases which further led to minimum treatment process efficiency. But when j increased, the removal efficiency (Y_1) of pollutants were found maximum because of the increased generation of $OH^{\bullet}$ at the surface of MMO anode as well as maximize the oxidation of chloride into RCS in the electrolyte solution. Moreover, at lower values of j, the EO process is not kinetically limited by mass transport of pollutants to the anode surface. Therefore, the increase in j value led to maximum removal efficiency (Martínez-Huitle et al., 2015). But at high values of j, the EO process is controlled by mass transport and an increase in j value could lead to the enhancement of OER from the electrolysis of water as shown in Equation 4.3.12. Due to which $OH^{\bullet}$, $HO_2^{\bullet}$, etc. were consumed rapidly and decreases the Y_1 (Song et al., 2008). Hence, lowers the overall treatment process efficiency. While in the case of intermediate j values, the EO process is under the mixed kinetic regime and a further increase in j values could lead to increases in pollutant removal rate but decreases the current efficiency. Hence for maximum removal rate without a decrease in current efficiency and overall process efficiency, optimum values of j should be chosen.

$$2H_2O \rightarrow O_2 + 4H^+ + 4e^- \quad \textbf{(4.3.12)}$$

4.3.2.2 Effect of pH on % Degradation, (Y_1) of uric acid, creatinine and urea

The pH of the solution is a crucial factor as it influences the performance of the EO process. It explains the adsorption rate of $OH^{\bullet}$, as well as the type of reactive chlorine species that are predominant. Figure 4.3.2b has shown the effect of pH and t on Y_1 (uric acid). The results of graphs showed that with increasing pH value, a decrease in Y_1 was observed at all t values. However, for pH ≈ 5.5, Y_1 was increasing with t value while beyond 5.5 pH, Y_1 was first to become constant for t up to 4 min and then increases gradually with time. The increase in Y_1 was much faster at lower values of pH than high values of pH.

In the case of creatinine, Figure 4.3.3a shows the interaction between pH and j as well as their effect on Y_1. The results depict that at lower values of j up to 10.71 mA/cm^2 no significant effect of pH was observed in Y_1. For j> 10.71 mA/cm^2, a marginal increase in Y_1 was observed at

low values of pH≈ 5.5 while at pH> 5.5, Y_1 was increased constantly. Further increase in j >17.85 mA/cm^2, Y_1 decreases gradually at pH≈ 5.5 while for pH >5.5 Y_1 first became constant and then decreases marginally. This shows that oxidation of creatinine was little more at high values of pH than low values of pH.

For urea, Figure 4.3.4b shows the effect of pH and t on Y_1. The result shows that at lower values of pH≈ 6, Y_1 first increases gradually for t up to 150 min and then found decreasing with increasing t. A similar trend was observed for pH> 6 up to t≈ 120 min and then decreases gradually with increasing t values.

In previous studies, it has been reported that removal efficiency of the pollutants was maximum at lower pH values because the adsorption rate of the $OH^{\bullet}$ on the surface of MMO at acidic pH is high, hence led to direct oxidation of compound as shown in Equation 4.3.13. Whereas at highly basic pH adsorption rate of $OH^{\bullet}$ on anode surface decreases, which lead to the transformation of $OH^{\bullet}$ into H_2O_2 and $HO_2^{\bullet}$ (oxidants of lower potential) as shown in Equations 4.3.19 - 4.3.21, thus corresponds to mediated oxidation. Furthermore, it was also observed that at acidic pH, HOCl oxidant species generation was maximum which dominates over all other oxidant species like Cl_2, ClO^-, etc., shown in Equations 4.3.14 - 4.3.18 and hence led to indirect oxidation. While in the case of alkaline pH, lower chloro-oxidant species like ClO_3^- and ClO_4^- were generated with time and thus reduces the Y_1 as shown in Equations 4.3.22 - 4.3.24. Thus, the oxidation of the target pollutant was found to be maximum at acidic pH because of the involvement of both mechanisms, direct and indirect EO.

At acidic pH:

$$H_2O \longrightarrow OH^{\bullet} + H^+ + e^- \quad \textbf{(4.3.13)}$$

$$Cl_2 + 2e^- \longrightarrow 2Cl^- \quad \textbf{(4.3.14)}$$

$$Cl_2 + H_2O \longrightarrow HClO + Cl^- + H^+ \quad \textbf{(4.3.15)}$$

$$HClO \longrightarrow ClO^- + H^+ \quad \textbf{(4.3.16)}$$

$$ClO^- + H_2O + 2e^- \longrightarrow Cl^- + 2OH^- \quad \textbf{(4.3.17)}$$

$$Cl^- + OH^{\bullet} \longrightarrow ClO^- + H^+ + e^- \quad \textbf{(4.3.18)}$$

At basic pH:

$OH^{\bullet} + OH^{-} \longrightarrow \bullet O^{-} + H_2O$ **(4.3.19)**

$H_2O_2 + OH^{-} \longrightarrow HO_2^{-} + H_2O$ **(4.3.20)**

$HO_2^{\bullet} + OH^{-} \longrightarrow O_2\bullet^{-} + H_2O$ **(4.3.21)**

$ClO^{-} + OH^{-} \longrightarrow ClO_2^{-} + H^{+} + e^{-}$ **(4.3.22)**

$ClO_2^{-} + OH^{-} \longrightarrow ClO_3^{-} + H^{+} + e^{-}$ **(4.3.23)**

$ClO_3^{-} + OH^{-} \longrightarrow ClO_4^{-} + H^{+} + e^{-}$ **(4.3.24)**

4.3.2.3 Effect of NaCl dose (n) on % Degradation, (Y_1) of uric acid, creatinine and urea

Figure 4.3.2c (uric acid) showed the interaction between n and t and their effect on Y_1. The results of Figure 4.3c showed that at n ≈ 0.25 g/L, Y_1 was increasing with t up to 8 min and then become constant. However, for 0.25 <n> 1.0 g/L, Y_1 increases with t up to 6 min and then become with increasing t value. Further increase in n value beyond 1.0 g/L, Y_1 continuously increases with increasing values of t ≈ 8 min and then decreases with increasing t.

In the case of creatinine, the results of Figure 4.3.3b depicts that with increasing t value up to 90 min, Y_1 increases with increasing n values. However, a further increase in t value beyond 90min, a gradual decrease in Y_1 was observed at all values of n.

Figure 4.3.4a (urea) showed the interaction between n and j and their effect on Y_1. The results showed that at lower values of j up to 14.28 mA/cm^2, Y_1 increases with increasing n values. However, at n up to 1.13 g/L, Y_1 increases with increasing j values. Further increase in n ≈ 1.44 g/L, Y_1 increases marginally and then decreases with increasing j values.

The dose of NaCl plays a significant role because it influences the efficiency of the EO process as it defines the amount of RCS such as HClO, ClO^{-}, etc. formed during the treatment process. It was observed that an increase in n values lead to the rise in metabolites degradation. This was due to the increase in the synergistic effects of RCS and $OH^{\bullet}$ (Singh et al., 2016). During EO treatment, with increasing n, the concentration of Cl^{-} and OCl^{-} also increases in the solution which adsorbed on the surface of the anode and reacts with urine metabolites (uric acid, creatinine, and urea) resulting in their decomposition either directly by RCS and $OH^{\bullet}$ generated on the anode surface

or in the bulk through hypochlorite. In addition to this, the average rate of the degradation process increased due to the improvement in the solution conductivity which substantially decreased the drop in the voltage along with energy consumption. On further increase in the n values, it was found that the degradation of metabolites was minimum. This might be due to the reactions between NH_4^+ and HOCl acid as shown in Equation 4.3.25.

$$2NH_4^+ + 3HClO \longrightarrow N_2 + 3H_2O + 5H^+ + 3Cl^- \quad \textbf{(4.3.25)}$$

Hence, an optimum dose of NaCl is very important from the stability point of view. Besides this, it has been observed that MMO anode has proven to be very effective in promoting the indirect oxidation along with direct oxidation and hence prevents the fouling of anodes.

4.3.2.4 Effect of time (t) on % Degradation, (Y_1) of uric acid, creatinine and urea

Figure 4.3.2a,b,c (uric acid) shows the interaction of j, n, pH with t and their effect on Y_1. From the result of all figures, it was concluded that Y_1 increases with increasing t value up to 8 min. However further increase in t value beyond 8 min, Y_1 increases marginally. In other words, further, an increase in t> 8 min has no significant effect on Y_1.

Similar trends were observed in Figure 4.3.3b (creatinine), in which the effect of t and n on Y_1 was observed. For t value up to 90 min, Y_1 was found maximum for all values of n. Further increase in t values, decreased the Y_1 marginally. While in the case of urea, Figure 4.3.4b has shown the interaction between t and pH. At lower values of pH, Y_1 increases with increasing t value up to 150 min and then found constant at t> 150 min. However, at high values of pH, Y_1 increases with t up to 120 min and then decreases gradually with increasing t.

Various studies reported that during electrolysis, an impermeable film generates on the surface of the electrode causing passivation on the surface of the electrode, which in turn increases the treatment time as well as decreases the process efficiency. But in this experimental study, no such problem was observed because the MMO used has the advantage of coupling both direct and mediated oxidation processes in the presence of sodium chloride. Thus, prevents the passivation of the anode during the electrolysis. However, the optimization of time is very important for maximum degradation efficiency and longer stability of anodes.

4.3.2.5 Effect of j, pH, n and t on Energy consumption, (Y_2) of uric acid, creatinine and urea

Figure 4.3.2d (uric acid) shows the effect of n and pH on Y_2. The results showed that at higher values of pH i.e. (3.75>pH>7.25) and lower values of n i.e. (0.5> n>1.00 g/L), Y_2 was found maximum. It was observed at lower values of pH, Y_2 decreases gradually with increasing n values. While at higher values of pH it was found that with increasing n value Y_2 increases. However, Y_2 was decreasing with increasing pH at lower values of n. This might be due to the generation of the lower potential of oxidant species in solution at alkaline pH which in turn reduces the energy consumed during the treatment process. Figure 4.3.2e (uric acid) shows the effect of t and j on Y_2. The results depict that Y_2 was found constant at lower values of j ≈ 4.76 mA/cm^2 for all t values. However, an increase in j values up to 9.52 mA/cm^2, Y_2 was found constant for t ≈ 2 to 8 min and then increases sharply. Further increase in j>9.52 mA/cm^2, first increases Y_2 very sharply and then found constant for t> 8min.

Figure 4.3.3c (creatinine) shows the interaction between j and pH as well as their effect on Y_2. The results showed that Y_2 was found maximum at higher values of pH and j while the minimum at lower values of j for all pH. Figure 4.3.3d (creatinine) shows the effect of n and t as well on Y_2. From the results, it depicts that at lower values of n, Y_2 increases with increasing t values. However, on increasing n values, Y_2 was found decreasing sharply with increasing t values. At higher and lower values of n, Y_2 was found increasing gradually with increasing t.

Figure 4.3.4c (urea) shows the interaction between n and pH as well as their effect on Y_2. The results show a similar trend i.e. higher values of pH and lower values of n, Y_2 was found maximum. While at lower values of pH and higher values of n, Y_2 was found the minimum. Figure 4.3.4d (urea) shows the effect of t and j on Y_2. The results showed that Y_2 was found maximum at higher values of j and t. It was also observed that at lower values of j, Y_2 was found constant at all t values.

Energy consumption (Y_2) depends on the type of electrode used as well as the process parameters. From experimental results, it was found that with an increase in j value, Y_2 varies directly, at all t values due to various factors like might electrode deactivation, a decrease in the concentration of ions and an increase in solution temperature. It was also observed that at higher values of pH, Y_2 was found to be maximum while minimum with a decrease in solution pH. However, n shows the contrary effect, because at its higher values, Y_2 was found minimal, it could

be due to the ease of flow of current through the electrolyte solution. However, at lower values of n with increasing j values, Y_2 was found maximum because of the lower conductivity of the solution as well as an increase in the voltage drop.

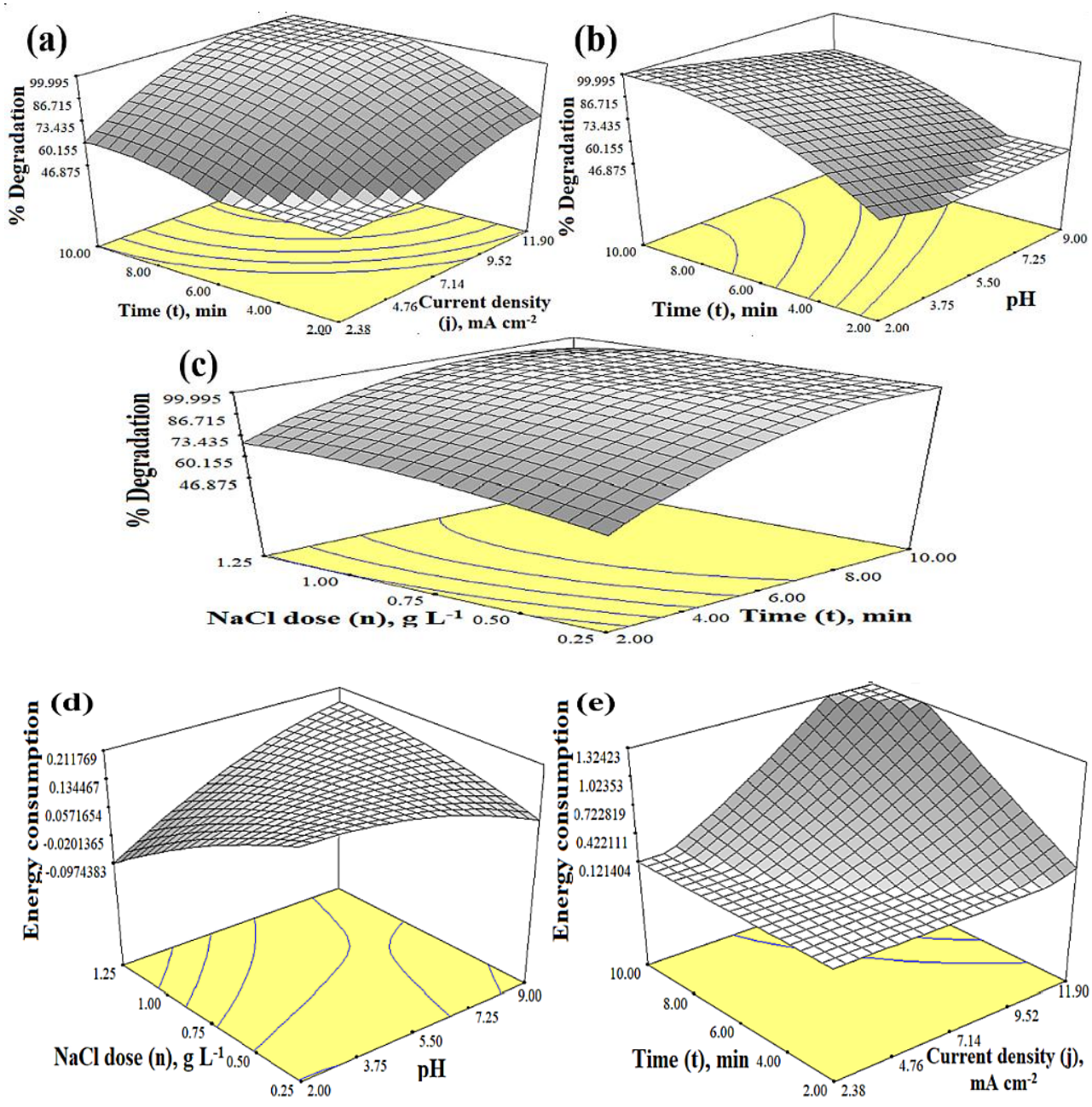

Figure 4.3.2 3D response graphs for EO treatment of uric acid using MMO (a) %Degradation versus t and j; (b) %Degradation versus pH and t; (c) %Degradation versus n and t; (d) Energy consumption versus n and pH and (e) Energy consumption versus t and j

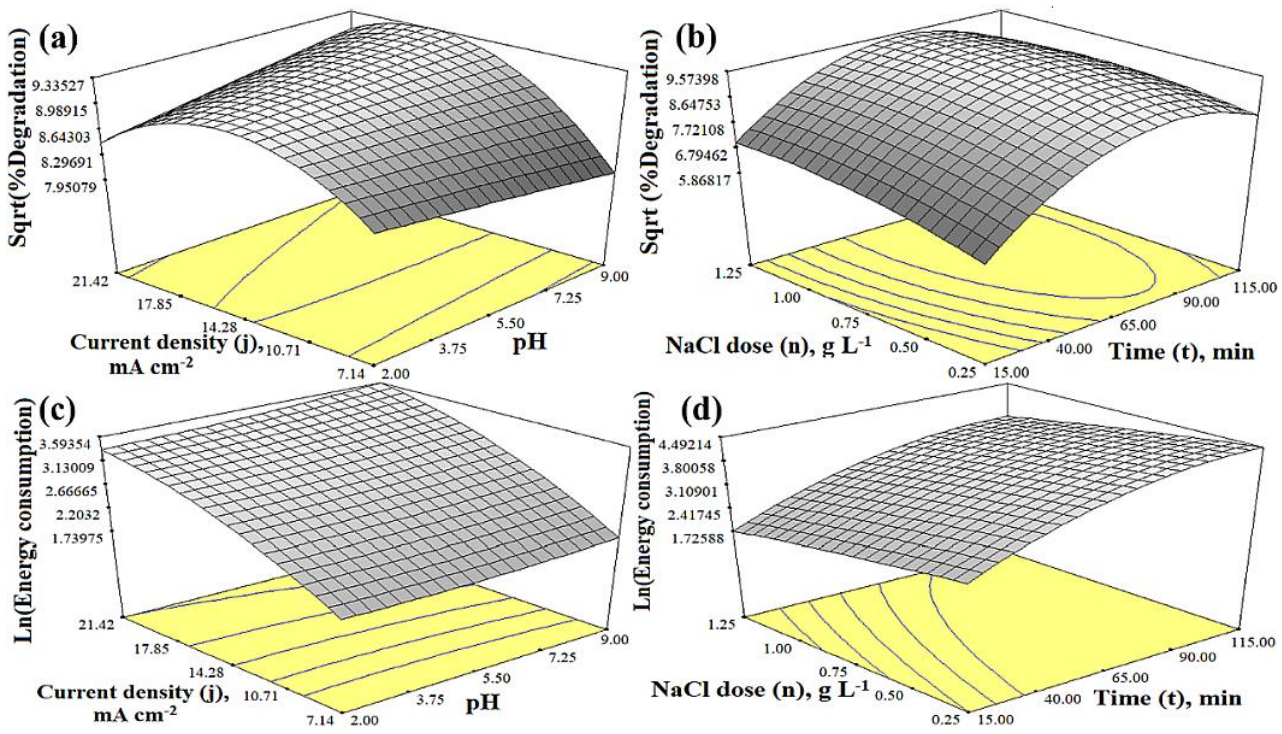

Figure 4.3.3 3D response graphs for EO treatment of creatinine using MMO (a) Sqrt (%Degradation) versus pH and j; (b) Sqrt(%Degradation) versus n and t; (c) Ln(Energy consumption) versus j and pH and (d) Ln(Energy consumption) versus t and n.

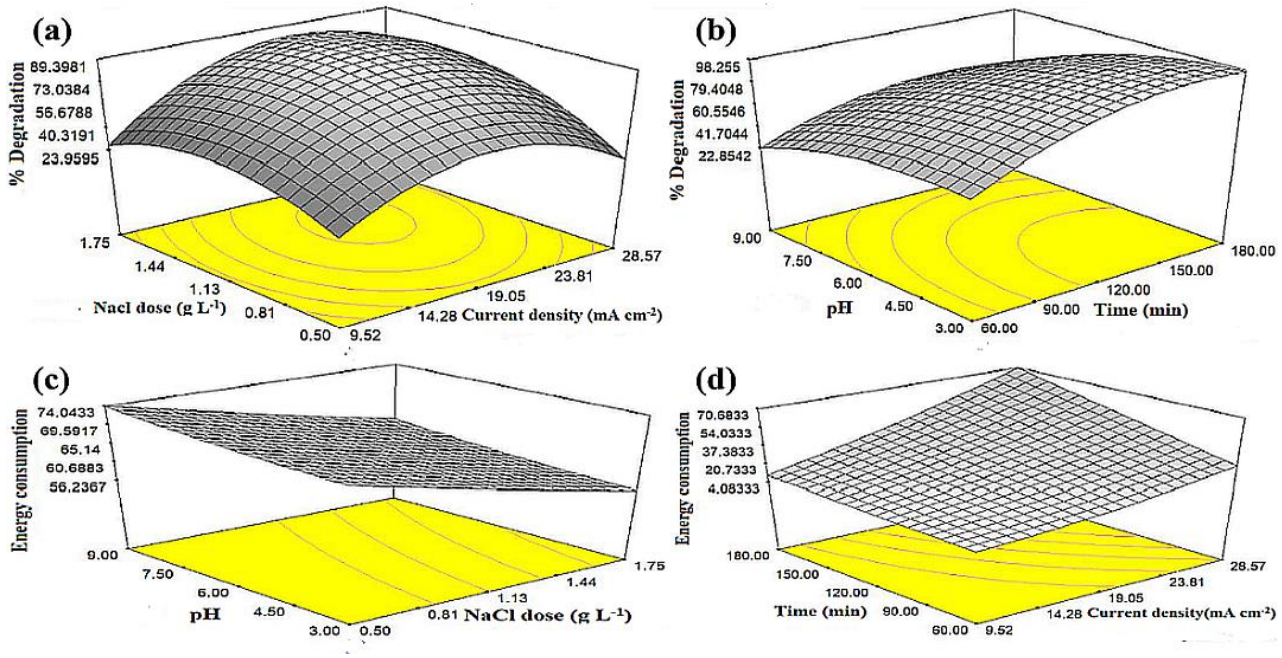

Figure 4.3.4 3D response graphs for EO treatment of urea using MMO (a) %Degradation versus n and j; (b) %Degradation versus pH and t; (c) Energy consumption versus n and pH and (d) Energy consumption versus t and j.

Optimization of operating parameters with the responses (Y_1 and Y_2) for the treatment of all urine metabolites using the EO process with MMO anode were carried out by multi-response process optimization by the desirability function approach. One-sided desirability (di) and overall desirability (D) for all urine metabolites were calculated by using maximum (Y_1) and minimum (Y_2) acceptable values of both responses as shown in Table 4.3.5. The desirability for response Y_1 for uric acid is calculated by Equation 3.8.5 with acceptable values of $Y_{1\text{-}min}$ as 9.25% and $Y_{1\text{-}max}$ as 98.4% as shown in Equation 4.3.26. Similarly for response Y_2 of uric acid is calculated by taking $Y_{2\text{-}min}$ as 0.05625 and $Y_{2\text{-}max}$ as 2.15625 kWh/m^3 respectively as shown in Equation 4.3.27.

$$d_{1(uric\ acid)} = \begin{cases} 0 & if\ Y_1 \leq 9.25 \\ \left[\frac{Y_1 - 9.25}{98.4 - 9.25}\right] & if\ 9.25 < Y_1 < 98.4 \\ 1 & if\ Y_1 \geq 98.4 \end{cases} \quad \textbf{(4.3.26)}$$

$$d_{2\ (uric\ acid)} = \begin{cases} 0 & if\ Y_2 \leq 0.05625 \\ \left[\frac{Y_2 - 0.05625}{2.15625 - 0.05625}\right] & if\ 0.05625 < Y_2 < 2.15625 \\ 1 & if\ Y_2 \geq 2.15625 \end{cases} \quad \textbf{(4.3.27)}$$

The desirability for both responses of the other two metabolites i.e. creatinine and urea were calculated by Equations 4.3.28- 4.3.31.

$$d_{1\ (creatinine)} = \begin{cases} 0 & if\ Y_1 \leq 4.5 \\ \left[\frac{Y_1 - 4.5}{87.94 - 4.5}\right] & if\ 4.5 < Y_1 < 87.94 \\ 1 & if\ Y_1 \geq 87.94 \end{cases} \quad \textbf{(4.3.28)}$$

$$d_{2\ (creatinine)} = \begin{cases} 0 & if\ Y_2 \leq 1.1625 \\ \left[\frac{Y_2 - 1.1625}{64.8355 - 1.1625}\right] & if\ 1.1625 < Y_2 < 64.8355 \\ 1 & if\ Y_2 \geq 64.8355 \end{cases} \quad \textbf{(4.3.29)}$$

$$d_{1\ (urea)} = \begin{cases} 0 & if\ Y_1 \leq 11.5 \\ \left[\frac{Y_1 - 11.5}{98.0 - 11.5}\right] & if\ 11.5 < Y_1 < 98.0 \\ 1 & if\ Y_1 \geq 98.0 \end{cases} \quad \textbf{(4.3.30)}$$

$$d_{2\ (urea)} = \begin{cases} 0 & if\ Y_2 \leq 3.63 \\ \left[\frac{Y_2 - 3.63}{65.7 - 3.63}\right] & if\ 3.63 < Y_2 < 65.7 \\ 1 & if\ Y_2 \geq 65.7 \end{cases} \quad \textbf{(4.3.31)}$$

In above all equations value of r was taken as 1. Therefore, overall desirability (D) for all urine metabolites was calculated using Equation 3.8.6. The simultaneous optimization of process parameters for all urine metabolites was done for maximizing the % Degradation and minimizing

the Energy consumption by keeping the input factors in the range. Table 4.3.5 shows the set of constraints applied during the EO process optimization of each urine metabolite i.e. uric acid, creatinine and urea. The best optimized conditions of process parameters for uric acid were obtained at pH= 2, n = 0.875 g/L, j= 7.142 mA/cm^2, t = 6.95 min and showed highest overall desirability, D = 0.899. While for creatinine most appropriate optimized conditions were obtained at pH= 2.4, n = 0.75 g/L, j= 12.005 mA/cm^2, t = 85 min with, D = 0.899. The optimal operating conditions for maximum removal of urea were found to be j=18.14 mA/cm^2, n=1.45 g/L, pH= 4 and t= 135 min which produced combined desirability value, D =0.857. At these optimized conditions, the value for responses Y_1 and Y_2 suggested by BBD were shown in Table 4.3.6a,b,c. In order to confirm these suggested values of responses, experiments for all urine metabolites were conducted in triplicate at the optimized condition. The average experimental value of both responses Y_1 and Y_2 for urine metabolites were found very close to the predicted values and listed in Table 4.3.7. This concludes that the optimization of EO treatment of urine metabolites using BBD under RSM was successfully done

Table 4.3.5 Constraints applied for optimization of EO treatment of each urine metabolite i.e. uric acid, creatinine and urea with MMO.

Urine metabolites	Variables	Goal	Lower limit	Upper limit
(a) Uric acid	pH	is in range	2	9
	t (min)	is in range	2	10
	j (mA/cm^2)	is in range	2.38	11.9
	n (g/L)	is in range	0.25	1.25
	Y_1, (%Degradation)	maximize	9.25	98.4
	Y_2, (Energy consumption)	minimize	0.05625	2.15625
(b) Creatinine	pH	is in range	2	9
	t (min)	is in range	15	115
	j (mA/cm^2)	is in range	7.14	21.42
	n (g/L)	is in range	0.25	1.25
	Y_1, Sqrt(%Degradation)	maximize	2.12132	9.37763
	Y_2, Ln(Energy consumption)	minimize	0.150573	4.17185
(c) Urea	pH	is in range	3	9
	t (min)	is in range	60	180
	j (mA/cm^2)	is in range	9.52	28.57
	n (g/L)	is in range	0.5	1.75
	Y_1, (%Degradation)	maximize	11.5	98
	Y_2, (Energy consumption)	minimize	3.63	65.7

Table 4.3.6a Individual and multi-response optimization results of uric acid treated with MMO for desirability calculations					
Response	j (mA/cm^2)	n (g/L)	t (min)	pH	Desirability
Individual response optimization					
%Degradation, Y_1 = 98.47%	11.90	0.85	6.37	2.25	1
Energy consumption, Y_2 = 0.1408 kWh/m^3	6.42	0.87	2	2.15	1
Synchronized optimization of responses					
%Degradation, Y_1 = 93.319%	7.142	0.875	6.95	2	0.899
Energy consumption, Y_2 = 0.5814 kWh/m^3					

Table 4.3.6b Individual and multi-response optimization results of creatinine treated with MMO for desirability calculations					
Response	j (mA/cm^2)	n (g/L)	t (min)	pH	Desirability
Individual response optimization					
%Degradation, Y_1 = 87.98%	16.35	0.96	107.21	2.31	1
Energy consumption, Y_2 = 1.1097 kWh/m^3	8.575	1.22	16.22	2.39	1
Simultaneously optimization of responses					
%Degradation, Y_1 = 85.97%	12.005	0.75	85	2.4	0.899
Energy consumption, Y_2 = 17.986 kWh/m^3					

Table 4.3.6c Individual and multi-response optimization results of urea treated with MMO for desirability calculations					
Response	j (mA/cm^2)	n (g/L)	t (min)	pH	Desirability
Individual Response optimization					
%Degradation, Y_1 = 97.08%	20.75	1.6	142	4.17	1
Energy consumption, Y_2 = 11.4 kWh/m^3	17.84	0.5	61.02	4	0.935
Synchronized optimization of responses					
%Degradation, Y_1 = 96.06%	18.14	1.45	135	4	0.857
Energy consumption, Y_2 = 21.11 kWh/m^3					

Table 4.3.7 Comparison between the predicted and actual experimental value of each urine metabolite treated with MMO at optimized conditions						
	Urine metabolites					
	Uric acid		Creatinine		Urea	
Responses	Predicted	Actual	Predicted	Actual	Predicted	Actual
%Degradation	93.319	91.571	85.97	85.41	96.06	94.78
Energy consumption (kWh/m^3)	0.5814	0.526	17.986	16.826	21.11	20.54

During the EO treatment process, it has been observed that the pH of all urine metabolites was found to be changed as shown in Figure 4.3.5. In this study, EO experiments were performed at optimized conditions of each urine metabolite with MMO. The initial set pH of urine metabolites solution was between 2 to 4, which was increasing during the treatment test and reaching final values i.e. 4.15 (uric acid), 6.9 (creatinine) and 7.5 (urea). The rapid and gradual increase in pH at the beginning of the treatment test was observed and then it kept almost constant at around 6.9 and 7.5 until the end of the process. During the EO treatment, the shift of pH from acidic towards neutral was due to the production of hydroxyl ion (OH^-) by water reduction at the surface of the cathode. Furthermore, pH during electrolysis between 90 min to 150 min was found stabilized to ≈ 7.0 (creatinine) and ≈7.5 (urea) due to the formation of the buffer which formed from produced CO_2 while degrading the metabolites as shown in Equation 4.3.32.

$$CO_2 + H_2O \longrightarrow H^+ + HCO_3^- \quad \textbf{(4.3.32)}$$

Besides this, the change in pH was might be due to the involvement of both mechanisms i.e. direct and indirect oxidation method. The degradation of all urine metabolites was happened due to the generation of strong oxidant species such as $OH^{\bullet}$ which generated from water discharge on the surface of the MMO anode during anodic oxidation. However, due to low adsorption rate (as pH shift towards neutral), $OH^{\bullet}$ readily converted to H_2O_2 and $HO_2^{\bullet}$ thus helps in mediated oxidation (Dbira et al., 2015). Furthermore, mediated oxidation also took place due to the presence of RCS like HOCl and Cl_2 at acidic pH which oxidizes the urine metabolites rapidly. In the present study, the degradation of urine metabolites i.e. uric acid, creatinine, and urea was happened largely because of indirect oxidation (HOCl, Cl_2, ClO^-, H_2O_2, etc.) than direct oxidation ($OH^{\bullet}$). Since, during EO treatment of metabolites some chloro-oxidant species such as HOCl, ClO^-, chloramines were found to be participating, which have been reported toxic, might be present in the treated wastewater samples. Moreover, the metabolites were also oxidized into byproducts which could be toxic to the environment and human health. Therefore, from the safe disposal point of view, it becomes necessary to verify as well as identify these toxic compounds if present in treated wastewater through various analytical techniques as discussed in section 4.3.4.

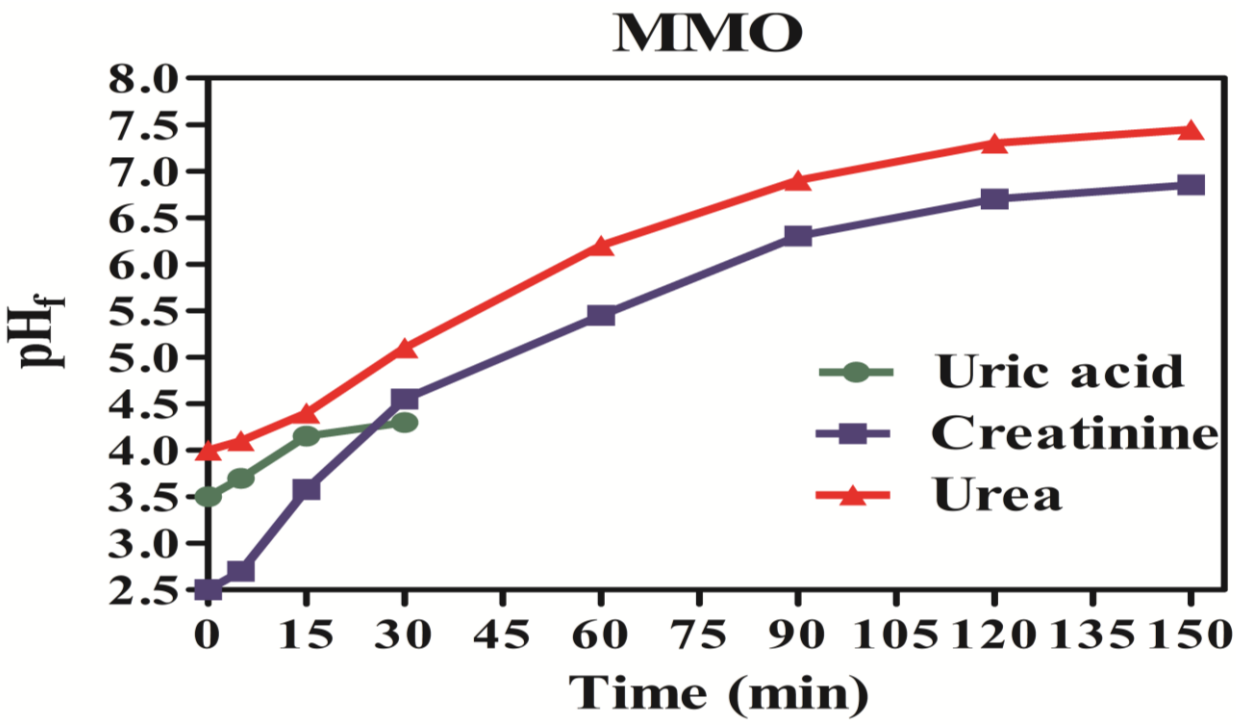

Fig 4.3.5 Graph of pH_f versus time at optimized conditions for all urine metabolites treated with MMO

4.3.3 Spectrophotometric Analysis

This test analysis was done initially in order to confirm the oxidation of target compounds (i.e. urine metabolites). In other words, it helps in getting the primary information regarding the degradation of target pollutants. The treated and untreated samples of urine metabolites were analyzed in the range of 200-500 nm. The UV-vis spectra for untreated and treated samples of urine metabolites by EO treatment were shown in Figure 4.3.6a,b,c. From results, it can be concluded that the absorbance peak of all pure urine metabolites untreated samples i.e. uric acid (290 nm), creatinine (238 nm) and urea (420 nm) were got reduced to a minimum after EO treatment of 7 min, 85 min and 135 min respectively. During test analysis, it was observed that some peaks disappeared while other peaks formed at different λ_{max} for certain time intervals confirming the formation and destruction of various unstable intermediate byproducts. This change in the λ_{max} approves the electrolytic degradation of urine metabolites by the attack of various oxidant species such as $OH^{\bullet}$, $HO_2^{\bullet}$ and HOCl which were generated in-situ during the EO treatment process.

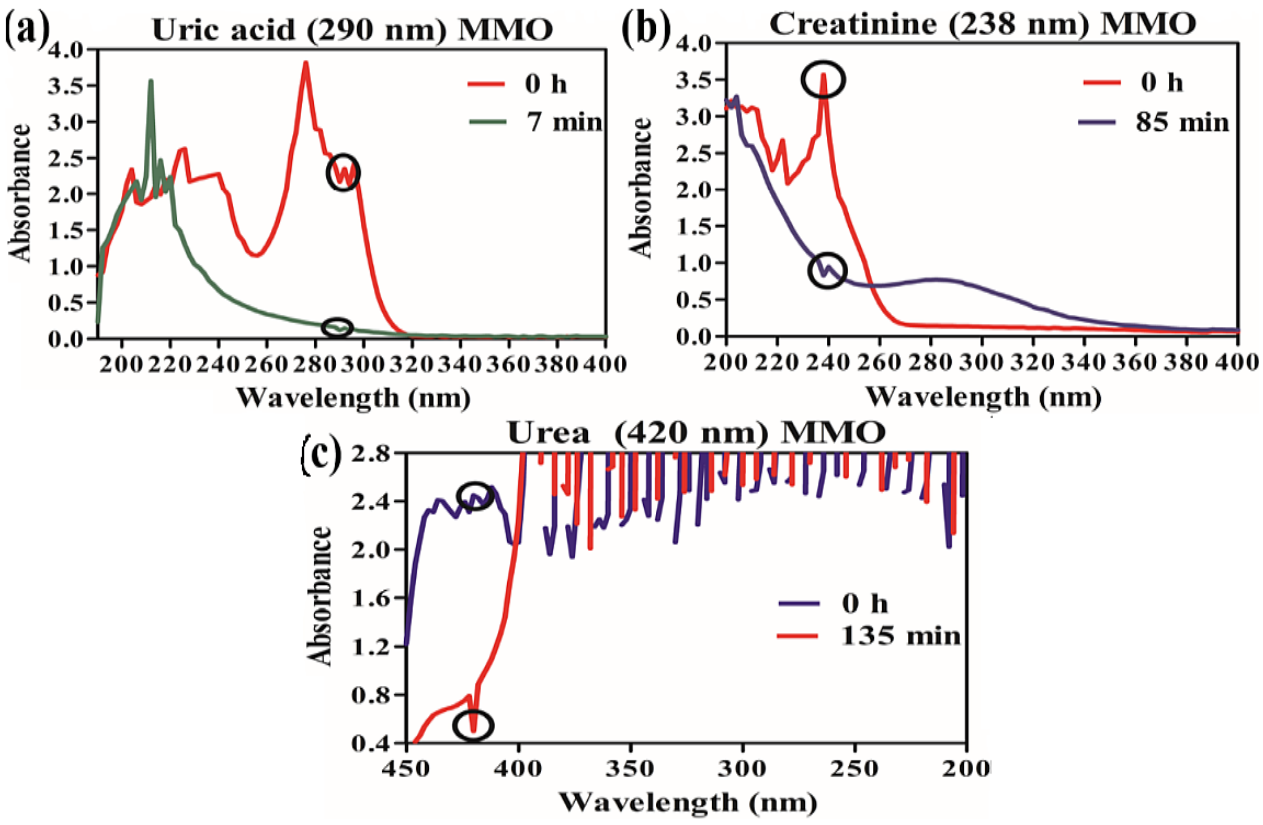

Figure 4.3.6 UV-vis spectra for untreated and treated samples of (a) uric acid, (b) creatinine and (c) urea with MMO at optimum conditions suggested by BBD.

4.3.4 Mineralization Studies

For monitoring the quality of EO treated urine metabolite samples, mineralization studies were performed at optimized conditions in terms of in-situ chemical analysis, CV, FT-IR and LC-MS analysis.

Chemical analysis: To further analyze the quality of treated and untreated samples in-situ chemical analysis was performed. This analysis would depict the results of a reduction in TOC and COD along with the quantification of various anions. Mineralization of uric acid was confirmed through a reduction in COD (87.05%) and TOC (84.62%) at optimized conditions which reached up to 91.0% and 87.89% when the reaction was extended to 15 min as shown in Figure 4.3.7a. In the case of creatinine, around 83.75% removal in COD and 80.5% decay in TOC were attained in 85min as shown in Figure 4.3.7b. Further extension in treatment time upto 150 min has reduced COD and TOC around 3.0% more only. Figure 4.3.7c shows the results of urea TOC decay around 90.5%, achieved after 135 min of electrolysis which further reached 93.16% when the reaction extended to 240 min. The reduction in COD concentration depicts the degradation of initial pollutants and the formation of intermediates chemical species during the process treatment. While decay in TOC value during the EO treatment process corresponds to the conversion of organic carbon into CO_2 (Dbira et al., 2019).

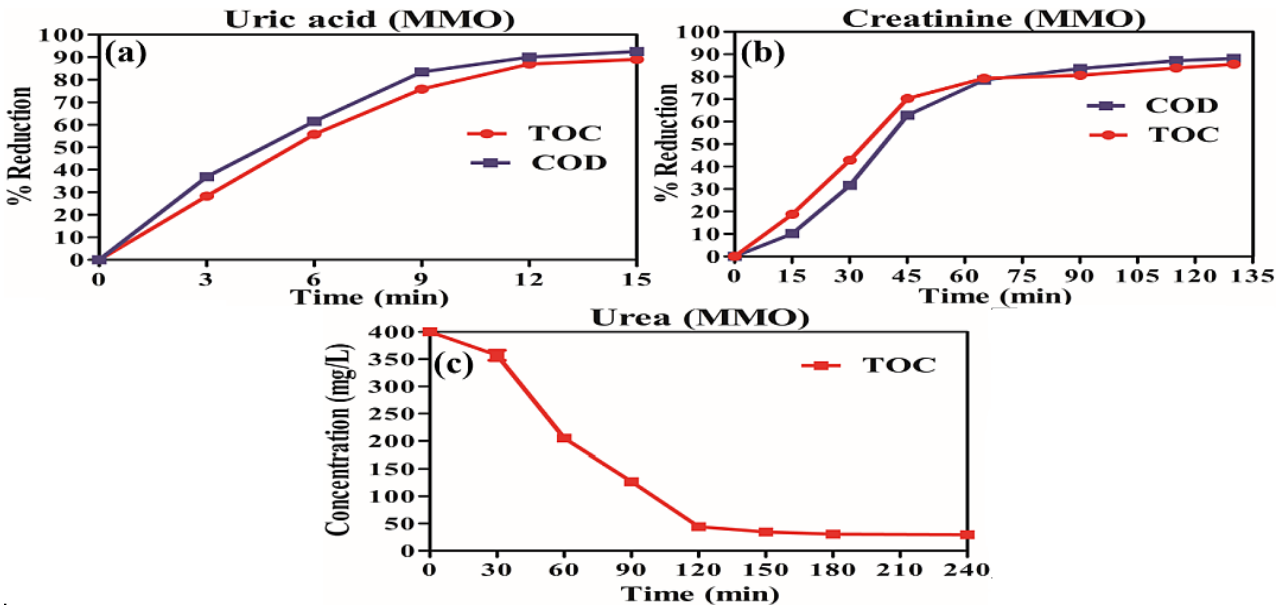

Figure 4.3.7 Plot of % COD and TOC removal versus time for (a) uric acid, (b) creatinine and (c) urea treated with MMO anodes at optimized conditions of each urine metabolite

To further verify the oxidation of urine metabolites into inorganic ions such as (NO_2^-, NO_3^-, NH_4^+) ion testing analysis was carried out along with the estimation of total nitrogen and total available chlorine. The total nitrogen present in each urine metabolites were found almost converted into NO_2^-, NO_3^-, NH_4^+, etc. A similar type of results was also reported for uric acid (Dbira et al., 2016), creatinine (Antoniou et al., 2007) and urea (Hernández et al., 2014) where nitrogen atoms in these urine metabolites were dissipated into these inorganic ions. A slowly continuous increasing trend was observed for the generation of NO_3^- ions while the concentration of NO_2^- and NH_4^+ started decreasing after 6 min and 9 min of treatment of uric acid respectively as depicted in Figure 4.3.8a. In the case of creatinine, an increasing trend was observed for generated NO_2^-, NO_3^- and NH_4^+ at the beginning of the EO treatment process as shown in Figure 4.3.8b. However, NO_3^- were started depleting after 30 min of electrolysis only and completely oxidized into a higher state when treatment was extended to 130 min. While NH_4^+ continuously increased upto 75 min of treatment and then found decreasing gradually till the end of the process. The concentration of NO_3^- ions showed a marginal increase up to 45 min, then increased sharply till 105 min of electrolysis and become at the end of the process as shown in Figure 4.3.8b.

In the case of uric acid and creatinine (Figure 4.3.8a,b), it was observed that the concentration of NO_2^- and NH_4^+ decreases during the electrolysis because of its conversion into NO_3^- ions as reported in the literature. Figure 4.3.8c showed results of NO_3^- and NH_4^+ ions generated during the EO treatment of urea with MMO anode. An increasing and then decreasing trend was seen in NH_4^+ generation while in case NO_3^- the continuous increasing trend was seen only. This might be due to the reaction between NH_4^+ and HOCl. In the case of NO_3^-, the increase was observed due to the oxidation of the chloramines by free chlorine. From Figure 4.3.9a,b,c, it can be observed that chloride level was continuously decreasing during the electrolysis of each urine metabolites. This is because of the oxidation of chloride on the MMO anode surface to produce strong oxidant species like Cl_2, HOCl, OCl^-, etc. for the destruction of each urine metabolites (i.e. uric acid, creatinine and urea).

In the case of urea, some other tests such as total nitrogen and TAC were also performed in order to understand the oxidation mechanism of urea in presence of reactive chlorine species as well as to analyze the nitrogen to chloride ratio. Figure 4.3.10a shows the results of the reduction in total nitrogen present in urea at different time intervals of electrolysis. In comparison to total nitrogen,

the low yield of nitrates was found during urea degradation which could be due to the less availability of free chlorine to urea ratio. From this above discussion, it may conclude that during electro-oxidation of urea molecular nitrogen may also generate (Cho and Hoffmann, 2014). The level of TAC increased gradually during the electro-oxidation treatment of urea and then increased sharply to higher values when urea was depleted to the maximum as shown in Figure 4.3.10b. During the treatment process TAC, an aggregate part of reactive intermediates does not remain constant. This might be due to the balance between the oxidation of urea and the generation of chlorine species along with their bond forms during the treatment process as reported in the literature (Hernlem, 2005).

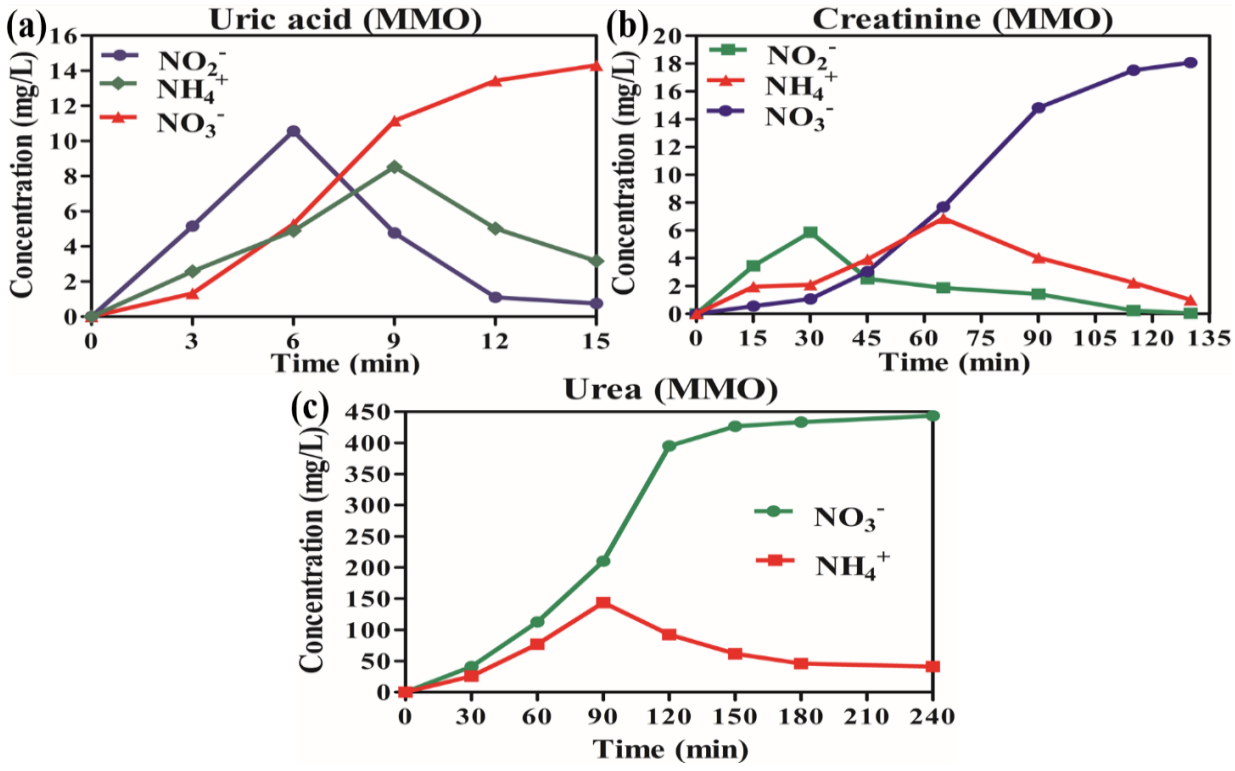

Figure 4.3.8 Production of inorganic ions (NO_2^-, NO_3^- and NH_4^+) ions during electrolysis of (a) uric acid, (b) creatinine and (c) urea with MMO anodes at optimized conditions.

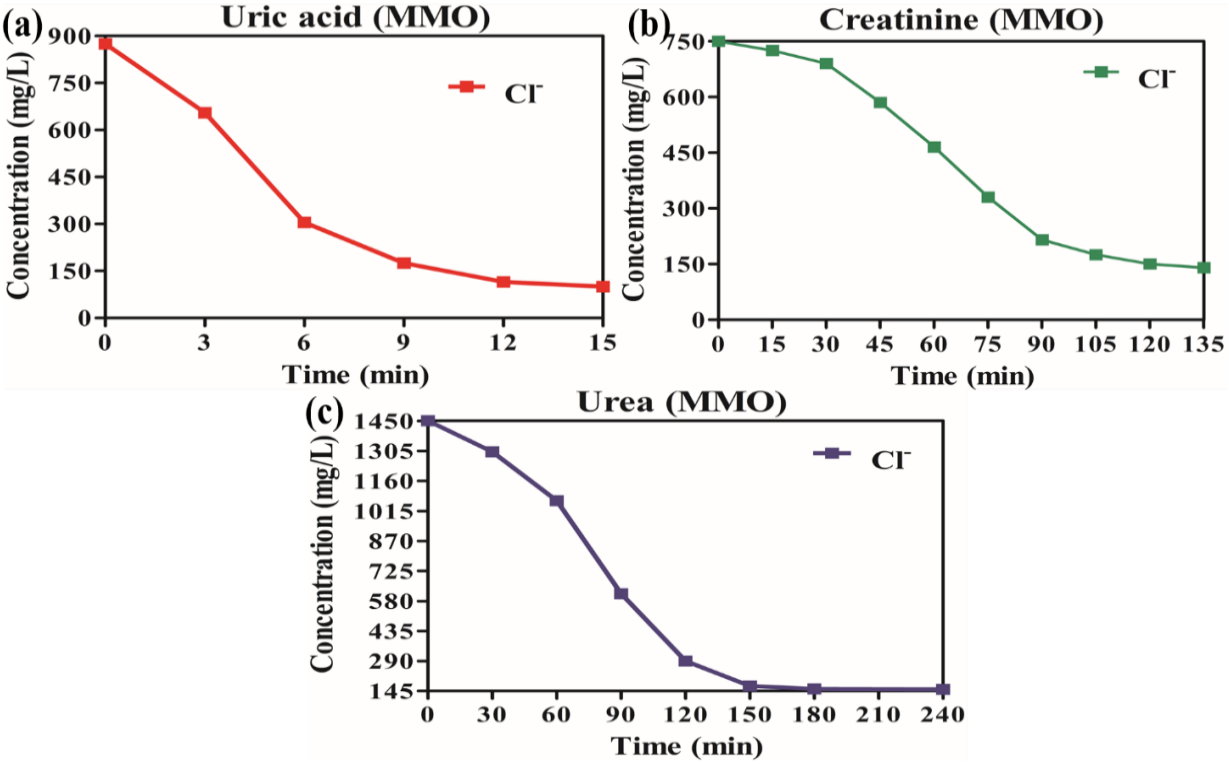

Figure 4.3.9 Mineralization plots of total chloride versus time at optimized conditions for (a) uric acid, (b) creatinine and (c) urea treated with MMO anodes

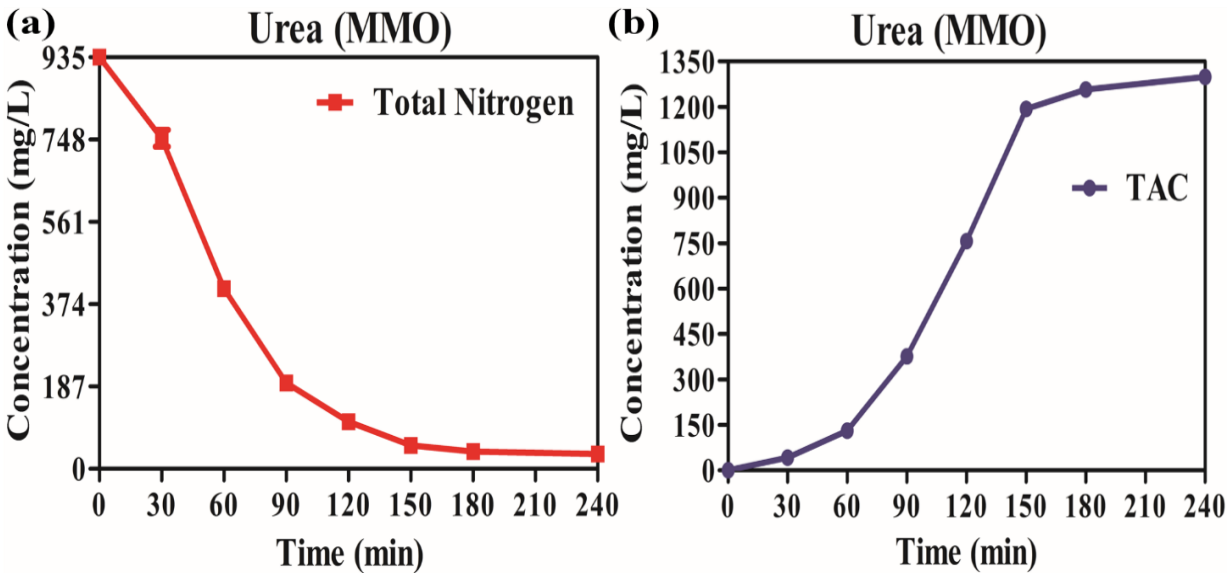

Figure 4.3.10 Mineralization plots of (a) total nitrogen versus time and (b) TAC versus time for urea treated with MMO at optimized conditions.

Cyclic Voltammetry (CV): Figure 4.3.11a,b,c shows the continuous CV for the EO treatment of uric acid (50 mg/L), creatinine (50 mg/L) and urea (2000 mg/L) respectively at Pt rod with potential range of -1.2 to 1.2 V. The anodic part of voltammogram was measured by occurrence of anodic peaks which corresponds to oxidation of pollutants while cathodic part of voltammogram was characterized by the existence of cathodic peaks which corresponds to reduction of pollutants. Along with the redox peaks of electrolyte, the samples of urine metabolites have also shown a few visible peaks in the potential range window (Mudila et al., 2018). As it can be seen that in 0 h samples (untreated) of all urine metabolites, one oxidation peak at ≈ -0.4 V (0.000025 A and 0.00005) potential in a first cycle and one reduction peak at ≈ – 0.8 V (-0.00010 A and 0.00015 A) were observed.

However, in the case of treated samples of all urine metabolites, cycle 1 shows the disappearance of the oxidation peak while cycle 2 exhibits a remarkable decrease in reduction peak (< -0.00005A). These quasi-reversible peaks attribute the oxidation and reduction mechanism that occur during the electrolysis of all urine metabolites (Hiwarkar et al., 2017). The dissolution/shifting of the peaks depicts the generation of simpler oxidative and reductive species during the degradation of uric acid, creatinine and urea with MMO anode. Moreover, an increase in oxidation peak current and decrease in oxidation peak potential indicates the great electro-catalytic activity towards the oxidation of all urine metabolites as well as amplified active electrochemical surface area (Zhang and Yin, 2014).

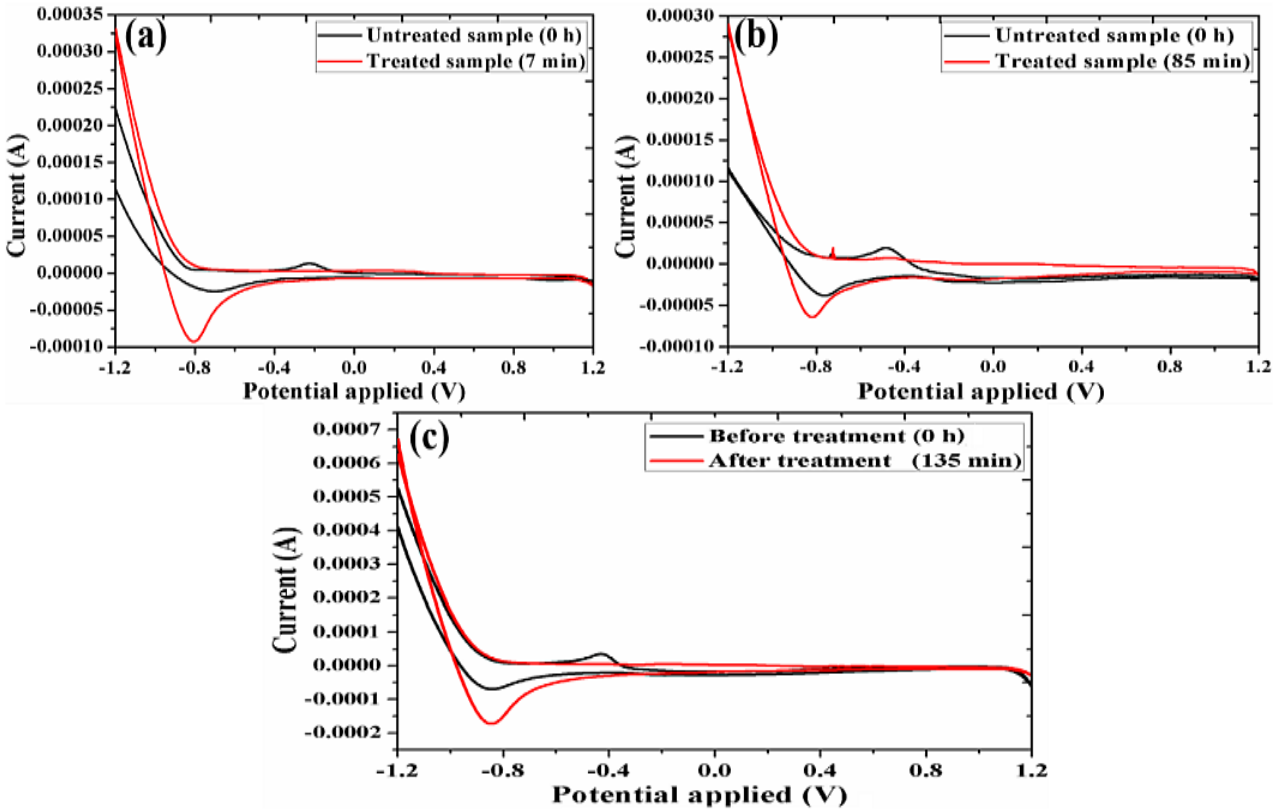

Figure 4.3.11 Cyclic Voltammetry measurements for untreated and EO treated samples of (a) uric acid, (b) creatinine and (c) urea with MMO at optimized conditions.

FT-IR (Fourier transformed infrared spectroscopy) analysis: To examine the removal phenomenon of uric acid, creatinine and urea from aqueous solution through the EO process with MMO anode, FT-IR was performed under optimal conditions. Figure 4.3.12 represents the FT-IR spectra of untreated and treated samples of uric acid taken at fixed time intervals. The result showed that most of the peaks were got shifted at distinct wavenumber, might be due to the structural changes occurred during the EO process. Some of the broad and sharp peaks during electrolysis were found to disappear due to the oxidation of uric acid and its intermediates via reactive oxidant species. Furthermore, few peaks during electrolysis were seemed to appear which accounts for $OH^{\bullet}$ and chlorine species as reported in the literature (Rajkumar and Muthukumar, 2012). Moreover, the % transmittance for maximum peaks was found increased after a treatment time of 6 min, which indicates that the oxidation of uric acid was complete and converted into simple compounds.

Figure 4.3.13 shows the FT-IR spectra of creatinine samples at different time intervals. The peaks at 1671.23, 1036.00 and 607.36 cm^{-1} accounts for –C=O stretch. A broad peak at 3252.44

cm^{-1} and an intense peak at 1590.51 cm^{-1} shows the presence of N-H and peak at 1330.25 cm^{-1} indicate the presence of the C-N group. Other peaks were also observed at 2800–3100 cm^{-1} and 600–800 cm^{-1} were accounts for C-H (stretch and bending). Some other small peaks were also observed in the spectra of raw creatinine sample (t= 0 h) which got disappeared completely during the electrolysis process.

Broad and sharp peaks at 3400 cm^{-1} and 1600 cm^{-1} were formed (t > 20 min) due to OH radical generation as well as due to C=O stretching of intermediates formed during the EO process (Hiwarker et al., 2017). The peaks at 1100–800 cm^{-1} (t > 40 min) were formed for chloride an inorganic anion, present in the hypochlorite solution. During EO treatment of creatinine, shifting of peaks was observed because of the breaking of the bonds at a particular wavenumber. In addition to this, an increase in the % transmittance was observed for most of the peaks after electrolysis, indicates the complete oxidation of the cyclic structure of creatinine.

Figure 4.3.14 gives the FT-IR spectra of untreated urea and its EO treated samples taken at fixed time intervals. The C=O stretching frequency appeared at 1672 cm^{-1}. The C–N stretching frequency appears at 1452 cm^{-1} (Singh et al., 2016). The N–H stretching and deformation frequencies appear at 3450 cm^{-1} and 1628 cm^{-1} respectively. Few other small peaks also appeared in the fingerprint region of the raw sample of urea (t= 0 h). Broad and sharp peaks at 3450 cm^{-1} and 1672 cm^{-1} were shifted to 3427 cm^{-1} and 1647 cm^{-1} after 45 min due to the production of $OH^{\bullet}$ at MMO as well as C=O stretching during the initial stage of EO treatment (Piasek and Urbanski, 1962). The peaks at 1100–800 cm^{-1} (t > 45 min) have also appeared which accounts for Cl^{-}, normally present in hypochlorite solution. The peak at 1381 cm^{-1} at 135 min shows the degradation of urea into nitrate ions. During electrolysis, most of the peaks were deviated due to the breakage of the bonds at distinct wavenumber. Moreover, an increase in the % transmittance was observed for most of the peaks after electrolysis, indicates destruction and oxidation of urea.

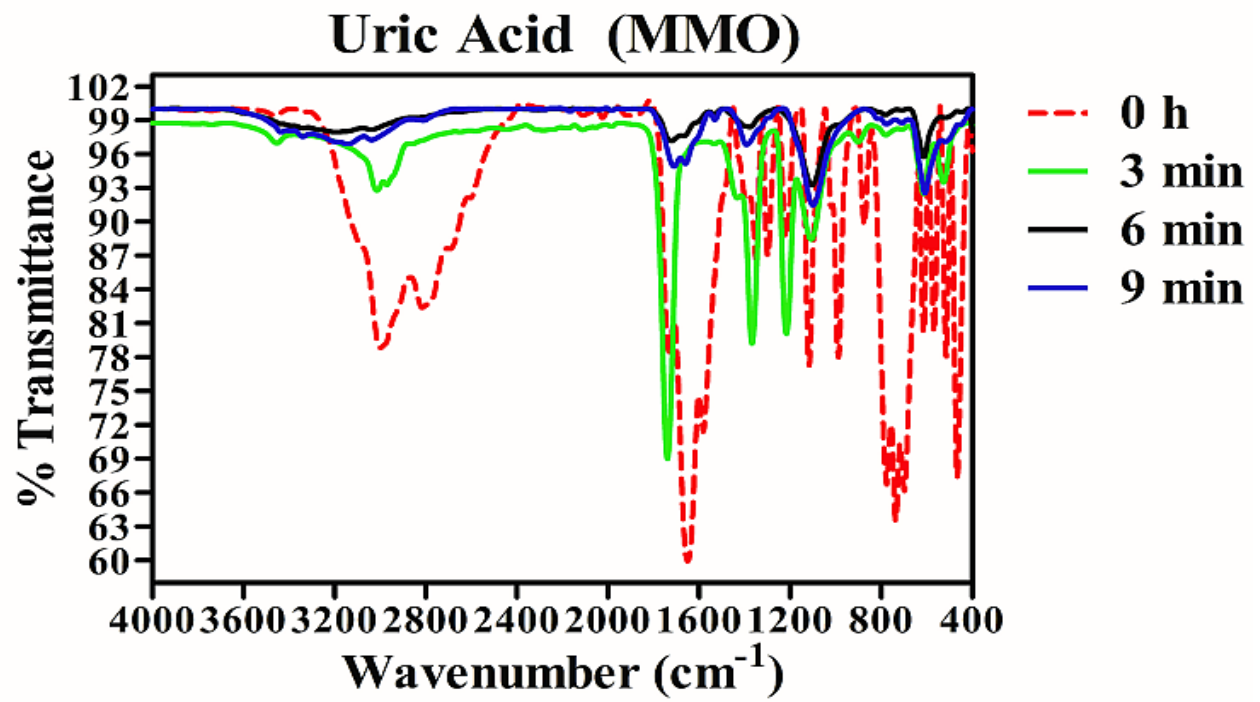

Figure 4.3.12 FT-IR spectra for uric acid of untreated and treated (MMO) samples taken at different time intervals (pH 2, the current density of 7.142 mA/cm^2 and NaCl dose 0.875 g/L).

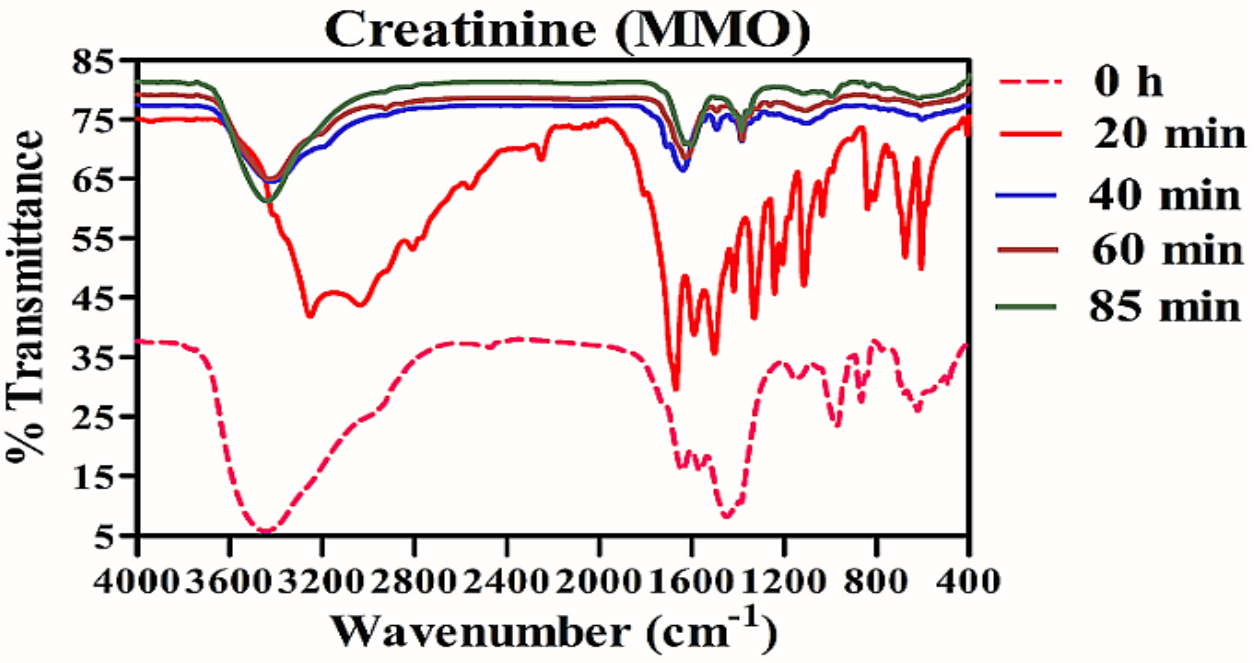

Figure 4.3.13 FT-IR spectra for creatinine of untreated and treated (MMO) samples taken at different time intervals (pH 2.4, current density 12.005 mA/cm^2 and NaCl dose 0.75 g/L).

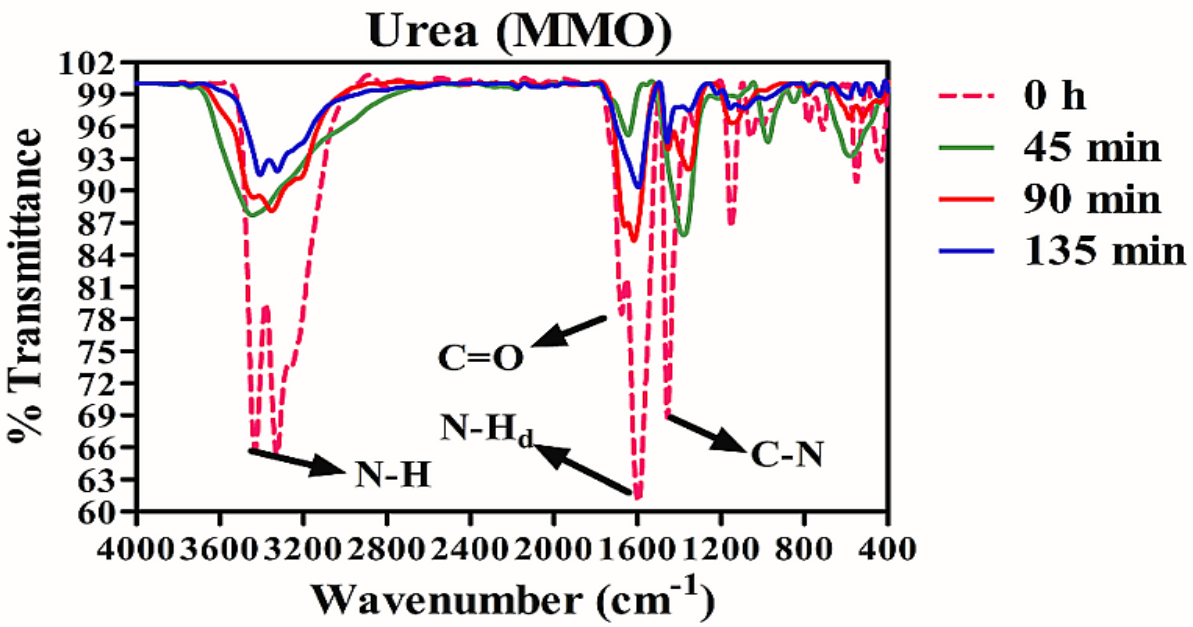

Figure 4.3.14 FT-IR spectra for urea of untreated and treated (MMO) samples taken at different time intervals (pH 4, current density 18.14 mA/cm^2 and NaCl dose 1.45 g/L).

LC-MS analysis: The intermediates and degradation by-products formed during the EO treatment of uric acid and creatinine were identified through LC-MS analysis shown in Figure 4.3.15a,c respectively. Based on these intermediates (1–10), a tentative degradation pathway for uric acid has been proposed shown in Figure 4.3.15b. The reduction of uric acid in route A led to the formation of 5-(aminomethylamino)pyrimidine-2,4(1H,3H)-dione from which 5-(ethylamino)pyrimidine-2,4(1H,3H)-dione was formed by deamination. Further, the demethylation of this compound occurs which formed 5-aminopyrimidine-2,4(1H,3H)-dione. The reduction and oxidation with deamination of this formed compound led to the generation of two compounds i.e. 5-amino-3,4-dihydropyrimidine-2(1H)-one and pyrimidine-2,4,5,6(1H,3H)-tetraone respectively. The subsequent reduction followed by benzene ring cleavage of pyrimidine-2,4,5,6(1H,3H)-tetraone led to the production of an unknown compound whose further fragmentation generated end compound urea and fragmentation with hydroxylation generated oxalic acid an end compound of degradation pathway. On the other hand reduction of uric acid in route, B led to the production of 2,3-dihydro-1H-purine-6,8(7H,9H)-dione from which 5-amino-3,4-dihydropyrimidine-2(1H)-one was formed by successive reduction and C-N bond cleavage. The subsequent benzene ring cleavage and deamination of 3,4-dihydropyrimidine-2(1H)-one led to the generation of 1-methyl-3-vinylurea. Further demethylation of 1-methyl-3-vinylurea has produced 1,3-dimethylurea compound and subsequent demethylation of 1,3-dimethylurea generated end product that is urea. Hence, the

oxidation of uric acid has generated two by-products urea and oxalic acid, which has also been reported in the literature by (Dbira et al., 2016).

The degradation pathway for creatinine has been proposed based on the intermediates (1–5) identified as shown in Figure 4.3.15d. The cleavage of C-N bond followed by oxidation of the target pollutant led to the formation of intermediate (1). While the fragmentation of (1) followed by oxidation and reduction could lead to the generation of (2) and (4) respectively. Removal of a methyl group from (2) could ultimately lead to the production of urea (3). Whereas, further oxidation of (4) could possibly form (5). Similar kind of products (3 and 5) has been reported in the literature (Antoniou et al., 2009).

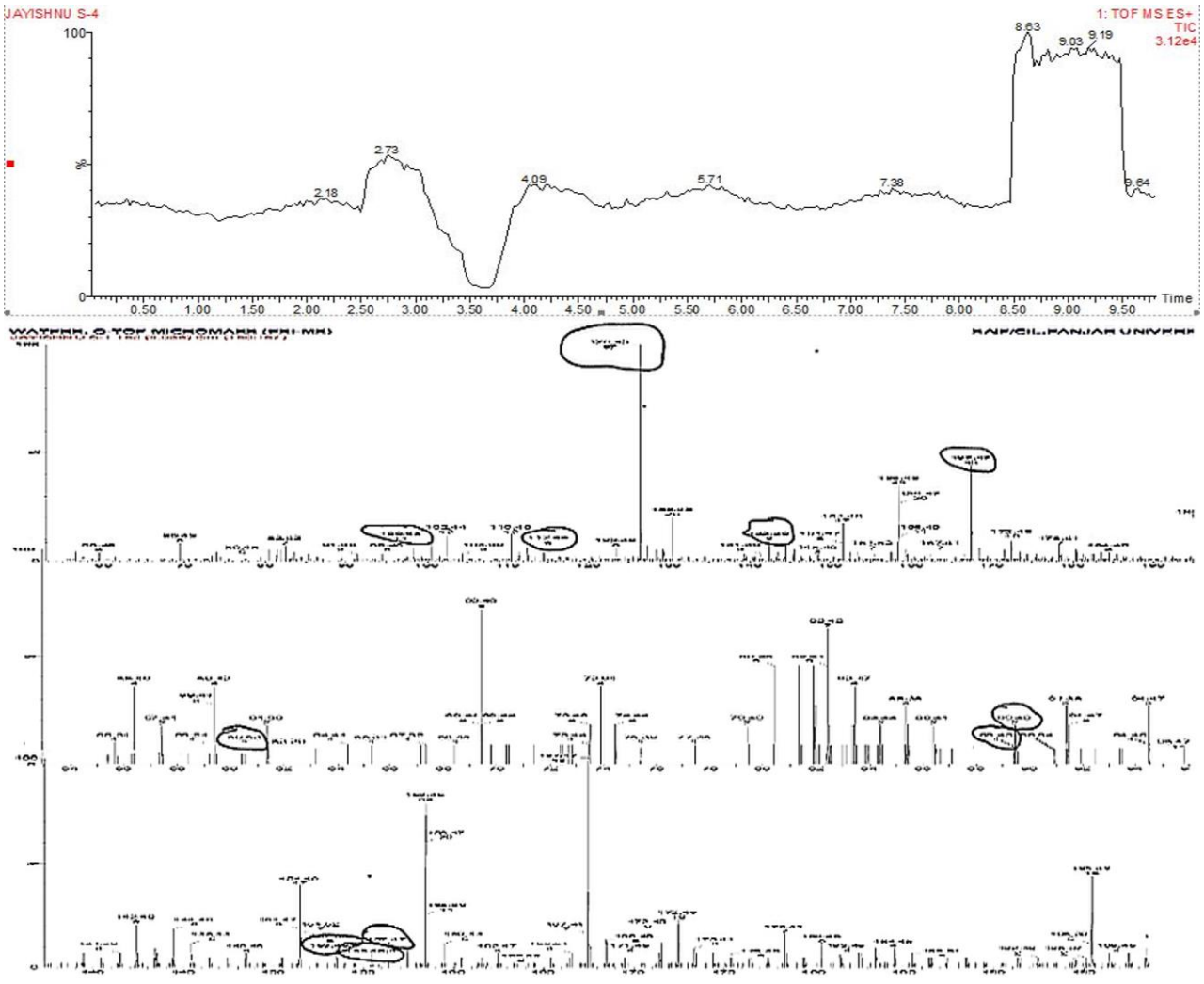

Figure 4.3.15 (a) GC chromatogram and mass spectra analysis for the identification of intermediates during the EO treatment of uric acid with MMO at the optimized condition.

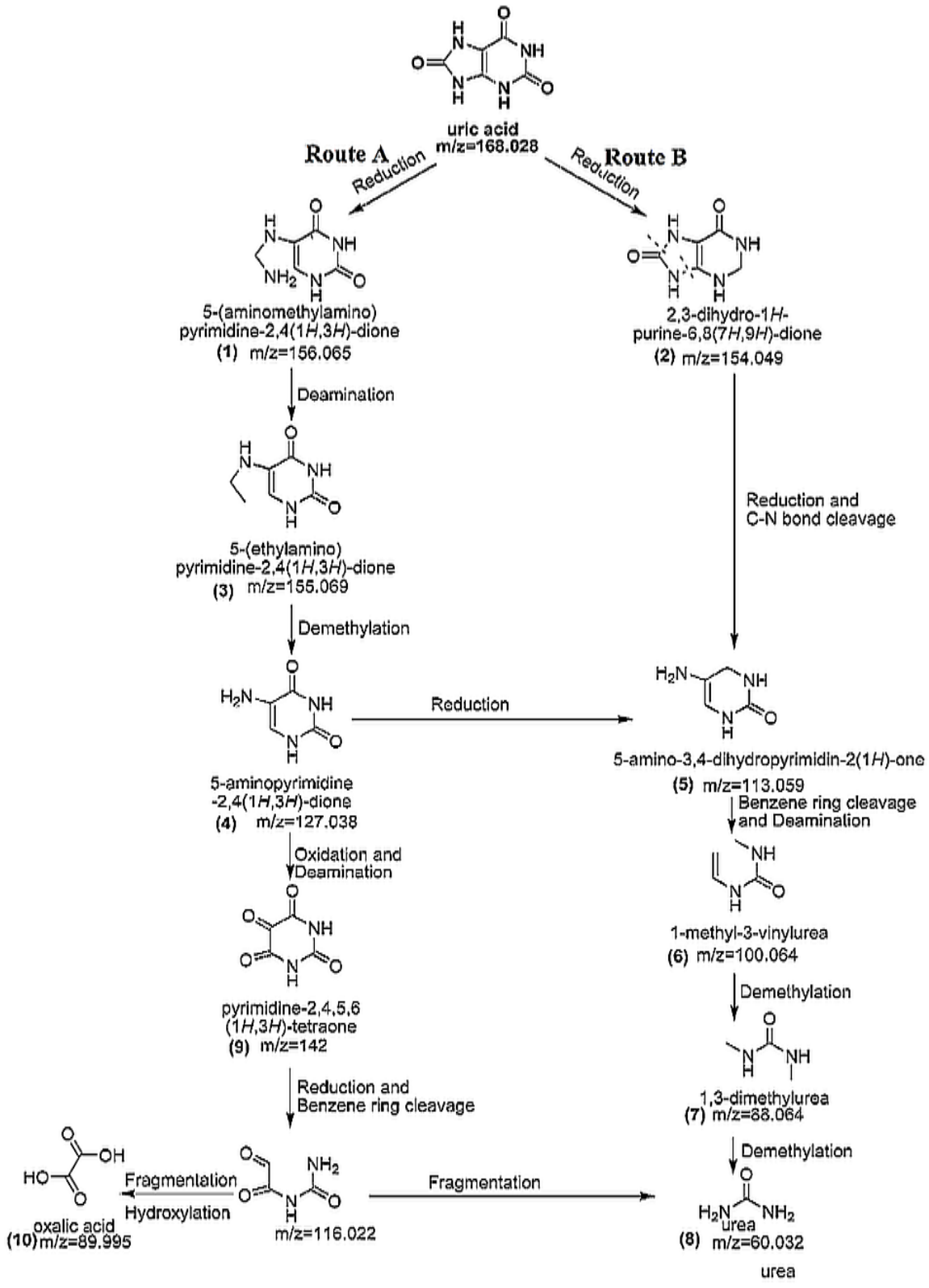

Figure 4.3.15 (b) Proposed degradation pathway for Uric acid treated with MMO

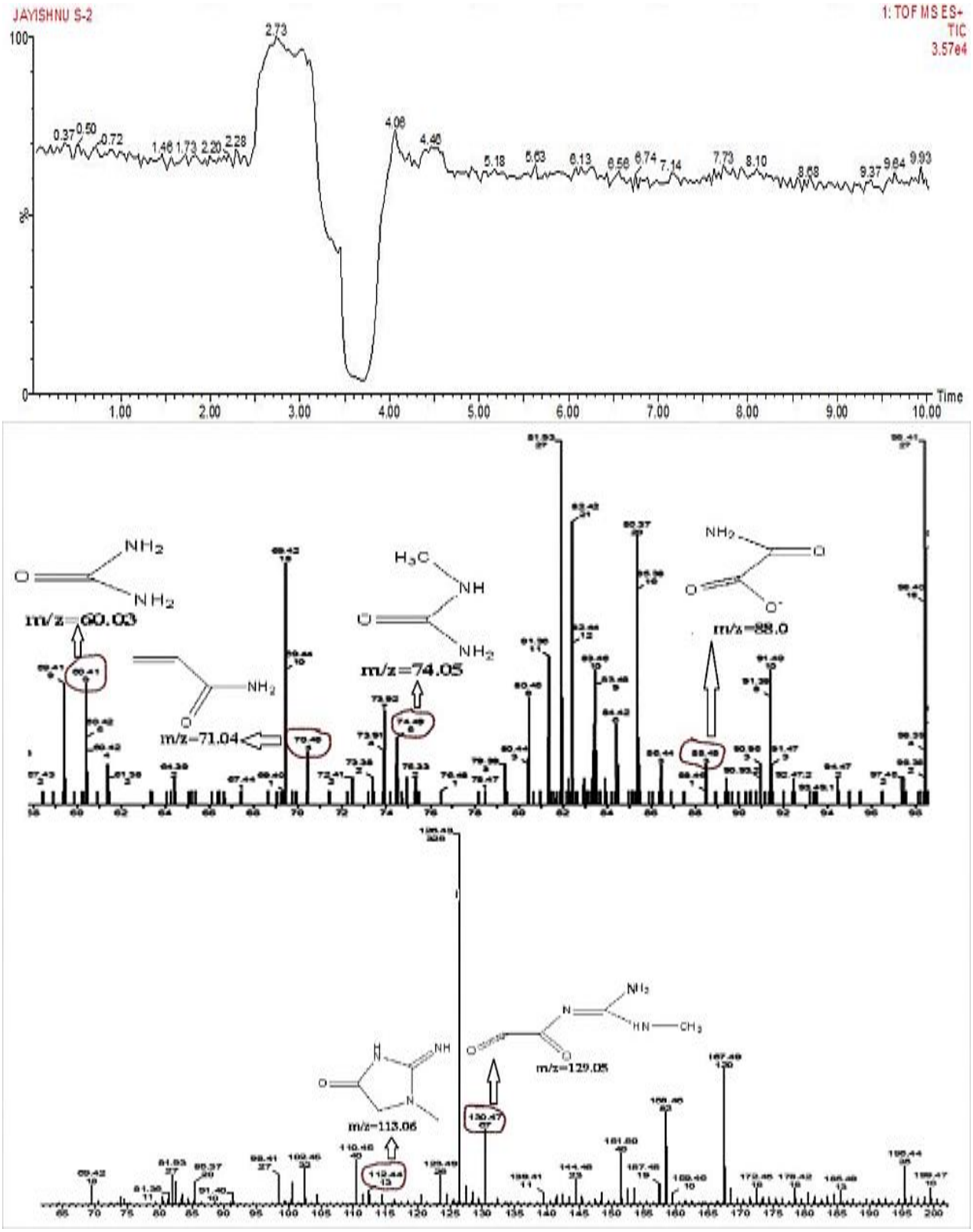

Figure 4.3.15 (c) GC chromatograms and mass spectra analysis for the identification of intermediates during the EO treatment of creatinine with MMO at the optimized condition.

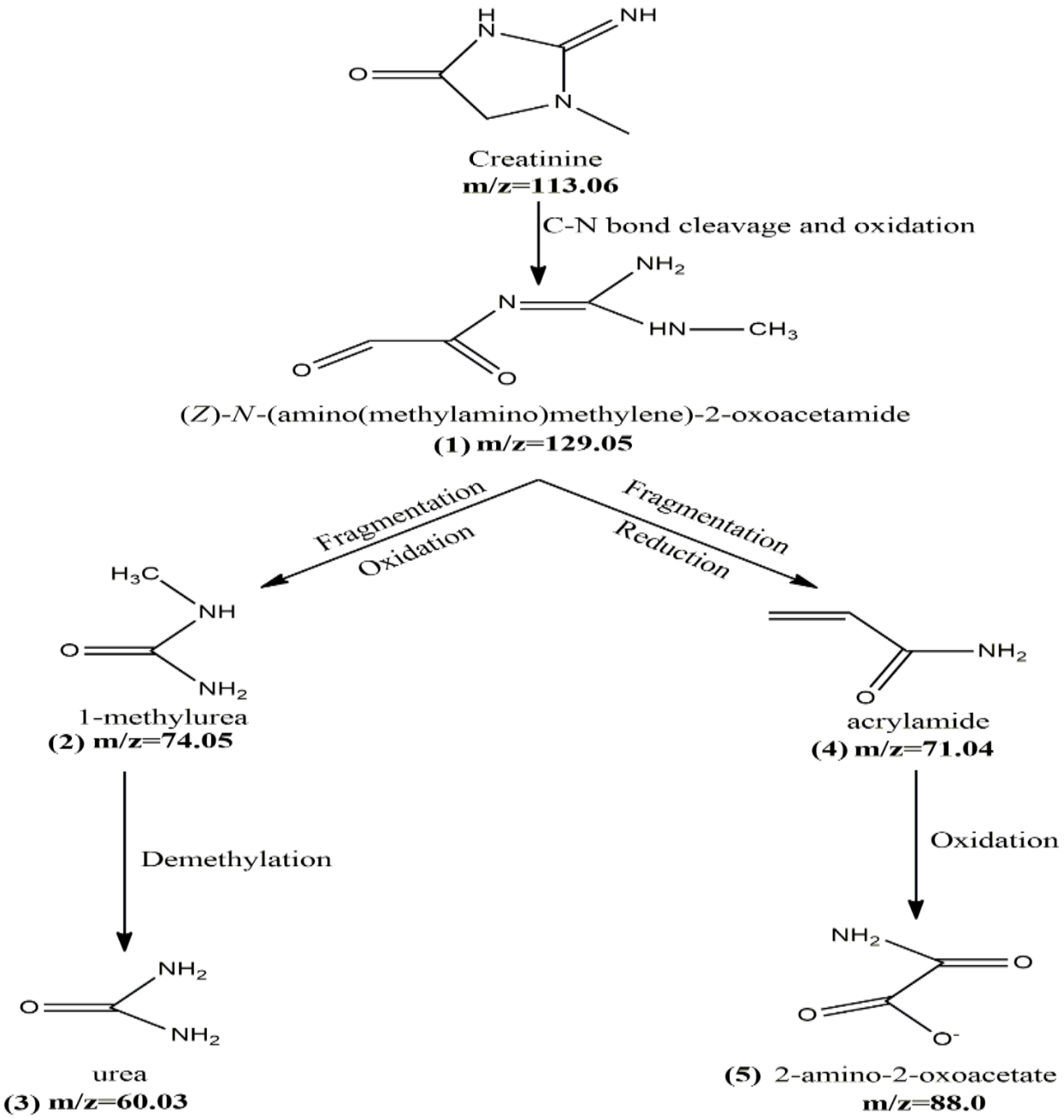

Figure 4.3.15 (d) Proposed degradation pathway for Creatinine treated with MMO.

4.3.5 Kinetic Study

The kinetic study of the degradation for batch EO treatment of each urine metabolite with MMO anode was studied at optimized conditions. The experimental data of each urine metabolite i.e. uric acid, creatinine and urea were tested for fitting to L-H (Langmuir Hinshelwood) kinetic model of

the first order. According to the results, the EO degradation process data was the best fit in the pseudo-first-order kinetic model which defined as follows:

$$\frac{-dC}{dt} = k_r KC \quad \textbf{(4.3.33)}$$

Where, k_r = reaction rate constant (min^{-1}); C = bulk substrate concentration (mg/L) at different time intervals; K= equilibrium adsorption constant; t= time (min). For the low concentration of pollutants (substrate), K can be ignored. Therefore, on integrating the Equation 4.3.33, the EO degradation rate can be defined as shown in Equation 4.3.34.

$$-\ln \frac{C_0}{C_t} = k_1 t \quad \textbf{(4.3.34)}$$

Where, C_0 = initial substrate concentration (mg/L); C_t= substrate concentration at any time of treatment (mg/L); k_1= apparent first-order rate constant (min^{-1}) and value of k comes from the slope of a plot between time and C_0/C_t.

4.3.6 Synergistic Studies

In order to investigate the photo-activity of MMO anode, synergistic studies were performed by three different techniques which include PC (interaction of light with anode surface), EO (constant applied current only) and PEC (constant applied current and light) at optimized conditions (Zhao et al., 2007). The synergistic studies were performed in order to check the degradation efficiency of the dual-process over the single process as well as some of both processes. In the present work, the synergy of one process over other for dual effect has been quantified using kinetic rate constant obtained through pseudo-first-order reactions as discussed in section 3.9.1. The oxidation experiments of urine metabolites i.e. uric acid, creatinine and urea were performed with MMO in a batch reactor under UV and solar light. The results of PEC under natural solar radiations for each urine metabolite were found almost similar to EO experimental results. Hence, the results for metabolites under solar radiation were not discussed in this experimental research study. Figure 4.3.16a,b,c shows the results for % removal of urine metabolites treated with different processes i.e. PC, EO, and PEC. Among all the processes, %Degradation of each urine metabolite was found maximum in the dual process i.e. PEC over individual processes. Furthermore, treatment time for each urine metabolite through PEC was also found to be reduced for achieving the same %Degradation during EO treatment. PC treatment was found less efficient for the removal treatment

of metabolites as compared to the other two processes. Negligible or very less amount of reduction in the concentration of uric acid (only 5%), creatinine (20%) and urea (28%) was observed when treated with PC. Based on the results of synergistic studies, the rate of degradation was studied at optimized conditions. The plot between C_t/C_o and time (pseudo-first-order kinetic) has been studied as shown in Figure 4.3.17a,b,c. From the Figure 4.3.18a, it was depicted that there was an immense increase in the first-order rate constant (as calculated from Equation 3.9.3) in case of PEC (0.3405 min^{-1}) was observed, which was 103 times of PC (0.0033 min^{-1}) and 1.14 times as compared to EO (0.2982 min^{-1}).

Similarly in the case of creatinine and urea first-order rate constant for the dual-process was much higher than individual processes i.e. PC and EO as shown in Figure 4.3.18b,c respectively. Thus, proves the viability of the dual-process over single treatment processes. Moreover, a synergistic effect of the dual-process for over EO came out to be 12.42%, 16.59%, 31.75% and over PC was observed 99.03%, 91.03%, 92.90 for uric acid, creatinine and urea respectively as quantified from Equation 3.9.1. The overall % synergy for urine metabolites such as uric acid (11.45%), creatinine (7.62%) and urea (24.66%) was calculated from Equation 3.9.2. Therefore, it concludes that the dual-process with synergistic results prompts its field-scale applications for the wastewater treatment with a significant decrease in treatment time from 7 min to 5 min (uric acid), 85 to 60 min (creatinine) and 135 to 95 min (urea). To further confirm our claim, experimental studies were carried out using fluorescence spectroscopy for the estimation of $OH^{\bullet}$ production at MMO under different light sources, pH, time intervals and current.

Fluorescence spectroscopy: In order to detect and quantify the short-lived $OH^{\bullet}$ species production on MMO anodes during treatment processes, fluorescence spectroscopy was performed. Figure 4.3.19a showed that maximum $OH^{\bullet}$ production was found during PEC under UV radiations than PEC (under solar radiations) and EO at 425 nm. This might happen due to the activation of photoactive layers i.e. TiO_2 of anode under light sources leading to the photo-generated e^-/h^+ pairs on the surface of the anode which oxidizes the compound adsorbed on the surface (Khan et al., 2015). Hence, resulting in more % COD removal in less time. From the results, it was also concluded that MMO is more photoactive under UV radiations than in solar radiation might be due to the high band-gap which lies in the UV range. Therefore, resulting in less production of reactive oxidant species like $OH^{\bullet}$ under solar radiation. Hence, it confirms that along with RCS, $OH^{\bullet}$ was also

involved during the treatment of all urine metabolites. From the literature survey, it was also observed that the pH of the solution has a great effect on the generation of $OH^{\bullet}$ during the treatment process (Wu et al., 2014). In order to verify the effect of pH on the generation of $OH^{\bullet}$, experiments were performed at different pH. From the results, as shown in Figure 4.3.19b it was found that more $OH^{\bullet}$ production was observed at acidic pH over basic and neutral pH. Moreover, with increasing time, the generation of $OH^{\bullet}$ at MMO was also increasing. Figure 4.3.19c shows the production of $OH^{\bullet}$ at different values of applied current. As it can be seen that $OH^{\bullet}$ production first increases with increasing current up to 0.7A after that it has been found that $OH^{\bullet}$ production decreases with increasing current values. This might be due to the consumption of $OH^{\bullet}$ by OER at higher values of current. Hence, from the experimental results, it concludes that the degradation of all urine metabolites was found to be majorly due to indirect oxidation via RCS and precisely by $OH^{\bullet}$ at optimized conditions. Hence, the effectiveness of the dual-process over a discrete process i.e. EO was proved.

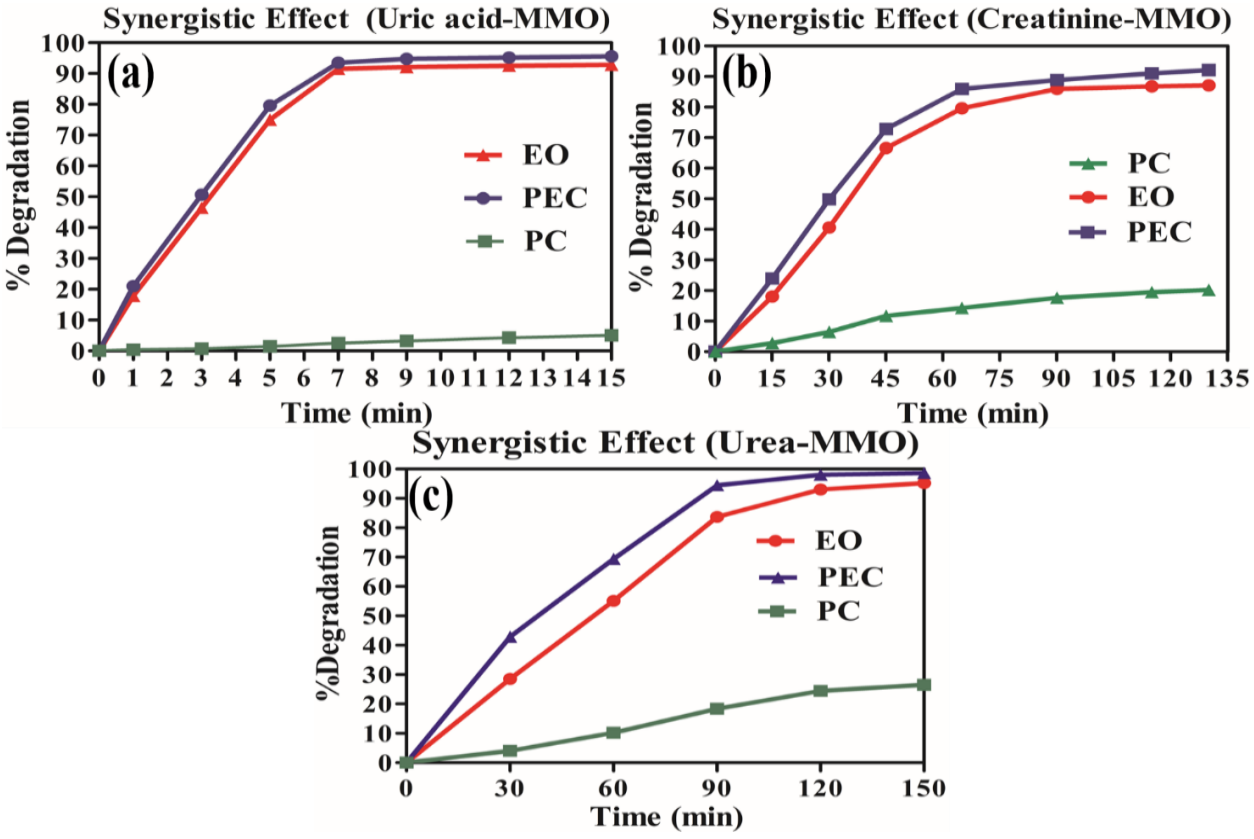

Figure 4.3.16 Comparison between different processes for the treatment of (a) uric acid, (b) creatinine and (c) urea with MMO at optimized conditions.

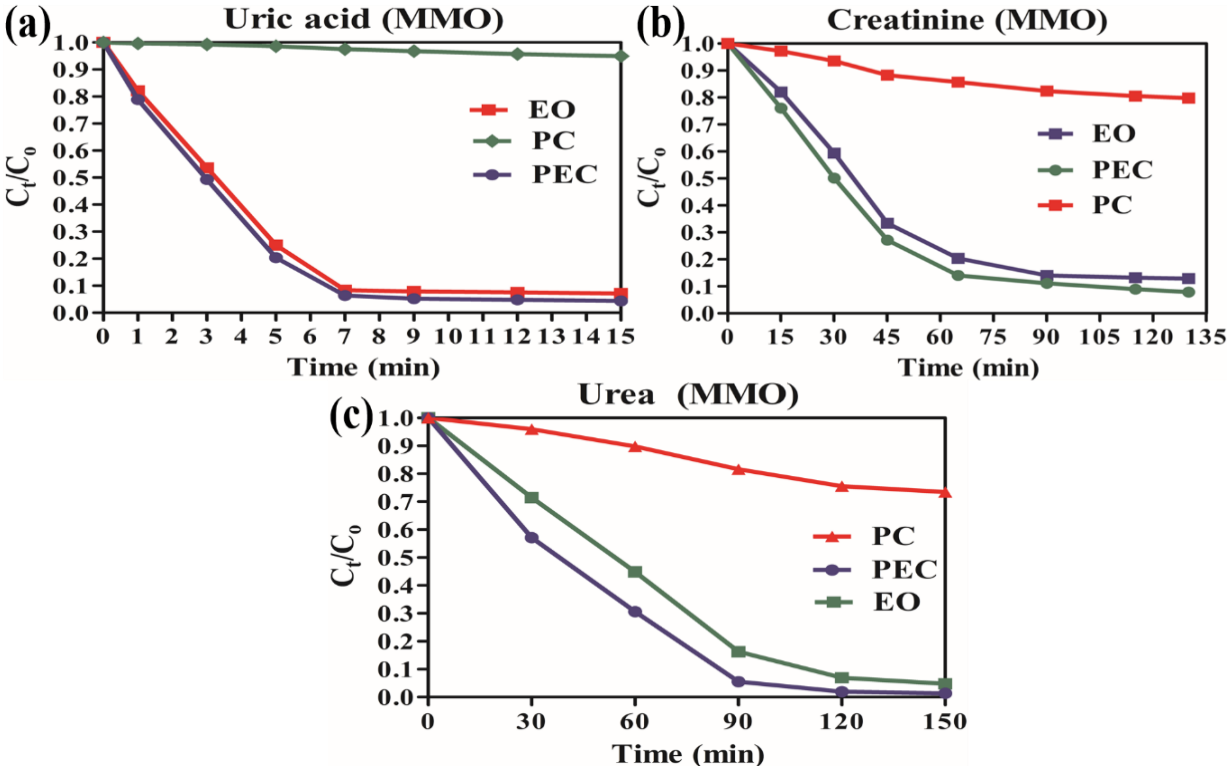

Figure 4.3.17 Plot of C_0/C_t versus time for each urine metabolites i.e. (a) uric acid, (b) creatinine and (c) urea treated with MMO at optimized conditions.

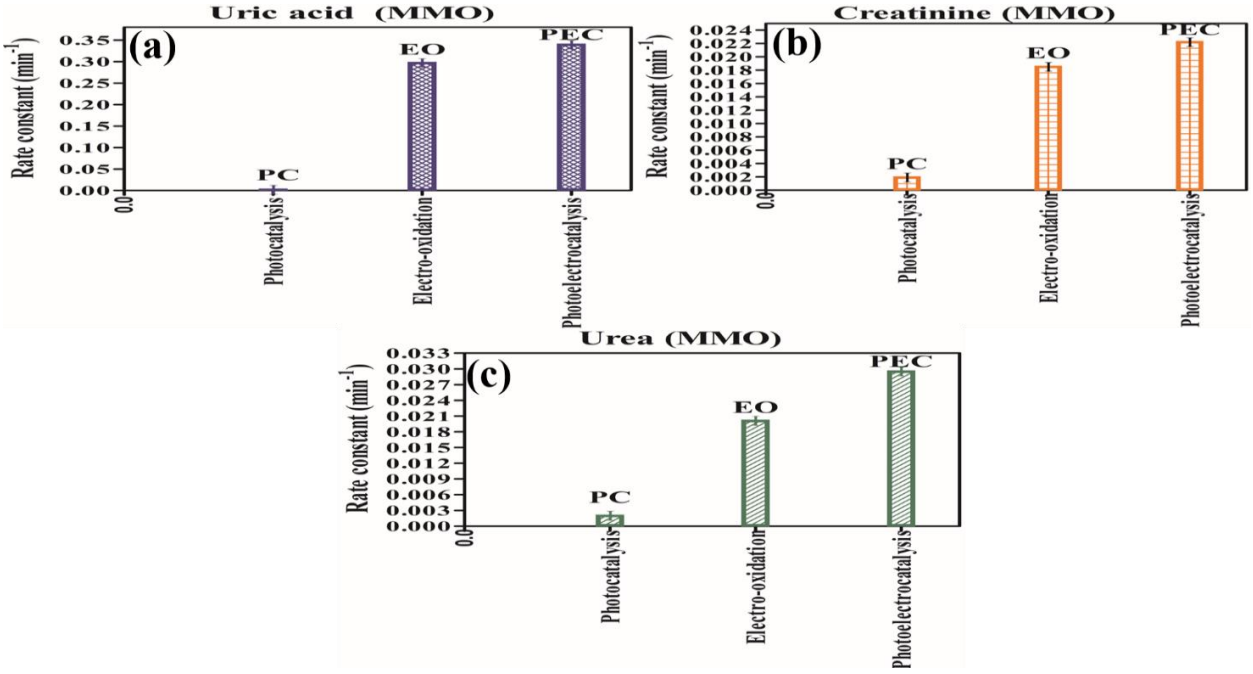

Figure 4.3.18 Plot of First-order rate constant versus different processes for the treatment of (a) uric acid, (b) creatinine and (c) urea with MMO.

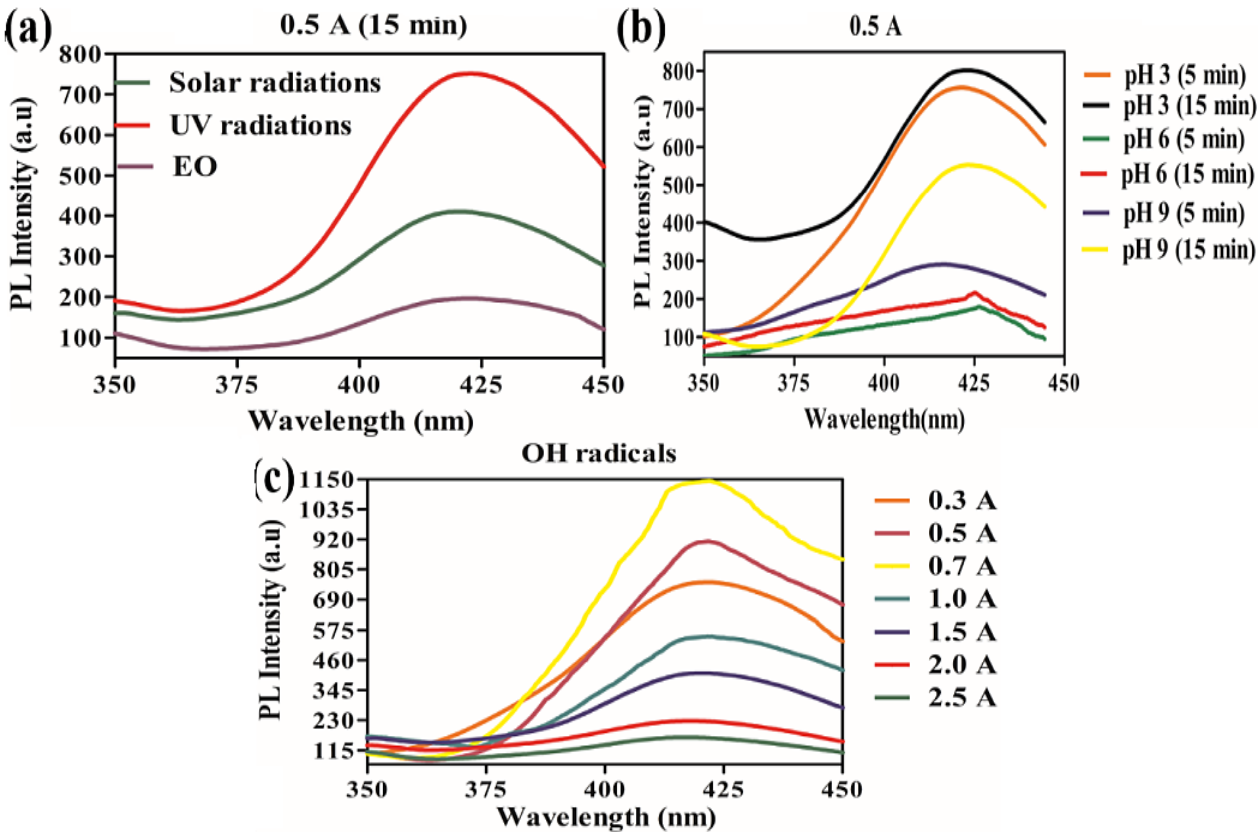

Figure 4.3.19 PL spectra of OH• (a) for different light sources at 0.5A; (b) for different pH at different time intervals and (c) at different current values using MMO anode.

4.3.7 Economic Evaluation

In literature, several studies deal with the EO process for the treatment of various organic pollutants without much pay attention to economic evaluation. The total operational cost for EO treatment process includes the expenses of electrodes, cost of stirring, cost of chemical and electrical energy consumed. However, the treatment process is being energy-intensive, the total cost for operation is mainly due to the cost of the electrode and electrical power employed. In the present study, the overall cost of the treatment process for the removal of each urine metabolites from aqueous solution was calculated using Equation 4.3.35.

$$\text{Operating cost} = C_{EC} + C_{EL} \quad \textbf{(4.3.35)}$$

Where C_{EC} = cost of energy consumed (kWh/m^3) and C_{EL}= cost of electrodes (Rs). The cost of an electrode and electrical energy consumed to remove per kg of each urine metabolite i.e. urea

from aqueous solution were calculated from the responses of the EO experiment conducted at optimized conditions as shown in Table 4.3.8.

Table 4.3.8: Evaluation of operating cost of the EO treatment process for urea treated with MMO
(A) Cost of Electrical Energy consumption
Electrical energy consumed = 20.54 kWh/m^3
Electricity price in Punjab, (India) = Rs 5.00/kWh
Cost of electrical energy consumed (C_{EC}) = Rs 102.7/m^3
Cost of electrical energy consumed to remove per kg of urea ($C_{EC)}$ = Rs 54.178/m^3
(B) Cost of Electrodes
Initial urea concentration in wastewater = 2000 mg/L= 2 kg/m^3
With 94.78% Degradation, concentration of urea removed =1.8956 kg/m^3
Urea concentration (1.8956 kg/m^3) reduced in time = 135 min = 2.25 h
Concentration of urea removed in 1h = 0.8425kg/m^3
Cost of one MMO anode = Rs 720/-
The life span of anode specified by manufacturer/supplier = 5 years
Cost of anode for 43800 h = Rs 720/-
Cost of anode for 1 h = Rs 0.01644/-
Cost of electrodes to remove per kg urea from wastewater = Rs 0.0195/m^3
(C) Operating cost analysis
Total operating cost for per kg of urea removal = 0.0195/m^3 + 54.178/m^3 = Rs 54.198/m^3
The overall operating cost of EO treatment of urea in US dollars = 0.778 \$/m^3 ≈ 0.78 \$/m^3

Similarly, the total operating cost for treating per kg of uric acid and creatinine at optimized conditions came out to be 0.83 \$/m^3 and 28.27 \$/m^3 respectively. Although this is a close approximation of the cost analysis for EO treatment yet the cost factor can be minimized further for scale-up studies with effective reactor designing. The results show that the economic feasibility of the EO process for the treatment of synthetic urine wastewater using MMO anode.

4.4 Study on EO Treatment of Urine Metabolites (i.e. Uric Acid, Creatinine and Urea) with Doped-MMO.

4.4.1 Model Fitting and Statistical Analysis

For designing the EO experimental runs for the treatment of each urine metabolite with doped-MMO, BBD coupled RSM has been employed. Four independent operational parameters such as initial pH (X_1), current density (X_2), treatment time (X_3) and NaCl dose (X_4), while %Degradation (Y_1) and Energy consumption (Y_2) were chosen as responses. The coded values along with the selected range of chosen parameters based on preliminary data were listed in Table 4.4.1. Total 30 number of experimental runs designed by BBD for all urine metabolites i.e. uric acid, creatinine and urea were conducted and calculated values of both responses were shown in Table 4.4.2a,b,c respectively.

Table 4.4.1 Range and coded levels of selected input operational variables for EO treatment of all urine metabolites with doped-MMO

			Range of actual and coded variables		
Compounds	Factors	Variables	-1	0	+1
(a) Uric Acid	X_1	Initial pH	3	7	11
	X_2	Current density , j (mA/cm^2)	2.38	7.14	11.90
	X_3	Treatment time, t (min)	5	30	55
	X_4	NaCl dose (n) (g/L)	0.25	0.75	1.25
(b) Creatinine	X_1	Initial pH	3.5	6.5	9.5
	X_2	Current density , j (mA/cm^2)	9.50	19.04	28.57
	X_3	Treatment time, t (min)	60	120	180
	X_4	NaCl dose (n) (g/L)	0.75	1.38	2.00
(c) Urea	X_1	Initial pH	2	5	8
	X_2	Current density , j (mA/cm^2)	19.04	33.33	47.61
	X_3	Treatment time, t (min)	80	160	240
	X_4	NaCl dose (n) (g/L)	1.5	3.25	5.00

Table 4.4.2a BBD matrix for EO treatment of uric acid with doped-MMO and their experimental results.

Run	Std	Block	pH	j (mA/cm^2)	t (min)	n (g/L)	% Degradation, Y_1	Energy consumption, Y_2 (kWh/m^3)
1	2	Block1	7	11.90	30	0.25	15	6.68
2	1	Block1	7	2.38	30	0.25	19	0.5
3	5	Block1	3	7.14	5	0.75	27	0.34
4	8	Block1	11	7.14	55	0.75	50	3.93
5	4	Block1	7	11.90	30	1.25	60	4.2
6	3	Block1	7	2.38	30	1.25	17	0.35
7	10	Block1	7	7.14	30	0.75	65	2.1
8	6	Block1	3	7.14	55	0.75	98	3.45
9	7	Block1	11	7.14	5	0.75	24	0.37
10	9	Block1	7	7.14	30	0.75	65	2.1
11	18	Block 2	7	7.14	55	1.25	55	3.2
12	20	Block 2	7	7.14	30	0.75	65	2.1
13	17	Block 2	7	7.14	55	0.25	31	6.83
14	11	Block 2	3	2.38	30	0.75	36	0.39
15	12	Block 2	3	11.90	30	0.75	75	4.86
16	14	Block 2	11	11.90	30	0.75	40	5.2
17	13	Block 2	11	2.38	30	0.75	29	0.45
18	19	Block 2	7	7.14	30	0.75	65	2.1
19	15	Block 2	7	7.14	5	0.25	7	0.64
20	16	Block 2	7	7.14	5	1.25	10	0.31
21	26	Block 3	3	7.14	30	1.25	88	1.69
22	25	Block 3	3	7.14	30	0.25	42	3.68
23	22	Block 3	7	11.90	5	0.75	12	0.86
24	29	Block 3	7	7.14	30	0.75	65	2.1
25	23	Block 3	7	2.38	55	0.75	22	0.74
26	21	Block 3	7	2.38	5	0.75	4	0.07
27	24	Block 3	7	11.90	55	0.75	44	9.08
28	30	Block 3	7	7.14	30	0.75	65	2.1
29	27	Block 3	11	7.14	30	0.25	20	3.86
30	28	Block 3	11	7.14	30	1.25	48	1.86

Table 4.4.2b BBD matrix for EO treatment of creatinine with doped-MMO and their experimental results.

Run	Std	Block	pH	j (mA/cm^2)	t (min)	n (g/L)	%Degradation Y_1	Energy consumption Y_2, (kWh/m^3)
1	6	1	5.5	14.28	65	0.75	32	28.5
2	7	1	5.5	14.28	115	0.25	38	14.61
3	3	1	9	21.42	65	0.75	88	24.8
4	5	1	5.5	14.28	15	0.25	14	5
5	4	1	5.5	14.28	115	1.25	29	27.4
6	10	1	2	7.14	65	0.75	68	28.4
7	1	1	5.5	14.28	15	1.25	46	29.32
8	9	1	2	21.42	65	0.75	68	28.4
9	2	1	5.5	14.28	65	0.75	20.5	31.6
10	8	1	9	7.14	65	0.75	77	84.33
11	19	2	5.5	21.42	15	0.75	68	28.4
12	15	2	5.5	14.28	65	0.75	27	11.2
13	17	2	5.5	7.14	15	0.75	39.5	61.38
14	13	2	9	14.28	65	0.25	92	39.42
15	20	2	5.5	14.28	65	0.75	68	28.4
16	11	2	5.5	7.14	115	0.75	42	13.8
17	16	2	2	14.28	65	0.25	25.5	7.8
18	14	2	5.5	21.42	115	0.75	34	44.1
19	12	2	9	14.28	65	1.25	12	14.9
20	18	2	2	14.28	65	1.25	71.5	44.4
21	30	3	5.5	7.14	65	0.25	68	28.4
22	26	3	2	14.28	115	0.75	37.5	13.2
23	22	3	5.5	14.28	65	0.75	22	10.4
24	21	3	5.5	14.28	65	0.75	49	9.46
25	25	3	9	14.28	115	0.75	19	15.4
26	24	3	9	14.28	15	0.75	24	58.2
27	27	3	2	14.28	15	0.75	51	45.12
28	28	3	5.5	7.14	65	1.25	83.5	38.82
29	23	3	5.5	21.42	65	1.25	78	54.6
30	29	3	5.5	21.42	65	0.25	68	28.4

Table 4.4.2c BBD matrix for EO treatment of urea with doped-MMO and their experimental results.

Std	Run	Block	j (mA/cm^2)	n (g/L)	t (min)	pH	% Degradation, Y_1	Energy consumption, Y_2 (kWh/m^3)
7	1	1	33.33	3.25	240.00	2.00	93	74.55
2	2	1	47.61	1.50	160.00	5.00	36	107.56
1	3	1	19.04	1.50	160.00	5.00	39	27.38
4	4	1	47.61	5.00	160.00	5.00	80	87.12
5	5	1	33.33	3.25	80.00	2.00	41	26.59
3	6	1	19.04	5.00	160.00	5.00	44	21.87
10	7	1	33.33	3.25	160.00	5.00	72	55.07
9	8	1	33.33	3.25	160.00	5.00	72	55.07
6	9	1	33.33	3.25	80.00	8.00	20	29.16
8	10	1	33.33	3.25	240.00	8.00	49.5	86.1
16	11	2	33.33	5.00	160.00	2.00	85	46.98
15	12	2	33.33	1.50	160.00	2.00	47.5	56.01
19	13	2	33.33	3.25	160.00	5.00	72	55.07
20	14	2	33.33	3.25	160.00	5.00	72	55.07
13	15	2	19.04	3.25	240.00	5.00	53	37.2
14	16	2	47.61	3.25	240.00	5.00	76	145
11	17	2	19.04	3.25	80.00	5.00	18.5	12.66
18	18	2	33.33	5.00	160.00	8.00	52	53.21
12	19	2	47.61	3.25	80.00	5.00	31	48.99
17	20	2	33.33	1.50	160.00	8.00	32.5	59.42
27	21	3	33.33	1.50	240.00	5.00	46	86.1
24	22	3	47.61	3.25	160.00	8.00	40	100.45
29	23	3	33.33	3.25	160.00	5.00	72	55.07
30	24	3	33.33	3.25	160.00	5.00	72	55.07
22	25	3	47.61	3.25	160.00	2.00	84	92.41
21	26	3	19.04	3.25	160.00	2.00	50	23.47
26	27	3	33.33	5.00	80.00	5.00	34	25.66
25	28	3	33.33	1.50	80.00	5.00	17	29.16
23	29	3	19.04	3.25	160.00	8.00	42.5	26.14
28	30	3	33.33	5.00	240.00	5.00	78	74.2

The quadratic model was suggested for all urine metabolites by exploiting the sequential model sum of square and model summary statistics. For analyzing the particular response for further analysis, some transformations were applied in order to check the high predicted R^2 value of the

chosen model. For uric acid, square root for a response Y_1 was applied while for urea and creatinine no such transformation was required. In the case of response Y_2, natural log transformation was applied to all urine metabolites. After applying particular transformations, values of R^2, predicted R^2 and adjusted R^2 for each urine metabolite were listed in Table 4.4.3. The R^2 value in the process depicts that the selected regression model could be used to predict the degradation efficiency for all urine metabolites in the EO reactor. Moreover, values of R^2 indicate that 98- 99% of variations can be explained by input variables within the range of factors studied whereas only 1-2% of variation cannot be explained by the model. Furthermore, high values of R^2 indicates the satisfactory interaction between predicted and observed values of experimental runs as well as confirmed that the model fit is significant for the manual regression analysis of experimental data.

Table 4.4.3 Various R-squared values for the quadratic model suggested by BBD for responses %Degradation (Y_1) and Energy consumption (Y_2) of all urine metabolites treated with doped-MMO

Compound	Responses	R-Squared	Adj R-Squared	Pred R Squared
(a) Uric acid	Y_1	0.9851	0.9691	0.8836
	Y_2	0.9978	0.9954	0.9834
(b) Creatinine	Y_1	0.9875	0.9740	0.8997
	Y_2	0.9980	0.9959	0.9845
(c) Urea	Y_1	0.9954	0.9905	0.9632
	Y_2	0.9995	0.9989	0.9957

The quadratic model for all urine metabolites was further analyzed using ANOVA. Table 4.4.4a,b,c shows the results of the quadratic model fitting in the form of analysis of variance (ANOVA). The higher F values and lower p values ($p<0.0001$) for both responses of all urine metabolites indicate that model terms are significant with a 95% confidence level and there may be a chance of only less than 0.01% that F-value of the chosen model could occur due to noise. Additionally, the values of an adequate precision ratio came out to be more than 4 shows the good fitting model to navigating the % degradation of urine metabolites in design space. The high value of mean square depicts that lack of fit is not significant and the model has favorable prediction ability. On the other hand, the coefficient of variance (CV) for all urine metabolites has exhibited the good accuracy and reproducibility of the results of the experimental runs. The relationship

between the responses and independent input parameters in terms of coded factors for all urine metabolites were expressed by the quadratic model equation, shown in Equations 4.4.1 - 4.4.6.

Uric acid:

$$Sqrt(Y_1) = + 8.06 + 0.85*X_1 + 0.95*X_2 + 1.66*X_3 – 0.88*X_4 – 1.81*X_1^2 – 1.44*X_2^2 – 1.88*X_3^2 + 0.37*X_4^2 + 1.03*X_1*X_2 + 0.12*X_1*X_3 – 0.43*X_1*X_4 + 0.33*X_2*X_3 – 0.11*X_2*X_4 – 0.63*X_3*X_4 \quad \textbf{(4.4.1)}$$

$$Ln(Y_2) = +0.74 + 1.26*X_1 – 0.32*X_2 + 1.17*X_3 + 0.047*X_4 - 0.43*X_1^2 + 0.15*X_2^2 - 0.57*X_3^2 + 0.025*X_4^2 - 0.027*X_1*X_2 - 3.145E\text{-}004*X_1*X_3 - 0.019*X_1*X_4 – 8.319E\text{-}003*X_2*X_3 + 0.012*X_2*X_4 + 0.011*X_3*X_4 \quad \textbf{(4.4.2)}$$

Creatinine:

$$Y_1 = + 68.00 – 21.12*X_1 + 11.00*X_2 + 12.21*X_3 + 18.25*X_4 – 10.77*X_1^2 – 10.58*X_2^2 – 15.65*X_3^2 – 11.33*X_4^2 - 8.37*X_1*X_2 - 6.75*X_1*X_3 – 7.00*X_1*X_4 + 8.37*X_2*X_3 + 3.50*X_2*X_4 + 5.25*X_3*X_4 \quad \textbf{(4.4.3)}$$

$$Ln(Y_2) = + 3.35 + 0.044*X_1 – 0.11*X_2 + 0.87*X_3 + 0.54*X_4 + 7.879E\text{-}003*X_1^2 - 0.027*X_2^2 - 0.20*X_3^2 - 0.14*X_4^2 + 6.203E\text{-}003*X_1*X_2 - 7.720E\text{-}003*X_1*X_3 + 8.873E\text{-}003*X_1*X_4 + 9.486E\text{-}003*X_2*X_3 + 9.402E\text{-}004*X_2*X_4 + 3.141E\text{-}003*X_3*X_4 \quad \textbf{(4.4.4)}$$

Urea:

$$Y_1 = + 72.00 + 8.33*X_1 + 12.92*X_2 - 13.67*X_3 + 19.50*X_4 – 11.31*X_1^2 – 11.69*X_2^2 – 5.94*X_3^2 - 15.94*X_4^2 + 9.75*X_1*X_2 - 9.12*X_1*X_3 + 2.62*X_1*X_4 – 4.50*X_2*X_3 + 3.75*X_2*X_4 – 5.62*X_3*X_4 \quad \textbf{(4.4.5)}$$

$$Ln(Y_2) = + 4.01 + 0.68*X_1 – 0.083*X_2 + 0.051*X_3 + 0.54*X_4 – 0.11*X_1^2 - 0.061*X_2^2 - 9.483E\text{-}003*X_3^2 - 0.15*X_4^2 + 3.484E\text{-}003*X_1*X_2 - 6.080E\text{-}003*X_1*X_3 + 1.814E\text{-}003*X_1*X_4 + 0.016*X_2*X_3 - 5.220E\text{-}003*X_2*X_4 + 0.013*X_3*X_4 \quad \textbf{(4.4.6)}$$

Table 4.4.4a ANOVA results of uric acid treated with doped-MMO suggested by BBD for responses (Y_1 and Y_2)										
Sources	% Degradation, (Y_1)					Energy Consumption, (Y_2)				
	Sum of square	DF	Mean square	F-value	Prob>F	Sum of square	DF	Mean square	F-value	Prob>F
Block	0.50	2	0.25			0.043	2	0.021		
Model	122.87	14	8.78	61.41	< 0.0001	40.42	14	2.89	421.12	< 0.0001
X_1	8.57	1	8.57	60.00	< 0.0001	18.91	1	18.91	2757.60	< 0.0001
X_2	10.75	1	10.75	75.23	< 0.0001	1.21	1	1.21	176.62	< 0.0001
X_3	33.04	1	33.04	231.18	< 0.0001	16.56	1	16.56	2415.40	< 0.0001
X_4	9.25	1	9.25	64.75	< 0.0001	0.027	1	0.027	3.94	0.0688
X_1^2	22.37	1	22.37	156.54	< 0.0001	1.28	1	1.28	186.06	< 0.0001
X_2^2	14.30	1	14.30	100.08	< 0.0001	0.16	1	0.16	23.68	0.0003
X_3^2	24.31	1	24.31	170.11	< 0.0001	2.20	1	2.20	320.74	< 0.0001
X_4^2	0.96	1	0.96	6.70	0.0225	4.122E-003	1	4.122E-003	0.60	0.4520
X_1X_2	4.22	1	4.22	29.53	0.0001	2.881E-003	1	2.881E-003	0.42	0.5281
X_1X_3	0.057	1	0.057	0.40	0.5376	3.956E-007	1	3.956E-007	5.769E-005	0.9941
X_1X_4	0.74	1	0.74	5.18	0.0404	1.424E-003	1	1.424E-003	0.21	0.6561
X_2X_3	0.44	1	0.44	3.10	0.1016	2.769E-004	1	2.769E-004	0.040	0.8438
X_2X_4	0.049	1	0.049	0.34	0.5671	5.782E-004	1	5.782E-004	0.084	0.7761
X_3X_4	1.60	1	1.60	11.21	0.0052	5.223E-004	1	5.223E-004	0.076	0.7869
Residual	1.86	13	0.14			0.089	13	6.856E-003		
Lack of fit	1.86	10	0.19			0.089	10	8.913E-003		
Pure error	0.000	3	0.000			0.000	3	0.000		
Core total	125.23	29				40.55	29			

Table 4.4.4b ANOVA results of creatinine (doped-MMO) suggested by BBD for responses (Y_1 and Y_2)										
Sources	% Degradation, (Y_1)					Energy consumption, (Y_2)				
	Sum of square	DF	Mean square	F-value	Prob>F	Sum of square	DF	Mean square	F-value	Prob>F
Block	26.72	2	13.36			4.684E-003	2	2.342E-003		
Model	16632.23	14	1188.02	73.12	< 0.0001	13.03	14	0.93	473.08	< 0.0001
X_1	5355.19	1	5355.19	329.60	< 0.0001	0.023	1	0.023	11.54	0.0048
X_2	1452.00	1	1452.00	89.37	< 0.0001	0.14	1	0.14	71.58	< 0.0001
X_3	1788.52	1	1788.52	110.08	< 0.0001	9.03	1	9.03	4587.58	< 0.0001
X_4	3996.75	1	3996.75	245.99	< 0.0001	3.46	1	3.46	1759.10	< 0.0001
X_1^2	795.50	1	795.50	48.96	< 0.0001	4.256E-004	1	4.256E-004	0.22	0.6496
X_2^2	768.05	1	768.05	47.27	< 0.0001	4.876E-003	1	4.876E-003	2.48	0.1395
X_3^2	1678.57	1	1678.57	103.31	< 0.0001	0.28	1	0.28	142.95	< 0.0001
X_4^2	880.76	1	880.76	54.21	< 0.0001	0.13	1	0.13	63.97	< 0.0001
X_1X_2	280.56	1	280.56	17.27	0.0011	1.539E-004	1	1.539E-004	0.078	0.7841
X_1X_3	182.25	1	182.25	11.22	0.0052	2.384E-004	1	2.384E-004	0.12	0.7334
X_1X_4	196.00	1	196.00	12.06	0.0041	3.150E-004	1	3.150E-004	0.16	0.6956
X_2X_3	280.56	1	280.56	17.27	0.0011	3.600E-004	1	3.600E-004	0.18	0.6759
X_2X_4	49.00	1	49.00	3.02	0.1061	3.536E-006	1	3.536E-006	1.797E-003	0.9668
X_3X_4	110.25	1	110.25	6.79	0.0218	3.947E-005	1	3.947E-005	0.020	0.8896
Residual	211.22	13	16.25	73.12	< 0.0001	0.026	13	1.968E-003		
Lack of fit	211.22	10	21.12	329.60	< 0.0001	0.026	10	2.558E-003		
Pure error	0.000	3	0.000			0.000	3	0.000		
Core total	16870.17	29				13.07	29			

Table 4.4.4c ANOVA results of urea treated with doped-MMO suggested by BBD for responses (Y_1 and Y_2)

Sources	% Degradation, (Y_1)					Energy consumption, (Y_2)				
	Sum of square	DF	Mean square	F-value	Prob>F	Sum of square	DF	Mean square	F-value	Prob>F
Block	6.20	2	3.10			3.837E-005	2	1.919E-005		
Model	13464.05	14	961.72	201.89	< 0.0001	9.33	14	0.67	1767.96	< 0.0001
X_1	833.33	1	833.33	174.94	< 0.0001	5.58	1	5.58	14791.52	< 0.0001
X_2	2002.08	1	2002.08	420.30	< 0.0001	0.083	1	0.083	220.25	< 0.0001
X_3	2241.33	1	2241.33	470.53	< 0.0001	0.031	1	0.031	82.54	< 0.0001
X_4	4563.00	1	4563.00	957.92	< 0.0001	3.44	1	3.44	9112.96	< 0.0001
X_1^2	877.53	1	877.53	184.22	< 0.0001	0.081	1	0.081	213.57	< 0.0001
X_2^2	936.67	1	936.67	196.64	< 0.0001	1.838E-003	1	1.838E-003	4.88	0.0458
X_3^2	241.74	1	241.74	50.75	< 0.0001	6.166E-004	1	6.166E-004	1.64	0.2233
X_4^2	1741.74	1	1741.74	365.65	< 0.0001	0.14	1	0.14	383.67	< 0.0001
X_1X_2	380.25	1	380.25	79.83	< 0.0001	4.854E-005	1	4.854E-005	0.13	0.7255
X_1X_3	333.06	1	333.06	69.92	< 0.0001	1.479E-004	1	1.479E-004	0.39	0.5420
X_1X_4	27.56	1	27.56	5.79	0.0318	1.316E-005	1	1.316E-005	0.035	0.8547
X_2X_3	81.00	1	81.00	17.00	0.0012	1.070E-003	1	1.070E-003	2.84	0.1159
X_2X_4	56.25	1	56.25	11.81	0.0044	1.090E-004	1	1.090E-004	0.29	0.5999
X_3X_4	126.56	1	126.56	26.57	0.0002	6.702E-004	1	6.702E-004	1.78	0.2053
Residual	61.93	13	4.76			4.902E-003	13	3.770E-004		
Lack of fit	61.93	10	6.19			4.902E-003	10	4.902E-004		
Pure error	0.000	3	0.000			0.000	3	0.000		
Core total	13532.17	29				9.34	29			

To confirm the accuracy of developed models, plots of normal % probability versus studentized residuals, studentized residuals versus predicted and predicted versus actual for the experimental data of both responses (i.e. % Degradation and Energy consumption) were examined as shown in Figure 4.4.1a,b,c. Diagnostic plots like predicted versus actual aims to find out the relationship between predicted and actual experimental values. The data points in this plot for all urine metabolites treated electrochemically with doped-MMO were found are in the proximity of the diagonal line indicating the good correlation between experimental data and predicted. The plot such as normal % probability versus studentized residuals depicts a suitable graphical method for judging the normality of residuals. From the results of the plot, it was found that residuals lie reasonably close to the straight diagonal line confirms the normal distribution of the observed data. In the case of studentized residuals versus predicted, the experimental data were scattered randomly scattered into a constant range of crossing residual graph, which indicates that the proposed model is sufficient and suitable for experimental data.

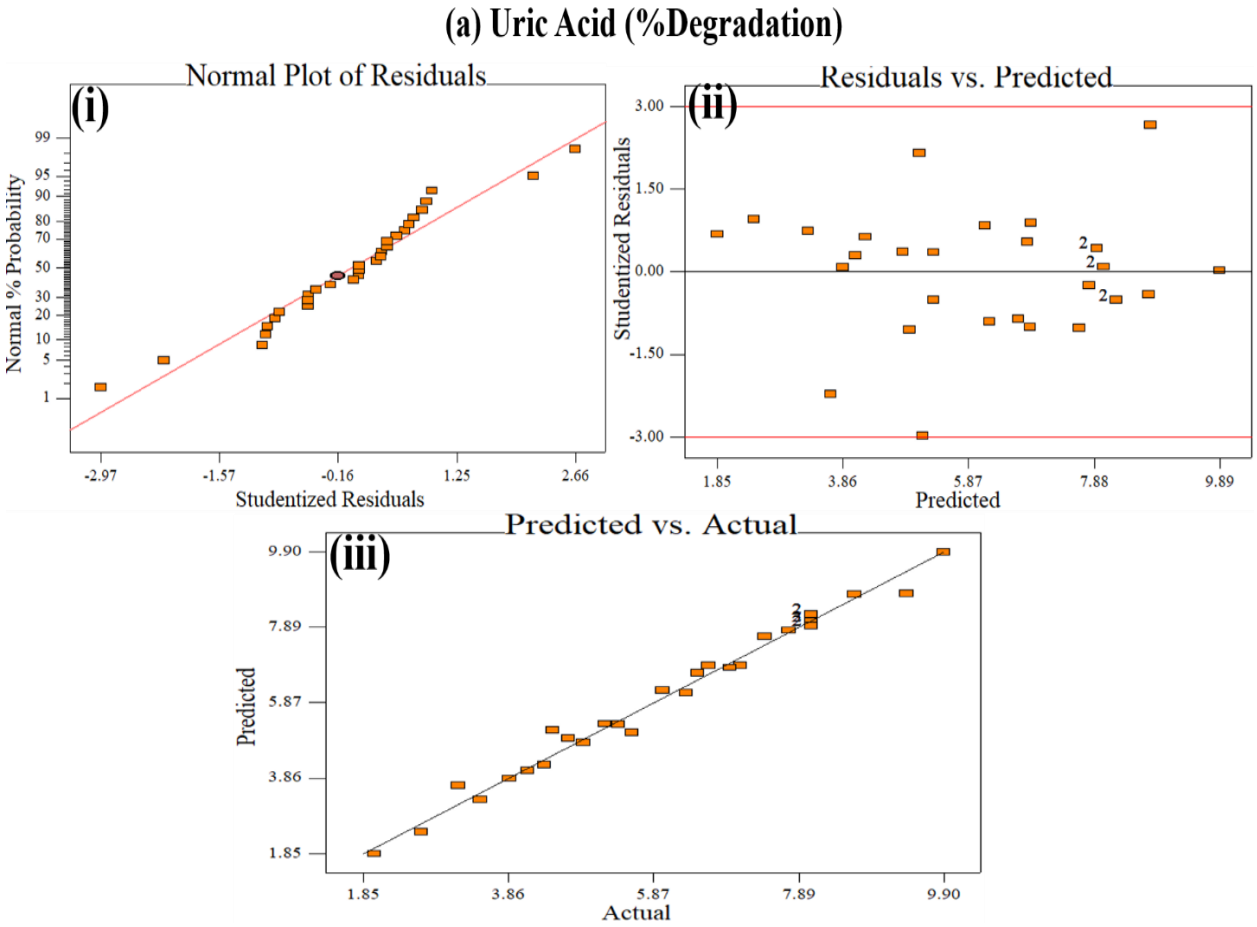

(a) Uric Acid (Energy consumed)

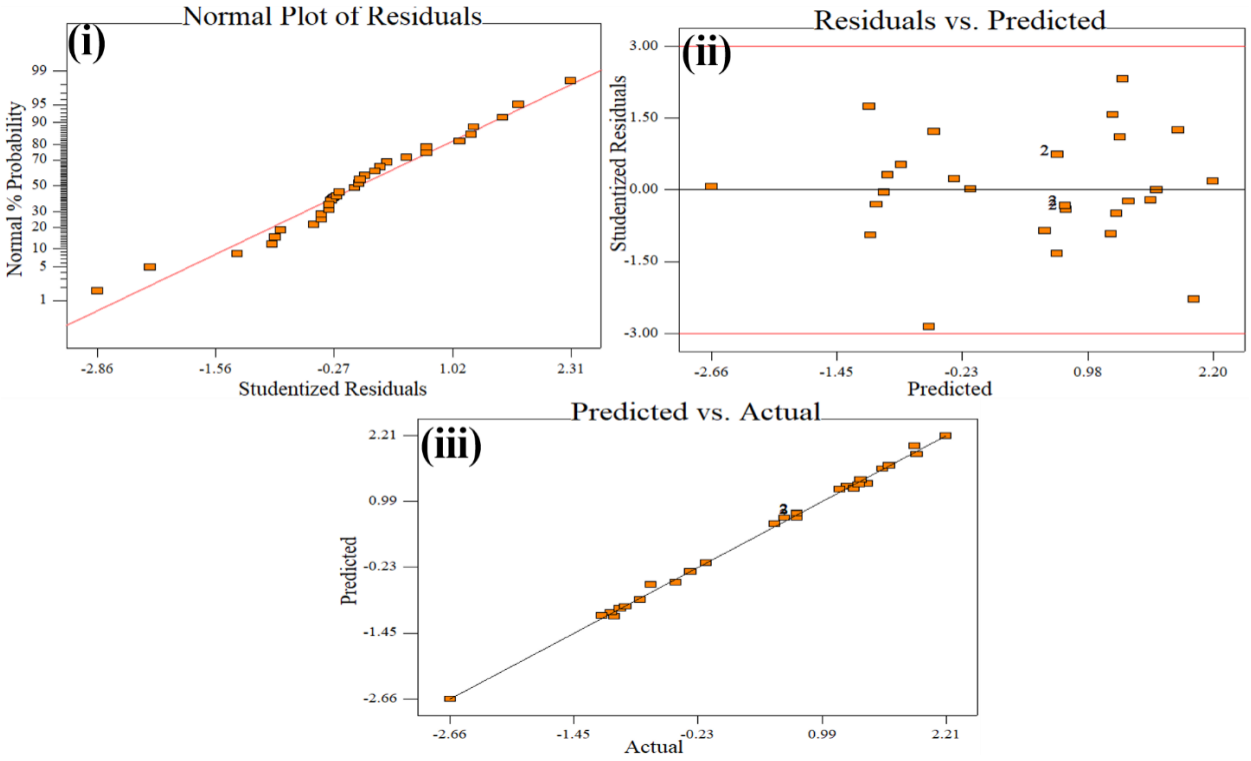

(b) Creatinine (%Degradation)

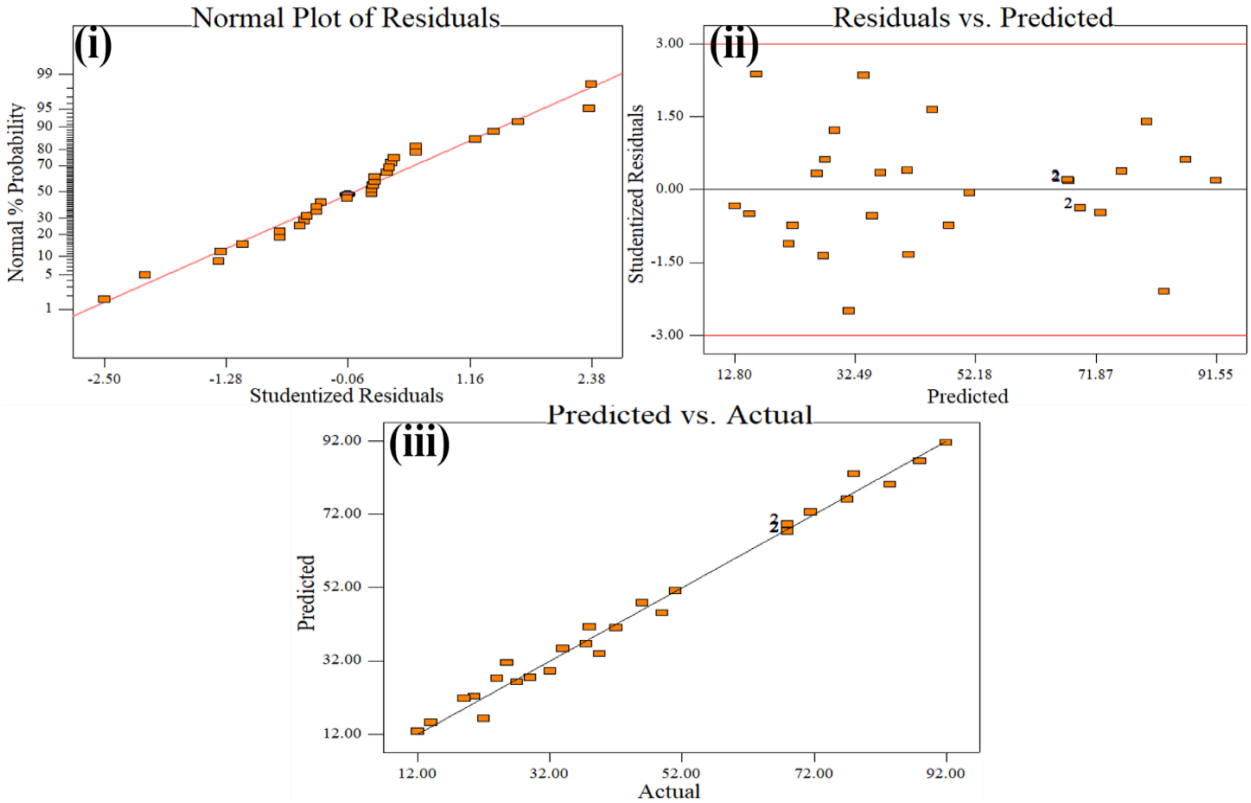

(b) Creatinine (Energy consumed)

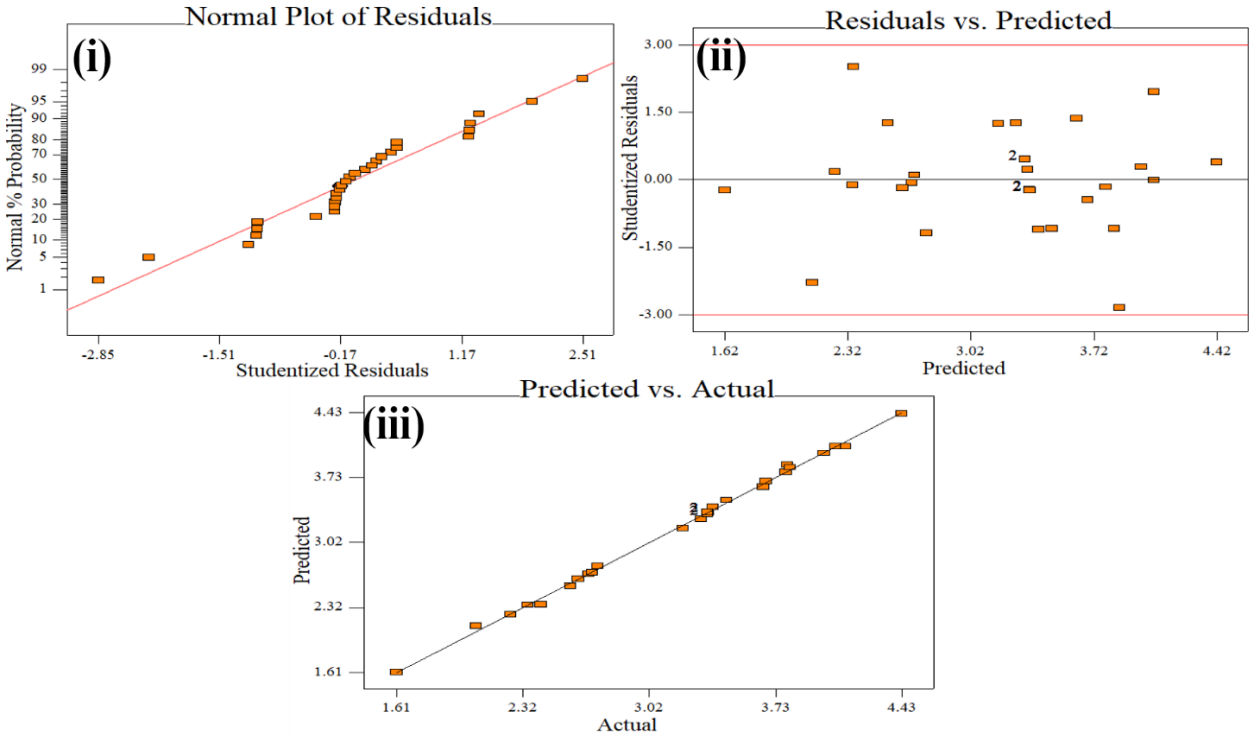

(c) Urea (%degradation)

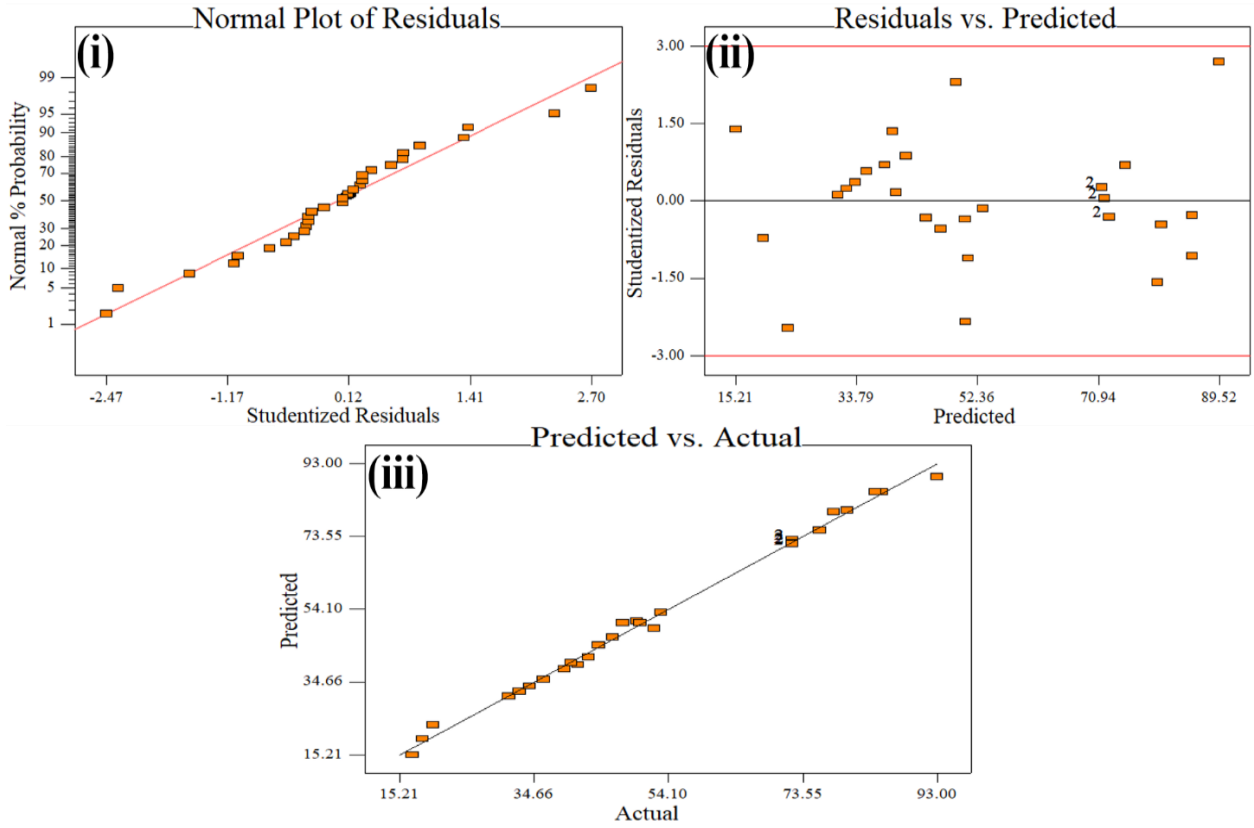

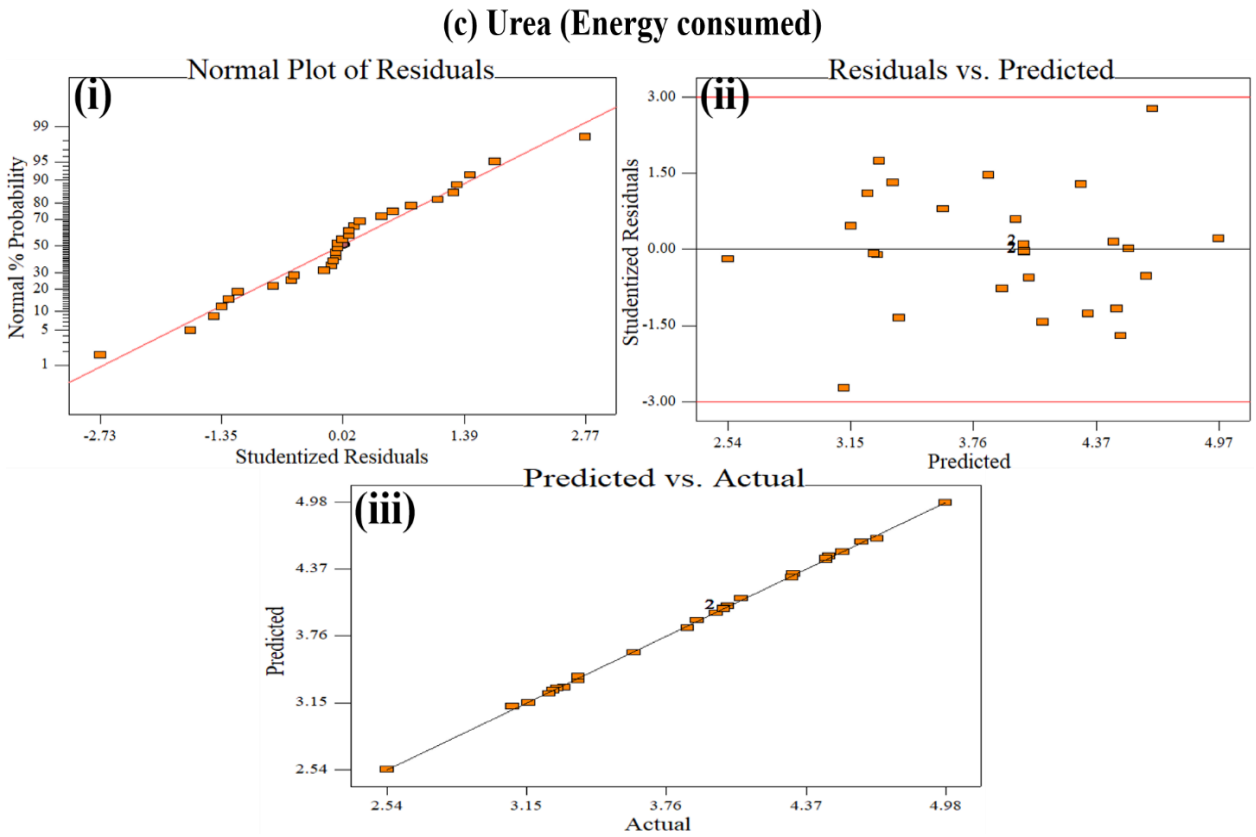

Figure 4.4.1 Plots of (i) normal % probability versus studentized residuals; (ii) studentized residuals versus predicted and (iii) predicted versus actual for responses (%Degradation and Energy consumed) of each urine metabolites i.e. (a) uric acid, (b) creatinine and (c) urea treated electrochemically with doped-MMO.

4.4.2 Effect of Process Parameters and Optimization

To visualize the effects of operational parameters on both responses, 3D response surface graphs obtained from RSM were investigated.

4.4.2.1 Effect of current density (j) and pH on % Degradation, (Y_1) of uric acid, creatinine and urea

Figure 4.4.2a shows the inter-parametric interaction of current density and pH as well as their effect on the response, Y_1 of (i) uric acid, (ii) creatinine and (iii) urea. In the EO treatment study, current density (j) is considered an important operating process factor because of the cost-effective analysis. Moreover, the generation of oxidant species, transferring of electrons and process efficiency all depends upon applied j. The effect of j on oxidation of (uric acid) was inspected by varying j from 2.38 mA/cm^2 from 11.90 mA/cm^2. From the results, it could be seen that at a lower

value of j ≈ 2.38 mA cm^{-2}, Y_1 was found constant for pH values up to 7. Further increase in pH > 7, Y_1 increased marginally. It was observed that at pH value 3, Y_1 found increasing with j values upto 9.52 mA/cm^2, then became constant with j value beyond 9.52 mA/cm^2. Further increase in pH value >5, Y_1 first increases with an increasing j value of 7.14 mA/cm^2 and then found decreasing with increasing values of j. At very high values of pH>9 Y_1 was found constant at the lower value of j upto 2.38 mA/cm^2, then increases with increasing j value ≈ 7.14 mA/$cm^2$and then decreases gradually with increasing j value > 7.14 mA/cm^2. This concludes that oxidation of uric acid was maximum at lower pH values while the minimum at high values of pH. Moreover, Y_1 was found increasing with increasing j from lower to high values. But at very high values of j, Y_1 found the minimum.

In the case of (ii) creatinine, Figure 4.4.2a showed that at lower values of j upto 14.27 mA/cm^2, Y_1 found decreasing with increasing values of pH upto 8 and then became constant when pH increased from 8 to 9.50. Thereafter, it has been seen that when the value of j increased from 14.27 mA/cm^2 to 19.04 mA/cm^2, a continuous decrease in Y_1 was observed with increasing values of pH. However, further, an increase in j value from 19.04 mA/cm^2 to 28.57 mA/cm^2, it has been observed that Y_1 was constant till pH≈ 5 and then found decreasing with increasing values of pH upto 9.5. Hence, Y_1 was found maximum at lower values of pH and middle values of j.

From Figure 4.4.2a (iii urea), it has been observed that pH has a marginal effect on Y_1. At lower values of pH upto 3.5, Y_1 was found increasing with increasing values of j upto 33.33 mA/cm^2 and thereafter Y_1 became constant when j increased from 33.33 mA/cm^2 to 47.61 mA/cm^2. However, when pH was increased from 3.5 to 8, a continuous decrease in Y_1 has been observed with increasing values of j.

From the graph results, it was also concluded that at lower values of the other two input parameters i.e. t and n, there was not much effect of j and pH was observed on Y_1. But when values of n and t increases, the effect of j and pH on Y_1 was clearly seen. This happened because, at lower values of j, generation of ROS and RCS on doped-MMO were falling down gradually with time. Due to which the current efficiency of other side reactions such as oxygen evolution reaction increased. But on increasing, j values with increasing n value helps in the generation of more oxidant species.

As discussed in the previous section, the pH of the solution is considered as a crucial factor for influencing the performance of the EO process. From experimental results, it was analyzed that maximum degradation of uric acid was achieved at lower values of pH. This was due to the high adsorption rate of generated $OH^{\bullet}$ in the oxide lattice of the anode at acidic pH (Kaur et al., 2015). Many studies in the literature have confirmed that doped-MMO acts as active anode and reactions occur on its surface during the EO treatment is the water oxidation reactions which in turn leading to the formation of adsorbed $OH^{\bullet}$. Furthermore, at acidic pH the generation of the oxidant species which high oxidant potential such as $OH^{\bullet}$, HClO, ClO^- in the bulk was more which indirectly oxidize the target pollutant. While, in the case of basic pH, it was found that the concentration of lower potential oxidant species such as H_2O_2, $HO^{\bullet}_2$, ClO_3^- and ClO_4^- was more. Thus, degradation of uric acid, creatinine and urea were found minimum at neutral and basic pH.

The concentration of electrolyte always plays a significant role because it influences the efficiency of the process by indirect oxidation. From the response graph (Figure. 4.4.2b) for (i) uric acid, it was observed that for lower values of n ≈ 0.5 g/L, Y_1 was found the minimum and constant with time up to 17.5 min. On further increase in n beyond 0.5 g/L, a gradual continuous increase in Y_1 was observed with time up to 42 min but after 42 min Y_1 remained almost unchanged.

In the case of another metabolite i.e. (ii) creatinine (Figure 4.4.2b), at lower values of n (≈1.06 g/L) and t≈ 90 min respectively, Y_1 was found constant. However, when values of n and t increased from 1.06 to 1.69 g/L and 90 to 150 min respectively, a gradual continuous increase in Y_1 was observed. Thereafter, an increase in values of n (≈ 2.00 g/L) and t ≈ (180 min) has shown no or marginal effect on Y_1. This depicts that very high and very low values of n and t have a marginal effect on Y_1.

A similar observation was observed in the case of (iii) urea (Figure 4.4.2b), where at high (≈ 4.12 mA/cm^2, 200 min) and low (≈ 2.38 mA/cm^2, 120 min) values of n and t, Y_1 was found maximum and minimum. Further increase in values of n and t beyond 4.12 mA/cm^2 at 240 min, has shown no effect as Y_1 was found constant. However, at middle values of n from 2.38 to 4.12 mA/cm^2 at t 120 min to 200 min, Y_1 was found gradually increasing with increasing values of n and t.

From the results, it was concluded that an increase in the Y_1 may be attributed due to the change in the ionic strength of the solution. The increase in ionic strength at higher values of n will generally cause an increase in current density in the same cell voltage and hence maximum Y_1 was achieved (Asaithambi and Matheswaran, 2016). It observed that after certain values of n and j, Y_1

was found the minimum. This might be happening due to the (1) scavenging of $OH^{\bullet}$ by high chloride dose, (ii)formation of more chloramines in the system (Pillai et al., 2015), (2) metal dissolution which leads to the formation of bigger flocs, (3) most of the applied current consume by gas evolution and side reactions and (4) increases the temperature of the solution.

Moreover, it was observed that prolonged electro-oxidation at higher j values always lead to the fouling of the anode because of the bond formation between pollutant and oxide lattice of an anode which grows like an impermeable film with time. Hence, for better process performance and longer service life of anodes optimization of process variables is very important.

4.4.2.2 Effect of j, n, t, and pH on Energy consumption, Y_2 of uric acid, creatinine and urea

Figure 4.4.2c has shown the effect of n and pH on Y_2 for (i) uric acid, (ii) creatinine and (iii) urea. From the response graph for (i) uric acid, it was observed that at a lower value of n ≈ 0.25 g/L, Y_2 was found maximum for all values of pH. Further increase in n values upto 0.75 g/L, a continuous decrease in Y_2 was observed at all values of pH. However, when n was increased further from 0.75 to 1.25 g/L, a gradual increase in Y_2 has been observed. This trend was seen at all values of pH. This shows that pH has no or marginal effect on Y_2. This might happen because, at lower values of n, the conductivity of solution was less due to which voltage drop increases which ultimately maximized the consumption of energy. However, when the concentration of electrolyte increases, the conductivity of the solution also increases which led Y_2 to be minimal because of the ease of current flow through the electrolyte solution. But at very high values of n, consumption of energy was more this might due to the (1) current was not enough to produce ROS and RCS species; (2) oxidation of high potential reactive species into lower potential species due to high applied current density and (3) no more formation of RCS and ROS as oxidation of pollutant completes (García-Espinoza et al., 2018). In the case of (ii) creatinine (Figure 4.4.2c), the effect of pH on Y_2 was found insignificant. From Figure 4.4.2c it has been seen that at low values on n, Y_2 was found maximum while at high values, Y_2 was observed minimum. This trend was observed at all values of pH. Similar results were also observed in the case of (iii) urea (Figure 4.4.2c).

Figure 4.4.2d has shown the effect of j and t on Y_2 of each urine metabolite i.e. (i) uric acid, (ii) creatinine and (iii) urea. From the graphs results of each urine metabolites, it was observed that with increasing values of j and t, Y_2 was also found increasing. This might happened because electrical power consumption is directly proportional to the current and time (Mondel et al., 2013). However,

it was found that the effect of pH on Y_2 was found to be marginal or less when compared to other parameters.

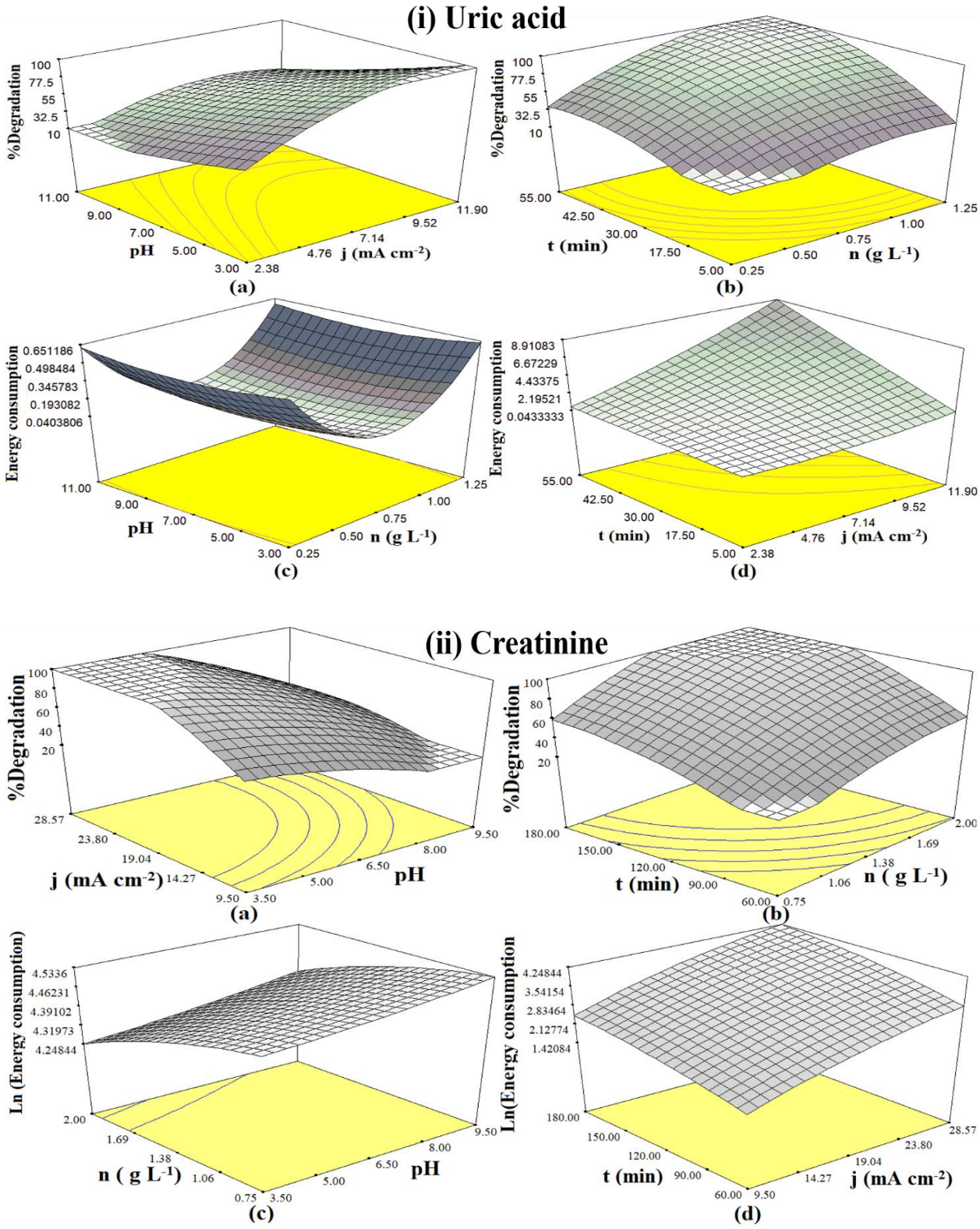

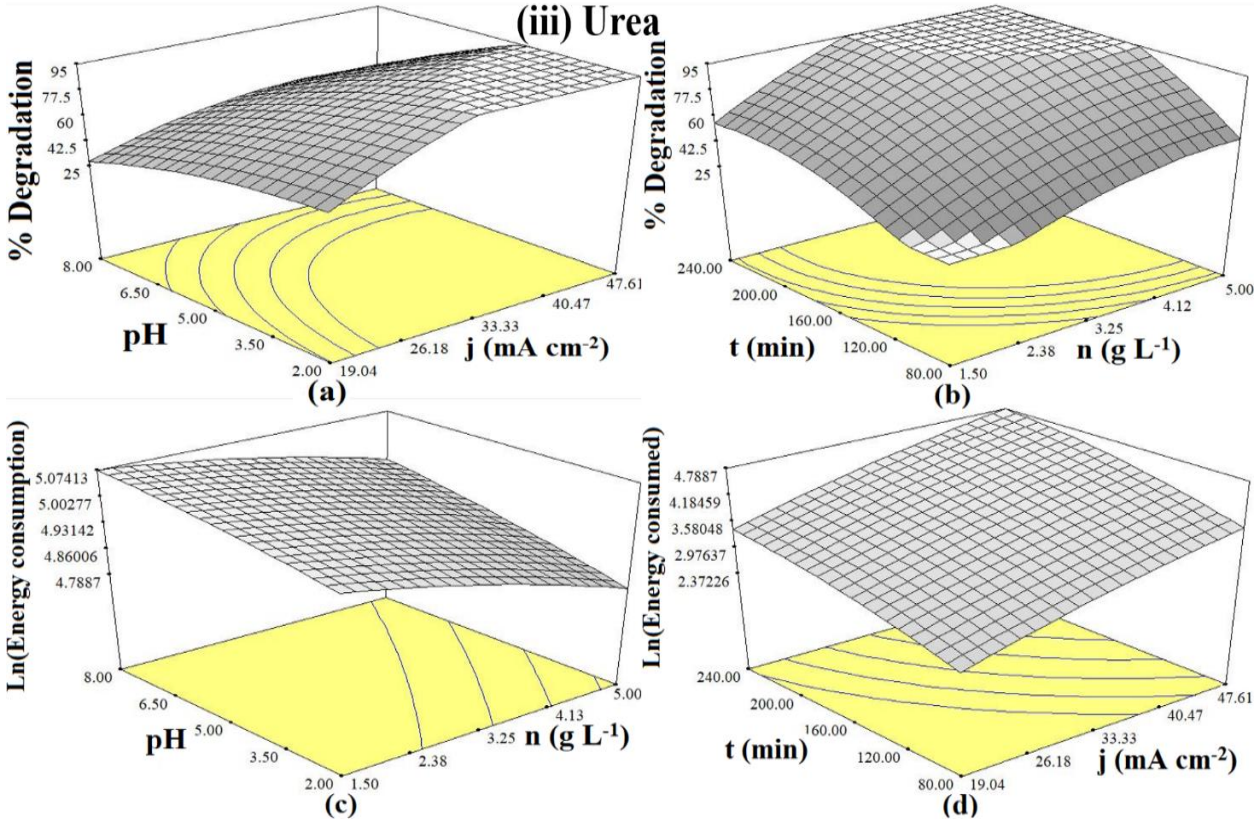

Figure 4.4.2 Effect of various input parameters (a) pH and j versus %Degradation; (b) t and n versus %Degradation; (c) n and pH versus Energy consumption and (d) t and j versus Energy consumption during the EO treatment of (i) uric acid, (ii) creatinine and (iii) urea with doped-MMO.

The statistical optimization of various input factors for the EO treatment of urine metabolites with doped-MMO anode was carried out by multi-response process optimization by desirability function approach One-sided desirability (di) and overall desirability (D) for each urine metabolite (i.e. uric acid, creatinine and urea) were calculated by using maximum and minimum acceptable values of both responses Y_1 and Y_2 as shown in Table 4.4.5 and represented in Equations 4.4.7–4.4.12.

Table 4.4.5 Constraints applied for optimization of EO treatment of each urine metabolite (a) uric acid (b) creatinine and (c) urea with doped-MMO				
Compound	Variables	Goal	Lower limit	Upper limit
(a) Uric acid	pH	is in range	3	11.0
	t (min)	is in range	5	55
	j (mA/cm^2)	is in range	2.38	11.9
	n (g/L)	is in range	0.25	1.25
	Y_1, (%Degradation)	maximize	4	98
	Y_2, (Energy consumption)	minimize	0.07	9.08
(b) Creatinine	pH	is in range	3.5	9.5
	t (min)	is in range	60	180
	j (mA/cm^2)	is in range	9.5	28.57
	n (g/L)	is in range	0.75	2
	Y_1, Sqrt(%Degradation)	maximize	12	92
	Y_2, Ln(Energy consumption)	minimize	5	84.33
(c) Urea	pH	is in range	2	8
	t (min)	is in range	80	240
	j (mA/cm^2)	is in range	19.04	47.61
	n (g/L)	is in range	1.5	5
	Y_1, (%Degradation)	maximize	17	93
	Y_2, (Energy consumption)	minimize	12.66	145

The desirability for response Y_1 for uric acid was calculated with acceptable values of $Y_{1\text{-}min}$ as 4.0% and $Y_{1\text{-}max}$ as 98.0%. Similarly, for response Y_2 of uric acid is calculated by taking $Y_{2\text{-}min}$ as 0.07 and $Y_{2\text{-}max}$ as 9.08 kWh/m^3 respectively as shown in Equation 4.4.7-4.4.8.

$$d_{1(uric\ acid)} = \begin{cases} 0 & if\ Y_1 \leq 4.00 \\ \left[\frac{Y_1 - 4.00}{98.0 - 4.00}\right] & if\ 4.00 < Y_1 < 98.0 \\ 1 & if\ Y_1 \geq 98.0 \end{cases} \quad \textbf{(4.4.7)}$$

$$d_{2\ (uric\ acid)} = \begin{cases} 0 & if\ Y_2 \leq 0.07 \\ \left[\frac{Y_2 - 0.07}{9.08 - 0.07}\right] & if\ 0.07 < Y_2 < 9.08 \\ 1 & if\ Y_2 \geq 9.08 \end{cases} \quad \textbf{(4.4.8)}$$

The desirability for both responses of the other two metabolites i.e. creatinine and urea were calculated by Equations 4.4.9- 4.4.12.

$$d_{1\,(creatinine)}= \begin{cases} 0 & if\ Y_1 \le 12.00 \\ \left[\frac{Y_1 - 12.00}{92 - 12.00}\right] & if\ 12.00 < Y_1 < 92 \\ 1 & if\ Y_1 \ge 92 \end{cases} \quad \textbf{(4.4.9)}$$

$$d_{2\,(creatinine)}= \begin{cases} 0 & if\ Y_2 \le 5.00 \\ \left[\frac{Y_2 - 5.00}{84.33 - 5.00}\right] & if\ 5.00 < Y_2 < 84.33 \\ 1 & if\ Y_2 \ge 84.33 \end{cases} \quad \textbf{(4.4.10)}$$

$$d_{1\,(urea)}= \begin{cases} 0 & if\ Y_1 \le 17.00 \\ \left[\frac{Y_1 - 17.00}{93.00 - 17.00}\right] & if\ 17.00 < Y_1 < 93.00 \\ 1 & if\ Y_1 \ge 93.00 \end{cases} \quad \textbf{(4.4.11)}$$

$$d_{2\,(urea)}= \begin{cases} 0 & if\ Y_2 \le 12.66 \\ \left[\frac{Y_2 - 12.66}{145.0 - 12.66}\right] & if\ 12.66 < Y_2 < 145.0 \\ 1 & if\ Y_2 \ge 145.0 \end{cases} \quad \textbf{(4.4.12)}$$

The simultaneous optimization of different process operating parameters was done by keeping all input factors in the range. The set of constraints were applied during the EO process optimization of urine metabolites in order to maximize the response Y_1 and minimize the response Y_2. The best optimized conditions of process parameters for uric acid were obtained at pH= 3.0, n= 1.11 g/L, j= 7.46 mA/cm^2, t = 42.79 min and showed highest D = 0.880. While for creatinine most appropriate optimized conditions were obtained at pH= 3.52, n= 1.80 g/L, j= 18.08 mA/cm^2, t = 140.65 min with D = 0.850. The optimal operating conditions for maximum removal of urea were found to be j=32.08 mA/cm^2, n= 4.66 g/L, pH= 3.4 and t= 195 min which produced combined desirability value, D =0.900. At these optimized conditions, the value for responses Y_1 and Y_2 suggested by BBD were shown in Table 4.4.6a,b,c. In order to confirm these suggested values of responses, experiments for all urine metabolites were conducted in triplicate at the optimized condition. The average experimental value of both responses Y_1 and Y_2 for urine metabolites were found very close to the predicted values and listed in Table 4.4.7. This concludes that the optimization of EO treatment of urine metabolites using BBD under RSM was successfully done.

Table 4.4.6a Individual and multi-response optimization results of uric acid treated with doped-MMO for desirability calculations					
Response	j (mA/cm^2)	n (g/L)	t (min)	pH	Desirability
Individual response optimization					
%Degradation, Y_1 = 98.02%	9.15	1.16	39.76	3.36	1
Energy consumption, Y_2 = 0.067 kWh/m^3	5.50	0.70	5.57	3.42	1
Synchronized optimization of responses					
%Degradation, Y_1 = 97.20%	7.46	1.11	42.79	3.0	0.880
Energy consumption, Y_2 = 2.588 kWh/m^3					

Table 4.4.6b Individual and multi-response optimization results of creatinine treated with doped-MMO for desirability calculations					
Response	j (mA/cm^2)	n (g/L)	t (min)	pH	Desirability
Individual response optimization					
%Degradation, Y_1 = 93.15%	28.09	1.96	119.62	4.73	1.00
Energy consumption, Y_2 = 7.85 kWh/m^3	10.56	1.89	60.00	3.81	0.964
Simultaneously optimization of responses					
%Degradation, Y_1 = 91.99%	18.08	1.80	140.65	3.52	0.850
Energy consumption, Y_2 = 26.98 kWh/m^3					

Table 4.4.6c Individual and multi-response optimization results of urea treated with doped-MMO for desirability calculations					
Response	j (mA/cm^2)	n (g/L)	t (min)	pH	Desirability
Individual Response optimization					
%Degradation, Y_1 = 97.98%	45.99	4.27	221.20	3.89	1
Energy consumption, Y_2 = 20.25 kWh/m^3	29.41	4.90	85.50	3.52	0.943
Synchronized optimization of responses					
%Degradation, Y_1 = 93.001%	32.08	4.66	195	3.4	0.900
Energy consumption, Y_2 = 53.61 kWh/m^3					

Table 4.4.7 Comparison between the predicted and actual experimental value of all urine metabolites treated with doped-MMO at optimized conditions.						
	Urine metabolites					
	Uric acid		Creatinine		Urea	
Responses	Predicted	Actual	Predicted	Actual	Predicted	Actual
%Degradation	97.20	95.35	91.99	90.002	93.001	91.15
Energy consumption (kWh/m^3)	2.588	2.479	26.98	25.83	53.61	51.53

Furthermore, the pH of all urine metabolites was found to be changed during the EO treatment with doped-MMO. EO treatment experiments were performed at optimized conditions for each urine metabolite i.e. urea, uric acid and creatinine. By analyzing Figure 4.4.3, it was found that a sharp and continuous increase in pH from 3.0 to 4.30 (uric acid), 3.5 to 7.48 (creatinine) and 3.4 to 8.4 (urea) within 60 min, 120 min, and 180 min respectively of EO treatment. However, further increase in treatment time i.e. t>60, t> 120 and t> 180 min shows the final pH (pH_f) stabilizes to ≈ 4.55 (uric acid), ≈7.60 (creatinine) and ≈8.50 (urea). The shift of pH from acidic towards alkaline could be attributed to the OER at the anode and hydrogen evolution reaction (HER) at the cathode, which involves the drastic hydroxyl ion (OH^-) generation and consumption (Wu et al., 2014). Furthermore, pH during electrolysis was found stabilized at alkaline pH due to the bicarbonate buffering effect as discussed in the earlier section (4.3.2). This change in pH depicts the involvement of both mechanisms i.e. direct and indirect oxidation method. In the present study, the degradation of urine metabolites i.e. uric acid, creatinine, and urea was happened because of both indirect

oxidation (HOCl, Cl_2, ClO^-, ClO_2^-, chloramines, H_2O_2, etc.) and direct oxidation ($OH^•$). However, the metabolites were oxidized into byproducts majorly due to the generated RCS during electrolysis which could be reported to be toxic. Therefore, it becomes necessary to verify as well as identify these toxic compounds if present in treated samples through various in-situ analytical techniques as discussed in the next section 4.4.4.

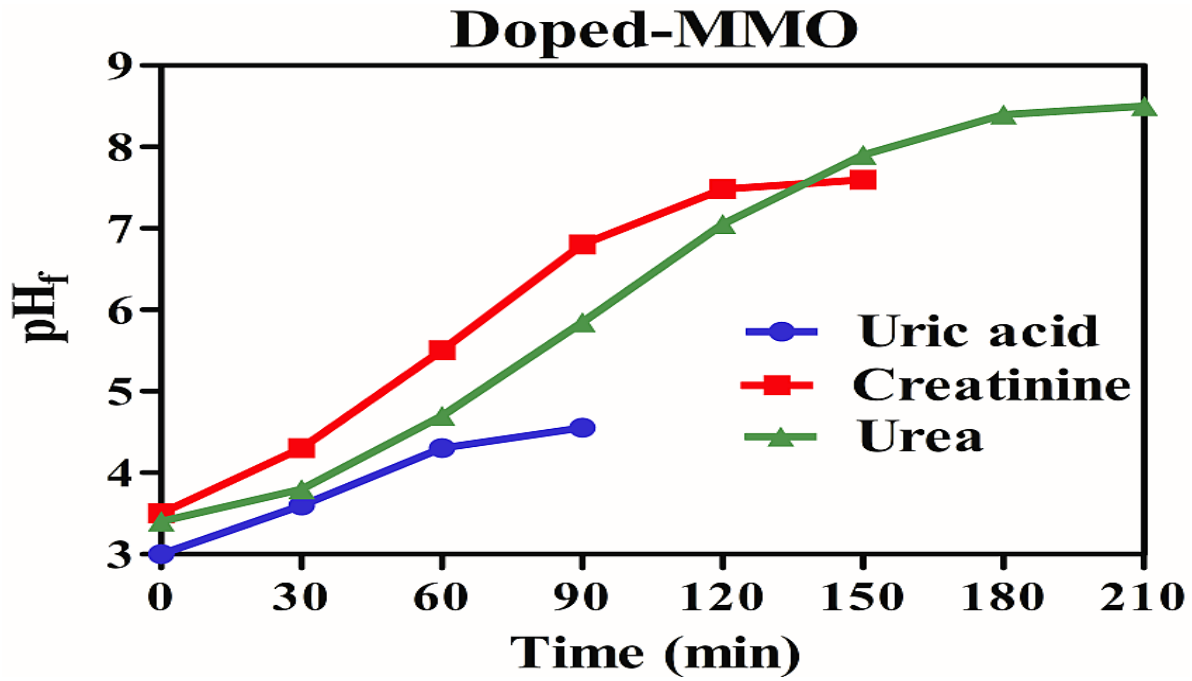

Figure 4.4.3 Graph of pH_f versus time during EO treatment of all urine metabolites with doped-MMO at optimized conditions.

4.4.3 Spectrophotometric Analysis: This analysis was performed in order to get the initial supportive information regarding the oxidation of urine metabolites i.e. uric acid, creatinine and urea with doped-MMO. The UV-vis spectra of both untreated and treated samples of urine metabolites by EO treatment were analyzed in the wavelength range of 200-500 nm as shown in Figure 4.4.4a,b,c. From the results of untreated samples of all urine metabolites, a sharp peak at λ_{max} values 290 nm (uric acid), 238 nm (creatinine) and 420 nm (urea) with narrower bandwidth and high absorption intensity. However, small and wide intensity peaks (of added salt like $NaCl/Na_2SO_4$ and reagent like para-Dimethylaminobenzaldehyde used for urea analysis) were also observed at λ values (a) 250-225 nm, (b) 220 nm and (c) 400-200 nm. During electrolysis, the absorption spectra of treated urine metabolites at the optimum time shows only reduced small intensity band while other small peaks at other λ values got disappeared at the end of the treatment process. Therefore, it

concludes that all urine metabolites i.e. uric acid, creatinine and urea were oxidized to simple components after EO treatment of 43 min, 135 min, and 195 min respectively with doped MMO. The formation of new peaks and reduction in the λ_{max} values has proved the electrocatalytic degradation of urine metabolites through the attack of various generated strong oxidant species such as $OH^{\bullet}$, Cl_2, HOCl, OCl^-, etc.

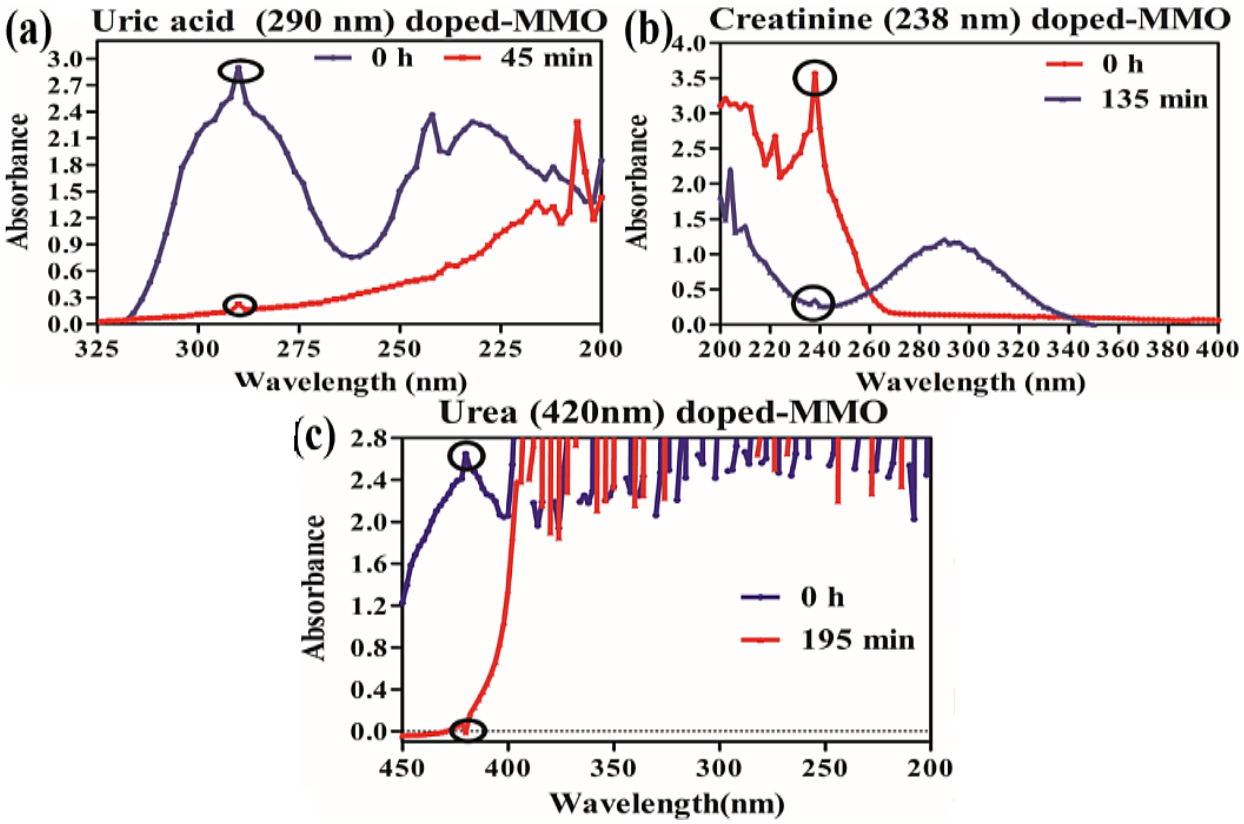

Figure 4.4.4 UV-vis spectra of untreated and treated samples of (a) uric acid, (b) creatinine and (c) urea with doped-MMO at optimum conditions.

4.4.4 Mineralization Studies

In order to view the quality of EO treated urine metabolites wastewater samples, mineralization studies were carried out at optimized conditions. The final electrolysis transformed products were identified by in-situ chemical analysis, CV, FT-IR and LC-MS analysis. Furthermore, untreated samples of urine metabolites were also analyzed using the same mentioned techniques in order to compare the results.

Chemical analysis: In order to inspect the quality of treated samples further analysis had been done and results were compared to untreated samples. Uric acid oxidation into byproducts was evaluated

in terms of decay in COD (90.5%) and TOC (87.51%) at optimized conditions as shown in Figure 4.4.5a. While in the case of creatinine, around 93.10% removal in COD and 89.55% in TOC were attained in 150 min as shown in Figure 4.4.5b. Figure 4.4.5c shows the results of a reduction in %TOC of urea, which was around 90.45% achieved after 210 min of electrolysis. Further extension in electrolysis i.e. 70 min (uric acid), 180 min (creatinine) and 240 min (urea) has shown the marginal effect on COD and TOC reduction i.e. approximately 2.0% to 6%.

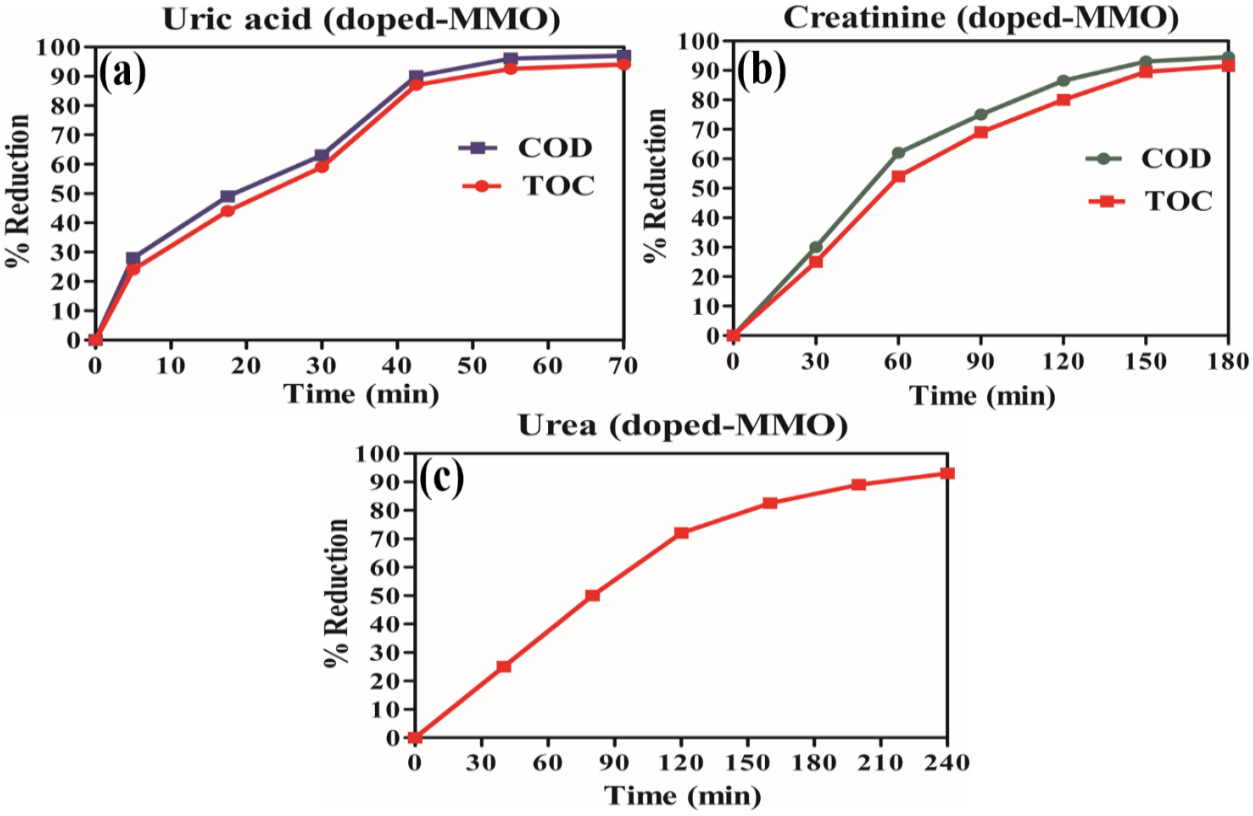

Figure 4.4.5 Plot of % COD and TOC reduction versus time during electrolysis of (a) uric acid, (b) creatinine and (c) urea with doped-MMO anodes at optimized conditions of each urine metabolite.

Taking into account the above results, further test analysis was done in order to authenticate the degradation of nitrogen-based components i.e. uric acid, creatinine and urea into CO_2, H_2O and inorganic ions. Production of inorganic ions such as NO_2^-, NO_3^- and NH_4^+ ion was observed after 5 min of EO treatment of uric acid as shown in Figure 4.4.6a. Furthermore, it also observed that the concentration of NO_2^- ion decreases after 15 min of electrolysis while NH_4^+ gets reduced after 30 min of EO treatment. In the case of NO_3^- concentration, a continuously increasing trend was observed. This might be due to the oxidation of NO_2^- and NH_4^+ by strong oxidants such as $OH^•$,

HOCl, etc. into NO_3^- ions as reported in literature studies (Dbira et al., 2016). Moreover, the same trend was also observed in case creatinine, where an increasing trend in NO_2^-, NH_4^+ and NO_3^- were observed after 60 min of EO treatment as shown in Figure 4.4.6b. However, after 60 min of reaction, the concentration of NH_4^+ was found gradual decreasing till the end of the electrolysis. The concentration of NO_2^- was found decreasing gradually after 90 min of electrolysis, whereas nitrate ion followed an increasing trend in their concentration with the probability of conversion of NO_2^-, into NO_3^-.

In the present study, the quantitative analysis of the inorganic ions generated during electrolysis of urea indicates the release of NO_3^- and NH_4^+ only. However, no other anion such as NO_2^- was generated during the EO treatment of urea. Figure 4.4.6c (urea) depicts that the amount of generated NO_3^- and NH_4^+ in the solution increased proportionally up to 90 min. However, after 90 min of treatment time, it had been observed that the concentration of NH_4^+ was found decreased while the concentration of NO_3^- was increased gradually till the end of electrolysis.

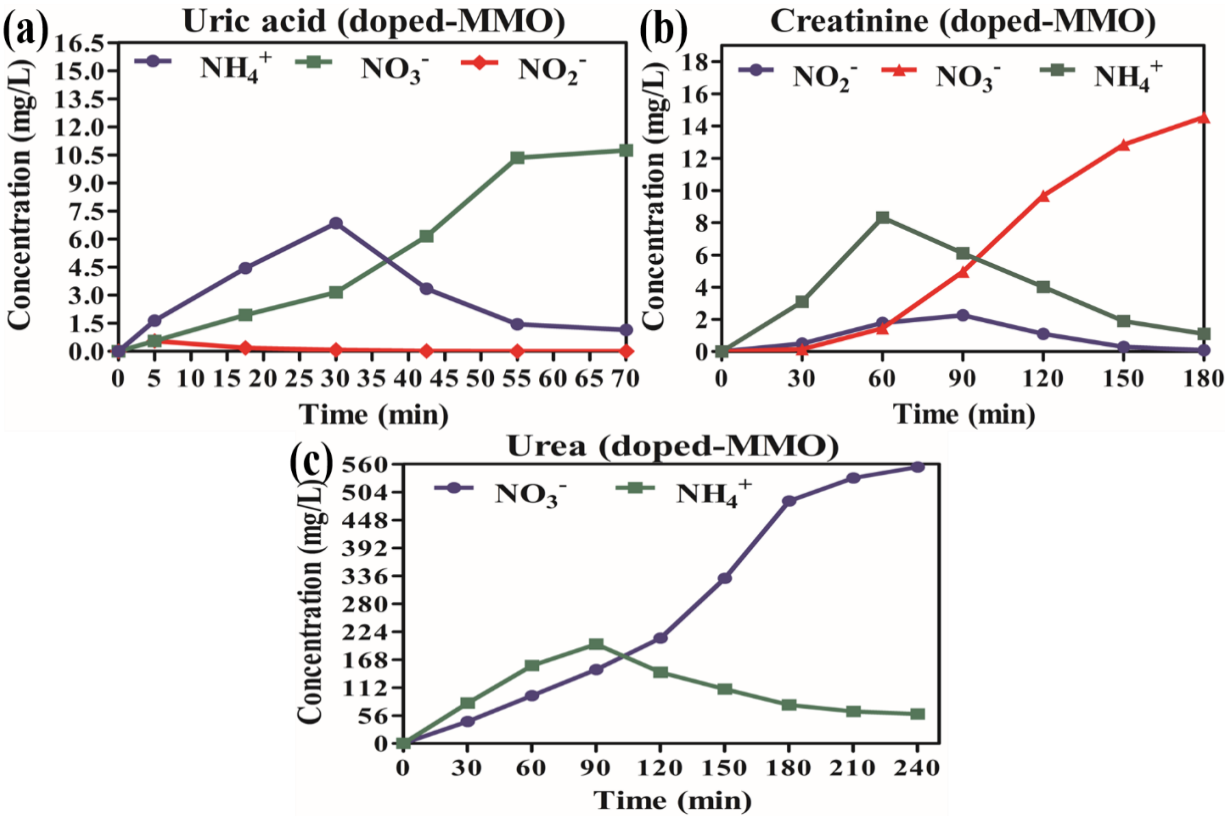

Figure 4.4.6 Production of inorganic ions (NO_2^-, NO_3^- and NH_4^+) during electrolysis of (a) uric acid, (b) creatinine and (c) urea with doped-MMO anodes at optimized conditions.

Figure 4.4.7a,b,c shows the profile of chloride concentration and TAC versus treatment time for all urine metabolites. From the results for each urine metabolite, it can be observed that the concentration of chloride was found continuously decreasing during the EO treatment depicting the conversion of Cl^- into RCS such as Cl_2, HOCl, OCl^-, etc. In addition to this, the level of TAC was found to increase gradually with time during electrolysis of all urine metabolites. The TAC is an aggregate mixture of reactive intermediates i.e. the sum of free chlorine (Cl_2, HOCl) and combined chlorine (chloramines such as NH_2Cl).

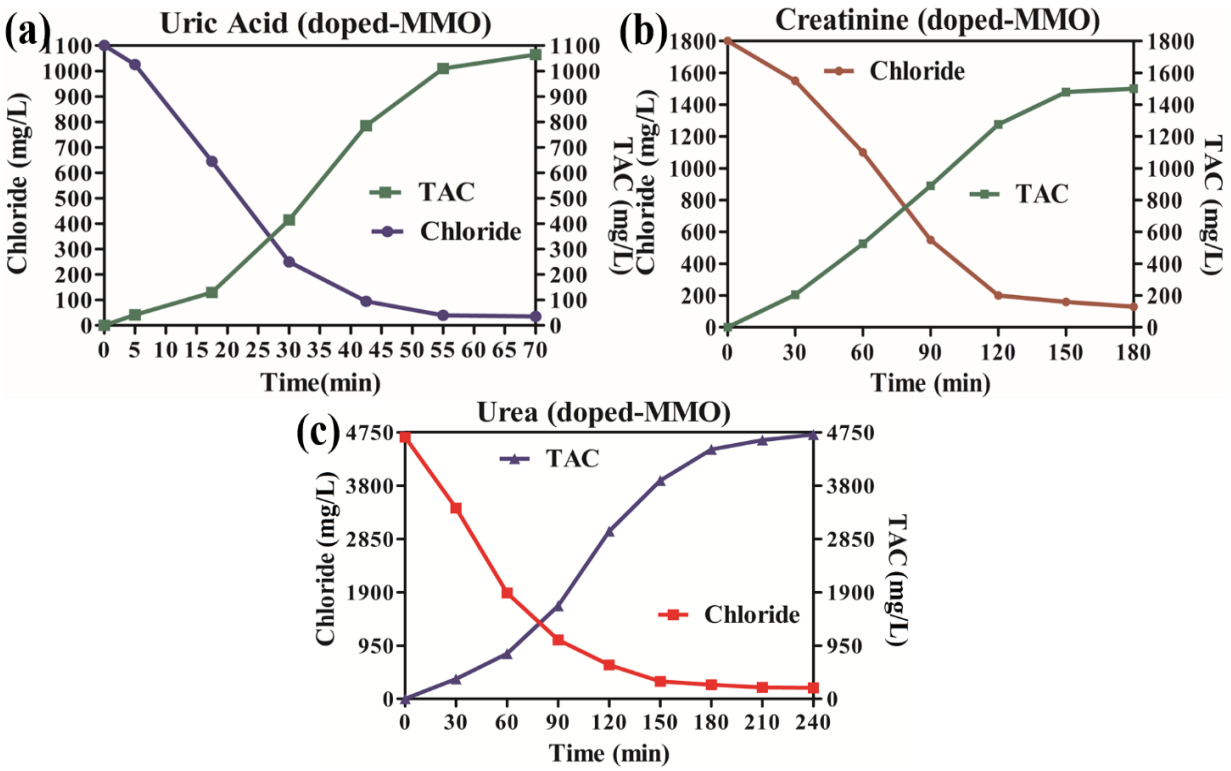

Figure 4.4.7 Mineralization plots of chloride and TAC versus time at optimized conditions for (a) uric acid, (b) creatinine and (c) urea treated with doped-MMO.

Cyclic Voltammetry (CV): The technique was required for the explanation of EO behavior of the anode during the treatment of all urine metabolites and gives the supporting information regarding the intermediates generated. Figure 4.4.8 shows the continuous CVs for the untreated and EO treated samples of uric acid (50 mg/L), creatinine (50 mg/L) and urea (2000 mg/L) at platinum rod with a potential range of -1.2 to 1.2 V. (Mudila et al., 2018). As it can be seen that in 0 h samples (untreated) of all urine metabolites, one small oxidation peak at ≈ -0.4 V potential in a first cycle and one small broad reduction peak at – 0.8 V were observed. This depicted the reduction of chlorine to chloride

and then oxidation of chloride to chlorine. However, in the case of treated samples of all urine metabolites, cycle 1 shows the disappearance of oxidation peak and shift towards -0.2 V while cycle 2 exhibits a large sharp reduction peak at -0.8V. This dissolution/shifting of the peaks indicates the degradation of urine metabolites through indirect oxidation by $OH^{\bullet}$ and chloro-oxidant species which might have generated intermediates and chlorinated organic byproducts in treated samples (Hiwarkar et al., 2017). Moreover, these changes in the redox peaks indicate the high electro-catalytic activity towards the oxidation of all urine metabolites as well as enhanced active surface area of doped-MMO (Zhang and Yin, 2014).

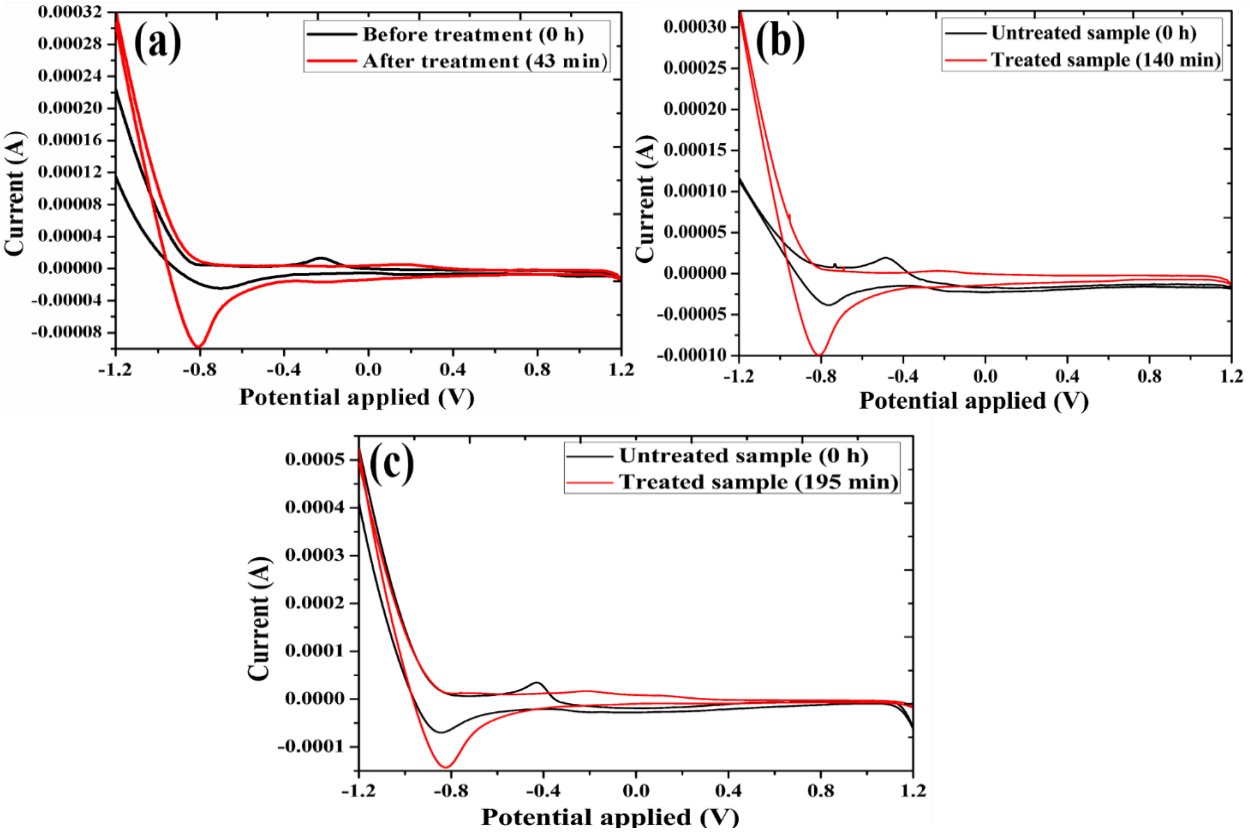

Figure 4.4.8 Cyclic Voltammetry measurements for untreated and treated samples of (a) uric acid, (b) creatinine and (c) urea with doped-MMO at optimized conditions.

FT-IR spectra studies: Figure 4.4.9 represents the FT-IR spectra of untreated and treated samples (at different time intervals) of all urine metabolites (i.e. uric acid, creatinine and urea). The characteristic absorption broad peaks with wavenumber (cm^{-1}) at 2806.49, 3003.95, 3254.8, 3388.64, 3455.08, 612.10, 698.80 and 781.84, respectively were formed due to the $OH^{\bullet}$ and chloro-oxidant species generated during EO of urine metabolites. The sharp peaks at 1675.93, 1738.41,

3012.38, 1600.69, 3356.12 and 3455.08, respectively were due to the presence of characteristic absorption of C=O, C-H and N-H groups. The vibrational frequency of C≡N, C=N, C-N, C=C stretching linked with the heterocyclic structure was around at 2242.90, 1101.36, 1215.1, 1349.93, 1216.76, 1581.68, 1656.12 and 1738.40, respectively.

However, few small peaks during electrolysis were also appeared in treated samples of all urine metabolites at 1349.93, 1366.65, 1380.46, 905.44, 1097.97 and 1119.19, respectively which corresponds to N-O and C-O groups. The results show that most of the peaks were got shifted at distinct wavenumber, might be due to the structural changes occurred during the EO process. Some of the broad and sharp peaks present in raw samples (t= 0 h) were found disappeared in treated samples due to the oxidation of urine metabolites into intermediates via RCS and ROS generated during the EO treatment process with doped-MMO (Rajkumar and Muthukumar, 2012). Moreover, the % transmittance for maximum peaks was found increased at optimized electrolysis treatment time, indicating the destruction and oxidation of the cyclic structure of urine metabolites.

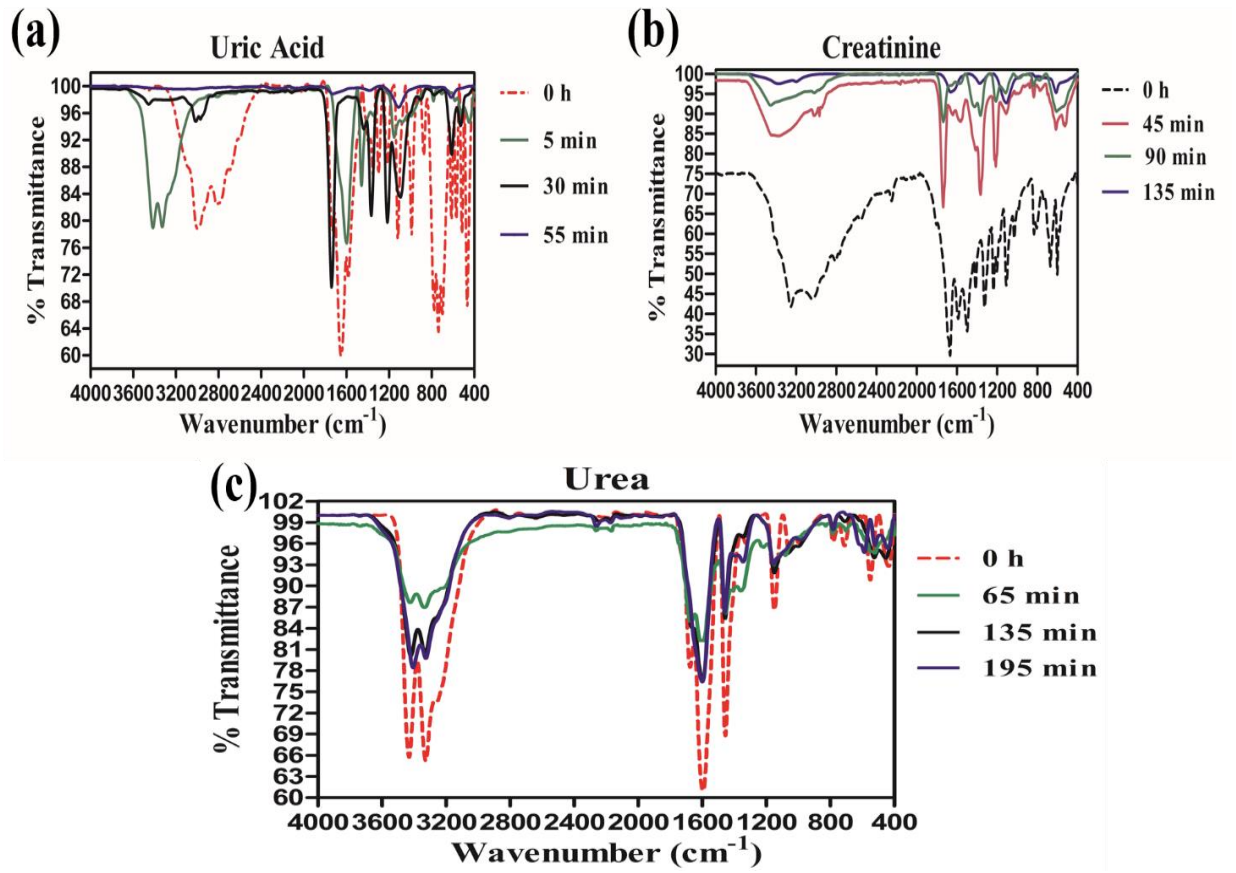

Figure 4.4.9 FT-IR spectra for untreated and treated samples of (a) uric acid, (b) creatinine and (c) urea with doped-MMO at optimized conditions.

LC-MS analysis: To explore the degraded and non-degraded compounds during EO treatment of uric acid, creatinine and urea as well identification of generated intermediates, LCMS analysis was performed for untreated and treated samples. The LCMS chromatograms indicate the identified intermediates generated during electrolysis of uric acid and creatinine using doped-MMO are shown in Figure 4.4.10a,b. Based on these produced byproducts (2-11), an oxidative mechanism along with a tentative degradation pathway for uric acid has been proposed and displayed in Figure 4.4.10c. The reduction of uric acid (1) led to the formation of a byproduct (2). After that intermediate (2) could undergo C-N bond cleavage to form (3) which on subsequent dehydroxylation could produce (4). Further, descendant (4) led to the formation of another intermediate (5) due to the cleavage of the C-N bond. The demethylation and deamination of (5) led to the formation of product (6), which on successive demethylation could yield intermediate (7). However, intermediate (7) undergo two different mechanisms simultaneously. Deamination of (7) could be led to the formation of intermediate (8) followed by deamination could finally yield the end product (9). On the other hand, intermediate (7) after going through C-N bond cleavage, could possibly yield final products (10) and (11).

In the case of creatinine, the intermediates (1-10) formed during electrolysis are shown in Figure 4.4.10d. The demethylation of creatinine in route A led to the formation of intermediate (1) from which (2) was formed by successive C-N bond cleavage. The deamination of (2) led to the generation of intermediate (3). The subsequent hydroxylation of (3) produced intermediate (4). The deamination and hydroamination of (4) ultimately led to the production of final products (8) and (9). On the other hand, the oxidation and C-N bond cleavage of creatinine in route B could lead to the production of intermediate (6). However, oxidation of (6) led to the production of intermediate (7) while fragmentation of (6) could possibly yield the final product (10). The fragmentation of intermediate also led to the generation of final products (8) and (9). To the best of our knowledge, this is one of the few reported studies, depicting the oxidative degradation mechanism for uric acid and creatinine.

Based on the experimental results, a tentative reaction pathway for urea has been proposed in the present study as shown in Figure 4.4.10e. The degradation of urea was mostly due to the generation of RCS and partially by ROS during electrolysis using doped-MMO/ MMO anodes. The end products produced through the electrolysis of urea are carbon dioxide, nitrate, molecular

nitrogen and chloramines. Most of the part of this pathway was formed based on the reported studies (Cho and Hoffmann, 2014; Hoffmann et al., 2014).

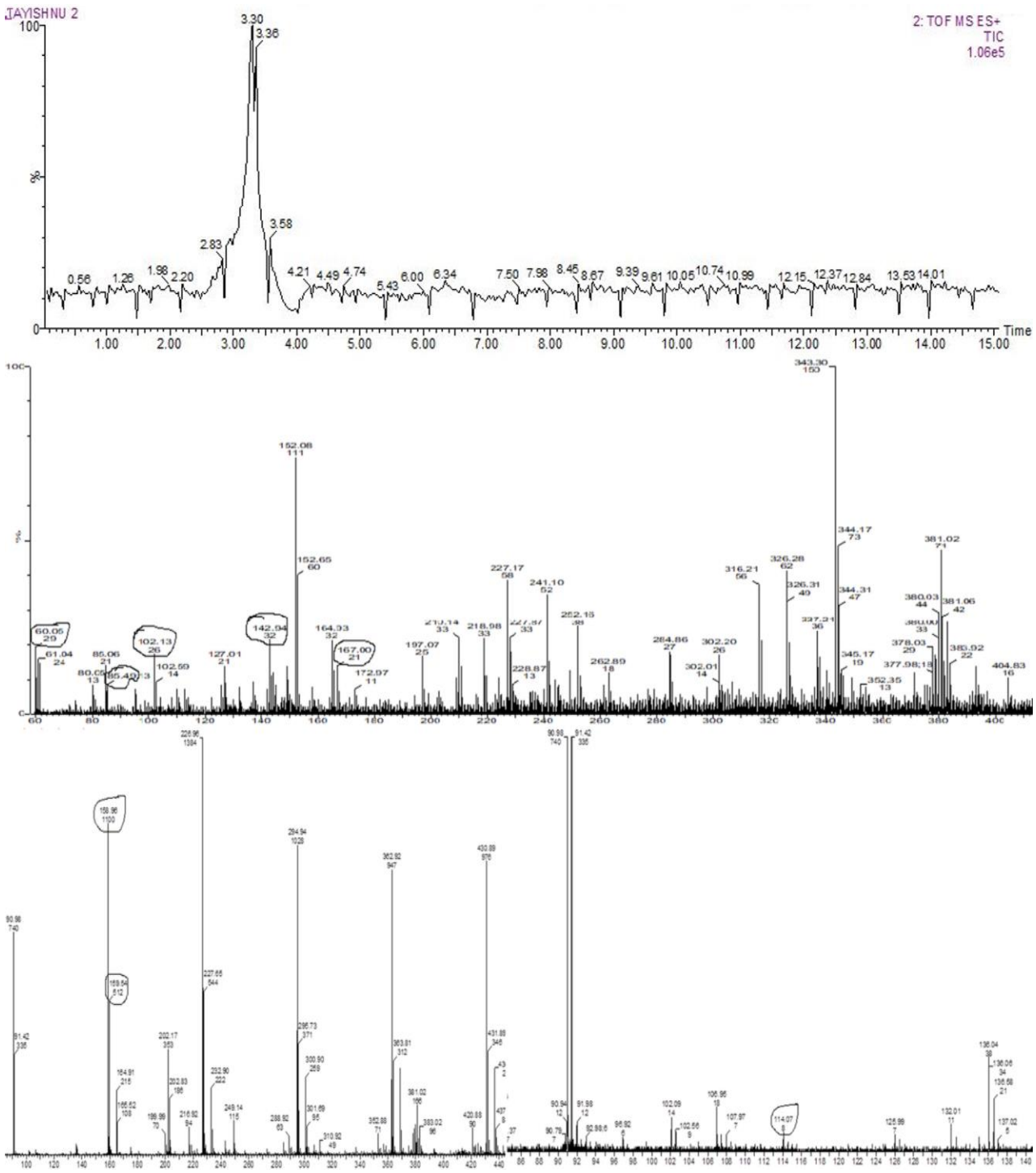

Figure 4.4.10a Mass spectra analysis for the identification of intermediates during the EO treatment of uric acid with doped-MMO at the optimized condition.

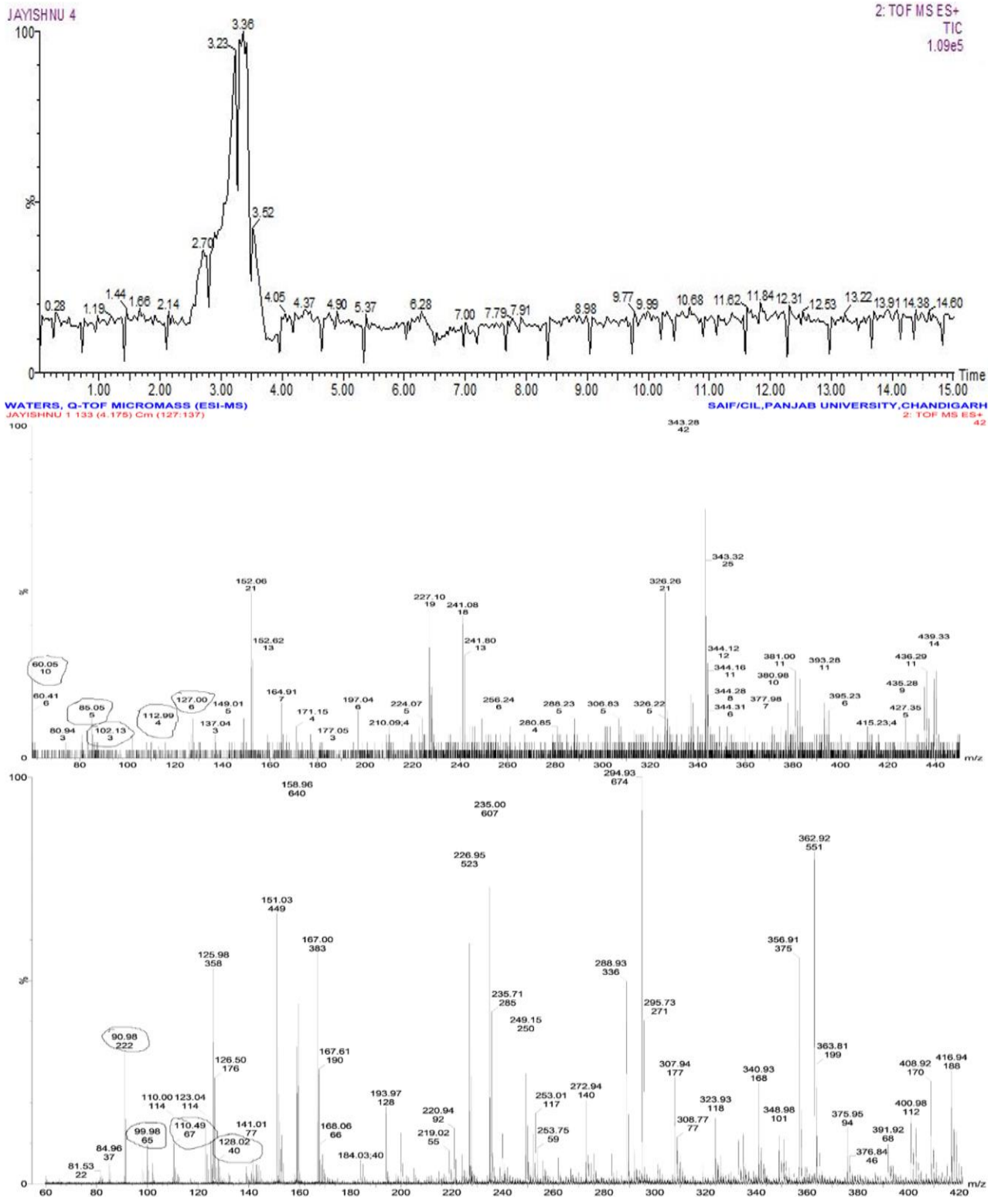

Figure 4.4.10b Mass spectra analysis for the identification of intermediates during the EO treatment of creatinine with doped-MMO at the optimized condition

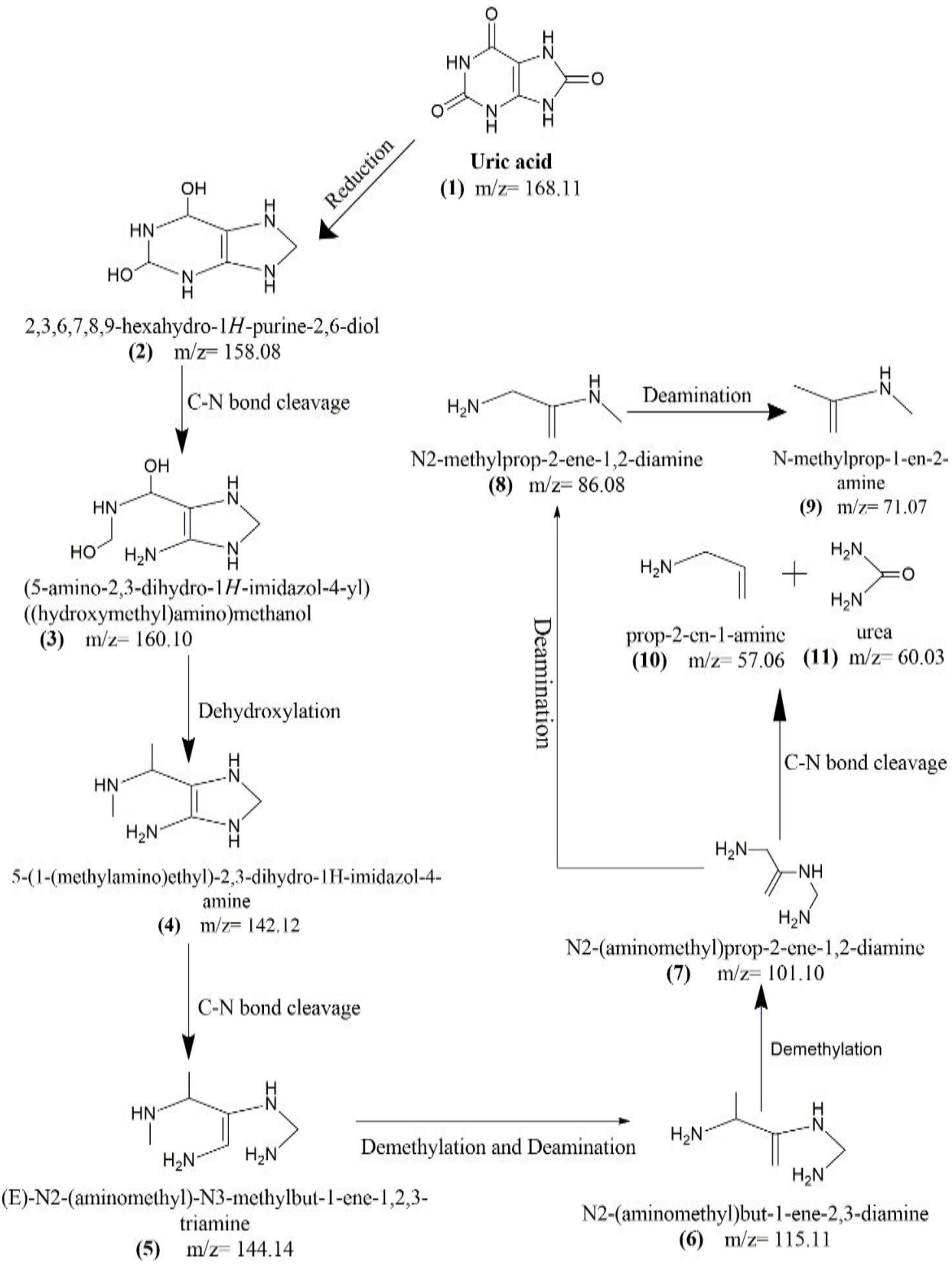

Figure 4.4.10c Proposed degradation pathway for Uric acid treated with doped-MMO

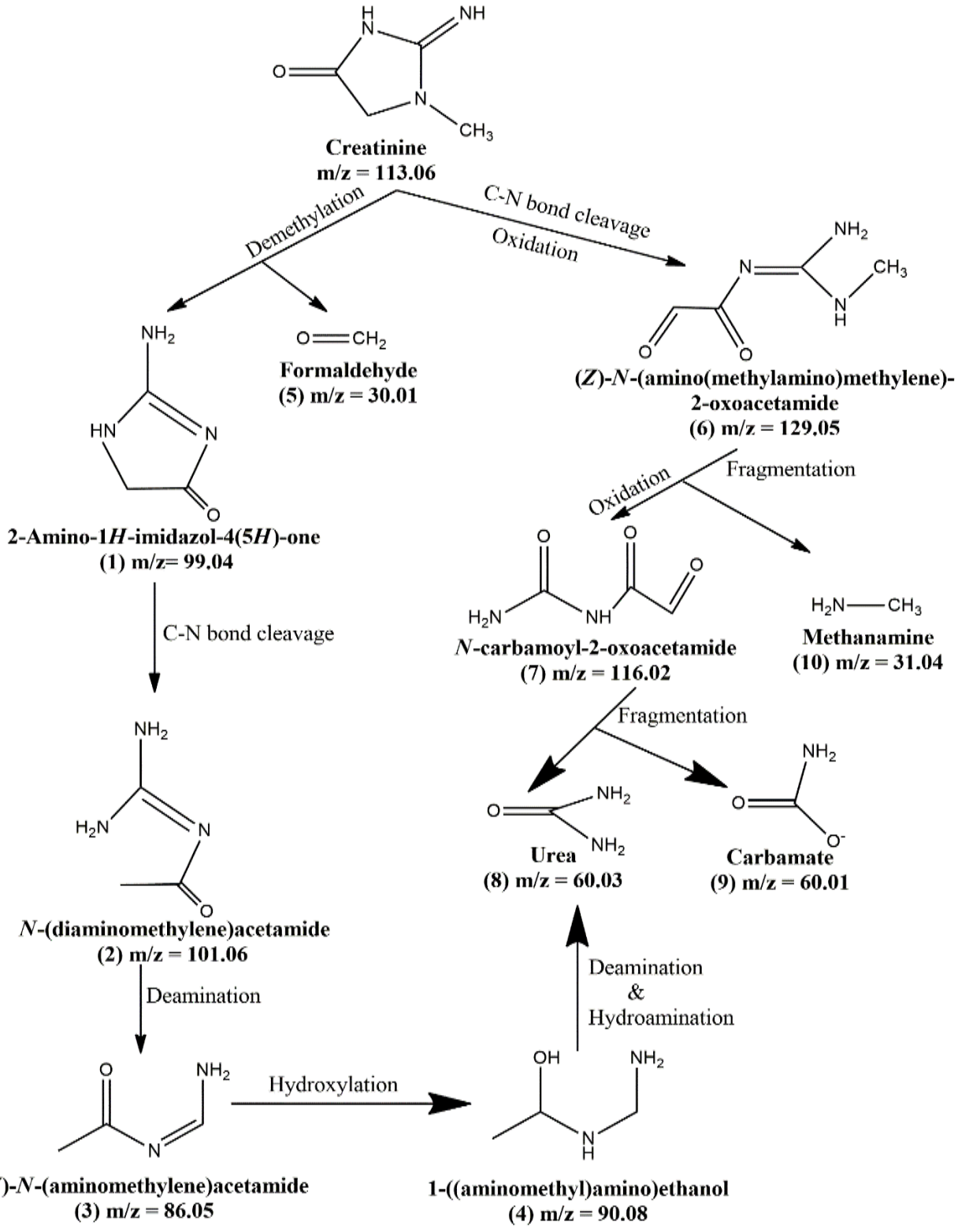

Figure 4.4.10d Proposed degradation pathway for Creatinine treated with doped-MMO

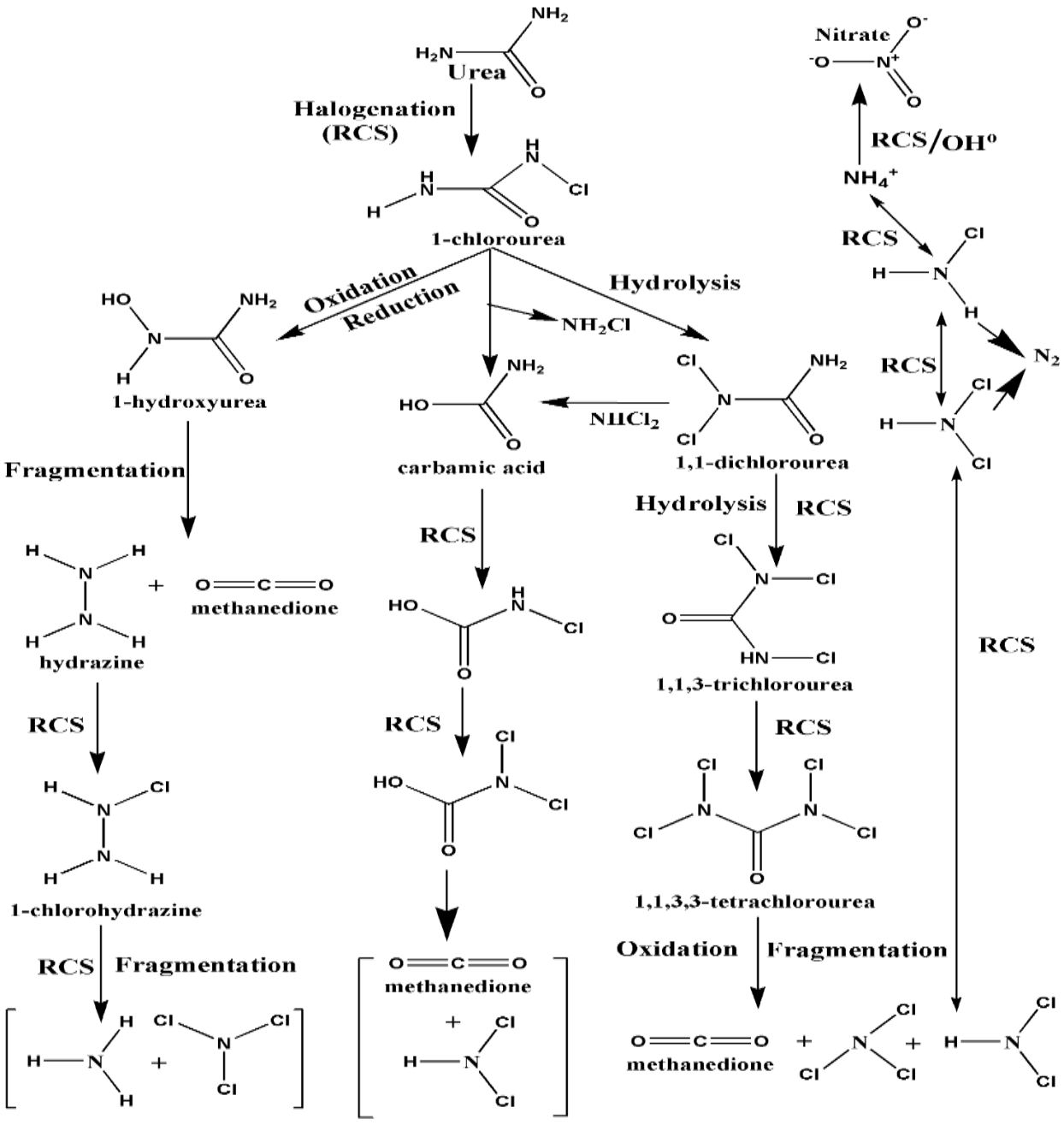

Figure 4.4.10e Proposed common degradation pathway for Urea treated by both anodes.

4.4.5 Synergistic Studies

The photo-activity of the doped-MMO anode was studied under both UV and solar radiation. The synergistic studies using doped-MMO were performed in order to check the removal efficiency of dual-process over single processes. In the present work, the synergy of one process over other for dual effect has been calculated and quantified using kinetic rate constant obtained through pseudo-

first-order reactions. The degradation of each metabolite under UV light was found relatively the same as of EO experimental results. This might be due to the low band-gap of doped-MMO due to which absorption of light by anode in the UV spectrum was less. Figure 4.4.11a,b,c shows the results of the synergistic effect of three different processes i.e. PC, EO and PEC, performed for the treatment of uric acid, creatinine and urea. The %Degradation of each urine metabolite was found maximum through PEC over PC and EO. Furthermore, time for electrolysis of each urine metabolite was also found to be significantly reduced for the same % degradation. PC treatment was found inefficient for the removal treatment over other processes. The % degradation through PC treatment process was found 12.0% (uric acid), 16.5% (creatinine) and 30% (urea). Similar kind of results was also observed when the plot between C_t/C_o and time has been studied as shown in Figure 4.4.12a,b,c. From the results (Figure 4.4.13a) it was depicted that an immense increase in the first-order rate constant in the case of PEC (0.0854 min^{-1}) was observed which was 3.4 times of PC (0.0025 min^{-1}) and 1.4 times as compared to EO (0.0616 min^{-1}).

Similarly, in the case of creatinine and urea, the first-order rate constant of the dual-process was much higher than individual processes i.e. PC and EO as shown in Figure 4.4.13b,c. Thus, proves the viability of the dual-process over single treatment processes. Moreover, a synergistic effect of the dual-process for over EO came out to be 27.86%, 13.77%, 19.87% and over PC was observed 97.07%, 93.41%, 88.81 for uric acid, creatinine and urea respectively. The overall % synergy for urine metabolites such as uric acid (24.94%), creatinine (7.19%) and urea (8.69%). Therefore, it concludes that the dual-process with synergistic results has significantly reduced the treatment time from 43 min to 30 min (uric acid), 140 to 120 min (creatinine) and 195 to 150 min (urea). To further verify the experimental results, similar studies were carried out for the estimation of $OH^{\bullet}$ production using fluorescence spectroscopy.

Fluorescence spectroscopy: Fluorescence studies were carried out for the quantification of generated $OH^{\bullet}$ at doped-MMO during the treatment process. Figure 4.4.14a showed that maximum $OH^{\bullet}$ production was found under solar radiations (PEC) than UV and EO. This may happen due to the activation of photoactive layers i.e. TiO_2 and SnO_2 of anode under light sources leading to the generation of more $OH^{\bullet}$ on the surface of anode resulting in more percentage degradation of uric acid in less time. Some researchers have also reported that doping can improve the photoactivity of the anode by increasing the charge separation of holes and electrons **(**Chen et al., 2009; Singh et al.,

2016). From the above results, it was concluded that doped-MMO is more photoactive under solar radiation than in UV.

From the literature survey, it was also observed that the pH of the solution has a great effect on the generation of $OH^{\bullet}$ during the treatment process. In order to verify the effect of pH on the generation of $OH^{\bullet}$, experiments were performed at different pH. From the results, as shown in Figure 4.4.14b it was found that more $OH^{\bullet}$ production was observed at basic pH over acidic and neutral pH. But at the same time, it was also observed that in the case of basic and neutral pH generation of $OH^{\bullet}$ decreases with increasing time which might be due to the scavenging of $OH^{\bullet}$ by bicarbonate and carbonate ions (Wu et al., 2014). While in the case of acidic pH it was found increasing. This might be due to the inhibition of OER by water oxidation resulting in more $OH^{\bullet}$ production. Hence, it concludes that the degradation of all urine metabolites with doped-MMO was found maximum under solar radiations (PEC) at acidic pH. Therefore, the effectiveness of dual-process over discrete process i.e. EO was proved.

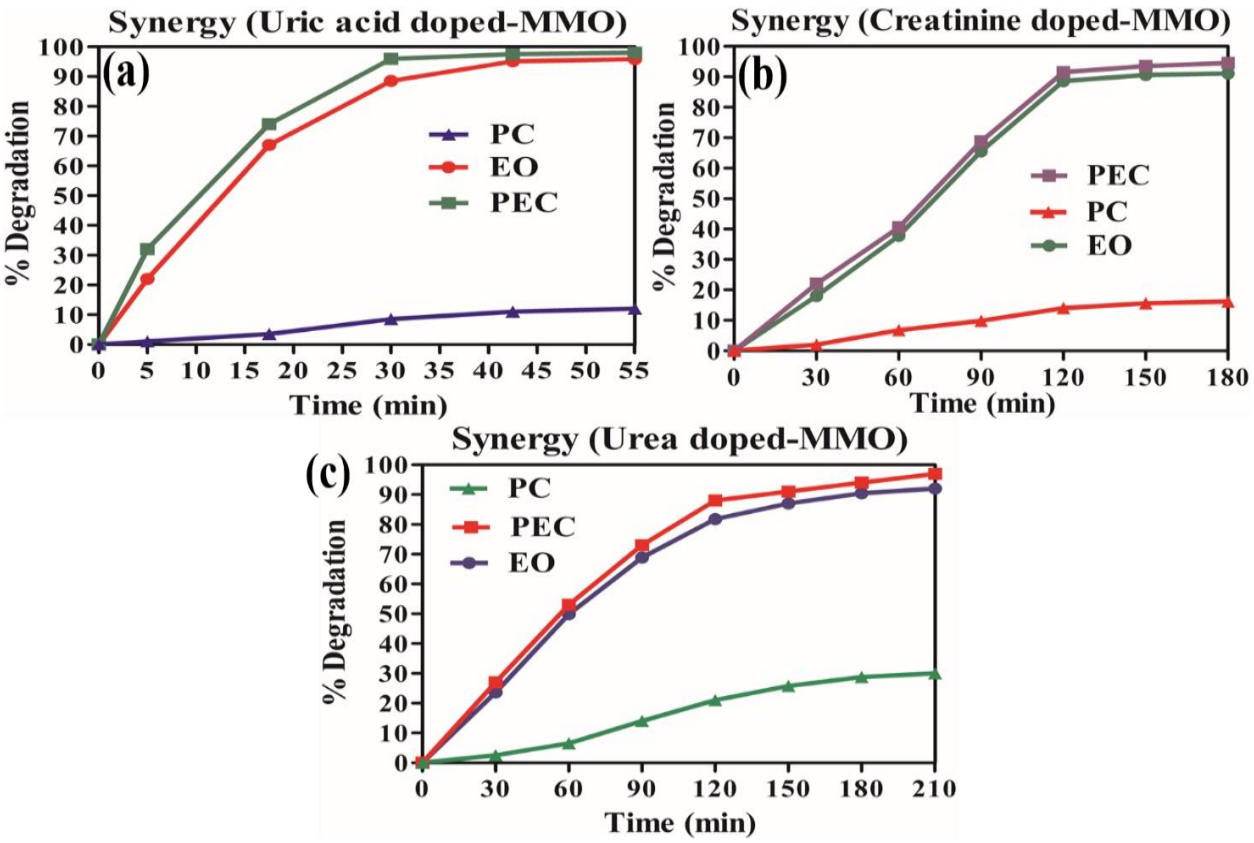

Figure 4.4.11 Comparison between different processes using doped-MMO for the treatment of (a) uric acid, (b) creatinine and (c) urea at optimized conditions.

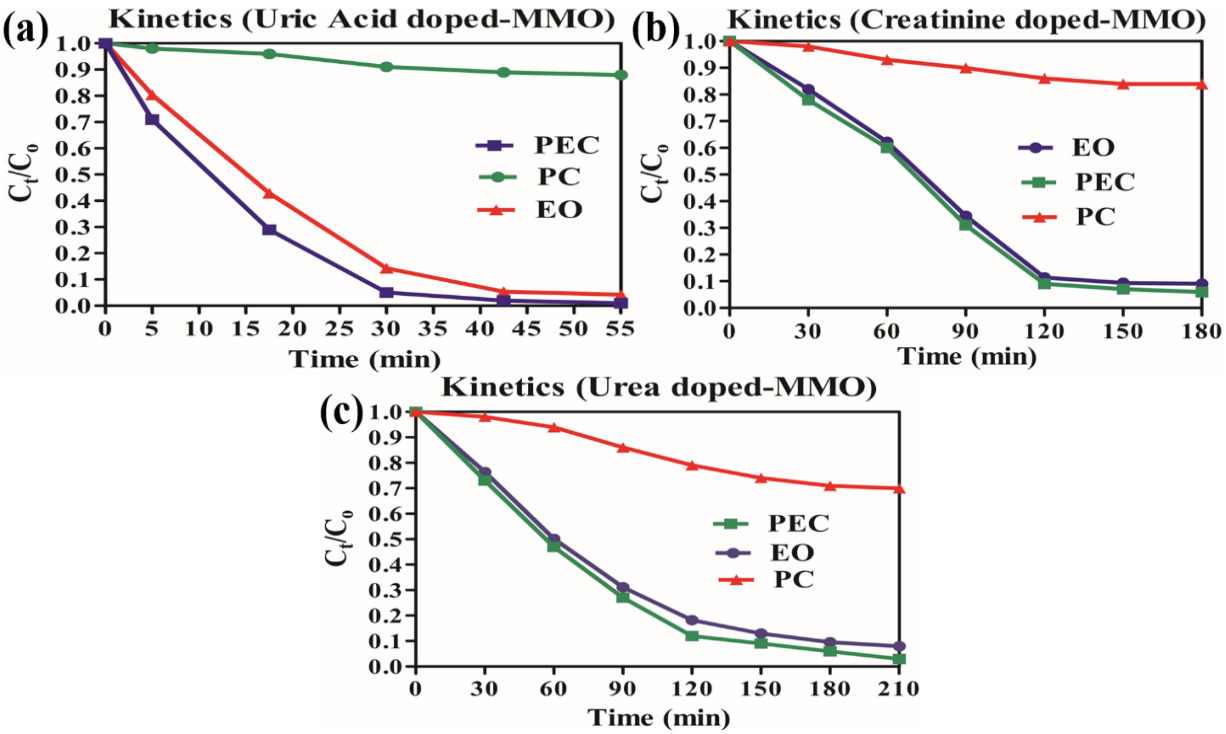

Figure 4.4.12 Plot of C_0/C_t versus time for each urine metabolite i.e. (a) uric acid, (b) creatinine and (c) urea treated with doped-MMO at optimized conditions.

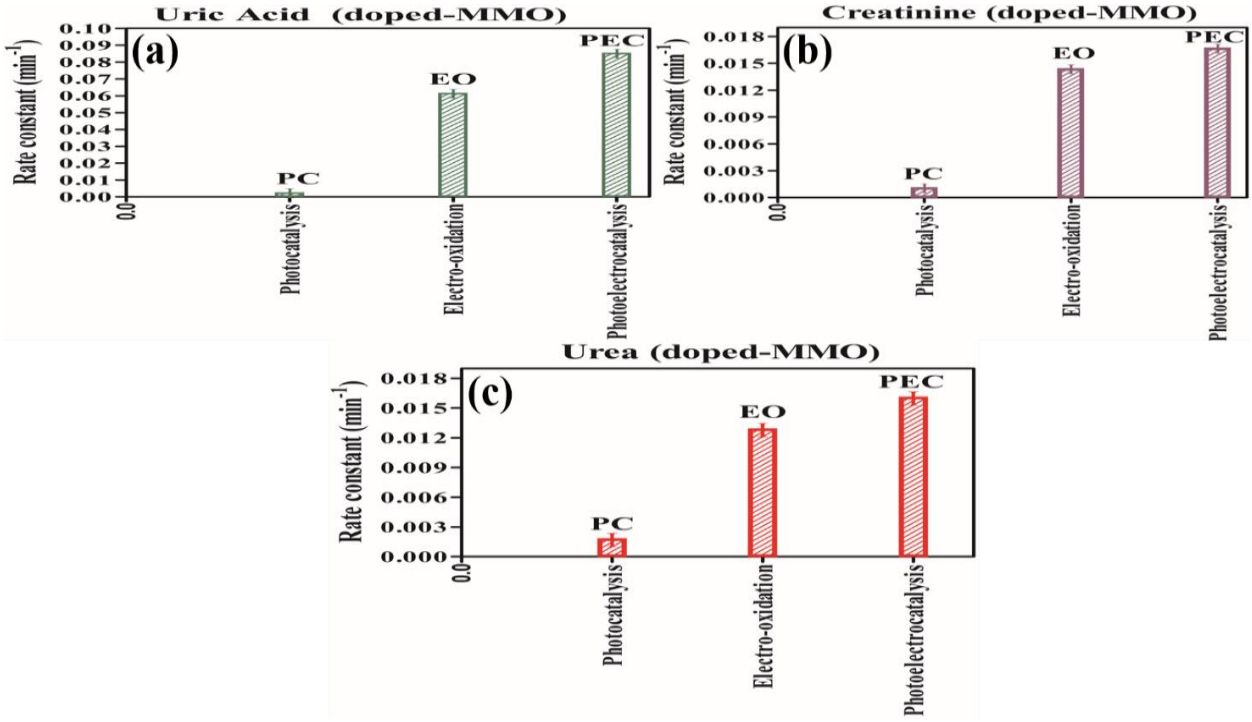

Figure 4.4.13 Values of the rate constant for the degradation of (a) uric acid, (b) creatinine and (c) urea via different processes with doped-MMO.

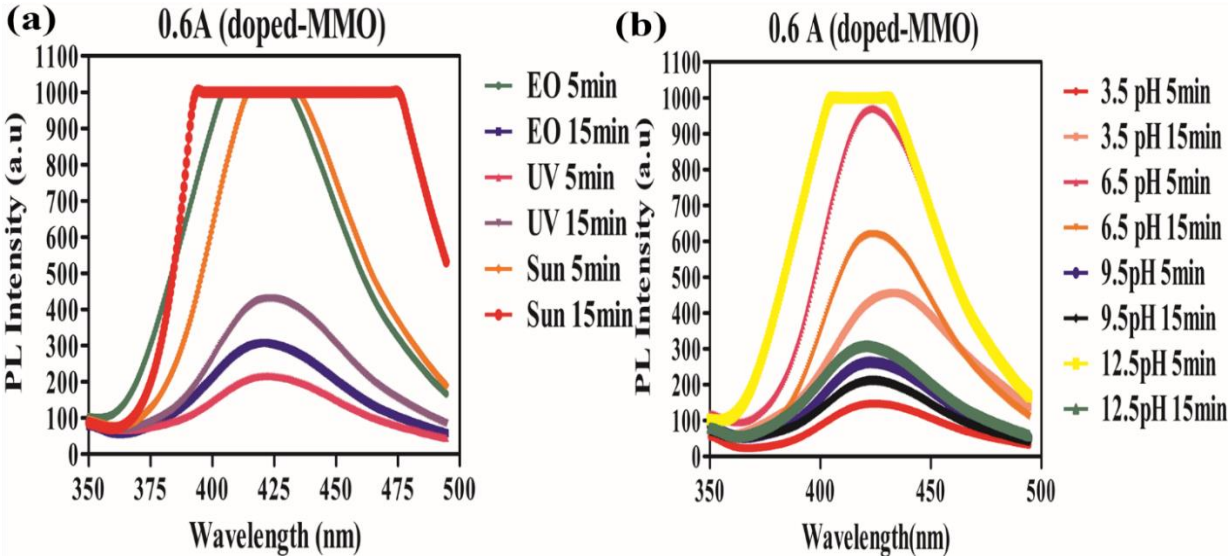

Figure4.4.14 PL spectra of $OH^{\bullet}$ at doped-MMO (a) for different light sources at 0.6A and (b) for different pH at different time intervals at 0.6A.

4.4.6 Operating Cost Analysis In the present study, the overall cost of the treatment process for the removal of each urine metabolites from aqueous solution using doped-MMO was calculated and shown in Table 4.4.8.

Table 4.4.8: Evaluation of operating cost of EO treatment process for uric acid treated with doped-MMO
(A) Cost of Electrical Energy consumption
Electrical energy consumed = 2.479 kWh/m^3
Electricity price in Punjab, (India) = Rs 5.00/kWh
Cost of electrical energy consumed (C_{EC}) = Rs 12.395 m^3
Cost of energy consumed to remove per kg of uric acid ($C_{EC)}$ = Rs 12.395/0.0477 = 259.85 kWh/m^3
(B) Cost of Electrodes
Initial uric acid concentration in wastewater = 50 mg/L= 0.05 kg/m^3
With 95.35% degradation, concentration of uric acid removed = 0.0477kg/m^3
Time of treatment = 43 min = 0.716 h ≈ 0.72 h
Concentration of uric acid removed in 1h = 0.0662 kg/m^3
Cost of one MMO anode = Rs 820/-
The life span of anode = 5 years

Cost of anode for 43800 h = Rs 820/-
Cost of anode for 1 h = Rs 0.0187/-
Cost of electrodes to remove per kg uric acid from wastewater = Rs 0.2825/m^3
(C) Operating cost analysis
Total operating cost for per kg of uric acid removal = 0.2825/m^3 + 259.85/m^3 = Rs 260.133/m^3
The overall operating cost of EO treatment of uric acid in US dollars = 3.740 \$/m^3

Similarly, the total operating cost for treating per kg of creatinine and urea came out to be 41.68 \$/m^3 and 2.05\$/m^3 respectively. The results show that the economic feasibility of the EO process for the treatment of synthetic urine wastewater using doped-MMO. However, the cost can be further minimized during scale-up studies by modifying the design of the electrolytic reactor and operating conditions accordingly.

SECTION-B

4.5 Study on EO Treatment of SU with (i) MMO and (ii) Doped-MMO.

4.5.1 Model Fitting and Statistical Analysis

In this study, three-level BBD based RSM has been employed for the designing of EO experiments for SU using MMO and doped-anodes. The process conditions for the oxidation of pollutants from SU, four input operational parameters were selected such as initial pH (Y_1), applied current density (Y_2), treatment time (Y_3) and N/Cl ratio (Y_4). The actual ranges along with coded values of input parameters were selected on the basis of the reported studies and prior observations as shown in Table 4.5.1. The total number of experimentally designed by BBD for EO treated SU with MMO and doped-MMO was 30 with six replication runs at the center. The experimental results of responses like %COD removed (Z_1) and SEC (Z_2) for EO treatment of SU were calculated by conducting the experimental runs according to the suggested design matrix as shown in Table 4.5.2a,b.

Table 4.5.1 Range and coded levels of selected input operational variables for EO treatment of SU

			Range of actual and coded variables		
Electrodes	Factors	Variables	-1	0	+1
MMO	Y_1	Initial pH	3	6	9
	Y_2	Current density , j (mA/cm^2)	19.04	33.325	47.61
	Y_3	Treatment time, t (h)	6	9	12
	Y_4	N/Cl ratio	0.3	1.0	1.7
Doped-MMO	Y_1	Initial pH	3.5	6.5	9.5
	Y_2	Current density , j (mA/cm^2)	26.19	42.86	59.52
	Y_3	Treatment time, t (h)	7	10	13
	Y_4	N/Cl ratio	0.2	0.8	1.4

Table 4.5.2a BBD matrix and their experimental results for measured responses of SU treated with MMO

Std	Run	Block	j (mA/cm^2)	N/Cl ratio	t (h)	pH	% COD removed, Z_1	SEC, Z_2 (kWh/kg COD removed)
2	1	1	47.61	1.00	9.00	3.00	87	34.08
6	2	1	33.33	1.70	6.00	6.00	22	77.5
5	3	1	33.33	0.30	6.00	6.00	67	13.27
8	4	1	33.33	1.70	12.00	6.00	26	121.63
10	5	1	33.33	1.00	9.00	6.00	65.5	30.55
7	6	1	33.33	0.30	12.00	6.00	72	22.65
9	7	1	33.33	1.00	9.00	6.00	65.5	30.55
3	8	1	19.04	1.00	9.00	9.00	33	34.01
4	9	1	47.61	1.00	9.00	9.00	62	52.94
1	10	1	19.04	1.00	9.00	3.00	57	18.58
16	11	2	33.33	0.30	9.00	9.00	59	23.87
19	12	2	33.33	1.00	9.00	6.00	65.5	30.55
11	13	2	19.04	1.00	6.00	6.00	40	18.35
20	14	2	33.33	1.00	9.00	6.00	65.5	30.55
14	15	2	47.61	1.00	12.00	6.00	69	60.36
17	16	2	33.33	1.70	9.00	3.00	31	75.31
15	17	2	33.33	0.30	9.00	3.00	88.5	12.98
18	18	2	33.33	1.70	9.00	9.00	24.5	102.86
12	19	2	47.61	1.00	6.00	6.00	64	33.64
13	20	2	19.04	1.00	12.00	6.00	45	32
29	21	3	33.33	1.00	9.00	6.00	65.5	30.55
21	22	3	19.04	0.30	9.00	6.00	53	11.19
23	23	3	19.04	1.70	9.00	6.00	28	55
25	24	3	33.33	1.00	6.00	3.00	74	17.36
26	25	3	33.33	1.00	6.00	9.00	53	26.57
24	26	3	47.61	1.70	9.00	6.00	23	140
22	27	3	47.61	0.30	9.00	6.00	80.5	24.33
30	28	3	33.33	1.00	9.00	6.00	65.5	30.55
27	29	3	33.33	1.00	12.00	3.00	79	30.65
28	30	3	33.33	1.00	12.00	9.00	58	49

Table 4.5.2b BBD matrix and their experimental results for measured responses of SU treated with doped-MMO								
Std	Run	Block	j (mA/cm^2)	N/Cl ratio	t (h)	pH	% COD removed, Z_1	SEC, Z_2 (kWh/kg COD removed)
3	1	1	26.19	0.80	10.00	9.50	26	52.64
4	2	1	59.52	0.80	10.00	9.50	65	61.09
5	3	1	42.86	0.20	7.00	6.50	61	11.3
6	4	1	42.86	1.40	7.00	6.50	8.5	220.32
1	5	1	26.19	0.80	10.00	3.50	32	31.5
2	6	1	59.52	0.80	10.00	3.50	83	38.76
9	7	1	42.86	0.80	10.00	6.50	68	34.68
10	8	1	42.86	0.80	10.00	6.50	68	34.68
8	9	1	42.86	1.40	13.00	6.50	19.5	275.87
7	10	1	42.86	0.20	13.00	6.50	78	32.67
11	11	2	26.19	0.80	7.00	6.50	20	34.38
13	12	2	26.19	0.80	13.00	6.50	30	56.78
14	13	2	59.52	0.80	13.00	6.50	80	66.31
15	14	2	42.86	0.20	10.00	3.50	70	20.32
18	15	2	42.86	1.40	10.00	9.50	10	301.78
16	16	2	42.86	0.20	10.00	9.50	62	23.06
19	17	2	42.86	0.80	10.00	6.50	68	34.68
17	18	2	42.86	1.40	10.00	3.50	22	174.34
12	19	2	59.52	0.80	7.00	6.50	63	33.56
20	20	2	42.86	0.80	10.00	6.50	68	34.68
27	21	3	42.86	0.80	13.00	3.50	81	39.51
22	22	3	59.52	0.20	10.00	6.50	92	25.78
26	23	3	42.86	0.80	7.00	9.50	50	41.65
28	24	3	42.86	0.80	13.00	9.50	57	63.39
29	25	3	42.86	0.80	10.00	6.50	68	34.68
23	26	3	26.19	1.40	10.00	6.50	18	165
25	27	3	42.86	0.80	7.00	3.50	60	21.4
24	28	3	59.52	1.40	10.00	6.50	47	190
21	29	3	26.19	0.20	10.00	6.50	38	16.47
30	30	3	42.86	0.80	10.00	6.50	68	34.68

The results of the model summary statistic for both responses (Z_1 and Z_2) of SU showed the highest R^2 values for the quadratic model only, which advocates that the model has explained the experimental data very well and indicates the satisfactory interaction between predicted and

observed values of experimental runs. The natural log transformation for a response (Z_2) and no transformation for a response (Z_1) was applied for EO treated SU with MMO and doped MMO. After exploiting sequential F–test and other adequacy measures, the model suggested for SU was quadratic as shown in Table 4.5.3.

Table 4.5.3 Various R-squared values for the quadratic model suggested by BBD for responses %COD removed (Z_1) and SEC (Z_2) of SU treated with MMO and doped-MMO

Electrodes	Responses	R-Squared	Adj R-Squared	Pred R Squared
MMO	Z_1	0.9801	0.9586	0.8424
	Z_2	0.9930	0.9855	0.9472
Doped-MMO	Z_1	0.9737	0.9453	0.8180
	Z_2	0.9920	0.9835	0.9409

Table 4.5.4a,b shows the result of the quadratic model fitting in the form of analysis of variance (ANOVA). ANOVA with higher F values and lower p values ($p<0.0001$) i.e. "Prob>F" for both responses (Z_1 and Z_2), supports the quadratic model. The significant and highly significant terms of batch EO process for both responses Z_1 and Z_2 of SU were observed from the ANOVA tables. The values of adequate precision ratio for both responses have come out above 4, which depicts the goodness of the fitted model and can be used for design space navigation. An empirical relationship between the responses and the operational parameters in terms of independent coded factors obtained from the design-expert software for all urine metabolites was expressed by the quadratic model equation as shown in Equations 4.5.1-4.5.4.

SU treated with MMO:

$$Z_1 = +65.50 + 10.79*Y_1 - 10.58*Y_2 - 22.13*Y_3 + 2.42*Y_4 - 6.54*Y_1^2 + 1.52*Y_2^2 - 14.92*Y_3^2 - 3.10*Y_4^2 - 0.25*Y_1*Y_2 - 8.12*Y_1*Y_3 + 0.00*Y_1*Y_4 + 5.75*Y_2*Y_3 + 0.00*Y_2*Y_4 - 0.25*Y_3*Y_4 \quad \textbf{(4.5.1)}$$

$$Z_2 = +3.42 + 0.33*Y_1 + 0.24*Y_2 + 0.83*Y_3 + 0.28*Y_4 + 0.040*Y_1^2 - 0.011*Y_2^2 + 0.24*Y_3^2 + 0.015*Y_4^2 - 0.041*Y_1*Y_2 - 0.039*Y_1*Y_3 + 7.126E\text{-}003*Y_1*Y_4 - 0.074*Y_2*Y_3 + 0.011*Y_2*Y_4 - 0.021*Y_3*Y_4 \quad \textbf{(4.5.2)}$$

SU treated with doped-MMO:

$Z_1 = + 68.00 + 22.17*Y_1 - 6.50*Y_2 - 23.00*Y_3 + 6.92*Y_4 - 8.63*Y_1^2 - 5.63*Y_2^2 - 17.13*Y_3^2 - 6.87*Y_4^2 - 3.00*Y_1*Y_2 - 6.25*Y_1*Y_3 + 1.75*Y_1*Y_4 - 1.00*Y_2*Y_3 - 3.50*Y_2*Y_4 - 1.50*Y_3*Y_4$ **(4.5.3)**

$Ln(Z_2) = + 3.55 + 0.090Y_1 + 0.23*Y_2 + 1.18*Y_3 + 0.29*Y_4 + 0.11*Y_1^2 + 0.10*Y_2^2 + 0.54*Y_3^2 + 0.10*Y_4^2 - 0.015*Y_1*Y_2 - 0.015*Y_1*Y_3 + 0.045*Y_1*Y_4 + 0.11*Y_2*Y_3 - 0.048*Y_2*Y_4\ 0.21*Y_3*Y_4$ **(4.5.4)**

Table 4.5.4a ANOVA results EO treated SU with MMO suggested by BBD for responses (Z_1 and Z_2).

Sources	% COD removed (Z_1)					SEC (Z_2)				
	Sum of square	DF	Mean square	F-value	Prob> F	Sum of square	DF	Mean square	F-value	Prob> F
Block	42.92	2	21.46			0.037	2	0.019		
Model	10875.95	14	776.85	45.70	< 0.0001	11.72	14	0.84	132.37	< 0.0001
Y_1	1397.52	1	1397.52	82.21	< 0.0001	1.33	1	1.33	210.82	< 0.0001
Y_2	1344.08	1	1344.08	79.07	< 0.0001	0.68	1	0.68	107.79	< 0.0001
Y_3	5874.19	1	5874.19	345.57	< 0.0001	8.34	1	8.34	1318.86	< 0.0001
Y_4	70.08	1	70.08	4.12	0.0633	0.91	1	0.91	144.00	< 0.0001
Y_1^2	293.44	1	293.44	17.26	0.0011	0.011	1	0.011	1.73	0.2112
Y_2^2	15.86	1	15.86	0.93	0.3517	8.320E-004	1	8.320E-004	0.13	0.7227

Y_3^2	1525.76	1	1525.76	89.76	< 0.0001	0.40	1	0.40	63.04	< 0.0001
Y_4^2	66.07	1	66.07	3.89	0.0703	1.610E-003	1	1.610E-003	0.25	0.6224
Y_1Y_2	0.25	1	0.25	0.015	0.9053	6.734E-003	1	6.734E-003	1.06	0.3211
Y_1Y_3	264.06	1	264.06	15.53	0.0017	6.211E-003	1	6.211E-003	0.98	0.3399
Y_1Y_4	0.000	1	0.000	0.000	1.0000	2.031E-004	1	2.031E-004	0.032	0.8606
Y_2Y_3	132.25	1	132.25	7.78	0.0153	0.022	1	0.022	3.50	0.0842
Y_2Y_4	0.000	1	0.000	0.000	1.0000	4.747E-004	1	4.747E-004	0.075	0.7885
Y_3Y_4	0.25	1	0.25	0.015	0.9053	1.762E-003	1	1.762E-003	0.28	0.6066
Residual	220.98	13	17.00			0.082	13	6.327E-003		
Lack of fit	220.98	10	22.10			0.082	10	8.225E-003		
Pure error	0.000	3	0.000			0.000	3	0.000		
Core total	11139.84	29				11.84	29			

Table 4.5.4b ANOVA results EO treated SU with doped-MMO suggested by BBD for responses (Z_1 and Z_2).

Sources	% COD removed (Z_1)					SEC (Z_2)				
	Sum of square	DF	Mean square	F-value	Prob> F	Sum of square	DF	Mean square	F-value	Prob> F
Block	418.40	2	209.20			0.095	2	0.048		
Model	15993.97	14	1142.43	34.34	< 0.0001	20.70	14	1.48	115.70	< 0.0001
Y_1	5896.33	1	5896.33	177.26	< 0.0001	0.097	1	0.097	7.56	0.0166
Y_2	507.00	1	507.00	15.24	0.0018	0.65	1	0.65	50.48	< 0.0001
Y_3	6348.00	1	6348.00	190.84	< 0.0001	16.63	1	16.63	1301.35	< 0.0001
Y_4	574.08	1	574.08	17.26	0.0011	1.02	1	1.02	79.99	< 0.0001
Y_1^2	510.11	1	510.11	15.34	0.0018	0.082	1	0.082	6.41	0.0250
Y_2^2	216.96	1	216.96	6.52	0.0240	0.073	1	0.073	5.71	0.0327
Y_3^2	2010.96	1	2010.96	60.45	< 0.0001	2.03	1	2.03	158.93	< 0.0001
Y_4^2	324.11	1	324.11	9.74	0.0081	0.074	1	0.074	5.81	0.0315
Y_1Y_2	36.00	1	36.00	1.08	0.3172	8.564E-004	1	8.564 E-004	0.067	0.7998
Y_1Y_3	156.25	1	156.25	4.70	0.0494	0.024	1	0.024	1.84	0.1976
Y_1Y_4	12.25	1	12.25	0.37	0.5544	8.037E-003	1	8.037 E-003	0.63	0.4420

Y_2Y_3	4.00	1	4.00	0.12	0.7343	0.045	1	0.045	3.49	0.0846
Y_2Y_4	49.00	1	49.00	1.47	0.2465	9.328E-003	1	9.328 E-003	0.73	0.4084
Y_3Y_4	9.00	1	9.00	0.27	0.6117	0.18	1	0.18	13.70	0.0027
Residual	432.43	13	33.26			0.17	13	0.013		
Lack of fit	432.43	10	43.24			0.17	10	0.017		
Pure error	0.000	3	0.000			0.000	3	0.000		
Core total	16844.80	29				20.96	29			

The reliability of developed models for both responses of SU treated with MMO and doped-MMO was examined by constructing diagnostic plots of normal % probability versus studentized residuals, studentized residuals versus predicted and predicted versus actual for the experimental data as shown in Figure 4.5.1 and Figure 4.5.2 respectively. From the plots of normal % probability versus studentized residuals, it was observed that residuals are in the proximity of the straight diagonal line which confirms the normal distribution of observed data.

In the case of studentized residuals versus predicted, the random scatter in the plot indicates that the standard deviation separating the predicted values from actual. Therefore, developed models are considered to be satisfactory because the residuals for the prediction of each response are minimum. The data points predicted versus the actual plot for SU were found very close to the diagonal line indicating the adequate agreement between experimental data and predicted data.

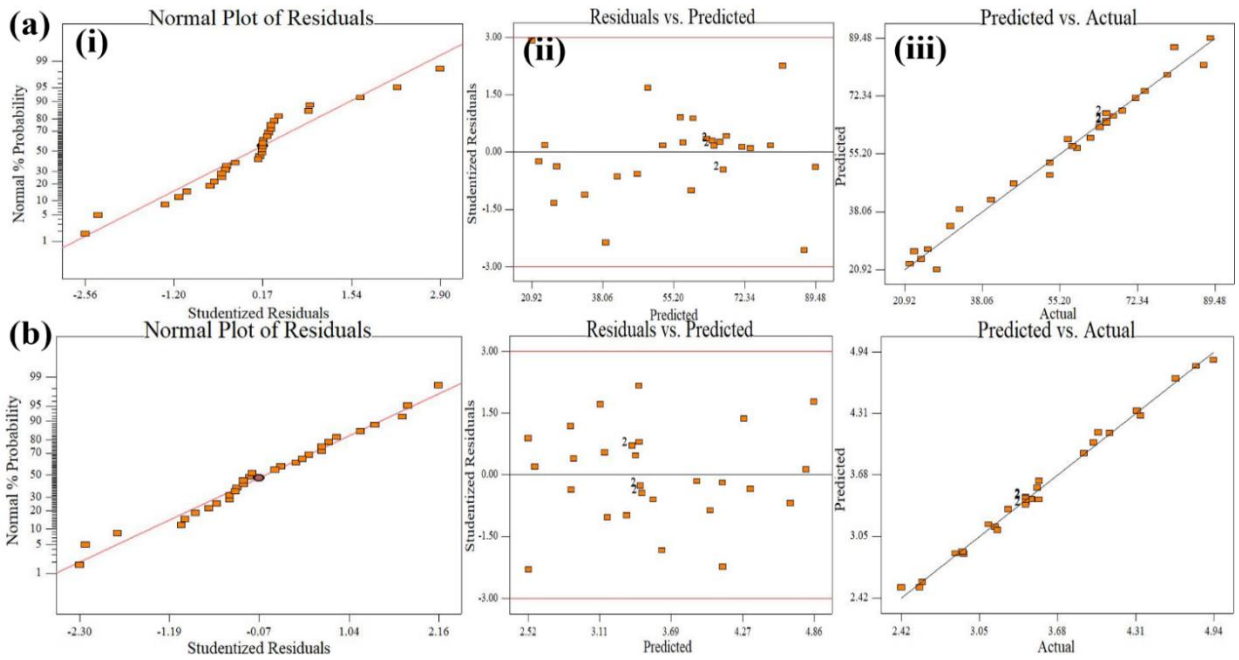

Figure 4.5.1 Plots of (i) normal % probability versus studentized residuals; (ii) studentized residuals versus predicted and (iii) predicted versus actual for responses (a) %COD removed and (b) SEC of SU treated with MMO.

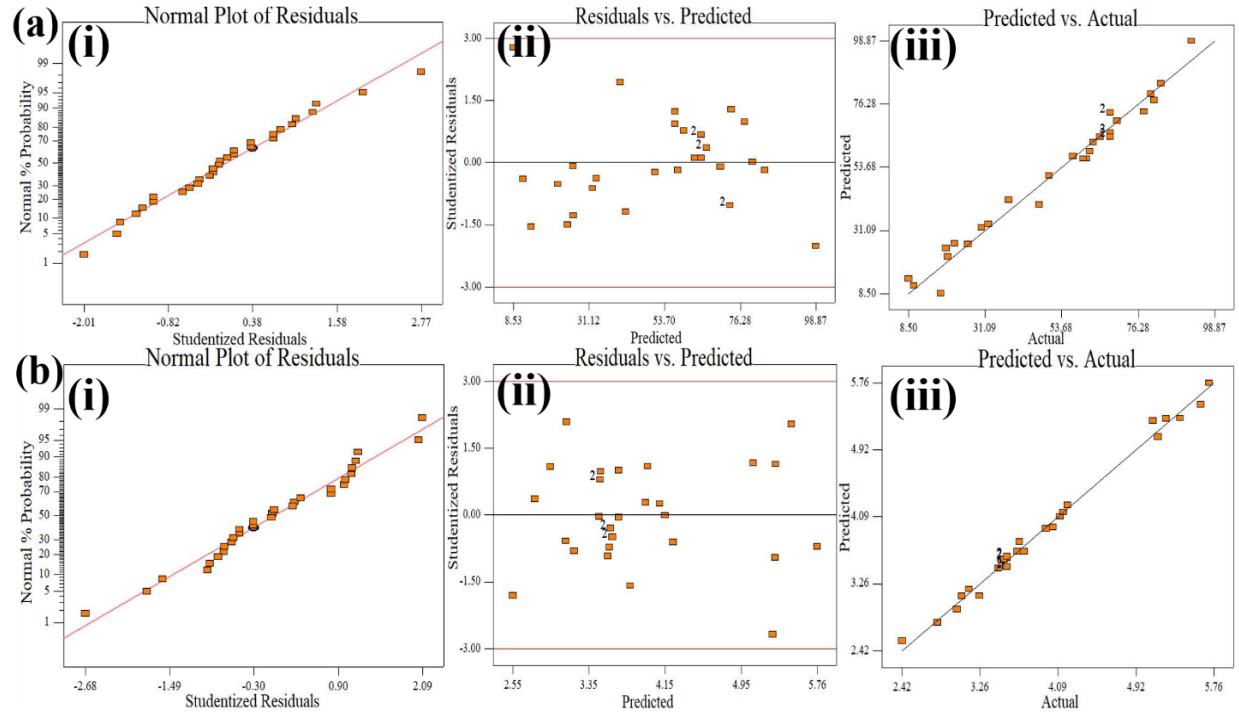

Figure 4.5.2 Plots of (i) normal % probability versus studentized residuals; (ii) studentized residuals versus predicted and (iii) predicted versus actual for responses (a) %COD removed and (b) SEC of SU treated with doped-MMO.

4.5.2 Effect of Process Parameters and Optimization

To explore the effect of EO operational parameters, 3D response surface graphs obtained from RSM were observed.

4.5.2.1 Effect of j and N/Cl ratio on % COD removed, (Z_1) of SU treated with MMO and doped-MMO

Several researchers have reported the successful use of MMO and doped-MMO for the treatment of mixed wastewaters such as industrial, leachate, domestic wastewater, etc. via producing in-situ strong oxidants (Cui et al., 2009; Rio et al., 2009; Wu et al., 2014). SU contains many dissolved ionic inorganic species resulting in good conductivity and makes the EO method suitable for its treatment as no additional chemical is required. Hence it becomes necessary to study the effect of various operational parameters on oxidation of SU using MMO and doped-MMO. Several studies have reported j as an important operating parameter in the EO remediation process because it regulates the amount of ROS produced on the surface of the anode. In this experimental work, the effect of j and N/Cl ratio on EO treated SU with MMO was analyzed by varying j from 19.04 to 47.61 mA/cm^2 and N/Cl ratio from 0.3 to 1.7. Figure 4.5.3a has shown the interaction between j and N/Cl as well as their simultaneous effect on Z_1. The graph results showed that Z_1 was maximum at lower values of N/Cl ratio upto 0.65 and then found decreasing gradually with an increasing ratio of ≈ 1.7. This trend was found on all values of j. However, with increasing values of j, a marginal gradual increase in Z_1 was observed at the N/Cl ratio of ≈ 0.45. Further increase in N/Cl ratio from 1 to 1.7, it was found that Z_1 first increased upto 33.33 mA/cm^2 and then decreased with increasing j values ≈ 47.61 mA/cm^2.

While in the case of SU treated with doped-MMO (Figure 4.5.4a), results showed that at lower values of N/Cl ratio from 0.2 to 0.5, Z_1 was found increasing with increasing value of j from 26.19 to 51.19 mA/cm^2. However further increase in j value from 51.19 mA/cm^2 to 59.52 mA/cm^2 showed no significant change in values of Z_1 for N/Cl ratio upto 0.5. While in the case of N/Cl ratio it has been observed that with increasing values of N/Cl ratio from 0.2 to 0.8, Z_1 was found increasing marginally for all values of j. But the further increase in N/Cl ratio from 0.8 to 1.4, showed a gradual decrease in Z_1. This trend was observed for all values of j. The results depict the changes in values of Z_1 during the EO at different values of applied j. From the experimental results it was found that at lower values j and higher values of N/Cl ratio, the Z_1 was minimum. However, when j was

increased and N/Cl ratio decreased, Z_1 was found maximum. This happens because, at lower values of j, generation of reactive oxidant species on MMO and doped-MMO anodes was fallen down gradually with time. Due to which rate of pollutant removal decreased which further led to minimum treatment process efficiency. But when j increased, the Z_1 was found maximum because of the increased generation of $MO_x(OH^{\bullet})$ and MO_{x+1} at the surface of anodes. This could be due to a concomitant acceleration of reaction as shown in Equations 4.5.5 and 4.5.6 respectively.

$$MO_x + H_2O \longrightarrow MO_x(OH^{\bullet}) + H^+ + e^- \quad \textbf{(4.5.5)}$$

$$MO_x(OH^{\bullet}) \longrightarrow MO_{x+1} + H^+ + e^- \quad \textbf{(4.5.6)}$$

Where M = anode (MMO/doped-MMO). However, further increase in j from values led to the marginal increase from 40.47 mA/cm^2 to 47.61 mA/cm^2 because of higher increase in rate of reaction occurred in Equation 4.5.6 compared to reaction occurred in Equation 4.5.5 resulting in generation of MO_{x+1} radicals as well as enhancement of OER. Moreover, the side reactions relatively decreased the amount of these oxidants, and further oxidized into O_2, weak oxidants like peroxodisulfate (4.5.7), peroxodiphosphate (4.5.8) and percarbonate (4.5.9) and ozone (4.5.10) in bulk.

$$2\ SO_4^{2-} \longrightarrow S_2O_8^{2-} + 2\ e^- \quad \textbf{(4.5.7)}$$

$$2\ PO_4^{3-} \longrightarrow P_2O_8^{2-} + 4\ e^- \quad \textbf{(4.5.8)}$$

$$2\ CO_3^{2-} \longrightarrow C_2O_6^{2-} + 2\ e^- \quad \textbf{(4.5.9)}$$

$$3H_2O \longrightarrow O_3 + 6\ H^+ + 6\ e^- \quad \textbf{(4.5.10)}$$

The N/Cl ratio plays a significant role because it influences the efficiency of the EO process by increasing the conductivity of a solution and makes the process less expensive. It defines the amount of RCS such as HClO, ClO^-, etc. formed during EO treatment of pollutants. At a higher N/Cl ratio the amount of nitrogen content was much more than the amount of chloride which leads to the blockage of active sites on anode surface and decreases the oxidation of chloride into RCS. Hence, it decreases the treatment efficiency. However, on increasing the amount of chloride in solution, depletes the pollutants rapidly from solution by generating more RCS from the oxidation of chloride at the surface of anode resulting in more COD removal. Moreover, MMO (containing active metals) exhibits better electrocatalytic properties for chlorine evolution. It concludes that lower values of the N/Cl ratio lead to the rise in organic degradation in SU.

However, in case of doped-MMO (containing non-active metals) showed maximum Z_1 at very low values of N/Cl ratio than MMO because the generation of RCS at these types of anodes is less as compared to MMO anode. Although the % COD removed with doped-MMO has been due to the

synergistic effects of RCS and ROS (Hiwarkar et al., 2017). During EO treatment, with decreasing N/Cl ratio, the concentration of Cl^- increases in the solution, resulting in the generation of more RCS which reacts with pollutants resulting in maximum Z_1. Therefore, for maximum removal rate without a decrease in current efficiency and overall process efficiency, optimum values of j and N/Cl ratio should be chosen.

4.5.2.2 Effect of pH and t on % COD removed, Z_1 of SU treated with MMO and doped-MMO

Figure 4.5.3b shows the interaction between pH and t as well their effect on, Z_1 (MMO anode). To see the effect of time and pH on oxidation of SU, values of t varied from 6.0 h to 12.0 h while pH was varied from 3 to 9. The graph results showed that Z_1 was found maximum with increasing values of t. this pattern was observed at all pH values. However, in the case of pH, Z_1 was found decreasing with increasing values of pH for all t values. The maximum value of Z_1 was observed at higher values of t upto 10.5 h, however, a further increase in t values ≈ 12.0 h, Z_1 was found constant. While in the case of pH, Z_1 was found maximum at lower values of pH ≈ 4.5 and minimum at higher values of pH ≈ 9.

Figure 4.5.4b shows the interaction between pH and t as well their effect on, Z_1 (doped-MMO). The results showed that an increase in values of t from 7.0 h to 10.0 h, Z_1 was found increasing at all values of pH. However, a further increase in values of t from 10.0 h to 13.0 h showed maximum values of Z_1 for pH values upto 6, while minimum in case of pH values 6 to 9.5. From the results, it has been observed that the oxidative power of electro-generated species is strongly dependent on solution pH. The standard reduction potential of Cl_2 and HCl is considerably higher than ClO^-, indicates faster oxidation of pollutants when mediated by RCS is obtained under acidic pH acidic conditions in case of MMO anodes. While in the case of doped-MMO it has been reported that in acidic solution, oxygen evolution was controlled to such an extent, so as the generation of $OH^\bullet$ and H_2O_2 in the solution could be increased. Therefore, the COD removal rate in acidic conditions is preferable over alkaline conditions. Moreover, the formation of strong oxidizing substances such as H_2O_2 and $OH^\bullet$ was inhibited under alkaline conditions and hence did not help the oxidation of pollutants present in SU. The optimization of time is very important for maximum Z_1 and longer stability of anodes because during EO an impermeable film developed which causes passivation of anode surface, thus increases the oxygen gas evolution.

4.5.2.3 Effect of j, pH, n, and t on SEC, Z_2 of SU treated with MMO and doped-MMO

Figure 4.5.3c shows the interaction between pH and N/Cl ratio as well as their effect on, Z_2 (MMO). The results depict that Z_2 was found decreasing with increasing N/Cl ratio upto 1.0, for all values of pH. Further increase in N/Cl ratio from 1.0 to 1.7, led to an increase in values of Z_2 for all values of pH. However, the values of Z_2 was found maximum at higher values of pH from 7.5 to 9.0 at N/Cl ratio ≈ 1.7. At lower values of N/Cl ratio upto 0.3, Z_2 was found constant for all values of pH. It depicts that at lower values of the N/Cl ratio, there was no effect of pH was observed on Z_2. While at higher values of N/Cl ratio ≈1.7, Z_2 was found increasing with increasing values of pH.

However, in the case of doped-MMO (Figure 4.5.4c), the result showed that an increase in values N/Cl ratio from 0.2 to 1.4 has increased the values of Z_2 for all values of pH. This could be due to the lower conductivity of the solution as well as an increase in the voltage drop. Furthermore, it has been observed that Z_2 was found increasing with increasing values of pH. This was due to the production of strong RCS and ROS such as (HOCl, Cl_2, $OH^{\bullet}$, etc.) at lower pH lead to maximum oxidation in lesser time and required minimum energy. While at alkaline pH, low oxidation potential reactive species such as (OCl^-, H_2O_2, $HO_2^{\bullet}$, etc.) were dominant due to which degradation efficiency was found minimum resulting in more energy consumption.

Figure 4.5.3d (MMO) and Figure 4.5.4d (doped-MMO) show the interaction between j and t as well as their effect on Z_2. The results of the graph (4.5.3d) for MMO showed that at lower values of t upto 7.5 h and j upto 26.18 mA/cm^2, Z_2 was found to be minimum. However, a further increase in j and t values i.e. 47.61 mA/cm^2 and 12.0 h respectively showed a gradual increase in values of Z_2. While in the case of doped-MMO, the results of the response graph (Figure 4.5.4d) showed that at a lower value of t ≈ 7.0 h, Z_2 was found increasing with increasing values of j from 26.19 mA/cm^2 to 59.52 mA/cm^2. Furthermore, it has been observed that with an increasing value of t from 7.0 h to 10.0 h, Z_2 was found decreasing first and then increased with increasing values of t from 10 to 13 h. this trend was found on all values of j. Moreover, at a higher value of t ≈ 13.0 h, Z_2 was found increasing values of j. In general, SEC (Z_2) highly dependent upon the type of anode and operational input parameters. As it can be seen that with increasing j values, Z_2 varies directly at all values of t due to various factors like electrode deactivation, decrease in the concentration of ions and an increase in solution temperature.

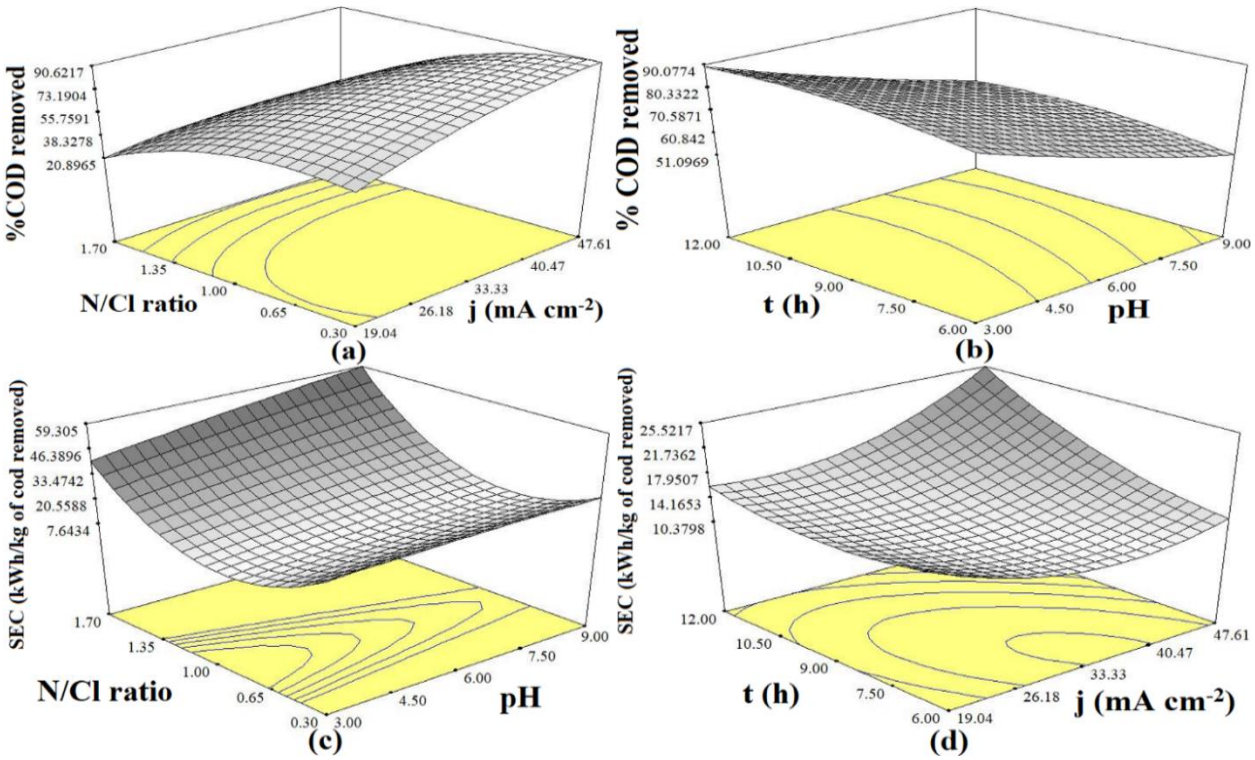

Figure 4.5.3 3D response graphs for EO treatment of SU with MMO (a) %COD removed versus N/Cl ratio and j; (b) %COD removed versus pH and t; (c) SEC versus N/Cl ratio and pH and (d) SEC versus t and j

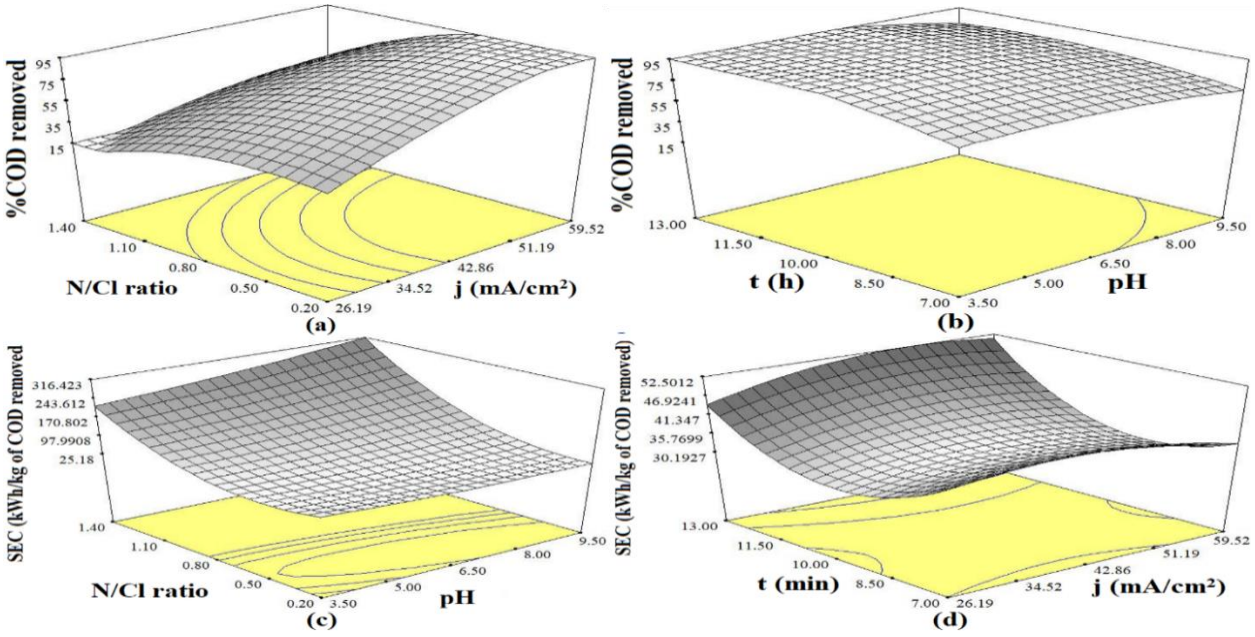

Figure 4.5.4 3D response graphs for EO treatment of SU with doped-MMO (a) %COD removed versus N/Cl ratio and j; (b) %COD removed versus pH and t; (c) SEC versus N/Cl ratio and pH and (d) SEC versus t and j

Optimization of operating parameters with the responses (Z_1 and Z_2) for the treatment of SU using the EO process with MMO and doped-MMO anode were carried out by multi-response process optimization by desirability function approach. One-sided desirability (di) and overall desirability (D) were calculated by using maximum (Z_1) and minimum (Z_2) acceptable values of both responses. The desirability for response Z_1 for SU was calculated with acceptable values of $Z_{1\text{-}min}$ as 22.0% and $Z_{1\text{-}max}$ as 88.5%. Similarly, for the response, Z_2 was calculated by taking $Z_{2\text{-}min}$ as 11.19 and $Z_{2\text{-}max}$ as 140.00 kWh/kg of COD removed respectively as shown in Equations 4.5.11 and 4.5.12. Similarly, desirability for responses Z_1 and Z_2 were calculated and shown in Equations 4.5.13 and 4.5.14.

$$d_{1(SU)} = \begin{cases} 0 & if\ Z_1 \leq 22.0 \\ \left[\frac{Z_1 - 22.0}{88.5 - 22.0}\right] & if\ 22.0 < Z_1 < 88.5 \\ 1 & if\ Z_1 \geq 88.5 \end{cases} \quad \textbf{(4.5.11)}$$

$$d_{2\ (SU)} = \begin{cases} 0 & if\ Z_2 \leq 11.19 \\ \left[\frac{Z_2 - 11.19}{140.00 - 11.19}\right] & if\ 11.19 < Z_2 < 140.00 \\ 1 & if\ Z_2 \geq 140.00 \end{cases} \quad \textbf{(4.5.12)}$$

$$d_{1(SU)} = \begin{cases} 0 & if\ Z_1 \leq 8.5 \\ \left[\frac{Z_1 - 8.5}{92 - 8.5}\right] & if\ 8.5 < Z_1 < 92 \\ 1 & if\ Z_1 \geq 92 \end{cases} \quad \textbf{(4.5.13)}$$

$$d_{2\ (SU)} = \begin{cases} 0 & if\ Z_2 \leq 11.30 \\ \left[\frac{Z_2 - 11.30}{301.78 - 11.30}\right] & if\ 11.30 < Z_2 < 301.78 \\ 1 & if\ Z_2 \geq 301.78 \end{cases} \quad \textbf{(4.5.14)}$$

Synchronized optimization of all input variables was done for maximizing the %COD removed, Z_1 and minimizing the SEC, Z_2 by keeping the operational parameters in range. The best optimized conditions of process parameters and value for responses Z_1 and Z_2 suggested by BBD for each electrode were shown in Table 4.5.5a,b. In order to confirm these suggested values of responses, further experiments were conducted in triplicate at the optimized condition. The average experimental value of each response i.e. Z_1 and Z_2 for SU were found very close to the predicted values as shown in Table 4.5.6. This concludes that the optimization of EO treatment of SU with MMO and doped-MMO using BBD under RSM was successfully done.

Table 4.5.5a Individual and multi-response optimization results of SU treated with MMO for desirability calculations					
Response	j (mA/cm^2)	N/Cl ratio	t (h)	pH	Desirability
Individual Response optimization					
% COD removed (Z_1)= 91.234%	43.06	0.46	10.26	4.42	1
SEC (Z_2) = 2.400 kWh/ kg of COD removed	21.82	0.35	7.00	5.51	1
Simultaneously optimization of responses					
% COD removed (Z_1)= 86.056%	30.33	0.42	8.79	3.42	0.985
SEC (Z_2) = 11.78 kWh/kg of COD removed					

Table 4.5.5b Individual and multi-response optimization results of SU treated with doped-MMO for desirability calculations					
Response	j (mA/cm^2)	N/Cl ratio	t (h)	pH	Desirability
Individual Response optimization					
% COD removed (Z_1)= 94.89%	54.80	0.35	10.47	4.13	1
SEC (Z_2) = 11.86 kWh/ kg of COD removed	42.86	0.27	7.65	4.09	0.985
Simultaneously optimization of responses					
% COD removed (Z_1)= 91.99%	53.91	0.25	10.05	4.20	0.941
SEC (Z_2) = 21.175 kWh/kg of COD removed					

Table 4.5.6 Comparison between the predicted and actual EO experimental values of SU at optimized conditions			
Electrodes	Responses	Predicted	Actual
MMO	% COD removed	86.056	85.25
	SEC (kWh/kg of COD removed)	11.88	11.75
Doped-MMO	% COD removed	91.99	90.55
	SEC (kWh/kg of COD removed)	21.157	20.851

Figure 4.5.5 represents the changes in conductivity and pH during the electrolysis of SU with MMO and doped-MMO at optimized conditions. From the results (Figure 4.5.5a), it has been observed that not much significant change in conductivity was seen during the treatment of SU with MMO (17.0 to 18.0 mS/cm) and doped-MMO (17.0 to 18.6 mS/cm) anodes. This depicts the lower formation of additional inorganic ionic species from the oxidation of salts or mineralization of organic nitrogen during the treatment of SU by both anodes (Dbira et al., 2019). Additionally, a significant difference in the pH change was observed during the treatment of SU by both anodes (4.5.5b). The initial pH was maintained constant i.e. 3.42 (MMO) and 4.20 (doped-MMO) during the electrolysis of SU.

In the case of MMO, a rapid and gradual increase in pH from 3.42 to 6.75 was observed within 4.5 h of EO treatment, and for all t> 4.5 h, pH_f stabilizes to 8.0. While in the case of doped-MMO, a continuous increase from 4.2 to 7.7 was observed within 6.0 h of EO treatment, and a further increase in t> 6.0 h led to a marginal increase from 7.7 to 8.5 pH_f. This increase in pH during the EO treatment of SU is related to the electrochemical reaction taking place on the surface of both anodes. This might be due to the conversion of calcium and magnesium ions into precipitates at alkaline conditions. Moreover, a gradual decrease of phosphate ion concentration (graph shown in section 4.5.4) due to the formation of soluble complexes of calcium and magnesium, and hence resulting in a significant change in pH of SU solution (Li et al., 2015).

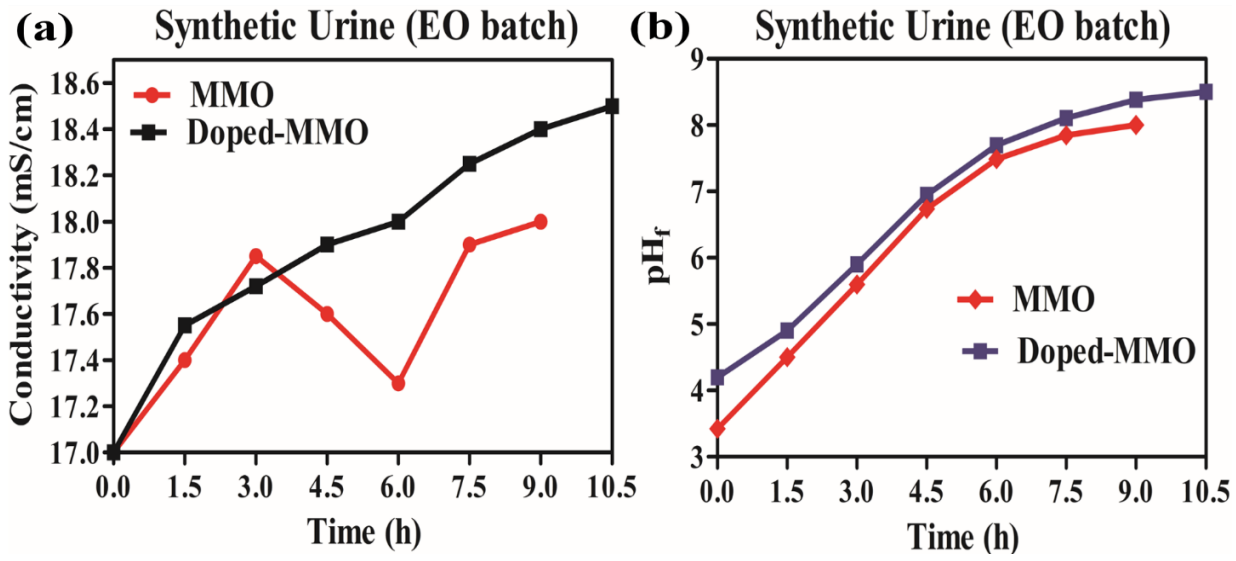

Figure 4.5.5 Changes in the (a) conductivity and (b) pH of the electrolyte during the EO treatment of SU treated by both anodes at optimized conditions.

4.5.3 Synergistic Studies

In the present work, the synergy of one process over the other for dual effect has been calculated and quantified using kinetic rate constant obtained through pseudo-first-order reactions. The oxidation experiments for SU were performed with MMO in a batch reactor under UV and with doped-MMO under solar light. Figure 4.5.6a,b shows the results for COD removal of SU treated with MMO through different processes i.e. PC, EO, and PEC (UV). Among all the processes, %COD removal of SU was found maximum in the dual process i.e. PEC over individual processes. Furthermore, treatment time for SU through PEC was also found to be reduced from 8.8 h to 6.0 h. PC treatment was found less efficient for %COD removal as compared to the other two processes. Figure 4.5.6c shows the plot of the rate constant versus different treatment processes. From the results, it was depicted that an immense increase in the first-order rate constant in case of the integrated process (0.2991 h^{-1}) which was 10.2 times of PC (0.0294 h^{-1}) and 1.25 times to EO (0.2334 h^{-1}). Thus, proves the viability of the dual-process over a single treatment process. Moreover, a synergistic effect of the dual-process i.e. PEC for over EO came out to be 22.0% and over PC was observed 99.17% respectively. The overall % synergy for SU came out to be 12.14%. -

In contrast, % COD removal of SU treated with doped-MMO through PC, EO, and PEC (solar light) was found higher than the MMO treated SU. As expected, among all the processes % COD removal of SU was found maximum in the dual PEC (under solar radiation) over individual processes. Furthermore, treatment time for SU through PEC was also found to be significantly reduced from 10.05 h to 6.5 h as shown in Figure 4.5.7a,b. Furthermore, the results of Figure 4.5.7c has shown a maximum value of k for PEC (0.3264 h^{-1}) over PC (0.0339 h^{-1}) and EO (0.261 h^{-1}). Moreover, the % synergy of PEC for over EO and PC came out to be 20.04% and 89.61% respectively. The overall % synergy for SU treated with doped-MMO was came out to be 9.65%.

This happened because, in the case of PEC, the production of a strong oxidant such as $OH^{\bullet}$ under UV light (MMO) and under sunlight (doped-MMO) was more than the EO treatment process and hence resulted in more % COD removal. Hence, this proves that $OH^{\bullet}$ (ROS) was also being involved during the oxidation of pollutants present in SU along with RCS. Therefore, it concludes that the dual-process with synergistic results has cued its large scale application for the treatment of urinal wastewater with a significant reduction in electrolysis time.

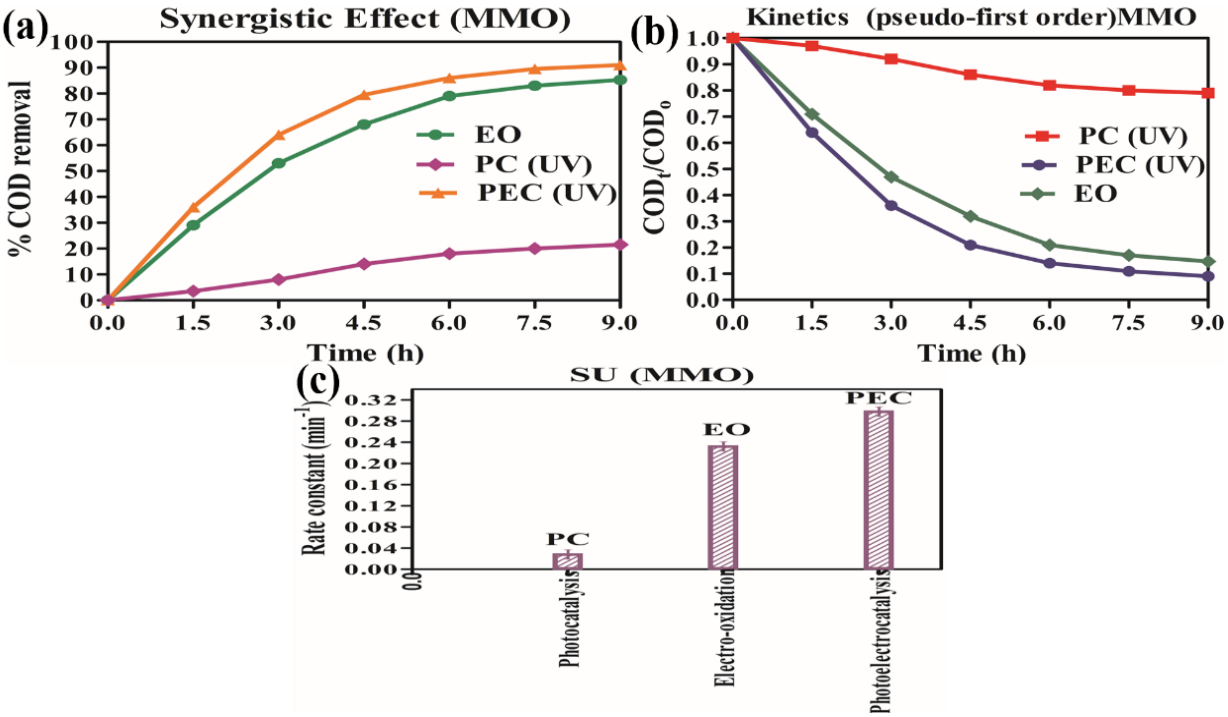

4.5.6 Plot of synergistic effect for treatment of SU through different processes with MMO (a) % COD removal versus treatment time; (b) plot of C_t/C_0 versus time and (c) pseudo-first-order rate constant versus different processes

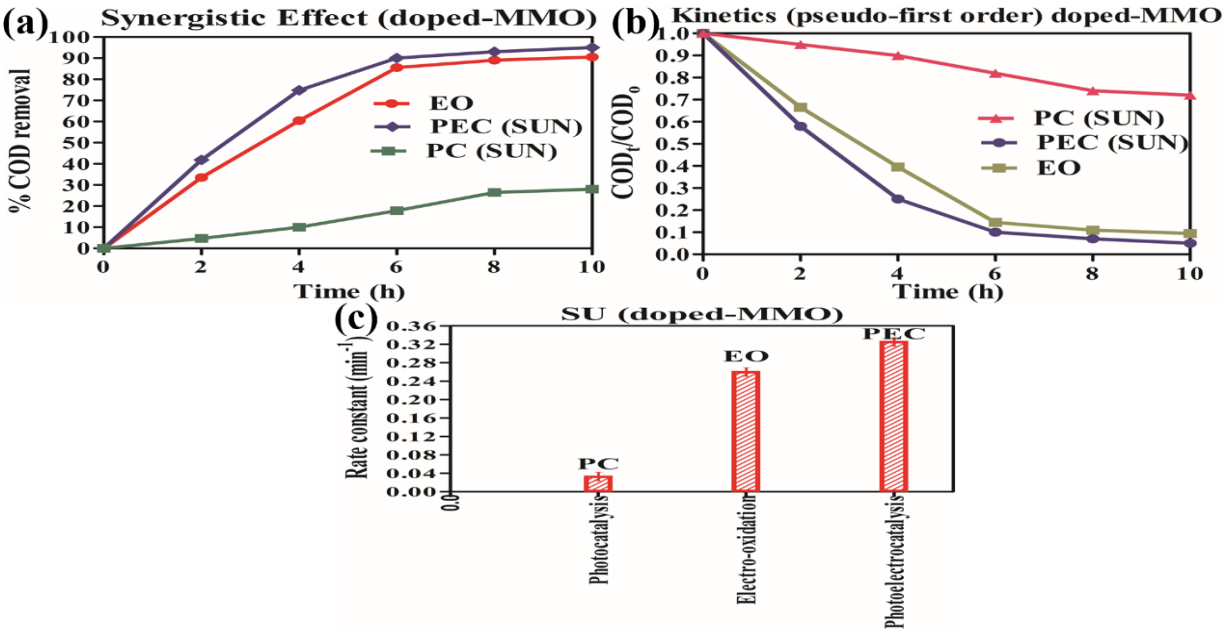

4.5.7 Plot of synergistic effect for treatment of SU through different processes with doped-MMO (a) % COD removal versus treatment time; (b) plot of C_t/C_0 versus time and (c) pseudo-first-order rate constant versus different processes

4.5.4 Mineralization Studies

In view of EO treated SU samples quality, mineralization studies were performed at optimized conditions in terms of in-situ chemical analysis, CV, FT-IR and LC-MS analysis.

Chemical analysis: The quality of treated and untreated samples were checked by performing in-situ chemical analysis. This analysis would depict the results of the transformation of organic and inorganic pollutants into carbon dioxide, water and inorganic salts. Mineralization of SU was confirmed through a reduction in COD (87.25%) and TOC (85.88%) at optimized conditions as shown in Figure 4.5.8a. While in the case of doped-MMO, the reduction was found slightly higher than MMO at optimized conditions as shown in Figure 4.5.9a.

The oxidation of nitrogen-based organic matter (present in SU i.e. uric acid, creatinine and urea) into inorganic ions such as NO_2^-, NO_3^- and NH_4^+ were checked by ion testing analysis. The total nitrogen present in SU was around 6300 mg/L. The most of the nitrogen (≈ 95%) associated with urea present in untreated SU, rest is being free NH_4^+ and organic nitrogen associated with creatinine and uric acid respectively. A continuous sharp increasing trend was observed for the generation of $NO_2^-$and NH_4^+ while the concentration of NO_3^- increases slowly as depicted in Figure 4.5.8b. However, the concentration of NO_2^- and NH_4^+ were found depleting after 3.0 h and 4.5 h of electrolysis indicating the conversion of NO_2^- into NO_3^-. While in the case of NO_3^-, a continuous increase in concentration was observed until the end of electrolysis. This might be due to the reaction between NH_4^+ and HOCl. In the case of NO_3^-, the increase was observed due to the oxidation of chloramines by free chlorine. An important observation was observed that the difference between the concentration of nitrogen and its generated species was not much indicating the almost conversion of nitrogen into inorganic ions during electrolysis with MMO. Similar kind of results has been observed when SU was treated with doped-MMO at optimized conditions as shown in Figure 4.5.9b.

From Figure 4.5.8c (MMO) and Figure 4.5.9c (doped-MMO), it can be observed that chloride level was continuously decreasing during the electrolysis of SU. This is because of the oxidation of chloride on the anode to produce strong RCS like Cl_2, HOCl, OCl^-, etc. for the destruction of organic matter present in SU. The level of TAC increased gradually during the EO treatment of urea and then increased sharply to higher values when urea was depleted to the maximum. During the treatment process, TAC an aggregate part of reactive intermediates does not

remain constant. This might be due to the balance between the oxidation of nitrogen-based components and the generation of chlorine species along with their bond forms during the treatment process as reported in the literature (Hernlem, 2005).

Figure 4.5.8d (MMO) and Figure 4.5.9d (doped-MMO) represent changes in the concentration of sulfates (SO_4^{2-}) and phosphates (PO_4^{3-}) with time during the EO treatment of SU wastewater. From the plot, it can be observed that the concentration of PO_4^{3-} was found decreasing with increasing time. This might be happening due to the acid-base distribution and solubility dependence of inorganic ions (PO_4^{3-}) on pH values, resulting in the formation of perphosphates. However in the case of SO_4^{2-} marginal or negligible change in concentration was found during the 8.8 h and 10.05 h of electrolysis, depicting the non-dependency on values of pH due to the higher solubility of sulfates in water (Dbira et al., 2015).

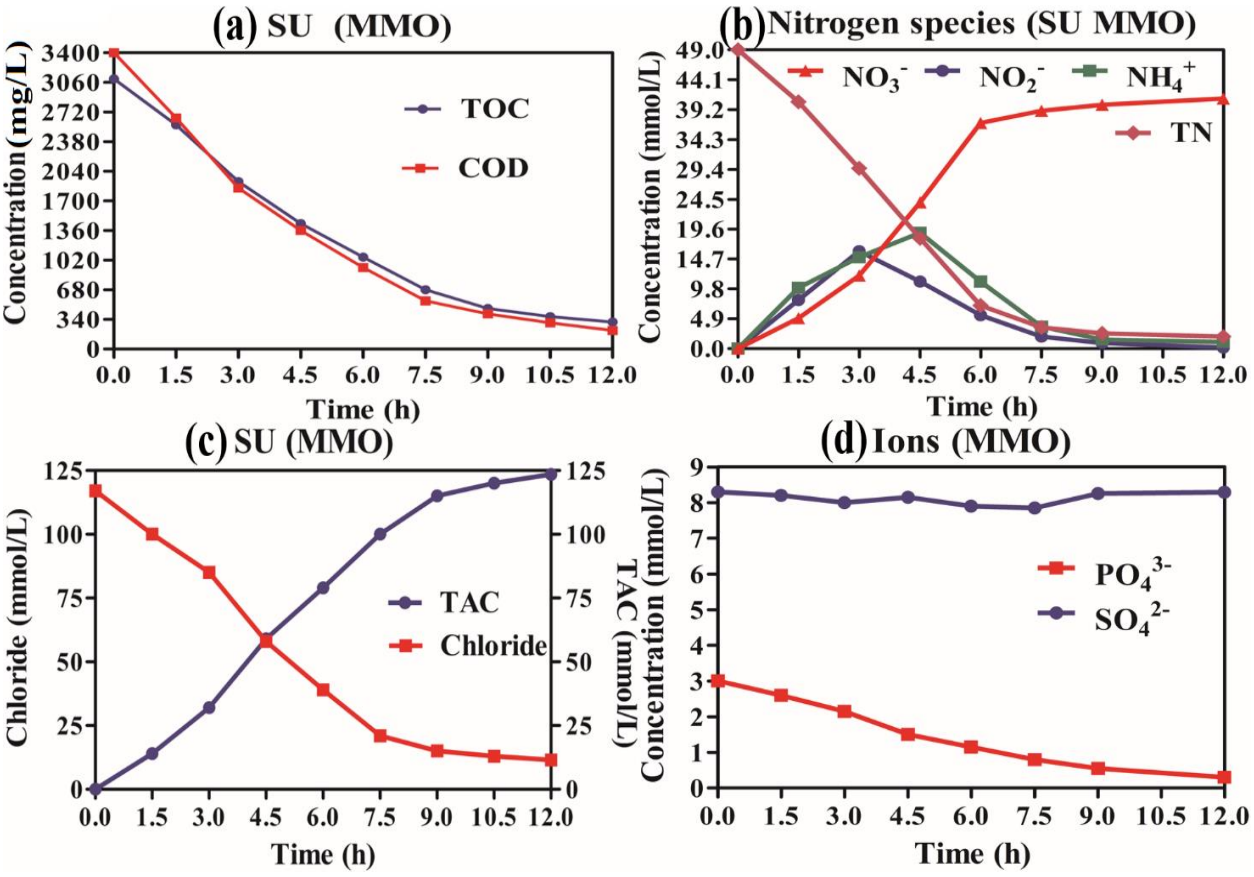

Figure 4.5.8 Plot of mineralization of SU treated with MMO anode at optimized conditions at different time intervals (a) concentration of COD and TOC; (b) generation of different nitrogen species; (c) concentration of chloride and TAC and (d) concentration of ions

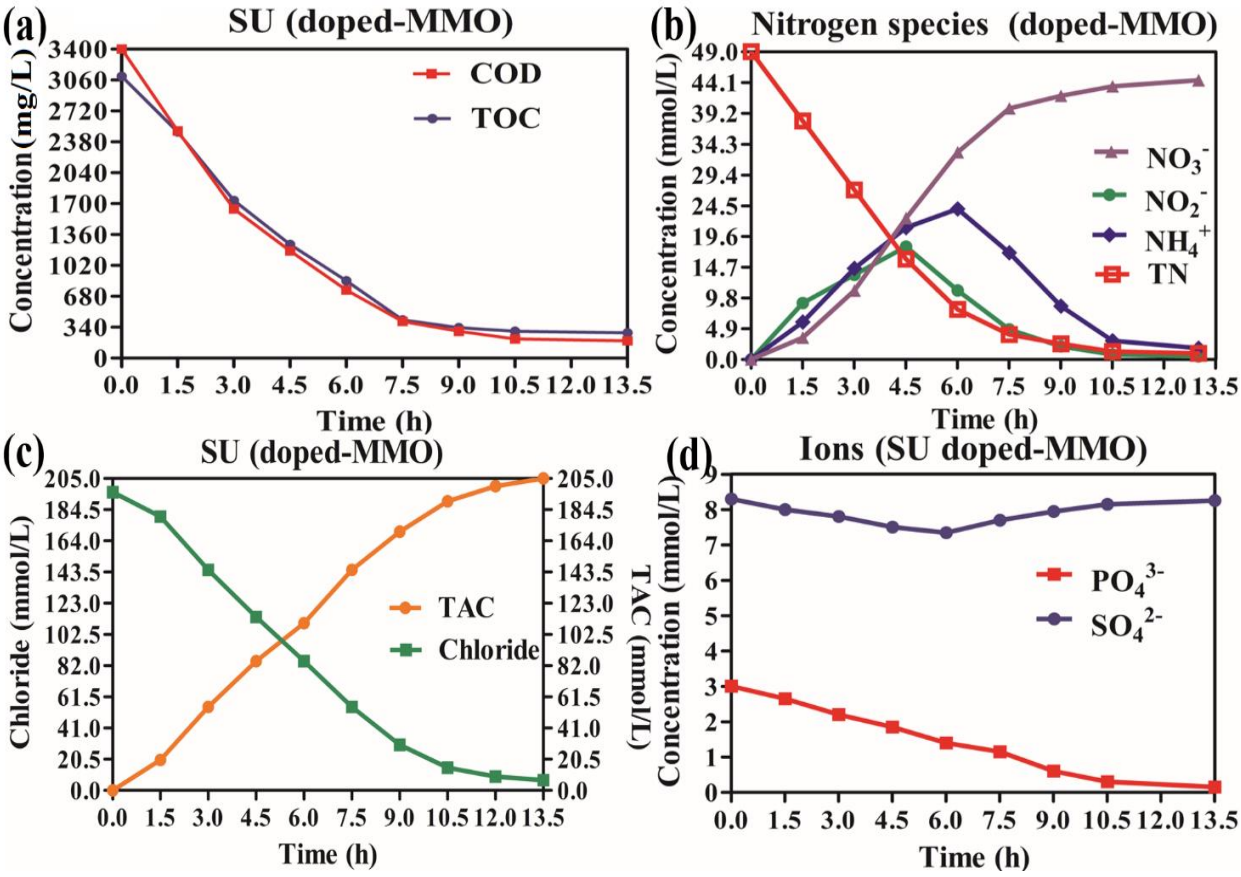

Figure 4.5.9 Plot of mineralization of SU treated with doped-MMO anode at optimized conditions at different time intervals (a) concentration of COD and TOC; (b) generation of different nitrogen species; (c) concentration of chloride and TAC and (d) concentration of ions

Cyclic Voltammetry (CV): Figure 4.5.10a,b shows the continuous CV for raw and final samples of SU treated with MMO and doped-MMO respectively, with a potential range of -1.2 to 0.0 V. The EO treated and untreated samples of SU has also shown a few visible peaks in the potential range window. As it can be seen that in 0 h samples (MMO) one oxidation peak at ≈ 0.0001 A while in the case of doped-MMO two oxidation peaks (0.00015 A, 0.0000 A) in a first cycle and one reduction peak at ≈ -0.0001 A (MMO and doped-MMO) has been observed. However, in the case of the treated sample, cycle 1 showed the disappearance of oxidation peak (MMO) and shifting of oxidation peaks (doped-MMO) while cycle 2 exhibit a remarkable decrease and shift in reduction peak from [(-0.9V to -0.85V (MMO); -0.9V to -0.7V (doped-MMO)]. These irreversible peaks attribute the oxidation and reduction mechanism that occurs during the electrolysis of SU on both anodes.

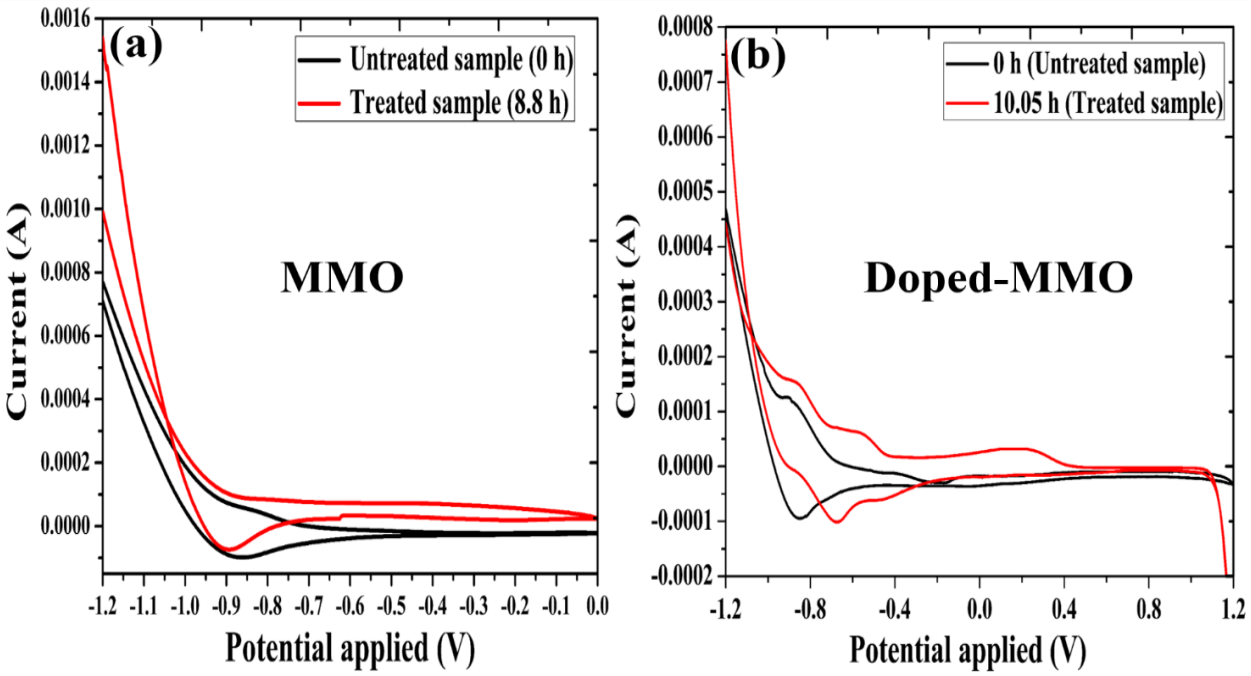

Figure 4.5.10 Cyclic Voltammetry measurements for untreated and treated samples of SU with (a) MMO and (b) doped-MMO at optimized conditions.

FT-IR analysis: To analyze the removal phenomenon of nitrogen-based organic pollutants from SU, FT-IR analysis of untreated and EO treated samples were done. Figure 4.5.11a,b represents the FT-IR spectra of SU treated with MMO and doped-MMO anode. The results showed that characteristic absorption broad peaks with wavenumber at 3254.8, 3388.64, 3455.08, 612.10, 698.80 and 781.84 cm^{-1}, respectively were formed due to the $OH^{\bullet}$ and chloro-oxidant species generated during EO treatment of SU. The sharp peaks at 1600.69, 1738.41, 3356.12 and 3455.08, respectively were due to the presence of characteristic absorption of C=O, C-H and N-H groups (Naz et al., 2017).

The vibrational frequency of C≡N, C=N, C-N, C=C stretching linked with the heterocyclic structure was around at 1101.36, 1215.1, 1349.93, 1581.68, 1656.12 and 1738.40, respectively (Kumar and Srivastava, 2018). However, few small peaks during electrolysis were also appeared in treated samples of SU at 1349.93, 1380.46, 905.44 and 1119.19, respectively which corresponds to N-O and C-O groups. The results show that most of the peaks were got shifted at distinct wavenumber, might be due to the structural changes occurred during the EO process. Some of the broad and sharp peaks present in raw samples (t= 0 h) were found disappeared in treated samples due to the oxidation of organic pollutants into intermediates via RCS and ROS generated during EO treatment of SU with MMO and doped-MMO anodes**.** Moreover, the % transmittance for maximum

peaks was found increased at optimized electrolysis treatment time, indicating the destruction and oxidation of the cyclic structure of organic pollutants. The FT-IR results of SU were almost similar to the FT-IR results of urine metabolites such as uric acid, creatinine and urea when treated individually (as discussed in section I, Chapter 4).

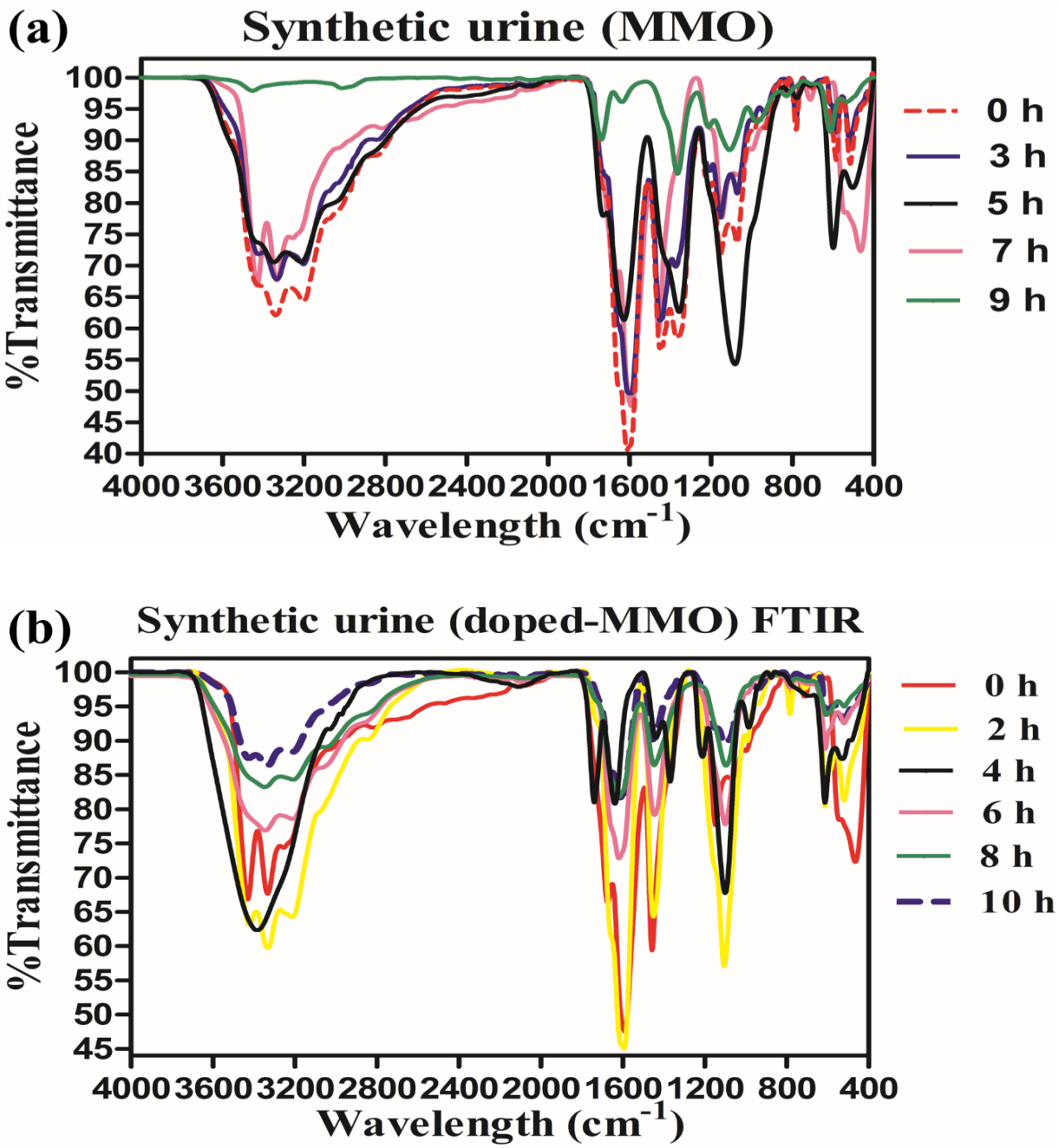

Figure 4.5.11 FT-IR spectra of SU treated with (a) MMO and (b) doped-MMO at optimized conditions for different time intervals

LC-MS analysis: The organic and inorganic components present in untreated and treated samples of SU with MMO and doped-MMO were identified through LCMS as shown in Figure 4.5.12a.The results of the untreated sample (0 h) have shown the sharp peaks of metabolites like urea, uric acid and creatinine while some few peaks were also observed which might belong to the inorganic components/salts. However, it was observed that after electrolysis most of the diagnosed organic components got eliminated and converted into intermediates like oxalic acid, 1-methylurea, guanidine, etc. while some new components were also diagnosed in trivial proportions. Further, oxidation of these intermediates via RCS and ROS might have produced products like carbon dioxide, water, nitrate, chloramines, etc. Based on the above discussion, a provisional common mechanism has been proposed for the treated SU with both anodes and shown in Figure 4.5.12b. Moreover, most of the intermediates generated during the electrolytes of SU were found almost similar to the intermediates generated during electrolysis of urine metabolites alone as discussed in former sections (4.3.4 and 4.4.4).

Further to confirm the oxidation of organic components such as urea, uric acid and creatinine, a spectrophotometric analysis was done. Figure 4.5.13a (MMO) shows that 97.5% of uric acid remove in 1.0 h only while urea (91.0%) and creatinine (87.5%) took 7.5 h to oxidize into non-toxic simpler compounds. However, in the case of doped-MMO, 98.50% of uric acid removed in 3.0 h, while 93.0% urea and 89.80% creatinine took 10.5 h to oxidize during EO treatment of SU as shown in Figure 4.5.13b. The results depict that EO treatment of SU with MMO took less time to oxidize organic components present in SU into byproducts as compared to doped-MMO. This might be due to the less formation of RCS at doped-MMO as compared to MMO. Several authors reported the significant amount of RCS generation at active metals (i.e. Pt, IrO_2, RuO_2, etc.) over non-active metals (i.e. SnO_2, Ta_2O_5) (Scialdone, 2009; Martinez-Huitle and Andrade, 2011). Furthermore, the non-toxicity of diagnosed components in the final samples of both anodes for SU was confirmed through the toxicity analysis test discussed in the next section 4.5.6.

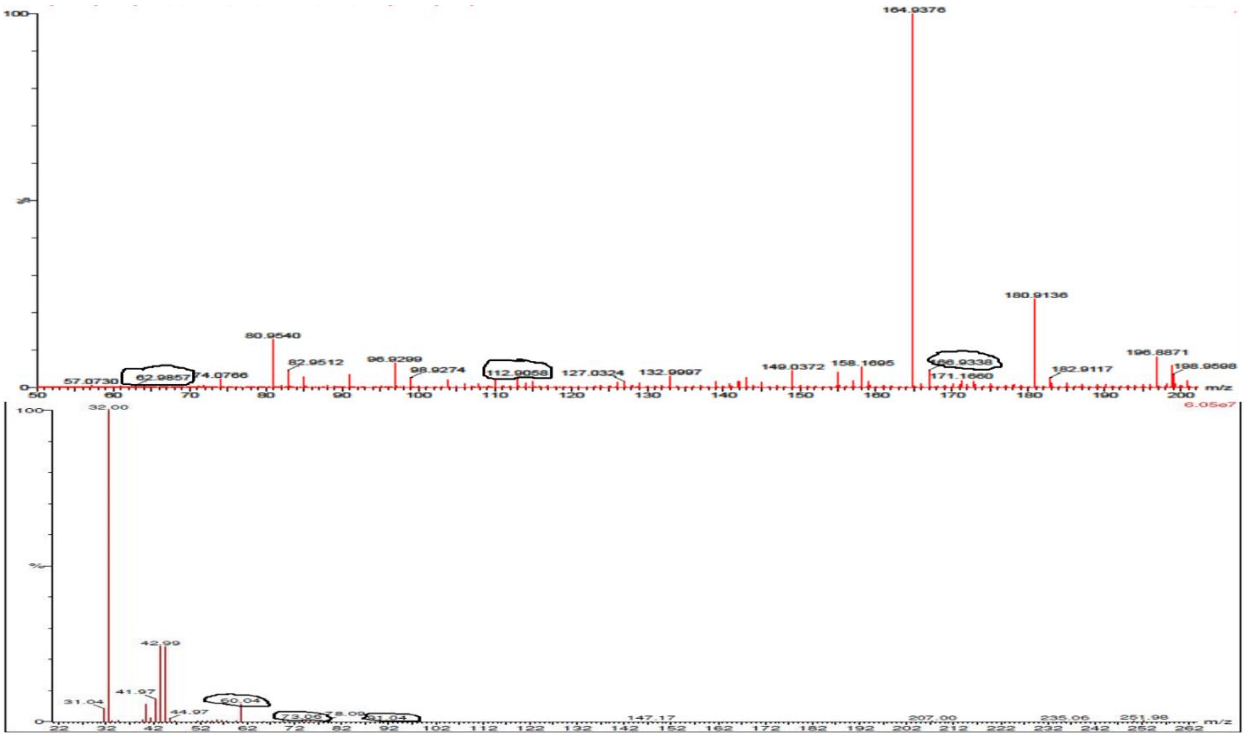

Figure 4.5.12a Mass spectra analysis for the identification of intermediates during the EO treatment of SU by both MMO and doped-MMO anodes at the optimized conditions.

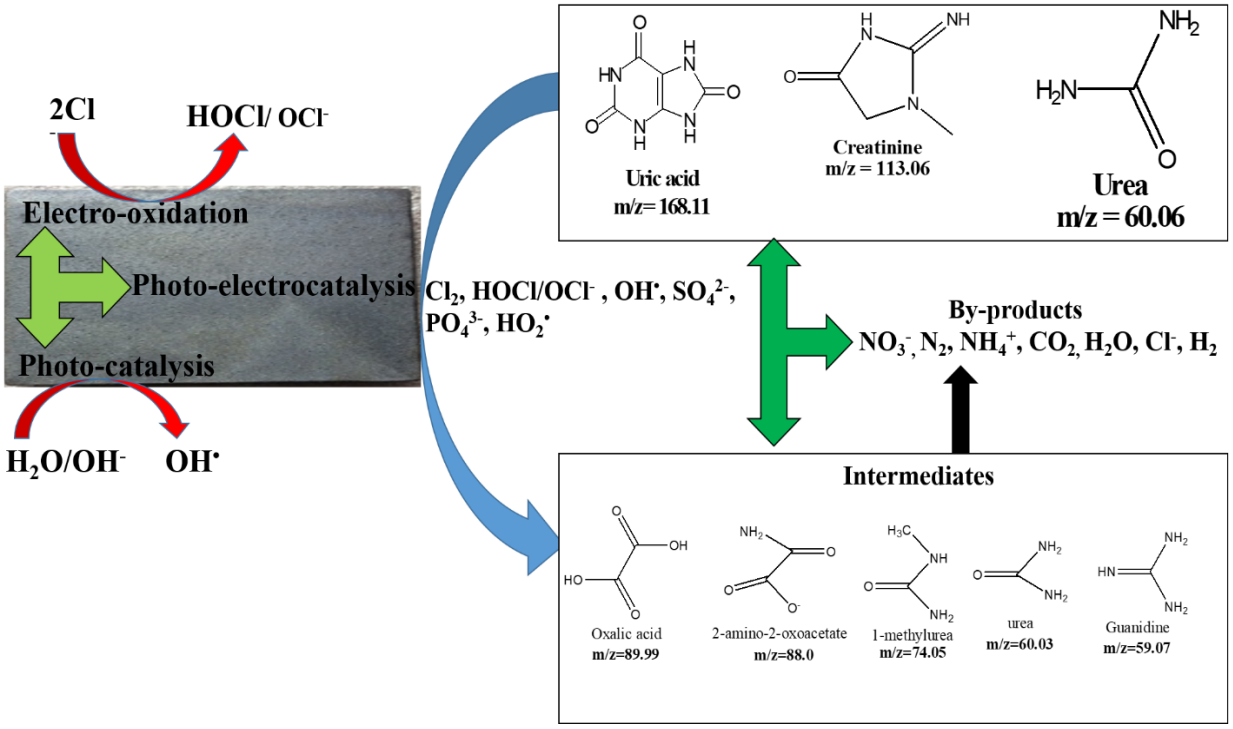

Figure 4.5.12b Common tentative proposed degradation pathway for SU treated by both MMO and doped-MMO anodes.

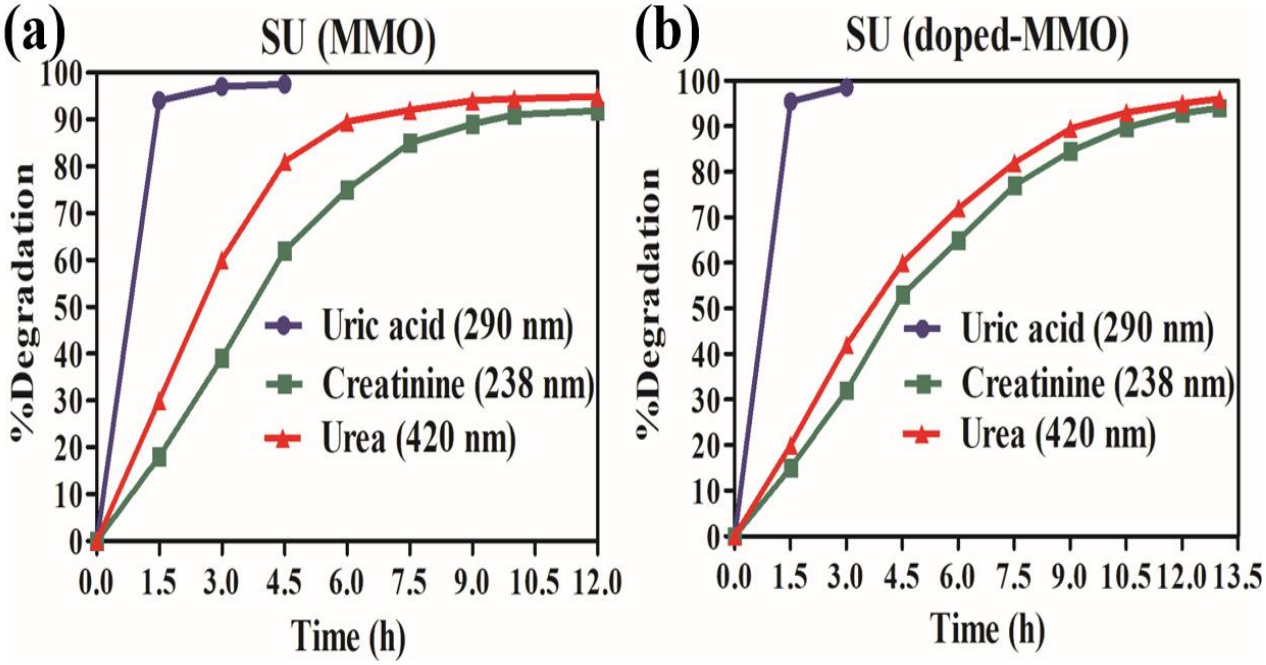

Figure 4.5.13 Plot of % Degradation of organic pollutants present in SU versus time treated with (a) MMO and (b) doped-MMO.

4.5.6 Toxicity Analysis

In order to check the quality of EO treated SU sample with MMO and doped-MMO, toxicity analysis (Kirby-Bauer test) was executed using agar well diffusion assay against *E. coli* taking untreated sample as a control. Muller Hinton agar (MHA) plates were taken in which 0.5 cm well was punched using a sterile cork borer. Thereafter, approx. 50 µl of treated and untreated samples were poured in well and allowed to disperse properly for 10 min. Further, the culture of *E. coli* was swabbed in plates and placed in an incubator for overnight at 37 $^{\circ}$C. The toxicity of samples was inspected through the zone of inhibition that occurred around the well. The zone was found only in control (untreated samples) of 0 h without acid and with acid addition while in case of final EO treated samples of SU with MMO and doped-MMO, no zone of inhibition was observed implying that toxic organics got mineralized into simpler non-toxic components as shown in Figure 4.5.14.

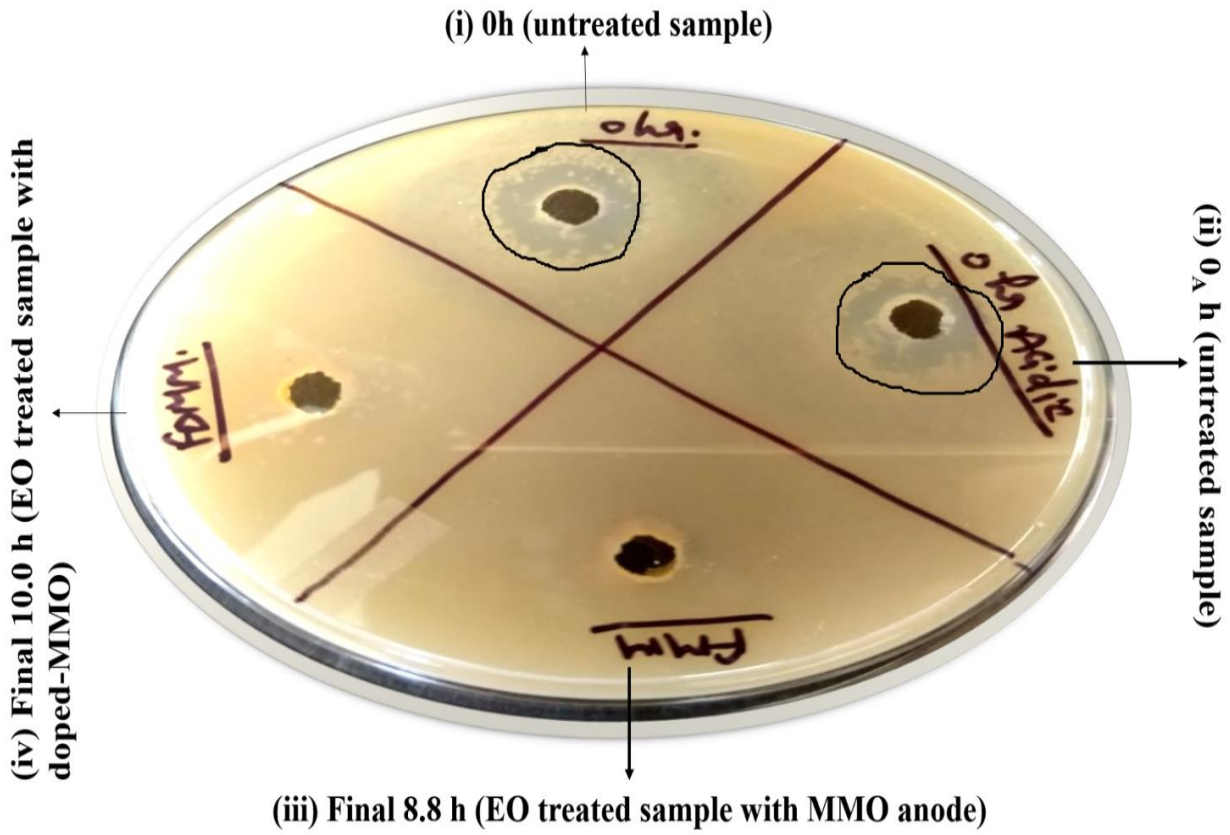

Figure 4.5.14 Toxicity analysis of untreated and EO treated samples of SU for both MMO and doped-MMO anodes.

4.5.7 Disinfection Studies

Besides its efficacy towards oxidation of organic components, the disinfection efficiency of EO and PEC was also studied using *E. coli* as (pathogenic microorganism) spiked SU. The experimental study was carried out at optimized conditions using MMO and doped-MMO anodes. The untreated and treated samples of volume 1 mL was poured in plates containing media called MacConkey agar. After that, media plates were then placed at 37 ^{o}C for getting discreet colonies of *E. coli*. The concentration of coliform in SU samples was estimated in terms of CFU 100 mL^{-1}. Figure 4.5.15a showed the total removal of *E. coli* from SU has been achieved within 30 min through PEC and 45 min via EO when treated with MMO. Based on these observations a plot was made between CFU 100 mL^{-1} versus treatment time. Whereas in the case of doped-MMO, the total removal of *E. coli* from SU has been achieved within 35 min through PEC and 75 min via EO as shown in Figure 4.5.16a.

Figure 4.5.15b and Figure 4.5.16b represents the changes in the concentration of *E. coli* during electrolysis of SU at different time intervals at optimized conditions. As it can be seen that the concentration of *E. coli* was found decreasing rapidly with time under UV and solar radiations. However, it was observed that the time required to disinfect SU wastewater was very less as compared to complete/ partial oxidation of organic matter present in SU. The complete disinfection of wastewater was seemed dependent directly on the production of disinfectants which further depends on the concentration of chlorides added and the concentration of reduced nitrogen species present in solution. Additionally, the treatment processes convert the organic matter into inorganic ions such as NO_3^-, SO_4^{2-}, PO_4^{3-}, Cl^-, etc., H_2O and CO_2 (Örmeci and Linden, 2002; Cotillas et al., 2018).

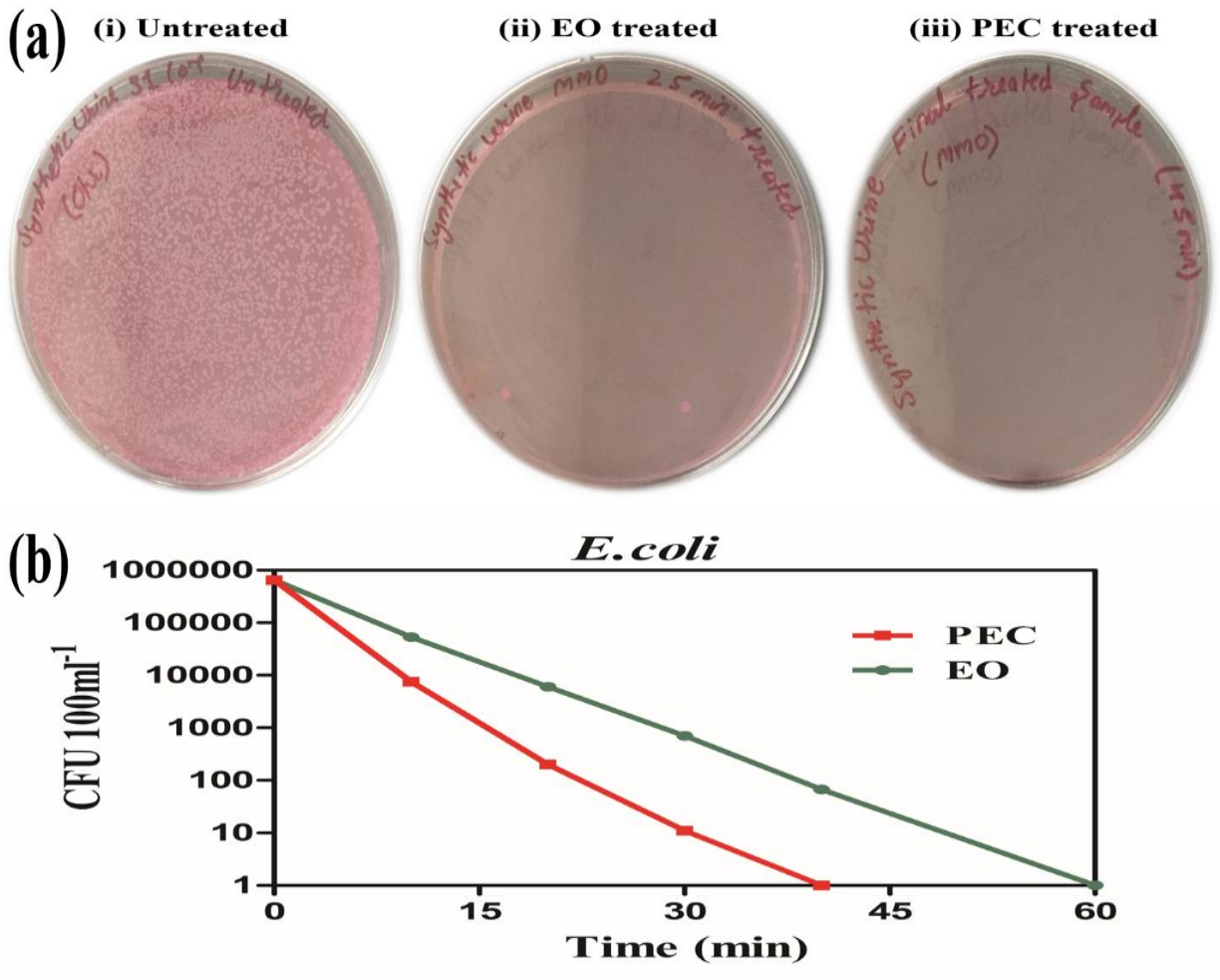

Figure 4.5.15 (a) Total coliform (*E.coli*) count images of untreated and treated (EO and PEC) samples of SU with MMO and (b) plot of CFU 100 mL^{-1} versus treatment time.

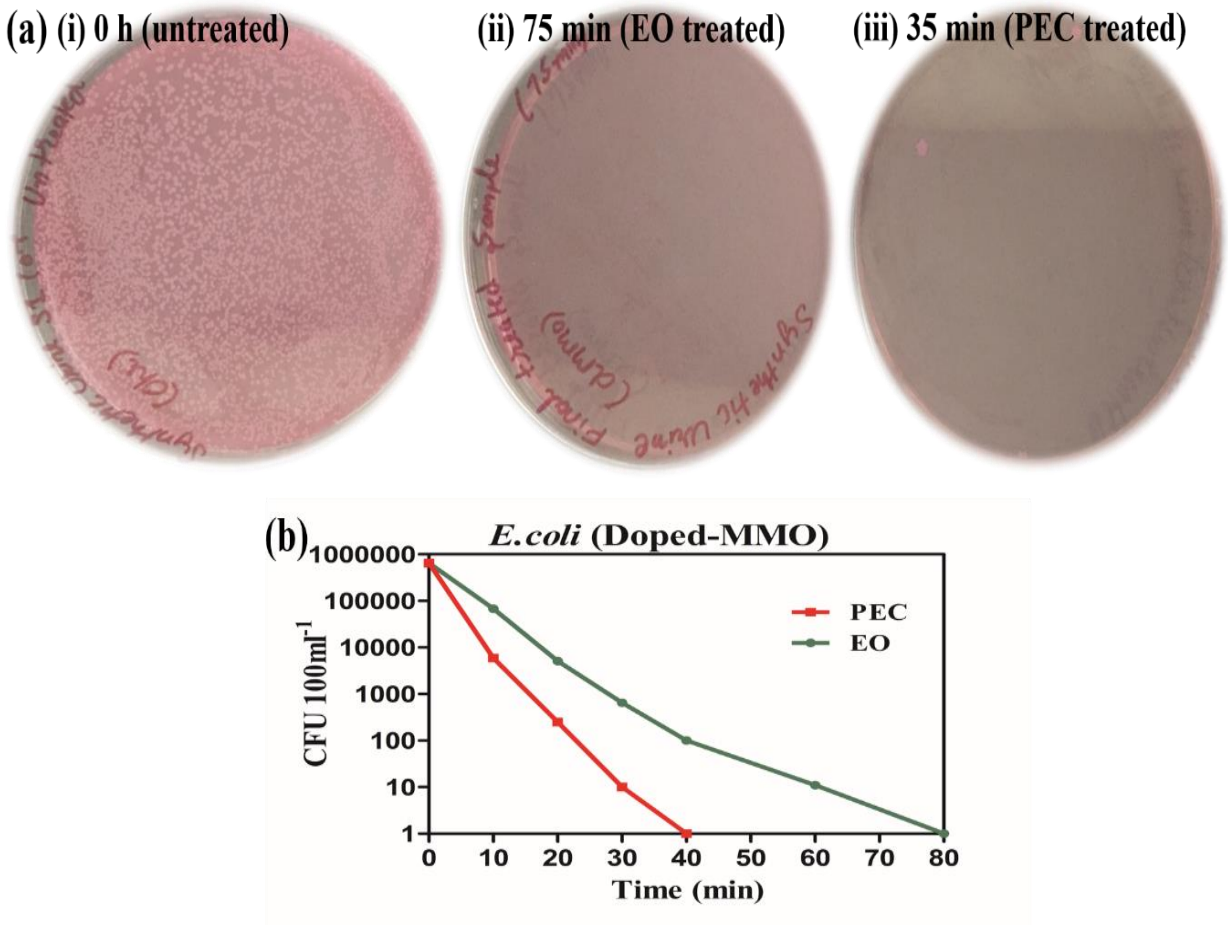

Figure 4.5.16 (a) Total coliform (*E.coli*) count images of untreated and treated (EO and PEC) samples of SU with doped-MMO and (b) plot of CFU 100 mL^{-1} versus treatment time.

4.5.8 Total Operational Cost

In order to visualize the successful commercialization of the proposed method, treatment technology must provide viable solutions economically and as well as socially over traditional methods. In the case of the EO treatment unit, the overall cost for the treatment process with MMO came out to be 0.85 $/kg of COD removed as shown in Table 4.5.7. Similarly, the total operational cost for treated SU wastewater treated with doped-MMO has been calculated and which came out to be 1.50 $/ kg of COD removed. The results depict a sustainable solution for the on-site treatment of urinal wastewaters in terms of the economic feasibility of the EO process as well as the stability of anodes. Moreover, the overall cost could be reduced further during scale-up studies by modifying the reactor design, operating conditions, recycling the urine as flush water and coupling the decentralized molecular hydrogen production accordingly.

Table 4.5.7 Evaluation of operating cost of the EO treatment process for SU treated with MMO
(A)Cost of Electrical Energy consumption
Electrical energy consumed = 11.75 kWh/ kg of COD removed
Electricity price in India, (Punjab) = Rs 5.00/kWh
Cost of electrical energy consumed (C_{EC}) = Rs 58.75/ kg of COD removed
(B) Cost of Electrodes
Initial COD concentration in wastewater = 3400 mg/L= 3.4 kg/m^3
With 85.25% degradation, concentration of COD removed = 2898.5 ≈ 2899 mg/L= 2.899 kg/m^3
Time of treatment = 8.8 h
Concentration of COD removed in 1h = 329.432 mg/L ≈ 0.33 kg/m^3
Cost of one MMO anode = Rs 720/-
The Life span of anode = 5 years
Cost of anode for 43800 h = Rs 720/-
Cost of anode for 1 h = Rs 0.01644/-
Cost of electrodes to remove per kg COD from wastewater = Rs 0.0498 ≈ Rs 0.05
(C) Operating cost analysis
Total operating cost for per kg of COD removal = 0.05 + 12.01 = Rs 58.8 /kg of COD removed
The overall operating cost of EO treatment of SU in US dollars = 0.85 $/kg of COD removed

Section C

Scale-up Studies

4.6 Continuous Recirculation EO Treatment of SU by MMO and Doped-MMO Coupled with Molecular Hydrogen Production

In order to visualize the field scale applications for the on-site treatment of urine, mandatory scale-up trials are required with human urine samples. Besides this, there is a strong possibility of harnessing molecular H_2 production as commercial fuel during EO treatment of urine (Cho et al., 2014). In this context, optimized results from lab-scale trials have been used to execute the scaled-up version of EO treatment of SU under continuous recirculation mode in a PV driven wastewater electrolytic reactor. Figure 4.6.1a,b shows the plot of % Removal (COD, urea, creatinine and uric acid) versus treatment time for both anodes. As it can be seen that, 83.43% (MMO) and 74.20% (doped-MMO) reduction in COD was achieved within 6 h of electrolytic treatment of SU under continuous recirculation mode. The degradation of nitrogen-based organic components such as uric acid, creatinine, and urea was also checked. From Figure 4.6.1a it has been observed that 78.78% (urea), 85.16% (uric acid) and 72.67% (creatinine) were oxidized during the continuous EO treatment of SU with doped-MMO.

In contrast, the % Degradation of these organic compounds in the case of MMO was found higher i.e. 84.95% (urea), 90.77% (uric acid) and 88.02% (creatinine) as compared to doped-MMO as shown in Figure 4.6.1b. As expected, the results clearly indicate the oxidation of these organic compounds present in SU was majorly due to the generated RCS and precisely by $OH^{\bullet}$ during the treatment process. In addition, the volumetric fraction of molecular hydrogen (XH_2) along with other gases i.e. molecular N_2 and CO_2 during continuous EO treatment of SU was also checked. The volumetric fraction of H_2 generated during 6 h of electrolysis in the range of 70.58% -1.7190% (MMO) and 59.142% – 3.340% (doped-MMO) as shown in Figure 4.6.2a,b. Other by-product gases such as N_2, CO_2, CH_4, and CO has also been generated during electrolysis of SU by both anodes as shown in Figure 4.6.3. However, the volumetric molecular fraction of these gaseous byproducts was found increasing with treatment time due to the oxidation of pollutants into molecular N_2 and CO_2. Figure 4.6.3 showed the graph of (i) reference gas, SU wastewater treated with (ii) MMO anode and (iii) doped MMO. The reference gas was a mixture of known gases with known concentration containing carbon dioxide (11.85%), hydrogen (15.20%), carbon monoxide (19.70%), nitrogen

(17.80%), methane (5.20%) and argon (balance). Whereas, the other two graphs i.e. (SU samples treated with MMO and doped-MMO) represents the generation of gaseous byproducts after 2 h of electrolytic treatment of SU.

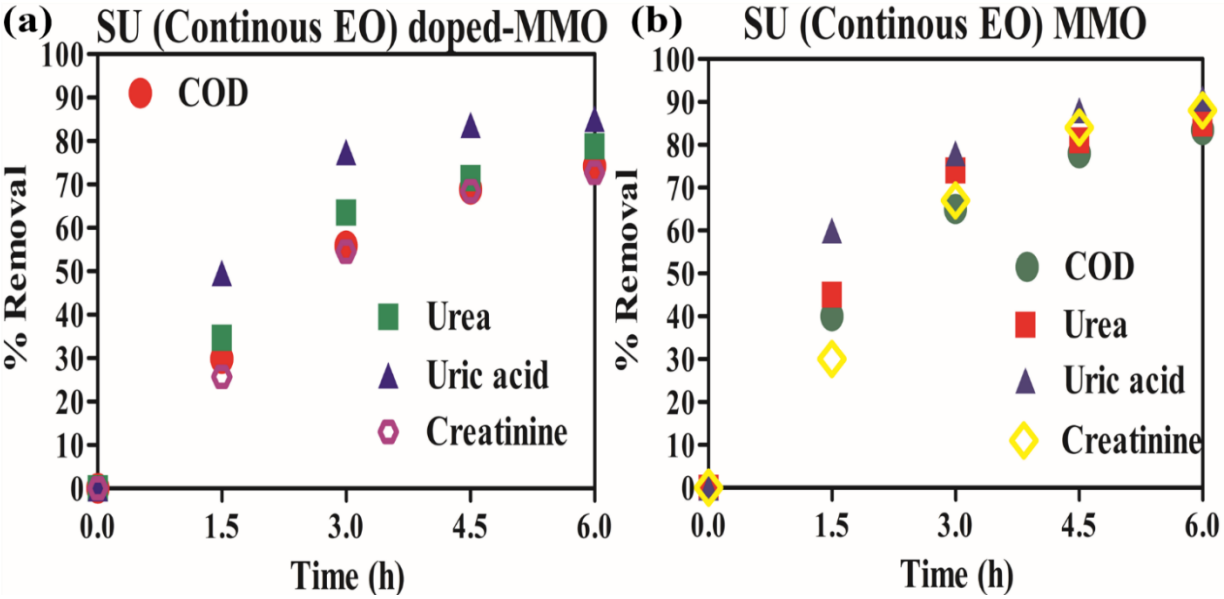

Figure 4.6.1 Plot of % Removal of COD and organic components (urea, uric acid and creatinine) versus treatment time during continuous electrolysis of SU with (a) doped-MMO and (b) MMO.

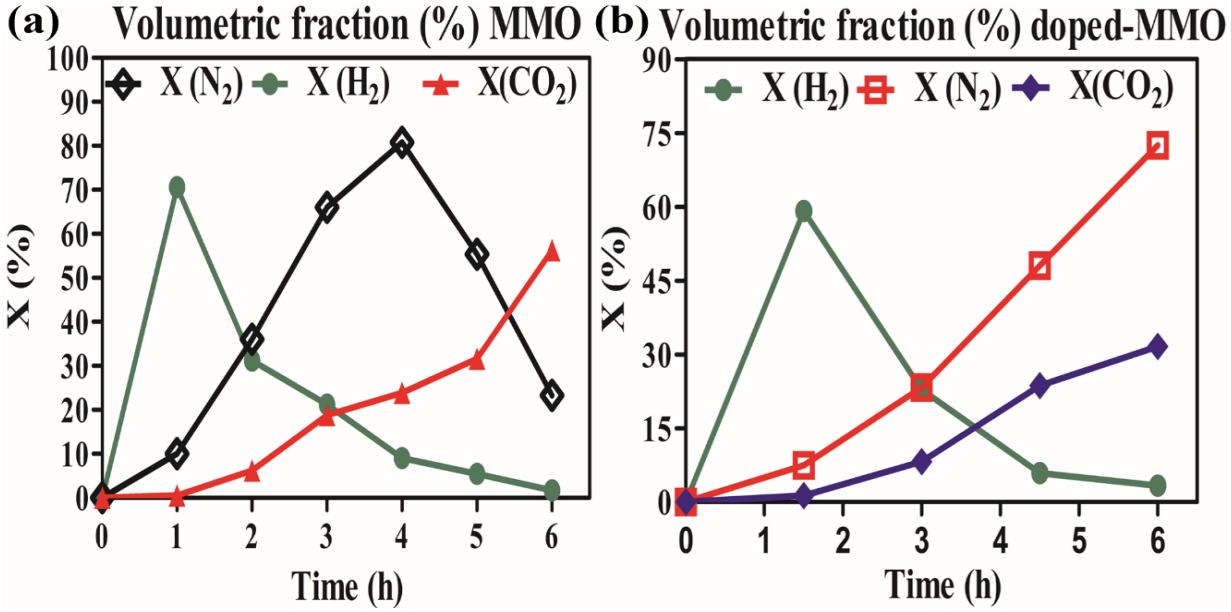

Figure 4.6.2 Plot of the volumetric fraction (X) of generated gases versus treatment time during continuous electrolysis of SU with (a) MMO and (b) doped-MMO.

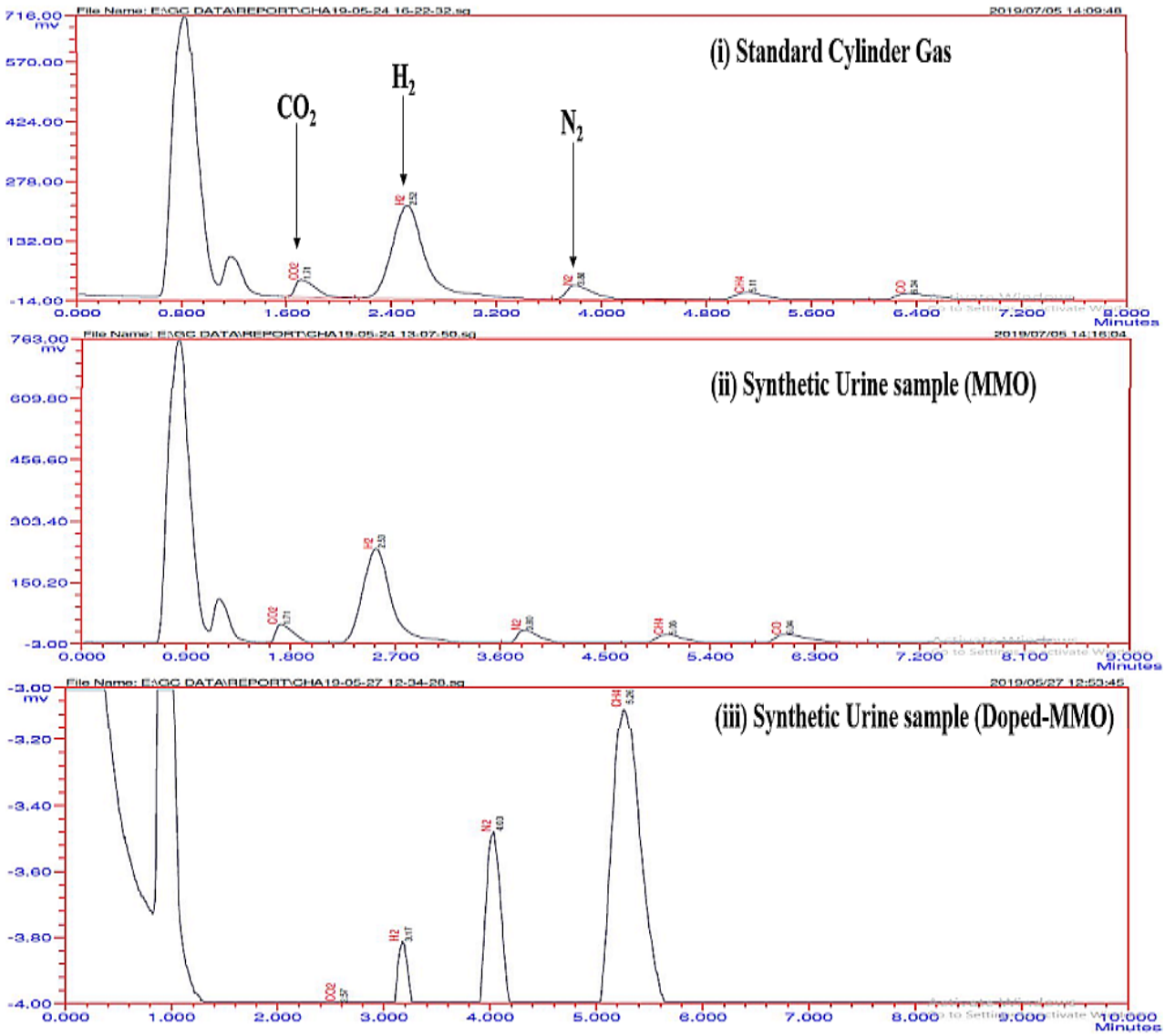

Figure 4.6.3 Gas Chromatograms for (i) standard gas, (ii) SU sample treated with MMO and (iii) SU sample treated with doped-MMO.

4.6.1 Total Capital Expenditure

Total capital expenditure (Capex) cost for continuous EO treatment of SU includes the cost of a pump, cost of the battery, cost solar cell, cost of piping & fitting, cost reactor, cost of electrodes and cost of operation.

Total cost= Rs 1800 (pump) + Rs 2500 (battery) + Rs 500 (solar cell) + Rs 200 (piping and fitting) + Rs 900 (reactor) + Rs 720 (MMO)

Total Capex = Rs 6620 ≈ Rs 6700 for 5years (1825 days).

The volume of SU wastewater treated per day = 2L

The COD removal achieved during the treatment process = 5.6 kg/m^3

Cost of treatment (per day) to remove 5.6 kg/m^3 COD = Rs 3.70/-

Hence total cost = cost of operation + Capex = Rs 0 + 3.70 = Rs 3.70/- = 0.054 $

Similarly calculation were done for doped MMO = Rs 3.80/- = 0.055$ for removal of 5.0 kg/m^3.

The overall cost for EO treated SU effluent (2L) was came out to be 0.054 $ which was in comparison to other AOPs such as fenton, ozonation, photocatalysis, etc. was found less (Canizares et al., 2009; Gupta et al., 2012). The feasibility of any water recycling technique at a commercial level depends on the cost of construction, maintenance and operation. Moreover, these other AOPs techniques are used for specific purposes but their use is restricted at potable and industrial levels as well as have technical and operational glitches. However, EO treatment process is suggested to be cheaper than other AOPs for satisfying discharge limits of treated effluents. Economically cheap MMO and Doped-MMO with years of service life can make this process more economically feasible. Taking all points into consideration scale-up factors like power consumption, volume handle, and energy factors are going to decide the real economy of the treatment process. However, the reduced cost of treatment at the lab scale definitely boost up the process economy during its commercial-scale visualization.

Treatment of Actual Human Urine (AHU)

4.7 Continuous Recirculation EO Treatment of AHU Wastewater with MMO in PV Driven Reactor

This section deal with the prominent application of studied EO technology for the treatment of AHU wastewater. For this application of the treatment process, AHU wastewater has been treated in a PV driven EO reactor. Actual validation of results would be possible only if the tested electrodes i.e. MMO and doped-MMO with optimized parameters would be suitable to treat AHU. In fact, this is the most challenging part where real type effluent would be subjected to studied EO process. Furthermore, in order to economize the treatment process, the energy required for the treatment of AHU was actually derived by installing solar panel (325W/24V). Moreover, to visualize its commercial-scale applications, the EO process was operated in a

continuous manner. The main emphasis of the study was to oxidize the recalcitrant organic pollutants present in urine wastewater into non-toxic byproducts so that this treated wastewater can be reused further as flush water or this technology could be successfully employed as primary/tertiary treatment option prior to biological methods in sewage treatment plants.

The AHU wastewater was initially characterized for the parameters including COD, TDS, pH, conductivity, chloride, total nitrogen, and concentration of urine metabolites (urea, uric acid, and creatinine) as listed in Table 4.7. The concentrations in AHU are much relating to the literature studies (Udert et al., 2006; Cho et al., 2014; Cid et al., 2018).

Table 4.7 Characterization of AHU wastewater

Parameters	Values
COD (mg/L)	8500-9600
TDS (mg/L)	11.55-13.10
Total nitrogen (mg/L)	8100-8800
pH	6.2-6.8
Conductivity (mS/cm)	14.55-16.80
Urea (mg/L)	7500-8500
Creatinine (mg/L)	1300-1500
Uric acid (mg/L)	380-490
Chloride (mg/L)	3000-3500

The EO experiments for the treatment of AHU were conducted at optimized conditions using MMO anodes. Figure 4.7.1a shows the plot of % removal (COD, urea, creatinine and uric acid) versus treatment time. As it can be seen that 68.33% reduction in COD was achieved in 6 h of electrolytic treatment of AHU under continuous recirculation mode. The degradation of nitrogen-based organic components such as uric acid, creatinine, and urea was also checked. Furthermore, it has also been observed that 69.09% (urea), 95.180% (uric acid) and 67.95% (creatinine) were oxidized via generated RCS and ROS during the treatment process. However, with an increase in the size of the reactor and electrodes, the power of oxidation capacity to treat these pollutants could be further improved (Kete et al., 2018). Figure 4.7.1b represents the changes in the pH and conductivity of the AHU wastewater during the EO treatment process. The results indicate no significant change in the conductivity of treated urine wastewater. In contrast, a significant change in the pH of urine wastewater was observed during the treatment process.

The initial pH of urine wastewater was maintained constant around 6.46. However, the pH of the wastewater was found decreasing rapidly to 4.45 pH within 3 h of electrolysis. Afterward, it was found increased from 4.45 to 6.97 pH and then remain unchanged until the end of the treatment. The decrease in the pH might be due to the electrochemical reactions occurred on the surface of MMO anode during the EO treatment process as discussed in former section A and B. This acidic pH expected to have an important role in prevention of volatilization of ammonia as well as helps in the speciation of the intermediates during the electrolysis process (Dbira et al., 2019). Thus concludes that change in pH depends largely on the type of electrode used for the particular treatment process.

In addition, the volumetric fraction of XH_2 along with other gases i.e. N_2 and CO_2 during continuous EO treatment of AHU was also checked. The volumetric fraction of H_2 and N_2 generated during 6 h of electrolysis were in the range 69.74% – 2.617% and 18.019% – 62.133% respectively as shown in Figure 4.7.1c. Other by-product gases have also been generated in small fractions (not shown here) during electrolysis of AHU. However, the volumetric molecular fraction of H_2 was found decreasing due to the oxidation of pollutants into molecular N_2 and CO_2.

Figure 4.7.2 showed the GCMS spectra of untreated and EO treated samples of urine wastewater, depicting the elimination of most of the organic components after the treatment process. Moreover, the detected identified byproducts present in the treated solution were found non-toxic as compared to the untreated sample as confirmed through toxicity analysis and shown in Figure 4.7.3.

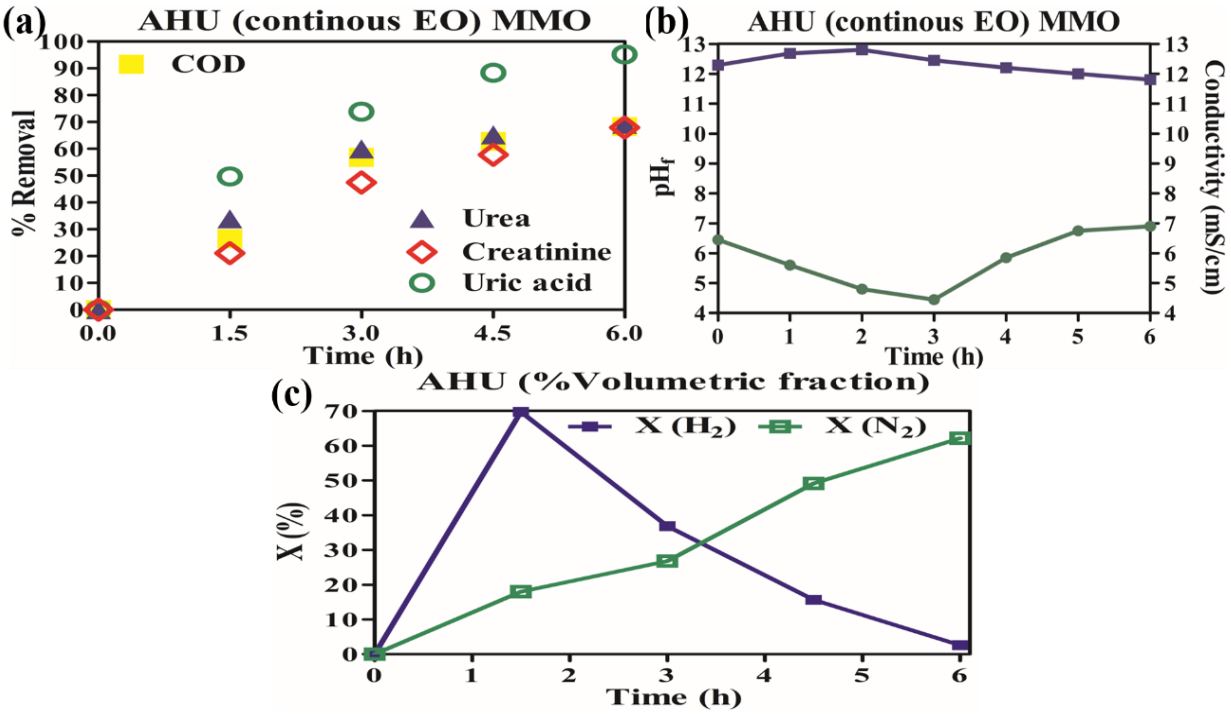

Figure 4.7.1 Plot of (a) % Removal of COD and organic components (i.e. urea, uric acid and creatinine) present in AHU versus treatment time; (b) change in pH and conductivity versus treatment time and (c) volumetric fraction (X) of generated gases versus treatment time during continuous electrolysis of AHU with MMO.

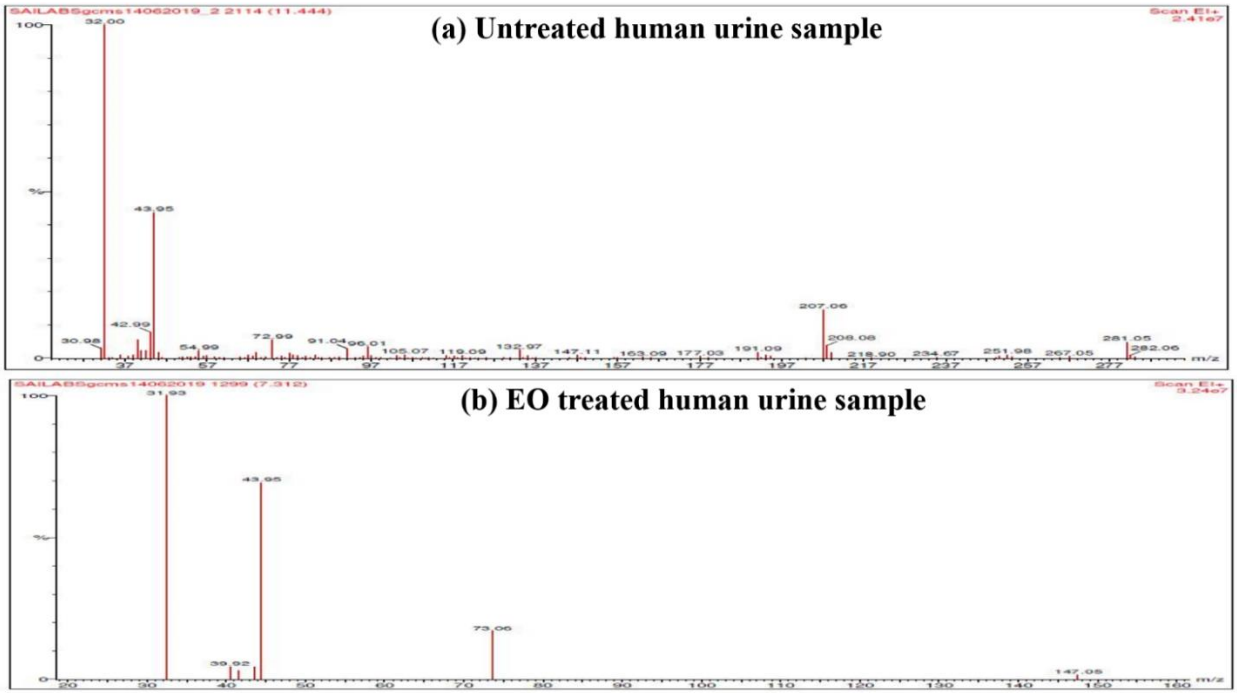

Figure 4.7.2 GC-MS spectra of untreated and treated samples of AHU with MMO anode.

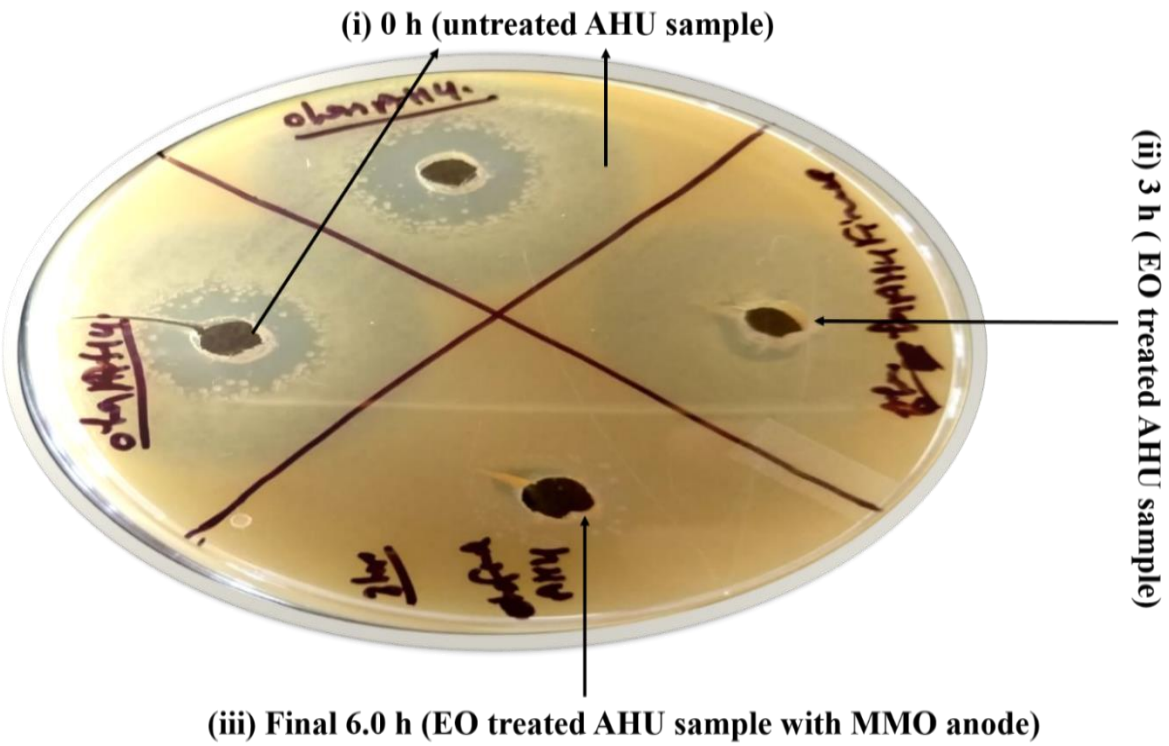

Figure 4.7.3 Toxicity analysis of untreated and treated samples of AHU with MMO.

Section-D

4.8 Durability Studies

In order to visualize the practical applicability and economy of the EO process towards field-scale applications, the durability and stability of the MMO and doped-MMO anodes were studied. In this context, efforts have been made to evaluate the stability and durability in terms of a number of recycles and % removal. From Figure 4.8a,b, it was observed that MMO and doped-MMO anodes were magnificently reused for approximately ≈400 times (1242.5 h) and ≈500 times (1853.166 h) respectively without any much substantial reduction in process efficiency. Generally, at acidic pH, high NaCl and high current density values, the life span of anodes decreased due to passivation and dissolution (Martinez-Huitle and Ferro, 2006; Scialdone, 2009). Several studies in the literature have reported the stability of MMO anodes upto 100-300 h or a maximum of 600 days only (Wang et al., 2013; Herrada et al., 2018; Zahedi et al., 2018; Liu et al., 2015). Whereas, MMO and doped-MMO used in the present study exhibits immense stability even after 1242.5 h (MMO) and 1853.166

h (doped-MMO) under extreme conditions and could be used further for a maximum of 5 years due to the presence of the appropriate amount of IrO_2 in both anodes. These anode offers the advantage of generating a significant amount of ROS and RCS due to the high concentration of SnO_2, Ta_2O_5, Pt, TiO_2, and RuO_2, in the oxide mixture which helps in the occurrence of both mechanism i.e. direct and indirect oxidation during the treatment process by both anodes (Chaplin, 2014).

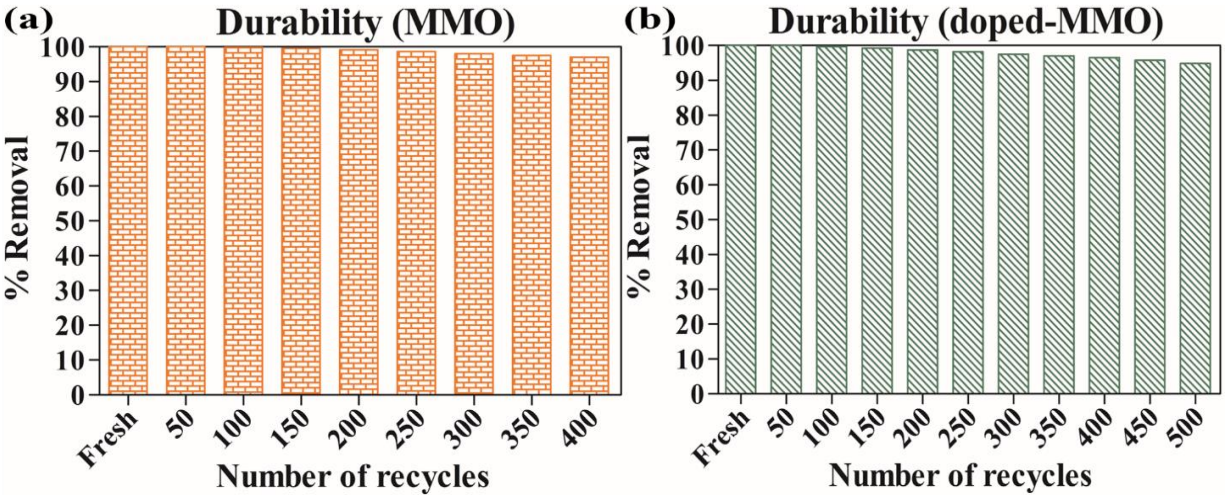

Figure 4.8 Recyclability studies of (a) MMO and (b) doped-MMO anodes for the % Removal of target pollutants

4.9 Characterization of MMO and Doped-MMO anodes

4.9.1 SEM/EDS Analysis

To characterize the surface morphology and structural properties of the MMO anodes SEM was performed. While for the elemental composition of the different metal oxide layers coated on the anode surface, EDS was used. The Ti plate (Figure 4.9.1a) showed an almost flat surface with some small grooves. From the SEM images of freshly coated MMO (Figure 4.9.1b), it can be seen that the appearance of anode generally corresponds to mud cracked morphology along with agglomerated points (Coteiro et al., 2006). This happens because electrodes were prepared via thermal anodic decomposition and after then successive cooling was done. The presence of Ti in the sheet has made the consequence for the formation of TiO_2 as the first layer, which further allowed the better fixing of the oxide layers of other metals (Wu et al., 2014). Furthermore, the incorporation of oxides of Ruthenium, iridium, and titanium in the metal sheet has increased the surface area as well as making the structure relatively porous, smooth and uniform with wide and deep cracks hence

prevents the anode from corrosion along with greater stability for a longer period of time (Kumar et al., 2007; Goudarzi and Ghorbani, 2016). The addition of platinum in the anodes has affected the morphology by improving its homogeneity of the coated layers along with the formation of smaller size particles which formed due to the compacting effect **(**Rio et al., 2010). Figure 4.9.1c showed the surface allied characteristics of recycled MMO, which further implying intact homogeneous layers of the metal oxides even after 400 (1242.5 h) recycles.

Durability and stability of anodes were further proven with the presence of prominent peaks of all three metals i.e. Pt, Ir, Ru, Ti, and O even in a recycled plate. The quantitative analysis through EDS shows that the molecular concentration of these metals in the oxide mixture was found almost equal in both fresh and recycles MMO, thus confirming the stability of anodes even after multiple numbers of recycles. In addition, the elemental mapping images as shown in Figure 4.9.1d was obtained by analyzing the distribution of the different metal elements coated on the whole surface of the titanium metal sheet. The results reveal that the distribution of Ti, Ru, O, Ir and Pt are homogeneous throughout the oxide film, but the distribution of Ir and Pt is limited.

In order to determine the surface morphology and structural properties of doped-MMO, SEM was performed. Figure 4.9.2a,b,c has shown the SEM images of the Ti sheet without any coating, freshly coated anode and recycled anodes. From the image of freshly coated doped-MMO (Figure 4.9.2b), it was observed that thermally decomposed prepared doped-MMO anode exhibits a slightly rough, porous, smaller and shallower mud cracked type structure which indicates anode with enhanced working area. A larger active working area results in an increased catalytic activity which further facilitates the lowering of effective current density (Msindo et al., 2010). The appearance of cracks on the fabricated anode surface depicts that the islands (white bright spots) are made up of different oxide layers with an average width of 5 µm (Tian et al., 2007). The presence of Ti as a substrate in the anode has helped in the formation of the oxide layer of TiO_2 which is UV active helps in the generation of $OH^{\bullet}$ at the anode surface (Rodríguez et al., 2013). The addition of Ta in the anode has enabled the anode to work at higher values of current without causing any damage to an anode (Shestakova et al., 2014). Moreover, the results are consistent with other reported studies that show the incorporation of Sb along with Sn has affected the morphology by improving the structure of coatings. The SEM image of recycling anode (Figure 4.9.2c) showed relatively identical

surface characteristics and morphology thus confirms the uniformity of different metal oxide layers even after 500 (1853.166 h) recycles.

Similarly, for the elemental composition of the different metal oxides coated on anode surface (freshly as well as recycled doped-MMO), EDS was performed. The stability of novel doped-MMO was further proven with the presence of a predominant peak of all the five elements i.e. Sb, Sn, Ir, Ta, O, and Ti even in the recycled sheet. EDS data (Inset) depicts the quantitative analysis in terms of molecular concentration of different metals in the oxide mixture which seemed almost the same in both fresh and recycle anode, thus confirming the stability of anodes even after 500 (1853.166 h) recycles. In addition, the elemental mapping images as shown in Figure 4.9.2d was obtained by analyzing the distribution of the different metals coated on the whole surface of the Ti sheet. The results reveal that the distribution of Ti, Sn, Ir, O, Sb and Ta are homogeneous throughout the oxide film, but the distribution of Sb is limited.

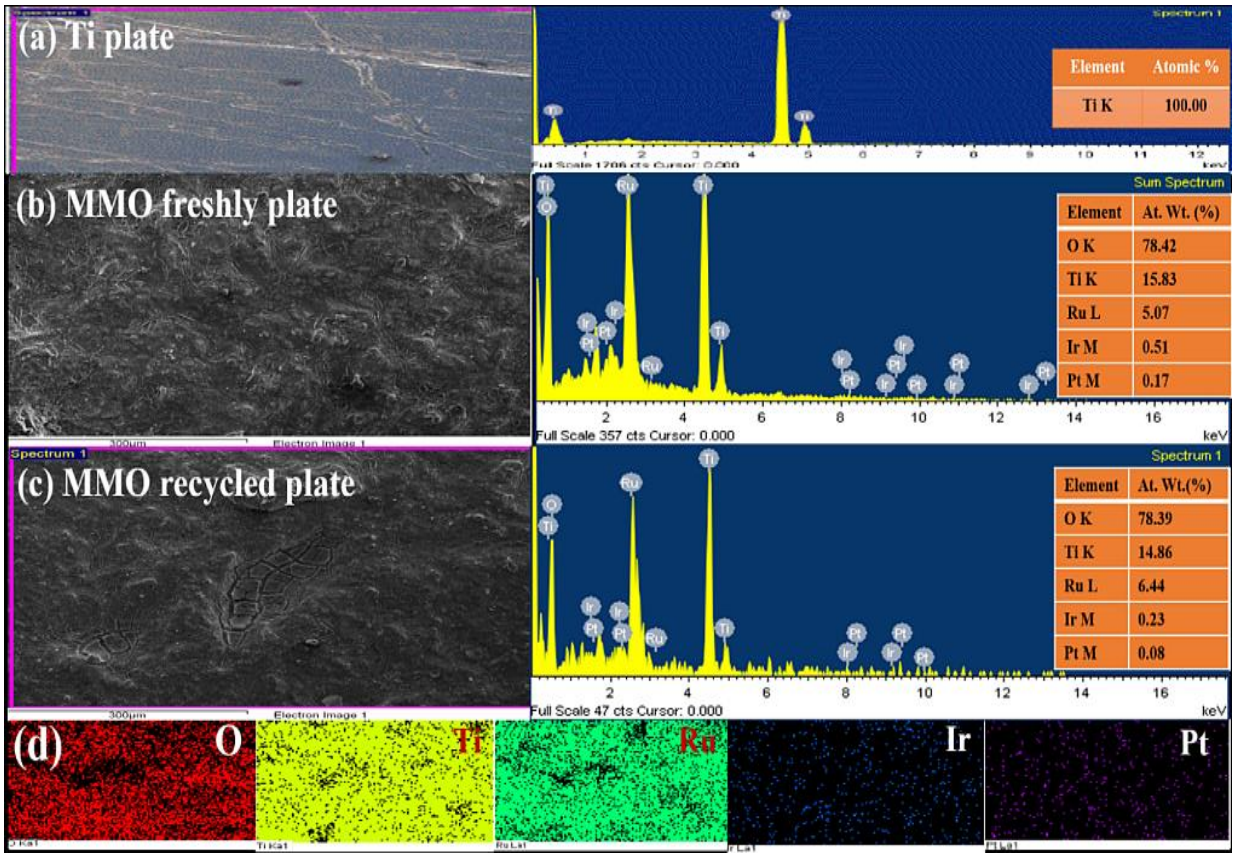

Figure 4.9.1 SEM-EDS images (a) Ti sheet, (b) MMO freshly coated plate and (c) MMO recycled plate; (d) Elemental mapping images.

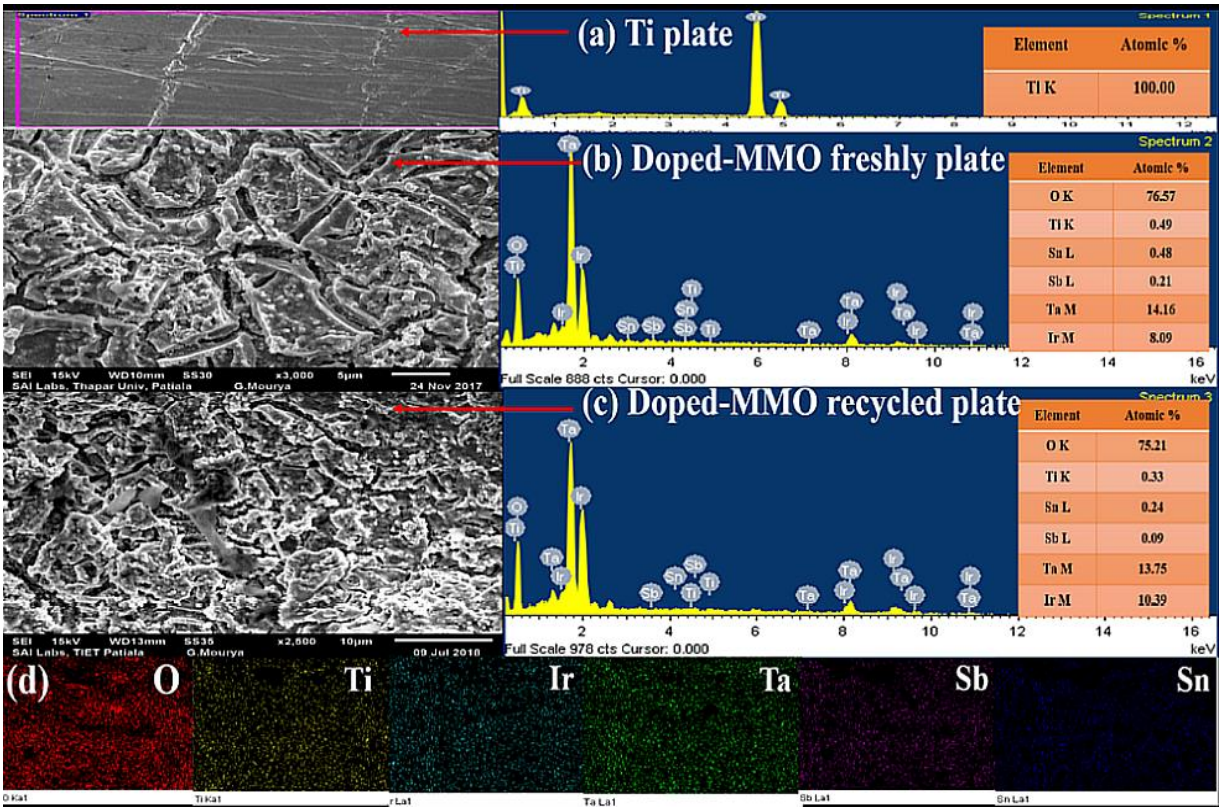

Figure 4.9.2 SEM-EDS images (a) Ti sheet, (b) doped-MMO freshly coated plate and (c) doped-MMO recycled plate; (d) Elemental mapping images.

4.9.2 XRD Analysis

Figure 4.9.3 shows an X-ray diffractogram of a Ti plate, a freshly coated sample of MMO and a recycled sample of MMO. XRD basically determines the crystalline planes of the structure of the oxide films which coated on the titanium sheet. Through XRD it became possible to distinctively identify the existence of oxides of Ru, Ir, and Ti in rutile structure. The presence of TiO_2 and other oxide layers of metals have made a tetragonal structure and ionic radii of the same magnitude. Furthermore, the same peaks of oxides of metal have also been observed in recycled sheet, thus indicating the retention of all coated metal oxides even after 400 (1242.5 h) recycles. It was also observed that similar peaks were found even in the recycled MMO. But at the same time, it was also found that some metal peaks were deviated from their original position due to the loss of some amount of metals in the multiple runs of the experiment. Diffraction peaks corresponds to titanium (JCPDS No. 00-005-0682), titanium dioxide (JCPDS No. 00-034-0180) indicated as rutile syn, ruthenium (JCPDS No. 01-071-2273) referred to as ruthenium (IV) oxide, iridium (JCPDS No. 00-015-0870) were indicated as iridium oxide and platinum (JCPDS No. 01-072-2997) were indicated

as platinum titanium. Most of the similar peaks were already reported in the literature (Makgae, 2005).

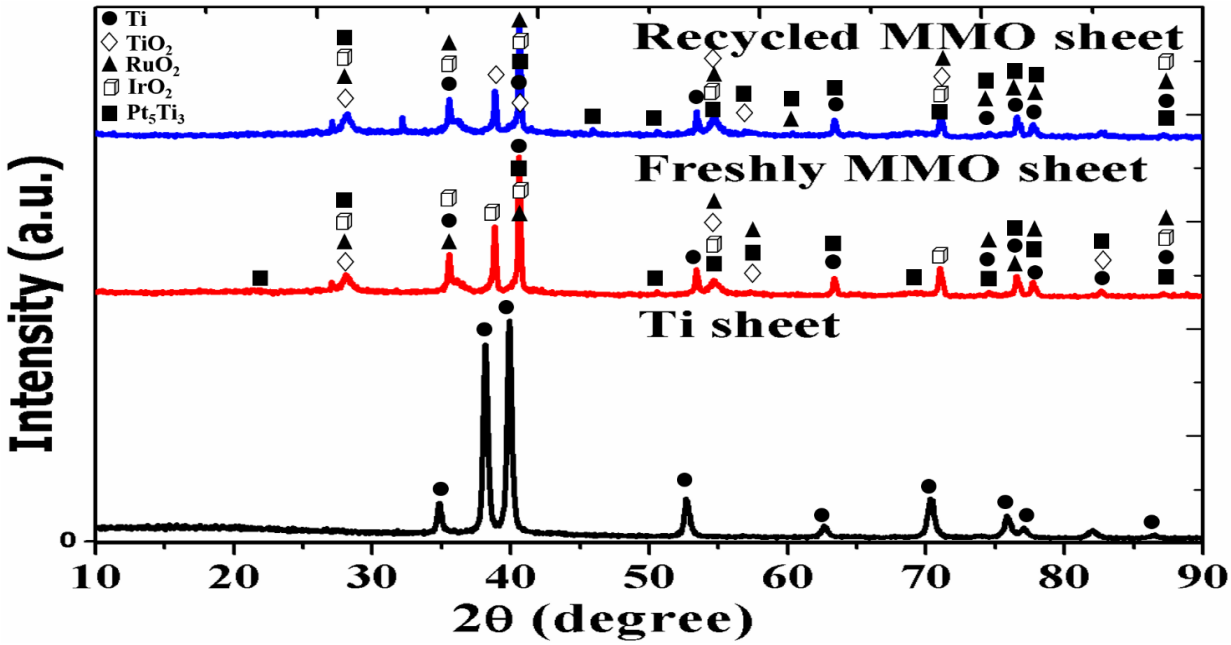

Figure 4.9.3 XRD pattern of Ti plate, freshly coated MMO plate and recycled MMO plate.

Figure 4.9.4 shows X-ray diffractogram (XRD) of a Ti sheet only, the freshly coated doped-MMO and recycled doped-MMO plate. XRD helps to identify the existence of different metals in the oxide mixture. From results, it was clearly seen that the sharp peaks of TiO_2 with rutile phase, few peaks of anatase Ti along with the characteristic reflection of SnO_2 with rutile-type structure. This indicates that the mixed coating of different metals has covered the surface of the Ti substrate significantly (Chen et al., 2010). Despite the incorporation of doping ions into SnO_2 with a low doping level, few diffraction peaks of Sb was still observed in XRD spectra (Wang et al., 2013). The peak of IrO_2 and Ta_2O_5 were also confirmed from XRD spectra. Furthermore, the same peaks of oxides of metal were observed in recycled doped-MMO, hence confirming the confinement of all metal oxide even after 500 (1853.166 h) recycles. It was observed that few metal oxide peaks were deviated from their original position due to the loss of some amount of metals in the multiple runs of the experiment. The diffraction peaks of all metals such as SnO_2 (JCPDS No. 01-072-1147), Ti (JCPDS No. 01-089-3725), TiO_2 (JCPDS No. 01-088-1175), IrO_2 (JCPDS No. 01-088-0288), Ta_2O_5 (JCPDS No. 01-070-4776) and Sb_2O_4 (JCPDS No. 01-074-8714) were identified. Most of the similar

peaks were already reported in the literature (Tian et al., 2007; Polonský et al., 2012; Shestakova et al., 2014; Qin et al., 2019).

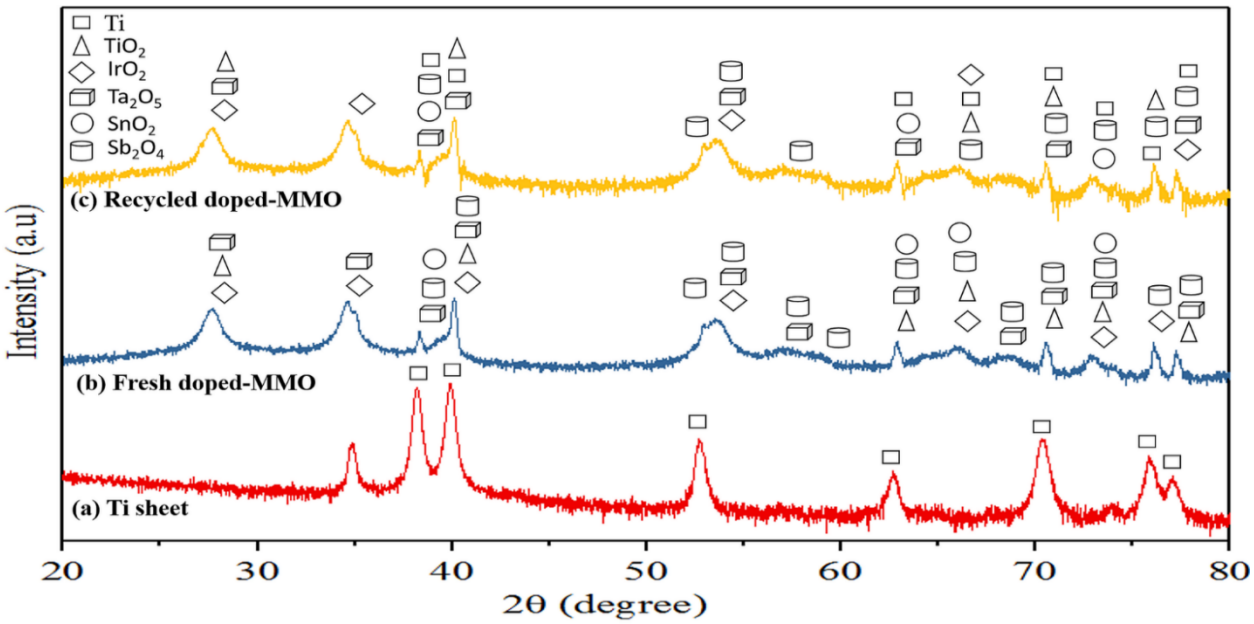

Figure 4.9.4 XRD pattern of Ti plate, freshly coated doped-MMO plate and recycled doped-MMO plate.

4.9.3 XPS Analysis

Figure 4.9.5 (i) depicts the XPS spectra of freshly coated MMO and recycled MMO anodes in order to analyze the surface compositions and electronic nature i.e. oxidation state of metal elements. From the results, it has been observed that no significant change in the oxidation state of metals, as well as the presence of each element, was found even after multiple recycles. The occurrence of carbon (C 1s) in both samples could be attributed to adventitious carbon employed for appropriate binding energy shifts generated by samples. Figure 4.9.5 (ii) indicates the Ti 2p spectrum of MMO anode in which peaks correspond to binding energies of Ti $2p_{3/2}$ and Ti $2p_{1/2}$ states and were observed at 458.91 eV and 461.43 eV respectively (Tseng et al., 2014). Figure 4.9.5 (iii) shows the spectra shape of the O 1s signal in which one broad peak was visible at 530. 48 eV and could be assigned Ti─O bonds.

Figure 4.9.5 (iv),(v),(vi) demonstrates the spectrum of Ru 3d, Ir 4f, and Pt 4f signals, confirming their presence in MMO anode. In contrast to Ru and Ir, Pt signal indicates a single oxidation state i.e. Pt (V), belonging to Pt $4f_{5/2}$ level was observed around 74.93 eV and further

indicate the interstitial formation of Pt─Ti bonds. However, in the case of Ru and Ir spectrum, two individual characteristic peaks of each element were observed at 279.87 eV, 284.10 eV, 60.43 eV, and 63.43 eV respectively. The data derived for Ru and Ir region from respective signals were correlated with Ru $3d_{5/2}$, Ru $3d_{3/2}$, Ir $4f_{7/2}$, and Ir $4f_{5/2}$ thus proposing the formation of hydrated RuO_2 and IrO_2 metal oxides. The results in the present study are in good correlation with the reported studies in the literature (Reetz et al., 2003; Wang et al., 2015; Egorov et al., 2017).

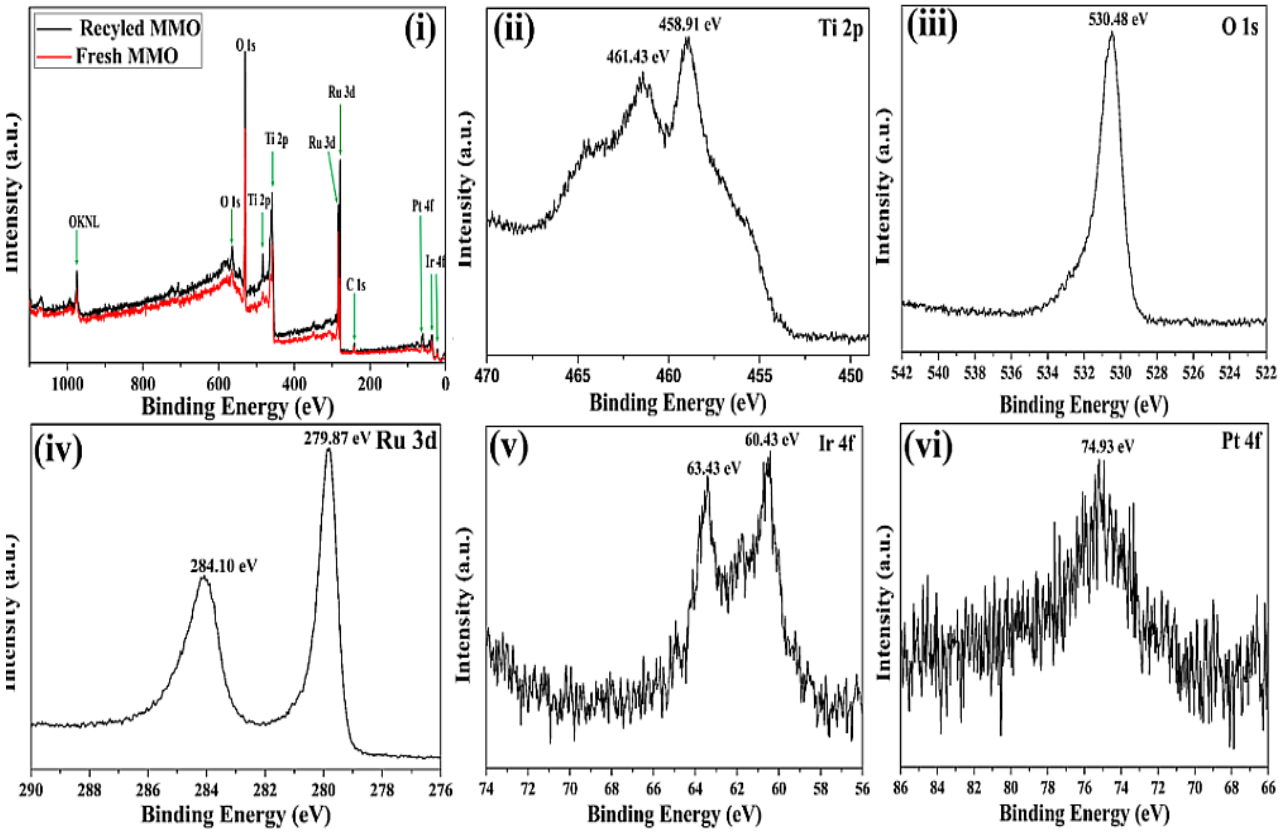

Figure 4.9.5 XPS analysis of (i) Fresh MMO and recycled MMO along with (ii) Ti 2p spectrum, (iii) O 1s spectrum, (iv) Ru 3d spectrum, (v) Ir 4f spectrum and (vi) Pt 4f spectrum.

Figure 4.9.6a depicts the XPS spectra of freshly coated doped-MMO and recycled doped-MMO anodes in order to inspect the molecular information relevant to the electrode surface chemistry (Rio et al., 2009). The results depict the marginal change in the intensity of freshly coated samples and a recycled sample of doped-MMO without affecting the oxidation state of metals. The binding energies of metal elements in the XPS spectra were calibrated by using C 1s. The XPS examination was mainly focused on the detailed analysis of each element present in doped-MMO.

Figure 4.9.6b showed the spectrum of Ti 2p, which clearly indicated the prominent peaks at 458.88 eV and 467.25 eV corresponds to binding energies of Ti $2p_{3/2}$ and Ti $2p_{1/2}$ states.

Figure 4.9.6c showed the core level O 1s spectra in which a symmetric peak appeared at 530.66 eV, attributed to the low binding energy and could be ascribed to O^{2-} ion in the doped-MMO lattice. Figure 4.9.6d indicates the profile of doublet Ta 4f photoelectron spectra, exhibiting the four peaks centered at 28.0 eV, 26.17 eV, 24.79 eV, and 22.87 eV, which could be assigned to $4f_{5/2}$ and $4f_{7/2}$ core level Ta^{5+}, Ta^{4+}, $Ta^{2+,}$ and Ta^{1+} respectively. Figure 4.9.6e showed the spectrum of Ir 4f signal, exhibits two characteristics peak at 63.49 eV and 60.43 eV, which could be ascribed to Ir $4f_{5/2}$ and Ir $4f_{7/2}$. Figure 4.9.6f showed the binding energy of Sn 3d core-level spectra at around 496.0 eV, could be assigned to the $3d_{3/2}$ core level. Figure 4.9.6g demonstrates the Sb 3d core-level spectra at around 530.83 eV for Sb $3d_{5/2}$. The peak position showed the Sn^{4+} and Sb^{5+} were the major oxidation states of the Sn and Sb species. These peaks in Figure 4.9.6 correspond to the respective binding energies of fully oxidized stoichiometric TiO_2, IrO_2, Ta_2O_5, SnO_2 and Sb_2O_5, which are in good agreement with other works (Kong et al., 2010; Wang et al., 2013; Denny et al., 2016).

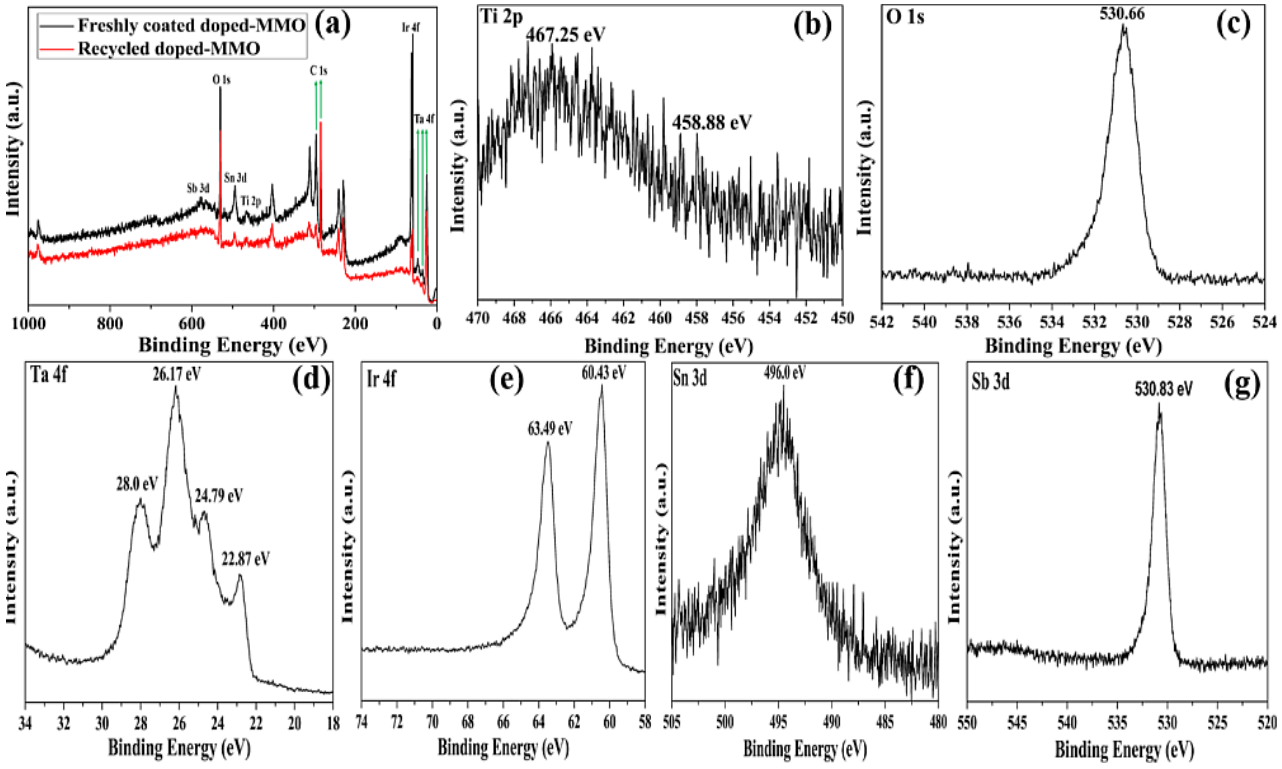

Figure 4.9.6 XPS analysis of (a) Fresh doped-MMO and recycled doped-MMO along with (b) Ti 2p spectrum, (c) O 1s spectrum, (d) Ta 4f spectrum, (e) Ir 4f spectrum, (f) Sn 3d spectrum and (g) Sb 3d spectrum.

4.9.4 Raman Spectroscopy

In Figure 4.9.7, the Raman spectrum of the oxide film for both electrode samples (freshly coated MMO anode and recycled MMO anode) were compared in order to confirm the presence of the same respective oxide peaks. The results showed small peaks at 133 cm^{-1} for TiO_2 (Lagopati et al., 2014), 525 cm^{-1} for RuO_2, 728 cm^{-1} for IrO_2 (Korotcov et al., 2007) and 1600 cm^{-1} for Pt (Singh et al., 2014). Raman spectrum of recycled anode shows the same peaks as freshly coated yet somewhat moved to 520 cm^{-1} and 751 cm^{-1} along with changed amplitude. From both the spectrums it can be seen that there was no change happen after utilization of MMO anode for electrochemical oxidation treatment of synthetic urine and its metabolites even after 400 (1242.5 h) recycles. Hence, it can be concluded that the addition of Ru and Ir metals has increased the stability of the coatings for a longer period of time.

In Figure 4.9.8 the Raman spectra of freshly coated doped-MMO and recycled doped-MMO were compared. The result depicts two crests in number at 553 cm^{-1} and 798 cm^{-1} which could be attributed to SnO_2/ IrO_2 and Ta_2O_5. In addition, a small peak was also observed at 132 cm^{-1} for TiO_2 spectra. No separate peaks were found for oxides of Sb because of its low concentration in oxide mixture. The Raman spectra of recycled anode showed top with relatively same amplitude like freshly coated sample without any shift in wavenumber (cm^{-1}). Therefore, both spectrum indicates that no change happens in the oxide lattice of recycling doped-MMO even after used for approximately 500 times. Hence, it concludes that the addition of Ir has increased the stability of doped-MMO anodes.

Table 4.9 demonstrates the examination made between the Raman spectrums measured in this particular study and those found in the literature for different metal oxides present in the doped-MMO anode. In literature, studies reported that SnO_2 depicts rutile structure at around peaks in the range 400-500 cm^{-1} while crystalline at 630-640 cm^{-1}. Few weak peaks were found in range 200-300 cm^{-1} and 700-1000 cm^{-1} could be attributed to TiO_2, formed due to the oxidation of the Ti surface (non-conductive substrate). Furthermore, the incorporation of other metal oxides on the Ti surface was done to increase the conductivity as well as the reactivity of the process. SnO_2, n-type semiconductor with a wide ban gap was further upgraded by including other metal oxides in order to enhance its mechanical stability and electro-catalytic activity. Sb was added as a dopant in order

to have more oxygen opening in the oxide lattice of Sn (as Sb as higher valence (+5)) and could present more dynamic destinations for the EO treatment process.

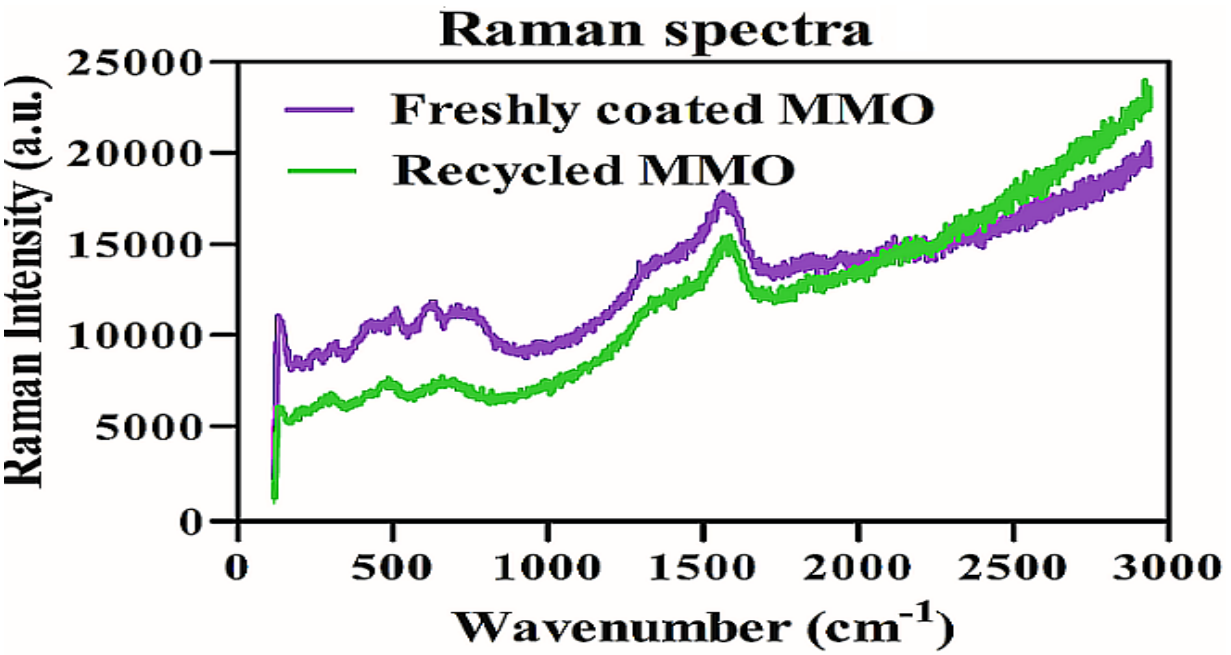

Figure 4.9.7 Raman spectra of MMO anodes (before and after application to EO treatment process).

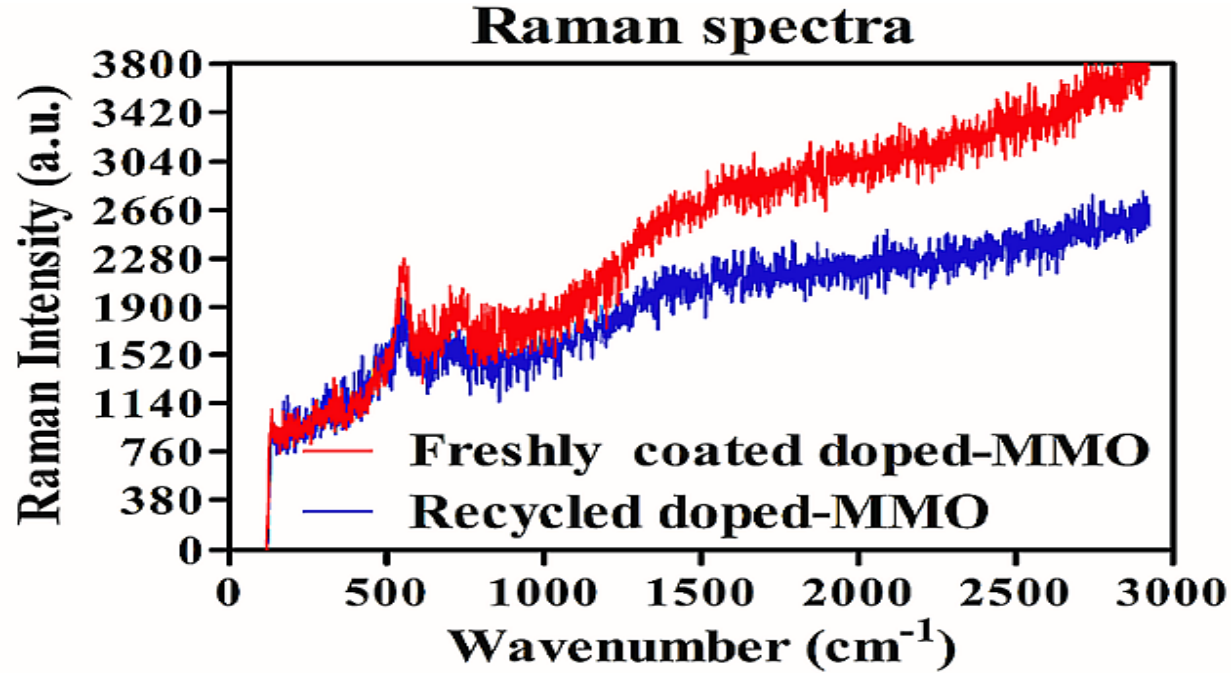

Figure 4.9.8 Raman spectra of doped-MMO anodes (before and after application to EO treatment process).

Table 4.9 Peak position of various metal oxides in doped-MMO in the Raman spectrum		
Oxides	Raman shift (cm^{-1})	References
Tin oxides (SnO_2)	430, 474, 478, 550, 627 and 778 cm^{-1}	Yaqub et al., 2015
Iridium oxides (IrO_2)	465, 527, 600 and 702 cm^{-1}	Pavlovic et al., 2017
Tantalum oxides (Ta_2O_5)	100, 251, 340, 490, 621, 705, and 843 cm^{-1}	Chen et al., 2003
Titanium oxides (TiO_2)	143, 197, 232, 399, 447, 519, 610, 639 and 826 cm^{-1}	Lubas et al., 2014; Ekoi et al., 2019
Antimony oxides (Sb_2O_4)	439, 499, 595 and 679 cm^{-1}	Yaqub et al., 2015
Doped-MMO ($Ti/IrO_2/Ta_2O_5/SnO_2$-Sb_2O_4)	132, 553 and 798 cm^{-1}	This thesis

Chapter-5

CONCLUSION AND RECOMMENDATIONS

5.1 Conclusion

In the present study, the potential application of novel MMO ($Ti/IrO_2/RuO_2/Pt$) and doped-MMO ($Ti/IrO_2/Ta_2O_5/SnO_2$-Sb_2O_4) anodes as an alternative source to costly electrodes have been visualized for the EO treatment of urine metabolites (i.e. uric acid, urea, and creatinine), SU and AHU. On the basis experimental results of the treatment study, some of the major conclusions are listed below.

5.1.1 EO treatment of urine metabolites i.e. uric acid, creatinine and urea with MMO and doped-MMO anodes:

- Parametric optimization for the treatment of each urine metabolite through the EO process by MMO and doped-MMO has been done successfully.
- The high R^2 values of both responses i.e. %Degradation and energy consumption for quadratic suggested by BBD under RSM advocates a good correlation between predicted and experimental data of EO treated urine metabolites by both anodes.
- The maximum %Degradation and energy consumption at optimized conditions by EO treatment with MMO anodes was found to be (91.571%, 0.526 kWh/m^3) for uric acid, (85.41%, 16.826 kWh/m^3) for creatinine and (94.78%, 20.54 kWh/m^3) for urea respectively.
- The maximum % Degradation and energy consumption at optimized conditions by EO treatment with doped-MMO anodes was found to be (95.35%, 2.479 kWh/m^3) for uric acid, (90.002%, 25.83 kWh/m^3) for creatinine and (91.15%, 51.53 kWh/m^3) for urea respectively.
- The degradation of uric acid, creatinine, and urea were found to be high at optimum conditions because of the involvement of both mechanisms direct and indirect oxidation. At low values of current density, NaCl and acidic pH, urine metabolites were oxidized directly by in-situ generated adsorbed $OH^{\bullet}$ on MMO anode surface, however, RCS such as Cl_2, HOCl, OCl^- degraded the target pollutants through mediated oxidation.
- While in the case of doped-MMO the maximum %Degradation of each urine metabolite was achieved at high values of current density, NaCl and acidic pH values as compared to with MMO anodes.

- The degradation of all urine metabolites was majorly happened due to the generation of strong chloro-oxidation species during EO treatment by both anodes.
- Kinetic study with both types of anodes shows that the %Degradation was much faster in the case of dual-process PEC than the EO and PC. The %Degradation of all urine metabolites in each treatment process has followed the first-order kinetics.
- Synergistic studies of both anodes showed maximum %Degradation for each urine metabolite was achieved in case of dual-process i.e. PEC over discreet process like EO and PC with a significant reduction in treatment time.
- The overall % synergy for each urine metabolite was calculated to be uric acid (11.45%), creatinine (7.62%) and urea (24.66%) during the oxidation treatment with MMO anode. while in the case of doped-MMO, it found to be uric acid (24.94%), creatinine (7.19%) and urea (8.69%) over other processes.
- Fluorescence spectroscopy results showed the maximum $OH^{\bullet}$ production during PEC i.e. under UV light (MMO) and under sunlight (doped-MMO) over the EO process. Moreover, the production of $OH^{\bullet}$ was found high in the case of doped-MMO as compared to MMO anode. This depicts that non-active anodes (doped-MMO) are more capable of producing $OH^{\bullet}$ while active anodes (MMO) is for RCS.
- Mineralization studies of uric acid and creatinine depict (87.05%, 83.75%) reduction in COD and (84.62%, 80.05%) decay in TOC respectively. However, in the case of doped-MMO maximum reduction in COD (90.05%, 93.10%) and (87.51%, 89.55%) removal in TOC was achieved at optimized conditions. While in the case of urea, approximately 90.05% and 90.45% reduction in TOC was achieved during EO treatment by MMO and doped-MMO anodes respectively. Further extension in treatment time has a lead marginal effect on both COD and TOC i.e. approximately 4.0-6.0%.
- Formations of inorganic ions such as NO_2^-, $NH_4^{+,}$ and NO_3^- have proved the almost complete mineralization of all urine metabolites (i.e. uric acid, creatinine, and urea) via EO treatment by both anodes.
- The results of analytic techniques such as FT-IR and CV for each urine metabolite have proved the complete destruction and oxidation of cyclic structure of each urine metabolite through the oxidation and reduction mechanism that occurs during the EO treatment at optimized conditions by both anodes.

- The intermediates formed during the oxidation process of each urine metabolites by both anodes were identified through LC-MS analysis, which further validated the degradation of uric acid, creatinine, and urea. Based on these identified intermediates, a tentative degradation pathway has been proposed in the present study.
- The total operating cost for treating per kg of uric acid, creatinine and urea with MMO came out to be 0.83 $/m^3$, 28.27 $/m^3$ and 0.78 $/m^3$ respectively.
- The total operating cost for treating per kg of uric acid, creatinine and urea with doped-MMO came out to be 3.740 $/m^3$, 41.68 $/m^3$ and 2.05 $/m^3$ respectively.
- The results show that the economic feasibility of the EO process for the treatment of synthetic urine wastewater by MMO and doped-MMO anodes.

5.1.2 EO treatment (batch) of SU with MMO and doped-MMO anodes:

- EO treatment of SU by both anodes i.e. MMO and doped-MMO has been done successfully. The statistical analysis showed a great correlation between predicted and experimental data.
- From 3D response surface graphs, it has been concluded that low values of N/Cl ratio in case of doped-MMO and high values in the case of MMO was responsible for maximum %COD removed during EO treatment of SU.
- Simultaneously optimization for the treatment of SU through the EO process by MMO and doped-MMO has been done successfully.
- The maximum %COD removed and SEC at optimized conditions by EO treatment was found to be 85.25% and 11.75 kWh/kg of COD removed with MMO and 90.55%, 20.851 kWh/kg of COD removed with doped-MMO.
- The overall % synergy for SU treated by MMO and the doped-MMO anode was calculated to be 12.14% and 9.65%. The combination of EO with light radiations (UV light in case of MMO) and (sunlight in case of doped-MMO) can significantly reduce the treatment time as well as avoid the formation of toxic chlorinated oxidant species.
- The in-situ chemical analysis depicts 87.25% reduction in COD and 85.88% reduction in TOC was achieved in 8.8 h at optimized conditions. While in the case of doped-MMO, the reduction was found slightly higher than MMO at optimized conditions.
- The urine metabolites i.e. uric acid, creatinine, and urea were also found degraded through the attack of in-situ electro-generated oxidants during the treatment process.

- The oxidation of these urine metabolites present in SU by both anodes leads to the release of nitrogen from their chemical structure which further got transformed into NO_2^-, NH_4^+, and NO_3^-. The maximum production of NO_2^-, NH_4^+, and NO_3^- was observed in the case of doped-MMO as compared to MMO anodes.
- LC-MS analysis clear that most of the diagnosed organic components got eliminated and converted into intermediates like oxalic acid, 1-methyl urea, guanidine, etc. during EO treatment of SU with MMO and doped-MMO.
- The non-toxicity of diagnosed components in the final samples of SU treated by both anodes was confirmed through the zone of inhibition by Kirby-Bauer toxicity analysis test.
- The electrochemical disinfection of SU wastewaters with MMO and doped-MMO allows the complete removal of *E.coli* within 45 and 75 min of the treatment process.

- During the EO treatment process by both anodes, large amounts of oxidants were produced from the oxidation of the ions present in SU which are responsible for the removal of pathogenic microorganisms

- The total operating cost for removing per kg of COD of SU during EO treatment with MMO and doped-MMO came out to be 0.85 $/kg of COD removed and 1.50 $/ kg of COD removed respectively.
- The results depict a sustainable solution for the on-site treatment of urinal wastewaters in terms of the economic feasibility of the EO process as well as the stability of both anodes.

5.1.3 EO treatment (continuous) of SU with MMO and doped-MMO anodes:

- The EO experiments conducted at optimized conditions (batch) shows that 83.43% COD removal (MMO) and 74.20% COD removal (doped-MMO) was achieved within 6 h of electrolytic treatment of SU in PV driven electrolytic cell under continuous recirculation mode.

- From the scale-up studies, the appropriate amount of molecular H_2, N_2, and CO_2 were produced, depicting the fruitful degradation of nitrogen-based components into simpler components that are non-toxic.

- The volumetric fraction of H_2 generated during 6 h of electrolysis in the range of 70.58% - 1.7190% (MMO) and 59.142% – 3.340% (doped-MMO). Other byproduct gases such as N_2, CO_2, CH_4, and CO has also been generated during electrolysis of SU by both anodes.

- Total capital expenditure (Capex) cost (per day) for continuous EO treatment of SU with MMO and doped-MMO was calculated to be 0.054 $ and 0.055 $ respectively.

5.1.4 EO treatment (continuous) of AHU with MMO anode:

- The continuous EO treatment of AHU wastewater conducted at optimized conditions using MMO anodes shows a 68.33% reduction in COD, 69.09% (urea), 95.180% (uric acid) and 67.95% (creatinine) was oxidized during 6 h of electrolytic treatment.
- The volumetric fraction of H_2 and N_2 generated during 6 h of electrolysis were found in the range of 69.74% – 2.617% and 18.019% – 62.133% respectively.
- GCMS spectra of untreated and EO treated samples of AHU wastewater confirms the elimination of most of the organic components after the treatment process. Moreover, the detected identified byproducts present in the treated solution were found non-toxic as compared to the untreated sample as confirmed through toxicity analysis.

5.1.5 Durability studies of both anodes:

- Various characterization techniques like SEM-EDS, XRD, Raman, XPS analysis have proved the durability and stability of MMO and doped-MMO even after 400 and 500 recycles respectively.
- Thus the extended durability and stability of both anodes further highlight its commercial applications.

5.2 Recommendations

EO coupled light radiations using cheap anodes has shown its great potential for the treatment of SU/AHU wastewater containing nitrogen-based recalcitrant compounds such as urea, uric acid, and creatinine. The use of a PV driven reactor for the treatment of this type of mixed wastewater has represented an alternative sustainable solution for minimizing the consumption of electric power used during the particular treatment process. Thus, future investigations would emphasize the more techno-economic analysis of field-scale applications such as on-site treatment of urinal wastewater and reuse as flush water. The concept is more viable in developing countries like India, where a lot of population require common urinals in their community. Thus having a strong potential of harnessing the molecular H_2 beside provides the eco-sanitation in terms of on-site treatment of urinal wastewaters. In addition, the use of these novel anodes with more efficient reactor design capable of handling large volume can open up new channels in the field of wastewater treatment (such as toilet wastewater, industrial wastewater, nitrogen-rich wastewater, and secondary waste) with electrochemical advanced oxidation technology.

REFERENCES

1. Abdel-Monem, N.M., Abdel-Salam, O.E., Nassar, A.F., Mahmoud, M.H., 2013. Oxidation of urea in human urine using flow-by porous graphite electrode. *International Journal of Scientific and Engineering Research* 4, 1715-1723.
2. Adams, C., Wang, Y., Loftin, K., Meyer, M., 2002. Removal of Antibiotics from Surface and Distilled Water in Conventional Water Treatment Processes. *Journal of Environmental Engineering* 128, 253–260. https://doi.org/10.1061/(ASCE)0733-9372(2002)128:3(253).
3. Aguilar, R., Dávila, M.M., Elizalde, M.P., Mattusch, J., Wennrich, R., 2004. Capability of a carbon–polyvinylchloride composite electrode for the detection of dopamine, ascorbic acid and uric acid. *Electrochimica Acta* 49, 851–859. https://doi.org/10.1016/j.electacta.2003.10.002
4. Alula, M.T., Yang, J., 2014. Photochemical decoration of magnetic composites with silver nanostructures for determination of creatinine in urine by surface-enhanced Raman spectroscopy. *Talanta* 130, 55–62. https://doi.org/10.1016/j.talanta.2014.06.047
5. American Health Public Association (APHA). Standard methods for the examination of water and wastewater. 17th ed., Standard method no. 4500-NO_3^- (E), Washington, DC: APHA; 1989c.
6. American Health Public Association (APHA). Standard Methods for the Examination of Water and Wastewater. 19th ed., Standard method no. (18th Edition), 5220-C, Washington, DC: APHA; 1992.
7. American Health Public Association (APHA). Standard Methods for the Examination of Water and wastewater. 17th ed., Standard method no. 4500-TN (A), Washington, DC: APHA; 1989a.
8. American Health Public Association (APHA). Standard Methods for the Examination of Water and wastewater. 17th ed., Standard method no. 4500-Cl^- (B), Washington, DC: APHA; 1989b.
9. American Health Public Association (APHA). Standard Methods for the Examination of Water and wastewater. 17th ed., Standard method no. 4500-NO_2^- (B), Washington, DC: APHA; 1989d.

10. American Health Public Association (APHA). Standard Methods for the Examination of Water and wastewater. 17th ed., Standard method no. 4500-NH_4^+ (C), Washington, DC: APHA; 1989e.
11. American Health Public Association (APHA). Standard Methods for the Examination of Water and wastewater. 17th ed., Standard method no. 4500-Cl^- (B), Washington, DC: APHA; 1989f.
12. Amstutz, V., Katsaounis, A., Kapalka, A., Comninellis, C., Udert, K.M., 2012. Effects of carbonate on the electrolytic removal of ammonia and urea from urine with thermally prepared IrO_2 electrodes. *Journal of Applied Electrochemistry* 42, 787–795. https://doi.org/10.1007/s10800-012-0444-y
13. An, H., Cui, H., Zhang, W., Zhai, J., Qian, Y., Xie, X., Li, Q., 2012. Fabrication and electrochemical treatment application of a microstructured TiO_2-NTs/Sb–SnO_2/PbO_2 anode in the degradation of C.I. Reactive Blue 194 (RB 194). *Chemical Engineering Journal* 209, 86–93. https://doi.org/10.1016/j.cej.2012.07.089
14. Andrade, L.S., Rocha-Filho, R.C., Bocchi, N., Biaggio, S.R., Iniesta, J., García-Garcia, V., Montiel, V., 2008. Degradation of phenol using Co- and Co, F-doped PbO_2 anodes in electrochemical filter-press cells. *Journal of Hazardous Materials* 153, 252–260. https://doi.org/10.1016/j.jhazmat.2007.08.046
15. Andres, L.A., Briceño, B., Chase, C., Echenique, J. A., 2017. Sanitation and externalities: evidence from early childhood health in rural India. *Journal of Water, Sanitation, and Hygiene for Development* 7, 272-289.
16. Anglada, A., Urtiaga, A., Ortiz, I., 2009. Contributions of electrochemical oxidation to waste-water treatment: fundamentals and review of applications. *Journal of Chemical Technology and Biotechnology* 84, 1747–1755. https://doi.org/10.1002/jctb.2214
17. Antoniou, M.G., Dionysiou, D.D., 2007. Application of immobilized titanium dioxide photocatalysts for the degradation of creatinine and phenol, model organic contaminants found in NASA's spacecraft wastewater streams. *Catalysis Today* 124, 215–223. https://doi.org/10.1016/j.cattod.2007.03.054
18. Antoniou, M.G., Nambiar, U., Dionysiou, D.D., 2009. Investigation of the photocatalytic degradation pathway of the urine metabolite, creatinine: The effect of pH. *Water Research* 43, 3956–3963. https://doi.org/10.1016/j.watres.2009.06.015.

19. Aquino, J.M., Rocha-Filho, R.C., Ruotolo, L.A.M., Bocchi, N., Biaggio, S.R., 2014. Electrochemical degradation of real textile wastewater using β-PbO_2 and DSA® anodes. *Chemical Engineering Journal* 251, 138–145. https://doi.org/10.1016/j.cej.2014.04.032
20. Araújo, W.R.D., Salles, M.O., Paixão, T.R.L.C., 2012. Development of an enzymeless electroanalytical method for the indirect detection of creatinine in urine samples. *Sensors and Actuators B: Chemical* 173, 847–851. https://doi.org/10.1016/j.snb.2012.07.114
21. Asaithambi, P., Matheswaran, M., 2016. Electrochemical treatment of simulated sugar industrial effluent: Optimization and modeling using a response surface methodology. *Arabian Journal of Chemistry* 9, S981–S987. https://doi.org/10.1016/j.arabjc.2011.10.004
22. Bagastyo, A.Y., Radjenovic, J., Mu, Y., Rozendal, R.A., Batstone, D.J., Rabaey, K., 2011. Electrochemical oxidation of reverse osmosis concentrate on mixed metal oxide (MMO) titanium coated electrodes. *Water Research* 45, 4951–4959. https://doi.org/10.1016/j.watres.2011.06.039
23. Bansal, P., Verma, A., 2018. In-situ dual effect studies using novel Fe-TiO_2 composite for the pilot-plant degradation of pentoxifylline. *Chemical Engineering Journal* 332, 682–694. https://doi.org/10.1016/j.cej.2017.09.121
24. Bansal, S., Kushwaha, J.P., Sangal, V.K., 2013. Electrochemical Treatment of Reactive Black 5 Textile Wastewater: Optimization, Kinetics, and Disposal Study. *Water Environment Research* 85, 2294–2306. https://doi.org/10.2175/106143013X13807328848414
25. Barbosa, M.P.R., Lima, N.S., de Matos, D.B., Alves Felisardo, R.J., Santos, G.N., Salazar-Banda, G.R., Cavalcanti, E.B., 2018. Degradation of pesticide mixture by electro-Fenton in the filter-press reactor. *Journal of Water Process Engineering* 25, 222–235. https://doi.org/10.1016/j.jwpe.2018.08.008
26. Barrera-Díaz, C., Cañizares, P., Fernández, F.J., Natividad, R., Rodrigo, M.A., 2017. Electrochemical Advanced Oxidation Processes: An Overview of the Current Applications to Actual Industrial Effluents. *Journal of the Mexican Chemical Society* 58, 256-275. https://doi.org/10.29356/jmcs.v58i3.133
27. Bergmann, M.E.H., Rollin, J., Iourtchouk, T., 2009. The occurrence of perchlorate during drinking water electrolysis using BDD anodes. *Electrochimica Acta* 54, 2102–2107. https://doi.org/10.1016/j.electacta.2008.09.040

28. Bezerra, M.A., Santelli, R.E., Oliveira, E.P., Villar, L.S., Escaleira, L.A., 2008. Response surface methodology (RSM) as a tool for optimization in analytical chemistry. *Talanta* 76, 965–977. https://doi.org/10.1016/j.talanta.2008.05.019
29. Bhatia, H., Bhatia, R., 2017. India Open-Defecation Free: Opportunities and Challenges. *International Journal for Innovative Research in Multidisciplinary Field* 3, 88-93.
30. Bińka, A.K., Sombra-Madej, S., 2012. Comparison of the Advanced Oxidation Processes (UV, UV/H_2O_2 and O_3) for the Removal of Antibiotic Substances during Wastewater Treatment. *Ozone: Science and Engineering* 34, 136–139. https://doi.org/10.1080/01919512.2012.650130
31. Borras, C., Berzoy, C., Mostany, J., Herrera, J.C., Scharifker, B.R., 2007. A comparison of the electrooxidation kinetics of p-methoxyphenol and p-nitrophenol on Sb-doped SnO_2 surfaces: Concentration and temperature effects. *Applied Catalysis B: Environmental* 72, 98–104. https://doi.org/10.1016/j.apcatb.2006.09.017
32. Borràs, N., Oliver, R., Arias, C., Brillas, E., 2010. Degradation of Atrazine by Electrochemical Advanced Oxidation Processes Using a Boron-Doped Diamond Anode. *The Journal of Physical Chemistry A* 114, 6613–6621. https://doi.org/10.1021/jp1035647
33. Brillas, E., Sirés, I., Oturan, M.A., 2009. Electro-Fenton Process and Related Electrochemical Technologies Based on Fenton's Reaction Chemistry. *Chemical Reviews* 109, 6570–6631. https://doi.org/10.1021/cr900136g
34. Brocklehurst, C., 2014. Scaling up Rural Sanitation in India. *PLoS Medicine* 11, e1001710. https://doi.org/10.1371/journal.pmed.1001710
35. Cañizares, P., Larrondo, F., Lobato, J., Rodrigo, M.A., Sáez, C., 2005. Electrochemical Synthesis of Peroxodiphosphate Using Boron-Doped Diamond Anodes. *Journal of The Electrochemical Society* 152, D191. https://doi.org/10.1149/1.2039936
36. Cañizares, P., Paz, R., Lobato, J., Sáez, C., Rodrigo, M.A., 2006. Electrochemical treatment of the effluent of a fine chemical manufacturing plant. *Journal of Hazardous Materials* 138, 173–181. https://doi.org/10.1016/j.jhazmat.2006.05.056
37. Cañizares, P., Paz, R., Sáez, C., Rodrigo, M.A., 2009. Costs of the electrochemical oxidation of wastewaters: A comparison with ozonation and Fenton oxidation processes. *Journal of Environmental Management* 90, 410–420. https://doi.org/10.1016/j.jenvman.2007.10.010

38. Catanho, M., Malpass, G.R.P., Motheo, A.J., 2006. Photoelectrochemical treatment of the dye reactive red 198 using DSA® electrodes. *Applied Catalysis B: Environmental* 62, 193–200. https://doi.org/10.1016/j.apcatb.2005.07.011
39. Černigoj, U., Štangar, U.L., Trebše, P., 2007. Evaluation of a novel Carberry type photoreactor for the degradation of organic pollutants in water. *Journal of Photochemistry and Photobiology A: Chemistry* 188, 169–176. https://doi.org/10.1016/j.jphotochem.2006.12.009
40. Chai, S., Zhao, G., Li, P., Lei, Y., Zhang, Y., Li, D., 2011. Novel Sieve-Like SnO_2 /TiO_2 Nanotubes with Integrated Photoelectrocatalysis: Fabrication and Application for Efficient Toxicity Elimination of Nitrophenol Wastewater. *The Journal of Physical Chemistry C* 115, 18261–18269. https://doi.org/10.1021/jp205228h
41. Chaplin, B.P., 2014. A critical review of electrochemical advanced oxidation processes for water treatment applications. *Environmental Science: Processes Impacts* 16, 1182–1203. https://doi.org/10.1039/C3EM00679D
42. Chauhan, R., Srivastava, V.C., 2019. Electrochemical denitrification of highly contaminated actual nitrate wastewater by Ti/RuO_2 anode and iron cathode. *Chemical Engineering Journal* 122065. https://doi.org/10.1016/j.cej.2019.122065
43. Chen, F., Yang, X., Mak, H.K.C., Chan, D.W.T., 2010. Photocatalytic oxidation for antimicrobial control in built environment: A brief literature overview. *Building and Environment* 45, 1747–1754. https://doi.org/10.1016/j.buildenv.2010.01.024
44. Chen, G., 2004. Electrochemical technologies in wastewater treatment. *Separation and Purification Technology* 38, 11-41. doi:10.1016/j.seppur.2003.10.006
45. Chen, G., Chen, X., Yue, P.L., 2002. Electrochemical Behavior of Novel Ti/IrOx−Sb_2O_5−SnO_2 Anodes. *The Journal of Physical Chemistry B* 106, 4364–4369. https://doi.org/10.1021/jp013547o
46. Chen, J.-C., Kumar, A.S., Chung, H.-H., Chien, S.-H., Kuo, M.-C., Zen, J.-M., 2006. An enzymeless electrochemical sensor for the selective determination of creatinine in human urine. *Sensors and Actuators B: Chemical* 115, 473–480. https://doi.org/10.1016/j.snb.2005.10.015

47. Chen, L.-C., Tsai, F.-R., Fang, S.-H., Ho, Y.-C., 2009. Properties of sol-gel SnO_2/TiO_2 electrodes and their photoelectrocatalytic activities under UV and visible light illumination. *Electrochimica Acta* 54, 1304–1311. https://doi.org/10.1016/j.electacta.2008.09.009
48. Chen, X., Gao, F., Chen, G., 2005. Comparison of Ti/BDD and Ti/SnO_2-Sb_2O_5 electrodes for pollutant oxidation. *Journal of Applied Electrochemistry* 35, 185–191. https://doi.org/10.1007/s10800-004-6068-0
49. Chen, Y., Fierro, J.L.G., Tanaka, T., Wachs, I.E., 2003. Supported Tantalum Oxide Catalysts: Synthesis, Physical Characterization, and Methanol Oxidation Chemical Probe Reaction. *The Journal of Physical Chemistry B* 107, 5243–5250. https://doi.org/10.1021/jp0276451
50. Chen, Y., Hong, L., Xue, H., Han, W., Wang, L., Sun, X., Li, J., 2010. Preparation and characterization of TiO_2-NTs/SnO_2-Sb electrodes by electrodeposition. *Journal of Electroanalytical Chemistry* 648, 119–127 https://doi.org/10.1016/j.jelechem.2010.08.004
51. Cheng, W., Yang, M., Xie, Y., Liang, B., Fang, Z., Tsang, E.P., 2013. Enhancement of mineralization of metronidazole by the electro-Fenton process with a Ce/SnO_2–Sb coated titanium anode. *Chemical Engineering Journal* 220, 214–220. https://doi.org/10.1016/j.cej.2013.01.055
52. Cho, K. and Hoffmann, M.R., 2014. Urea degradation by electrochemically generated reactive chlorine species: Products and reaction pathways. *Environmental Science and Technology* 48, 11504-11511. dx.doi.org/10.1021/es5025405
53. Cho, K., Kwon, D., Hoffmann, M.R., 2014. Electrochemical treatment of human waste coupled with molecular hydrogen production. *RSC Advances* 4, 4596–4608. https://doi.org/10.1039/C3RA46699J.
54. Cho, K., Qu, Y., Kwon, D., Zhang, H., Cid, C.A., Aryanfar, A., Hoffmann, M.R., 2014. Effects of Anodic Potential and Chloride Ion on Overall Reactivity in Electrochemical Reactors Designed for Solar-Powered Wastewater Treatment. *Environmental Science and Technology* 48, 2377–2384. https://doi.org/10.1021/es404137u
55. Chong, M.N., Jin, B., Chow, C.W.K., Saint, C., 2010. Recent developments in photocatalytic water treatment technology: A review. *Water Research* 44, 2997–3027. https://doi.org/10.1016/j.watres.2010.02.039

56. Cid, C.A., Qu, Y., Hoffmann, M.R., 2018. Design and preliminary implementation of onsite electrochemical wastewater treatment and recycling toilets for the developing world. Environmental Science: Water Research & Technology 4, 1439–1450. https://doi.org/10.1039/C8EW00209F
57. Comninellis, C., 1992. Electrochemical treatment of wastewater containing phenol. *In Institution of Chemical Engineers Symposium Series* 127, 189-201.
58. Correa-Lozano, B., Comninellis, C., Battisti, A. D., 1997. The service life of $Ti/SnO_2–Sb_2O_5$ anodes. *Journal of Applied Electrochemistry* 27, 970-974.
59. Cossu, R., Polcaro, A.M., Lavagnolo, M.C., Mascia, M., Palmas, S., Renoldi, F., 1998. Electrochemical Treatment of Landfill Leachate: Oxidation at Ti/PbO_2 and Ti/SnO_2 Anodes. *Environmental Science and Technology* 32, 3570–3573. https://doi.org/10.1021/es971094o
60. Costa, N.R., Lourenço, J., Pereira, Z.L., 2011. Desirability function approach: A review and performance evaluation in adverse conditions. *Chemometrics and Intelligent Laboratory Systems* 107, 234–244. https://doi.org/10.1016/j.chemolab.2011.04.004
61. Coteiro, R.D., Teruel, F.S., Ribeiro, J., Andrade, A.R. de, 2006. Effect of solvent on the preparation and characterization of DSA®-type anodes containing RuO_2-TiO_2-SnO_2. *Journal of the Brazilian Chemical Society* 17, 771–779. https://doi.org/10.1590/S0103-50532006000400020
62. Cotillas, S., de Vidales, M.J.M., Llanos, J., Sáez, C., Cañizares, P., Rodrigo, M.A., 2016. Electrolytic and electro-irradiated processes with diamond anodes for the oxidation of persistent pollutants and disinfection of urban treated wastewater. *Journal of Hazardous Materials* 319, 93–101. https://doi.org/10.1016/j.jhazmat.2016.01.050
63. Cotillas, S., Lacasa, E., Sáez, C., Cañizares, P., Rodrigo, M.A., 2018. Disinfection of urine by conductive-diamond electrochemical oxidation. *Applied Catalysis B: Environmental* 229, 63–70. https://doi.org/10.1016/j.apcatb.2018.02.013
64. Cui, Y.H., Li, X.Y. and Chen, G., 2009. Electrochemical degradation of bisphenol A on different anodes. *Water Research* 43, 1968-1976. https://doi.org/10.1016/j.watres.2009.01.026
65. Daghrir, R., Drogui, P., Robert, D., 2012. Photoelectrocatalytic technologies for environmental applications. *Journal of Photochemistry and Photobiology A: Chemistry* 238, 41–52. https://doi.org/10.1016/j.jphotochem.2012.04.009

66. Daghrir, R., Drogui, P., Delegan, N., El Khakani, M.A., 2014. Removal of chlortetracycline from spiked municipal wastewater using a photoelectrocatalytic process operated under sunlight irradiations. *Science of The Total Environment* 466–467, 300–305. https://doi.org/10.1016/j.scitotenv.2013.07.001
67. Daghrir, R., Drogui, P., Ka, I., El Khakani, M.A., 2012. Photoelectrocatalytic degradation of chlortetracycline using Ti/TiO_2 nanostructured electrodes deposited by means of a Pulsed Laser Deposition process. *Journal of Hazardous Materials* 199–200, 15–24. https://doi.org/10.1016/j.jhazmat.2011.10.022
68. da Silva, S.G., Silva, J.C.M., Buzzo, G.S., De Souza, R.F.B., Spinacé, E.V., Neto, A.O., Assumpção, M.H.M.T., 2014. Electrochemical and fuel cell evaluation of PtAu/C electrocatalysts for ethanol electro-oxidation in alkaline media. *International Journal of Hydrogen Energy* 39, 10121–10127. https://doi.org/10.1016/j.ijhydene.2014.04.169
69. Datta, M.K., Kadakia, K., Velikokhatnyi, O.I., Jampani, P.H., Chung, S.J., Poston, J.A., Manivannan, A., Kumta, P.N., 2013. High performance robust F-doped tin oxide-based oxygen evolution electro-catalysts for PEM based water electrolysis. *Journal of Materials Chemistry A* 1, 4026. https://doi.org/10.1039/c3ta01458d
70. Daudey, L., 2018. The cost of urban sanitation solutions: a literature review. *Journal of Water Sanitation and Hygiene for Development* 8, 176–195. https://doi.org/10.2166/washdev.2017.058
71. Dbira, S., Bensalah, N., Ahmad, M.I., Bedoui, A., 2019. Electrochemical Oxidation/Disinfection of Urine Wastewaters with Different Anode Materials. *Materials* 12, 1254. https://doi.org/10.3390/ma12081254
72. Dbira, S., Bensalah, N., Bedoui, A., 2016. Mechanism and kinetics of electrochemical degradation of uric acid using conductive-diamond anodes. *Environmental Technology* 37, 2993–3001. https://doi.org/10.1080/09593330.2016.1173115
73. Dbira, S., Bensalah, N., Bedoui, A., Cañizares, P., Rodrigo, M.A., 2015. Treatment of synthetic urine by electrochemical oxidation using conductive-diamond anodes. *Environmental Science and Pollution Research* 22, 6176–6184. https://doi.org/10.1007/s11356-014-3831-6

74. Dbira, S., Bensalah, N., Cañizares, P., Rodrigo, M.A., Bedoui, A., 2015. The electrolytic treatment of synthetic urine using DSA electrodes. *Journal of Electroanalytical Chemistry* 744, 62–68. https://doi.org/10.1016/j.jelechem.2015.02.026
75. Denny, Y.R., Firmansyah, T., Oh, S.K., Kang, H.J., Yang, D.-S., Heo, S., Chung, J., Lee, J.C., 2016. Effect of oxygen deficiency on electronic properties and local structure of amorphous tantalum oxide thin films. *Materials Research Bulletin* 82, 1–6. https://doi.org/10.1016/j.materresbull.2016.03.004
76. Ding, Y., Yang, C., Zhu, L., Zhang, J., 2010. The photoelectrochemical activity of liquid phase deposited TiO_2 film for the degradation of benzotriazole. *Journal of Hazardous Materials* 175, 96–103. https://doi.org/10.1016/j.jhazmat.2009.09.037
77. Diouf, A., Motia, S., El Alami El Hassani, N., El Bari, N., Bouchikhi, B., 2017. Development and characterization of an electrochemical biosensor for creatinine detection in human urine based on functional molecularly imprinted polymer. *Journal of Electroanalytical Chemistry* 788, 44–53. https://doi.org/10.1016/j.jelechem.2017.01.068
78. Dixit, A., Mishra, P.K., Alam, M.S., 2017. Titania Nanofibers: A Potential Adsorbent for Mercury and Lead Uptake. *International Journal of Chemical Engineering and Applications* 8, 75–81. https://doi.org/10.18178/ijcea.2017.8.1.633
79. Dominguez-Ramos, A., Irabien, A., 2013. Analysis and Modeling of the Continuous Electro-oxidation Process for Organic Matter Removal in Urban Wastewater Treatment. *Industrial and Engineering Chemistry Research* 52, 7534–7540. https://doi.org/10.1021/ie303021v
80. Dong, S., Feng, J., Fan, M., Pi, Y., Hu, L., Han, X., Liu, M., Sun, Jingyu, Sun, Jianhui, 2015. Recent developments in heterogeneous photocatalytic water treatment using visible light-responsive photocatalysts: a review. *RSC Advances* 5, 14610–14630. https://doi.org/10.1039/C4RA13734E
81. dos Santos, E.V., Sena, S.F.M., da Silva, D.R., Ferro, S., De Battisti, A., Martínez-Huitle, C.A., 2014. Scale-up of electrochemical oxidation system for the treatment of produced water generated by the Brazilian petrochemical industry. *Environmental Science and Pollution Research* 21, 8466–8475. https://doi.org/10.1007/s11356-014-2779-x
82. Egorov, K.V., Lebedinskii, Y.Y., Soloviev, A.A., Chouprik, A.A., Azarov, A.Yu., Markeev, A.M., 2017. Initial and steady-state Ru growth by atomic layer deposition studied by in situ

Angle-Resolved X-ray Photoelectron Spectroscopy. *Applied Surface Science* 419, 107–113. https://doi.org/10.1016/j.apsusc.2017.05.010

83. Ekoi, E.J., Gowen, A., Dorrepaal, R., Dowling, D.P., 2019. Characterization of titanium oxide layers using Raman spectroscopy and optical profilometry: Influence of oxide properties. *Results in Physics* 12, 1574–1585. https://doi.org/10.1016/j.rinp.2019.01.054
84. Feng, Y.J., Li, X.Y., 2003. Electro-catalytic oxidation of phenol on several metal-oxide electrodes in aqueous solution. *Water Research* 37, 2399–2407. https://doi.org/10.1016/S0043-1354(03)00026-5
85. Feng, Y., Cui, Y.-H., Liu, J., Logan, B.E., 2010. Factors affecting the electro-catalytic characteristics of the Eu doped SnO_2/Sb electrode. *Journal of Hazardous Materials* 178, 29–34. https://doi.org/10.1016/j.jhazmat.2009.12.101
86. Fernandes, A., Santos, D., Pacheco, M.J., Ciríaco, L., Lopes, A., 2014. Nitrogen and organic load removal from sanitary landfill leachates by anodic oxidation at Ti/Pt/PbO_2, Ti/Pt/SnO_2-Sb_2O_4, and Si/BDD. *Applied Catalysis B: Environmental* 148–149, 288–294. https://doi.org/10.1016/j.apcatb.2013.10.060.
87. Ferreira, S.L.C., Bruns, R.E., Ferreira, H.S., Matos, G.D., David, J.M., Brandão, G.C., da Silva, E.G.P., Portugal, L.A., dos Reis, P.S., Souza, A.S., dos Santos, W.N.L., 2007. Box-Behnken design: An alternative to the optimization of analytical methods. *Analytica Chimica Acta* 597, 179–186. https://doi.org/10.1016/j.aca.2007.07.011
88. Fóti, G., 1999. Oxidation of Organics by Intermediates of Water Discharge on IrO_2 and Synthetic Diamond Anodes. *Electrochemical and Solid-State Letters* 2, 228. https://doi.org/10.1149/1.1390792
89. Freeman, M.C., Garn, J.V., Sclar, G.D., Boisson, S., Medlicott, K., Alexander, K.T., Penakalapati, G., Anderson, D., Mahtani, A.G., Grimes, J.E.T., Rehfuess, E.A., Clasen, T.F., 2017. The impact of sanitation on infectious disease and nutritional status: A systematic review and meta-analysis. *International Journal of Hygiene and Environmental Health* 220, 928–949. https://doi.org/10.1016/j.ijheh.2017.05.007
90. Freitas, A.M.D., Sirtori, C., Peralta-Zamora, P., 2011. Photoelectrocatalytic degradation of camphor on TiO_2/RuO_2 electrodes. *Environmental Chemistry Letters* 9, 97–102. https://doi.org/10.1007/s10311-009-0252-8

91. Frolova, L., Lyskov, N., Dobrovolsky, Yu., 2012. Nanostructured Pt/SnO_2–SbOx–RuO_2 electrocatalysts for direct alcohol fuel cells. *Solid State Ionics* 225, 92–98. https://doi.org/10.1016/j.ssi.2012.02.013
92. Frontistis, Z., Daskalaki, V.M., Katsaounis, A., Poulios, I., Mantzavinos, D., 2011. Electrochemical enhancement of solar photocatalysis: Degradation of endocrine disruptor bisphenol-A on Ti/TiO_2 films. *Water Research* 45, 2996–3004. https://doi.org/10.1016/j.watres.2011.03.030
93. Fryda, M., Matthée, T., Mulcahy, S., Höfer, M., Schäfer, L., Tröster, I., 2003. Applications of DIACHEM® Electrodes in Electrolytic Water Treatment. The Electrochemical Society Interface 12, 40-44.
94. Fu, J., Zhao, Y., Wu, Q., 2007. Optimizing photoelectrocatalytic oxidation of fulvic acid using response surface methodology. *Journal of Hazardous Materials* 144, 499–505. https://doi.org/10.1016/j.jhazmat.2006.10.071
95. Gągol, M., Przyjazny, A., Boczkaj, G., 2018. Wastewater treatment by means of advanced oxidation processes based on cavitation – A review. *Chemical Engineering Journal* 338, 599–627. https://doi.org/10.1016/j.cej.2018.01.049
96. Ganzenko, O., Huguenot, D., van Hullebusch, E.D., Esposito, G., Oturan, M.A., 2014. Electrochemical advanced oxidation and biological processes for wastewater treatment: a review of the combined approaches. *Environmental Science and Pollution Research* 21, 8493–8524. https://doi.org/10.1007/s11356-014-2770-6
97. Ganesapillai, M., Simha, P., Gupta, K., Jayan, M., 2016. Nutrient Recovery and Recycling from Human Urine: A Circular Perspective on Sanitation and Food Security. *Procedia Engineering* 148, 346–353. https://doi.org/10.1016/j.proeng.2016.06.461
98. Gao, B., Chen, W., Liu, J., An, J., Wang, L., Sillanpää, M., 2019. The photoelectrocatalytic performance of $ZnIn_2S_4$ nanosheets and microspheres are grown on flexible graphite felt. *Journal of Electroanalytical Chemistry* 845, 144–153. https://doi.org/10.1016/j.jelechem.2019.05.030.
99. García, O., Isarain-Chávez, E., Garcia-Segura, S., Brillas, E., Peralta-Hernández, J.M., 2013. Degradation of 2,4-Dichlorophenoxyacetic Acid by Electro-oxidation and Electro-Fenton/BDD Processes Using a Pre-pilot Plant. *Electrocatalysis* 4, 224–234. https://doi.org/10.1007/s12678-013-0135-4

100. García-Espinoza, J.D., Mijaylova-Nacheva, P., Avilés-Flores, M., 2018. Electrochemical carbamazepine degradation: Effect of the generated active chlorine, transformation pathways, and toxicity. *Chemosphere* 192, 142–151. https://doi.org/10.1016/j.chemosphere.2017.10.147

101. Goudarzi, M., Ghorbani, M., 2016. Deposition of (Ti, Ru)O_2 and (Ti, Ru, Ir)O_2 oxide coatings prepared by the sol-gel method on titanium. *Journal of Sol-Gel Science and Technology* 79, 44–50. https://doi.org/10.1007/s10971-016-4009-0

102. Grimm, J., Bessarabov, D., Maier, W., Storck, S., Sanderson, R.D., 1998. Sol-gel film-preparation of novel electrodes for the electrocatalytic oxidation of organic pollutants in water. *Desalination* 115, 295–302. https://doi.org/10.1016/S0011-9164(98)00048-4.

103. Gupta, V.K., Ali, I., Saleh, T.A., Nayak, A., Agarwal, S., 2012. Chemical treatment technologies for waste-water recycling—an overview. RSC Advances 2, 6380. https://doi.org/10.1039/c2ra20340e

104. Guzmán-Duque, F.L., Palma-Goyes, R.E., González, I., Peñuela, G., Torres-Palma, R.A., 2014. Relationship between anode material, supporting electrolyte and current density during electrochemical degradation of organic compounds in water. *Journal of Hazardous Materials* 278, 221–226. https://doi.org/10.1016/j.jhazmat.2014.05.076

105. Han, L., Xin, Y., Liu, H., Ma, X., Tang, G., 2010. Photoelectrocatalytic properties of nitrogen-doped TiO_2/Ti photoelectrode prepared by plasma-based ion implantation under visible light. *Journal of Hazardous Materials* 175, 524–531. https://doi.org/10.1016/j.jhazmat.2009.10.037

106. Han, R., Ding, D., Xu, Y., Zou, W., Wang, Y., Li, Y., Zou, L., 2008. Use of rice husk for the adsorption of congo red from aqueous solution in column mode. *Bioresource Technology* 99, 2938–2946. https://doi.org/10.1016/j.biortech.2007.06.027

107. Hanrahan, G., Lu, K., 2006. Application of Factorial and Response Surface Methodology in Modern Experimental Design and Optimization. *Critical Reviews in Analytical Chemistry* 36, 141–151. https://doi.org/10.1080/10408340600969478

108. He, Z., Huang, C., Wang, Q., Jiang, Z., Chen, J., Song, S., 2011. Preparation of a Praseodymium Modified Ti/SnO_2-Sb/PbO_2 Electrode and its Application in the Anodic Degradation of the Azo Dye Acid Black 194. *International Journal Electrochemical Science* 6, 14

109. Hernández, M.C., Russo, N., Panizza, M., Spinelli, P. and Fino, D., 2014. Electrochemical oxidation of urea in aqueous solutions using a boron-doped thin-film diamond electrode. *Diamond and Related Materials* 44, 109-116. https://doi.org/10.1016/j.diamond.2014.02.006

110. Herrada, R.A., Acosta-Santoyo, G., Sepúlveda-Guzmán, S., Brillas, E., Sirés, I., Bustos, E., 2018. IrO_2-Ta_2O_5|Ti electrodes prepared by electrodeposition from different Ir: Ta ratios for the degradation of polycyclic aromatic hydrocarbons. *Electrochimica Acta* 263, 353–361. https://doi.org/10.1016/j.electacta.2018.01.056

111. Hernlem, B.J., 2005. Electrolytic destruction of urea in dilute chloride solution using DSA electrodes in a recycled batch cell. *Water Research* 39, 2245–2252. https://doi.org/10.1016/j.watres.2005.04.018

112. Hiwarkar, A.D., Singh, S., Srivastava, V.C., Mall, I.D., 2017. Mineralization of pyrrole, a recalcitrant heterocyclic compound, by the electrochemical method: Multi-response optimization and degradation mechanism. *Journal of Environmental Management* 198, 144–152. https://doi.org/10.1016/j.jenvman.2017.04.051

113. Hoffmann, M.R., Cho, K., Cid, C., Yan, Q., 2014. Development of a Self-Contained, PV-Powered Domestic Toilet and Electrochemical Wastewater Treatment System Suitable for the Developing World, in 3rd Annual International Conference on Sustainable Energy and Environmental Sciences (SEES 2014). Presented at the Annual International Conference on Sustainable Energy and Environmental Sciences, Global Science & Technology Forum (GSTF). https://doi.org/10.5176/2251-189X_SEES14.27.

114. Höglund, C., Ashbolt, N., Stenström, T.A., Svensson, L., 2002. Viral persistence in source-separated human urine. *Advances in Environmental Research* 6, 265–275. https://doi.org/10.1016/S1093-0191(01)00057-0.

115. Hu, M., Fan, B., Wang, H., Qu, B., Zhu, S., 2016. Constructing the ecological sanitation: a review on technology and methods. *Journal of Cleaner Production* 125, 1–21. https://doi.org/10.1016/j.jclepro.2016.03.012

116. Hua, Z., Dai, Z., Bai, X., Ye, Z., Wang, P., Gu, H., Huang, X., 2016. Copper nanoparticles sensitized TiO_2 nanotube arrays electrode with enhanced photoelectrocatalytic activity for diclofenac degradation. *Chemical Engineering Journal* 283, 514–523. https://doi.org/10.1016/j.cej.2015.07.072

117. Ikematsu, M., Kaneda, K., Iseki, M., Yasuda, M., 2007. Electrochemical treatment of human urine for its storage and reuse as flush water. *Science of The Total Environment* 382, 159–164. https://doi.org/10.1016/j.scitotenv.2007.03.028

118. Isunju, J.B., Schwartz, K., Schouten, M.A., Johnson, W.P., van Dijk, M.P., 2011. Socio-economic aspects of improved sanitation in slums: A review. *Public Health* 125, 368–376. https://doi.org/10.1016/j.puhe.2011.03.008.

119. Jafari, M., Ebrahimzadeh, H., Banitaba, M.H., 2015. Fast vaporization solid-phase microextraction and ion mobility spectrometry: A new approach for the determination of creatinine in biological fluids. *Talanta* 144, 474–479. https://doi.org/10.1016/j.talanta.2015.06.046

120. Jara, C., Di Giulio, S., Fino, D., Spinelli, P., 2008. Combined direct and indirect electrooxidation of urea containing water. *Journal of Applied Electrochemistry* 38, 915–922. https://doi.org/10.1007/s10800-008-9496-4

121. Jasper, J.T., Yang, Y., Hoffmann, M.R., 2017. Toxic Byproduct Formation during Electrochemical Treatment of Latrine Wastewater. *Environmental Science and Technology* 51, 7111–7119. https://doi.org/10.1021/acs.est.7b01002

122. Jüttner, K., Galla, U., Schmieder, H., 2000. Electrochemical approaches to environmental problems in the process industry. *Electrochimica Acta* 45, 2575–2594. https://doi.org/10.1016/S0013-4686(00)00339-X

123. Karuppiah, M.T., Raju, G.B., 2009. Anodic Degradation of CI Reactive Blue 221 Using Graphite and $IrO_2/TaO_2/RuO_2$ Coated Titanium Electrodes. *Industrial and Engineering Chemistry Research* 48, 2149–2156. https://doi.org/10.1021/ie801291h

124. Katukiza, A.Y., Ronteltap, M., Niwagaba, C.B., Foppen, J.W.A., Kansiime, F., Lens, P.N.L., 2012. Sustainable sanitation technology options for urban slums. *Biotechnology Advances* 30, 964–978. https://doi.org/10.1016/j.biotechadv.2012.02.007

125. Kaur, P., Sangal, V.K., Kushwaha, J.P., 2015. Modeling and evaluation of electro-oxidation of dye wastewater using artificial neural networks. *RSC Advances* 5, 34663–34671. https://doi.org/10.1039/C4RA14160A

126. Kaur, S., Singh, V., 2007. Visible light-induced sonophotocatalytic degradation of Reactive Red dye 198 using dye-sensitized TiO_2. *Ultrasonics Sonochemistry* 14, 531–537. https://doi.org/10.1016/j.ultsonch.2006.09.015

127. Kete, M., Pliekhova, O., Matoh, L., Štangar, U.L., 2018. Design and evaluation of a compact photocatalytic reactor for water treatment. *Environmental Science and Pollution Research* 25, 20453–20465. https://doi.org/10.1007/s11356-017-9895-3

128. Khan, M.M., Adil, S.F., Al-Mayouf, A., 2015. Metal oxides as photocatalysts. *Journal of Saudi Chemical Society* 19, 462–464. https://doi.org/10.1016/j.jscs.2015.04.003

129. Khandegar, V., Acharya, S., Jain, A.K., 2018. Data on the treatment of sewage wastewater by electrocoagulation using a punched aluminum electrode and characterization of generated sludge. *Data in Brief* 18, 1229–1238. https://doi.org/10.1016/j.dib.2018.04.020

130. Khuri, A.I., Mukhopadhyay, S., 2010. Response surface methodology. *Wiley Interdisciplinary Reviews: Computational Statistics* 2, 128–149. https://doi.org/10.1002/wics.73

131. Kim, J., Choi, W.J.K., Choi, J., Hoffmann, M.R., Park, H., 2013. Electrolysis of urea and urine for solar hydrogen. *Catalysis Today* 199, 2–7. https://doi.org/10.1016/j.cattod.2012.02.009

132. Kollu, K., Örmeci, B., 2012. Effect of particles and bioflocculation on the ultraviolet disinfection of Escherichia coli. *Water Research* 46, 750–760. https://doi.org/10.1016/j.watres.2011.11.046.

133. Kong, J., Shi, S., Kong, L., Zhu, X., Ni, J., 2007. Preparation and characterization of PbO_2 electrodes doped with different rare earth oxides. *Electrochimica Acta* 53, 2048–2054. https://doi.org/10.1016/j.electacta.2007.09.003

134. Kong, J.-Z., Li, A.-D., Li, X.-Y., Zhai, H.-F., Zhang, W.-Q., Gong, Y.-P., Li, H., Wu, D., 2010. Photo-degradation of methylene blue using Ta-doped ZnO nanoparticle. *Journal of Solid State Chemistry* 183, 1359–1364. https://doi.org/10.1016/j.jssc.2010.04.005

135. Koparal, A.S., Yavuz, Y., Gürel, C., Öğütveren, Ü.B., 2007. Electrochemical degradation and toxicity reduction of C.I. Basic Red 29 solution and textile wastewater by using diamond anode. *Journal of Hazardous Materials* 145, 100–108. https://doi.org/10.1016/j.jhazmat.2006.10.090

136. Korotcov, A.V., Huang, Y.S., Tiong, K.K. and Tsai, D.S., 2007. Raman scattering characterization of well-aligned RuO_2 and IrO_2 nanocrystals. *Journal of Raman Spectroscopy*: An International Journal for Original Work in all Aspects of Raman

Spectroscopy, Including Higher Order Processes, and also Brillouin and Rayleigh Scattering 38, 737-749. https://doi.org/10.1002/jrs.1655

137. Kotz, R., Stucki, S., Carcer, B., 1991. Electrochemical wastewater treatment using high overvoltage anodes. Part I: Physical and electrochemical properties of SnO_2 anodes. *Journal of Applied Electrochemistry* 21, 14–20. https://doi.org/10.1007/BF01103823

138. Kumar, A., Prasad, B. and Mishra, I.M., 2007. Process parametric study for ethene carboxylic acid removal onto powder activated carbon using Box-Behnken design. *Chemical Engineering and Technology: Industrial Chemistry*-Plant Equipment-Process Engineering-Biotechnology 30, 932-937. https://doi.org/10.1002/ceat.200700084

139. Kumar, N., Srivastava, V.C., 2018. Simple Synthesis of Large Graphene Oxide Sheets via Electrochemical Method Coupled with Oxidation Process. *ACS Omega 3*, 10233–10242. https://doi.org/10.1021/acsomega.8b01283

140. Lacasa, E., Llanos, J., Cañizares, P., Rodrigo, M.A., 2012. Electrochemical denitrification with chlorides using DSA and BDD anodes. *Chemical Engineering Journal* 184, 66–71. https://doi.org/10.1016/j.cej.2011.12.090

141. Lagopati, N., Tsilibary, E.P., Falaras, P., Papazafiri, P., Pavlatou, E.A., Kotsopoulou, E. and Kitsiou, P., 2014. Effect of nanostructured TiO_2 crystal phase on photoinduced apoptosis of breast cancer epithelial cells. *International Journal of Nanomedicine* 9, 3219. doi: 10.2147/IJN.S62972

142. Lakshmi, D., Whitcombe, M.J., Davis, F., Sharma, P.S., Prasad, B.B., 2011. Electrochemical Detection of Uric Acid in Mixed and Clinical Samples: A Review. *Electroanalysis* 23, 305–320. https://doi.org/10.1002/elan.201000525.

143. Langergraber, G., Muellegger, E., 2005. Ecological Sanitation—a way to solve global sanitation problems? *Environment International* 31, 433–444. https://doi.org/10.1016/j.envint.2004.08.006

144. Lee, K.M., Lai, C.W., Ngai, K.S., Juan, J.C., 2016. Recent developments of zinc oxide based photocatalyst in water treatment technology: A review. *Water Research* 88, 428–448. https://doi.org/10.1016/j.watres.2015.09.045

145. Lee, Y., Shin, H.-Y., Chun, S.H., Lee, J., Park, W.J., Baik, J.M., Yoon, S., Kim, M.H., 2012. Highly Single-Crystalline $Ir_xRu_{1-x}O_2$ Mixed Metal Oxide Nanowires. *The Journal of Physical Chemistry C* 116, 16300–16304. https://doi.org/10.1021/jp3048532

146. Leng, W.H., Zhu, W.C., Ni, J., Zhang, Z., Zhang, J.Q., Cao, C.N., 2006. Photoelectrocatalytic destruction of organics using TiO_2 as photoanode with simultaneous production of H_2O_2 at the cathode. *Applied Catalysis A: General* 300, 24–35. https://doi.org/10.1016/j.apcata.2005.10.053

147. Lester, Y., Ferrer, I., Thurman, E.M., Linden, K.G., 2014. Demonstrating sucralose as a monitor of full-scale UV/AOP treatment of trace organic compounds. *Journal of Hazardous Materials* 280, 104–110. https://doi.org/10.1016/j.jhazmat.2014.07.009.

148. Levenspiel, O., 1999. Chemical reaction engineering. Industrial and Engineering Chemistry research 38, 4140-4143.

149. Li, G., Wang, Y.-H., Chen, Q.-Y., 2013. Influence of fluoride-doped tin oxide interlayer on Ni–Sb–SnO_2/Ti electrodes. *Journal of Solid State Electrochemistry* 17, 1303–1309. https://doi.org/10.1007/s10008-013-1997-3

150. Li, H., Yu, Q., Yang, B., Li, Z., Lei, L., 2015. Electro-catalytic oxidation of artificial human urine by using BDD and IrO_2 electrodes. *Journal of Electroanalytical Chemistry* 738, 14–19. https://doi.org/10.1016/j.jelechem.2014.11.018.

151. Li, P., Zhao, G., Li, M., Cao, T., Cui, X., Li, D., 2011. Design and high efficient photoelectric-synergistic catalytic oxidation activity of 2D macroporous SnO_2/1DTiO_2 nanotubes. *Applied Catalysis B: Environmental.* https://doi.org/10.1016/j.apcatb.2011.11.010

152. Li, S., Wang, F., Xu, M., Wang, Y., Fang, W., Hu, Y., 2013. Fabrication and characteristics of a nanostructure PbO_2 anode and its application for degradation of phenol. *Journal of The Electrochemical Society* 160, 44-48. DOI: 10.1149/2.082304jes

153. Li, X.Z., Li, F.B., Fan, C.M., Sun, Y.P., 2002. Photoelectrocatalytic degradation of humic acid in aqueous solution using a Ti/TiO_2 mesh photoelectrode. *Water Research* 36, 2215–2224. https://doi.org/10.1016/S0043-1354(01)00440-7

154. Li, X., Zhao, B., Wang, P., 2007. Degradation of 2,4-dichlorophenol in aqueous solution by a hybrid oxidation process. *Journal of Hazardous Materials* 147, 281–287. https://doi.org/10.1016/j.jhazmat.2006.12.077

155. Li, X., Cui, Y., Feng, Y., Xie, Z., Gu, J.-D., 2005. Reaction pathways and mechanisms of the electrochemical degradation of phenol on different electrodes. *Water Research* 39, 1972–1981. https://doi.org/10.1016/j.watres.2005.02.021

156. Lin, H., Niu, J., Xu, J., Li, Y., Pan, Y., 2013. Electrochemical mineralization of sulfamethoxazole by Ti/SnO_2-Sb/Ce-PbO_2 anode: Kinetics, reaction pathways, and energy cost evolution. *Electrochimica Acta* 97, 167–174. https://doi.org/10.1016/j.electacta.2013.03.019

157. Liu, B., Wang, C., Chen, Y., Ma, B., 2019. Electrochemical behavior and corrosion mechanism of Ti/IrO_2-RuO_2 anodes in sulphuric acid solution. *Journal of Electroanalytical Chemistry* 837, 175–183. https://doi.org/10.1016/j.jelechem.2019.02.039

158. Liu, X., Chen, M., Bian, Z., Liu, C., 2008. Studies on urine treatment by biological purification using Azolla and UV photocatalytic oxidation. *Advances in Space Research* 41, 783–786. https://doi.org/10.1016/j.asr.2007.10.009

159. Liu, X., Chen, N., Han, B., Xiao, X., Chen, G., Djerdj, I. and Wang, Y., 2015. Nanoparticle cluster gas sensor: Pt activated SnO_2 nanoparticles for NH_3 detection with ultrahigh sensitivity. *Nanoscale* 7, 14872-14880. DOI: 10.1039/c5nr03585f.

160. Liu, Y., Liu, H., Ma, J., Li, J., 2011. Investigation on electrochemical properties of cerium doped lead dioxide anode and application for the elimination of nitrophenol. *Electrochimica Acta* 56, 1352–1360. https://doi.org/10.1016/j.electacta.2010.10.091

161. Liu, Y., Liu, H., Ma, J., Li, J., 2012. Preparation and electrochemical properties of Ce–Ru–SnO_2 ternary oxide anode and electrochemical oxidation of nitrophenols. *Journal of Hazardous Materials* 213–214, 222–229. https://doi.org/10.1016/j.jhazmat.2012.01.090

162. Liu, Z., Wang, F., Li, Y., Xu, T., Zhu, S., 2011. Continuous electrochemical oxidation of methyl orange wastewater using a three-dimensional electrode reactor. *Journal of Environmental Sciences* 23, S70–S73. https://doi.org/10.1016/S1001-0742(11)61081-4.

163. Lobato, J., Canizares, P., Rodrigo, M., Saez, C., Linares, J., 2006. A comparison of hydrogen cloud explosion models and the study of the vulnerability of the damage caused by an explosion of H2H2. *International Journal of Hydrogen Energy* 31, 1780–1790. https://doi.org/10.1016/j.ijhydene.2006.01.006

164. Lu, S.-J., Luo, J.-Y., Ji, S.-B., Li, N.-X., Li, H., Li, W.-S., 2014. Photoelectrocatalytic oxidation of uric acid on novel ruthenium(II) polypyridyl complex modified ZnO electrode for photo-stimulated fuel cells. *Electrochimica Acta* 136, 130–137. https://doi.org/10.1016/j.electacta.2014.05.061.

165. Lubas, M., Jasinski, J.J., Sitarz, M., Kurpaska, L., Podsiad, P., Jasinski, J., 2014. Raman spectroscopy of TiO_2 thin films formed by hybrid treatment for biomedical applications. *Spectrochimica Acta Part A: Molecular and Biomolecular Spectroscopy* 133, 867–871. https://doi.org/10.1016/j.saa.2014.05.045
166. Lüthi, C., McConville, J., Norström, A., Panesar, A., Ingle, R., Saywell, D., Schütze, T., 2010. Rethinking Sustainable Sanitation for the Urban Domain. *Proceedings of the Water Environment Federation* 2010, 449–465. https://doi.org/10.2175/193864710798285363
167. Macak, J.M., Gong, B.G., Hueppe, M., Schmuki, P., 2007. Filling of TiO_2 Nanotubes by Self-Doping and Electrodeposition. *Advanced Materials* 19, 3027–3031. https://doi.org/10.1002/adma.200602549
168. Maddikeri, G.L., Pandit, A.B., Gogate, P.R., 2013. Ultrasound-assisted interesterification of waste cooking oil and methyl acetate for biodiesel and triacetin production. Fuel Processing Technology 116, 241–249. https://doi.org/10.1016/j.fuproc.2013.07.004
169. Majorin, F., Torondel, B., Routray, P., Rout, M., Clasen, T., 2017. Identifying Potential Sources of Exposure Along the Child Feces Management Pathway: A Cross-Sectional Study Among Urban Slums in Odisha, India. *The American Journal of Tropical Medicine and Hygiene* 97, 861–869. https://doi.org/10.4269/ajtmh.16-0688
170. Makoś, P., Przyjazny, A., Boczkaj, G., 2019. Methods of assaying volatile oxygenated organic compounds in effluent samples by gas chromatography—A review. *Journal of Chromatography A* 1592, 143–160. https://doi.org/10.1016/j.chroma.2019.01.045
171. Makgae, M.E., Theron, C.C., Przybylowicz, W.J., Crouch, A.M., 2005. Preparation and surface characterization of $Ti/SnO_2–RuO_2–IrO_2$ thin films as electrode material for the oxidation of phenol. *Materials Chemistry and Physics* 92, 559–564. https://doi.org/10.1016/j.matchemphys.2005.02.022
172. Malato, S., Fernández-Ibáñez, P., Maldonado, M.I., Blanco, J., Gernjak, W., 2009. Decontamination and disinfection of water by solar photocatalysis: recent overview and trends. *Catalysis Today* 147, 1–59. https://doi.org/10.1016/j.cattod.2009.06.018
173. Malpass, G.R.P., Miwa, D.W., Machado, S.A.S., Olivi, P., Motheo, A.J., 2006. Oxidation of the pesticide atrazine at DSA® electrodes. *Journal of Hazardous Materials* 137, 565–572. https://doi.org/10.1016/j.jhazmat.2006.02.045

174. Martínez-Huitle, C.A., Andrade, L.S., 2011. Electrocatalysis in wastewater treatment: recent mechanism advances. *Química Nova* 34, 850–858. https://doi.org/10.1590/S0100-40422011000500021

175. Martínez-Huitle, C.A., Brillas, E., 2009. Decontamination of wastewaters containing synthetic organic dyes by electrochemical methods: A general review. *Applied Catalysis B: Environmental* 87, 105–145. https://doi.org/10.1016/j.apcatb.2008.09.017

176. Martínez-Huitle, C.A., Rodrigo, M.A., Sirés, I., Scialdone, O., 2015. Single and Coupled Electrochemical Processes and Reactors for the Abatement of Organic Water Pollutants: A Critical Review. *Chemical Reviews* 115, 13362–13407. https://doi.org/10.1021/acs.chemrev.5b00361

177. Martinez-Huitle, C.A., and Ferro, S., 2006. Electrochemical oxidation of organic pollutants for the wastewater treatment: direct and indirect processes. *Chemical Society Reviews* 35, 1324-1340. DOI: 10.1039/b517632h.

178. Meaney, K.L., Omanovic, S., 2007. $Sn_{0.86}$–$Sb_{0.03}$–$Mn_{0.10}$–$Pt_{0.01}$-oxide/Ti anode for the electro-oxidation of aqueous organic wastes. *Materials Chemistry and Physics* 105, 143–147. https://doi.org/10.1016/j.matchemphys.2007.04.046

179. Menon, S.H., Sadhik A, M., 2015. Design and Development of Packed Bed Electrochemical Reactors (PBER's) Using Scrap Lead Dioxide as Novel Electrodes. *Journal of Chemical Engineering and Process Technology* 06. https://doi.org/10.4172/2157-7048.1000253

180. Mohabbati-Kalejahi, E., Azimirad, V., Bahrami, M., Ganbari, A., 2012. A review of creatinine measurement techniques. *Talanta* 97, 1–8. https://doi.org/10.1016/j.talanta.2012.04.005

181. Mohapatra, G., 2019. Projected Behavioural Change in Swachh Bharat Mission: A Public Policy Perspective. *Indian Journal of Public Administration* 65, 451–474. https://doi.org/10.1177/0019556119863856

182. Molino-Lova, R., Prisco, D., Pasquini, G., Vannetti, F., Paperini, A., Zipoli, R., Luisi, M.L.E., Cecchi, F., Macchi, C., 2013. Higher uric acid levels are associated with better functional recovery in elderly patients receiving cardiac rehabilitation. *Nutrition, Metabolism and Cardiovascular Diseases* 23, 1210–1215. https://doi.org/10.1016/j.numecd.2013.04.009

183. Mondal, B., Srivastava, V.C., Kushwaha, J.P., Bhatnagar, R., Singh, S., Mall, I.D., 2013. Parametric and multiple response optimization for the electrochemical treatment of textile

printing dye-bath effluent. *Separation and Purification Technology* 109, 135–143. https://doi.org/10.1016/j.seppur.2013.02.026

184. Moreira, F.C., Boaventura, R.A.R., Brillas, E., Vilar, V.J.P., 2017. Electrochemical advanced oxidation processes: A review on their application to synthetic and real wastewaters. *Applied Catalysis B: Environmental* 202, 217–261. https://doi.org/10.1016/j.apcatb.2016.08.037.
185. Msindo, Z.S., Sibanda, V., Potgieter, J.H., 2010. Electrochemical and physical characterization of lead-based anodes in comparison to Ti–(70%) IrO_2/(30%) Ta_2O_5 dimensionally stable anodes for use in copper electrowinning. *Journal of Applied Electrochemistry* 40, 691–699. https://doi.org/10.1007/s10800-009-0044-7.
186. Mudila, H., Prasher, P., Rana, S., Khati, B., Zaidi, M.G.H., 2018. Electrochemical oxidation-reduction and determination of urea at enzyme-free PPY-GO electrode. *Carbon letters* 26, 88–94. https://doi.org/10.5714/CL.2018.26.088
187. Naz, A., Arun, S., Narvi, S.S., Alam, M.S., Singh, A., Bhartiya, P., Dutta, P.K., 2018. Cu(II)-carboxymethyl chitosan-silane schiff base complex grafted on nano-silica: Structural evolution, antibacterial performance, and dye degradation ability. *International Journal of Biological Macromolecules* 110, 215–226. https://doi.org/10.1016/j.ijbiomac.2017.11.112
188. Nidheesh, P.V., Gandhimathi, R., 2014. Removal of Rhodamine B from aqueous solution using graphite–graphite electro-Fenton system. *Desalination and Water Treatment* 52, 1872–1877. https://doi.org/10.1080/19443994.2013.790321
189. Neodo, S., Rosestolato, D., Ferro, S., De Battisti, A., 2012. On the electrolysis of dilute chloride solutions: Influence of the electrode material on Faradaic efficiency for active chlorine, chlorate, and perchlorate. *Electrochimica Acta* 80, 282–291. https://doi.org/10.1016/j.electacta.2012.07.017.
190. Neto, A. S., Andrade, A.R.D., 2009. Electrochemical degradation of glyphosate formulations at DSA® anodes in chloride medium: an AOX formation study. *Journal of Applied Electrochemistry* 39, 1863–1870. https://doi.org/10.1007/s10800-009-9890-6
191. Neumann-Spallart, M., 2007. Aspects of Photocatalysis on Semiconductors: Photo<I>electro</I>catalysis. *CHIMIA International Journal for Chemistry* 61, 806–809. https://doi.org/10.2533/chimia.2007.806.

192. Niu, J., Lin, H., Xu, J., Wu, H., Li, Y., 2012. Electrochemical Mineralization of Perfluorocarboxylic Acids (PFCAs) by Ce-Doped Modified Porous Nanocrystalline PbO_2 Film Electrode. *Environmental Science and Technology* 46, 10191–10198. https://doi.org/10.1021/es302148z

193. Niu, J., Maharana, D., Xu, J., Chai, Z., Bao, Y., 2013. High activity of Ti/SnO_2-Sb electrode in the electrochemical degradation of 2,4-dichlorophenol in aqueous solution. *Journal of Environmental Sciences* 25, 1424–1430. https://doi.org/10.1016/S1001-0742(12)60103-X.

194. Örmeci, B., Ishida, G.A. and Linden, K.G., 2001. Impact of chlorine and monochloramine on ultraviolet light disinfection. In First IUVA International UV Congress, Washington, DC, USA.

195. Örmeci, B., Linden, K.G., 2002. Comparison of UV and chlorine inactivation of particle and non-particle associated coliform. *Water Science and Technology: Water Supply* 2, 403–410. https://doi.org/10.2166/ws.2002.0197

196. Oturan, M.A., 2014. Electrochemical advanced oxidation technologies for the removal of organic pollutants from water. *Environmental Science and Pollution Research* 21, 8333–8335. https://doi.org/10.1007/s11356-014-2841-8

197. Özcan, A., Şahin, Y., 2010. Preparation of selective and sensitive electrochemically treated pencil graphite electrodes for the determination of uric acid in urine and blood serum. Biosensors and Bioelectronics 25, 2497–2502. https://doi.org/10.1016/j.bios.2010.04.020

198. Özer, A., Gürbüz, G., Çalimli, A., Körbahti, B.K., 2009. Biosorption of copper(II) ions on Enteromorpha prolifera: Application of response surface methodology (RSM). Chemical Engineering Journal 146, 377–387. https://doi.org/10.1016/j.cej.2008.06.041

199. Ozer, R.R., Ferry, J.L., 2001. Investigation of the Photocatalytic Activity of TiO_2 −Polyoxometalate Systems. *Environmental Science and Technology* 35, 3242–3246. https://doi.org/10.1021/es0106568

200. Özgen, S., Yildiz, A., 2010. Application of Box–Behnken design to modeling the effect of smectite content on swelling to hydrocyclone processing of bentonites with various geologic properties. *Clays and Clay Minerals* 58, 431–448. https://doi.org/10.1346/CCMN.2010.0580312

201. Pan, K., Tian, M., Jiang, Z.-H., Kjartanson, B., Chen, A., 2012. Electrochemical oxidation of lignin at lead dioxide nanoparticles photoelectrodeposited on TiO_2 nanotube arrays. *Electrochimica Acta* 60, 147–153. https://doi.org/10.1016/j.electacta.2011.11.025
202. Panizza, M., Cerisola, G., 2008. Removal of color and COD from wastewater containing acid blue 22 by electrochemical oxidation. *Journal of Hazardous Materials* 153, 83–88. https://doi.org/10.1016/j.jhazmat.2007.08.023
203. Panizza, M., Martinez-Huitle, C.A., 2013. Role of electrode materials for the anodic oxidation of real landfill leachate – Comparison between Ti–Ru–Sn ternary oxide, PbO_2, and boron-doped diamond anode. *Chemosphere* 90, 1455–1460. https://doi.org/10.1016/j.chemosphere.2012.09.006.
204. Panizza, M., Delucchi, M., Sirés, I., 2010. Electrochemical process for the treatment of landfill leachate. *Journal of Applied Electrochemistry* 40, 1721–1727. https://doi.org/10.1007/s10800-010-0109-7.
205. Pareek, V., Chong, S., Tadé, M., Adesina, A.A., 2008. Light intensity distribution in heterogeneous photocatalytic reactors. *Asia-Pacific Journal of Chemical Engineering* 3, 171–201. https://doi.org/10.1002/apj.129
206. Park, H., Bak, A., Ahn, Y.Y., Choi, J., Hoffmann, M.R., 2012. Photoelectrochemical performance of multi-layered BiOx–TiO_2/Ti electrodes for degradation of phenol and production of molecular hydrogen in water. *Journal of Hazardous Materials* 211–212, 47–54. https://doi.org/10.1016/j.jhazmat.2011.05.009
207. Park, H., Choo, K.-H., Park, H.-S., Choi, J., Hoffmann, M.R., 2013. Electrochemical oxidation and microfiltration of municipal wastewater with simultaneous hydrogen production: Influence of organic and particulate matter. *Chemical Engineering Journal* 215–216, 802–810. https://doi.org/10.1016/j.cej.2012.11.075
208. Paschoal, F.M.M., Anderson, M.A., Zanoni, M.V.B., 2009. Simultaneous removal of chromium and leather dye from simulated tannery effluent by photoelectrochemistry. *Journal of Hazardous Materials* 166, 531–537. https://doi.org/10.1016/j.jhazmat.2008.11.058
209. Pavlovic, Z., Ranjan, C., van Gastel, M., Schlögl, R., 2017. The active site for the water oxidizing anodic iridium oxide probed through in situ Raman spectroscopy. *Chemical Communications* 53, 12414–12417. https://doi.org/10.1039/C7CC05669A

210. Pelegrini, R., Peralta-Zamora, P., de Andrade, A.R., Reyes, J., Durán, N., 1999. Electrochemically assisted photocatalytic degradation of reactive dyes. *Applied Catalysis B: Environmental* 22, 83–90. https://doi.org/10.1016/S0926-3373(99)00037-5

211. Philippidis, N., Nikolakaki, E., Sotiropoulos, S., Poulios, I., 2010. Photoelectrocatalytic inactivation of E. coli XL-1 blue colonies in water. *Journal of Chemical Technology and Biotechnology* 85, 1054–1060. https://doi.org/10.1002/jctb.2394

212. Piasek Z, Urbanski T (1962) The infra-red absorption spectrum and structure of urea, B Pol Acad Sci-Tech X: 113-120

213. Pillai, I.M.S., Gupta, A.K., Tiwari, M.K., 2015. Multivariate optimization for electrochemical oxidation of methyl orange: Pathway identification and toxicity analysis. *Journal of Environmental Science and Health, Part A* 50, 301–310. https://doi.org/10.1080/10934529.2015.981119

214. Pinhedo, L., Pelegrini, R., Bertazzoli, R., Motheo, A.J., 2005. Photoelectrochemical degradation of humic acid on a $(TiO_2)_{0.7}(RuO_2)_{0.3}$ dimensionally stable anode. *Applied Catalysis B: Environmental* 57, 75–81. https://doi.org/10.1016/j.apcatb.2004.10.006

215. Polonský, J., Petrushina, I.M., Christensen, E., Bouzek, K., Prag, C.B., Andersen, J.E.T., Bjerrum, N.J., 2012. Tantalum carbide as a novel support material for anode electrocatalysts in polymer electrolyte membrane water electrolyzers. *International Journal of Hydrogen Energy* 37, 2173–2181. https://doi.org/10.1016/j.ijhydene.2011.11.035

216. Popa, E., Kubota, Y., Tryk, D.A., Fujishima, A., 2000. Selective Voltammetric and Amperometric Detection of Uric Acid with Oxidized Diamond Film Electrodes. *Analytical Chemistry* 72, 1724–1727. https://doi.org/10.1021/ac990862m

217. Pundir, C.S., Yadav, S., Kumar, A., 2013. Creatinine sensors. *TrAC Trends in Analytical Chemistry* 50, 42–52. https://doi.org/10.1016/j.trac.2013.04.013

218. Qin, X., Zhao, Y., Li, J., Chen, G., 2019. The effect of Ir content on the stability of Ti/IrO_2-SnO_2 -Sb_2O_5 electrodes for O_2 evolution. *The Canadian Journal of Chemical Engineering* 97, 743–754. https://doi.org/10.1002/cjce.23337

219. Radjenovic, J., Bagastyo, A., Rabaey, K., Batstone, D., Gernjak, W., Mu, Y., Rozendal, R.A., Escher, B., Poussade, Y. and Keller, J., 2012. Electrochemical Treatment of Problematic Water Recycle Waste Streams. *Urban Water Security Research Alliance*.

220. Radomska, A., Bodenszac, E., Głąb, S., Koncki, R., 2004. Creatinine biosensor based on ammonium ion-selective electrode and its application in flow-injection analysis. *Talanta* 64, 603–608. https://doi.org/10.1016/j.talanta.2004.03.033

221. Raghu, S., Lee, C.W., Chellammal, S., Palanichamy, S., Basha, C.A., 2009. Evaluation of electrochemical oxidation techniques for degradation of dye effluents—A comparative approach. *Journal of Hazardous Materials* 171, 748–754. https://doi.org/10.1016/j.jhazmat.2009.06.063

222. Rajasulochana, P., Preethy, V., 2016. Comparison on the efficiency of various techniques in the treatment of waste and sewage water – A comprehensive review. *Resource-Efficient Technologies* 2, 175–184. https://doi.org/10.1016/j.reffit.2016.09.004

223. Rajkumar, D., Kim, J., 2006. Oxidation of various reactive dyes with in situ electro-generated active chlorine for textile dyeing industry wastewater treatment. *Journal of Hazardous Materials* 136, 203–212. https://doi.org/10.1016/j.jhazmat.2005.11.096

224. Rajkumar, D., Song, B.J., Kim, J.G., 2007. Electrochemical degradation of Reactive Blue 19 in chloride medium for the treatment of textile dyeing wastewater with the identification of intermediate compounds. *Dyes and Pigments* 72, 1–7. https://doi.org/10.1016/j.dyepig.2005.07.015

225. Rajkumar, K., Muthukumar, M., 2012. Optimization of the electro-oxidation process for the treatment of Reactive Orange 107 using response surface methodology. *Environmental Science and Pollution Research* 19, 148–160. https://doi.org/10.1007/s11356-011-0532-2

226. Raju, T., Basha, C.A., 2005. Electrochemical cell design and development for mediated electrochemical oxidation-Ce(III)/Ce(IV)system. *Chemical Engineering Journal* 114, 55–65. https://doi.org/10.1016/j.cej.2005.09.004

227. Ranade, S.S., Thiagarajan, P., 2017. Selection of design for response surface. IOP Conference Series: Materials Science and Engineering 263, 022043. https://doi.org/10.1088/1757-899X/263/2/022043

228. Rao, S. A. N., Venkatarangaiah, V.T., Nagarajappa, G.B., Nataraj, S.H., Krishnegowda, P.M., 2017. Enhancement in the photo-electrocatalytic activity of SnO_2 -Sb_2O_4 mixed metal oxide anode by nano-WO_3 modification: Application to trypan blue dye degradation. Journal of Environmental Chemical Engineering 5, 4969–4979. https://doi.org/10.1016/j.jece.2017.09.033

229. Raut, A.S., Cunningham, G.B., Parker, C.B., Klem, E.J.D., Stoner, B.R., Deshusses, M.A., Glass, J.T., 2013. Electrochemical Disinfection of Human Urine for Water-Free and Additive-Free Toilets Using Boron-Doped Diamond Electrodes. ECS Transactions 53, 1–11. https://doi.org/10.1149/05317.0001ecst

230. Raut-Jadhav, S., Saharan, V.K., Pinjari, D.V., Saini, D.R., Sonawane, S.H., Pandit, A.B., 2013. Intensification of degradation of imidacloprid in aqueous solutions by the combination of hydrodynamic cavitation with various advanced oxidation processes (AOPs). *Journal of Environmental Chemical Engineering* 1, 850–857. https://doi.org/10.1016/j.jece.2013.07.029

231. Raut-Jadhav, S., Badve, M.P., Pinjari, D.V., Saini, D.R., Sonawane, S.H., Pandit, A.B., 2016. Treatment of the pesticide industry effluent using hydrodynamic cavitation and its combination with process intensifying additives (H_2O_2 and ozone). *Chemical Engineering Journal* 295, 326–335. https://doi.org/10.1016/j.cej.2016.03.019

232. Rautanen, S. L., Viskari, E. L., 2006. In search of drivers for dry sanitation. Land Use and Water Resources Research 6, 4-1.

233. Reetz, M.T., Lopez, M., Grünert, W., Vogel, W., Mahlendorf, F., 2003. Preparation of Colloidal Nanoparticles of Mixed Metal Oxides Containing Platinum, Ruthenium, Osmium, and Iridium and Their Use as Electrocatalysts †. *The Journal of Physical Chemistry* B 107, 7414–7419. https://doi.org/10.1021/jp027785a

234. Rincón, A.G., Pulgarin, C., 2003. Photocatalytic inactivation of E. coli: effect of (continuous–intermittent) light intensity and of (suspended–fixed) TiO_2 concentration. *Applied Catalysis B: Environmental* 44, 263–284. https://doi.org/10.1016/S0926-3373(03)00076-6

235. Río, A.I.D., Fernández, J., Molina, J., Bonastre, J., Cases, F., 2010. On the behavior of doped SnO_2 anodes stabilized with platinum in the electrochemical degradation of reactive dyes. *Electrochimica Acta* 55, 7282–7289. https://doi.org/10.1016/j.electacta.2010.07.008

236. Río, A.I.D., Molina, J., Bonastre, J., Cases, F., 2009. Study of the electrochemical oxidation and reduction of C.I. Reactive Orange 4 in sodium sulfate alkaline solutions. *Journal of Hazardous Materials* 172, 187–195. https://doi.org/10.1016/j.jhazmat.2009.06.147

237. Rodríguez, F.A., Mateo, M.N., Aceves, J.M., Rivero, E.P., González, I., 2013. Electrochemical oxidation of bio-refractory dye in a simulated textile industry effluent using

DSA electrodes in a filter-press type FM01-LC reactor. *Environmental Technology* 34, 573–583. https://doi.org/10.1080/09593330.2012.706645

238. Rosales, E., Pazos, M., Sanromán, M.A., 2012. Advances in the Electro-Fenton Process for Remediation of Recalcitrant Organic Compounds. *Chemical Engineering and Technology* 35, 609–617. https://doi.org/10.1002/ceat.201100321
239. Sahu, O.P., Chaudhari, P.K., 2015. Electrochemical treatment of sugar industry wastewater: COD and color removal. *Journal of Electroanalytical Chemistry* 739, 122–129. https://doi.org/10.1016/j.jelechem.2014.11.037
240. Sangal, V.K., Kumar, V., Mishra, I.M., 2014. Process parametric optimization of a divided wall distillation column. *Chemical Engineering Communications* 201, 72–87. https://doi.org/10.1080/00986445.2012.762625
241. Särkkä, H., Bhatnagar, A., Sillanpää, M., 2015. Recent developments of electro-oxidation in water treatment — A review. *Journal of Electroanalytical Chemistry* 754, 46–56. https://doi.org/10.1016/j.jelechem.2015.06.016
242. Särkkä, H., Kuhmonen, K., Vepsäläinen, M., Pulliainen, M., Selin, J., Rantala, P., Kukkamäki, E., Sillanpää, M., 2009. Electrochemical oxidation of sulfides in paper mill wastewater by using mixed oxide anodes. *Environmental Technology* 30, 885–892. https://doi.org/10.1080/09593330902927651
243. Sautin, Y.Y., Nakagawa, T., Zharikov, S., Johnson, R.J., 2007. Adverse effects of the classic antioxidant uric acid in adipocytes: NADPH oxidase-mediated oxidative/nitrosative stress. *American Journal of Physiology-Cell Physiology* 293, C584–C596. https://doi.org/10.1152/ajpcell.00600.2006
244. Schmalz, V., Dittmar, T., Haaken, D., Worch, E., 2009. Electrochemical disinfection of biologically treated wastewater from small treatment systems by using boron-doped diamond (BDD) electrodes – Contribution for direct reuse of domestic wastewater. *Water Research* 43, 5260–5266. https://doi.org/10.1016/j.watres.2009.08.036.
245. Scialdone, O., 2009. Electrochemical oxidation of organic pollutants in the water at metal oxide electrodes: A simple theoretical model including direct and indirect oxidation processes at the anodic surface. *Electrochimica Acta* 54, 6140-6147. https://doi.org/10.1016/j.electacta.2009.05.066

246. Scialdone, O., Guarisco, C., Galia, A., 2011. Oxidation of organics in water in microfluidic electrochemical reactors: Theoretical model and experiments. *Electrochimica Act*a 58, 463–473. https://doi.org/10.1016/j.electacta.2011.09.073

247. Selcuk, H., Sene, J.J., Anderson, M.A., 2003. Photoelectrocatalytic humic acid degradation kinetics and the effect of pH applied potential and inorganic ions. *Journal of Chemical Technology and Biotechnology* 78, 979–984. https://doi.org/10.1002/jctb.895

248. Shao, L., He, P., Xue, J., Li, G., 2006. Electrolytic degradation of biorefractory organics and ammonia in leachate from bioreactor landfills. *Water Science and Technology* 53, 143–150. https://doi.org/10.2166/wst.2006.347

249. Shestakova, M., Bonete, P., Gómez, R., Sillanpää, M., Tang, W.Z., 2014. Novel Ti/Ta_2O_5-SnO_2 electrodes for water electrolysis and electrocatalytic oxidation of organics. *Electrochimica Acta* 120, 302–307. https://doi.org/10.1016/j.electacta.2013.12.113

250. Shi, H.-X., Qu, J.-H., Wang, A.-M., Ge, J.-T., 2005. Degradation of microcystins in aqueous solution with in situ electrogenerated active chlorine. *Chemosphere* 60, 326–333. https://doi.org/10.1016/j.chemosphere.2004.11.070

251. Showkat, N., 2016. Coverage of Sanitation Issues in India. SAGE Open 6, 215824401667539. https://doi.org/10.1177/2158244016675395

252. Simha, P., Ganesapillai, M., 2017. Ecological Sanitation and nutrient recovery from human urine: How far have we come? A review. *Sustainable Environment Research* 27, 107–116. https://doi.org/10.1016/j.serj.2016.12.001

253. Simka, W., Piotrowski, J., Nawrat, G., 2007. Influence of anode material on the electrochemical decomposition of urea. *Electrochimica Acta* 52, 5696–5703. https://doi.org/10.1016/j.electacta.2006.12.017

254. Simka, W., Piotrowski, J., Robak, A., Nawrat, G., 2009. Electrochemical treatment of aqueous solutions containing urea. *Journal of Applied Electrochemistry* 39, 1137–1143. https://doi.org/10.1007/s10800-008-9771-4

255. Singh, H., Chauhan, G., Jain, A.K., Sharma, S.K., 2017. The adsorptive potential of agricultural wastes for the removal of dyes from aqueous solutions. *Journal of Environmental Chemical Engineering* 5, 122–135. https://doi.org/10.1016/j.jece.2016.11.030

256. Singh, N.B., Sarkar, U., 2014. Structure, vibrational, and optical properties of a platinum cluster: a density functional theory approach. *Journal of Molecular Modeling* 20. https://doi.org/10.1007/s00894-014-2537-5

257. Singh, S., Lo, S.L., Srivastava, V.C., Hiwarkar, A.D., 2016. Comparative study of electrochemical oxidation for dye degradation: Parametric optimization and mechanism identification. *Journal of Environmental Chemical Engineering* 4, 2911–2921. https://doi.org/10.1016/j.jece.2016.05.036

258. Singh, S., Srivastava, V.C., Lo, S.L., 2016. Surface Modification or Doping of WO_3 for Enhancing the Photocatalytic Degradation of Organic Pollutant Containing Wastewaters: A Review. *Materials Science Forum* 855, 105–126. https://doi.org/10.4028/www.scientific.net/MSF.855.105

259. Sirés, I., Brillas, E., 2012. Remediation of water pollution caused by pharmaceutical residues based on electrochemical separation and degradation technologies: A review. *Environment International* 40, 212–229. https://doi.org/10.1016/j.envint.2011.07.012

260. Sirés, I., Brillas, E., Oturan, M.A., Rodrigo, M.A., Panizza, M., 2014. Electrochemical advanced oxidation processes: today and tomorrow. A review. *Environmental Science and Pollution Research* 21, 8336–8367. https://doi.org/10.1007/s11356-014-2783-1

261. Socha, A., Chrzescijanska, E., Kusmierek, E., 2005. Electrochemical and photoelectrochemical treatment of 1-aminonaphthalene-3,6-disulphonic acid. *Dyes and Pigments* 67, 71–75. https://doi.org/10.1016/j.dyepig.2004.10.012

262. Song, S., Zhang, H., Ma, X., Shao, Z., Baker, R.T. and Yi, B., 2008. Electrochemical investigation of electrocatalysts for the oxygen evolution reaction in PEM water electrolyzers. *International Journal of Hydrogen Energy* 33, 4955-4961. https://doi.org/10.1016/j.ijhydene.2008.06.039

263. Spångberg, J., Tidåker, P., Jönsson, H., 2014. Environmental impact of recycling nutrients in human excreta to agriculture compared with enhanced wastewater treatment. *Science of The Total Environment* 493, 209–219. https://doi.org/10.1016/j.scitotenv.2014.05.123

264. Srivastava, V.K., Nigam, A.K. and Misra, R.P., 2015. Diarrhea in Rural Children–Some Environmental Correlates. *Journal of Statistics and Applications* 13, 59-63.

265. Stackelberg, P.E., Gibs, J., Furlong, E.T., Meyer, M.T., Zaugg, S.D., Lippincott, R.L., 2007. The efficiency of conventional drinking-water-treatment processes in the removal of

pharmaceuticals and other organic compounds. *Science of The Total Environment* 377, 255–272. https://doi.org/10.1016/j.scitotenv.2007.01.095

266. Sulaymon, A.H. and Abbar, A.H., 2012. Scale-up of electrochemical reactors. *Electrolysis* 17, 189-202 http://dx. doi. org/10. 5772/48728

267. Suzuki, H., Araki, S., Yamamoto, H., 2015. Evaluation of advanced oxidation processes (AOP) using O_3, UV, and TiO_2 for the degradation of phenol in water. *Journal of Water Process Engineering* 7, 54–60. https://doi.org/10.1016/j.jwpe.2015.04.011

268. Szpyrkowicz, L., Kaul, S.N., Molga, E., DeFaveri, M., 2000. Comparison of the performance of a reactor equipped with a Ti/Pt and an SS anode for simultaneous cyanide removal and copper recovery. *Electrochimica Acta* 46, 381–387. https://doi.org/10.1016/S0013-4686(00)00595-8

269. Tahir, A., Visaria, A., 2017. Sewage Pollution in Water Supply in Indore. Indian *Journal of Occupational and Environmental Medicine* 21, 149-151. https://doi.org/10.4103/ijoem.IJOEM_150_17.

270. Tarley, C.R.T., Silveira, G., dos Santos, W.N.L., Matos, G.D., da Silva, E.G.P., Bezerra, M.A., Miró, M., Ferreira, S.L.C., 2009. Chemometric tools in electroanalytical chemistry: Methods for optimization based on factorial design and response surface methodology. *Microchemical Journal* 92, 58–67. https://doi.org/10.1016/j.microc.2009.02.002

271. Tarrass, F., Benjelloun, M., 2012. The effects of water shortages on health and human development. *Perspectives in Public Health* 132, 240–244. https://doi.org/10.1177/1757913910391040

272. Thakur, C., Srivastava, V.C., Mall, I.D., Hiwarkar, A.D., 2018. Mechanistic Study and Multi-Response Optimization of the Electrochemical Treatment of Petroleum Refinery Wastewater. *Clean – Soil Air Water* 46, 1700624. https://doi.org/10.1002/clen.201700624

273. Thirugnanasambandham, K., Sivakumar, V., Maran, J.P., 2015. Response surface modeling and optimization of treatment of meat industry wastewater using the electrochemical treatment method. *Journal of the Taiwan Institute of Chemical Engineers* 46, 160–167. https://doi.org/10.1016/j.jtice.2014.09.021

274. Tian, M., Bakovic, L., Chen, A., 2007. Kinetics of the electrochemical oxidation of 2-nitrophenol and 4-nitrophenol studied by in situ UV spectroscopy and chemometrics. *Electrochimica Acta* 52, 6517–6524. https://doi.org/10.1016/j.electacta.2007.04.080.

275. Tseng, W.J., Cheng, C.-C., Hsieh, J.H., 2014. Rattle-Structured Ag/TiO_2 Nanocomposite Capsules with Bactericide and Photocatalysis Activities. *Journal of the American Ceramic Society* 97, 407–412. https://doi.org/10.1111/jace.12710

276. Udert, K.M., Larsen, T.A., Gujer, W., 2006. The fate of major compounds in source-separated urine. *Water Science and Technology* 54, 413–420. https://doi.org/10.2166/wst.2006.921

277. Urbańczyk, E., Sowa, M., Simka, W., 2016. Urea removal from aqueous solutions—a review. *Journal of Applied Electrochemistry* 46, 1011–1029. https://doi.org/10.1007/s10800-016-0993-6

278. Urtiaga, A.M., Pérez, G., Ibáñez, R., Ortiz, I., 2013. Removal of pharmaceuticals from a WWTP secondary effluent by ultrafiltration/reverse osmosis followed by electrochemical oxidation of the RO concentrate. *Desalination* 331, 26–34. https://doi.org/10.1016/j.desal.2013.10.010

279. Vanlangendonck, Y., Corbisier, D., Van Lierde, A., 2005. Influence of operating conditions on the ammonia electro-oxidation rate in wastewaters from power plants (ELONITA™ technique). *Water Research* 39, 3028–3034. https://doi.org/10.1016/j.watres.2005.05.013.

280. Vazhacharickal, P.J., Predotova, M., Chandrasekharam, D., Bhowmik, S., Buerkert, A., 2013. Urban and peri-urban agricultural production along railway tracks: a case study from the Mumbai Metropolitan Region. *Journal of Agriculture and Rural Development in the Tropics and Subtropics* 114, 145-157.

281. Vedharathinam, V., Botte, G.G., 2012. Understanding the electro-catalytic oxidation mechanism of urea on nickel electrodes in alkaline medium. *Electrochimica Acta* 81, 292–300. https://doi.org/10.1016/j.electacta.2012.07.007.

282. M., V., 2019. A study on open-air defecation practices among the population above 6 years in the rural field practice area of Santhiram Medical College, Nandyal, Kurnool dist, Andhra Pradesh. *International Journal Of Community Medicine And Public Health* 6, 1901-1907. https://doi.org/10.18203/2394-6040.ijcmph20191468.

283. Walsh, F.C. and de Leon, C.A.P., 2014. Electrochemical Cell Design for Water Treatment. *Encyclopedia of Applied Electrochemistry*, 462-464. DOI: https://doi.org/10.1007/978-1-4419-6996-5_134

284. Wang, F., Li, S., Xu, M., Wang, Y., Fang, W., Yan, X., 2013. Effect of Electrochemical Modification Method on Structures and Properties of Praseodymium Doped Lead Dioxide Anodes. *Journal of The Electrochemical Society* 160, D53–D59. https://doi.org/10.1149/2.057302jes

285. Wang, H., Wang, J.L., 2008. The cooperative electrochemical oxidation of chlorophenols in anode-cathode compartments. *Journal of Hazardous Materials* 154, 44–50. https://doi.org/10.1016/j.jhazmat.2007.09.102

286. Wang, H., Sun, D.-Z., Bian, Z.-Y., 2010. Degradation mechanism of diethyl phthalate with electrogenerated hydroxyl radical on a Pd/C gas-diffusion electrode. *Journal of Hazardous Materials* 180, 710–715. https://doi.org/10.1016/j.jhazmat.2010.04.095

287. Wang, N., Li, D., Yu, L., Yu, X., Sun, T., 2015. Preparation of RuO_2/Nano-Graphite Cathode for Electrocatalytic Degradation of Phenol. *International Journal of Electrochemical Science* 10, 9824-9836.

288. Wang, N., Li, X., Wang, Y., Quan, X., Chen, G., 2009. Evaluation of bias potential enhanced photocatalytic degradation of 4-chlorophenol with TiO_2 nanotube fabricated by anodic oxidation method. *Chemical Engineering Journal* 146, 30–35. https://doi.org/10.1016/j.cej.2008.05.025

289. Wang, Q., Jin, T., Hu, Z., Zhou, L., Zhou, M., 2013. TiO_2-NTs/SnO_2-Sb anode for efficient electrocatalytic degradation of organic pollutants: Effect of TiO_2-NTs architecture. *Separation and Purification Technology* 102, 180–186. https://doi.org/10.1016/j.seppur.2012.10.006

290. Wang, W.-Y., Yang, M.-L., Ku, Y., 2010. Photoelectrocatalytic decomposition of dye in aqueous solution using Nafion as an electrolyte. *Chemical Engineering Journal* 165, 273–280. https://doi.org/10.1016/j.cej.2010.09.039.

291. Wang, Y., Hong, C.-S., 2000. TiO_2-mediated photomineralization of 2-chlorobiphenyl: the role of O_2. Water Research 34, 2791–2797. https://doi.org/10.1016/S0043-1354(00)00009-9

292. Wang, Z., Srivastava, V., Ambat, I., Safaei, Z., Sillanpää, M., 2019. Degradation of Ibuprofen by UV-LED/catalytic advanced oxidation process. *Journal of Water Process Engineering* 31, 100808. https://doi.org/10.1016/j.jwpe.2019.100808

293. Wei, Z., Liang, F., Liu, Y., Luo, W., Wang, J., Yao, W., Zhu, Y., 2017. Photoelectrocatalytic degradation of phenol-containing wastewater by TiO_2/g-C_3N_4 hybrid heterostructure thin

film. *Applied Catalysis B: Environmental* 201, 600–606. https://doi.org/10.1016/j.apcatb.2016.09.003

294. WHO/UNICEF Joint Water Supply and Sanitation Monitoring Programme, 2014. Progress on drinking water and sanitation: 2014 Update. World Health Organization.
295. World Bank. World Development Indicators: http://data.worldbank.org/indicator.2015.
296. Wu, T., Zhao, G., Lei, Y., Li, P., 2011. Distinctive Tin Dioxide Anode Fabricated by Pulse Electrodeposition: High Oxygen Evolution Potential and Efficient Electrochemical Degradation of Fluorobenzene. *The Journal of Physical Chemistry* C 115, 3888–3898. https://doi.org/10.1021/jp110149v
297. Wu, W., Huang, Z.H., Lim, T.T., 2014. The recent development of mixed metal oxide anodes for electrochemical oxidation of organic pollutants in water. *Applied Catalysis A: General* 480, 58–78. https://doi.org/10.1016/j.apcata.2014.04.035
298. Wu, X., Schuyler House, R., Peri, R., 2016. Public-private partnerships (PPPs) in water and sanitation in India: lessons from China. *Water Policy* 18, 153–176. https://doi.org/10.2166/wp.2016.010
299. Wu, X., Yang, X., Wu, D., Fu, R., 2008. Feasibility study of using carbon aerogel as particle electrodes for decoloration of RBRX dye solution in a three-dimensional electrode reactor. *Chemical Engineering Journal* 138, 47–54. https://doi.org/10.1016/j.cej.2007.05.027
300. Xie, Y.-B., Li, X.-Z., 2006. Degradation of bisphenol A in aqueous solution by H_2O_2-assisted photoelectrocatalytic oxidation. *Journal of Hazardous Materials* 138, 526–533. https://doi.org/10.1016/j.jhazmat.2006.05.074
301. Xu, H., Li, A.-P., Qi, Q., Jiang, W., Sun, Y.-M., 2012. Electrochemical degradation of phenol on the La and Ru doped Ti/SnO_2-Sb electrodes. *Korean Journal of Chemical Engineering* 29, 1178–1186. https://doi.org/10.1007/s11814-012-0014-3
302. Yadav, A., Pandey, J., 2017. Contribution of point sources and non-point sources to nutrient and carbon loads and their influence on the trophic status of the Ganga River at Varanasi, India. *Environmental Monitoring and Assessment* 189. https://doi.org/10.1007/s10661-017-6188-8.
303. Yan, W., Wang, D., Botte, G.G., 2012. Nickel and cobalt bimetallic hydroxide catalysts for urea electro-oxidation. *Electrochimica Acta* 61, 25–30. https://doi.org/10.1016/j.electacta.2011.11.044

304. Yang, L., Liu, Z., 2007. Study on light intensity in the process of photocatalytic degradation of indoor gaseous formaldehyde for saving energy. *Energy Conversion and Management* 48, 882–889. https://doi.org/10.1016/j.enconman.2006.08.023

305. Yaqub, A., Isa, M.H., Ajab, H., 2015. Electrochemical Degradation of Polycyclic Aromatic Hydrocarbons in Synthetic Solution and Produced Water Using a Ti/SnO_2-Sb_2O_5-RuO_2 Anode. *Journal of Environmental Engineering* 141, 04014074. https://doi.org/10.1061/(ASCE)EE.1943-7870.0000900

306. Yavuz, Y., Shahbazi, R., 2012. Anodic oxidation of Reactive Black 5 dye using boron-doped diamond anodes in a bipolar trickle tower reactor. *Separation and Purification Technology* 85, 130–136. https://doi.org/10.1016/j.seppur.2011.10.001

307. Zahedi, M., Jafarzadeh, K., Mirjani, M., Abbasi, H.M., 2018. The effect of anodizing time on the electrochemical behavior of the Ti/TiO_2 NTs/IrO_2-RuO_2-Ta_2O_5 anode. *Ionics* 24, 451–458. https://doi.org/10.1007/s11581-017-2210-y

308. Zanta, C.L.P.S., Michaud, P.-A., Comninellis, C., De Andrade, A.R., Boodts, Julien.F.C., 2003. Electrochemical oxidation of p -chlorophenol on SnO_2–Sb_2O_5 based anodes for wastewater treatment. *Journal of Applied Electrochemistry* 33, 1211–1215. https://doi.org/10.1023/B:JACH.0000003863.13587.b7

309. Zhang, C., Jiang, Y., Li, Y., Hu, Z., Zhou, L., Zhou, M., 2013. Three-dimensional electrochemical process for wastewater treatment: A general review. *Chemical Engineering Journal* 228, 455–467. https://doi.org/10.1016/j.cej.2013.05.033

310. Zhang, D., 2008. Reuse oriented decentralized wastewater treatment based on ecological sanitation in fast-growing agglomerations (Doctoral dissertation).

311. Zhang, R., Sun, P., Boyer, T.H., Zhao, L., Huang, C.-H., 2015. Degradation of Pharmaceuticals and Metabolite in Synthetic Human Urine by UV, UV/H_2O_2, and UV/PDS. *Environmental Science and Technology* 49, 3056–3066. https://doi.org/10.1021/es504799n

312. Zhang, W., 2003. Photoelectrocatalytic degradation of reactive brilliant orange K-R in a new continuous flow photoelectrocatalytic reactor. *Applied Catalysis A: General* 255, 221–229. https://doi.org/10.1016/S0926-860X(03)00593-3

313. Zhang, Z., Yin, J., 2014. Sensitive detection of uric acid on partially electro-reduced graphene oxide modified electrodes. *Electrochimica Acta* 119, 32–37. https://doi.org/10.1016/j.electacta.2013.12.033.

314. Zhao, G., Cui, X., Liu, M., Li, P., Zhang, Y., Cao, T., Li, H., Lei, Y., Liu, L., Li, D., 2009. Electrochemical Degradation of Refractory Pollutant Using a Novel Microstructured TiO_2 Nanotubes/Sb-Doped SnO_2 Electrode. *Environmental Science and Technology* 43, 1480–1486. https://doi.org/10.1021/es802155p

315. Zhao, H., Gao, J., Zhao, G., Fan, J., Wang, Yanbin, Wang, Yujing, 2013. Fabrication of novel SnO_2-Sb/carbon aerogel electrode for ultrasonic electrochemical oxidation of perfluorooctanoate with high catalytic efficiency. *Applied Catalysis B: Environmental* 136–137, 278–286. https://doi.org/10.1016/j.apcatb.2013.02.013

316. Zhao, X., Qu, J., Liu, H., Hu, C., 2007. Photoelectrocatalytic Degradation of Triazine-Containing Azo Dyes at γ-Bi_2MoO_6 Film Electrode under Visible Light Irradiation ($\lambda > 420$ Nm). *Environmental Science and Technology* 41, 6802–6807. https://doi.org/10.1021/es070598b

317. Zhou, M., He, J., 2008. Degradation of cationic red X-GRL by electrochemical oxidation on the modified PbO_2 electrode. *Journal of Hazardous Materials* 153, 357–363. https://doi.org/10.1016/j.jhazmat.2007.08.056

318. Zhou, M., Särkkä, H., Sillanpää, M., 2011. A comparative experimental study on methyl orange degradation by electrochemical oxidation on BDD and MMO electrodes. *Separation and Purification Technology* 78, 290–297. https://doi.org/10.1016/j.seppur.2011.02.013

319. Zhu, K., Zhang, W., Wang, H., Xiao, Z., 2008. Electro-Catalytic Degradation of Phenol Organics with SnO_2-Sb_2O_3/Ti Electrodes. *CLEAN – Soil Air Water* 36, 97–102. https://doi.org/10.1002/clen.200700037

320. Zhuo, Q., Deng, S., Yang, B., Huang, J., Yu, G., 2011. Efficient Electrochemical Oxidation of Perfluorooctanoate Using a Ti/SnO_2-Sb-Bi Anode. *Environmental Science and Technology* 45, 2973–2979. https://doi.org/10.1021/es1024542

321. Zöllig, H., Remmele, A., Fritzsche, C., Morgenroth, E., Udert, K.M., 2015. Formation of Chlorination Byproducts and Their Emission Pathways in Chlorine Mediated Electro-Oxidation of Urine on Active and Nonactive Type Anodes. *Environmental Science and Technology* 49, 11062–11069. https://doi.org/10.1021/acs.est.5b01675.

LIST OF CONTRIBUTIONS

- **Published Articles**

  - Singla, J., Verma, A., Sangal, V.K., 2017. Performance and Evaluation of Electro-Oxidation Treatment of Human Urine Metabolite Uric Acid Using Response Surface Methodology. ***Journal of The Electrochemical Society*** 164, E312–E320. https://doi.org/10.1149/2.0681712jes
  - Singla, J., Verma, A., Sangal, V.K., 2018. Parametric optimization for the treatment of human urine metabolite, creatinine using electro-oxidation. ***Journal of Electroanalytical Chemistry*** 809, 136–146. https://doi.org/10.1016/j.jelechem.2017.12.061
  - Singla, J., Sangal, V.K., Verma, A., 2019. Evaluation and optimization of the process parameters for the photo-electrochemical treatment of urea using mixed metal oxide anodes. ***Process Safety and Environmental Protection*** 130, 197–208. https://doi.org/10.1016/j.psep.2019.08.017
  - Singla, J., Sangal, V. K., Verma, A., 2019. Applications of doped mixed metal oxide anode for the electro-oxidation treatment and mineralization of urine metabolite, uric acid. ***Journal of Water Process and Engineering*** 32, 100944. https://doi.org/10.1016/j.jwpe.2019.100944
  - Singla, J., Sangal, V. K., Singh, A., Verma A., 2020. Application of mixed metal oxide anode for the electro-oxidation/disinfection of synthetic urine: Potential of harnessing molecular hydrogen generation. ***Journal of Environmental Management*** 255, 109847. https://doi.org/10.1016/j.jenvman.2019.109847

- **Conference Presentation**

  - Poster presentation on "Electrochemical advanced oxidation treatment of uric acid and creatinine present in human urine" International Conference on Advanced Oxidation Processes, AOP-2016, BITS GOA. December 17-20, 2016.
  - Oral presentation on " Application of Electro-oxidation process for the treatment of human urine metabolites" International conference on Harnessing Engineering Technology and Innovation for Sustainable Growth, HETIS 2016, Punjab University, Chandigarh.

Journal of The Electrochemical Society, **164** (12) E312-E320 (2017)
0013-4651/2017/164(12)/E312/9/$37.00 © The Electrochemical Society

Performance and Evaluation of Electro-Oxidation Treatment of Human Urine Metabolite Uric Acid Using Response Surface Methodology

Jayishnu Singla,[a] Anoop Verma,[a,z] and Vikas K. Sangal[b,z]

[a]*School of Energy and Environment, Thapar University, Patiala, Punjab, India*
[b]*Department of Chemical Engineering, Thapar University, Patiala, Punjab, India*

In this work, electrocatalytic treatment of uric acid has been performed by anodic oxidation using mixed metal oxide (MMO) anode and stainless steel as a cathode. A full factorial Box-Behnken design under response surface methodology was applied to evaluate the effect of various operating parameters such as current applied (i), pH of the solution, NaCl concentration (n) and treatment time (t) in an electrochemical cell. 92% degradation of uric acid (C_0 = 50 mg L^{-1}) was achieved with all the optimal conditions e.g. current intensity 0.3 A, pH of 2 and treatment time of 6.95 min. The main strength of the study lies in the reporting the durability of electrodes besides being cost-effective. The electrodes were durable enough to be used even after sixty cycles as confirmed through SEM/EDS and XRD. The mineralization of uric acid was confirmed through a reduction in COD and TOC along with generation of nitrite and nitrate ions. A degradation pathway for uric acid has been proposed based on the intermediates formed as identified through LC-MS analysis. Hence the attempts in the present study will open up new opportunities in the field of eco-sanitation especially in developing countries for the on-site treatment of human urine.
 [DOI: 10.1149/2.0681712jes]

Manuscript submitted June 9, 2017; revised manuscript received August 2, 2017. Published August 11, 2017.

In developing country like India, water demand for the treatment of domestic wastewater is growing exponentially high. Urine makes more than 1% volume of domestic wastewater and contains a large part of the plant nutrients and organic compounds such as urea, creatinine and uric acid.[1] Human urine is a special type of wastewater with very complex chemical composition. When it left from human body it becomes unpleasant, smelly and unstable with high biochemical oxygen demand (BOD) which makes the degradation process more complicated.[2,3] Uric acid (UA) is one of the persistent polluting components of urine wastewaters. It is an enzymatic final oxidation product of dietary purine metabolism which works as an antioxidant in human blood plasma and protects against oxidative stress.[4–6] Its high concentration in human body results in several diseases like leukemia, kidney diseases arthritis and cardiovascular diseases.[7] In addition, this effluent is extensively used in agriculture as fertilizer as it contains high nitrogen, phosphorous and potassium content.[8] At the same time, it is considered as toxic for human health and environment because of pathogen's transmission as well as the high content of nitrogen. Same time it is rebellious to many conventional and biological treatments.[9] Moreover, conventional treatment methods demand a huge amount of water as well as consume a large percentage of energy.[10] Moreover, these techniques have proven to be inefficient for the treatment of persistence and recalcitrant compounds.

Literature has consolidated the performance of advanced oxidation processes (AOPs) as promising technologies for the treatment of wide variety of bio-recalcitrant pollutants present in water/wastewater.[11–13] Studies have been reported in the literature for the treatment of human urine and its metabolites[14–16] using heterogeneous photo catalysis. However, continuous requirement of UV, as well as longer time for complete disinfection, necessitates an immediate requirement for an effective alternative technology. Electrochemical advanced oxidation processes (EAOPs), have come-up in recent years as a promising technology for degrading of a wide variety of pollutants.[17–20]

Electro-oxidation (EO) process is cost effective and eco-friendly technique[21,22] which offers better removal efficiencies as compared to other processes. The effectiveness of the process and its feasibility at a commercial level largely depend upon the innovation of new electrodes material which is capable of generating a lot of strong oxidizing agents such as hydroxyl radicals OH• and various chloro-oxidant species.[23]

Different kinds of electrodes such as boron doped diamond (BDD), dimensionally stable type electrodes (DSA), mixed metal oxides types (MMO) have been studied for the degradation of a wide variety of pollutants.[24–26] EO using BDD proved to be efficient because of its high overvoltage and oxidation potential[27,28] along with an important drawback that is a generation of toxic byproducts like chlorates and perchlorates hence require additional treatment for the removal of these toxic products. Moreover, the known high cost of conductive diamonds anodes makes there large scale industrial application unfeasible. In particular, various authors have reported that MMO anodes are one of the effective and electrochemically stable electrodes which possess high quality for chlorine evolution and presents longer service life as compared to other electrodes.[29,30] Electrochemical water splitting at MMO generate adsorbed hydroxyl radicals which further evolve towards oxygen evolution reactions and likely to cause complete degradation of organic compounds.[25] These MMO anodes have established their worth in treating a wide variety of pollutants like paper mill water,[31] reverse osmosis concentrate,[32] synthetic wastewater,[33] and landfill leachate.[34] Thus there is need to study the concept of application of using these MMO anodes for the degradation of UA.

The present study attempts to explore the use of low-cost MMO anodes for the degradation of UA by EO process. Attempts have been made to reduce the treatment time along with maintaining the durability of electrodes. Thus citing its novelty. Furthermore, the effect of operating input parameters like pH, current (i), chloride concentration and time (t) on %degradation (Y_1) and energy consumed (Y_2) were investigated. The Box-Behnken design (BBD) under response surface methodology (RSM) was used for the optimization of process parameters. Process efficiency was analyzed by different analytical techniques which include total organic carbon (TOC), chemical oxygen demand (COD) along with an investigation of mineralization end products (i.e, NO_3^-, NO_2^- and NH_4^+ ions). The formations of organic intermediates were analyzed by LC-MS. Hence, based on these intermediates generation oxidative degradation pathway for UA has been proposed in this study. Stability and durability studies have been performed by characterizing the electrodes using SEM-EDS and XRD techniques.

Materials and Methods

Chemicals.—All chemicals of analytical grade were used in the present study. UA ($C_5H_4N_4O_3$) with (99.5% purity) was purchased from Sigma- Aldrich, Missouri, U.S. Sodium chloride (NaCl), sulfuric acid (H_2SO_4) and sodium hydroxide (NaOH) were purchased from Loba Chemi Pvt. Ltd. Mumbai, India. All the solutions were prepared with high-purity water obtained from a Millipore Milli-Q system, with resistivity >18 MΩ cm^{-1} at 25°C. HPLC grade acetonitrile and formic acid were purchased from Sigma Aldrich for HPLC analysis.

[z]E-mail: anoop.kumar@thapar.edu; vksangal@gmail.com

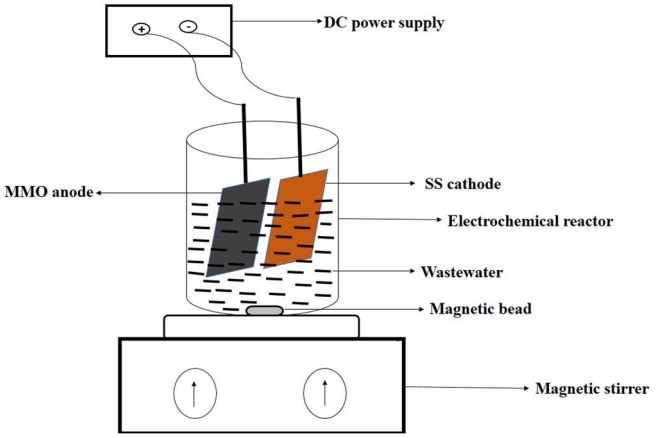

Figure 1. Schematic diagram of experimental setup used for the electrochemical treatment of Uric acid.

Sample preparation and experimental setup.—Synthetic wastewater solution was prepared by dissolving 100 mg of UA in one liter (L) double distilled water. All samples and other reagents were stored at 4°C to prevent unwanted degradation. The initial concentration of UA was selected be 50 mg/L accordingly for this study.

EO treatment UA was carried out in a single compartment electrochemical cell of working volume 500 ml under a batch operation mode is shown in Figure 1. MMO was used as anode purchased from (Exotic Elements Pvt. Ltd., Mumbai, India) having dimension 70 mm∗70 mm∗1 mm, whereas stainless steel as the cathode of the same dimension was purchased from (Bio age Pvt. Ltd., Mohali, India). These electrodes were connected parallel with 10 mm inter-electrode spacing. While performing scientific procedure current was maintained using DC (DIGITECH, Ambala, India, Model: 0–30 V, 0–2 A). A magnetic stirrer was used to stir the sample properly in a reactor at 650 rpm.

Experimental procedure.—An experimental study was carried out under galvanostatic conditions. 0.1N HCl and 0.1N NaOH were used for adjusting the pH of the solution during the experiment and NaCl was used as supporting electrolyte to improve the electrical conductivity of the solution. At fixed time intervals, 1 ml of sample volume was taken from the solution and filtered through 0.20 μm nylon filters and analyzed with double beam UV Visible spectrophotometer at λ max 290 nm. The adsorption studies were carried out under dark conditions using only MMO anode without providing current with continuous stirring. There was no significant reduction in concentration of UA. This confirmed that degradation of UA was because of EO only.

Analytical methods.—Electrochemical degradation studies were carried out by analyzing the samples using high-performance liquid chromatography (HPLC) and UV-Visible spectrophotometer (HITACHI model no. U-2800) at 290 nm wavelength. The degradation of the model compound was also confirmed by HPLC (Shimadzu, SED-20A) having communication module, CBM-20A with diode array detector, SPDM-20A, and pump, LC-20AD. The column temperature was adjusted to 25°C while sample injection volume used was 20 μl. The HPLC was carried out in a binary system with 25 mM formic acid and acetonitrile as mobile phase using C-18 column (250 mm × 4.60 mm) having a particle size of 5 μm with detection wavelength set at 290 nm for uric acid. Initially, 10% of acetonitrile was run for using linear gradient which was incremented to 100% within 40 min. Mineralization efficacy of UA was studied by the reduction in total organic carbon (TOC) and chemical oxygen demand values (COD). COD was checked with closed reflux method according to APHA standard methods.[35] TOC was analyzed with multi N/C 2100Analytik Jena TOC analyzer. The inorganic ions which include nitrate, nitrite, NH_4^+, total nitrogen formed during experimental work were determined using APHA standard methods.[36–38] The intermediates and final products formed during the EO process were detected by LC-MS. Sample analysis was conducted under an isocratic condition with a mobile phase of solvent A (50%) and solvent B (50%). Solvent A was composed of 0.1% formic acid in water solution and solvent B was 0.1%formic acid in acetonitrile. Samples were diluted to 1:1 ratio (sample: solvent) and then directly injected into the electrospray mass spectrometer at a flow rate of 200 μl/min for data analysis in the positive ion mode. The instrument used was the Q-TOF mass spectrometer from Micromass UK Ltd. The surface morphology and composition of the coatings of purchased MMO anodes were characterized using a JEOL 5900LV scanning electron microscope (SEM) along with X-ray energy dispersive spectrometry (EDS). The crystalline phases of the prepared electrodes were identified by X-ray diffraction (XRD) using a Rigaku D/Max. III.V X-ray diffractometer with Cu K_ irradiation.

Experimental design and analysis.—Response Surface Methodology (RSM) is a statistical technique which is used to optimize the effective operational parameters with reduced the number of experiments as well as to analyze the inter-parametric interaction and their effects on responses.[39] Box-Behnken design (BBD) under RSM was used for the parametric study. Several researchers in their studies have applied BBD for the optimization of various chemical and physical.[40–42]

The sequential F-test, lack of fit test and other adequacy measures are normally used for choosing the predominant model. To generate the statistical and response plots, Design-Expert software V-6.0.8 was used. To fit the experimental data and to identify the relevant model terms a second-order polynomial, Eq. 1, was used through nonlinear regression analysis. Considering all the linear terms, square terms and the linear by linear interaction terms, the quadratic response model[43,44] can be described as:

$$Y = \gamma_o + \sum_{i=1}^{4} \gamma_i Z_i + \sum_{i=1}^{4} \gamma_{ii} Z_i^2 + \sum_{i=j}^{3} \sum_{i=j+1}^{4} \gamma_{ij} Z_{ij} \quad [1]$$

Where Y is response; γ_o, γ_i, γ_{ii}, γ_{ij} are constant quadratic coefficients and Zi, the uncoded input factors. There are two responses (%degradation, Y_1 and energy consumption, Y_2) in present study. Therefore, multi-response process optimization with desirability function approach was used for the optimization of the multiple responses simultaneously. The desirability (Di) value lies between 0 and 1, representing the closeness of response to its ideal value.[45]

In multi-response optimization, all the individual desirability function are combined in order to obtain overall desirability function, Di as shown below in Eq. 2.

$$Di = (d_1 \times d_2)^{1/2} \quad [2]$$

Where d_1 is desirability of %degradation and d_2 is desirability of energy consumption.

In the present study, four operational parameters, pH, current (i), time (t) and NaCl concentration (n) with three levels coding (−1(low) and +1(high)), were followed by RSM modeling and (%degradation, Y_1 and energy consumption, Y_2) were taken as responses of the system. The energy consumption during EO treatment was calculated by following Eq. 3.

$$E = \left[\frac{V * I * T}{S_v}\right] \quad [3]$$

Where V = voltage; I = current (A); T = treatment time (h); Sv = Sample volume (m^3)

By conducting preliminary experiments for %degradation and energy consumption at various operational parameters, working ranges of parameters were decided accordingly. The center of experiments was defined by preliminary experimental runs so that RSM technique could be used with confidence for defining the range of variables. Levels of the operational parameter are shown in Table I. Table II provides experimental design matrix of experimental runs, designed using BBD.

Table I. Range of variables and coded levels of design model.

Factors	Variables	Range of actual and coded variables −1	0	+1
A	Initial pH	2	5.5	9
B	Current, i (A)	0.1	0.3	0.5
C	Time of electrolysis, t (min)	2	6	10
D	NaCl conc., (n) (g/400 ml)	0.1	0.3	0.5

Results and Discussion

Model fitting and statistical analysis with BBD.—The statistical design expert software version 6.0.8 (STAT-Ease INC., Minneapolis, US) was applied for the regression analysis of experimental data. The results of response Y_1 and Y_2 respectively for the EO treatment of UA were determined according to the design matrix are listed in Table II.

For selecting the best model, sequential F –test and other adequacy measures were exploited as shown in Table III.[46] The regression process was adopted to fit the 2nd order polynomial equation and for analyzing the statistical significance of relevant model terms. The sequential model sum of square and model summary statistic are two different test that was performed in order to check the adequacy of the model for both the responses (Y_1 and Y_2). The p value for a response (Y_1 and Y_2) were found to be <0.0001 and hence model advised was quadratic. This indicates that at least one term in regression equation had a significant correlation with the response variables.[47] The insignificant model terms in the manual regression method were evicted automatically which in turn provides the summarize results of analysis of variance (ANOVA) for each response with reduced quadratic equation and shows significant model terms.

The ANOVA results obtained from regression analysis for the %degradation and energy consumption for EO treatment of UA, with model F-value of 14.12 and 76.75 respectively, implies model is significant. The significant and highly significant model terms are dependent upon the value of ANOVA results came for both responses Y_1 and Y_2 respectively. The significant terms for response Y_1 are n, i^2, t^2, n^2 while i and t are highly significant whereas for response Y_2, the significant model terms are n, i^2, pH∗n while i, t, i∗t are shown as highly significant. The model summary statistic showed the R^2 (regression coefficient) value for both the responses were 0.933 and 0.987 respectively, implies a good correlation between observed and predicted experimental values. For the %degradation and energy consumed, the adequate precision ratio was found to be 13.813 and 35.407 respectively. An adequate precision ratio above 4 indicates that adequate model is fit and can be used for navigating the design space.[48] Second order polynomial equation of responses Y_1 (% degradation) and Y_2 (energy consumed) respectively in terms of independent coded factors for MMO anodes are summarized in (Eq. 4-5).

$$\begin{aligned}\%\,\mathrm{Deg} = {} & +87.61 - 3.09 * A + 17.31 * B + 23.71 * C \\ & + 6.86 * D - 1.05 * A^2 - 12.70 - 14.68 * C^2 - 7.06 * D^2 \\ & - 2.98 * A * B + 2.04 * A * C + 5.97 * A * D \\ & - 4.45 * B * C + 0.57 * B * D - 5.48 * C * D \end{aligned} \quad [4]$$

$$\begin{aligned}\mathrm{Energy\ consumed} = {} & \\ & + 618.75 + 33.75 * A + 561.56 * B + 438.75 * C \\ & - 97.19 * D - 41.09 * A^2 + 132.81 * B^2 + 17.03 * C^2 - 24.69 * D^2 \\ & + 7.50 * A * B + 0.00 * A * C + 108.75 * A * D + 375.00 * B * C \\ & - 21.56 * B * D - 33.75 * C * D \end{aligned} \quad [5]$$

Where A, B, C, and D are pH, current (i), time (t) and NaCl concentration (n) respectively.

Table II. Full factorial BBD matrix and their experimental results.

Run	Std	pH	i (A)	t (min)	n (g/400 ml)	% Degradation, Y_1	Energy consumed, Y_2 (kWh/m^3)
1	3	2	0.5	6	0.3	98.4	1293.75
2	17	2	0.3	2	0.3	51.04	206.25
3	19	2	0.3	10	0.3	95.05	1031.25
4	1	2	0.1	6	0.3	71.5	168.75
5	9	2	0.3	6	0.1	78.8	675
6	11	2	0.3	6	0.5	74.22	138.75
7	29	5.5	0.3	6	0.3	95.05	618.75
8	25	5.5	0.3	6	0.3	85.95	618.75
9	24	5.5	0.5	6	0.5	96.07	1200
10	14	5.5	0.5	2	0.3	61.25	431.25
11	16	5.5	0.5	10	0.3	96.7	2156.25
12	7	5.5	0.3	2	0.5	58.4	191.25
13	26	5.5	0.3	6	0.3	75.5	618.75
14	6	5.5	0.3	10	0.1	93.5	1125
15	28	5.5	0.3	6	0.3	87.5	618.75
16	13	5.5	0.1	2	0.3	9.25	56.25
17	21	5.5	0.1	6	0.1	37.2	258.75
18	8	5.5	0.3	10	0.5	97.28	956.25
19	23	5.5	0.1	6	0.5	55.1	138.75
20	5	5.5	0.3	2	0.1	32.7	225
21	27	5.5	0.3	6	0.3	94.05	618.75
22	22	5.5	0.5	6	0.1	75.89	1406.25
23	15	5.5	0.1	10	0.3	62.5	281.25
24	4	9	0.5	6	0.3	79.45	1293.75
25	10	9	0.3	6	0.1	67.23	675
26	12	9	0.3	6	0.5	86.25	573.75
27	20	9	0.3	10	0.3	93.24	1031.25
28	18	9	0.3	2	0.3	41.07	206.25
29	2	9	0.1	6	0.3	64.48	138.75

Table III. Selection of adequate model for degradation of Uric Acid.

Source	Sum of squares	DF	Mean Square	F Value	p	Remark
			Sequential model sum of squares			
Mean	1.542E + 005	1	1.542E + 005			
Linear	11022.08	4	2755.52	18.55	< 0.0001	
2FI	395.30	6	65.88	0.37	0.8859	
Quadratic	2205.12	4	551.28	8.00	0.0014	Suggested
Cubic	461.15	8	57.64	0.69	0.6968	Aliased
Residual	246.25	4	61.56	-	-	
Total	1.688E + 005	29	5821.40	-	-	
			Lack of fit tests			
Linear	3319.18	20	165.96	2.70	0.1735	
2FI	2923.87	14	208.85	3.39	0.1235	
Quadratic	718.75	10	71.88	1.17	0.4783	Suggested
Cubic	257.61	2	128.80	2.09	0.2389	Aliased
Pure Error	246.25	4	61.56			
			Model Summary statistics			
Source	Std. dev	R^2	Adj. R^2	Pre.R^2	Press	Remark
Linear	12.19	0.7556	0.7148	0.6619	4932.49	
2FI	13.27	0.7827	0.6620	0.4825	7548.36	
Quadratic	80.67	0.9338	0.8677	0.6898	4524.79	Suggested
Cubic	9.16	0.9655	0.8388	−1.5693	37480.10	Aliased

Figure 2a shows the residual points on normal probability plot and dot diagram of these residuals lie very close to a straight line signifies that the underlying assumptions of the analysis were satisfied. Figure 2b shows the relationship between the actual and predicted values of Y (% degradation). It can be seen that the residuals are in the proximity of the straight diagonal line between actual and predicted. Hence it can be concluded that the developed model is considered to be satisfactory and accurate because the residuals for the prediction of each response are minimum.[49,50]

Effect of parameters.—The 3-D response surface graphs obtained from RSM were investigated to look out the effects of various input parameters on both the responses for EO treatment of UA.

pH as parameter defines which kind of Cl^- species is predominant as well as the adsorption rate of OH• radicals. In Figure 3a for pH value 2 to 9 it can be observed that %degradation was increasing on increasing i value from 0.1 A to 0.35 A. Further increase in i values from 0.35 A to 0.5 A, a marginal increase in Y_1 was seen. Also, it can be observed that Y_1 was maximum at acidic pH and thereafter Y_1 decreases gradually with further increase in pH. Therefore it can be concluded that, at highly acidic pH, %degradation was maximum while at highly basic pH %degradation was found to be minimum.

In EO treatment both direct and indirect process is involved. In previous studies it has been reported that the adsorption rate of the OH• radicals on the anodes is high in highly acidic pH leads to the direct oxidation of compound at the anode. While in the case of highly

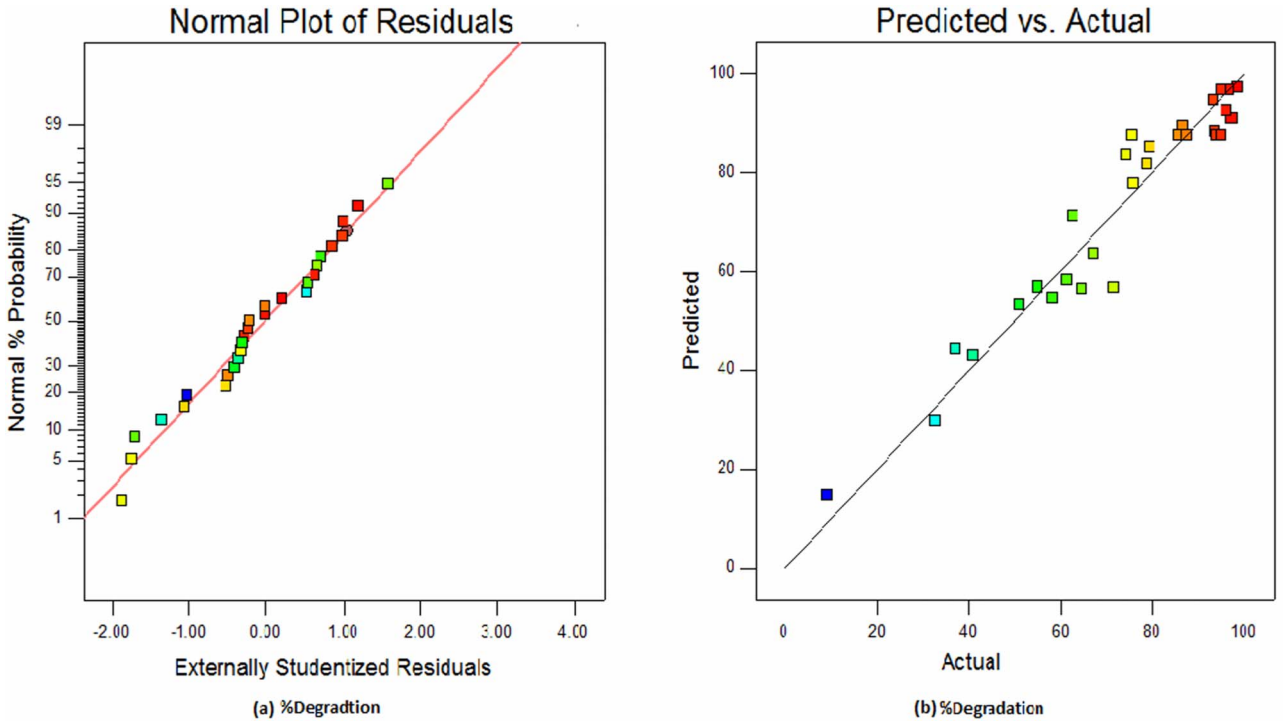

Figure 2. (a) The normal plot of Residuals for %degradation and (b) The regression plots of predicted vs actual for %degradation.

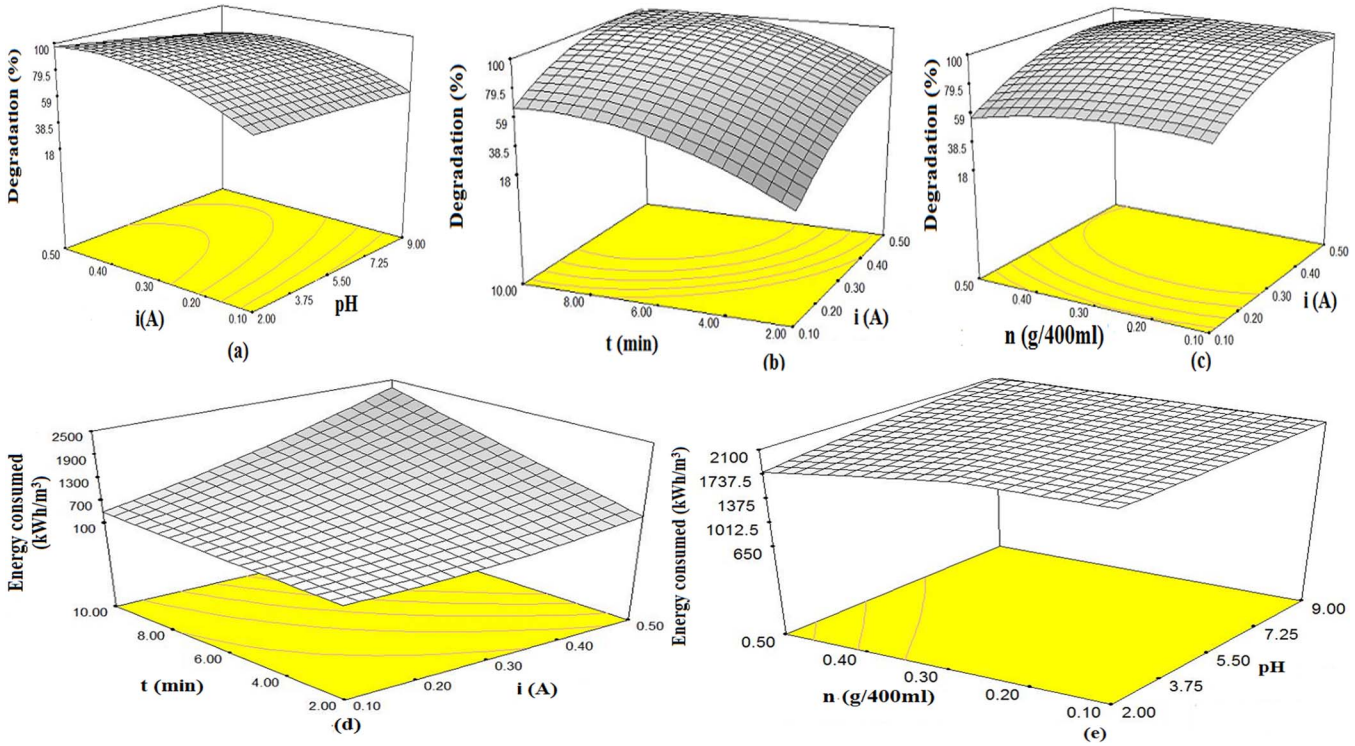

Figure 3. 3-D response surface graph for the electro-oxidation of Uric acid (a) %degradation versus pH and i (b) %degradation versus t and i. (c) %degradation versus i and n (d) energy consumed versus t and i and (e) energy consumed versus pH and n.

basic pH the adsorption rate of the OH• radicals on the anode surface is decreased leads to the transformation of OH• radicals into H_2O_2 and HO_2• (oxidants of lower potential) shown in (Eqs. 6–10)[51] which corresponds to indirect oxidation**.**

$$O_2 + 2H^+ + 2e^- \rightarrow H_2O_2 \quad [6]$$

$$2H_2O \rightarrow 2 \bullet OH + 2H^+ + 2e^- \quad [7]$$

$$2 \bullet OH \rightarrow H_2O_2 \quad [8]$$

$$\bullet OH + H_2O_2 \rightarrow HO_2 \bullet + H_2O \quad [9]$$

$$2H_2O \rightarrow O_2 + 4H^+ + 4e^- \quad [10]$$

Moreover, in addition to this in highly acidic pH generation of HOCl oxidant species in bulk was maximum which dominates over all other oxidant species like Cl_2, ClO^- etc, and leads to indirect oxidation. While in basic pH, ClO- species were generated. On increasing current these species increases and hence, enhances the % degradation. With the time ClO- species get converted to lower chloro-oxidant species like ClO_3^- and ClO_4^- in alkaline pH (Eqs. 11–17)[1,9] and hence reduces the response (Y_1).[52,53] Also on increasing *i* value beyond 0.35 A in both acidic and basic pH, side reactions takes place leads to reduction in OH• radical generation and hence reduces the degradation efficiency.[54,23] Hence on increasing pH, response Y_1 decreases for all i values.

$$2Cl^- \rightarrow Cl_2 + 2e^- \quad [11]$$

$$Cl_2 + H_2O \rightarrow HClO + Cl^- + H^+ \quad [12]$$

$$HClO \rightarrow ClO^- + H^+ \quad [13]$$

$$Cl^- + \bullet OH \rightarrow ClO^- + H^+ + e^- \quad [14]$$

$$ClO^- + \bullet OH \rightarrow ClO_2^- + H^+ + e^- \quad [15]$$

$$ClO_2^- + \bullet OH \rightarrow ClO_3^- + H^+ + e^- \quad [16]$$

$$ClO_3^- + \bullet OH \rightarrow ClO_4^- + H^+ + e^- \quad [17]$$

Figure 3b shows the effect of i and t on Y_1 (%degradation). It was seen that increasing t value up to 7 mins, Y_1 increases rapidly. But for t > 7 mins, it was found that Y_1 increases marginally. This was followed for all i and all pH values. In previous studies, it has been reported that during electrolysis passivation of electrodes occur with time in which the interaction between the contaminant and anode surface build up like an impermeable film. And this film resists the MMO dissolution and electron transfer from electrode surface and hence limits the process efficiency.[40] More than 90% of degradation was observed up to 7 mins of reaction time at highly acidic pH, however, at higher pH for complete degradation more than 10 mins is required.

Figure 3c shows the effect of n and i on %degradation (Y_1). On increasing electrolyte concentration (n) up to 0.3 g leads to higher degradation. But on further increase in (n > 0.3 g), marginal decrease in degradation efficiency was observed for all i values. Actually, the amount of electrolyte concentration defines the amount of reactive chlorine species formed. With a higher amount of chloride concentration, more reactive chlorine species would be formed leading to increases in Y_1.[55] At the same time, corrosion and fouling of the electrodes could be observed at higher electrolyte concentrations. Keeping this in consideration, the electrolyte concentration was kept at 0.3

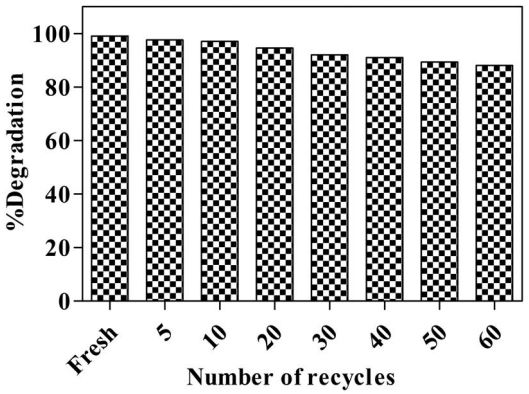

Figure 4. Plot of % degradation of uric acid vs number of recycles of MMO anode.

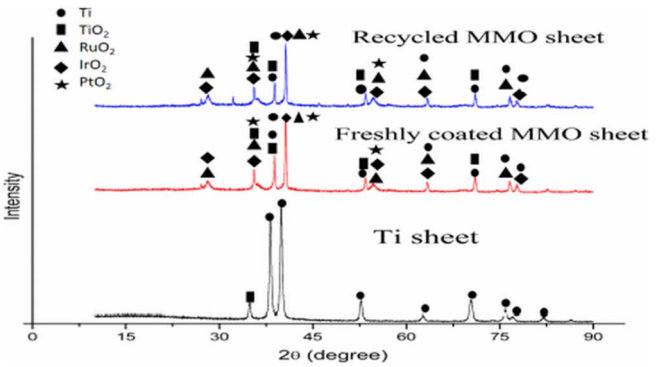

Figure 6. XRD patterns of electrodes (Ti sheet, freshly coated MMO sheet and recycled MMO sheet).

g/400 ml for the present study. Besides this, the selected MMO electrodes promote the direct oxidation which leads considerably higher efficiency along with preventing fouling of electrodes.

Energy consumption (Y_2) depends on the type of electrode varies with each of the process parameters, the current applied is a most important parameter. With an increase in i value the electrical consumption varies directly. Higher pH shows higher energy consumption even at lower i values as shown in Figure 3(d, e). NaCl concentration shows contrary effect, with higher NaCl concentration showing lower energy consumption due to ease of flow of current through the electrolyte.

Durability studies.—In electrochemical processes, the recyclability, as well as stability of electrodes, decide the practical viability of process towards its commercial applications. In this context, attempts have been made in the present study to evaluate the durability of electrodes in terms of a number of recycles and degradation efficiency of uric acid. The electrodes were successfully recycled for at-least 60 cycles without any significant loss in degradation efficiency (~10%) shown in Figure 4. Generally, the life of electrodes is largely dependent upon fouling and passivation of the electrodes due to high electrolyte concentration along with higher values of current.[56,25] The main reason for high durability of the electrodes in our present study is due to moderate electrolyte concentration and lower values of current. The stability of the electrodes after 60th cycle (180 h) was further confirmed through SEM/EDS and XRD analysis as discussed in next subsection.

Characterization of MMO anodes.—SEM and EDS were used to study the surface morphology and elemental composition of electrodes (Ti sheet, freshly coated MMO sheet and recycled MMO sheet) respectively as shown in Figure 5. The SEM image of freshly coated and recycled MMO sheet depicts almost similar surface characteristics thus indicating a uniform layer of metals even after sixty cycles. The prominent peaks of all three metals i.e. Ru, Ir and Pt along with Ti and O even in recycled MMO sheet further confirms the durability and stability of electrodes after sixty experimental runs.

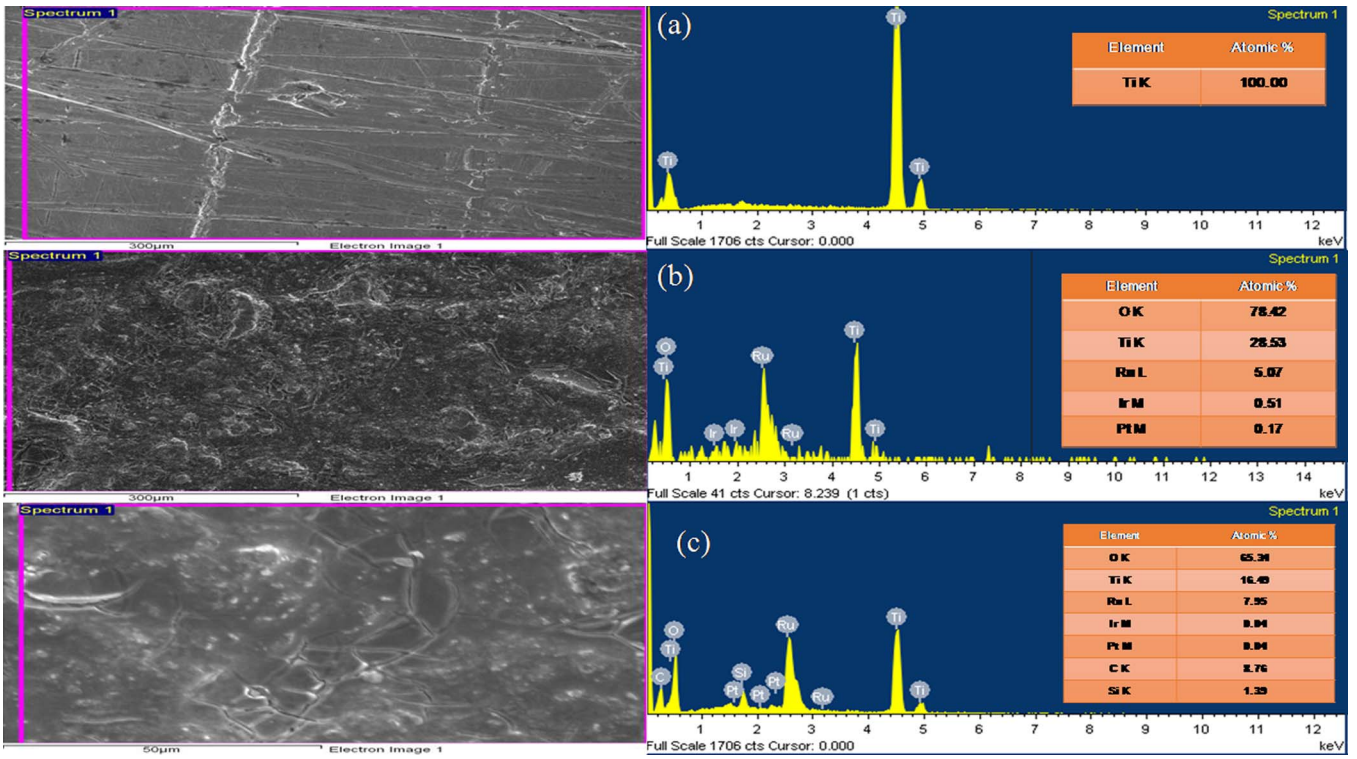

Figure 5. SEM images of (a) Ti sheet, (b) freshly coated MMO sheet and (c) recycled MMO sheet along with EDS data.

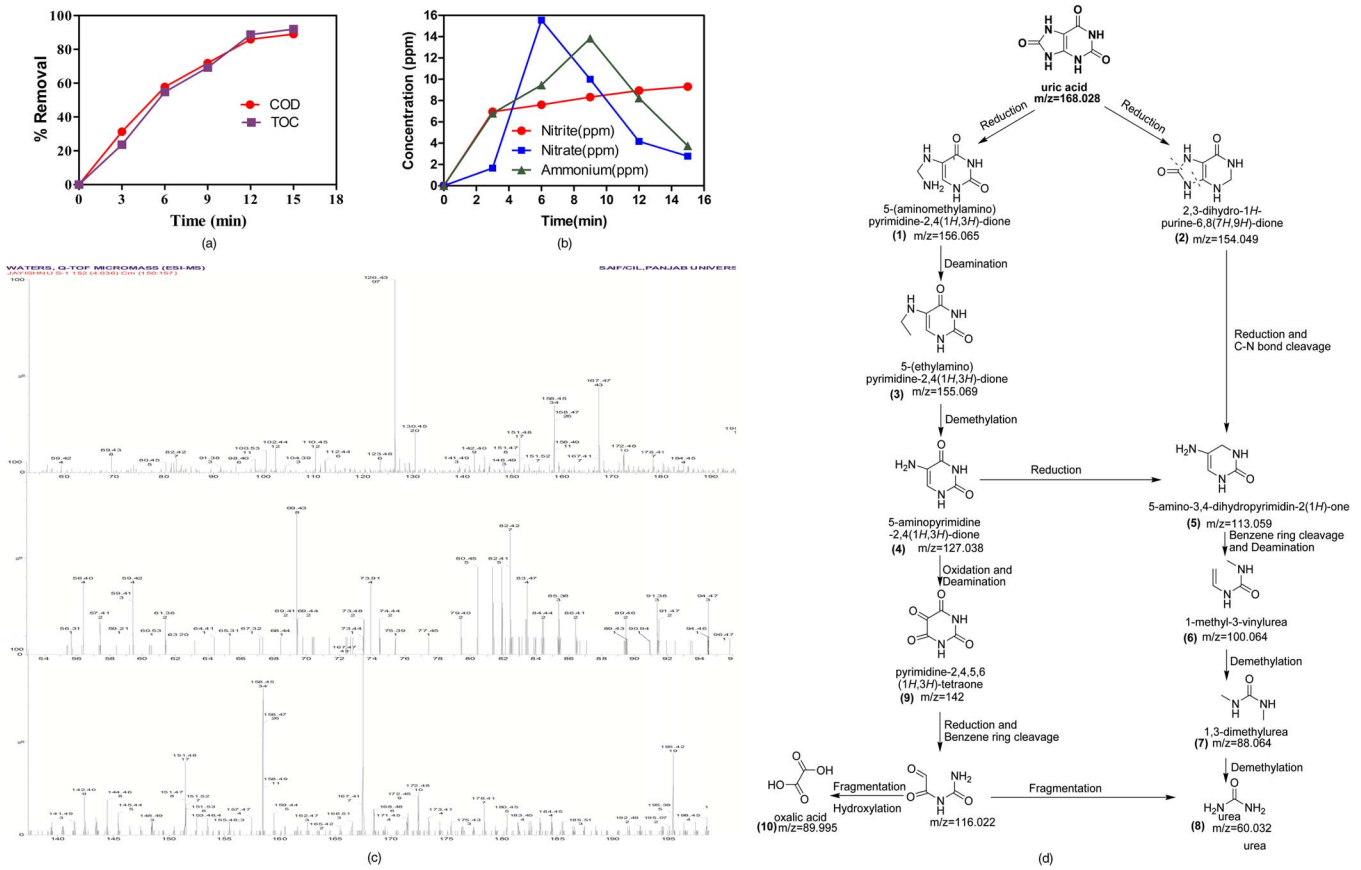

Figure 7. (a) Plot of % COD and TOC removal vs. time during electrolysis of uric acid (50 mg L^{-1}) on MMO anodes. (b) Production of nitrite, nitrate and ammonium ions during electrolysis of uric acid on MMO anodes. (c) Mass spectra analysis for the identification of intermediates during the electrolysis of uric acid. (d) Suggested degradation pathway for Uric acid.

The XRD pattern of freshly coated MMO sheet and recycled MMO sheet along with Ti sheet is depicted in Figure 6. The crystalline planes of Pt, Ru, and Ir along with Ti have been observed even in recycled MMO sheet thus confirming the retention of all metals even after sixty cycles. The diffraction peaks of titanium (reference code: 01-089-2762), titanium dioxide (reference code: 01-078-1508), ruthenium oxide (reference code: 00-021-1172), iridium (IV) oxide (reference code: 01-088-0288) and Platinum oxide (reference code: 01-074-1870) were also identified. An additional peak in recycled MMO sheet may pertain to some ionic species which may use in electrolyte preparation. Almost similar peaks are reported earlier in the literature.[57–60]

Table IV. Individual and simultaneously optimization results (with maximization of Y_1 and minimization of Y_2) for desirability calculation.

Individual response optimization					
Response	pH	i (A)	t (min)	n (g/400 ml)	Desirability
$Y_1 = 98.47\%$	2.10	0.5	6.37	0.35	1.00
$Y_2 = 140.849$ kWh/m^3	2.00	0.27	2.00	0.35	1.00
Simultaneous optimization of responses					
$Y_1 = 93.319\%$	2	0.30	6.95	0.35	0.899
$Y_2 = 581.491$ kWh/m^3					

Optimization

The simultaneous optimization of process parameters was done for maximizing the degradation for UA and minimizing the energy consumption keeping the factor in the range. The optimum values of input parameters and responses with corresponding desirability value for individual and simultaneously optimization (%degradation, Y_1 maximization, and energy consumption, Y_2 minimization) has been shown in Table IV. The optimized value of process parameters obtained was pH 2, NaCl concentration 0.35 g/400 ml and current 0.3 A. Time of reaction obtained was 6.95 min with overall desirability, D = 0.899 for degradation of uric acid. At optimum condition, Y_1 and Y_2 predicted by BBD were to be 93.319% and 581.491 kWh/m^3 respectively. The actual value obtained in same time and following optimum conditions were ~91.571% and 525.593 kWh/m^3 given in Table V. During electrolysis of water, the formation of OH• radicals takes place which directly oxidizes the compound. Further, these generated OH• species with time transformed into H_2O_2 and HO_2• which aids in the indirect oxidation process. In addition to this, the presence of chloro-oxidant species also helps in performing indirect oxidation. Therefore the degradation of the target compound is due to both direct and indirect oxidation at optimized conditions.

Table V. Comparison between predicted and experimental values of responses at optimum conditions for electro-oxidation treatment.

Responses	Predicted Value	Experimental Value
%Degradation (Y_1)	93.319%	91.571%
Energy consumption (Y_2)	581.491 kWh/m^3	525.593 kWh/m^3

Mineralization Studies

Mineralization of UA was confirmed in our study through a reduction in COD and TOC along with generation of anions like nitrite and nitrate. Around 60% removal in COD and 55% removal in TOC were achieved at optimized conditions which reached to more than 90% when the reaction was extended to 15 min as shown in Figure 7a. An increasing trend was observed for the generation of nitrate ions while the concentration of nitrite ions started decreasing after 6 min of treatment as depicted in Figure 7b. The nitrite ions could possibly convert into nitrate ions as reported in literature.[3] In addition to this, the peak of the parent compound at 291 nm got disappeared after 10 mins of treatment time as depicted by HPLC chromatograms. The intermediates formed during the degradation of UA were identified through LC-MS analysis shown in Figure 7c. Based on these intermediates (1–10), a degradation pathway has been proposed as shown in Figure 7d. The end products (8 and 10) has also been earlier reported for the degradation of UA.[9]

Conclusions

Removal of UA by EO through MMO anode using Multi-response process optimization under RSM has been done successfully. In the electro-oxidation process, degradation of UA was found to be maximum because of the involvement of both direct and indirect processes. This includes (a) direct oxidation of compound and its intermediated on the anode surface, (b) indirect oxidation with highly generated oxidant species like HOCl, ClO-, H_2O_2, $HO_2\bullet$ etc and (c) oxidation via in-situ electrochemically generated hydroxyl radicals on the surface of electrodes. At optimum conditions, more than 90% degradation was achieved. Complete removal of COD and TOC were obtained when reaction time extended to 15 mins. The organic intermediates (oxalic acid and urea) formed during the anodic oxidation treatment were confirmed by HPLC and LC-MS analysis. Based on these intermediates the oxidative degradation pathway of UA has been proposed in the study. During electrolysis, the transformation of the nitrogen content of UA into ammonium ion, nitrate and nitrite has been analyzed by APHA standard methods (4500). Results obtained from SEM-EADX and XRD indicates the stability and efficacy of the electrodes for the efficient degradation of compound even after 60 cycles of the experimental run. Results indicate the efficacy of EO process as a promising technique for the treatment of recalcitrant compounds.

References

1. S. Dbira, N. Bensalah, A. Bedoui, P. Cañizares, and M. A. Rodrigo, Treatment of synthetic urine by electrochemical oxidation using conductive-diamond anodes, *Environmental Science and Pollution Research*, **22**, 6176 (2015).
2. K. Cho, D. Kwon, and M. R. Hoffmann, Electrochemical treatment of human waste coupled with molecular hydrogen production, *RSC Advances*, **4**, 4596 (2014).
3. H. Li, Q. Yu, B. Yang, Z. Li, and L. Lei, Electrocatalytic oxidation of artificial human urine by using BDD and IrO_2 electrodes, *Journal of Electroanalytical Chemistry*, **738**, 14 (2015).
4. A. Özcan, Ali, and Y. Şahin, Preparation of selective and sensitive electrochemically treated pencil graphite electrodes for the determination of uric acid in urine and blood serum, *Biosensors and Bioelectronics*, **25**, 2497 (2010).
5. R. Molino-Lova, D. Prisco, G. Pasquini, F. Vannetti, A. Paperini, R. Zipoli, M. L. E. Luisi, F. Cecchi, and C. Macchi, Higher uric acid levels are associated with better functional recovery in elderly patients receiving cardiac rehabilitation, *Nutrition, Metabolism and Cardiovascular Diseases*, **23**, 1210 (2013).
6. Y. Y. Sautin, T. Nakagawa, S. Zharikov, and R. J. Johnson, Adverse effects of the classic antioxidant uric acid in adipocytes: NADPH oxidase-mediated oxidative/nitrosative stress, *American Journal of Physiology-Cell Physiology*, **293**, 584 (2007).
7. D. Lakshmi, M. J. Whitcombe, F. Davis, P. S. Sharma, and B. B. Prasad, Electrochemical detection of uric acid in mixed and clinical samples: a review, *Electroanalysis*, **23**, 305 (2011).
8. B. Vinnerås, H. Palmquist, P. Balmér, and H. Jönsson, The characteristics of household wastewater and biodegradable solid waste—a proposal for new Swedish design values, *Urban Water Journal*, **3**, 3 (2006).
9. S. Dbira, N. Bensalah, and A. Bedoui, Mechanism and kinetics of electrochemical degradation of uric acid using conductive-diamond anodes, *Environmental Technology*, **37**, 2993 (2016).
10. H. Park, K. H. Choo, H. S. Park, J. Choi, and M. R. Hoffmann, Electrochemical oxidation and micro filtration of municipal wastewater with simultaneous hydrogen production: Influence of organic and particulate matter, *Chemical Engineering Journal*, **215**, 802 (2013).
11. Y. Lester, I. Ferrer, E. M. Thurman, and K. G. Linden, Demonstrating sucralose as a monitor of full-scale UV/AOP treatment of trace organic compounds, *Journal of Hazardous Materials*, **280**, 104 (2014).
12. H. Suzuki, S. Araki, and H. Yamamoto, Evaluation of advanced oxidation processes (AOP) using O_3, UV, and TiO_2 for the degradation of phenol in water, *Journal of Water Process Engineering*, **7**, 54 (2015).
13. K. M. Lee, C. W. Lai, K. S. Ngai, and J. C. Juan, Recent developments of zinc oxide based photocatalyst in water treatment technology: a review, *Water research*, **88**, 428 (2016).
14. X. Liu, M. Chen, Z. Bian, and C. C. Liu, Studies on urine treatment by biological purification using Azolla and UV photocatalytic oxidation, *Advances in Space Research*, **41**, 783 (2008).
15. M. G. Antoniou, U. Nambiar, and D. D. Dionysiou, Investigation of the photocatalytic degradation pathway of the urine metabolite, creatinine: the effect of pH, *Water research*, **43**, 3956 (2009).
16. R. Zhang, P. Sun, T. H. Boyer, L. Zhao, and C. H. Huang, Degradation of pharmaceuticals and metabolite in synthetic human urine by UV, UV/H_2O_2, and UV/PDS, *Environmental Science and Technology*, **49**, 3056 (2015).
17. E. Brillas, I. Sirés, and M. A. Oturan, Electro-Fenton process and related electrochemical technologies based on Fenton's reaction chemistry, *Chemical Reviews*, **109**, 6570 (2009).
18. H. Zhang, X. Ran, and X. Wu, Electro-Fenton treatment of mature landfill leachate in a continuous flow reactor, *Journal of hazardous materials*, **241**, 259 (2012).
19. B. P. Chaplin, Critical review of electrochemical advanced oxidation processes for water treatment applications, *Environmental Science: Processes & Impacts*, **16**, 1182 (2014).
20. S. J. Lu, J. Y. Luo, S. B. Ji, N. X. Li, H. Li, and W. S. Li, Photo electrocatalytic oxidation of uric acid on a novel ruthenium (II) poly pyridyl complex modified ZnO electrode for photo-stimulated fuel cells, *Electrochimica Acta*, **136**, 130 (2014).
21. R. Daghrir, P. Drogui, and J. Tshibangu, Efficient treatment of domestic wastewater by an electrochemical oxidation process using bored doped diamond anode, *Separation and Purification Technology*, **131**, 79 (2014).
22. R. Jelena and D. L. Sedlak, Challenges and opportunities for electrochemical processes as next-generation technologies for the treatment of contaminated water, *Environmental Science and Technology*, **49**, 11292 (2015).
23. J. Wu, H. Zhang, N. Oturan, Y. Wang, L. Chen, and M. A. Oturan, Application of response surface methodology to the removal of the antibiotic tetracycline by an electrochemical process using carbon-felt cathode and DSA (Ti/RuO_2–IrO_2) anode, *Chemosphere*, **87**, 614 (2012).
24. N. Borràs, O. Ramon, C. Arias, and E. Brillas, Degradation of atrazine by electrochemical advanced oxidation processes using a boron-doped diamond anode, *The Journal of Physical Chemistry A*, **114**, 6613 (2010).
25. O. Scialdone, Electrochemical oxidation of organic pollutants in water at metal oxide electrodes: A simple theoretical model including direct and indirect oxidation processes at the anodic surface, *Electrochimica Acta*, **54**, 6140 (2009).
26. J. M. Aquino, R. C. R. Filho, L. A. M. Ruotolo, N. Bocchi, and S. R. Biaggio, Electrochemical degradation of a real textile wastewater using β-PbO_2 and DSA anodes, *Chemical Engineering Journal*, **251**, 138 (2014).
27. A. S. Raut, G. B. Cunningham, C. B. Parker, E. J. D. Klem, B. R. Stoner, M. A. Deshusses, and J. T. Glass, Electrochemical disinfection of human urine for water-free and additive-free toilets using boron-doped diamond electrodes, *ECS Transactions*, **53**, 1 (2013).
28. S. Dbira, N. Bensalah, P. Cañizares, M. A. Rodrigo, and A. Bedoui, The electrolytic treatment of synthetic urine using DSA electrodes, *Journal of Electroanalytical Chemistry*,. **744** , 62 (2015).
29. G. Chen, Electrochemical technologies in wastewater treatment, *Separation and Purification Technology*, **38**, 11 (2004).
30. E. Lacasa, J. Llanos, P. Cañizares, and M. A. Rodrigo, Electrochemical denitrification with chlorides using DSA and BDD anodes, *Chemical Engineering Journal*, **184**, 66 (2012).
31. H. Särkkä, K. Kuhmonen, M. Vepsäläinen, M. Pulliainen, J. Selin, P. Rantala, E. Kukkamäki, and M. Sillanpää, Electrochemical oxidation of sulfides in paper mill wastewater by using mixed oxide anodes, *Environmental Technology*, **30** , 885 (2009).
32. A. Y. Bagastyo, J. Radjenovic, Y. Mu, R. A. Rozendal, D. J. Batstone, and K. Rabaey, Electrochemical oxidation of reverse osmosis concentrate on mixed metal oxide (MMO) titanium coated electrodes, *Water Research*, **45**, 4951 (2011).
33. M. Zhou, H. Särkkä, and M. Sillanpää, A comparative experimental study on methyl orange degradation by electrochemical oxidation on BDD and MMO electrodes, *Separation and Purification Technology*, **78**, 290 (2011).
34. M. Panizza and C. A. Martinez-Huitle, Role of electrode materials for the anodic oxidation of a real landfill leachate–Comparison between Ti–Ru–Sn ternary oxide, PbO_2 and boron-doped diamond anode, *Chemosphere*, **90**, 1455 (2013).
35. American Health Public Association (APHA). Standard methods for the Examination of Water and Wastewater. 19th ed., Standard method no. (18th Edition), 5220-C, Washington, DC: APHA; 1992.
36. American Health Public Association (APHA). Standard methods for the Examination of Water and Wastewater. 17th ed., Standard method no. 4500-NO_2^- (B), Washington, DC: APHA; 1989.
37. American Health Public Association (APHA). Standard methods for the Examination of Water and Wastewater. 17th ed., Standard method no. 4500-NO_3^- (E), Washington, DC: APHA; 1989.

38. American Health Public Association (APHA). Standard methods for the Examination of Water and Wastewater. 17th ed., Standard method no. 4500-NH_4^+ (C), Washington, DC: APHA; 1989.
39. S. Bansal, J. P. Kushwaha, and V. K. Sangal, Electrochemical treatment of reactive black 5 textile wastewater: optimization, kinetics, and disposal study, *Water Environment Research*, **85**, 2294 (2013).
40. H. Zhang, X. Ran, X. Wu, and D. Zhang, Evaluation of electro-oxidation of biologically treated landfill leachate using response surface methodology, *Journal of Hazardous Materials*, **188**, 261 (2011).
41. V. K. Sangal, V. Kumar, and I. M. Mishra, Optimization of structural and operational variables for the energy efficiency of a divided wall distillation column, *Computers, and Chemical Engineering*, **40**, 33 (2012).
42. P. Singh, A. Dhir, and V. K. Sangal, Optimization of photocatalytic process parameters for the degradation of acrylonitrile using Box Behnken Design, *Desalination and Water Treatment*, **55**, 1501 (2015).
43. A. Kumar, B. Prasad, and I. M. Mishra, Process Parametric Study for Ethene Carboxylic Acid Removal onto Powder Activated Carbon using Box-Behnken Design, *Chemical Engineering, and Technology*, **30**, 932 (2007).
44. S. Singh, S. Singh, S. L. Lo, and N. Kumar, Electrochemical treatment of Ayurveda pharmaceuticals wastewater: Optimization and characterization of sludge residue, *Journal of the Taiwan Institute of Chemical Engineers*, **67**, 385 (2016).
45. A. D. Hiwarkar, S. Singh, V. C. Srivastava, and I. D. Mall, Mineralization of pyrrole, a recalcitrant heterocyclic compound, by the electrochemical method: Multi-response optimization and degradation mechanism, *Journal of Environmental Management*, **198**, 144 (2017).
46. V. K. Sangal, V. Kumar, and M. I. Mishra, Optimization of a divided wall column for the separation of C4-C6 normal paraffin mixture using Box-Behnken design, *Chemical Industry, and Chemical Engineering Quarterly/CICEQ.*, **19**, 107 (2013).
47. K. Thirugnanasambandham, V. Sivakumar, and J. P. Maran, Response surface modeling and optimization of treatment of meat industry wastewater using electrochemical treatment method, *Journal of the Taiwan Institute of Chemical Engineers*, **46**, 160 (2015).
48. K. Rajkumar and M. Muthukumar, Optimization of an electro-oxidation process for the treatment of Reactive Orange 107 using response surface methodology, *Environmental Science, and Pollution Research*, **19**, 148 (2012).
49. A. Garg, V. K. Sangal, and P. K. Bajpai, Decolorization and degradation of Reactive Black 5 dye by photocatalysis: modeling, optimization and kinetic study, *Desalination and Water Treatment*, **57**, 18003 (2016).
50. V. K. Sangal, V. Kumar, and I. M. Mishra, Process parametric optimization of a divided wall distillation column, *Chemical Engineering Communications*, **201**, 72 (2014).
51. P. Kaur, V. K. Sangal, and J. P. Kushwaha, Modeling and evaluation of electro-oxidation of dye wastewater using artificial neural networks, *RSC Advances*, **5**, 34663 (2015).
52. C. A. Martínez-Huitle and E. Brillas, Electrochemical alternatives for drinking water disinfection, *Angewandte Chemie International Edition*, **47**, 1998 (2008).
53. C. Comninellis and G. Chen, eds. *Electrochemistry for the Environment*, Vol. 2015. New York: Springer, 2010.
54. Y. J. Jung, K. W. Baek, B. S. Oh, and J.-W. Kang, An investigation of the formation of chlorate and perchlorate during electrolysis using Pt/Ti electrodes: The effects of pH and reactive oxygen species and the results of kinetic studies, *Water Research*, **44**, 5345 (2010).
55. K. K. Garg and B. Prasad, Electrochemical treatment of benzoic acid (BA) from aqueous solution and optimization of parameters by response surface methodology (RSM), *Journal of the Taiwan Institute of Chemical Engineers*, **56**, 122 (2015).
56. C. A. Martinez-Huitle and S. Ferro, Electrochemical oxidation of organic pollutants for the wastewater treatment: direct and indirect processes, *Chemical Society Reviews*, **35**, 1324 (2006).
57. M. E. Makgae, C. C. Theron, W. J. Przybylowicz, and A. M. Crouch, Preparation and surface characterization of Ti/SnO_2–RuO_2–IrO_2 thin films as an electrode material for the oxidation of phenol, *Materials Chemistry and Physics*, **92**, 559 (2005).
58. S. Song, H. Zhang, X. Ma, Z. Shao, R. T. Baker, and B. Yi, Electrochemical investigation of electrocatalysts for the oxygen evolution reaction in PEM water electrolyzers, *International Journal of Hydrogen Energy*, **33**, 4955 (2008).
59. Y.-H. Cui, X.-V. Li, and G. Chen, Electrochemical degradation of bisphenol A on different anodes, *Water Research*, **43**, 1968 (2009).
60. X. Liu, N. Chen, B. Han, X. Xiao, G. Chen, I. Djerdj, and Y. Wang, Nanoparticle cluster gas sensor: Pt activated SnO_2 nanoparticles for NH_3 detection with ultra high sensitivity, *Nanoscale*, **7**, 14872 (2015).

Journal of Electroanalytical Chemistry 809 (2018) 136–146

Contents lists available at ScienceDirect

Journal of Electroanalytical Chemistry

journal homepage: www.elsevier.com/locate/jelechem

Parametric optimization for the treatment of human urine metabolite, creatinine using electro-oxidation

Jayishnu Singla[a], Anoop Verma[a,*], Vikas K. Sangal[b]

[a] School of Energy and Environment, Thapar University, Patiala, Punjab, India
[b] Department of Chemical Engineering, Thapar University, Patiala, Punjab, India

ARTICLE INFO

Keywords:
Electro-oxidation
Dimensionally stable anode
Response surface methodology
Box-Behnken design
Mineralization

ABSTRACT

The efficacy and durability studies of the dimensionally stable anode (DSA) have been carried out for the treatment of human urine metabolite, creatinine using electro-oxidation process. The influence of various input parameters such as current density, treatment time, pH and concentration of electrolyte on responses like % degradation and energy consumption were explained using Box-Behnken design. 85.41% pollutant degradation along with complete mineralization was achieved at optimum conditions like pH-(2.4), current density-(10.29 mA cm^{-2}), NaCl concentration-(0.75 g L^{-1}) and treatment time-(85 min). Interestingly, a treatment time of was significantly lower than the reported values with similar kind of advanced technologies. Further reduction in treatment time i.e. 60 min was achieved by incorporating synergistic effect through Photoelectrocatalysis for the same %degradation. The electrodes used were durable enough even after forty-five cycles as confirmed through SEM/EDS and Raman Spectra. Further, mineralization studies were carried out by measuring the reduction in COD (81.25%) and TOC (84.37%) along with generation of various ions such as nitrite, nitrate and ammonium ion under the optimized conditions. Based upon the detected intermediates analyzed through FT-IR and LC-MS, a degradation mechanism for creatinine has been proposed.

1. Introduction

Creatinine (2-amino 1-methyl-5H-imidazol-4-one) is one of the components present in human blood and eliminated through the body via urine excretion [1,2]. Creatinine is the final end product of creatine catabolism in skeletal muscle and considered as helpful in maintaining the efficiency of kidney, thyroid, and muscles. Its high concentration in human blood and serum can cause renal failure, muscular abnormalities, thyroid malfunction and vascular diseases [3]. Furthermore, creatinine is one of the principal nitrogen-based compound present in the human urine [4]. Because of the high nitrogen content its direct exposure and accumulation into the water streams can cause an adverse effect on the environment, eutrophication of surface waters and transmission of the pathogen as well [5]. Treatment of such wastewater becomes a challenge because of its complexity and composition which varies every day [6]. Hence require effective and strong technologies for the treatment as well as removal of persistent and recalcitrant compounds from wastewater.

Literature in the recent past has shown that efficiency of advanced oxidation processes (AOP's) for the treatment of such complex, toxic and persistent compounds present in water/wastewater [6–8]. However, continuous requirement of energy for a longer period of time for complete degradation along with HO· scavenging makes this technology relatively expensive which necessitates a requirement for an effective alternative technology. Studies pertaining to electrochemical-based advanced treatment technologies (EAOP's) have confirmed that these technologies are strong bet for the treatment of toxic and persistent bio-refractive compounds [9]. These technologies (EAOP's) do not require any chemical addition like H_2O_2 for the generation of $HO^{\cdot}$ moreover the $HO^{\cdot}$ generate directly from the oxidation of water. Further, in addition to this, the compounds which are unreactive to $HO^{\cdot}$ radicals can be degraded through direct electron transfer (DET) reactions [10].

One of the most attractive and affordable technology that have come under EAOP is the electrooxidation (EO). EO is considered as highly efficient, versatile and eco-friendly technology with high oxidation stability and has made considerably huge progress in water/wastewaters treatment [11,12]. Despite, of such advantages, EAOP carries certain deficiencies such as the cost of electrodes, the short lifespan of anodes, mass transfer limitations and low current efficiencies which actually limit their use on field-scale [13]. To overcome these limitations, the recent studies have come up with use of dimensionally

* Corresponding author.
E-mail address: anoop.kumar@thapar.edu (A. Verma).

https://doi.org/10.1016/j.jelechem.2017.12.061
Received 13 August 2017; Received in revised form 17 December 2017; Accepted 25 December 2017
Available online 29 December 2017

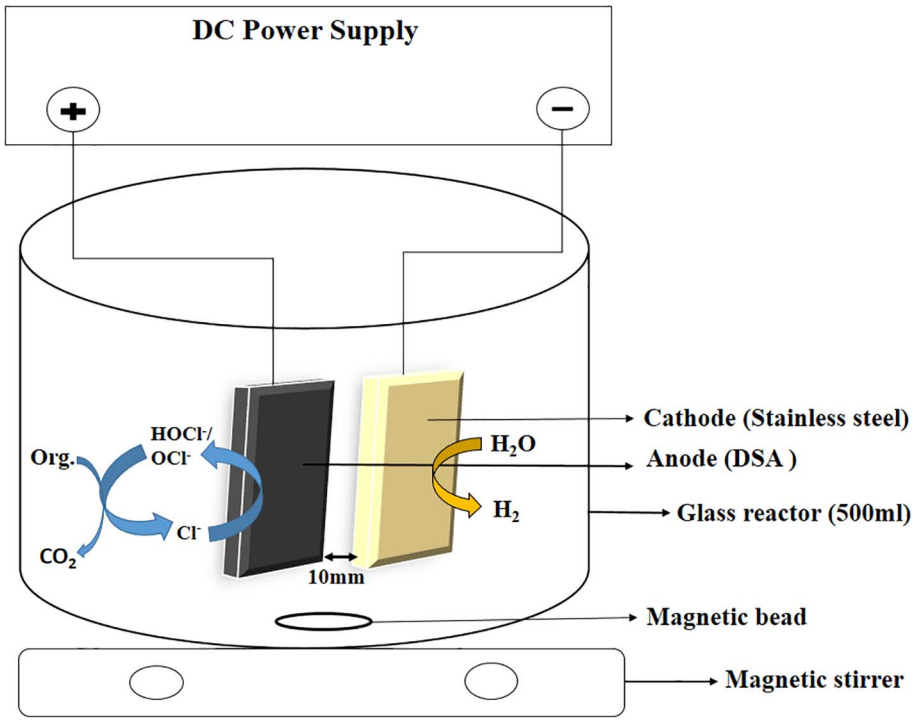

Fig. 1. Schematic diagram of experimental setup used for the electrochemical treatment of creatinine.

stable anodes (DSA) for the treatment of wastewater containing recalcitrant organics. DSA as anodes such as Sn-Sb binary DSA, Ir-Ru binary DSA, Ir-Ta binary DSA, Ti-Ru binary DSA, Ti-Bi binary DSA, Ir-Ru-Sn ternary DSA, Ce-Ru-Sn ternary DSA and Ru-Ir-Sn-Ti quaternary DSA anodes [14] have been used for the EO treatment of large variety of wastes such as dyes effluent [15,16] pesticides and herbicides [17,18], phenolic compounds[19], pharmaceutical waste [20,21], plasticizers[22], chelating agents [23] and Microcystin toxins [24]. These electrodes exhibit better process efficiency, has good electrochemical stability properties as well as proven to be highly competent in the production of the chloro-oxidant species like hypochlorite and hydroxyl radicals during EO treatment [25,26].

From the literature survey, it has been observed that several research groups have presented the use of DSA such as Ti/(Pt-Ir), Pt-Ti, Ti/(RuO_2-IrO_2), Ti/RuO_2 and Ti/IrO_2 for the treatment of synthetic/human urine and its metabolites [27–32]. In this present study, the novel combination of Pt-Ru-Ir-Ti quaternary DSA anode has been selected to get the good resistance properties of Ru-Ir. The Pt layer decreases the adsorption of Cl- ions which further increases the process efficiency at low current densities [33].

Further efforts have been made to increase the process efficiency by incorporating photo-catalysis along with EO i.e. photo-electrocatalysis (PEC). In PEC, the photogenerated electrons in the excited TiO_2 coated anode are taken towards cathode via external circuit hence preventing its combination with photogenerated holes on the anode surface [34]. Photo-electrocatalytic oxidation process has received considerable attention in the field of environmental protection and has been applied for the treatment of different effluents like dye [35], phenolic compounds [36], Humic substances [37], microbial pollutants [38] present in water/wastewater. Hence photo-electrocatalysis can be considered as a good alternative to conventional photo-catalysis for improving the degradation rate by incorporating synergistic effect along with the overcoming of pit-falls of photo-catalysis process [14].

The goal of this study is to evaluate the efficacy of DSA electrodes for the EO as well as PEC treatment of human urine metabolite, creatinine. Besides reporting its novelty in terms of first-time use of this type of anode, efforts have also been done to reduce the treatment time as reported in the literature. Box-Behnken design (BBD) under response surface methodology (RSM) is used for investigating the effect of the input parameters namely, initial pH, current density, electrolyte concentration (NaCl concentration) and time on percentage degradation (% degradation) and energy consumption. Additionally, durability and stability of electrodes are checked using various characterization techniques such as SEM-EDS and Raman spectroscopy. The efficiency of the process is investigated using various analytical methods such total organic carbon (TOC), chemical oxygen demand (COD) along with mineralization end products (i.e, NO_3^-, NO_2^- and NH_4^+ ions). The oxidative degradation pathway of creatinine during EO treatment is also proposed in this study as analyzed by Fourier transformed infrared spectroscopy (FT-IR) and cross-confirmed through liquid chromatography-mass spectroscopy (LC-MS).

2. Material and methods

2.1. Chemicals

Creatinine ($C_4H_7NO_3$) with 99.5% purity, acetonitrile and formic acid of analytical grade were purchased from Sigma-Aldrich, Missouri, (U.S.). Sodium chloride (NaCl), sulfuric acid (H_2SO_4) and sodium hydroxide (NaOH) were purchased from Loba Chemicals Pvt. Ltd. Mumbai, India. All the solutions were prepared in double distilled water with resistivity $> 18\ M\Omega\ cm^{-1}$ at 25 °C obtained from a Millipore Milli-Q system.

2.2. Sample preparation and experimental setup

Standard synthetic wastewater sample was prepared by dissolving 50 mg creatinine in 1 L double distilled water. The sample was prepared freshly each time. EO experiments for the treatment of creatinine were carried out in a Glass reactor of working volume 500 ml under a batch operation mode as shown in Fig. 1. The anode used in the study was titanium sheet coated with oxides of (titanium, iridium and ruthenium), purchased from (Exotic Elements Pvt. Ltd., Mumbai, India) having dimension (70 mm ∗ 70 mm ∗ 1 mm), whereas stainless steel as cathode of the same dimension was purchased from (Bio age Pvt. Ltd., Mohali, India). The effective surface area of the anode was 42 cm^2. In

the present study, the electrodes were positioned vertically in parallel mode with 10 mm inter-electrode spacing. DC supply (DIGITECH, Ambala, India, Model: 0–30 V, 0–2 A) was used to maintain the current during the experimental runs. To maintain the uniform concentration of the electrolyte, the solution was continuously agitated at 600 rpm using a magnetic stirrer.

2.3. Experimental procedure

EO treatment was carried out under galvanostatic conditions. Before starting the process experiments the pH of the solution was adjusted by 0.1 N HCl and 0.1 N NaOH while NaCl was used as supporting electrolyte to improve the ionic strength of the wastewater solution. At certain time intervals, 1 ml of sample volume was withdrawn from the system, filtered using 0.20 μm nylon filters and analyzed by UV–Visible spectrophotometer at λmax 238 nm. The adsorption of creatinine using DSA was checked under dark without any current supply with continuous stirring. It was observed that no significant change in the optical density occurred. Thus, the effectiveness of EO process was proved in context to the degradation of creatinine.

2.4. Analytical methods

Analytical studies for creatinine were carried out by analyzing the samples through UV–Visible spectrophotometer (HITACHI, model U-2800) and HPLC (Shimadzu) with maximum absorption of creatinine at 238 nm wavelength. Total organic carbon (TOC) and chemical oxygen demand (COD) analysis for the treated samples were monitored to check the mineralization efficiency of EO process. APHA standard methods (4500) were used to determine the reduction in COD as well as the generation of inorganic ions such as nitrate, nitrite, and ammonium ion during the treatment process [39–42]. TOC of the samples was monitored using multi N/C 2100Analytik Jena TOC analyzer. The intermediates formed during the degradation of creatinine were confirmed through LC-MS analysis. Q-TOF mass spectrometer (Micromass UK Ltd) was used for LC-MS analysis. The temperature of the ion spray injector was adjusted to 480 °C while declustering potential was 73 V. The analysis was carried out under isocratic mode using mobile phase of 0.1% formic acid in water (50%) and 0.1% formic acid in acetonitrile (50%). Data analysis was conducted in the positive ion mode with a flow rate of 200 μl min^{-1}. In order to analyze the structural and functional characteristics of the pure sample and its complexes, FT-IR was performed. The FT-IR spectrometer used in the present study was the Perkin Elmer Spectrum 2. The FT-IR spectra were recorded in the range 4100–400 cm^{-1}. The surface morphology and elemental composition of the coatings of purchased DSA anodes were examined using a JEOL 5900LV scanning electron microscope (SEM) along with energy dispersive X-ray spectrometry (EDX) mapping. Before the analysis, samples were coated with the thin layer of gold. Raman spectra were recorded on a confocal micro Raman spectrophotometer (STR 500, Airix Corporation, Japan) with a green diode laser source of 532 nm.

2.5. Experimental design

In the present study, Response Surface Methodology (RSM) was used to optimize process parameters by reducing the number of experiments as well as to investigate the inter-parametric interactions of the independent variables and their effects on the responses [43]. Box-Behnken design (BBD) under RSM, requires an experimental run according to $N = s^2 + s + m_p$, where, s is the factor number and m_p is the replicate number of the central point [44]. The four input operating variables used in the study were initial pH(X_1), current density(X_2), time(X_3) and NaCl concentration (X_4). The factor level coded for these process parameters were designated as −1(low), 0(center) and +1(high), shown in Table 1. The experimental range for each variable was decided based on the literature studies and preliminary experiments. The total number of experiments designed by BBD for the present study based on 3 level factorial experimental design was 29, as illustrated in Table 2.

Table 1
Range and coded levels of chosen variables for electro-oxidation of creatinine.

Factors	Variables	Range of actual and coded variables		
		−1	0	+1
A	Initial pH	2	5.5	9
B	Current density (mA cm^{-2})	6.12	12.24	18.36
C	Time of electrolysis (min)	15	65	115
D	NaCl conc. (g L^{-1})	0.25	0.75	1.25

To fit the second order polynomial equation (Eq. (1)) to the experimental data and to analyze the relevant model terms, a manual regression process was used. Considering all the linear terms, square terms and the linear by linear interaction terms, the quadratic response model [45] can be described as:

$$Z = \alpha_o + \sum_{i=1}^{4} \alpha_i X_i + \sum_{i=1}^{4} \alpha_{ii} X_i^2 + \sum_{i=j}^{3} \sum_{i=j+1}^{4} \alpha_{ij} X_{ij} + ei \quad (1)$$

where Z is the response; α_o, α, α_{ii}, α_{ij} are constant coefficients, X_i, X_{ii}, X_{ij} are independent input variables and e_i is the error. In the present case, due to the involvement of the two responses %degradation and energy consumption, multi-response process optimization with desirability function approach was used for the optimization of the multiple responses simultaneously [46,47]. In multi response optimization, each response is converted into an individual desirability function whose value lies between 0 and 1 [48]. All the individual desirability functions are combined in order to obtain overall desirability function, by converting multi-response into single response.

3. Result and discussion

3.1. Statistical analysis with BBD

For designing as well as for analyzing the experimental data through multiple regression analysis, statistical design expert software version 6.0.8 (STAT-Ease Inc., Minneapolis, US) was used. The results of responses like % degradation and energy consumption for the EO treatment of creatinine were calculated by conducting the experimental runs at suggested set of process parameters shown in Table 2 by BBD.

The sequential model sum of square and model summary statistic were two different test, performed in order to obtain best regression model among various models like linear, 2FI, quadratic and cubic [49,50]. A Logit transformation for % degradation and square root transformation for energy consumed were applied to the experimental data. From the results of the adequacy tests, the *p*-value for the quadratic model was < 0.05 which indicates that the model to be statistically significant [51]. Similarly, R^2 0.9726, 0.9770 for % degradation and energy consumption were found to be maximum for the quadratic model when compared with other models. The insignificant model terms in the manual regression method were evicted automatically which in turn provided the summarize results of analysis of variance (ANOVA) for each response with reduced quadratic equation and showed significant model terms [52].

The Second order polynomial equation of responses % degradation and energy consumption, respectively in terms of independent coded factors for DSA electrode are summarized in Eqs. (2)–(3).

Table 2
BBD matrix and experimental results for electro-oxidation of creatinine.

Std	Run	pH	Current density (mA cm^{-2})	Time (min)	NaCl conc. (g L^{-1})	%Degradation	Energy consumption (kWh m^{-3})
3	1	2	18.36	65	0.75	84.63	37,536.3
2	2	2	6.12	65	0.75	40.222	5524.83
23	3	2	6.12	65	1.25	42.22	3818.63
21	4	2	6.12	65	0.25	52.09	5687.32
20	5	2	12.24	115	0.75	81.11	35,925
24	6	2	18.36	65	1.25	80.89	25,593
29	7	5.5	12.24	65	0.75	77.99	18,199.4
4	8	5.5	18.36	65	0.75	77.06	47,529.8
18	9	5.5	12.24	15	0.75	15.73	4575
27	10	5.5	12.24	65	0.75	80.74	18,199.4
5	11	5.5	12.24	15	0.25	8.86	5512.5
6	12	5.5	12.24	115	0.25	85.3	42,822.6
9	13	5.5	12.24	65	0.25	76.36	25,593
26	14	5.5	12.24	65	0.75	81.89	18,199.4
8	15	5.5	12.24	115	1.25	87.79	22,417.2
28	16	5.5	12.24	65	0.75	76.47	18,199.4
1	17	5.5	6.12	65	0.75	60.85	5118.59
19	18	5.5	12.24	115	0.75	87.94	32,763.6
13	19	5.5	6.12	15	0.75	7.124	1162.5
14	20	5.5	18.36	15	0.75	37.36	9956.25
12	21	5.5	12.24	65	1.25	73.84	12,837.1
11	22	5.5	12.24	65	1.25	82.74	11,699.6
16	23	5.5	18.36	115	0.75	86.6	47,991.7
7	24	9	12.24	15	1.25	21.63	2850
17	25	9	12.24	15	0.75	40.15	4050
25	26	9	18.36	65	0.75	78.78	18,199.4
22	27	9	12.24	65	0.25	74.13	64,835.5
15	28	9	12.24	115	0.75	81.85	9196.8
10	29	9	12.24	65	0.25	66.04	24,374.3

$$\%\text{degradation} = +79.17 - 6.56*X_1 + 13.03*X_2 + 31.64*X_3 + 2.19*X_4 - 1.77*X_1^2 - 9.48*X_2^2 - 19.93*X_3^2 - 6.12*X_4^2 + 3.26*X_1*X_2 + 4.40*X_1*X_3 + 0.36*X_1*X_4 - 6.37*X_2*X_3 + 4.16*X_2*X_4 - 2.57*X_3*X4 \quad (2)$$

$$\text{Energy consumption} = +18199.44 - 1167.07*X_1 + 16911.15*X_2 + 13584.22*X_3 - 7467.47*X_4 + 1450.71*X_1^2 + 3503.72*X_2^2 - 2087.29*X_3^2 + 1514.90*X_4^2 + 2396.80*X_1*X_2 + 659.10*X_1*X_3 + 589.04*X_1*X_4 + 7500.29*X_2*X_3 - 9343.46*X_2*X_4 - 4435.72*X_3*X4 \quad (3)$$

where X_1, X_2, X_3 and X_4 are initial pH, current density, time and NaCl concentration respectively.

Table 3 shows the ANOVA results obtained from the second order quadratic equation for the responses % degradation and energy consumption respectively, for EO treatment of creatinine using DSA. The model F-value of 38.85 and 42.39 respectively, implies suggested the model is significant. Values of "Prob > F" < 0.05 at the 95%probability level indicate that model terms are significant and highly significant [53]. From the ANOVA results, the significant model term for response % degradation are pH, current density, NaCl concentration, current density^2, NaCl concentration^2, and current density ∗ time while current density ∗ time are highly significant. For response energy consumption, the significant model terms are time^2, current density ∗ time and current density ∗ NaCl concentration whereas current density, time, and NaCl concentration are shown as highly significant. The model summary statistic showed the R^2 (regression coefficient) value for both the responses were 0.9753 and 0.9770 respectively, implies a good correlation between response and the factors [54]. For responses % degradation and energy consumption, the adequate precision ratio was found to be 22.544 and 25.768, respectively. An adequate precision ratio above 4 indicates that adequate model is fit and can be used for navigating the design space [55].

To come to decision for adequacy of the developed mathematical model, construction of diagnostic plots between the actual versus predicted for experimental data were evaluated. These plots represent the relationship between predicted and experimental values [56]. The data points on the plot (Fig. 2a) were in the proximity of the straight diagonal line, which concludes that there is a good adequate agreement between the experimental data and data predicted by developed mathematical model [57]. Fig. 2b shows the residual points on normal probability plot and dot diagram of these residuals lies reasonably close to a straight line signifies that the underlying assumptions of the analysis were satisfied [58].

3.2. Effect of process parameters

3.2.1. Effect of initial pH on %degradation

pH of the solution is a crucial factor influencing the performance of the electro-oxidation process. It explains the adsorption rate of $HO^{\cdot}$ radicals as well as the type of Cl^- species is predominant. Fig. 3a shows the interaction between pH and current density on % degradation. From the results, it was found that for pH value ≈ 2, % degradation was increasing at all the current density values. However, for pH > 2, % degradation was first increasing for current density values up to 15.30 mA cm^{-2} and then started decreasing gradually for current density > 15.30 mA cm^{-2}.

In previous studies, it has been reported that the removal efficiency of the pollutant tends to increase at lower pH values because at highly acidic pH the adsorption rate of the $HO^{\cdot}$ radicals on the DSA is high and hence, leads to the direct oxidation of compound at the anode surface shown in Eq. (6). Whereas at highly basic pH, the adsorption rate of the $HO^{\cdot}$ radicals on the anode surface is decreased leads to the transformation of $HO^{\cdot}$ radicals into H_2O_2 and $HO_2^{\cdot}$ (oxidants of lower potential) shown in Eqs. (10)–(12) [14] thus, corresponds to mediated oxidation. Furthermore, it was also observed that at highly acidic pH, HOCl oxidant species generation was maximum which dominates over all other oxidant species like Cl_2, ClO^- etc., shown in Eqs. (5)–(9) [31] and hence led to indirect oxidation. While in the case of alkaline pH, lower chloro-oxidant species like ClO_3^- and ClO_4^- were generated with time and thus reducing the degradation efficiency shown in Eqs.

Table 3
ANOVA suggested by BBD for %degradation and energy consumption.

Sources	%Degradation (Y_1)					Energy consumption (Y_2): (kWh/m^3)				
	Sum of square	DF	Mean square	F-value	Prob > F	Sum of square	DF	Mean square	F-value	Prob > F
Model	119.02	14	8.50	35.44	< 0.0001	91,610.54	14	6543.61	42.39	< 0.0001
pH	4.97	1	4.97	20.74	0.0005	139.17	1	139.17	0.90	0.3585
Current density	14.61	1	14.61	60.91	< 0.0001	44,668.49	1	44,668.49	289.35	< 0.0001
Time	85.62	1	85.62	356.96	< 0.0001	35,142.24	1	35,142.24	227.64	< 0.0001
NaCl conc.	1.80	1	1.80	7.51	0.9433	6579.03	1	6579.03	42.62	< 0.0001
pH^2	$1.257 * 10^{-3}$	1	$1.257 * 10^{-3}$	$5.241 * 10^{-3}$	0.0013	91.67	1	91.67	0.59	0.4538
Current density^2	3.82	1	3.82	15.94	0.0001	7.59	1	7.59	0.049	0.8277
Time^2	6.63	1	6.63	27.63	0.0761	1765.50	1	1765.50	11.44	0.0045
NaCl conc.^{2}	0.88	1	0.88	3.67	0.9268	4.59	1	4.59	0.030	0.8656
pH * current density	$2.097 * 10^{-3}$	1	$2.097 * 10^{-3}$	$8.741 * 10^{-3}$	0.6355	115.41	1	115.41	0.75	0.4018
pH * time	0.056	1	0.056	0.23	0.7979	5.14	1	5.14	0.033	0.8579
pH * NaCl conc.	0.016	1	0.016	0.068	0.0144	20.21	1	20.21	0.13	0.7229
Current density * time	1.87	1	1.87	7.79	0.0433	826.12	1	826.12	5.35	0.0364
Current density * NaCl conc.	0.35	1	0.35	1.46	0.2470	1641.50	1	1641.50	10.63	0.0057
Time * NaCl conc.	0.13	1	0.13	0.55	0.4713	330.36	1	330.36	2.14	0.1656
Residual	3.36	14	0.24			2161.25	14	154.37		
Lack of fit	3.09	10	0.31	4.64	0.0762	2161.25	10	216.12		
Pure error	0.27	4	0.067			0.000	4	0.000		
Cor total	122.38	28				93,771.79	28			

(13)–(15) [59]. Thus, the oxidation of the target pollutant was found to be maximum at acidic pH because of the involvement of both mechanisms, direct and indirect EO.

At acidic pH:

$$H_2O \rightarrow HO^{\cdot} + H^+ + e^- \quad (4)$$

$$Cl_2 + 2e^- \rightarrow 2Cl^- \quad (5)$$

$$Cl_2 + H_2O \rightarrow HClO + Cl^- + H^+ \quad (6)$$

$$HClO \rightarrow ClO^- + H^+ \quad (7)$$

$$ClO^- + H_2O + 2e^- \rightarrow Cl^- + 2OH^- \quad (8)$$

$$Cl^- + {}^{\cdot}OH \rightarrow ClO^- + H^+ + e^- \quad (9)$$

At basic pH:

$$HO^{\cdot} + OH^- \rightarrow {}^{\cdot}O^- + H_2O \quad (10)$$

$$H_2O_2 + OH^- \rightarrow HO_2^- + H_2O \quad (11)$$

$$HO_2^{\cdot} + OH^- \rightarrow O_2^{\cdot -} + H_2O \quad (12)$$

$$ClO^- + OH^- \rightarrow ClO_2^- + H^+ + e^- \quad (13)$$

$$ClO_2^- + OH^- \rightarrow ClO_3^- + H^+ + e^- \quad (14)$$

$$ClO_3^- + OH^- \rightarrow ClO_4^- + H^+ + e^- \quad (15)$$

3.2.2. Effect of current density on %degradation

Current density is one of the most important operating parameters for EO treatment process for the analysis of both mechanistic study and cost effectiveness. In EO process, the generation rate of oxidant species like $HO^{\cdot}$, ozone, $HO_2\cdot$ and chloro-oxidant species along with the capability of electron transfer is highly dependent upon the current density. From the literature it was found that chloro-oxidant species generation rate was significantly increased by increasing the current density [60] thus, increasing the process efficiency. But at the same time at higher current densities Oxygen evolution reaction was more favored over chloro-oxidant species and thus lowering the process efficiency of electrodes [61]. At higher current densities the oxidation of the pollutant may lead to side reactions such as OER in which the $OH^{\cdot}$ radicals were consumed. Moreover it would lead to increase in energy consumption due to rise in temperature of the solution [14].

To examine the effect of the current density and time on the response % degradation, the value of current density was varied from 6.12 to 18.36 mA cm^{-2}. From Fig. 3b it was observed that % degradation first increase gradually for current density up to ≈ 12.24 mA cm^{-2}, then become constant for current density < 15.30 mA cm^{-2}. Further increase in current density value > 15.30

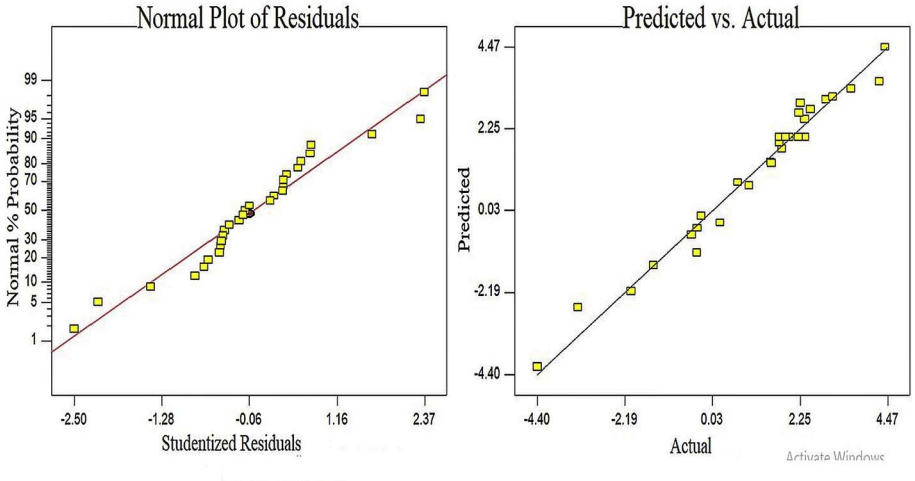

Fig. 2. (a) The normal plot of Residuals for %degradation and (b) The regression plots of predicted vs actual for % degradation.

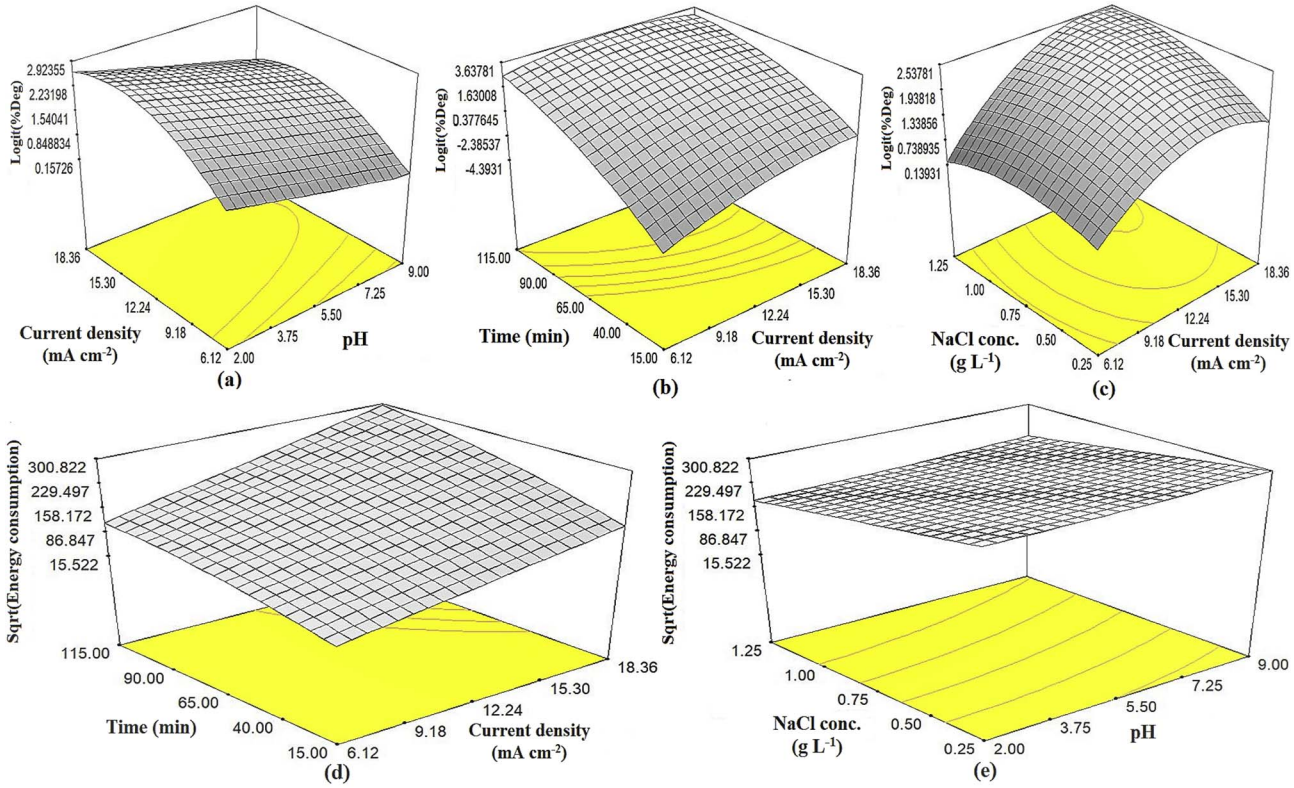

Fig. 3. 3-D response surface graph for the electro-oxidation of creatinine (a) %degradation versus pH and current density (b) %degradation versus time and current density (c) % degradation versus current density and chloride concentration (d) energy consumption versus time and current density and (e) energy consumption versus pH and chloride concentration.

mA cm^{-2}, % degradation was decreased marginally. This trend was observed at all time values. This concludes that DSA performs better oxidation at lower current densities.

3.2.3. Effect of NaCl concentration (c) on %degradation

Electrolyte concentration in EO process defines the quantity of reactive chlorine species formed during the process. Fig. 3c shows the effect of NaCl concentration and current density on % degradation. It can be observed that for current density value from 6.12 to ≈ 15.30 mA cm^{-2}, % degradation increases with increase in electrolyte concentration values. Further increase in current density value beyond 15.30 mA cm^{-2}, an increase in % degradation was observed for NaCl concentration values up to 1 g L^{-1} and then % degradation become constant for high values of NaCl concentration > 1.0 g L^{-1} showing complete degradation of the target compound. The increase in the % degradation is because of the increase in the synergistic effects of both HO· and chloro-oxidant species [62]. At the same time, high concentration of chloride values leads to the corrosion and fouling of the electrodes, thus affecting its stability. Hence, optimum dose of NaCl concentration is very important from the stability point of view. Besides this, it has been observed that DSA electrodes have proven to be very effective in promoting the direct oxidation along with mediated oxidation and hence prevents the fouling of electrodes.

3.2.4. Effect of electrolysis time on %degradation

In EO process the treatment time is an important parameter as it controls the rate of the reaction. In order to evaluate the effect of treatment time on response % degradation, time was varied from 10 to 115 min and result was shown in Fig. 3b. From the observation, it was found that with an increase in time value, % degradation increases gradually for all values of current density. Various studies also reported that during electrolysis an impermeable film generates on the surface of the electrode and hence increase the passivation on the electrode surface which in turn increases the treatment time and further decreases the process efficiency [57]. But in this case, no such problem was observed because the DSA used has the advantage of coupling both direct and mediated oxidation processes and thus, prevents the passivation of the anode during the electrolysis.

3.2.5. Effect of initial pH, current density, time and NaCl concentration on energy consumption

Energy consumption depends on the type of electrode used as well as the process parameters. From Fig. 3d it was found that with an increase in current density value the energy consumption varies directly, at all-time values. From Fig. 3e it was observed that at higher values of pH, energy consumption was found to be maximum. While NaCl concentration shows contrary effect, because at its higher concentration values the energy consumption was found to be less, this could be due to the ease of flow of current through the electrolyte solution [31].

3.3. Durability studies

In electrochemical oxidation processes, the durability study of the anode was an important factor in deciding the economy as well as the practical viability of the process towards commercial applications. In the present study, attempts have been made to check the durability of electrodes in terms of a number of recycles and degradation efficiency of creatinine. The electrodes were successfully recycled for at-least 45 cycles without any much significant loss in degradation efficiency (~8%) shown in Fig. 4. Generally at high electrolyte concentration and higher current values, life of the electrodes decreases due to fouling and passivation [31]. The reason for high robustness of the DSA electrodes in our study is due to the temperate amount of electrolyte concentration used as well as lower values of applied current. The stability of the electrodes after 45th cycle (110 h) was further confirmed through SEM/EDS and Raman spectroscopy analysis as discussed in Section 3.5.

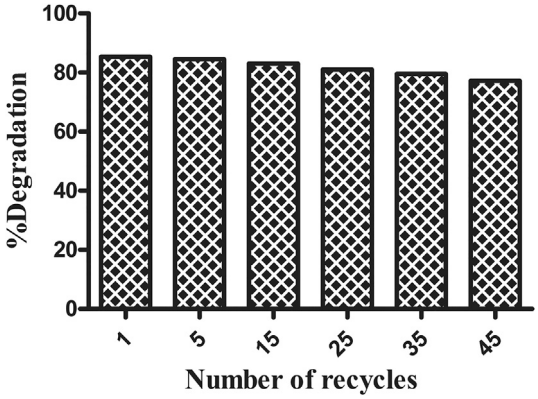

Fig. 4. Recyclability pattern of DSA electrode up-to 45 experimental runs.

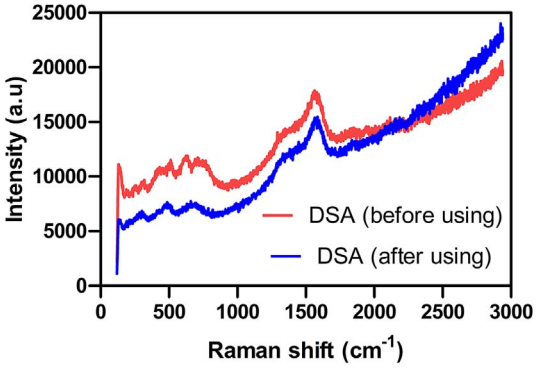

Fig. 6. Raman spectra of DSA electrodes (before and after application to Electro-oxidation process).

3.4. Characterization of DSA electrodes

SEM was performed to characterize the morphology and surface structure of the electrodes (freshly coated anode and recycled anode) respectively. As shown in Fig. 5a and b SEM image of the freshly coated anode and recycled anode shows almost similar surface characteristics. Thus indicating a uniform layer of metals even after forty-five cycles. The incorporation of Ruthenium, irridium and platinum in the metal sheet has made the structure of electrode relatively smooth, porous and uniform with minor cracks, which in turn prevents the electrode from corrosion thereby, enhancing the stability of electrode for a longer period of time [58]. The prominent peaks of all three metals i.e. Ru, Ir and Pt along with Ti and O even in recycled anode further confirms the durability and stability of electrodes after forty-five experimental runs. Further, quantitative analysis shows that the atomic concentration of various metals Ti, Ru, Ir, O, and Pt in the oxide mixture were quietly same for both the samples shown in Fig. 5a and b, thus confirming the stability of electrodes even after multiple numbers of experimental runs. In addition, the elemental mapping images as shown in Fig. 5c was obtained by analyzing the distribution of the different metal elements coated on the whole surface of titanium metal sheet. The results reveal that the distribution of Ti, Ru, O, Ir and Pt are homogeneous throughout the oxide film, but the distribution of iridium and platinum are limited.

In Fig. 6, Raman spectrum of the oxide film for both electrode samples (freshly coated anode and recycled anode) were compared in order to confirm the presence of the same respective oxide peaks. Fig. 5 shows small peaks at 133 cm^{-1} for TiO_2 [63], 525 cm^{-1} for RuO_2, 728 cm^{-1} for IrO_2 [64] and 1600 cm^{-1} for Pt [65]. Raman spectrum of recycled anode shows the same peaks like freshly coated yet somewhat moved to 520 and 751 cm^{-1} along with changed amplitude as shown in Fig. 5. From both the spectrums it can be seen that there was no change happen after utilization of DSA electrode for electrochemical oxidation treatment of creatinine even after forty-five runs. Hence, it can be concluded that the addition of Ru and Ir metals has increased the stability of the coatings for a longer period of time. Spectrophotometric studies for DSA electrode were conducted to check the valence state of metallic coatings of the purchased anode.

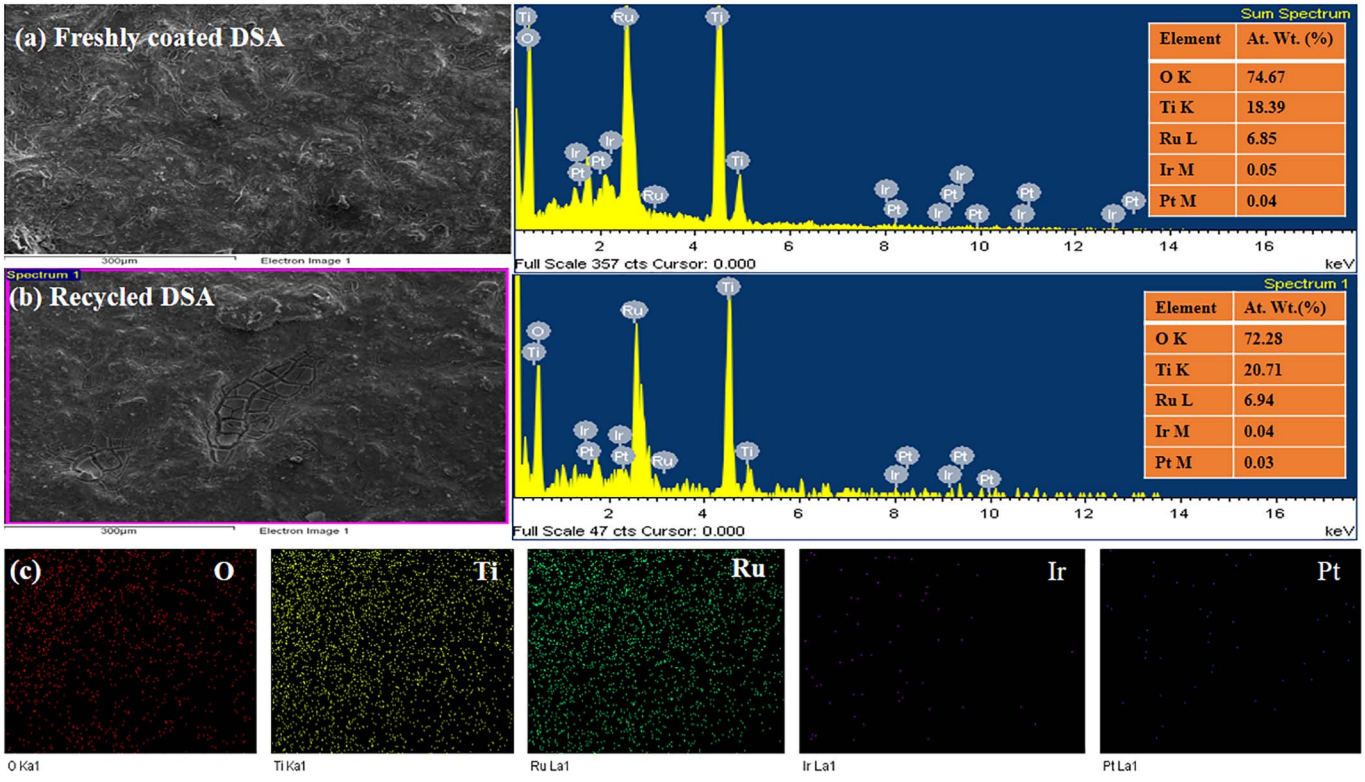

Fig. 5. SEM and EDS images (a) freshly coated sheet and (b) recycled sheet (c) EDS elemental mapping images.

Table 4
Individual and simultaneously optimization results for desirability calculations.

Response	pH	Current density (mA cm^{-2})	Time (min)	NaCl conc. (g L^{-1})	Desirability
Individual response optimization					
% Degradation = 87.98%	2.31	14.02	107.21	0.96	1.00
Energy consumption = 1109.75 kWh m^{-3}	2.39	7.35	16.22	1.22	1.00
Simultaneous optimization of responses					
% Degradation = 85.97%					
Energy consumption = 17,986.028 kWh m^{-3}	2.4	10.29	85	0.75	0.899

3.5. Optimization

In this study, the optimum conditions for the electro-oxidation treatment of creatinine were carried out through simultaneous optimization of multiple responses %degradation and energy consumption respectively. For simultaneous optimization, the process parameters were kept within range while the response % degradation was fixed as maximum and response energy consumption was fixed as minimum respectively. Table 4 shows the optimum conditions for input parameters and responses along with the corresponding desirability value for individual and simultaneously optimization. The optimum conditions for process parameters were found out to be pH = 2.4, current density = 10.29 mA cm^{-2}, time = 85 min and electrolyte concentration = 0.75 g L^{-1}. At these optimized conditions, the value of responses %degradation and energy consumption proposed by BBD were 85.97% and 17,986.028 kWh/m^3along with overall desirability, D = 0.899. In order to confirm the adequacy of the developed model, actual experiments were performed at these optimized conditions. The values of responses at these optimum conditions were found out to be 85.41% and 16,826.875 kWh/cm^3 respectively, which came out to be very close to the predicted values as shown in Table 5. During electrolysis, due to the generation of various oxidant species like ($HO^{\cdot}$, H_2O_2, $HO_2^{\cdot}$ HOCl, and OCl^-) at optimized conditions, concludes that both direct and indirect oxidation mechanisms were responsible for the degradation of creatinine. The PEC was also conducted at optimized conditions to observe the synergistic effect of dual effect (EO + PC) for the degradation of creatinine. The treatment time was further reduced to 60mins with the dual process, thus proving the effectiveness of dual process over individual processes respectively. Actually, the process would lead to activation of TiO_2 coating on DSA under UV irradiation, leading to the generation of more hydroxyl radicals which subsequently reduce the treatment time. During this dual process, the recombination of electrons and holes was inhibited by taking away the photo-generated electrons towards cathode via external circuit leaving behind photogenerated holes or $OH^{\cdot}$ at the surface of the anode which subsequently attacks the pollutant and degrades it [34].

3.6. Mineralization studies

In order to check the quality of treated effluent, samples were analyzed for identification of latter transformed products through various techniques like UV–vis, FTIR, COD, TOC, inorganic ions(NO_3^-, NO_2^- and NH_4^{+}) and LC-MS analysis. Fig. 7 shows the UV–vis spectrophotometer results for untreated and treated samples after 85mins of treatment time. From results, it can be concluded that the initial value

Table 5
Comparison between predicted and actual experimental value at optimized conditions suggested by BBD.

Responses	Predicted	Actual experimental value
% Degradation	85.97%	85.41%
Energy consumption	17,986.028 kWh m^{-3}	16,826.875 kWh m^{-3}

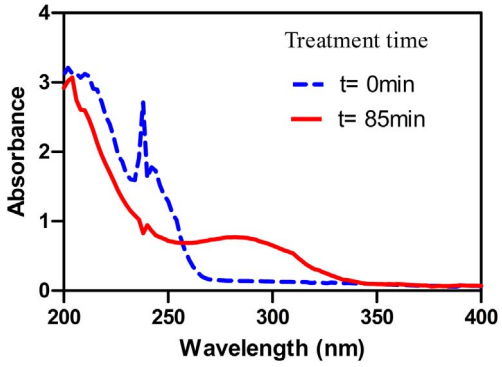

Fig. 7. UV–visible spectra of treated and untreated creatinine at optimized parameters (pH-2.4, current density-10.29 mA cm^{-2}, NaCl concentration-0.75 g L^{-1} and treatment time- 85 min).

of absorbance for pure creatinine got changed during the electrolytic treatment and some other peaks were seems to be formed at different lambda max at different time intervals. This change in the lambda max confirms the formation and destruction of various unstable intermediate byproducts through oxidant species such as $HO^{\cdot}$, $HO_2\cdot$, and HOCl which were generated in-situ during the EO process [48,66].

To examine the phenomenon of creatinine removal from aqueous solution through the electro-oxidation process, FT-IR was performed under optimal conditions. Fig. 8 shows the FT-IR spectra of creatinine samples at different time intervals. The peaks at 1671.23, 1036.00 and 607.36 cm^{-1} accounts for –C═O stretch. A broad peak at 3252.44 cm^{-1} and intense peak at 1590.51 cm^{-1} shows the presence of N—H and peak at 1330.25 cm^{-1} indicate the presence of C—N group. Other peaks were also observed at 2800–3100 cm^{-1} and 600–800 cm^{-1} were accounts for C—H (stretch and bending). Some other small peaks were also observed in the fingerprint region of raw creatinine sample (t = 0 min) which got disappeared completely during the electrolysis process. Broad and sharp peaks at 3400 cm^{-1} and 1600 cm^{-1} were formed (t > = 15 min) due to OH radical generation as well as due to- C═O stretching of intermediates formed during EO process [48]. The peaks at 1100–800 cm^{-1} (t > 45 min) were formed

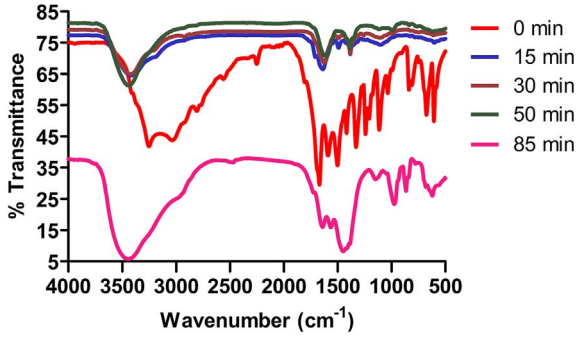

Fig. 8. FT-IR spectra of treated creatinine at different time intervals at optimized parameters (pH-2.4, current density-10.29 mA cm^{-2} and NaCl concentration-0.75 g L^{-1}).

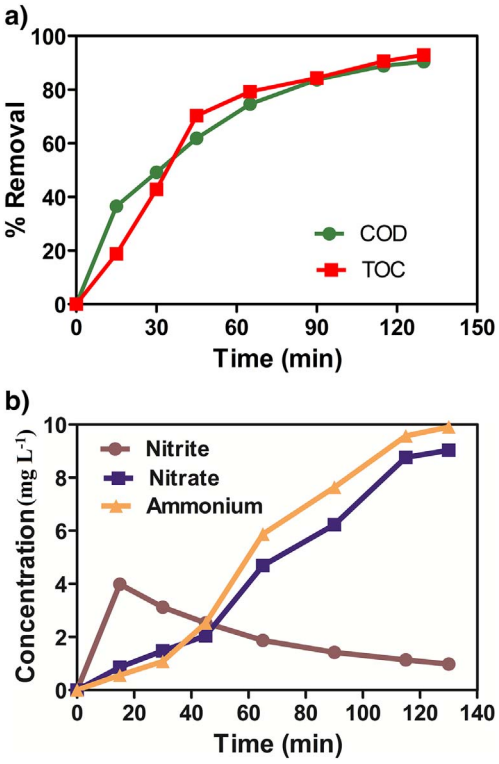

Fig. 9. (a) Percentage of COD and TOC removal with time during electrolysis of creatinine at optimized parameters (pH-2.4, current density-10.29 mA cm^{-2} and NaCl concentration-0.75 g L^{-1}).
(b) Nitrite, nitrate and ammonium ions concentration (mg L^{-1}) during electrolysis of creatinine at optimized parameters (pH-2.4, current density-10.29 mA cm^{-2} and NaCl concentration-0.75 g L^{-1}).
(c) Proposed degradation pathway for creatinine.

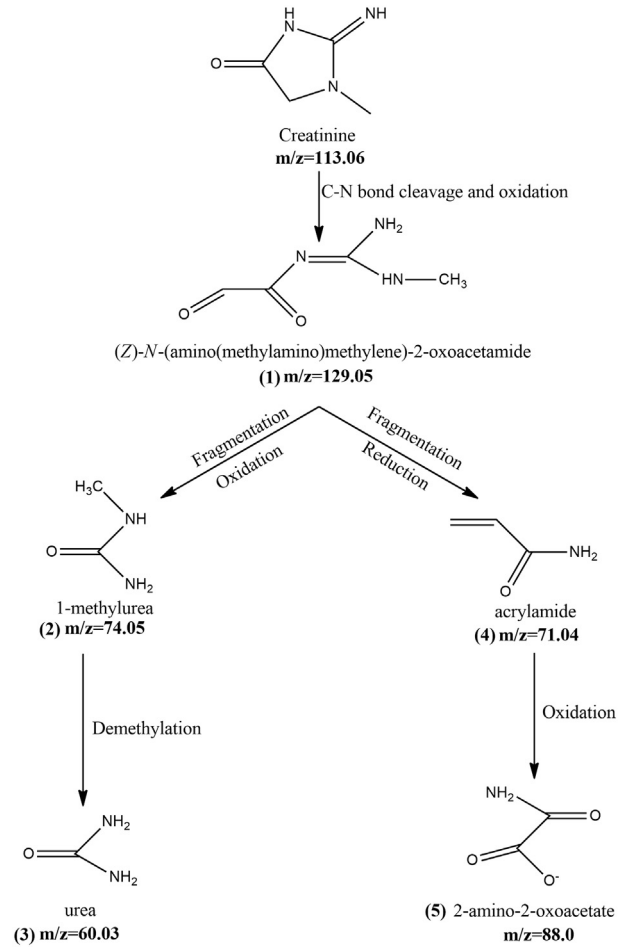

Fig. 9. (*continued*)

which accounts for chloride inorganic anion, normally present in hypochlorite solution [52].During EO treatment of creatinine, shifting of peaks was observed because of the breaking of the bonds at particular wavenumber. In addition to this, an increase in the % transmittance was observed for most of the peaks after electrolysis, indicates the complete oxidation of cyclic structure of creatinine.

The mineralization of creatinine by EO process was confirmed in the study through a reduction in COD and TOC along with generation of ions like nitrite, nitrate and ammonium ion. Around 80% removal in COD and TOC were attained in 85mins at optimized conditions be pH = 2.4, current density = 10.29 mA $cm^{-2}$and electrolyte concentration = 0.75 g L^{-1} which reached to > 90% when the reaction was extended to 130 min as shown in Fig. 9a. An increasing trend was observed for the generated nitrate and ammonium ions while in the case of nitrite, ion concentration started decreasing after 20 min of treatment time as shown in Fig. 9b. This could be possible due to the conversion of nitrite ion into nitrate ions as reported in the literature [6]. During EO treatment of creatinine, the intermediates formed were identified through LC-MS analysis (Supplementary Information, S1). Based on these intermediates (1–5), a degradation pathway has been proposed as shown in Fig. 9c. The cleavage of C—N bond followed by oxidation of the target pollutant led to the formation of intermediate (1). While the fragmentation of (1) followed by oxidation and reduction could lead to the generation of (2) and (4) respectively. Removal of a methyl group from (2) could ultimately lead to the production of urea (3). Whereas, further oxidation of (4) could possibly form (5). Similar kind of products (3 and 5) has been reported in the literature [4].

4. Conclusion

EO removal of creatinine through titanium based DSA has been studied successfully using BBD for parametric optimization. The optimal process parameters for obtaining the maximum degradation were found to be pH ≈ 2.4, current density ≈ 10.29 mA cm^{-2}, time ≈ 85 min and electrolyte concentration ≈ 0.75 g L^{-1}. Multi-response optimization by desirability function was found to be useful for simultaneous maximization of % degradation and minimization of energy consumption. Actual experimental values for responses % degradation and energy consumption were found to be very close to the predicted values at optimized conditions. The degradation of creatinine was found to be maximum because of the involvement of both mechanisms, direct and indirect processes. Primarily, due to the generation of $OH^{\cdot}$ and chloro-oxidant species like HOCl, ClO and partially due to the involvement of other electrochemically generated oxidants such as H_2O_2 and $HO_2\cdot$. More than 90% reduction in COD and TOC values were achieved when the reaction was further extended to 130 min. Organic and inorganic intermediates formed at the different time of the treatment were confirmed FT-IR and LC-MS analysis. Based on these intermediates the oxidative degradation pathway of creatinine has been proposed in the study. Characterization results obtained from SEM, EDS and Raman spectroscopy has confirmed the stability and potency of DSA electrodes for effective degradation of creatinine even after forty-five cycles of the experimental run. Results indicate the efficiency of EO process as a promising technique for eco-sanitation applications in developing for the on-site treatment of human urine.

Supplementary data to this article can be found online at https://doi.org/10.1016/j.jelechem.2017.12.061.

References

[1] M.K. Elham, V. Azimirad, M. Bahrami, A. Ganbari, A review on creatinine measurement techniques, Talanta 97 (2012) 1–8.
[2] M.T. Alula, J. Yang, Photochemical decoration of magnetic composites with silver nanostructures for determination of creatinine in urine by surface-enhanced Raman spectroscopy, Talanta 130 (2014) 55–62.
[3] C.S. Pundir, S. Yadav, A. Kumar, Creatinine sensors, Trends Anal. Chem. 50 (2013) 42–52.
[4] M.G. Antoniou, U. Nambiar, D.D. Dionysiou, Investigation of the photocatalytic degradation pathway of the urine metabolite, creatinine: the effect of pH, Water Res. 43 (2009) 3956–3963.
[5] S. Dbira, N. Bensalah, A. Bedoui, P. Cañizares, M.A. Rodrigo, Treatment of synthetic urine by electrochemical oxidation using conductive-diamond anodes, Environ. Sci. Pollut. Res. 22 (2015) 6176–6184.
[6] M.G. Antoniou, D.D. Dionysios, Application of immobilized titanium dioxide photocatalysts for the degradation of creatinine and phenol, model organic contaminants found in NASA's spacecraft wastewater streams, Catal. Today 124 (2007) 215–223.
[7] X. Liu, M. Chen, Z. Bian, C.C. Liu, Studies on urine treatment by biological purification using Azolla and UV photocatalytic oxidation, Adv. Space Res. 41 (2008) 783–786.
[8] R. Zhang, P. Sun, H.B. Treavor, L. Zhao, C.H. Huang, Degradation of pharmaceuticals and metabolite in synthetic human urine by UV, UV/H_2O_2, and UV/PDS, Environ. Sci. Technol. 49 (2015) 3056–3066.
[9] I. Sirés, E. Brillas, M.A. Oturan, M.A. Rodrigo, M. Panizza, Electrochemical advanced oxidation processes: today and tomorrow. A review, Environ. Sci. Pollut. Res. 21 (2014) 8336–8367.
[10] B.P. Chaplin, A critical review of electrochemical advanced oxidation processes for water treatment applications, Environ. Sci. Process Impacts. 16 (2014) 1182–1203.
[11] Q. Zhuo, S. Deng, B. Yang, J. Huang, G. Yu, Efficient electrochemical oxidation of perfluorooctanoate using a Ti/SnO_2-Sb-Bi anode, Environ. Sci. Technol. 45 (2011) 2973–2979.
[12] O.P. Sahu, P.K. Chaudhari, Electrochemical treatment of sugar industry wastewater: COD and color removal, J. Electroanal. Chem. 739 (2015) 122–129.
[13] C. Zhang, Y. Jiang, Y. Li, Z. Hu, L. Zhou, M. Zhou, Three-dimensional electrochemical process for wastewater treatment: a general review, J. Chem. Eng. 228 (2013) 455–467.
[14] W. Wu, Z.H. Huang, T.T. Lim, The recent development of mixed metal oxide anodes for electrochemical oxidation of organic pollutants in water, Appl. Catal. A: General. 480 (2014) 58–78.
[15] D. Rajkumar, J.G. Kim, Oxidation of various reactive dyes with in situ electrogenerated active chlorine for textile dyeing industry wastewater treatment, J. Hazard. Mater. 136 (2006) 203–212.
[16] S. Raghu, C.W. Lee, Chellammal, S. Palanichamy, C.A. Basha, Evaluation of electrochemical oxidation techniques for degradation of dye effluents—a comparative approach, J. Hazard. Mater. 171 (2009) 748–754.
[17] S.A. Neto, A.R.D. Andrade, Electrochemical degradation of glyphosate formulations at DSA® anodes in chloride medium: an AOX formation study, J. Appl. Electrochem. 39 (2009) 1863–1870.
[18] G.R.P. Malpass, G.R. Salazar-Banda, D.W. Miwa, S.A.S. Machado, A.J. Motheo, Comparing atrazine and cyanuric acid electro-oxidation on mixed oxide and boron-doped diamond electrodes, Environ. Technol. 34 (2013) 1043–1051.
[19] H. Wang, J.L. Wang, The cooperative electrochemical oxidation of chlorophenols in anode-cathode compartments, J. Hazard. Mater. 154 (2008) 44–50.
[20] W. Cheng, M. Yang, Y. Xie, B. Liang, Z. Fang, E.P. Tsang, Enhancement of mineralization of metronidazole by the electro-Fenton process with a Ce/SnO_2–Sb coated titanium anode, Chem. Eng. J. 220 (2013) 214–220.
[21] D. Santos, M.J. Pacheco, A. Gomes, A. Lopes, L. Ciríaco, Preparation of Ti/Pt/SnO_2–Sb_2O_4 electrodes for anodic oxidation of pharmaceutical drugs, J. Appl. Electrochem. 43 (2013) 407–416.
[22] H. Wang, D.Z. Sun, Z.Y. Bian, Degradation mechanism of diethyl phthalate with electrogenerated hydroxyl radical on a Pd/C gas-diffusion electrode, J. Hazard. Mater. 180 (2010) 710–715.
[23] L. Shao, P. He, J. Xue, G. Li, Electrolytic degradation of biorefractory organics and ammonia in leachate from bioreactor landfill, Water Sci. Technol. 53 (2006) 143–150.
[24] H.X. Shi, J.H. Qu, A.M. Wang, J.T. Ge, Degradation of microcystins in aqueous solution with in-situ electrogenerated active chlorine, Chemosphere 60 (2005) 326–333.
[25] G. Chen, Electrochemical technologies in wastewater treatment, Sep. Purif. Technol. 38 (2004) 11–41.
[26] O. Scialdone, Electrochemical oxidation of organic pollutants in water at metal oxide electrodes: a simple theoretical model including direct and indirect oxidation processes at the anodic surface, Electrochim. Acta 54 (2009) 6140–6147.
[27] M. Ikematsu, K.K.M. Iseki, M. Yasuda, Electrochemical treatment of human urine for its storage and reuse as flush water, Sci. Total Environ. 382 (2007) 159–164.
[28] H. Li, Q. Yu, B. Yang, Z. Li, L. Lei, Electro-catalytic oxidation of artificial human urine by using BDD and IrO 2 electrodes, J. Electroanal. Chem. 738 (2015) 14–19.
[29] S. Dbira, N. Bensalah, P. Cañizares, M.A. Rodrigo, A. Bedoui, The electrolytic treatment of synthetic urine using DSA electrodes, J. Electroanal. Chem. 744 (2015) 62–68.
[30] B.J. Hernlem, Electrolytic destruction of urea in dilute chloride solution using DSA electrodes in a recycled batch cell, Water Res. 39 (2005) 2245–2252.
[31] J. Singla, A. Kumar, V.K. Sangal, Performance and evaluation of electro-oxidation treatment of human urine metabolite uric acid using response surface methodology, J. Electrochem. Soc. 164 (2017) 312–320.
[32] W. Simka, J. Piotrowski, G. Nawrat, Influence of anode material on electrochemical decomposition of urea, Electrochim. Acta 52 (2007) 5696–5703.
[33] W. Simka, J. Piotrowski, A. Robak, G. Nawrat, Electrochemical treatment of aqueous solutions containing urea, J. Appl. Electrochem. 39 (2009) 1137–1143.
[34] R. Daghrir, P. Drogui, D. Robert, Photoelectrocatalytic technologies for environmental applications, J. Photochem. Photobiol. A Chem. 238 (2012) 41–52.
[35] Y. Xu, D. Zhong, J. Jia, 2nd International Conference on Bioinformatics and Biomedical Engineering, (2008), pp. 3696–3699.
[36] X.Z. Li, B.X. Zhao, P. Wang, Degradation of 2, 4-dichlorophenol in aqueous solution by a hybrid oxidation process, J. Hazard. Mater. 147 (2007) 281–287.
[37] H. Selcuk, J.J. Sene, M.A. Anderson, Photoelectrocatalytic humic acid degradation kinetics and effect of pH applied potential and inorganic ions, J. Chem. Technol. Biotechnol. 78 (2003) 979–984.
[38] N. Philippidis, E. Nikolakaki, S. Sotiropoulos, I. Poulios, Photoelectrocatalytic inactivation of *E. coli* XL-1 blue colonies in water, J. Chem. Technol. Biotechnol. 85 (2010) 1054–1060.
[39] American Health Public Association (APHA), Standard Methods for the Examination of Water and Wastewater. 19th ed., Standard Method No. (18th Edition), APHA, 5220-C, Washington, DC, 1992.
[40] American Health Public Association (APHA), Standard Methods for the Examination of Water and Wastewater. 17th ed., Standard Method No. 4500-NO_2^- (B), APHA, Washington, DC, 1989.
[41] American Health Public Association (APHA), Standard Methods for the Examination of Water and Wastewater. 17th ed., Standard Method No. 4500-NO_3^- (E), APHA, Washington, DC, 1989.
[42] American Health Public Association (APHA), Standard Methods for the Examination of Water and Wastewater. 17th ed., Standard Method No. 4500-NH_4^+ (C), APHA, Washington, DC, 1989.
[43] A. Garg, V.K. Sangal, P.K. Bajpai, Decolorization and degradation of Reactive Black 5 dye by photocatalysis: modeling, optimization and kinetic study, Desalin. Water Treat. 57 (2016) 18003–18015.
[44] P. Singh, A. Dhir, V.K. Sangal, Optimization of photocatalytic process parameters for the degradation of acrylonitrile using Box Behnken Design, Desalin. Water Treat. 55 (2015) 1501–1508.
[45] V.K. Sangal, V. Kumar, I.M. Mishra, Optimization of structural and operational variables for the energy efficiency of a divided wall distillation column, Comput. Chem. Eng. 40 (2012) 33–40.
[46] M. Bhaskar, V.C. Srivastava, J.P. Kushwaha, R. Bhatnagar, S. Singh, I.D. Mall, Parametric and multiple response optimizations for the electrochemical treatment of textile printing dye-bath effluent, Sep. Purif. Technol. 109 (2013) 135–143.
[47] V.K. Sangal, V. Kumar, I.M. Mishra, Process parametric optimization of a divided wall distillation column, Chem. Eng. Commun. 201 (2014) 72–87.
[48] A.D. Hiwarkar, S. Singh, V.C. Srivastava, I.D. Mall, Mineralization of pyrrole, a recalcitrant heterocyclic compound, by the electrochemical method: multi-response optimization and degradation mechanism, J. Environ. Manag. 198 (2017) 144–152.
[49] P. Kaur, V.K. Sangal, J.P. Kushwaha, Modeling and evaluation of electro-oxidation of dye wastewater using artificial neural networks, RSC Adv. 5 (2015) 34663–34671.
[50] K. Thirugnanasambandham, V. Sivakumar, J.P. Maran, Response surface modeling and optimization of treatment of meat industry wastewater using electrochemical treatment method, J. Taiwan Inst. Chem. Eng. 46 (2015) 160–167.
[51] H. Zhang, X. Ran, X. Wu, D. Zhang, Evaluation of electro-oxidation of biologically treated landfill leachate using response surface methodology, J. Hazard. Mater. 188 (2011) 261–268.
[52] K. Rajkumar, M. Muthukumar, Optimization of an electro-oxidation process for the treatment of Reactive Orange 107 using response surface methodology, Environ. Sci. Pollut. Res. 19 (2012) 148–160.
[53] P. Asaithambi, M. Matheswaran, Electrochemical treatment of simulated sugar industrial effluent: optimization and modeling using a response surface methodology, Arab. J. Chem. 9 (2016) 981–987.
[54] P. Kaur, A.P. Singh, A.K. Prince, J.P. Kushwaha, Optimization and evaluation of CBSOL LE red wool dye adsorption from aqueous solution onto commercial activated carbon, Int. J. Environ. Sci. Technol. 12 (2015) 3755–3766.
[55] V.S. Jagati, V.C. Srivastava, B. Prasad, Multi-response optimization of parameters for the electrocoagulation treatment of electroplating wash-water using aluminum electrodes, Sep. Sci. Technol. 50 (2015) 181–190.
[56] V.K. Sangal, V. Kumar, I.M. Mishra, Optimization of a divided wall column for the separation of C4-C6 normal paraffin mixture using Box-Behnken design, Chem. Ind. Chem. Eng. Q. 19 (2013) 107–119.
[57] S. Singh, S. Singh, S.L. Lo, N. Kumar, Electrochemical treatment of Ayurveda pharmaceuticals wastewater: optimization and characterization of sludge residue, J. Taiwan Inst. Chem. Eng. 67 (2016) 385–396.
[58] A. Kumar, B. Prasad, I.M. Mishra, Process parametric study for ethene carboxylic acid removal onto powder activated carbon using Box-Behnken design, Chem. Eng. Technol. 30 (2017) 932–937.
[59] C. Barrera-Diaz, P. Canizares, F.J. Fernandez, R. Natividad, M.A. Rodrigo, Electrochemical advanced oxidation processes: an overview of the current applications to actual industrial effluents, J. Mex. Chem. Soc. 58 (2014) 256–275.
[60] S. Dbira, N. Bensalah, A. Bedoui, Mechanism and kinetics of electrochemical degradation of uric acid using conductive-diamond anodes, Environ. Technol. 3 (2016) 2993–3001.
[61] A. Singh, A. Kumar, P. Bansal, J. Singla, Evaluation of the process parameters for electro fenton and electro chlorination treatment of reactive black 5 (RB5) dye, J. Electrochem. Soc. 164 (2017) 203–212.

[62] A. Yaqub, M.H. Isa, H. Ajab, Electrochemical degradation of polycyclic aromatic hydrocarbons in synthetic solution and produced water using a Ti/SnO_2-Sb_2O_5-RuO_2 anode, J. Environ. Eng. 141 (2014) 04014074.
[63] N. Lagopati, E.P. Tsilibary, P. Falaras, P. Papazafiri, E.A. Pavlatou, E. Kotsopoulou, P. Kitsiou, Effect of nanostructured TiO_2 crystal phase on photo-induced apoptosis of breast cancer epithelial cells, Int. J. Nanomedicine 9 (2014) 3219–3230.
[64] A.V. Korotcov, Y.S. Huang, K.K. Tiong, D.S. Tsai, Raman scattering characterization of well-aligned RuO_2 and IrO_2 nanocrystals, J. Raman Spectrosc. 38 (2007) 737–749.
[65] N.B. Singh, U. Sarkar, Structure, vibrational, and optical properties of the platinum cluster: a density functional theory approach, J. Mol. Model. 20 (2014) 2537–2548.
[66] P. Kaur, J.P. Kushwaha, V.K. Sangal, Evaluation and dispensability study of actual textile wastewater treatment by an electro-oxidation method using Ti/RuO_2 anode, Process. Saf. Environ. Prot. 111 (2017) 13–22.

Process Safety and Environmental Protection 130 (2019) 197–208

Contents lists available at ScienceDirect

Process Safety and Environmental Protection

journal homepage: www.elsevier.com/locate/psep

Evaluation and optimization of the process parameters for the photo-electrochemical treatment of urea using mixed metal oxide anodes

Jayishnu Singla [a], Vikas K. Sangal [b,*], Anoop Verma [a,*]

[a] School of Energy and Environment, Thapar Institute of Engineering and Technology, Patiala, Punjab, India
[b] Department of Chemical Engineering, Malaviya National Institute of Technology, Jaipur, Rajasthan, India

ARTICLE INFO

Article history:
Received 21 June 2019
Received in revised form 4 August 2019
Accepted 19 August 2019
Available online 21 August 2019

Keywords:
Electro-oxidation
Urea
Mixed metal oxide
Energy consumed
Box-Behnken design
Optimization

ABSTRACT

The present study investigates the electro-oxidation (EO) treatment of urea containing wastewater using mixed metal oxide (MMO) anodes. Box-Behnken design (BBD) was employed to analyze the effects of various operational process parameters like current density (j), NaCl dose (n), treatment time (t) and pH in an EO reactor in batch mode. The performance of the treatment process was evaluated in terms of % degradation and energy consumption. Under optimum conditions, the experimental results showed that more than 94.78% of degradation of urea was achieved. Electro-oxidation has effectively reduced the TOC (90%) under optimum conditions. Attempts were made to integrate the two process electro-oxidation and photocatalysis i.e. Photoelectrocatalysis within the same treatment unit for the enhanced degradation of target pollutant. The electro-oxidation process with mixed metal oxide anode has also attained a significant removal of nitrogen by transforming into the NO_3^- and NH_4^+ through the formation of $OH^\bullet$ and reactive chlorine species. Characterization techniques like SEM-EDX and XRD have confirmed the durability of mixed metal oxide anodes even after 90 recycles of the experimental run. The total operating cost for electro-oxidation treatment of urea under optimized conditions is found to be 0.78 $/m^3.

1. Introduction

Lack of proper sanitation along with rampant agriculture activities in developing countries like India had led to inflated concentrations of nitrogen in surface water, groundwater and rivers (Amin et al., 2017). A recent study has shown that in India more than 20 million ton of urea, which is a potential source of nitrogen, was used for the agriculture activities and apparently it has put indirect and direct potential ill effects on human health as well as on aquatic life (Yadav and Pandey, 2017). Apart from this, many industries like pharmaceuticals, chemical industry, fertilizer companies, etc are adding woes to the concern of pollution in water due to continuous discharge of nitrogen-based components during the manufacturing of chemicals and treatment of wastewater. Thus, causing serious health problems as well as increasing the biological oxygen demand (BOD) of surface and ground waters (Gupta et al., 2017). Combined agriculture and open defecation contribute more than 70% of the total nitrogen nuisance in terms of urea discharge in rivers (Showkat, 2016).

Urea, known as carbamide, is an organic compound which plays an essential role in the living organisms. It participates in the biological processes and metabolic pathways such as protein decomposition (Urbańczyk et al., 2016). It is colorless, highly soluble in water, odorless and non-toxic compound. In spite of its low toxicity, its continuous discharge in the streams from sources like toilet wastewater (contains 9 to 24 gm L^{-1}), industries, and fertilizers waste leads to the excessive N-loading in surface water and cause algal blooming leaving adverse effects on the ecosystem as well as human well-being (Cho and Hoffmann, 2014). Moreover, its readily automatic conversion to ammonia via enzymatic hydrolyzes by urease leads to the serious environmental and health problems such as an increase in the pH of the soil and release of free ammonia into the atmosphere contributing toxic compounds like ammonium, nitrates, and sulfates (Yan et al., 2012).

The technical feasibility of conventional processes like adsorption, biological decomposition, enzymatic decomposition, and chemical oxidation is still under debate (Amstutz et al., 2012; Cataldo Hernández et al., 2014). With the variable sources of contamination, there is a requirement for effective on-site treatment

* Corresponding authors.
E-mail addresses: vksangal.chem@mnit.ac.in (V.K. Sangal), anoop.kumar@thapar.edu (A. Verma).

https://doi.org/10.1016/j.psep.2019.08.017
0957-5820/

of urea-rich wastewater for removing the nitrogen loading as well as avoiding the issues came from the storage of toilet wastewater (Maurer et al., 2006).

In recent years, the electrochemical oxidation (EO) process has shown promising results for the treatment of the different types of bio refractory organic pollutants which are not amenable to the conventional biological treatment technologies (Barrera-Díaz et al., 2017). For instance, the nitrogen removal through biological processes for urea treatment may have hydraulic retention time up to a few days while electrochemical treatment can execute the removal within a few hours (Cho and Hoffmann, 2014). It is a technique based on the transfer of electrons, with inherent advantages of high energy efficiency, compatible, amenability to automation, easy handling and safe as they operate under mild conditions. Same time it is versatile with a wide range of applications to treat bio-recalcitrant compounds and a variety of effluents (Sirés et al., 2014).

A few studies have reported the EO treatment of urea because of its complex removal mechanism, which depends on several factors such as pH, the concentration of electrolyte, applied current and type of electrode used (Mahmoud et al., 2013). Several researchers have tested different electrodes such as glassy carbon, Ti/Ir, Ti/RuO_2, Ti/Pt, boron-doped diamond (BDD), Ni/Ni(OH_2), PbO_2, graphite, etc. for the removal of urea in presence of chloride (Cataldo Hernández et al., 2014; Simka et al., 2007; Osetrova and Skundin, 2002). Although successful, yet the problem of dissolution of Pb, low stability of Ni, deactivation of Pt anodes at high applied potentials, the formation of hydrazine on Ir anode and production of chlorates, perchlorates on BDD during the treatment process (Bergmann et al., 2009). Moreover, the high cost of BDD anodes made their pilot-scale applications impractical. Hence, prompted the scientist to work with cost-effective mixed metal oxides (MMO) anodes.

MMO has exhibited a wide variety of applications for the treatment of dyes, pesticides, phenols, pharmaceuticals, landfill leachate and even real wastewaters (Wu et al., 2014; Zöllig et al., 2015; Isarain-Chávez et al., 2017; Gurung et al., 2018). These anodes are electrochemically stable, cheap, efficient and having good electrocatalytic properties in terms of anodically generated reactive chloro-oxidant species such as (Cl_2, HOCl, ClO^-, $Cl^•$) which likely to cause complete degradation of pollutants (Subba Rao and Venkatarangaiah, 2014).

In this experimental study, Ti/Ir/Ru/Pt (ternary) MMO anode was chosen for EO treatment of urea. This novel combination of different metal oxides was incorporated on titanium anodes in order to have a more electro-active surface area (more active sites), better stability in acidic solutions as well as a high temperature, good resistance properties, durable enough at high anodic potentials and electrochemically effective even at lower current densities (Singla et al., 2017). Through this study, authors claim the novelty in terms of first-time use of ternary anodes for urea treatment.

The present study aims to understand the EO mechanism of urea by identifying the optimal relationship between initial chloride content and applied current density. Box-Behnken design (BBD) was applied to design the experiments and to evaluate the inter-parametric relation among different input process parameters such as NaCl dose (n), pH, applied current density (j) and treatment time (t) as well as their effect on % degradation (Q_1) and energy consumed (Q_2). Further, the durability and stability of novel anodes were studied through different characterization techniques such as XRD and SEM-EDS. Fourier transformed infrared spectroscopy (FTIR), cyclic voltammetry (CV), total organic carbon (TOC), total available chlorine (TAC), total nitrogen along with an examination of inorganic ions (i.e., Cl^-, NO_3^- and NH_4^+ ions) were used to analyze the quality of treated effluent.

2. Materials and methods

2.1. Materials

All chemicals used in the present study were analytical grade. Urea (CH_4N_2O) with (>99% purity) was procured from Sigma-Aldrich. Sodium sulfate, Na_2SO_4 and sodium chloride, NaCl were supplied from Loba Chemie, India. H_2SO_4 (0.1 N) and NaOH (0.1 N) used for initial pH adjustments were obtained from SD Fine Chemicals Ltd. (India). The solutions were prepared with double-distilled at 25 °C and collected through a Millipore Milli-Q system.

2.2. Experimental setup

The EO batch reactor (Fig. 1a) was used in the present study for the treatment of urea (2 g L^{-1}) with a working volume of 400 mL. MMO (as an anode) and stainless steel (as a cathode) with dimensions (70 mm *70 mm *1 mm) and total effective surface area of 42 cm^2 (20 mm inter-electrode spacing) was used for each experimental run. The current density desired for each experimental run was maintained constant by the digital current power supply (5 A, 30 V).

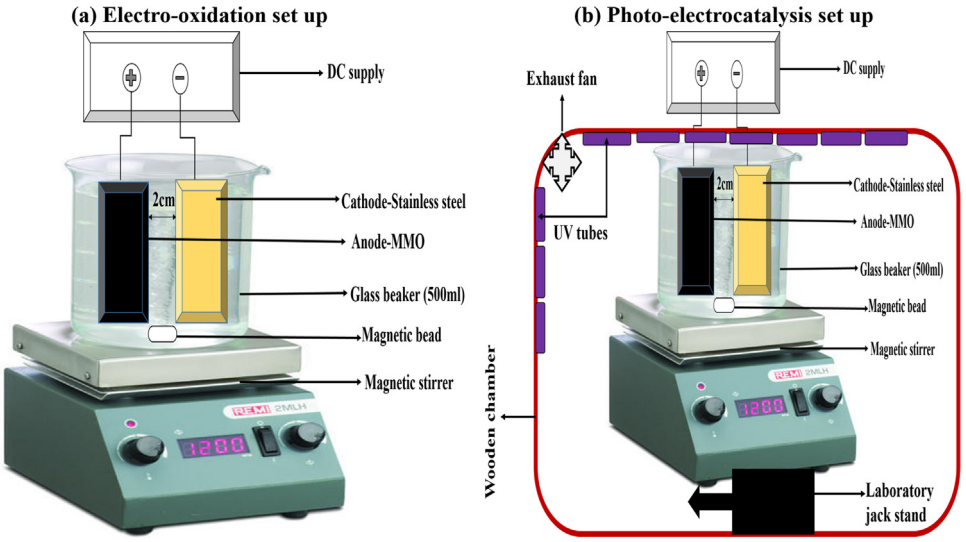

Fig. 1. Schematic diagram of the experimental setup used for the treatment of urea (a) electro-oxidation and (b) photoelectrocatalysis.

Table 1
Range of choose variables for electro-oxidation treatment of urea and their levels.

	Variables	Range of actual and coded variables		
		−1	0	+1
X_1	Current Density (mA cm^{-2})	9.52	19.04	28.57
X_2	NaCl dose (g L^{-1})	0.5	1.13	1.75
X_3	Time (min)	60	120	180
X_4	pH	3	6	9

Table 2
BBD matrix and their experimental results.

Std	Run	Block	Current density (mA cm^{-2})	NaCl dose (g L^{-1})	Time (min)	pH	% Degradation	Energy consumption (kWhr m^{-3})
4	1	1	28.57	1.75	120	6	65	37.2
9	2	1	19.05	1.13	120	6	82	22.4
7	3	1	19.05	1.13	60	9	20	11.86
3	4	1	9.52	1.75	120	6	26	6.76
2	5	1	28.57	0.50	120	6	17	49.92
5	6	1	19.05	1.13	60	3	52	11
8	7	1	19.05	1.13	180	9	46	34.97
10	8	1	19.05	1.13	120	6	82	22.4
1	9	1	9.52	0.50	120	6	15	7.96
6	10	1	19.05	1.13	180	3	98	31.8
15	11	2	19.05	0.50	60	6	19	13.06
13	12	2	9.52	1.13	120	9	23	8.44
18	13	2	19.05	1.75	180	6	76	30
20	14	2	19.05	1.13	120	6	82	22.4
12	15	2	28.57	1.13	120	3	73	43.68
11	16	2	9.52	1.13	120	3	39	6.8
14	17	2	28.57	1.13	120	9	30	46.32
19	18	2	19.05	1.13	120	6	82	22.4
17	19	2	19.05	0.50	180	6	59	37.8
16	20	2	19.05	1.75	60	6	37	10.4
29	21	3	19.05	1.13	120	6	82	22.4
23	22	3	9.52	1.13	180	6	41	10.52
30	23	3	19.05	1.13	120	6	82	22.4
28	24	3	19.05	1.75	120	9	35	21.52
25	25	3	19.05	0.50	120	3	56	25.28
21	26	3	9.52	1.13	60	6	11.5	3.63
24	27	3	28.57	1.13	180	6	62	65.7
22	28	3	28.57	1.13	60	6	22	22.5
26	29	3	19.05	1.75	120	3	88	19.6
27	30	3	19.05	0.50	120	9	28	26.72

For each experimental run, the electrolytic solution in a reactor was mixed homogeneously by a magnetic stirrer at 600 rpm.

For photo-electrocatalysis, the EO reactor (mentioned above) has been placed in a fabricated wooden chamber. However, the DC supply was placed outside the chamber for safety purposes. The chamber contains 10 UV tubes, out of which 7 tubes (Philips) of 36 W (365 nm) were attached beneath of the top roof while other 3 UV tubes of 18 W (365 nm) attached to the one sidewall of the wooden chamber and aligned horizontally as shown in Fig. 1b. The experiments under UV light were executed at a UV intensity of 23 ± 2 W m^{-2} measured by a radiometer (Eppley; model no. 33,013). For getting the appropriate intensity of UV light throughout the reaction, the distance of the EO reactor was fixed from the tubes accordingly.

2.3. Electro-oxidation experiments

Electrochemical decomposition of urea was performed under galvanostatic conditions. The pH of urea wastewater was adjusted with NaOH (0.1 N) and H_2SO_4 (0.1 N) solution as per the requirement for a particular experimental run. For improving the conductivity of the urea wastewater sample, necessitate an amount of Na_2SO_4 (1 g L^{-1}) was added. The chemical analysis was carried out periodically by withdrawing a sample volume of 1 mL after filtering through 0.20 μm nylon filters and analyzed spectrophotometrically. Urea adsorption studies on MMO were performed under dark conditions without applying any voltage with continuous stirring and negligible reduction in the concentration of urea was noticed. Hence, the efficacy of the treatment process was proven in context to urea degradation using EO. All experiments were performed thrice to check the reproducibility of results. For validation of results, suitable statics were applied. The mean value of results has been quoted in the study along with the standard deviation that has been represented in the form of bar graphs wherever required.

2.4. Analytical analysis

Double beam UV–vis spectrophotometer (U-2800, HITACHI, Japan) was used to determine the percentage degradation of urea in treated samples at λ_{max} 420 nm. Urea concentration was determined on spectrophotometer by addition of hydrochloric acid and p-dimethylaminobenzaldehyde in order to obtain a yellow color solution, which formed due to the formation of the complex. TOC of urea samples were analyzed with TOC analyzer (Multi N/C 2100 Analytik Jena). The oxidative and reductive reaction occurred during electrolysis of urea were measured through CV [auto lab, model-CHI660C] by using three-electrode assembly with Pt wire as the counter electrode, Ag/AgCl as a reference and commercially available Pt rod with $1cm^2$ area as a working electrode. APHA standard methods were performed to analyze the mineral-

ization by-products of urea such as inorganic ions which include (NO_3^-, NH_4^+, and Cl^-), total available chlorine (TAC), total nitrogen. The study of $OH^•$ production during electro-oxidation and photoelectrocalatysis (PEC) were checked using a fluorescence spectrophotometer (PerkinElmer, LS 45). Terephthalic acid (TPA) was used as a robe which readily reacts with the $OH^•$ and produces a fluorescence compound named 2-hydroxyterephthalic acid (TAOH). The intensity of fluorescence compound was taken at an excitation wavelength at 315 nm and emission wavelength at 425 nm. The surface morphology and elemental composition were checked through an SEM-EDS (scanning electron microscope, [model-JSM-6510LV, JEOL, Japan]) and (energy dispersive spectrometry [model-INCAX-act, Oxford instruments, U.K]. The crystalline structure of MMO anode was analyzed by XRD (X-ray diffraction) using X'Pert pro diffractometer from 2 Theta = 20-90°. To analyze the functional and structural characteristics of samples, FT-IR (Perkin Elmer Spectrum 2, 4100–400 cm^{-1}) was performed.

2.5. Experimental design

In this study, three-level Box-Behnken design (BBD) based RSM has employed for the experimental design, data analysis and parametric optimization of the EO treatment for urea. Each factor in BBD was coded at three levels −1(low), 0 (neutral) and +1(high). The design level limit of selected input parameters i.e. current density (j) (X_1), NaCl dose (n) (X_2), treatment time (t) (X_3) and pH (X_4) has been shown in Table 1. Process parameters and their ranges for the experimental study were determined on the basis of the literature survey and preliminary experiments performed. The total number of experimental runs were established based on BBD was 30 with six replication runs at the center as shown in Table 2. The performance of the EO process was evaluated by analyzing the responses; percentage degradation (Q_1) and energy consumed (Q_2). During EO treatment of urea the response (Q_2) i.e. energy consumption, E (kWhr m^{-3}) was calculated by following Eq. (1).

$$E = \left[\frac{V^*I^*t}{S_v}\right] \quad (1)$$

where, I = current (A); V = voltage; t = treatment time (h); Sv = Sample volume (m3). In the optimization process, the mathematical relationship of the response Q on these significant input factors can be estimated by the second-order polynomial equation. The experimental data obtained were fitted to a second-order polynomial equation, described in Eq. (2):

$$Q = \beta_\circ + \sum_{i=1}^{4}\beta_i X_i + \sum_{i=1}^{4}\beta_{ii}X_i^2 + \sum_{i=j}^{3}\sum_{i=j+1}^{4}\beta_{ij}X_{ij} + ei \quad (2)$$

where Q is the response; ß$_0$, ß$_i$, ß$_{ii}$, ß$_{ij}$ are constant coefficients; X_i, X_{ii}, X_{ij} are input factors and e_i is the error (Nair et al., 2014). The quality of the resultant polynomial model was expressed by the coefficient of determination R^2 while statistical significance was checked by F-Test. For the present case, due to the involvement of more than one response multi-response optimization with desirability approach was used to optimize the EO operational parameters.

2.6. Operating cost analysis

The overall cost for EO treatment comprises of cost of electrodes, cost of stirring, cost of chemical and electrical energy consumed. However the treatment process is energy-intensive, therefore total cost for operation is due to the electrode cost and electrical power employed. Hence, in the present study, the total cost for EO operation was calculated using the following equation:

$$\text{Operatingcost} = C_{EC} + C_{EL} \quad (3)$$

Where, C_{EC} = cost of energy consumed (kWh m^{-3}) and C_{EL} = cost of electrodes (Kg m^{-3}). The price of electricity in Punjab, (India) = ₹s 5.00/kWh. In the present study, the cost of MMO anode was Rs 720 per piece. The manufacturer/supplier has specified the life span of the electrode is 5 years.

3. Result and discussion

In the present study, Box-Behnken design with (4-factors, 3-levels, 2-responses) under RSM was developed by statistical Design-Expert software version 6.0.8 (STAT-Ease Inc., Minneapolis, US). All the experimental runs were performed according to the design given by BBD. The data obtained from the experimental runs were analyzed by two different tests in order to obtain effective regression models among various models. The model summary statistics showed the highest regression coefficient R^2 values for the quadratic model. The R^2 values for both response variables were 0.9900 and 0.9986 respectively, indicating that models have explained the experimental data very well and advocates satisfactory adjustments between observed and predicted values.

Table 3 shows the results of the quadratic model fitting in the form of analysis of variance (ANOVA). It is a statistical technique which subdivides the total variation into parts i.e. variation related to model and variation related to residual error for the purpose of testing hypotheses on the parameters of the model (Fu et al., 2007). The results of ANOVA implying that the model is highly significant, with F values 92.35 and 647.44, respectively which further indicate that adequate model is fit and can be used for design space navigation (Sangal et al., 2012). The non-significant value lack-of-fit (P > F = 0.0001) indicate that the model is statistically significant for responses (Q_1 and Q_2) and can be used for further analysis and very low probability value.

An empirical relationship between the responses and the operational parameters in terms of independent coded factors obtained from the design-expert software were expressed by the quadratic model equation as shown in Eqs. (4)–(5):

$$\begin{aligned} Q_1 = {} & +82.00 + 9.46*X_1 + 11.08*X_2 + 18.37*X_3 - 18.67*X_4 \\ & -31.21*X_1^2 - 19.15*X_2^2 - 16.33*X_3^2 - 10.77*X_4^2 \\ & +9.25*X_1*X_2 - 2.62*X_1*X_3 - 6.75*X_1*X_4 - 0.25*X_2*X_3 \\ & -6.25*X_2*X_4 - 5.00*X_3*X_4 \end{aligned} \quad (4)$$

$$\begin{aligned} Q_2 = {} & +22.40 + 18.43*X_1 - 2.94*X_2 + 11.53*X_3 + 0.97*X_4 \\ & +3.17*X_1^2 + 0.27*X_2^2 - 0.10*X_3^2 + 0.49*X_4^2 - 2.88*X_1*X_2 \\ & +9.08*X_1*X_3 + 0.25*X_1*X_4 - 1.29*X_2*X_3 + 0.12*X_2*X_4 \\ & +0.58*X_3*X_4 \end{aligned} \quad (5)$$

where X_1, X_2, X_3 and X_4 are current density, electrolyte concentration, treatment time and pH while Q_1 and Q_2 are % degradation and energy consumed respectively. The important part of the data analysis procedure is to evaluate the adequacy of developed mathematical models by constructing diagnostic plots such as predicted versus actual for the experimental data. The data points on this plot lie were found very close to the diagonal line, indicating the good correlation between experimental data and predicted data developed by the chosen model (Thirugnanasambandham et al., 2015)

Table 3
ANOVA results suggested by BBD for responses (Q_1 and Q_2).

Sources	% Degradation (Q_1)					Energy Consumed (Q_2)				
	Sum of square	DF	Mean square	F-value	Prob > F	Sum of square	DF	Mean square	F-value	Prob > F
Block	15.52	2	7.76			1.41	2	0.71		
Model	20575.85	14	1469.70	92.35	< 0.0001	6229.86	14	444.99	647.44	<0.0001
X_1	1073.52	1	1073.52	67.46	< 0.0001	4077.82	1	4077.82	5933.06	< 0.0001
X_2	1474.08	1	1474.08	92.63	< 0.0001	103.61	1	103.61	150.74	< 0.0001
X_3	4051.69	1	4051.69	254.60	< 0.0001	1594.83	1	1594.83	2320.41	< 0.0001
X_4	4181.33	1	4181.33	262.75	< 0.0001	11.35	1	11.35	16.51	0.0013
X_1^2	6678.58	1	6678.58	419.67	< 0.0001	68.85	1	68.85	100.18	< 0.0001
X_2^2	2513.57	1	2513.57	157.95	< 0.0001	0.49	1	0.49	0.71	0.4134
X_3^2	1829.33	1	1829.33	114.95	< 0.0001	0.076	1	0.076	0.11	0.7454
X_4^2	795.50	1	795.50	49.99	< 0.0001	1.64	1	1.64	2.38	0.1466
X_1X_2	342.25	1	342.25	21.51	0.0005	33.18	1	33.18	48.27	< 0.0001
X_1X_3	27.56	1	27.56	1.73	0.2109	329.60	1	329.60	479.56	< 0.0001
X_1X_4	182.25	1	182.25	11.45	0.0049	0.25	1	0.25	0.36	0.5568
X_2X_3	0.25	1	0.25	0.016	0.9022	6.60	1	6.60	9.61	0.0084
X_2X_4	156.25	1	156.25	9.82	0.0079	0.058	1	0.058	0.084	0.7768
X_3X_4	100.00	1	100.00	6.28	0.0263	1.33	1	1.33	1.94	0.1869
Residual	206.88	13	15.91			8.93	13	0.69		
Lack of fit	206.88	10	20.69			8.93	10	0.89		
Pure error	0.000	3	0.000			0.000	3	0.000		
Core total	20798.24	29				6240.21	29			

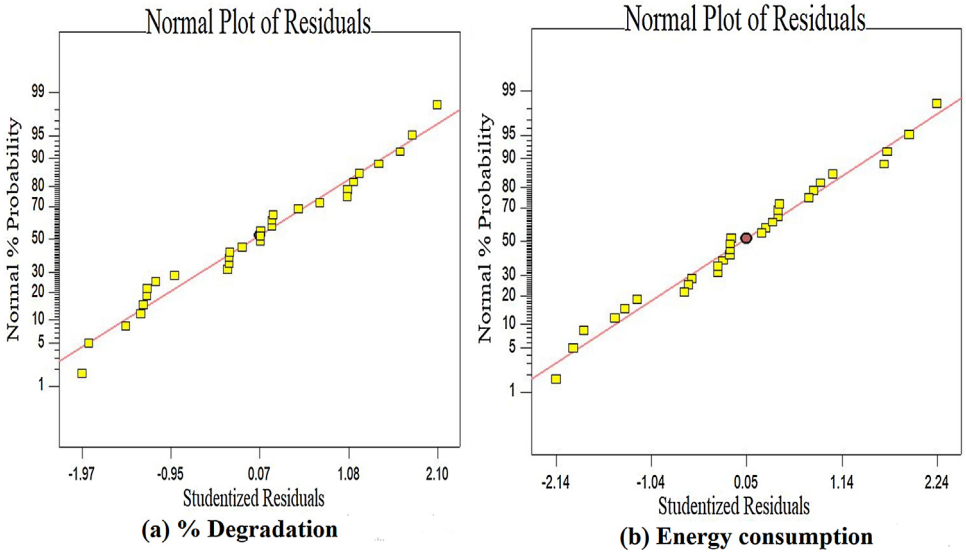

Fig. 2. The plot of Normal % probability vs Studentized Residuals for (a) %degradation and (b) energy consumption.

as shown in Fig. 2. To visualize the effect of operational parameters on responses and to find out the optimal condition of these parameters, 3D response surface graphs were studied.

3.1. *Effect of process variables*

3.1.1. *Effect of current density (j), NaCl dose (n), treatment time(t) and pH on % degradation, (Q_1)*

Current density, j is an important operating parameter in the EO process because of the cost-effectiveness analysis and mechanistic study. Furthermore, the capability of transfer of electron and generation of oxidant species all depend upon j (Wu et al., 2014). For j values from 9.52 to ≈ 20 mA cm^{-2}, it can be observed (Fig. 3a) that, Q_1 increases with increasing n values up to 1.13 g L^{-1}. Further increase in j values upto 28.57 mA cm^{-2} showed a gradual decrease in Q_1. While at each n value beyond 1.13 g L^{-1}, shows a marginal effect on Q_1 value. Urea degradation is highly dependent upon current and non-linear. In literature, it has been reported that at very lower values of current applied, generation of chlorine species on MMO anodes has fallen down gradually with time and hence decreases the process efficiency (Hernlem, 2005). But on increasing j values, it appeared that the generation of $OH^{\bullet}$ and oxidation of chloride in reactive chlorine oxidant species (RCS) increased, which helped in the better degradation of urea in the aqueous solution. From the experimental results it has been found that after certain values of j and n, the removal efficiency of urea becomes minimum. This might be due to the metal dissolution at higher values of j, which propagated the growth of the flocs in the solution as well as increase the temperature of the solution which further interferes the degradation process and hence decreased the process efficiency (Garg and Prasad, 2015). Furthermore, it has also been reported that MMO exhibits better process efficiency at lower values of j because of the low oxygen evolution potential which disfavored the other side reactions and hence provides effective degradation of pollutant.

The concentration of sodium chloride plays a significant role because it influences the efficiency of the EO process. Actually, the dose of NaCl defines the amount of RCS such as HClO, ClO^-, etc. formed during EO treatment of urea at MMO anodes. It has been observed that an increase in n values lead to the rise in urea

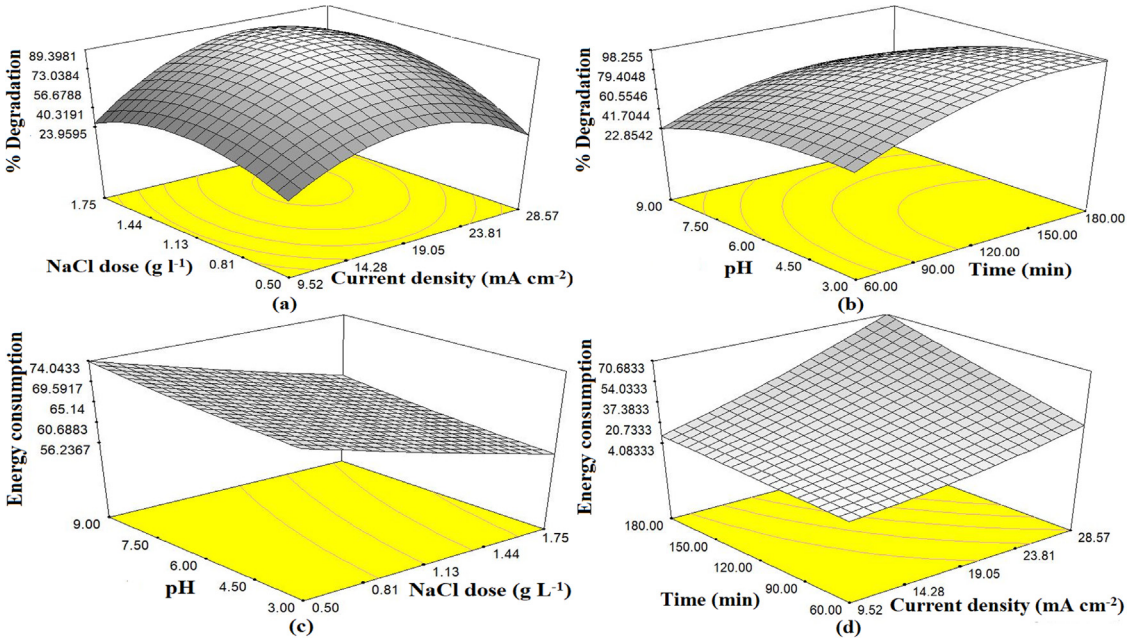

Fig. 3. Effect of different operational parameters on % degradation and energy consumption during electrolysis of urea (a) j and n (b) t and pH (c) n and pH and (d) t and. j.

degradation. RuO_2 and Pt, metal oxides are known to be the most widely used electro-catalyst due to their enhanced performance for Cl_2 and oxygen evolution potential upto 1.7 V to 1.9 V (Martínez-Huitle and Andrade, 2011). Furthermore, it has been observed that during EO treatment with increasing NaCl dose, the concentration of chloride ions and hypochlorite ions might have also increased in the solution which gets adsorbed on the surface of the anode. These ions react with urea resulting in its decomposition either directly on the surface of the anode or $OH^{\bullet}$ and indirectly by chlorine species and H_2O_2 species generated in the bulk. Hence, the synergistic effects of chloro active species and $OH^{\bullet}$ radicals have led to the maximum degradation efficiency during the treatment process (Hiwarkar et al., 2017). In addition to this, the average rate of the degradation process increases due to the improvement in the solution conductivity which substantially decreases the drop in the voltage along with energy consumption. On further increase in the n values, it has been found that urea degradation was minimum, which might be due to the reactions between ammonium ion and hypochlorous acid (Cataldo Hernández et al., 2014) as shown in following Eq. (6):

$$2NH_4^+ + 3HClO \rightarrow N_2 + 3H_2O + 5H^+ + 3Cl^- \quad (6)$$

From Fig. 3b it can be seen that at lower values of pH ≈ 4.5, with increasing t values up to 140 min an increase in Q_1 has been found. On further increase in t values beyond 140 min showed a marginal effect on Q_1. Further, an increase in the pH value ≈ 6 showed a marginal effect on Q_1 with increasing t value. While at alkaline conditions i.e. beyond 7 pH, showed a gradual decrease in the Q_1 with time. Few studies in the literature have reported that during EO treatment, at high values of j with increasing t values always lead to the passivation of the electrode due to the bond formation between pollutant and anode which grows like an impermeable film. Moreover, at higher values of j, an increase in the oxygen evolution reactions was there which ultimately affect the performance of the EO process. However, the MMO used for present experimental work exhibit enhanced service life for longer period of time as well as are more electrochemical stable due to the presence of IrO_2 metal oxide (Liu et al., 2019). Yet, for better EO performance and longer service life of anodes, optimization of process variables is also very important. More than 95% of degradation was observed in 135 min at acidic pH.

In the EO treatment process, both mechanisms i.e. direct and indirect oxidation takes place simultaneously. The direct oxidation method at the surface of anode takes place by adsorption of $OH^{\bullet}$, generated in oxide lattice of ternary anode due to which oxidation of pollutant was there. Also, it was observed that adsorption of $OH^{\bullet}$ was found high at lower values of pH. Further, in addition to this, at acidic pH with increasing j also increases the generation rate of chloro-oxidant species such as HClO, ClO-, which indirectly oxidize the urea in the bulk. While, in the case of basic pH, the adsorption rate of generated $OH^{\bullet}$ is decreased in oxide lattice and transformed into lower oxidation potential oxidants such as H_2O_2 and $HO^{\bullet}{}_2$. Also, the concentration of ClO^- decreases as well and further oxidized to lower oxidant potential such as ClO_3^- and ClO_4^-. Therefore, urea degradation is reduced in alkaline pH in comparison to the acidic pH (Kaur et al., 2015).

3.1.2. *Effect of current density (j), NaCl dose (n), time (t) and pH on energy consumption (Q2)*

Fig. 3c shows that at lower values of n with increasing j values, Q_2 has been found to be maximum because of the lower conductivity of the solution as well as an increase in the voltage drop. At higher n values, Q_2 found to be minimal because of the ease of current flow through the electrolyte solution. While in case of higher values of j, energy consumption gradually increased with time due to various factors like might electrode deactivation, a decrease in the concentration of ions and an increase in solution temperature. However, the value of Q_2 has been found to be minimum with a decrease in solution pH as shown in Fig. 3d. This was due to the production of high oxidation potential RCS at lower values of pH lead to the maximum degradation and consumed less energy. While at alkaline pH, low oxidation potential RCS was generated which results in minimum degradation efficiency with maximum energy consumption.

3.2. *Multi-response optimization*

In the present study, optimization of operational process variables such as NaCl dose, treatment time, current density, and pH has

Table 4
Constraint applied for optimization process.

Variables	Goal	Lower limit	Upper limit
j	Is in range	9.52	28.57
n	Is in range	0.5	1.75
t	Is in range	60	180
pH	Is in range	3	9
% Degradation	Maximize	11.5	98
Energy consumed	Minimize	3.63	65.7

been performed in order to get the maximum removal of urea from synthetic wastewater along with minimum consumption of energy using MMO anodes. There are two responses Q_1 and Q_2 and optimum conditions for these responses are not the same. Optimum conditions for Q_1 has been selected in such a way that it should come out to be maximum and Q_2 should be minimized using the desirability function approach. To get this particular entity some constraints have been applied on operational parameters as shown in Table 4.

Table 5 shows the optimized values for the operational parameters and output responses as well as corresponding individual and simultaneous optimization desirability value. The optimum conditions obtained at pH 4, the current density at 18.14 mA cm^{-2}, NaCl dose of 1.45 g L^{-1} and treatment time 135 min which produced combined desirability value of responses, D 0.857. At these conditions, the value for response Q_1 was 96.06% and response Q_2 was 21.11 kW h m^{-3} as suggested by BBD. An experiment was then performed in order to verify the optimum results obtained from the predicted model. The value of the response Q_1 and Q_2 came out to be 94.78% and 20.54 kW h m^{-3} which seemed almost close to the predicted values as depicted in Table 6. During electrolysis, both mechanism direct and indirect oxidation of urea takes place due to the generation of various ions like $OH^{\bullet}$, HOCl, OCl^{-}, Cl_2, etc. Furthermore, the $OH^{\bullet}$ generated during the process were highly unstable hence, readily converted to H_2O_2 and $HO_2^{\bullet}$ thus helps in mediated oxidation. In addition to direct oxidation, mediated oxidation takes place also due to dominant chloride species like HOCl and Cl_2 at acidic pH which oxidize the urea rapidly. Due to the presence of more of chloro-oxidant spices in the bulk, the degradation of urea was largely mediated because of indirect oxidation.

3.3. Durability studies

In order to check the practical applicability and economy of the EO process towards pilot-scale application, the durability and stability of the MMO anodes have been studied. In this context, efforts have been made to evaluate the stability and durability in terms of degradation efficiency of urea for subsequent recycles. Despite the high concentration of NaCl and acidic pH, MMO anodes have been magnificently reused for approximately 90 times without any substantial reduction in process efficiency as shown in Fig. 4. Generally, at low pH, in the presence of high NaCl and current density values, the life span of MMO anode decreases due to passivation and dissolution (Singla et al., 2018). Several studies in the literature have reported the stability of MMO anodes upto 100–200 h or a maximum of 600 days only (Wang et al., 2012; Herrada et al., 2018; Zahedi et al., 2018; Liu et al., 2019). Whereas, MMO used in this study exhibit immense stability even after 270 h under extreme conditions and could be used further for a maximum of 5 years due to the presence of the appropriate amount of IrO_2. This anode offers the advantage of generating a significant amount of ROS and RCS due to the high concentration of Pt, TiO_2, and RuO_2, in the oxide mixture which helps in the occurrence of both mechanism i.e. direct and indirect oxidation (Chaplin, 2014).

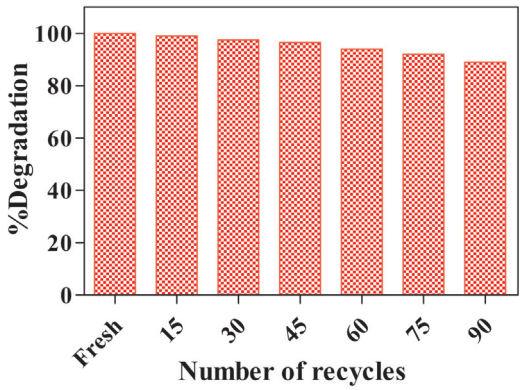

Fig. 4. Recyclability studies of MMO anode for the degradation of urea.

Table 6
Comparison between predicted and actual value at optimized conditions.

Responses	Predicted	Actual experimental values
% Degradation	96.06 %	94.78%
Energy consumed (kWh m^{-3})	21.11	20.54

To confirm the electrochemical stability of the MMO anodes even after the 90 recycles (270 h), anodes were further characterized by SEM, EDS and XRD as discussed in Section 3.4. In fact, this is the first reported study for such high durability of MMO electrodes in context to the degradation of urea or any other priority pollutants.

3.4. Anode characterization

3.4.1. SEM/EDS analysis

To characterize the surface morphology and structural properties of the MMO anodes, SEM was performed while for elemental composition of the different metal oxides layer coated on anode surface (freshly as well as recycled MMO), EDS was used respectively. The SEM images of fresh MMO and recycled MMO plates were illustrated in Fig. 5a, b. The results show the surface allied characteristics, which implying the even layers of metal oxides even after ninety recycles. From the SEM images, it has been observed that the appearance of the anode generally corresponds to mud cracked morphology along with agglomerated points (Coteiro et al., 2006). This happens because electrodes are prepared via thermal anodic decomposition and after then successive cooling has been done. The presence of titanium (Ti) in the sheet has made the con-

Table 5
Individual and MUlti-response optimization results for desirability calculations.

Response	Current density(mA cm^{-2})	NaCl dose(g L^{-1})	Time(min)	pH	Desirability
Individual Response optimization					
% Degradation (Q_1) = 97.08%	20.75	1.6	142	4.17	1
Energy consumed (Q_2) = 11.4 kW h m^{-3}	17.84	0.5	61.02	4	0.935
Simultaneously optimization of responses					
% Degradation(Q_1) = 96.06%	18.14	1.45	135	4	0.857
Energy consumed (Q_2) = 21.11 kW h m^{-3}					

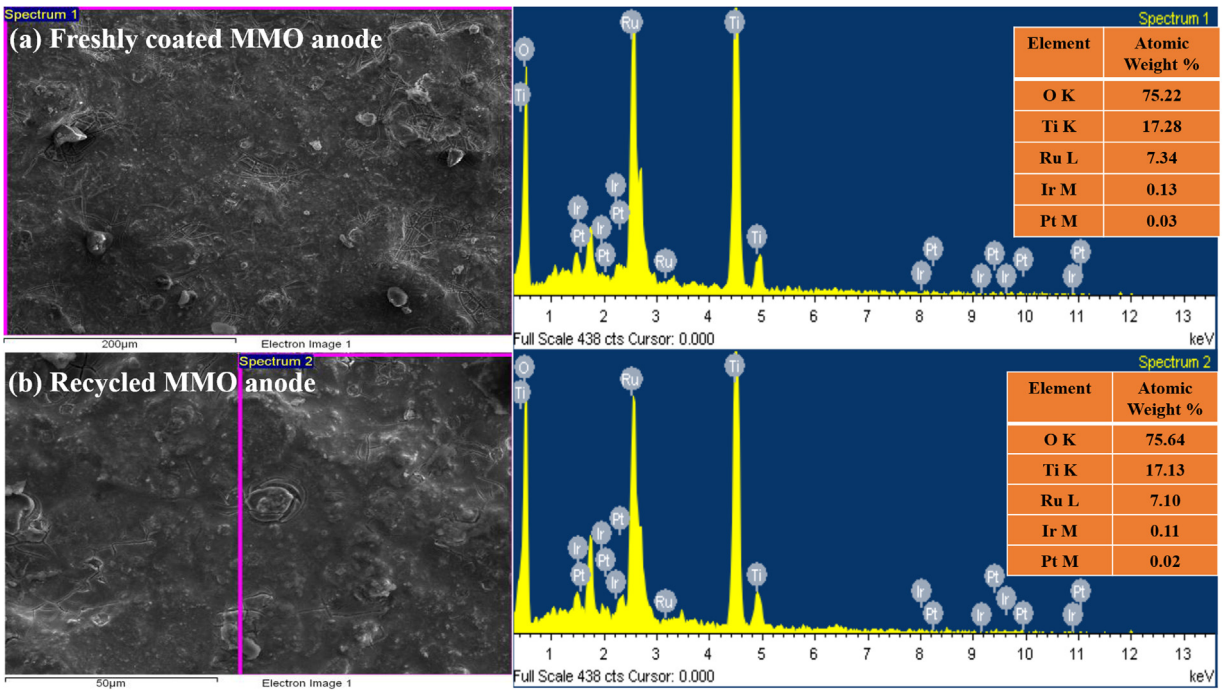

Fig. 5. SEM along with EDS images of MMO anode (a) freshly coated and (b) after 90 recycles.

sequence for the formation of TiO_2 as the first layer, which further allowed the better fixing of the oxide layers of other metals (Wu et al., 2014). Furthermore, the incorporation of oxides of Ti, iridium (Ir), ruthenium (Ru) and platinum (Pt) in the metal sheet has increased the surface area as well as making the structure relatively porous, smooth and uniform with wide and deep cracks hence prevents the anode from corrosion along with greater stability for a longer period of time (Goudarzi and Ghorbani, 2016). Addition of Pt in the anodes has affects the morphology by improving its homogeneity of the coated layers along with the formation of smaller size particles which formed due to the compacting effect (del Río et al., 2010). Furthermore, the appropriate content of Pt in MMO anode has increased the roughness factor as well as presented the higher capacitance. Durability and stability of anodes are further proven with the presence of extrusive peaks of all coated metals i.e. Pt, Ir, Ru, Ti, and O even in a recycled sheet. The quantitative analysis through EDS depicts the atomic concentration of elements coated in the oxide mixture, which has found almost equal in both fresh and recycles MMO, thus affirming that MMO can be used even for further studies.

3.4.2. XRD analysis

Fig. 6 shows X-ray diffractogram of a freshly coated sample of MMO and a recycled sample of MMO. XRD basically determine the crystalline planes of the structure of the oxide films which coated on the titanium sheet. Through XRD it became possible to distinctively identify the existence of oxides of Ru, Ir, and Ti in rutile structure. The presence of TiO_2 and other oxide layers of metals have made a tetragonal structure and ionic radii of the same magnitude (Singla et al., 2017). Furthermore, the same peaks of oxides of metal have also been observed in recycled sheet, thus indicating the retention of all coated metal oxides even after ninety recycles. It was also observed that similar peaks were found even in the recycled MMO. But at the same time, it was also found that some metal peaks were deviated from their original position due to loss of some amount of metals in the multiple runs of the experiment. Diffraction peaks corresponds to titanium (JCPDS card: 00-005-0682), titanium dioxide (JCPDS card: 00-034-0180) indicated as rutile syn, ruthenium

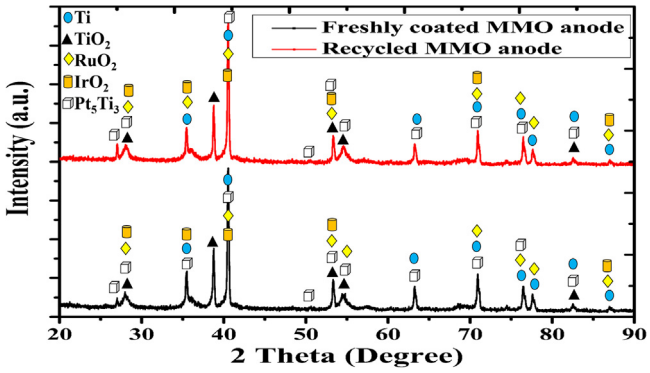

Fig. 6. XRD pattern of MMO anodes (Freshly coated and recycled plate).

(JCPDS card: 01-071-2273) referred to as ruthenium (IV) oxide, iridium (JCPDS card: 00-015-0870) were indicated as iridium oxide and platinum (JCPDS card: 01-072-2997) were indicated as platinum titanium. Most of the similar peaks were already reported in the literature (Makgae et al., 2005).

3.4.3. XPS analysis

Fig. 7 (i) depicts the XPS spectra of freshly coated MMO and recycled MMO anodes in order to analyze the electronic nature i.e. oxidation state of metal elements. From the results, it has been observed that no significant change in the oxidation state of metals, as well as the presence of each element, was found even after multiple recycles. The occurrence of carbon (C 1s) in both samples could be attributed to adventitious carbon employed for appropriate binding energy shifts generated by samples. Fig. 7 (ii) indicate the Ti 2p spectrum of MMO anode in which peaks corresponds to binding energies of Ti $2p_{3/2}$ and Ti $2p_{1/2}$ states and were observed at 458.91 eV and 461.43 eV respectively (Tseng et al., 2014). Fig. 7 (ii) shows the spectra shape of O 1s signal in which one broad peak was visible at 530. 48 eV and could be assigned ti Ti—O bonds. Fig. 7 (iii),(iv),(vi) demonstrates the spectrum of Ru 3d, Ir 4f, and Pt 4f signals, confirming their presence in MMO anode. In contrast to Ru

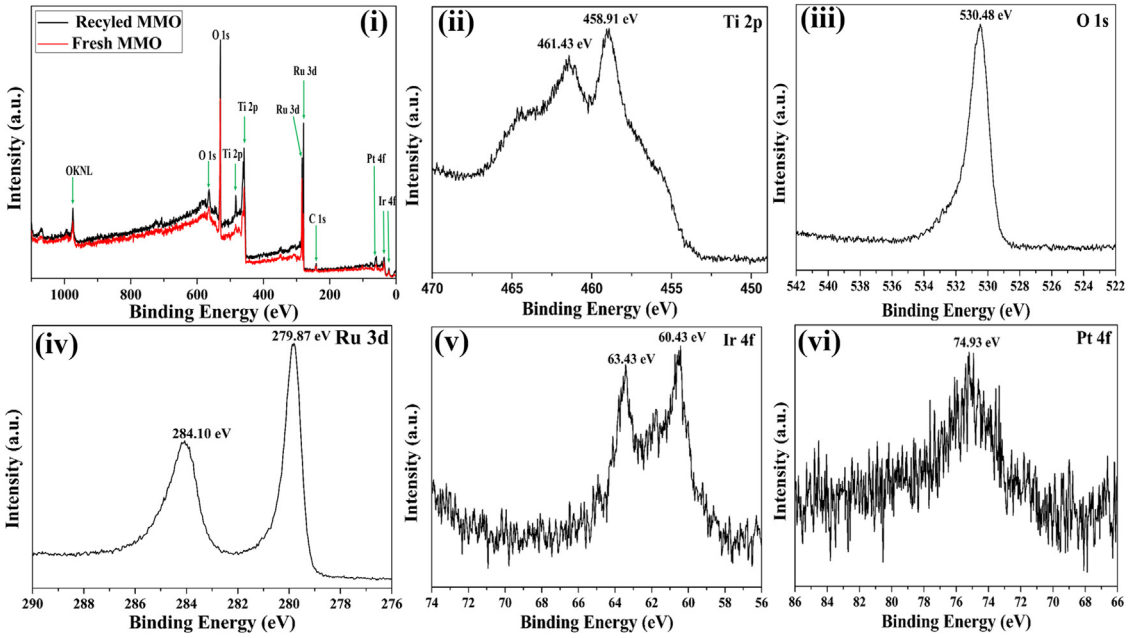

Fig. 7. XPS analysis of (i) Fresh MMO and recycled MMO along with (ii) Ti 2p spectrum (iii) O 1s spectrum (iv) Ru 3d spectrum (v) Ir 4f spectrum and (vi) Pt 4f spectrum.

and Ir, Pt signal indicates single oxidation state i.e. Pt (V), belonging to Pt $4f_{5/2}$ level was observed around 74.93 eV and further indicate the interstitial formation of Pt—Ti bonds. However, in the case of Ru and Ir spectrum, two individual characteristic peaks of each element were observed at 279.87 eV, 284.10 eV, 60.43 eV, and 63.43 eV respectively. The data derived for Ru and Ir region from respective signals were correlated with Ru $3d_{5/2}$, Ru $3d_{3/2}$, Ir $4f_{7/2,}$ and Ir $4f_{5/2}$ thus proposing the formation of hydrated RuO_2 and IrO_2 metal oxides. The results in the present study are in good correlation with the reported studies in the literature (Wang et al., 2015; Egorov et al., 2017).

3.5. Photoelectrocatalysis

In the present study, the synergistic effect of the dual process (photocatalysis and electro-oxidation) i.e. Photoelectrocatalysis (PEC) has been also performed under UV light at optimized con-

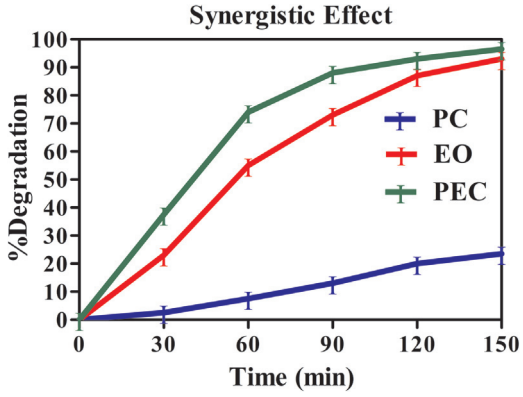

Fig. 8. Comparison of photocatalysis, electro-oxidation, and dual-process i.e. photoelectrocatalysis for the degradation of urea using MMO.

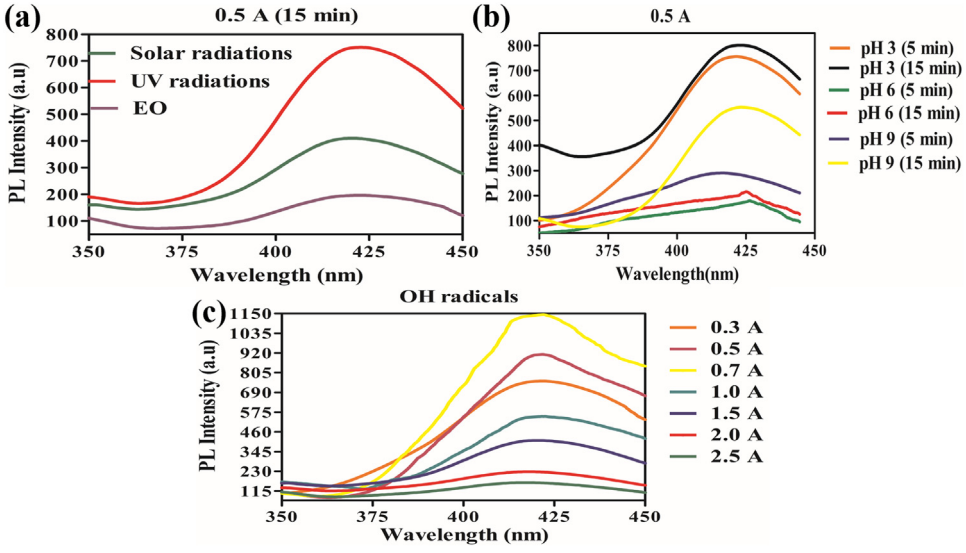

Fig. 9. PL spectra of $OH^{\bullet}$ (a) for different light sources at 0.5A (b) for different pH and different time intervals at 0.5A and (c) at different current densities using MMO anode.

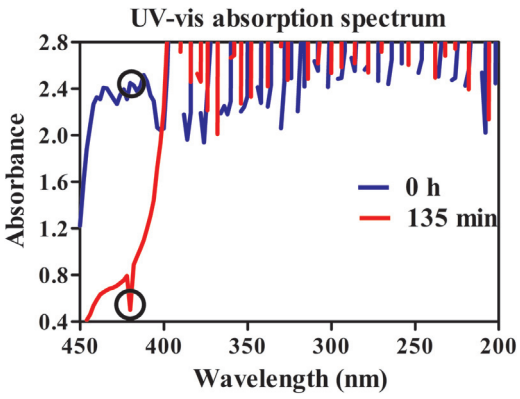

Fig. 10. UV–vis spectra of untreated (t = 0 min) and treated sample (t = 135 min) of urea at optimized conditions.

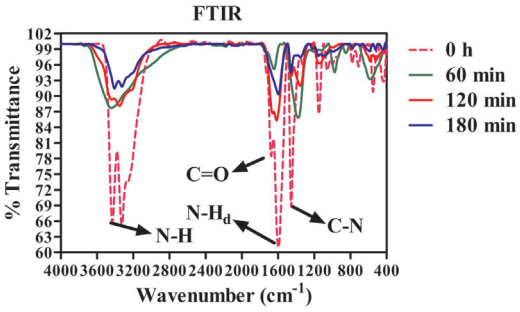

Fig. 11. FT-IR spectra of urea at different time intervals.

ditions. It has been found that treatment time got reduced further to 95 min from 135 min as depicted in Fig. 8. Hence, proving the effectiveness of dual-process over a single process. Further studies are performed in order to confirm the production of $OH^{\bullet}$ during EO and PEC at MMO. Various experiments have been performed with different parameters such as time, pH, current density and light source in an aqueous solution consists of 0.5 mM TPA in 5 mM NaOH. From Fig. 9a, it can be concluded that the production of $OH^{\bullet}$ at MMO is more in case of UV light over sunlight and EO alone. From the experimental results, as shown in Fig. 9b, it has been observed that more $OH^{\bullet}$ production are there at acidic and basic pH over neutral pH. Moreover, with increasing time generation of $OH^{\bullet}$ at MMO was also increasing. In the case of applied voltage, the production of $OH^{\bullet}$ at MMO first increases with increasing current up to 0.7A after that it has been found that $OH^{\bullet}$ production decreases with increasing current values as shown in Fig. 9c.

3.6. Mineralization

For monitoring the mineralization of urea, in-situ chemical analysis of the treated samples was carried out by spectrophotometric analysis and FT-IR. The UV–vis spectra for untreated and treated samples of urea by EO were shown in Fig. 10. From the results, it was seen that the absorbance peak of pure urea got reduced to a minimum after a treatment time of 135 min. Some other new peaks at different λ_{max} were formed for different time intervals. This change in λ_{max} confirms the electrolytic degradation of urea as well as the formation of other intermediate byproducts.

Further, to confirm the degradation of urea in aqueous solution through EO treatment, FT-IR was performed. Fig. 11 gives the FT-IR spectra of pure urea and its treated samples taken at fixed time intervals. The C=O stretching frequency appeared at 1672 cm^{-1}. The N—H stretching and deformation frequencies appear at 3450 cm^{-1} and 1628 cm^{-1} respectively. The C—N stretching frequency appears at 1452 cm^{-1}. Other small peaks have also appeared in the spectra of 0 h sample of urea (untreated). Broad and sharp peaks at 3450 cm^{-1} and 1672 cm^{-1} were shifted to 3427 cm^{-1} and 1647 cm^{-1} respectively after 60 min due to the production of $OH^{\bullet}$ at MMO and C=O stretching during the initial stage of EO treatment (Piasek and Urbanski, 1962). The peaks at 1100–800 cm^{-1} have also seen in spectra for sample t > 60 min, which generally accounts for Cl^{-}, present in hypochlorite solution. The peak at 1381 cm^{-1} at 180 min shows degradation of urea into nitrate ions. During electrolysis of urea, most of the peaks were deviated due to the breakage of the bonds at distinct wavenumber. Moreover, an increase in % transmittance was observed in a sample taken at 135 min, indicates oxidation of urea into byproducts.

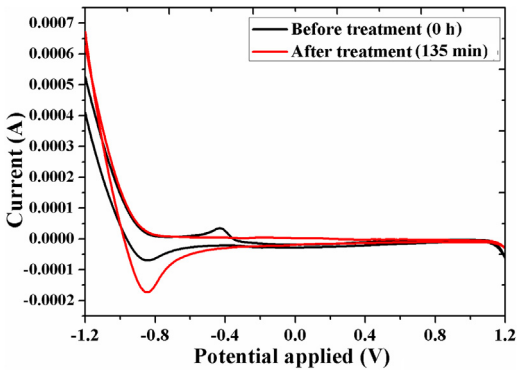

Fig. 12. Cyclic Voltammetric analysis for (a) untreated samples (0 h) and (b) treated samples (135 min) of urea.

To confirm the indirect EO mechanism of urea removal, cyclic voltammeter (CV) analysis were performed and studied. Fig. 12 shows the CV analysis graph of before and after treatment samples of urea at optimum conditions taking 2 g L^{-1} concentration with 0.1 M KCl and scanned at 50 mV s^{-1} using Pt anode as the working electrode. The full CV of urea was recorded in the potential range of −1.2 to 1.2 V. The experimental results of urea show that no additional peaks were found in the treated sample when compared to before treatment sample. This concludes that the degradation of urea was majorly due to indirect oxidation and $OH^{\bullet}$. However, few irreversible oxidation peaks in voltagramms were got disappeared in treated samples of urea at 135 min, which indicates the generation of some oxidizable and reducible species during electrolysis (Hiwarkar et al., 2017). Moreover, the difference in the anodic and cathodic parts of redox peaks for untreated and treated samples indicate the good electrical conductivity and high surface area properties of MMO anode (Mudila et al., 2018).

To further, analyze the quality of treated and untreated samples various analytical test was performed such as TOC, inorganic ions (NO_3^{-}, NH_4^{+}, Cl^{-}), total available chlorine (TAC) and total nitrogen at optimized conditions. Around 90% removal in TOC was observed after 135 min of treatment time which further reached 92% when the reaction continued to 240 min as shown in Fig. 13a. From Fig. 13b of anions shows an increasing and then decreasing trend in ammonium ion concentration while in case nitrate continuous increasing trend was observed. This might be due to the reaction between ammonium ion and hypochlorous acid. In the case of nitrate, the increase was observed due to the oxidation of the chloramines by free chlorine. In comparison to total nitrogen, the low yield of nitrates was found during urea degradation which could be due to the less availability of free chlorine to urea ratio as shown in Fig. 13c. From this above discussion, it may conclude that during electro-oxidation of urea molecular nitrogen may also generate.

From Fig. 13d it can be seen that chloride level was continuously decreasing during the electrolysis process. This is because of

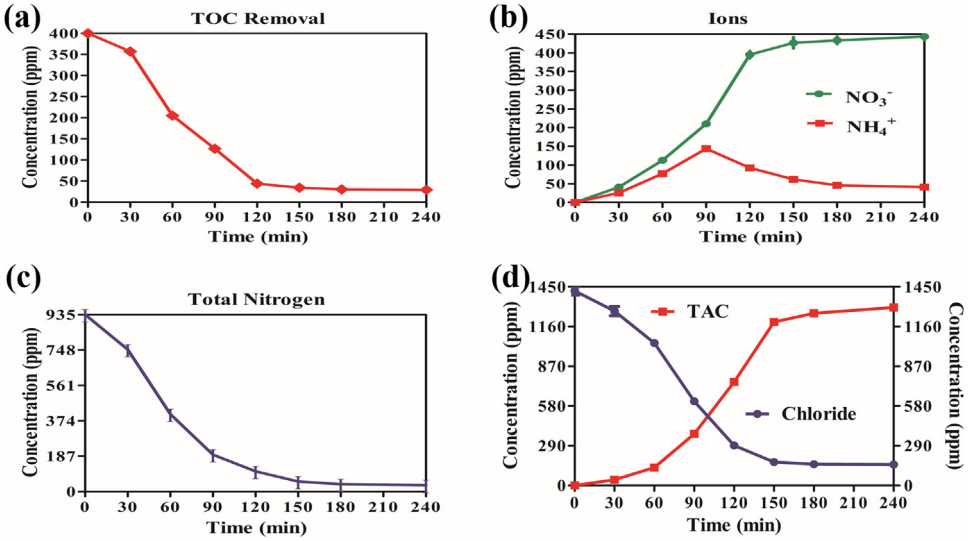

Fig. 13. Changes in the concentration of (a) TOC (b) inorganic ions (c) total nitrogen and (d) chloride concentration and TAC concentration at different time intervals.

the oxidation of chloride on the anode to produce strong oxidant species like HOCl/OCl^- for the destruction of urea. From this discussion, we may conclude that this intermediate step has followed the pseudo-first-order rate during course period of the process. The level of TAC increased gradually during the electro-oxidation treatment of urea and then increased sharply to higher values when urea was depleted to the maximum as shown in Fig. 13d. During the treatment process TAC, an aggregate part of reactive intermediates does not remain constant. This might be due to the balance between the oxidation of urea and generation of chlorine species along with their bond forms during the treatment process as reported in the literature (Hernlem, 2005).

3.7. Economic evaluation

In order to visualize the large scale applications of studied EO method, it becomes necessary to estimate the total cost of the treatment process. As discussed above in Section 2.6, the two effective parameters like cost of electrodes and electrical energy consumed have been considered for calculating the process economics. The detailed cost analysis for the EO process has been included in the supplementary information Table S1. By incorporating all the operating parameters, the total cost for removal of per kg urea from aqueous solution came out to be 0.78 $/m^3$. The results show that the economic feasibility of the EO process for the on-site treatment of urinal wastewaters. However, the cost can be further minimized during scale-up studies by modifying the design of the reactor and further optimizing the operating conditions accordingly.

4. Conclusion

The degradation studies of urea through EO with titanium-based MMO has been done successfully. The optimized parameters for urea electrolysis from BBD were found to be j=18.14 mA cm^{-2}; time = 135 min; NaCl dose=1.45 g L^{-1} and pH = 4, which has produced the combined desirability of both responses D = 0.857. At optimized conditions, the value of responses Q_1 and Q_2 found out to be 94.78% and 20.54 kW h m^{-3}, respectively. The degradation of urea was maximum because of the generation of strong oxidants like HOCl, OCl^-, $OH^•$ during both direct and indirect oxidation. Formations of ions such as nitrate and ammonium ion and reduction in TOC have proved the almost complete degradation of urea. Characterization techniques like SEM-EDS and XRD have proved the durability and stability of MMO anode for urea degradation even after 90 recycles. From the above results, it can be concluded that MMO anodes proved to be effective for the degradation of urea and can be used further research analysis which includes on-site treatment of urinal wastewater.

Acknowledgment

This research work did not receive any kind of specific grant from funding agencies in the commercial, public, or not-for-profit sectors. Authors are thankful to Dr. Neelam Verma, Professor in Department of Biotechnology and Dr. Pawan Krishan, Professor, in Department of Pharmaceutical Sciences and Drug Research, Punjabi University, Patiala, Punjab (India) for extending their lab facilities to carry out some part of experimental work.

Appendix A. Supplementary data

Supplementary material related to this article can be found, in the online version, at doi:https://doi.org/10.1016/j.psep.2019.08.017.

References

Amin, M.N., Kroeze, C., Strokal, M., 2017. Human waste: an underestimated source of nutrient pollution in coastal seas of Bangladesh, India and Pakistan. Mar. Pollut. Bull. 118, 131–140, http://dx.doi.org/10.1016/j.marpolbul.2017.02.045.

Amstutz, V., Katsaounis, A., Kapalka, A., Comninellis, C., Udert, K.M., 2012. Effects of carbonate on the electrolytic removal of ammonia and urea from urine with thermally prepared IrO_2 electrodes. J. Appl. Electrochem. 42, 787–795, http://dx.doi.org/10.1007/s10800-012-0444-y.

Barrera-Díaz, C., Cañizares, P., Fernández, F.J., Natividad, R., Rodrigo, M.A., 2017. Electrochemical advanced oxidation processes: an overview of the current applications to actual industrial effluents. J. Mex. Chem. Soc. 58, 256–275, http://dx.doi.org/10.29356/jmcs.v58i3.133.

Bergmann, M.E.H., Rollin, J., Iourtchouk, T., 2009. The occurrence of perchlorate during drinking water electrolysis using BDD anodes. Electrochim. Acta 54, 2102–2107, http://dx.doi.org/10.1016/j.electacta.2008.09.040.

Cataldo Hernández, M., Russo, N., Panizza, M., Spinelli, P., Fino, D., 2014. Electrochemical oxidation of urea in aqueous solutions using a boron-doped thin-film diamond electrode. Diamond Relat. Mater. 44, 109–116, http://dx.doi.org/10.1016/j.diamond.2014.02.006.

Chaplin, B.P., 2014. A critical review of electrochemical advanced oxidation processes for water treatment applications. Environ. Sci.- Proc. Imp. 16, 1182–1203, http://dx.doi.org/10.1039/C3EM00679D.

Cho, K., Hoffmann, M.R., 2014. Urea degradation by electrochemically generated reactive chlorine species: products and reaction pathways. Environ. Sci. Technol. 48, 11504–11511, http://dx.doi.org/10.1021/es5025405.

Coteiro, R.D., Teruel, F.S., Ribeiro, J., de Andrade, A.R., 2006. Effect of solvent on the preparation and characterization of DSA®-type anodes containing RuO_2-TiO_2-SnO_2. J. Braz. Chem. Soc. 17, 771–779, http://dx.doi.org/10.1590/S0103-50532006000400020.

del Río, A.I., Fernández, J., Molina, J., Bonastre, J., Cases, F., 2010. On the behavior of doped SnO_2 anodes stabilized with platinum in the electrochemical degradation of reactive dyes. Electrochim. Acta 55, 7282–7289, http://dx.doi.org/10.1016/j.electacta.2010.07.008.

Egorov, K.V., Lebedinskii, Y.Yu., Soloviev, A.A., Chouprik, A.A., Azarov, A.Yu., Markeev, A.M., 2017. Initial and steady-state Ru growth by atomic layer deposition studied by in situ angle resolved X-ray photoelectron spectroscopy. Appl. Surf. Sci. 419, 107–113, http://dx.doi.org/10.1016/j.apsusc.2017.05.010.

Fu, J., Zhao, Y., Wu, Q., 2007. Optimizing photoelectrocatalytic oxidation of fulvic acid using response surface methodology. J. Hazard. Mater. 144, 499–505, http://dx.doi.org/10.1016/j.jhazmat.2006.10.071.

Garg, K.K., Prasad, B., 2015. Electrochemical treatment of benzoic acid (BA) from aqueous solution and optimization of parameters by response surface methodology (RSM). J. Taiwan Inst. Chem. Eng. 56, 122–130, http://dx.doi.org/10.1016/j.jtice.2015.04.005.

Goudarzi, M., Ghorbani, M., 2016. Deposition of (Ti, Ru)O_2 and (Ti, Ru, Ir)O_2 oxide coatings prepared by sol-gel method on titanium. J. Solgel Sci. Technol. 79, 44–50, http://dx.doi.org/10.1007/s10971-016-4009-0.

Gupta, N., Pandey, P., Hussain, J., 2017. Effect of physicochemical and biological parameters on the quality of river water of Narmada, Madhya Pradesh, India. Water Sci. 31, 11–23, http://dx.doi.org/10.1016/j.wsj.2017.03.002.

Gurung, K., Ncibi, M.C., Shestakova, M., Sillanpää, M., 2018. Removal of carbamazepine from MBR effluent by electrochemical oxidation (EO) using a Ti/Ta_2O_5-SnO_2 electrode. Appl. Catal. B-Environ. 221, 329–338, http://dx.doi.org/10.1016/j.apcatb.2017.09.017.

Herrada, R.A., Acosta-Santoyo, G., Sepúlveda-Guzmán, S., Brillas, E., Sirés, I., Bustos, E., 2018. IrO_2-Ta_2O_5|Ti electrodes prepared by electrodeposition from different Ir:Ta ratios for the degradation of polycyclic aromatic hydrocarbons. Electrochim. Acta 263, 353–361, http://dx.doi.org/10.1016/j.electacta.2018.01.056.

Hernlem, B.J., 2005. Electrolytic destruction of urea in dilute chloride solution using DSA electrodes in a recycled batch cell. Water Res. 39, 2245–2252, http://dx.doi.org/10.1016/j.watres.2005.04.018.

Hiwarkar, A.D., Singh, S., Srivastava, V.C., Mall, I.D., 2017. Mineralization of pyrrole, a recalcitrant heterocyclic compound, by the electrochemical method: Multi-response optimization and degradation mechanism. J. Environ. Manage. 198, 144–152, http://dx.doi.org/10.1016/j.jenvman.2017.04.051.

Isarain-Chávez, E., Baró, M.D., Rossinyol, E., Morales-Ortiz, U., Sort, J., Brillas, E., Pellicer, E., 2017. Comparative electrochemical oxidation of methyl orange azo dye using Ti/Ir-Pb, Ti/Ir-Sn, Ti/Ru-Pb, Ti/Pt-Pd, and Ti/RuO_2 anodes. Electrochim. Acta 244, 199–208, http://dx.doi.org/10.1016/j.electacta.2017.05.101.

Kaur, P., Sangal, V.K., Kushwaha, J.P., 2015. Modeling and evaluation of electro-oxidation of dye wastewater using artificial neural networks. RSC Adv. 5, 34663–34671, http://dx.doi.org/10.1039/C4RA14160A.

Liu, B., Wang, C., Chen, Y., Ma, B., 2019. Electrochemical behavior and corrosion mechanism of Ti/IrO_2-RuO_2 anodes in sulphuric acid solution. J. Electroanal. Chem. 837, 175–183, http://dx.doi.org/10.1016/j.jelechem.2019.02.039.

Mahmoud, M.H., Abdel-Salam, O.E., Abdel-Monem, N.M., Nassar, A.F., El-Halwany, M.A., 2013. Removal of urea from industrial wastewater using electrochemical decomposition. Life Sci. 10, 2048–2055.

Makgae, M.E., Theron, C.C., Przybylowicz, W.J., Crouch, A.M., 2005. Preparation and surface characterization of Ti/SnO_2–RuO_2–IrO_2 thin films as electrode material for the oxidation of phenol. Mater. Chem. Phys. 92, 559–564, http://dx.doi.org/10.1016/j.matchemphys.2005.02.022.

Martínez-Huitle, C.A., Andrade, L.S., 2011. Electrocatalysis in wastewater treatment: recent mechanism advances. Quím. Nova. 34, 850–858, http://dx.doi.org/10.1590/S0100-40422011000500021.

Maurer, M., Pronk, W., Larsen, T.A., 2006. Treatment processes for source-separated urine. Water Res. 40, 3151–3166, http://dx.doi.org/10.1016/j.watres.2006.07.012.

Mudila, H., Prasher, P., Rana, S., Khati, B., Zaidi, M.G.H., 2018. Electrochemical oxidation-reduction and determination of urea at enzyme-free PPY-GO electrode. Carbon Lett. 26, 88–94, http://dx.doi.org/10.5714/CL.2018.26.088.

Nair, A.T., Makwana, A.R., Ahammed, M.M., 2014. The use of response surface methodology for modeling and analysis of water and wastewater treatment processes: a review. Water Sci. Technol. 69, 464–478, http://dx.doi.org/10.2166/wst.2013.733.

Osetrova, N.V., Skundin, A.M., 2002. Products of anodic oxidation of carbamide: effect of anionic composition of solution. Russ. J. Electrochem. 38, 266–269.

Piasek, Z., Urbanski, T., 1962. The infra-red absorption spectrum and structure of urea. Bull. Pol. Acad. Sci., Tech. Sci. X, 113–120.

Sangal, V.K., Kumar, V., Mishra, I.M., 2012. Optimization of structural and operational variables for the energy efficiency of a divided wall distillation column. Comput. Chem. Eng. 40, 33–40, http://dx.doi.org/10.1016/j.compchemeng.2012.01.015.

Showkat, N., 2016. Coverage of sanitation issues in India. SAGE Open 6, 1–6, http://dx.doi.org/10.1177/2158244016675395.

Simka, W., Piotrowski, J., Nawrat, G., 2007. Influence of anode material on an electrochemical decomposition of urea. Electrochim. Acta 52, 5696–5703, http://dx.doi.org/10.1016/j.electacta.2006.12.017.

Singla, J., Verma, A., Sangal, V.K., 2017. Performance and evaluation of electro-oxidation treatment of human urine metabolite uric acid using response surface methodology. J. Electrochem. Soc. 164, 312–320, http://dx.doi.org/10.1149/2.0681712jes.

Singla, J., Verma, A., Sangal, V.K., 2018. Parametric optimization for the treatment of human urine metabolite, creatinine using electro-oxidation. J. Electroanal. Chem. 809, 136–146, http://dx.doi.org/10.1016/j.jelechem.2017.12.061.

Sirés, I., Brillas, E., Oturan, M.A., Rodrigo, M.A., Panizza, M., 2014. Electrochemical advanced oxidation processes: today and tomorrow. A review. Environ. Sci. Pollut. Res. 21, 8336–8367, http://dx.doi.org/10.1007/s11356-014-2783-1.

Subba Rao, A.N., Venkatarangaiah, V.T., 2014. Metal oxide-coated anodes in wastewater treatment. Environ. Sci. Pollut. Res. 21, 3197–3217, http://dx.doi.org/10.1007/s11356-013-2313-6.

Thirugnanasambandham, K., Sivakumar, V., Maran, J.P., 2015. Response surface modeling and optimization of treatment of meat industry wastewater using electrochemical treatment method. J. Taiwan Inst. Chem. Ed. 46, 160–167, http://dx.doi.org/10.1016/j.jtice.2014.09.021.

Tseng, W.J., Cheng, C.C., Hsieh, J.H., 2014. Rattle-structured Ag/TiO2 nanocomposite capsules with bactericide and photocatalysis activities. J. Am. Ceram. Soc. 97, 407–412.

Urbańczyk, E., Sowa, M., Simka, W., 2016. Urea removal from aqueous solutions—a review. J. Appl. Electrochem. 46, 1011–1029, http://dx.doi.org/10.1007/s10800-016-0993-6.

Wang, N., Li, D., Yu, L., Yu, X., Sun, T., 2015. Preparation of RuO_2/nano-graphite cathode for electrocatalytic degradation of phenol. Int. J. Electrochem. Sci. 10, 13.

Wang, S., Xu, H., Yao, P., Chen, X., 2012. Ti/RuO_2-IrO_2-SnO_2-Sb_2O_5 anodes for Cl_2 evolution from seawater. Electrochemistry 80, 507–511, http://dx.doi.org/10.5796/electrochemistry.80.507.

Wu, W., Huang, Z.-H., Lim, T.-T., 2014. The recent development of mixed metal oxide anodes for electrochemical oxidation of organic pollutants in water. Appl. Catal. A 480, 58–78, http://dx.doi.org/10.1016/j.apcata.2014.04.035.

Yadav, A., Pandey, J., 2017. Contribution of point sources and non-point sources to nutrient and carbon loads and their influence on the trophic status of the Ganga River at Varanasi, India. Environ. Monit. Assess. 189, 475–493, http://dx.doi.org/10.1007/s10661-017-6188-8.

Yan, W., Wang, D., Botte, G.G., 2012. Nickel and cobalt bimetallic hydroxide catalysts for urea electro-oxidation. Electrochim. Acta 61, 25–30, http://dx.doi.org/10.1016/j.electacta.2011.11.044.

Zahedi, M., Jafarzadeh, K., Mirjani, M., Abbasi, H.M., 2018. The effect of anodizing time on the electrochemical behavior of the Ti/TiO_2 NTs/IrO_2-RuO_2-Ta_2O_5 anode. Ionics 24, 451–458, http://dx.doi.org/10.1007/s11581-017-2210-y.

Zöllig, H., Remmele, A., Fritzsche, C., Morgenroth, E., Udert, K.M., 2015. Formation of chlorination byproducts and their emission pathways in chlorine mediated electro-oxidation of urine on active and nonactive type anodes. Environ. Sci. Technol. 49, 11062–11069, http://dx.doi.org/10.1021/acs.est.5b01675.

Journal of Water Process Engineering 32 (2019) 100944

Contents lists available at ScienceDirect

Journal of Water Process Engineering

journal homepage: www.elsevier.com/locate/jwpe

Applications of doped mixed metal oxide anode for the electro-oxidation treatment and mineralization of urine metabolite, uric acid

Jayishnu Singla[a], Anoop Verma[a], Vikas K. Sangal[b,*]

[a] School of Energy and Environment, Thapar Institute of Engineering and Technology, Patiala, Punjab, India
[b] Department of Chemical Engineering, Malaviya National Institute of Technology, Jaipur, Rajasthan, India

ARTICLE INFO

Keywords:
Uric acid
Electro-oxidation
Response surface methodology
Photo-electrocatalysis
Doped-mixed metal oxide anode

ABSTRACT

Removal of nitrogen-based contaminants present in urine wastewater has become a considerable matter of concern because of its potentially harmful effects on human health and can cause alterations to aquatic life. Hence to avoid its dangerous effects, electro-assisted technology was employed for the voidance of this metabolite with the doped-mixed metal oxide. The influence of various input factors such as time, pH, current density and NaCl dose on treatment efficiency in terms of percent degradation and energy consumption were evaluated using response surface methodology. Electrolysis results showed that 95.35% degradation of uric acid was achieved at optimized conditions. In addition, to reduce the treatment time further, attempts have been made by incorporating dual effect i.e. Photoelectrocatalysis. The anode used for multiple runs were proven to be effectively stable through XRD and SEM/EDS. Analysis of treated uric acid solution was validated in terms of COD (92%) and TOC (89%) reduction. The transformation products of uric acid were identified through LC–MS. Based on these intermediates and literature survey, an oxidative mechanism for uric acid has been proposed. The total operating cost for electro-oxidation treatment process is found to be 0.18 $/m^3.

1. Introduction

In recent years, it was predicted that in a developing country like India around 66% of the population still practice open defecation and urination [1]. Moreover, it was observed that a great percent of underprivileged areas and urban slums are not connected to properly to any sewerage systems [2]. This will eventually lead to the discharge of generated hazardous waste into nearby areas, causing a wide range of health problems like malnutrition, diarrhea, anemia, retarded growth, etc. due to contamination of soil and surface water [3]. This depicts that huge proportion of the population living at risk of contamination of the environment by human fecal and urine wastewater. One of primitive way is the separation of urine and fecal. Out of which fecal can be handled by traditional solid waste management tools and the reuse of urine for re-flushing is something which can be worked on [4].

Human urine is mixed wastewater with complex chemical composition and contains most of the nitrogen-based compounds such as urea, uric acid, creatinine, etc. Among them, uric acid is a principal component of urinal wastewater. It is a primary enzymatic final breakdown product of dietary purine metabolism in the human body. It is mainly present in human blood with a normal range of 250 mg/day to 750 mg/day with a period of over 24 h [5]. In addition, uric acid is excreted via urine (2.4 mg/dL to 7.0 mg/dL) as bio refractory pollutant which leads to the serious alterations in the aquatic environment as well as can cause potential risk on human health [6,7]. Due to its toxicity, persistence and recalcitrant to conventional treatment technologies, there is an urgent requirement of some effective alternative technologies for the on-site treatment of urinal wastewater.

Electro-oxidation process (EO) have proven their potential for destroying as well as mineralize the recalcitrant pollutants into simpler compounds [8]. The process has received great attention for the treatment of mixed wastewater because of its effectiveness, environmental compatibility, economical (involvement of clean reagent i.e electron) and provides easy process control [9]. Generally, during electrolysis, the mineralization of toxic organic substances into inorganic ions and biocompatible compounds takes place due to the in-situ generation strong, powerful non-selective oxidant species of hydroxyl radicals ($OH^{\cdot}$) on the electrode surface [10]. In the development of the EO process technology, electrodes play a very important key role. Reviews have been reported for the EO treatment of various toxic organic pollutants present in wastewater with the different type of anodes such as graphite, glassy carbon, Pt, RuO_2, IrO_2, PbO_2, SnO_2, boron-doped diamond (BDD) and mixed metal oxide (MMO) [11,12]. Out of these, BDD is found superior for the destruction of refectory pollutants

* Correspondence author.
E-mail addresses: anoop.kumar@thapar.edu (A. Verma), vksangal.chem@mnit.ac.in (V.K. Sangal).

https://doi.org/10.1016/j.jwpe.2019.100944
Received 14 July 2019; Received in revised form 27 August 2019; Accepted 5 September 2019

and remediation of wastewaters [13] due to its high efficiency and exceptional compatibility. But the main issue encountered with the BDD is their high cost, difficulty in fabrication of coating complex shapes and formation of toxic byproducts such as chlorates, perchlorates, etc. [14,15]. Unlike BDD, MMO has low production cost, easy fabrication, highly stable with low oxygen potential, saves energy cost at industrial scale and show similar properties of BDD by producing $OH^{\cdot}$ on anode surface [16]. In past few years, MMO anodes such as binary (Ir-Ta, Ir-Ru, Sn-Sb), tertiary (Ir-Ru-Sn, Ir-Ru-Pt) and quaternary (Ru-Ir-Sn-Ti) have received a great deal of interest for removal of a wide range of toxic, organic components present in water and wastewater [17]. Unlike others, SnO_2 electrodes doped with antimony MMO have shown a high percentage of destruction along with the minimal formation of toxic byproduct [18]. Different type of electrodes have shown their worth in detecting the level of uric acid in serum and urine [19–26] but rarely discussed their removal. The reason could be the complexity of urinal wastewater, limitations for on-site treatment and process complications.

The present study attempts to cover some of these pitfalls using a novel combination of different active/ non-active metals that is Sb-Sn-Ta-Ir/Ti quaternary anode has been chosen for the treatment of uric acid. In order to get excellent resistance properties and good service life iridium (Ir) was incorporated. Tantalum (Ta) provides high current densities and enable the anode to work on high values of applied current without causing any damage. The integration of tin (Sn) was done to get more active sites for the generation of reactive oxygen species. Antimony (Sb) was doped in order to increases the conductivity of anode as well as lowers the oxygen evolution overpotential [27].

To our best knowledge, this is one of the few reported studies for the treatment of uric acid using novel quaternary doped-MMO. Systematic studies using response surface methodology were carried out in order to establish the process conditions where uric acid has been eliminated completely from an aqueous medium. The efficiency of the treatment process was evaluated in terms of responses, percent degradation and energy consumption. In fact, this is the first reported study of doped-MMO with more than 55 recycles for studying the degradation of uric acid in aqueous solution. The electrochemical stability of anode was analyzed through different characterization facilities. The quality of treated effluent was also validated using different analytical techniques.

2. Material and methods

2.1. Chemicals and materials

Uric acid ($C_5H_4N_4O_3$) of analytical grade (99.5% purity), supplied by Sigma-Aldrich (Missouri, U.S). Sulfuric acid, sodium hydroxide, sodium sulfate and sodium chloride were all of the analytical grade and purchased from Loba Chemi Pvt. Ltd, (India). The double-distilled water was utilized for the preparation of all solutions. Stainless steel (SS) used as cathode and doped-MMO used as an anode were procured from Bio age Pvt. Ltd. and Exotic Elements Pvt. Ltd. (India) respectively. DC supply with the model (0–30 V, 0–2 A) was purchased from DIGITECH, Ambala, India.

2.2. Experimental setup and procedure

The uric acid solution was prepared fresh every time by dissolving 50 mg in 1 L double distilled water. For EO experiments, a single compartment cell made up of borax glass beaker having a working volume of 400 mL was used (see graphical abstract). Single pair of doped-MMO and SS plates having dimensions (7 cm* 7 cm* 1 cm) with an effective working surface area of 42 cm^2 were used in each experimental run. In this study, both electrodes were placed parallel with inter-electrode spacing was maintained at ~2.0 cm for every experiment. During electrolysis, the current was maintained throughout the experiment run using DC power supply. For proper homogeneous mixing of the aqueous solution during experimental runs magnetic stirrer was used. All experiments were performed under controlled temperature conditions of 25 °C.

EO experiments for the treatment of uric acid were performed under galvanostatic conditions. Before electrolysis, aliquots of H_2SO_4 (0.1 N) and NaOH (0.1 N) were added in order to adjust the solution pH to the desired level. At certain time intervals, samples of 1 mL volume were taken out from the solution and filtered using 0.45 μm nylon filters and analyzed through UV–vis at λ_{max} 290 nm. All experiments were performed thrice in order to check the reproducibility of results and suitable statics were applied for the validation of results. The final pH of the uric acid solution was stabilized at 4.75.

2.3. Analytical methods

For the analytical evaluation of the withdrawn samples, several instruments were used in the present study [28–33]. The detailed procedure and information regarding the equipment have been provided in the supplementary information (Scheme S1).

2.4. Experimental design

For designing the experimental data for EO treatment of uric acid with doped-MMO, Box-Behnken design (BBD) under response surface methodology (RSM) was employed. The detailed description of experimental design using RSM has been given in supplementary information (Scheme S2) [34–36]. In order to evaluate the performance of EO treatment process, four input parameters like current density, NaCl dose, treatment time and pH and two responses i.e. %degradation and energy consumed were selected. The responses for EO treatment process were calculated by the following Eqs. (1) and (2) [37].

$$Y_1 = \frac{C_{0-C_t}}{C_0} \times 100 \tag{1}$$

$$Y_2 = \left[\frac{VIT}{V_s}\right] \times 10^3 \tag{2}$$

where, C_0 = initial uric acid concentration (mg/L); C_t = uric acid concentration at different time intervals (mg/L) ; I = current (A); V = cell voltage; t = treatment time (h); V_s = solution volume (L); Y_1 = % degradation and Y_2 = energy consumption (kWh/m^3).

2.5. Synergy calculations

In this present study, the synergy of the dual-process i.e. photoelectrocatalysis over individual processes has been calculated using the following Eqs. (3) and (4) [40].

Synergy over individual processes [photocatalysis or electro-oxidation]:

$$\%Synergy = 100 \times \left\{\frac{[k_{dual} - (k_{photocatalysis}\ or\ k_{electroxidation})]}{k_{dual}}\right\} \tag{3}$$

Overall Synergy:

$$\%Synergy = 100 \times \left\{\frac{[k_{dual} - (k_{photocatalysis} + k_{electroxidation})]}{k_{dual}}\right\} \tag{4}$$

Where 'k' = pseudo-first-order rate constant (min^{-1}) of each process and calculated from Eq. (5)

$$-\ln\frac{C_0}{C_t} = k_1 t \tag{5}$$

2.6. Operating cost analysis

The overall cost for the treatment process includes the cost of

Table 1
BBD matrix used for electro-oxidation treatment of Uric acid.

Std	Run	Block	Current density (mA cm^{-2})	NaCl dose (g L^{-1})	Time (min)	pH	% Degradation	Energy consumption (kWhr m^{-3})
2	1	1	11.90	0.25	30	7	15	6.68
1	2	1	2.38	0.25	30	7	19	0.5
5	3	1	7.14	0.75	5	3	27	0.34
8	4	1	7.14	0.75	55	11	50	3.93
4	5	1	11.90	1.25	30	7	60	4.2
3	6	1	2.38	1.25	30	7	17	0.35
10	7	1	7.14	0.75	30	7	65	2.1
6	8	1	7.14	0.75	55	3	98	3.45
7	9	1	7.14	0.75	5	11	24	0.37
9	10	1	7.14	0.75	30	7	65	2.1
18	11	2	7.14	1.25	55	7	55	3.2
20	12	2	7.14	0.75	30	7	65	2.1
17	13	2	7.14	0.25	55	7	31	6.83
11	14	2	2.38	0.75	30	3	36	0.39
12	15	2	11.90	0.75	30	3	75	4.86
14	16	2	11.90	0.75	30	11	40	5.2
13	17	2	2.38	0.75	30	11	29	0.45
19	18	2	7.14	0.75	30	7	65	2.1
15	19	2	7.14	0.25	5	7	7	0.64
16	20	2	7.14	1.25	5	7	10	0.31
26	21	3	7.14	1.25	30	3	88	1.69
25	22	3	7.14	0.25	30	3	42	3.68
22	23	3	11.90	0.75	5	7	12	0.86
29	24	3	7.14	0.75	30	7	65	2.1
23	25	3	2.38	0.75	55	7	22	0.74
21	26	3	2.38	0.75	5	7	4	0.07
24	27	3	11.90	0.75	55	7	44	9.08
30	28	3	7.14	0.75	30	7	65	2.1
27	29	3	7.14	0.25	30	11	20	3.86
28	30	3	7.14	1.25	30	11	48	1.86

electrodes, cost of stirring, cost of chemical and electrical energy consumed. However the process is found to be energy-intensive, therefore total cost for operation is due to the electrode cost and electrical power consumed. Hence, in this study, the total operating cost for the EO process was calculated using the following Eq. (6)

$$\text{Operating cost} = C_{EC} + C_{EL} \quad (6)$$

Where, C_{EC} = cost of energy consumed (kWh/m^3) and C_{EL} = cost of electrodes (Rs). The price of electricity in Punjab, (India) = ~ Rs 5.00 /kWh. The cost of the doped-MMO anode is Rs 820 per piece. The manufacturer/supplier has specified the life span of the electrode is 5 years

3. Result and discussion

The present statistical investigation was carried out through Design-Expert software version 6.0.8 (STAT-EASE Inc., Minneapolis, US) in order to minimize the void content and to optimize the experimental data. All the experimental runs were performed according to the design given by BBD as listed in Table 1. A quadratic model was suggested by exploiting sequential F-test and other adequacy measures [38]. The results of model summary statistics showed the highest R^2 values of both responses for the quadratic model i.e. 0.9629 and 0.9907 respectively. This advocates that model has explained the experimental data very well and indicate the satisfactory interaction between predicted and observed values of experimental runs. Hence, the model chosen was quadratic which was used to describe the effect of various operational process parameters on the treatment of uric acid using the EO process.

For processing the chosen quadratic model, manual regression method was applied in which insignificant model terms were evicted automatically and provide compiled results with a reduced quadratic equation. Table 2 shows the results of the quadratic model fitting in the form of analysis of variance (ANOVA). The detailed description of ANOVA results was given in supplementary information (Scheme S3) [41]. To check the reliability of chosen models for both responses, plots of normal % probability vs studentized residuals as depicted in Fig. 1 and studentized residuals vs predicted (discussed (Scheme S3). From the plots, it was observed that the points on this plot lie fairly close to the diagonal straight line which indicates that the model well satisfies the assumptions of the ANOVA [42]. Moreover, it also depicts that a normal plot is also a suitable graphical method for judging residuals normality and confirms the normal distribution of the observed data.

3.1. Effect of process parameters and Optimization

Three dimensional (3D) response graphs developed were studied in order to see the interactive effect of each operational parameters on responses as well as used to locate the optimal conditions for process parameters.

3.1.1. Effect of j, n, t, and pH on %degradation, Y_1

Fig. 2A shows the interaction between current density (j) and pH as well as their effect on Y_1. In the EO treatment study, it was always found that j considered an important operating process factor because of the cost-effective analysis. Moreover, transferring of electrons, generation of oxidant species, and process efficiency all depends upon applied j. It can be seen that when j increased from 2.38 mA/cm^2 to 9.52 mA/cm^2, Y_1 was also increased because of increase in production of electrons during electrolysis which in turn has increased the generation of strong oxidants. But the further increase in values of j from 9.52 mA/cm^2 to 11.90 mA/cm^2, Y_1 was found constant. This trend was observed at pH ≈ 3.5. Furthermore, when pH was increased from 3.5 to 11 it has been found that Y_1 increases gradually with increasing j values upto 7.14 mA/cm^2 then become decreasing with increasing j values. This happened because, at very low and high values of j, generation of reactive chlorine species (RCS) and reactive oxygen species (ROS) on doped-MMO were falling down gradually with time. Due to which the

Table 2
ANOVA results for responses Y_1 and Y_2.

Sources	% Degradation (Y_1)					Energy Consumed (Y_2)				
	Sum of square	DF	Mean square	F-value	Prob > F	Sum of square	DF	Mean square	F-value	Prob > F
Block	54.60	2	27.30			0.28	2	0.14		
Model	17617.12	14	1258.37	24.09	< 0.0001	148.68	14	10.62	98.98	< 0.0001
Z_1	1180.08	1	1180.08	22.59	0.0004	67.12	1	67.12	625.52	< 0.0001
Z_2	1728.00	1	1728.00	33.08	< 0.0001	9.33	1	9.33	86.93	< 0.0001
Z_3	3888.00	1	3888.00	74.44	< 0.0001	50.59	1	50.59	471.52	< 0.0001
Z_4	2002.08	1	2002.08	38.33	< 0.0001	0.13	1	0.13	1.23	0.2869
Z_1^2	3394.71	1	3394.71	65.00	< 0.0001	1.55	1	1.55	14.42	0.0022
Z_2^2	2070.11	1	2070.11	39.63	< 0.0001	1.91	1	1.91	17.78	0.0010
Z_3^2	2988.11	1	2988.11	57.21	< 0.0001	6.171E-003	1	6.171E-003	0.058	0.8142
Z_4^2	72.43	1	72.43	1.39	0.2601	0.027	1	0.027	0.25	0.6257
Z_1Z_2	552.25	1	552.25	10.57	0.0063	1.36	1	1.36	12.65	0.0035
Z_1Z_3	49.00	1	49.00	0.94	0.3504	14.25	1	14.25	132.81	< 0.0001
Z_1Z_4	196.00	1	196.00	3.75	0.0748	0.020	1	0.020	0.18	0.6761
Z_2Z_3	110.25	1	110.25	2.11	0.1700	2.72	1	2.72	25.37	0.0002
Z_2Z_4	81.00	1	81.00	1.55	0.2350	2.500E-005	1	2.500E-005	2.330E-004	0.9881
Z_3Z_4	506.25	1	506.25	9.69	0.0082	0.051	1	0.051	0.47	0.5042
Residual	678.98	13	52.23			1.39	13	0.11		
Lack of fit	678.98	10	67.90			1.39	10	0.14		
Pure error	0.000	3	0.000			0.000	3	0.000		
Core total	18350.70	29				150.36	29			

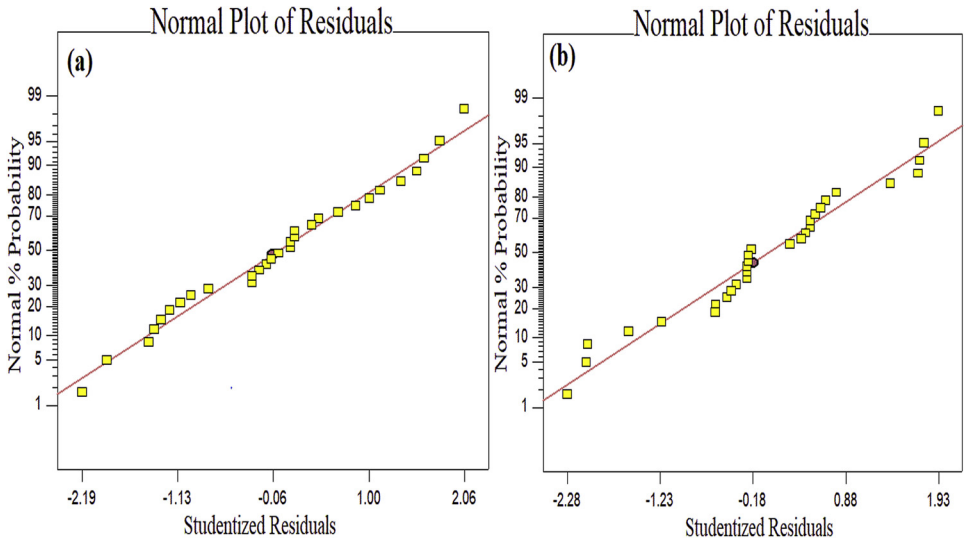

Fig. 1. Model adequacy plots for responses (a) %Degradation and (b) Energy consumption.

current efficiency of other side reactions such as oxygen evolution reaction increased. But on increasing, j values from lower value helps in generation of more oxidants such as $OH^{\cdot}$, HClO, ClO, etc.

The pH of the solution is considered as a crucial factor for influencing the EO process performance. From results, it was observed that maximum Y_1 was achieved at lower values of pH. This was due to the high adsorption rate of generated $OH^{\cdot}$ in the oxide lattice of the anode at acidic pH [43]. In the EO process, both mechanisms direct and indirect oxidation takes place simultaneously for the maximum degradation of target pollutant. The generation rate of reactive oxidant species like $OH^{\cdot}$, ozone, $HO_2^{\cdot}$ and RCS along with the capability of e-transfer is highly dependent upon the j and solution pH. Many studies in the literature have confirmed that doped-MMO acts as active anode and reactions occur on its surface during the EO treatment is the water oxidation reactions which in turn leading to the formation of adsorbed $OH^{\cdot}$ and led to direct oxidation of compound. Furthermore, at acidic pH, the generation of the strong oxidant species with high oxidant potential such as $OH^{\cdot}$, HClO, ClO- in the bulk was more which indirectly oxidize the target pollutant. While, in the case of basic pH, it was found that the concentration of lower potential oxidant species such as H_2O_2, $HO_2^{\cdot}$, ClO_3- and ClO_4- was more [44]. Thus, degradation of uric acid was found minimum at neutral and basic pH. Therefore, the oxidation of the target pollutant was found to be maximum at acidic pH because of the involvement of both mechanisms, direct and indirect EO.

The concentration of NaCl (n) always plays a significant role because it influences the efficiency of the process by generating RCS in the bulk. From the response graph (Fig. 2B), it has been observed that for lower values of n ≈ 0.5 g/L and t ≈ 17.5 min, Y_1 was found constant. Further increase in values of n ≈ 0.5–1.0 g/L and t ≈ 17.5 min–42.5 min, it was found that Y_1 was also increased. However, when n and t were increased further to 1.25 g/L at 55 min, Y_1 was found remained almost unchanged. From the results, it was concluded that an increase in the Y_1 may be attributed due to the change in the ionic strength of the solution. The increase in ionic strength at higher values of n will generally cause an increase in current density in the same cell voltage and hence maximum Y_1 was achieved [45]. It observed that after certain values of n and j, Y_1 was found the minimum. This might be happening due to the (i) scavenging of $OH^{\cdot}$ by high chloride dose,

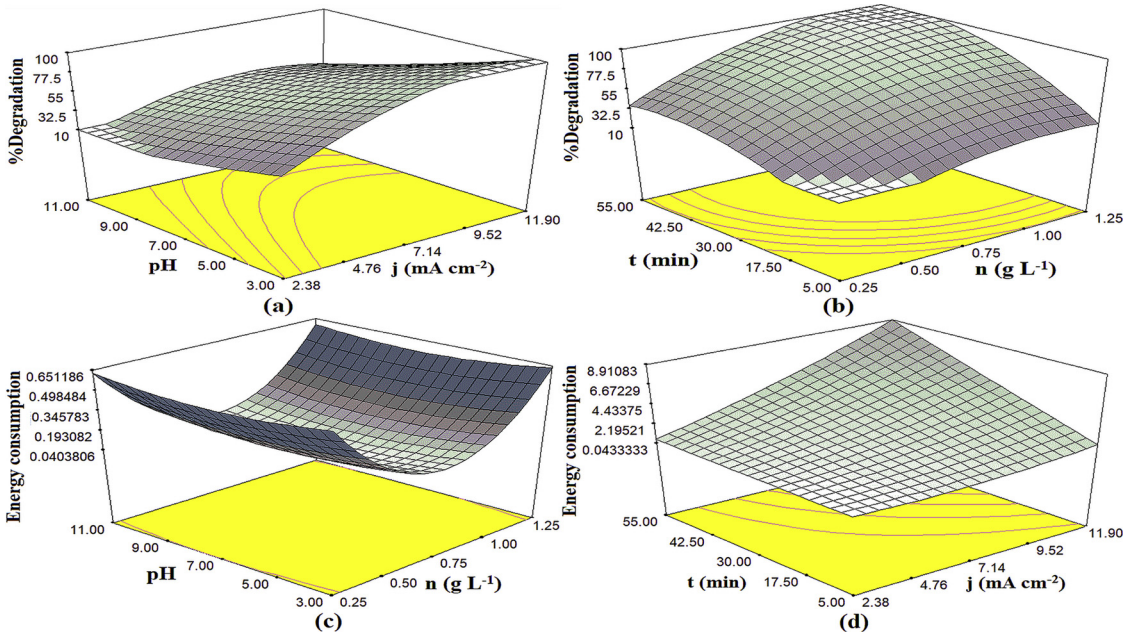

Fig. 2. Effect of various input parameters on %degradation and energy consumption during the EO treatment of uric acid (a) pH & j; (b) t & n; (c) n & pH and (d) t &. j.

Table 3
Individual and Synchronized optimization results.

Response	Current density (mA cm^{-2})	NaCl dose (g L^{-1})	Time (min)	pH	Desirability
Individual optimization					
% Degradation (Y_1) = 98.02	9.15	1.16	39.76	3.36	1.00
Energy consumed (Y_2) = 0.067 kW h m^{-3}	5.50	0.70	5.57	3.42	1.00
Synchronized optimization					
% Degradation(Y_1) = 97.20%	7.46	1.11	42.79	3.25	0.880
Energy consumed (Y_2) = 2.588 kW h m^{-3}					

(ii)formation of more chloramines in the system [46], (ii) metal dissolution which leads to the formation of bigger flocs, (iii) most of the applied current consume by gas evolution and side reactions and (iv) increases the temperature of the solution.

Moreover, it was observed that prolonged EO at higher j values always leads to the fouling of the anode because of the bond formation between pollutant and oxide lattice of an anode which grows like an impermeable film with time. Hence, for better process performance and longer service life of anodes optimization of process variables is very important.

3.1.2. Effect of j, n, t, and pH on energy consumption, Y_2

From Fig. 2C, it can be seen that at lower values of n ≈ 0.25 g/L, Y_2 was found maximum for all values of pH. But further increase in n values from 0.25 g/L to 0.75 g/L, Y_2 was found minimum. This trend was observed for all values of pH. However further increase in n value ≈ 1.0 g/L, Y_1 was found increased at all values of pH. Thereafter, it was observed that at very high values of n ≈ 1.25 g/L, Y_1 found maximum at lower (3) and higher (11) values of pH while minimum at pH from 5 to 9. At lower values of n, the conductivity of the solution was also lower due to which an increase in voltage drops took place which further leads to the increase in Y_2 value. While at higher values of n, Y_2 was found to be minimal because of the ease of current flow through the electrolyte solution. From Fig. 2D it can be seen that with increasing j and t values, Y_2 was also found increasing. This might happened because electrical power consumption is directly proportional to the current and time [47]. However, it was found that the effect of pH on Y_2 was found to be marginal or less when compared to other parameters.

3.1.3. Optimization

For the present study, simultaneous optimization of multi-responses was done in order to find out optimized conditions for EO treatment of uric acid using doped-MMO [39]. Optimum conditions selected for both responses were done in such a way that Y_1 should come out to be maximum and Y_2 should be minimized. This optimization technique basically evaluates a point that maximizes the desirability function. The optimum conditions obtained using desirability function approach were j = 7.46 mA/cm^2, n = 1.11 g/L, pH = 3.25 and t = 42.79 min along with combined desirability value D = 0.880. Under these conditions, value for responses Y_1 and Y_2 were 97.20% and 2.588 kW h/m^3 respectively as suggested by BBD as shown in Table 3. To validate these results further additional experiments have been performed at optimized conditions. The value of the response Y_1 = 95.35% and Y_2 = 2.479 kW h/m^3 which was found in close agreement to the predicted values as listed in Table 4. On seeing the good correlation between predicted and observed values depicts the reliability of incorporating the desirability function approach by BBD and has effectively optimized the process parameters for the EO treatment of uric acid.

3.2. Synergistic studies

As discussed in Section 2.5, synergistic studies have been performed using kinetic rate constant obtained through pseudo-first-order reactions. The oxidation experiments of uric acid were performed with doped-MMO in a batch reactor and three different techniques were

Table 4
Comparison between predicted and actual experimental values.

Responses	Predicted	Actual
% Degradation	97.20	95.35
Energy consumed (kWh m^{-3})	2.588	2.479

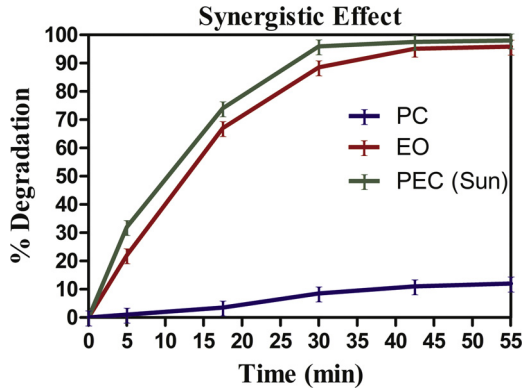

Fig. 3. Synergistic study of the dual-process Photo-electrocatalysis.

applied which include photo-catalysis (only light source), EO (constant current supply only) and photoelectrocatalysis (constant applied current and light). Fig. 3 shows that only 12% (under solar light) and 8.5% (under UV) degradation of uric acid were achieved through photo-catalysis after 1 h. In case of photoelectrocatalysis, 89.5% (under UV light) and 96% (under solar radiation) degradation of uric acid were achieved within 30 min of electrolysis, while EO took almost 1 h to reach that value (95.35%). Moreover, an immense increase in the first-order rate constant in case of the integrated process (0.0854 min^{-1}) which was 3.4 times of photo-catalysis (0.0025 min^{-1}) and 1.4 times as compared to EO (0.0616 min^{-1}) confirms the viability of dual-process over single treatment processes as shown in Fig. 4. The synergistic effect of the dual-process over EO came out to be 27.86% and over photo-catalysis, it was 97.07% as quantified from (Eq. (5)). While the overall synergy of the dual-process was found to be 24.94% as calculated from (Eq. (6)). Therefore, it concludes that the dual-process with synergistic results prompts it field-scale applications for the wastewater treatment with a significant decrease in treatment time.

To further confirm our claim, experimental studies were carried out using fluorescence spectroscopy for the estimation of $OH^{\cdot}$ production at doped-MMO under different light sources. Fig. 5A showed that maximum $OH^{\cdot}$ production was found under solar radiations (photoelectrocatalysis) than UV and EO. This might happen due to the activation of photoactive layers i.e TiO_2 and SnO_2 of anode under light sources leading to the generation of more $OH^{\cdot}$ on the surface of anode resulting more percentage degradation of uric acid in less time. Some researchers have also reported that doping can improve the photoactivity of the anode by increasing the charge separation of holes and electrons [48].

In order to verify the effect of pH on the generation of $OH^{\cdot}$, experiments were performed at different pH. From the results, it was found that more $OH^{\cdot}$ production was observed at basic pH over acidic and neutral pH (Fig. 5B). But at the same time, it was also observed that in the case of basic and neutral pH generation of $OH^{\cdot}$ decreases with increasing time. While in the case of acidic pH it was opposite. Hence, this advocates that degradation of uric acid was found to be largely due to indirect oxidation and minutely by $OH^{\cdot}$ at optimized conditions.

3.3. Durability studies

The economy of the treatment process for the pilot-scale applications majorly depends upon the stability of the anode [49]. Thus, in order to evaluate its ability to oxidize the pollutant, the doped-MMO anodes were used for multiple time in all extreme conditions. From Fig. 6, it was found that despite the harsh conditions, doped-MMO performed significantly well even after 55 recycles (64.166 h) without much substantial loss in electro-oxidation process efficiency. The stability of theses active doped-MMO was due to the incorporation of different metal oxide combinations which not only increased its service life as well as enhanced its electrochemical activity for a longer period of time. To further confirm its stability as well as to investigate the electrochemical and photochemical properties, anodes were characterized through SEM/EDS and XRD analysis as described in Section 3.4.

3.4. Characterization of a doped-MMO anode

Fig. 7(A–C) shows the SEM images of the Ti sheet without any coating, freshly coated anode and recycled anodes. From the image (Fig. 7B), it was observed that thermally decomposed prepared anode exhibits a slightly rough, porous, smaller and shallower mud cracked type structure, thus depicted anode with enhanced working area. A larger active working area resulted in an increased catalytic activity which further facilitates the lowering of effective current density [50]. The appearance of cracks on the fabricated anode surface depicts that the islands (white bright spots) are made up of different oxide layers with an average width of 5 μm [51]. The presence of Ti as a substrate in the anode has helped in the formation of the oxide layer of TiO_2 which is UV active helps in the generation of $OH^{\cdot}$ at the anode surface [52]. Addition of Ta in the anode has enabled the anode to work at higher values of current without causing any damage to an anode [53]. Moreover, the results are consistent with other reported studies that show the incorporation of Sb and Sn has affected the morphology by improving the structure of coatings. The SEM image of recycling anode (Fig. 7C) showed relatively identical surface characteristics and morphology thus confirms the uniformity of different metal oxide layer even after fifty-five recycles.

For an elemental composition of the different metal oxides coated on anode surface (freshly as well as recycled doped-MMO), EDS was

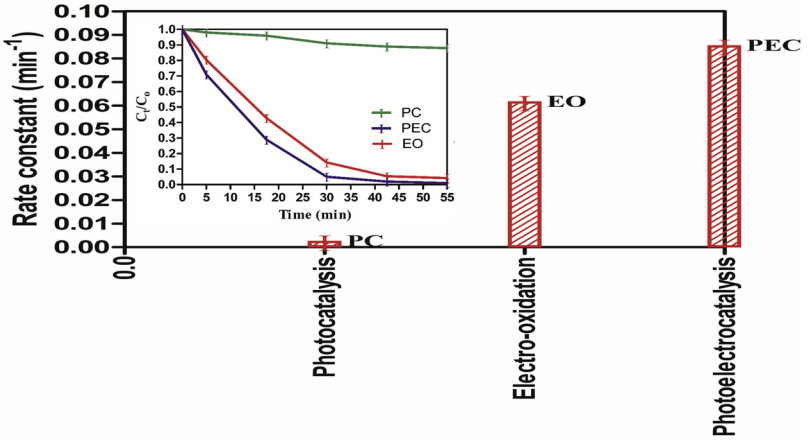

Fig. 4. Plot of pseudo-first-order rate constant for uric acid degradation through different processes. The plot of C_t/C_o vs time for different technologies (inset).

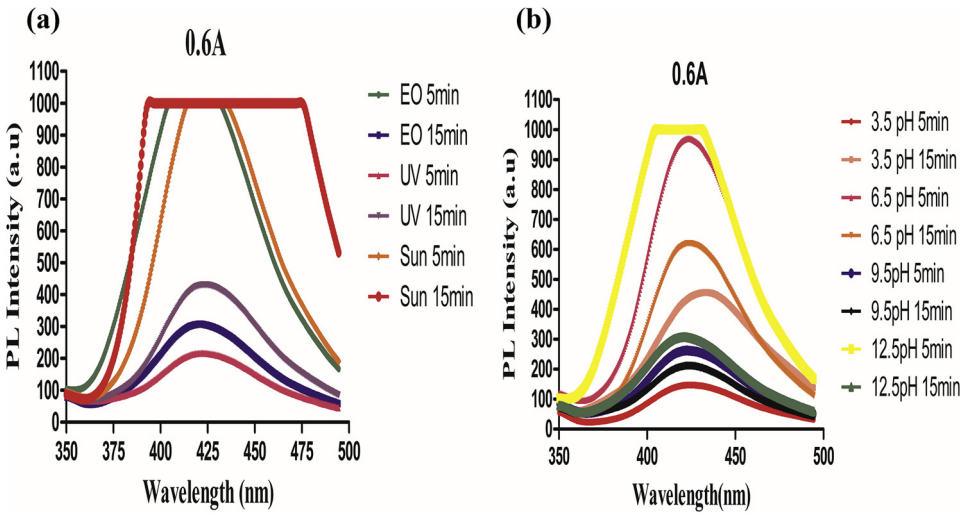

Fig. 5. PL spectra of $OH^{\cdot}$ at doped-MMO for (a) different light sources (b) different pH and time intervals at 0.6 A.

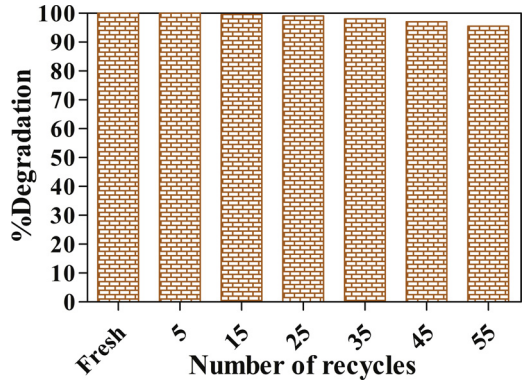

Fig. 6. Recyclability pattern of doped-MMO.

performed. The stability of novel doped-MMO was further proven with the presence of a predominant peak of all the five elements i.e. Sb, Sn, Ir, Ta, O, and Ti even in the recycled sheet. EDS data (Inset) depicts the quantitative analysis in terms of molecular concentration of different metals in the oxide mixture which seemed almost the same in both fresh and recycle anode, thus confirming the stability of anodes even after 55 recycles.

Fig. 8(A–C) shows X-ray diffractogram (XRD) of a Ti sheet only, the freshly coated and recycled plate. XRD helps to identify the existence of different metals in the oxide mixture. From results, it was clearly seen that the sharp peaks of TiO_2 with rutile phase, few peaks of anatase Ti along with the characteristic reflection of SnO_2 with rutile-type structure. This indicates that the mixed coating of different metals has covered the surface of the Ti substrate significantly [54]. Despite the incorporation of doping ions into SnO_2 with low doping level, few diffraction peaks of Sb was still observed in XRD spectra [55]. The peak of IrO_2 and Ta_2O_5 were also confirmed from XRD spectra. Furthermore, the same peaks of oxides of metal were observed in recycled doped-MMO, hence confirming the confinement of all metal oxide even after multiple runs. It was observed that few metal oxide peaks were deviated from their original position due to loss of some amount of metals in the multiple runs of the experiment. Further details regarding the

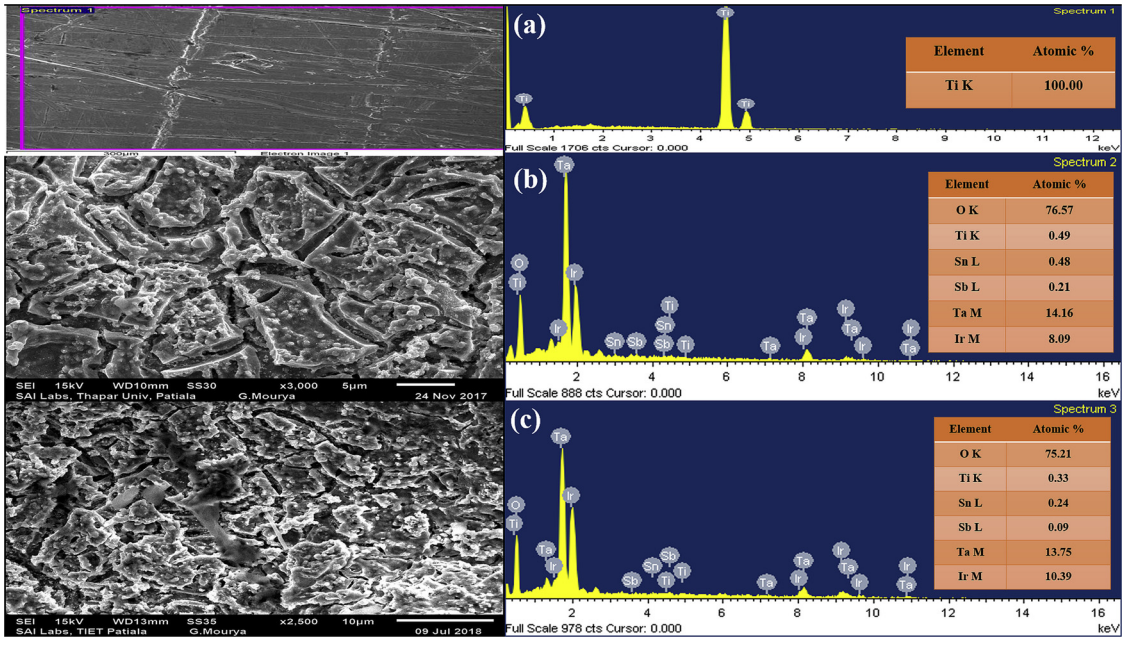

Fig. 7. The atomic percentage of different metals analyzed by EDS and SEM images of (a) Ti Sheet, (b) freshly coated doped-MMO (c) recycled doped-MMO.

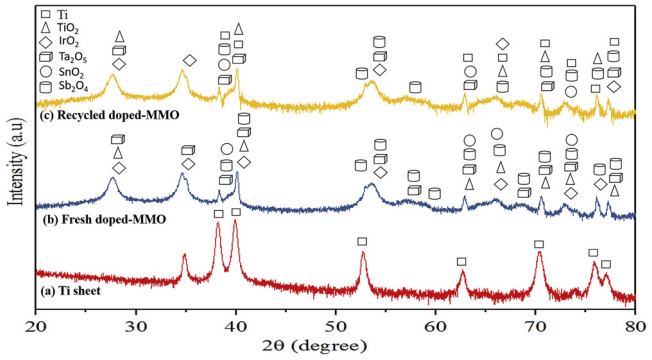

Fig. 8. XRD pattern of doped-MMO (Ti sheet, freshly coated and recycled plate).

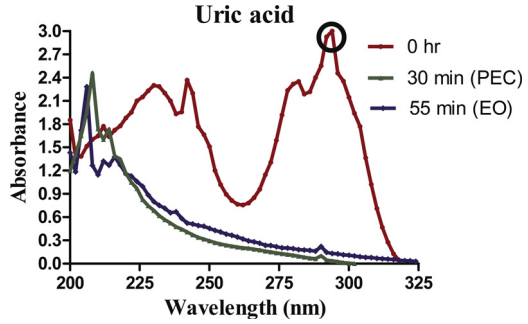

Fig. 9. UV–vis spectra of untreated (t = 0 min) and treated samples (EO [t = 55 min] & photoelectrocatalysis [t = 30 min]) at optimized conditions.

diffractions peaks have been discussed in Scheme S4 [56,57].

3.5. Mineralization studies

The mineralization studies of uric acid were performed using spectrophotometric analysis (Fig. 9) for the treated samples initially and to further confirm the degradation of uric acid, some analytical test such as COD, TOC, total available chlorine (TAC) and inorganic ions were performed at optimized conditions. Fig. 10A shows the results of

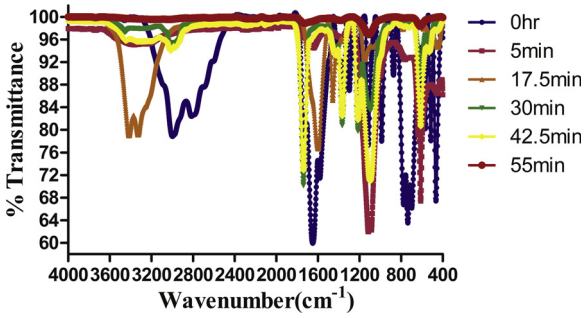

Fig. 11. FT-IR spectra of uric acid at certain intervals of time.

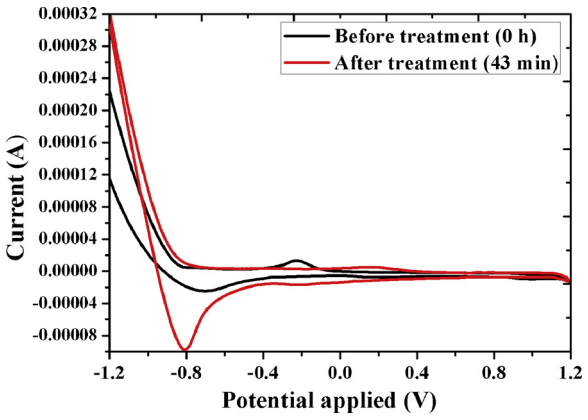

Fig. 12. Cyclic Voltammetric analysis of uric acid (a) untreated samples (0 h) and (b) treated samples (43 min).

mineralization of uric acid in terms of reduction of COD and TOC. More than 90% decrement in COD and 80% reduction in TOC were observed in 43 min. When treatment was further continued to 70 min it was found that reduction in COD and TOC became constant depicting that oxidation of uric acid into byproducts was completed.

Production of inorganic ions such as NO_2^-, NH_4^+ and NO_3^- were observed after 5 min of EO treatment of uric acid as shown in Fig. 10B. Furthermore, it was also observed that the concentration of nitrite ion

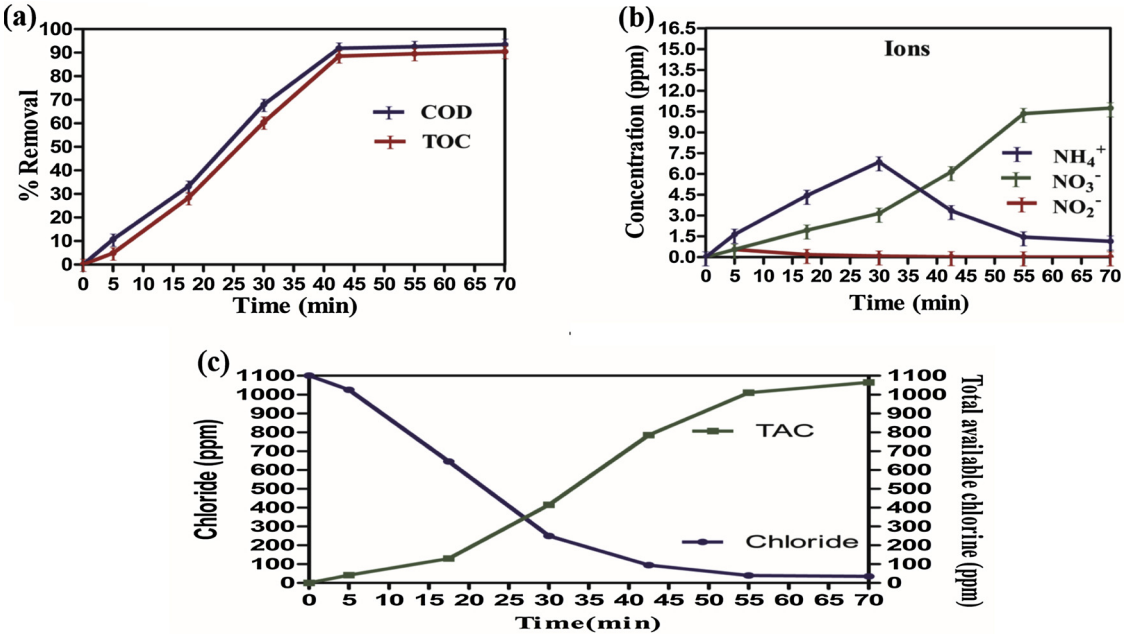

Fig. 10. Evolution plots of (a) COD and TOC (b) inorganic ions (c) chloride and TAC concentration at optimized conditions.

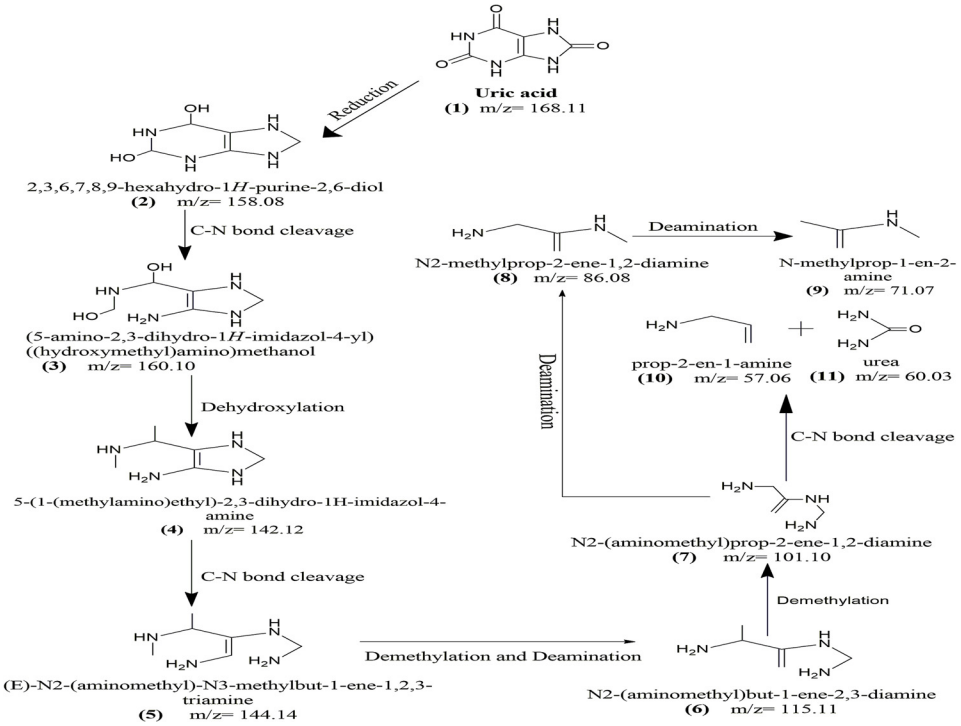

Fig. 13. Proposed oxidative pathway of uric acid with doped-MMO.

decreased after 15 min of electrolysis while NH_4^+ got reduced after 30 min of EO treatment. In the case of NO_3^- concentration, a continuously increasing trend was observed. This might be due to the oxidation of NO_2^- and NH_4^+ by strong oxidants such as $OH^{\cdot}$, HOCl, etc. into nitrate ions as per reported in literature studies [5]. Fig. 10C depicts the decreasing concentration of Cl^{-1} and increasing concentration of TAC, because of the oxidation of Cl^{-1} into strong oxidant species such as active chlorine, HOCl, OCl^- for the electrolytic treatment of uric acid. While TAC is comprised of the sum of all forms of chlorine species and combined chlorine species which results from a reaction with nitrogenous organic and inorganic ions [58].

During EO treatment of uric acid, its removal phenomena from aqueous solution at different time intervals were investigated through FT-IR spectra. From Fig. 11, it was found that most of the peaks were got shifted distinct wave number this might be due to the structural changes occurred during the EO process. Some of the broad and sharp peaks during electrolysis were found disappeared due to the oxidation of uric acid and its intermediates via reactive oxidant species. Furthermore, few peaks during electrolysis were seemed to appear which accounts for $OH^{\cdot}$ and chlorine species as reported in the literature [59,60]. Moreover, the % transmittance for maximum peaks was found increased after a treatment time of 55 min, which indicates that the oxidation of uric acid was complete and converted into simple compounds.

Fig. 12 shows the continuous CVs for the EO treatment of uric acid of 50 mg/L at platinum rod with potential range of −1.2 to 1.2 V. As it can be seen that in 0 h sample (untreated) of uric acid one oxidation peak at −0.2 V potential in cycle 1 and one reduction peak at – 0.7 V in cycle 2 were observed. However, in the case of the treated sample, cycle 1 shows the disappearance of oxidation peak while cycle 2 exhibit a remarkable decrease in reduction peak. The dissolution/shifting of peaks depicts the formation of simpler oxidative and reductive species during the degradation of uric acid with a doped-MMO anode [26]. Moreover, decreased oxidation peak potential and enhanced oxidation peak current indicates the great electro-catalytic activity towards the oxidation of uric acid and amplified active electrochemical surface area [25].

To further examine the possible intermediates formed during EO treatment were identified through LC–MS analysis. On the basis of the results of LC–MS analysis, a possible oxidative pathway of uric acid has been proposed in Fig. 13. The reduction in uric acid led to the formation of intermediates (2) which further undergo through successive mechanisms such as C—N bond cleavage, dehydroxylation, deamination, etc. and yield final byproducts (9)-(11). The final products of the oxidative pathway of uric acid have also been reported in the literature studies [5,44]. The mass spectra from which the degradation pathway proposed were shown in Fig. S3

3.6. Economic evaluation

In order to visualize the successful commercialization of a process, treatment technology must provide a significant reduction in the overall cost of the treatment process over conventional techniques. In the case of EO treatment unit, the overall economy for removal of per kg of uric acid came out to be 0.18 $/m^3 (Table S2). The results depict a sustainable solution for the on-site treatment of urinal wastewaters in terms of economic feasibility of EO process as well as the stability of anodes. However, the overall cost could be reduced further during scale-up studies by modifying the reactor design and operating conditions accordingly.

4. Conclusion

The present study depicts the successful applicability of novel fabricated doped-MMO for the EO treatment of target compound that is uric acid. Parametric optimization for the treatment process was done using BBD in which the desirability function approach found suitable for simultaneous minimization of energy consumption and maximization of %degradation. The degradation of uric acid was found maximum due to the generation of strong oxidants like HOCl, OCl^-, $OH^{\cdot}$ during electrolysis. The dual effect of two processes has shown the synergistic effect on the degradation of uric acid as better %degradation was achieved in lesser time. Characterization techniques like SEM-EDS and XRD have proved the durability and stability of doped-MMO in

terms of significant degradation of uric acid even after 55 recycles. UV–vis, FTIR and LC–MS analysis were used for the detection of intermediates formed during the treatment process at different time intervals. Furthermore, future investigations would emphasize more techno-economic analysis of field-scale applications such as on-site treatment of urinal wastewater and reuse as flush water.

Appendix A. Supplementary data

Supplementary material related to this article can be found, in the online version, at doi:https://doi.org/10.1016/j.jwpe.2019.100944.

References

[1] S.R. Patil, B.F. Arnold, A.L. Salvatore, B. Briceno, S. Ganguly, J.M. Colford, P.J. Gertler, The effect of India's total sanitation campaign on defecation behaviors and child health in rural Madhya Pradesh: a cluster randomized controlled trial, PLoS Med. 11 (2014) e1001709, , https://doi.org/10.1371/journal.pmed.1001709.

[2] X. Wu, R. Schuyler House, R. Peri, Public-private partnerships (PPPs) in water and sanitation in India: lessons from China, Water Policy 18 (2016) 153–176, https://doi.org/10.2166/wp.2016.010.

[3] V.K. Srivastava, A.K. Nigam, R.P. Misra, Diarrhea in rural children – some environmental correlates, J. Stat. Appl. 13 (2015) 59–63.

[4] M. Ganesapillai, P. Simha, K. Gupta, M. Jayan, Nutrient recovery and recycling from human urine: a circular perspective on sanitation and food security, Procedia Eng. 148 (2016) 346–353, https://doi.org/10.1016/j.proeng.2016.06.461.

[5] S. Dbira, N. Bensalah, A. Bedoui, Mechanism and kinetics of electrochemical degradation of uric acid using conductive-diamond anodes, Environ. Technol. 37 (2016) 2993–3001, https://doi.org/10.1080/09593330.2016.1173115.

[6] J. O'Shea, R.L. Bunch, Uric acid as a pollution Indicator, Journal (Water Pollution Control Federation) 37 (1965) 1444–1446.

[7] S.J. Lu, J.-Y. Luo, S.-B. Ji, N.-X. Li, H. Li, W.-S. Li, Photoelectrocatalytic oxidation of uric acid on novel ruthenium (II) polypyridyl complex modified ZnO electrode for photo-stimulated fuel cells, Electrochim. Acta 136 (2014) 130–137, https://doi.org/10.1016/j.electacta.2014.05.061.

[8] H. Särkkä, A. Bhatnagar, M. Sillanpää, Recent developments of electro-oxidation in water treatment — a review, J. Electroanal. Chem. 754 (2015) 46–56, https://doi.org/10.1016/j.jelechem.2015.06.016.

[9] A.H. Sulaymon, A.H. Abbar, Scale-up of electrochemical reactors, Electrolysis, IntechOpen, 2012, https://doi.org/10.5772/48728.

[10] H. Wang, J.L. Wang, The cooperative electrochemical oxidation of chlorophenols in anode-cathode compartments, J. Hazard. Mater. 154 (2008) 44–50, https://doi.org/10.1016/j.jhazmat.2007.09.102.

[11] M. Panizza, G. Cerisola, Removal of color and COD from wastewater containing acid blue 22 by electrochemical oxidation, J. Hazard. Mater. 153 (2008) 83–88, https://doi.org/10.1016/j.jhazmat.2007.08.023.

[12] C. Barrera-Díaz, P. Cañizares, F.J. Fernández, R. Natividad, M.A. Rodrigo, Electrochemical advanced oxidation processes: an overview of the current applications to actual industrial effluents, J. Mex. Chem. Soc. 58 (2017), https://doi.org/10.29356/jmcs.v58i3.133.

[13] B.P. Chaplin, The critical review of electrochemical advanced oxidation processes for water treatment applications, Environ. Sci.: Processes Impacts 16 (2014) 1182–1203, https://doi.org/10.1039/C3EM00679d.

[14] H. Zöllig, A. Remmele, C. Fritzsche, E. Morgenroth, K.M. Udert, Formation of chlorination byproducts and their emission pathways in chlorine mediated electrooxidation of urine on active and nonactive type anodes, Environ. Sci. Technol. 49 (2015) 11062–11069, https://doi.org/10.1021/acs.est.5b01675.

[15] J. Radjenovic, D.L. Sedlak, Challenges and opportunities for electrochemical processes as next-generation technologies for the treatment of contaminated water, Environ. Sci. Technol. 49 (2015) 11292–11302, https://doi.org/10.1021/acs.est.5b02414.

[16] R. Chaiyont, C. Badoe, C. Ponce de León, J.L. Nava, F.J. Recio, I. Sirés, P. Herrasti, F.C. Walsh, Decolorization of methyl orange dye at IrO_2-SnO_2-Sb_2O_5 coated titanium anodes, Chem. Eng. Technol. 36 (2013) 123–129, https://doi.org/10.1002/ceat.201200231.

[17] W. Wu, Z.H. Huang, T.T. Lim, The recent development of mixed metal oxide anodes for electrochemical oxidation of organic pollutants in water, Appl. Catal. A Gen. 480 (2014) 58–78, https://doi.org/10.1016/j.apcata.2014.04.035.

[18] B. Adams, M. Tian, A. Chen, Design and electrochemical study of SnO2-based mixed oxide electrodes, Electrochim. Acta 54 (2009) 1491–1498, https://doi.org/10.1016/j.electacta.2008.09.034.

[19] R. Kock, S. Seitz, B. Delvoux, H. Greiling, A method for the simultaneous determination of creatinine and uric acid in serum by high-performance-liquid-chromatography evaluated versus reference methods, Clin. Chem. Lab. Med. 33 (1995) 23–30, https://doi.org/10.1515/cclm.1995.33.1.23.

[20] J.-M. Zen, P.-J. Chen, A selective voltammetric method for uric acid and dopamine detection using clay-modified electrodes, Anal. Chem. 69 (1997) 5087–5093, https://doi.org/10.1021/ac9703562.

[21] E. Popa, Y. Kubota, D.A. Tryk, A. Fujishima, Selective voltammetric and amperometric detection of uric acid with oxidized diamond film electrodes, Anal. Chem. 72 (2000) 1724–1727, https://doi.org/10.1021/ac990862m.

[22] R. Aguilar, M.M. Dávila, M.P. Elizalde, J. Mattusch, R. Wennrich, The capability of a carbon–polyvinylchloride composite electrode for the detection of dopamine, ascorbic acid, and uric acid, Electrochim. Acta 49 (2004) 851–859, https://doi.org/10.1016/j.electacta.2003.10.002.

[23] D. Lakshmi, M.J. Whitcombe, F. Davis, P.S. Sharma, B.B. Prasad, Electrochemical detection of uric acid in mixed and clinical samples: a review, Electroanalysis 23 (2011) 305–320, https://doi.org/10.1002/elan.201000525.

[24] T.C. Canevari, P.A. Raymundo-Pereira, R. Landers, E.V. Benvenutti, S.A.S. Machado, Sol-gel thin-film based mesoporous silica and carbon nanotubes for the determination of dopamine, uric acid and paracetamol in the urine, Talanta 116 (2013) 726–735, https://doi.org/10.1016/j.talanta.2013.07.044.

[25] L. Zhang, D. Yang, Poly (2-mercaptobenzothiazole) modified electrode for the simultaneous determinations of dopamine, uric acid, and nitrite, Electrochim. Acta 119 (2014) 106–113, https://doi.org/10.1016/j.electacta.2013.12.031.

[26] Z. Zhang, J. Yin, Sensitive detection of uric acid on partially electro-reduced graphene oxide modified electrodes, Electrochim. Acta 119 (2014) 32–37, https://doi.org/10.1016/j.electacta.2013.12.033.

[27] A.N. Subba Rao, V.T. Venkatarangaiah, Metal oxide-coated anodes in wastewater treatment, Environ. Sci. Pollut. Res. - Int. 21 (2014) 3197–3217, https://doi.org/10.1007/s11356-013-2313-6.

[28] American Health Public Association (APHA), Standard Methods for the Examination of Water and Wastewater. 19th ed., Standard Method No. (18th Edition), APHA, 5220-C, Washington, DC, 1992.

[29] American Health Public Association (APHA), Standard Methods for the Examination of Water and Wastewater. 17th ed., Standard Method no. 4500-Cl (B), APHA, Washington, DC, 1989.

[30] American Health Public Association (APHA), Standard Methods for the Examination of Water and Wastewater. 17th ed., Standard Method no. 4500-NO_3^- (E), APHA, Washington, DC, 1989.

[31] American Health Public Association (APHA), Standard Methods for the Examination of Water and Wastewater. 17th ed., Standard Method no. 4500-NO_2^- (B), APHA, Washington, DC, 1989.

[32] American Health Public Association (APHA), Standard Methods for the Examination of Water and Wastewater. 17th ed., Standard Method no. 4500-NH_4^+ (C), APHA, Washington, DC, 1989.

[33] American Health Public Association (APHA), Standard Methods for the Examination of Water and Wastewater. 17th ed., Standard Method no. 4500-Cl^- (B), APHA, Washington, DC, 1989.

[34] C.R.T. Tarley, G. Silveira, W.N.L. Dos Santos, G.D. Matos, E.G.P. da Silva, M.A. Bezerra, M. Miró, S.L.C. Ferreira, Chemometric tools in electroanalytical chemistry: methods for optimization based on factorial design and response surface methodology, Microchem. J. 92 (2009) 58–67, https://doi.org/10.1016/j.microc.2009.02.002.

[35] G. Hanrahan, K. Lu, Application of factorial and response surface methodology in modern experimental design and optimization, Crit. Rev. Anal. Chem. 36 (2006) 141–151, https://doi.org/10.1080/10408340600969478.

[36] S. Singh, S. Singh, S.L. Lo, N. Kumar, Electrochemical treatment of Ayurveda pharmaceuticals wastewater: optimization and characterization of sludge residue, J. Taiwan Inst. Chem. Eng. 67 (2016) 385–396, https://doi.org/10.1016/j.jtice.2016.08.028.

[37] K. Thirugnanasambandham, V. Sivakumar, J.P. Maran, Response surface modeling and optimization of treatment of meat industry wastewater using electrochemical treatment method, J. Taiwan Inst. Chem. Eng. 46 (2015) 160–167, https://doi.org/10.1016/j.jtice.2014.09.021.

[38] J. Fu, Y. Zhao, Q. Wu, Optimizing photoelectrocatalytic oxidation of fulvic acid using response surface methodology, J. Hazard. Mater. 144 (2007) 499–505, https://doi.org/10.1016/j.jhazmat.2006.10.071.

[39] N.R. Costa, J. Lourenço, Z.L. Pereira, Desirability function approach: a review and performance evaluation in adverse conditions, Chemom. Intell. Lab. Syst. 107 (2011) 234–244, https://doi.org/10.1016/j.chemolab.2011.04.004.

[40] P. Bansal, A. Verma, In-situ dual effect studies using novel Fe-TiO_2 composite for the pilot-plant degradation of pentoxifylline, Chem. Eng. J. 332 (2018) 682–694, https://doi.org/10.1016/j.cej.2017.09.121.

[41] V.K. Sangal, V. Kumar, I.M. Mishra, Optimization of structural and operational variables for the energy efficiency of a divided wall distillation column, Comput. Chem. Eng. 40 (2012) 33–40, https://doi.org/10.1016/j.compchemeng.2012.01.015.

[42] A. Özer, G. Gürbüz, A. Çalimli, B.K. Körbahti, Biosorption of copper(II) ions on Enteromorpha prolifera: application of response surface methodology (RSM), Chem. Eng. J. 146 (2009) 377–387, https://doi.org/10.1016/j.cej.2008.06.041.

[43] P. Kaur, V.K. Sangal, J.P. Kushwaha, Modeling and evaluation of electro-oxidation of dye wastewater using artificial neural networks, RSC Adv. 5 (2015) 34663–34671, https://doi.org/10.1039/C4RA14160A.

[44] J. Singla, A. Verma, V.K. Sangal, Performance and evaluation of electro-oxidation treatment of human urine metabolite uric acid using response surface methodology, J. Electrochem. Soc. 164 (2017) E312–E320, https://doi.org/10.1149/2.0681712jes.

[45] P. Asaithambi, M. Matheswaran, Electrochemical treatment of simulated sugar industrial effluent: optimization and modeling using a response surface methodology, Arab. J. Chem. 9 (2016) S981–S987, https://doi.org/10.1016/j.arabjc.2011.10.004.

[46] I.M.S. Pillai, A.K. Gupta, M.K. Tiwari, Multivariate optimization for electrochemical oxidation of methyl orange: pathway identification and toxicity analysis, J. Environ. Sci. Health, Part A 50 (2015) 301–310, https://doi.org/10.1080/10934529.2015.981119.

[47] B. Mondal, V.C. Srivastava, J.P. Kushwaha, R. Bhatnagar, S. Singh, I.D. Mall,

Parametric and multiple response optimization for the electrochemical treatment of textile printing dye-bath effluent, Sep. Purif. Technol. 109 (2013) 135–143, https://doi.org/10.1016/j.seppur.2013.02.026.
[48] L.C. Chen, F.R. Tsai, S.H. Fang, Y.C. Ho, Properties of sol-gel SnO_2/TiO_2 electrodes and their photoelectrocatalytic activities under UV and visible light illumination, Electrochim. Acta 54 (4) (2009) 1304–1311.
[49] J. Singla, A. Verma, V.K. Sangal, Parametric optimization for the treatment of human urine metabolite, creatinine using electro-oxidation, J. Electroanal. Chem. 809 (2018) 136–146, https://doi.org/10.1016/j.jelechem.2017.12.061.
[50] Z.S. Msindo, V. Sibanda, J.H. Potgieter, Electrochemical and physical characterization of lead-based anodes in comparison to Ti–(70%) IrO_2/(30%) Ta_2O_5 dimensionally stable anodes for use in copper electrowinning, J. Appl. Electrochem. 40 (2010) 691–699, https://doi.org/10.1007/s10800-009-0044-7.
[51] M. Tian, L. Bakovic, A. Chen, Kinetics of the electrochemical oxidation of 2-nitrophenol and 4-nitrophenol studied by in situ UV spectroscopy and chemometrics, Electrochim. Acta 52 (2007) 6517–6524, https://doi.org/10.1016/j.electacta.2007.04.080.
[52] F.A. Rodríguez, M.N. Mateo, J.M. Aceves, E.P. Rivero, I. González, Electrochemical oxidation of bio-refractory dye in a simulated textile industry effluent using DSA electrodes in a filter-press type FM01-LC reactor, Environ. Technol. 34 (2013) 573–583, https://doi.org/10.1080/09593330.2012.706645.
[53] M. Shestakova, P. Bonete, R. Gómez, M. Sillanpää, W.Z. Tang, Novel Ti/Ta_2O_5-SnO_2 electrodes for water electrolysis and electrocatalytic oxidation of organics, Electrochim. Acta 120 (2014) 302–307, https://doi.org/10.1016/j.electacta.2013.12.113.
[54] Y. Chen, L. Hong, H. Xue, W. Han, L. Wang, X. Sun, J. Li, Preparation and characterization of TiO_2-NTs/SnO_2-Sb electrodes by electrodeposition, J. Electroanal. Chem. 648 (2010) 119–127, https://doi.org/10.1016/j.jelechem.2010.08.004.
[55] Q. Wang, T. Jin, Z. Hu, L. Zhou, M. Zhou, TiO_2-NTs/SnO_2-Sb anode for efficient electrocatalytic degradation of organic pollutants: effect of TiO_2-NTs architecture, Sep. Purif. Technol. 102 (2013) 180–186, https://doi.org/10.1016/j.seppur.2012.10.006.
[56] J. Polonský, I.M. Petrushina, E. Christensen, K. Bouzek, C.B. Prag, J.E.T. Andersen, N.J. Bjerrum, Tantalum carbide as a novel support material for anode electrocatalysts in polymer electrolyte membrane water electrolyzers, Int. J. Hydrogen Energy 37 (2012) 2173–2181, https://doi.org/10.1016/j.ijhydene.2011.11.035.
[57] X. Qin, Y. Zhao, J. Li, G. Chen, The effect of Ir content on the stability of Ti/IrO_2-SnO_2 -Sb_2O_5 electrodes for O_2 evolution, Can. J. Chem. Eng. 97 (2019) 743–754, https://doi.org/10.1002/cjce.23337.
[58] B.J. Hernlem, Electrolytic destruction of urea in dilute chloride solution using DSA electrodes in a recycled batch cell, Water Res. 39 (2005) 2245–2252, https://doi.org/10.1016/j.watres.2005.04.018.
[59] K. Rajkumar, M. Muthukumar, Optimization of the electro-oxidation process for the treatment of Reactive Orange 107 using response surface methodology, Environ. Sci. Pollut. Res. - Int. 19 (2012) 148–160, https://doi.org/10.1007/s11356-011-0532-2.
[60] A.D. Hiwarkar, S. Singh, V.C. Srivastava, I.D. Mall, Mineralization of pyrrole, a recalcitrant heterocyclic compound, by the electrochemical method: multi-response optimization and degradation mechanism, J. Environ. Manage. 198 (2017) 144–152, https://doi.org/10.1016/j.jenvman.2017.04.051.

Journal of Environmental Management 255 (2020) 109847

Contents lists available at ScienceDirect

Journal of Environmental Management

journal homepage: http://www.elsevier.com/locate/jenvman

Research article

Application of mixed metal oxide anode for the electro-oxidation/disinfection of synthetic urine: Potential of harnessing molecular hydrogen generation

Jayishnu Singla [a], Vikas K. Sangal [b], Amanjit Singh [c], Anoop Verma [a,*]

[a] School of Energy and Environment, Thapar Institute of Engineering and Technology, Patiala, Punjab, India
[b] Department of Chemical Engineering, Malaviya National Institute of Technology, Jaipur, Rajasthan, India
[c] Research and Development, Consumer Product Division, HSIL Limited, Gurgaon, Haryana, India

ARTICLE INFO

Keywords:
Electro-oxidation
Mixed metal oxide
Box behnken design
Disinfection
Synergy

ABSTRACT

The efficacy of electro-oxidation has been checked for the deterioration of synthetic urine (SU) using mixed metal oxide anode along with the potential of harnessing the commercially useful byproduct i.e. molecular hydrogen gas. The results from batch have been used to execute the scale-up studies for the continuous electro-oxidation treatment of SU in a photovoltaic driven reactor. The effect of different operational variables like pH, time, current density and N/Cl ratio on process efficiency was evaluated in terms of %COD removal and specific energy consumption using response surface methodology. The results showed that 87.25% removal in COD and 85.88% in TOC were achieved in 8.8 h. The complete deactivation of *E. coli* spiked synthetic urine wastewater was achieved in 45 min only. The main strength lies in the demonstration of the significant reduction in treatment time to 6 h by incorporating dual effect i.e. Photo-electrocatalysis. The anode used was proven to be stable and effective even after 100 recycles (207.5 h). The intermediates formed during the treatment process were analyzed through LC-MS. The techno-economic analysis for the proposed technology under optimized conditions was calculated to be 0.85 $/kg of COD removed.

1. Introduction

Despite socio-economic growth in the past several years, India has failed to provide proportionate sustainable development (Ganesapillai et al., 2016). According to the Joint Monitoring Programme (JMP) for Water Supply and Sanitation conducted by the WHO and the United Nations Children's Fund, approximately 2.4 billion people in word lack access to basic sanitation and waste disposal facilities while 66% population still practice open defecation (Daudey, 2018) and about a million people die from diseases like diarrhea, malnutrition, typhoid, dengue (Singh and Cheema, 2016). The eco-sanitation is a sustainable yet affordable solution for the safe disposal of human waste, which uses human urine as a resource of water (Simha and Ganesapillai, 2017).

Urine is a complex mixer containing both molecular and ionic compounds. It represents a small volume (≈1%) of domestic wastewater, but the major source of water pollution (Spångberg et al., 2014). Urine is difficult to describe as one particular formula because of its high dependence on various factors like climate, age, diet, physical activities. It also contains various micro-pollutants such as synthetic hormones, vitamins, organic acids, pharmaceutical residues which are considered as emerging environmental pollutants (Dbira et al., 2019). The principal organic fraction of urine is mainly comprised of nitrogen-based components such as urea, creatinine and uric acid.

The continuous discharge of untreated urinal wastewater is becoming a potential threat to the environment and human health (Cho et al., 2014), as pathogens present in human urine can remain alive for a longer period of time. The treatment of urinal wastewater could prevent environmental pollution by treating harmful micropollutants and recycling as flush water, which is a sustainable solution for water shortage (Ikematsu et al., 2007).

Recently several authors have reported the applications of electro-oxidation (EO) treatment technology for the treatment of several toxic effluents via in-situ reactive oxygen species (ROS) such as hydroxyl radical ($OH^{\bullet}$) (Zhuo et al., 2011). EO treatment process has been used for the treatment of *Escherichia coli* (*E. coli*) by producing disinfectants from the ions naturally contained in the water (Bergmann et al., 2009).

* Corresponding author.
E-mail addresses: vksangal.chem@mnit.ac.in (V.K. Sangal), anoop.kumar@thapar.edu (A. Verma).

https://doi.org/10.1016/j.jenvman.2019.109847
Received 24 August 2019; Received in revised form 7 October 2019; Accepted 7 November 2019
Available online 26 November 2019
0301-4797/

However, the effectiveness of a particular process is dependent upon electrodes, many authors have reported the removal of microorganisms from human urine using boron-doped diamond (BDD) as an anode (Cotillas et al., 2018). However, the drawback of this anode is the generation of hazardous chloro-oxidant species such as chlorates and perchlorates (Bergmann et al., 2009). Moreover, the high cost of BDD to treat a large volume of effluents made the pilot scale applications impractical.

In this context, mixed metal oxide (MMO) anode has been chosen because it is electrochemically stability, low in cost and promotes the generation of a significant amount of reactive chlorine species (RCS) and ROS at low current densities (Isarain-Chavez et al., 2017; Zahedi et al., 2018; Baddouh et al., 2018; Cruz-Diaz et al., 2018; Gurung et al., 2018).

In the experimental study, ternary MMO i. e Ti/Ir/Ru/Pt was chosen for EO treatment of synthetic urine (SU). The unique properties of ternary anode have been discussed in previous research works (Singla et al., 2018). The present study aims to investigate MMO anodes for the combined EO and disinfection of SU wastewaters by optimizing different process parameters such as nitrogen to chloride ratio (N/Cl), pH, applied current density and treatment time as well as their effect on responses using response surface methodology (RSM). Several analytical techniques were used to identify the intermediates formed during the electrolysis of synthetic urine. In addition, efforts have been made for the development of a photovoltaic (PV) driven electrolysis reactor for the EO treatment, a low-cost solution for on-site treatment of urinal wastewater for developing countries and providing a social-economic boost with the harnessing of hydrogen production.

2. Materials and methods

2.1. Chemicals and microorganisms

The bacterial strain i.e. *E. coli* (MTCC K-12) was procured from CSIR, Chandigarh, (India). The chemicals required for SU preparation, chemical oxygen demand (COD) estimation and anions test analysis have been discussed in detail in the Supplementary file (File S1).

2.2. Analytical methods

The analysis of untreated and treated samples of SU was carried out using various analytical techniques such as COD, total organic carbon (TOC), cyclic voltammetry (CV), FTIR along with the quantification of anions. The estimation of $OH^{\bullet}$ production was validated through a fluorescence spectrophotometer. The identification of intermediates generated during the process was checked through LC-MS. The MMO anode was characterized through SEM-EDS and XRD. The detailed description of these techniques has been discussed in File S2.

2.3. Electrodes fabrication

The MMO anodes were purchased from Exotic Elements Private Limited, Mumbai, while stainless steel (SS) from Bio age Private Limited, Mohali (India). The detailed discussion regarding the fabrication of MMO anode has been discussed in File S3.

2.4. Experimental reactor setup

EO experiments were carried out under batch operation mode in a single compartment electrochemical cell made up of glass with a total volume of 500 mL (Fig. 1A). Electrodes (MMO and SS) were used having dimensions of (7 cm x7 cm x 0.5 cm) and active surface area of 42 cm^2 and were connected parallel with an inter-electrode spacing of ~2.0 cm for every experiment and current was maintained using DC power supply (Model: 0–30 V with 0–2 A and 0–5 A) purchased from DIGITECH, Ambala, (India).

For photo-electrocatalysis (PEC), above mentioned EO reactor was placed in a wooden chamber, contains 10 UV tubes. Out of the 10 UV tubes, 7 tubes (Philips) of 36 W (365 nm) were attached beneath of the top roof while other 3 UV tubes of 18 W (365 nm) attached to the one sidewall of the wooden chamber and aligned horizontally (Fig. 1B) to maintain UV intensity of 23 ± 2 W/m^2 throughout the reaction measured by a radiometer (Eppley; model no. 33013).

For continuous EO experiments, a glass reactor fabricated with a plexiglass sheet having dimensions of 90 mm × 90 mm x 40 mm. The reactor was designed to treat 1–2 L of total sample volume, with one inlet and outlet along with one detachable baffle made up of acrylic fiber. An aqueous solution of SU with a working volume of 2 L was used for EO experiments. In order to capture different gases during EO treatment of SU, a glass box equipped with a sampling port (inlet and outlet) and a gas outlet port on top, was placed inversely over the EO

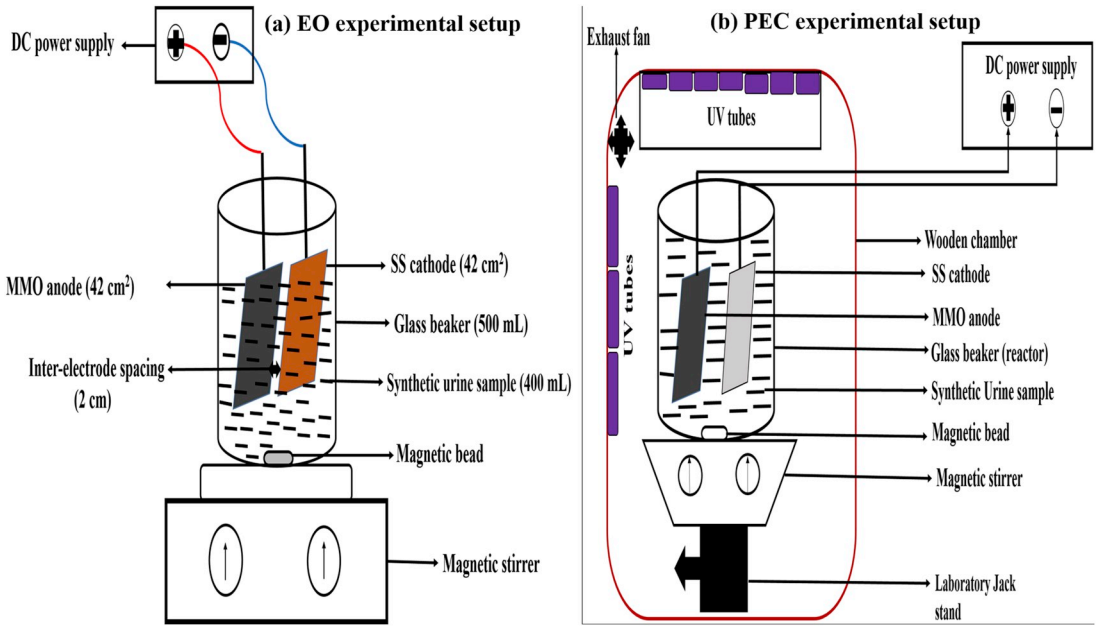

Fig. 1. Schematic diagram of the experimental setup used for the (a) EO and (b) PEC treatment of SU.

reactor. Furthermore, the whole setup was placed on a jack and the infiltration of air was stopped using clay (Fig. 2). The detailed discussion of cont. EO operation has been discussed under Section 3.6.

2.5. Experimental procedure

The lab-scale EO experiments for the treatment of SU working solution of 400 mL were freshly prepared and the pH of SU was adjusted with 0.1 N NaOH and 0.1 N H_2SO_4 solution as per the requirement. For homogeneous mixing of the aqueous solution during experimental runs; magnetic stirrer at 600 rpm was used. Prior to every EO experiment, electrodes were cleaned by dipping it into a 10% H_2SO_4 solution and then dried at room temperature. All experiments were performed at room temperature i.e. 25 °C ± 2 °C. The chemical analysis was carried out periodically by withdrawing a sample of appropriate volume. All experiments were performed thrice to check the reproducibility of results.

For continuous recirculation EO experiments for the treatment of SU, 2 L sample was stored in a tank and circulated through the single compartment EO reactor by a booster pump with 12 LPH flow rate. Further, to remove dissolved oxygen, molecular nitrogen was purged into the system for 1 h prior to the EO treatment process. The current to the electrodes were supplied through photovoltaic (PV) panels. At certain time intervals, samples of 10 mL were withdrawn and filtered for different test analysis and the sample for gas analysis was withdrawn by glass syringe through the inverted glass box.

2.6. Experimental design and statistical analysis

For designing the experimental matrix three-level Box-Behnken design (BBD) under RSM was employed. RSM is a chemometric tool which helps in the determination of the contribution of each operational parameters such as current density (j), pH, N/Cl ratio and treatment time (t) as well as the interaction between them. Two responses were selected i.e. % COD removed (Z_1) and specific energy consumption (Z_2) and calculated by the following Eqs. (1) and (2) (Kaur et al., 2017).

$$Z_1(\%\ \text{COD removal}) = \frac{COD_o - COD_t}{COD_0} X100 \tag{1}$$

$$Z_2(\text{SEC}) = \frac{\left(\left(\frac{Vit}{S_v}\right)\Big/ 10^3\right)}{COD_r/10^6} \tag{2}$$

where, COD_0 = Initial COD (mg/L); COD_t = COD at fixed time intervals (mg/L); SEC = specific energy consumption (kWh/kg of COD removed); i = current (A); V = voltage; t = electrolysis time (h) and Sv = Volume of sample (L). Further details has been discussed in File S4.

The total number of experimental runs established by BBD was 30 with six replication runs at the center as shown in Table 1. The adequacy of the chosen polynomial model was determined by two different tests i. e. model summary statistic and sequential model summary. The quality of the model was checked as the coefficient of determination R^2 while statistical significance was checked by F-Test. In the study of multi-response optimization with desirability, the approach was used to optimize the EO operational parameters and calculated by the following Eqs. (3) and (4) (Mondal et al., 2013).

$$\text{Di} = (d_1 X d_2)^{1/2} \tag{3}$$

$$d = \begin{cases} 0 & \\ \left[\dfrac{Z_i - Z_{i-min}}{Z_{i-max} - Z_{i-min}}\right]^k & \begin{matrix} if\ Z_i \le Z_{i-min} \\ if\ Z_{i-min} < Z_i < Z_{i-max} \end{matrix} \\ 1 & if\ Z_i \ge Z_{i-max} \end{cases} \tag{4}$$

where Di is the desirability function ($0 > d_i < 1$); d_1 and d_2 are desirabilities of responses Z_1 and Z_2.

2.7. Synergy calculations

The synergy of the dual-process i.e. PEC over single processes ie photocatalysis (PC) and EO in the present study was calculated by following Eqs. (5) and (6) (Bansal and Verma, 2018).

Synergy over single processes [PC or EO]:

$$\%Synergy = 100 \times \left\{\frac{[k_{dual} - (k_{PC}\ or\ k_{EO})]}{k_{dual}}\right\} \tag{5}$$

Overall Synergy:

$$\%Synergy = 100 \times \left\{\frac{[k_{dual} - (k_{PC} + k_{EO})]}{k_{dual}}\right\} \tag{6}$$

where 'k' = pseudo-first-order rate constant (h^{-1}) for every process and calculated from Eq. (7).

$$-\ln\frac{COD_0}{COD_t} = k_1 t \tag{7}$$

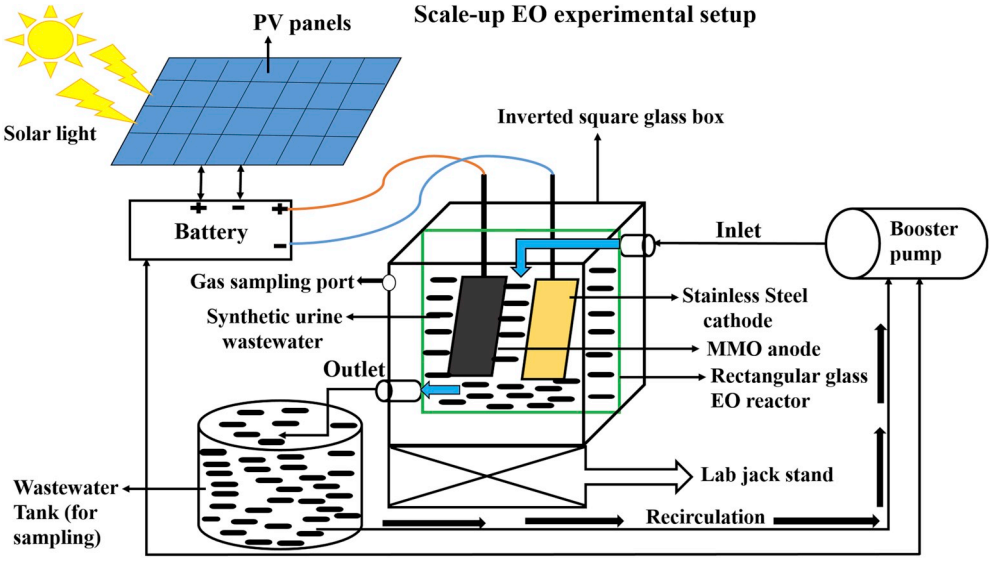

Fig. 2. Schematic diagram of the photovoltaic driven EO experimental setup.

Table 1
BBD matrix and their experimental results for measured responses.

Std	Run	Block	Current density (mA cm^{-2})	N/Cl ratio	Time (h)	pH	% COD removed, Z_1	SEC, Z_2 (kWhr/kg COD removed)
2	1	1	47.61	1.00	9.00	3.00	87	34.08
6	2	1	33.33	1.70	6.00	6.00	22	77.5
5	3	1	33.33	0.30	6.00	6.00	67	13.27
8	4	1	33.33	1.70	12.00	6.00	26	121.63
10	5	1	33.33	1.00	9.00	6.00	65.5	30.55
7	6	1	33.33	0.30	12.00	6.00	72	22.65
9	7	1	33.33	1.00	9.00	6.00	65.5	30.55
3	8	1	19.04	1.00	9.00	9.00	33	34.01
4	9	1	47.61	1.00	9.00	9.00	62	52.94
1	10	1	19.04	1.00	9.00	3.00	57	18.58
16	11	2	33.33	0.30	9.00	9.00	59	23.87
19	12	2	33.33	1.00	9.00	6.00	65.5	30.55
11	13	2	19.04	1.00	6.00	6.00	40	18.35
20	14	2	33.33	1.00	9.00	6.00	65.5	30.55
14	15	2	47.61	1.00	12.00	6.00	69	60.36
17	16	2	33.33	1.70	9.00	3.00	31	75.31
15	17	2	33.33	0.30	9.00	3.00	88.5	12.98
18	18	2	33.33	1.70	9.00	9.00	24.5	102.86
12	19	2	47.61	1.00	6.00	6.00	64	33.64
13	20	2	19.04	1.00	12.00	6.00	45	32
29	21	3	33.33	1.00	9.00	6.00	65.5	30.55
21	22	3	19.04	0.30	9.00	6.00	53	11.19
23	23	3	19.04	1.70	9.00	6.00	28	55
25	24	3	33.33	1.00	6.00	3.00	74	17.36
26	25	3	33.33	1.00	6.00	9.00	53	26.57
24	26	3	47.61	1.70	9.00	6.00	23	140
22	27	3	47.61	0.30	9.00	6.00	80.5	24.33
30	28	3	33.33	1.00	9.00	6.00	65.5	30.55
27	29	3	33.33	1.00	12.00	3.00	79	30.65
28	30	3	33.33	1.00	12.00	9.00	58	49

2.8. Operating cost analysis

The total cost for EO treatment comprises of cost of electrodes, the electrical energy consumed, calculated using the following Eq. (8) (Kaur et al., 2017).

$$\text{Operating cost} = C_{EC} + C_{EL} \quad (8)$$

where, C_{EC} = cost of energy consumed (kWh/m^3) and C_{EL} = cost of electrodes (Rs/per piece).

3. Results and discussion

The statistical investigation of experimental data was done using Design-Expert software version 6.0.8. The results of the model summary statistic showed the highest R^2 values of both responses i.e. 0.9801 and 0.9930 for a quadratic model, which indicates the satisfactory interaction between predicted and actual values of the experimental run. For further analysis, the manual regression method was applied with a reduced quadratic equation. Table 2 shows the results of the quadratic model fitting in the form of an analysis of variance (ANOVA). The detailed information has been discussed in File S5.

Table 2
ANOVA results suggested by BBD for responses (Z_1 and Z_2).

Sources	Z_1					Z_2				
	Sum of square	DF	Mean square	F-value	Prob > F	Sum of square	DF	Mean square	F-value	Prob > F
Block	42.92	2	21.46			0.037	2	0.019		
Model	10,875.95	14	776.85	45.70	<0.0001	11.72	14	0.84	132.37	<0.0001
Y_1	1397.52	1	1397.52	82.21	<0.0001	1.33	1	1.33	210.82	<0.0001
Y_2	1344.08	1	1344.08	79.07	<0.0001	0.68	1	0.68	107.79	<0.0001
Y_3	5874.19	1	5874.19	345.57	<0.0001	8.34	1	8.34	1318.86	<0.0001
Y_4	70.08	1	70.08	4.12	0.0633	0.91	1	0.91	144.00	<0.0001
Y_1^2	293.44	1	293.44	17.26	0.0011	0.011	1	0.011	1.73	0.2112
Y_2^2	15.86	1	15.86	0.93	0.3517	8.320E-004	1	8.320E-004	0.13	0.7227
Y_3^2	1525.76	1	1525.76	89.76	<0.0001	0.40	1	0.40	63.04	<0.0001
Y_4^2	66.07	1	66.07	3.89	0.0703	1.610E-003	1	1.610E-003	0.25	0.6224
Y_1Y_2	0.25	1	0.25	0.015	0.9053	6.734E-003	1	6.734E-003	1.06	0.3211
Y_1Y_3	264.06	1	264.06	15.53	0.0017	6.211E-003	1	6.211E-003	0.98	0.3399
Y_1Y_4	0.000	1	0.000	0.000	1.0000	2.031E-004	1	2.031E-004	0.032	0.8606
Y_2Y_3	132.25	1	132.25	7.78	0.0153	0.022	1	0.022	3.50	0.0842
Y_2Y_4	0.000	1	0.000	0.000	1.0000	4.747E-004	1	4.747E-004	0.075	0.7885
Y_3Y_4	0.25	1	0.25	0.015	0.9053	1.762E-003	1	1.762E-003	0.28	0.6066
Residual	220.98	13	17.00			0.082	13	6.327E-003		
Lack of fit	220.98	10	22.10			0.082	10	8.225E-003		
Pure error	0.000	3	0.000			0.000	3	0.000		
Core total	11,139.84	29				11.84	29			

3.1. Effect of process parameters and optimization

Three dimensional (3D) response graphs developed from the model were studied in order to analyze the interaction between operational parameters and their effect on responses.

3.1.1. Effect of j and N/Cl on % COD removed, Z_1

j is an important operating parameter in the EO remediation process because of cost-effectiveness analysis. The effect of j and N/Cl on EO of SU was analyzed by varying j from 19.04 to 47.61 mA/cm^2 and N/Cl ratio from 0.3 to 1.7. Fig. 3A has shown the interaction between them as well as their simultaneous effect on % COD removal, Z_1. The graph showed that Z_1 was maximum at low values of N/Cl ratio up to 0.65 and then decreases gradually with an increasing ratio of ≈1.70. This trend was visible on all values of j. However, with increasing values of j, a marginal increase in Z_1 was observed at the N/Cl ratio of ≈0.45. Further, an increase in N/Cl ratio from 1 to 1.7, it was found that Z_1 first increased to 33.33 mA/cm^2 and then decreased with increasing j values ≈ 47.61 mA/cm^2. From the experimental, it was found that at lower values j and higher values of N/Cl ratio, Z_1 was minimum. However, when j was increased and N/Cl ratio decreased, Z_1 was found maximum. This happens because, at lower values of j, generation of ROS on MMO anodes falls gradually with time. But when j increases, the removal efficiency of pollutants was maximum because of the increased generation of $OH^{\bullet}$ and RCS. At lower values of j, the EO process is not kinetically limited by mass transport of pollutants so, the increase in j value led to maximum removal efficiency. But at high values of j, the EO process is controlled by mass transport and an increase in j value leads to the enhancement of oxygen evolution reaction (Moreira et al., 2017). Due to which ROS was consumed rapidly decreasing the Z_1. While in the case of intermediate j values, an increase in j values leads to the increase in pollutant removal rate but decreases the current efficiency as discussed in File S5.

The N/Cl ratio plays a significant role as it influences the efficiency of the EO process by increasing the conductivity of a solution. It defines the amount of RCS formed during EO treatment of pollutants at MMO anodes. At higher values of N/Cl ratio, the concentration of chloride is less as compared to the concentration of nitrogen due to which the active sites on anode surface blocked, decreasing the oxidation of chloride into RCS. However, at lower values of the N/Cl ratio, depletion of pollutants rapid as more RCS is generated resulting in maximum Z_1. The increase in Z_1 values was due to the synergistic effect of RCS and $OH^{\bullet}$ (Moreira et al., 2017).

3.1.2. Effect of t and pH on Z_1

Fig. 3B shows the interaction between pH and t as well as their effect on Z_1. To see the effect of t and pH on the oxidation process, values of t varied from 6 h to 12 h while pH was varied from 3 to 9. The graph showed that Z_1 was found maximum with increasing values of t at all pH values. However, Z_1 was found decreasing with increasing values of pH for all t values. The maximum value of Z_1 was observed at higher values of t at 10.50 h, however, a further increase in t values ≈ 12 h, Z_1 was found constant. While in the case of pH, Z_1 was found maximum at lower values of pH ≈ 4.5 and minimum at higher values of pH ≈ 9. Several authors have reported the maximum removal efficiency at acidic pH because the adsorption rate of $OH^{\bullet}$ on the surface of MMO is high, hence led to direct oxidation of pollutants, as at basic pH, the adsorption rate of $OH^{\bullet}$ decreases, due to which $OH^{\bullet}$ transform into lower potential oxidants H_2O_2 and $HO_2^{\bullet}$ as shown in Eqs. (12) and (13). Furthermore, at acidic pH, the generation rate of high potential oxidants like HOCl, Cl_2, ClO^- was maximum as shown in Eqs. (9)–(11), which led to the maximum degradation. While in the case of alkaline pH, lower potential oxidants like ClO_2^-, ClO_3^- and ClO_4^- reducing degradation efficiency as shown in Eq. (14). Moreover, acidic pH helps to prevent the volatilization of ammonia during the electrolysis (Barrera-Díaz et al., 2017) and also stops the oxidization of other ions such as sulfate, phosphate, carbonate in bulk (Cotillas et al., 2018). Thus, the destruction of the organic pollutant was better at acidic pH than basic pH.

At acidic pH:

$$2Cl^- \longrightarrow Cl_2 + 2e^- \quad (9)$$

$$Cl_2 + H_2O \longrightarrow HClO + Cl^- + H^+ \quad (10)$$

$$HClO \longrightarrow ClO^- + H^+ \quad (11)$$

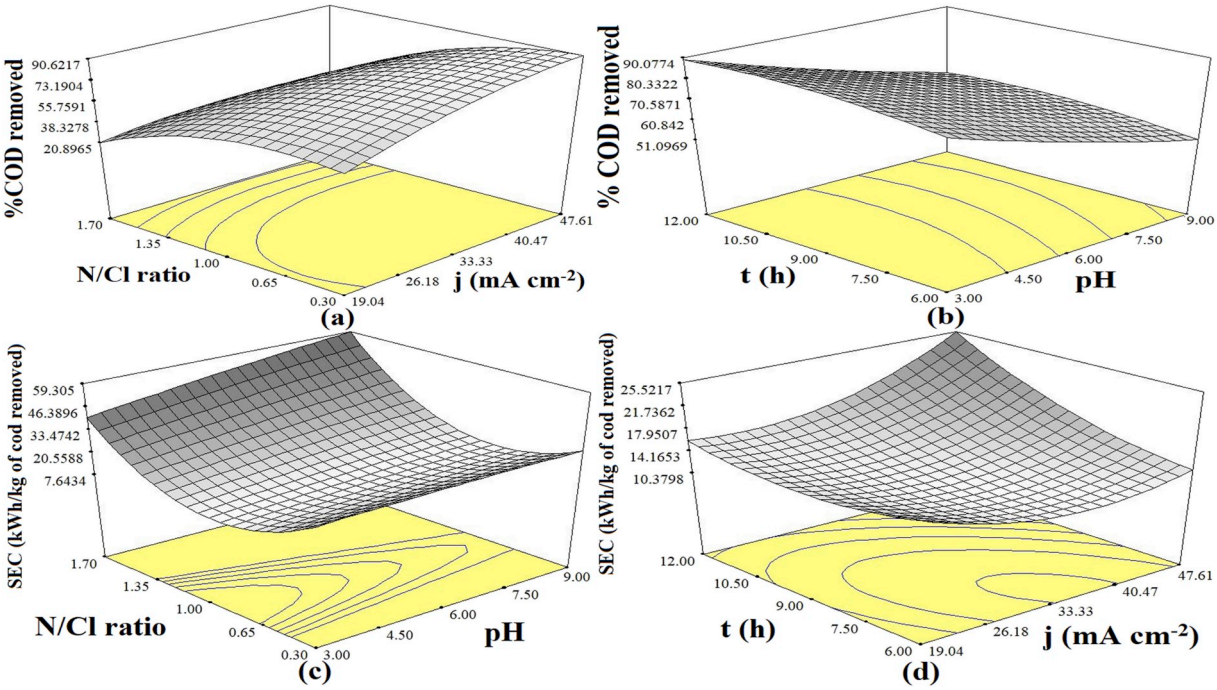

Fig. 3. Effect of different operational parameters on %COD removal and SEC during SU electrolysis (a) j and N/Cl ratio, (b) t and pH, (c) N/Cl ratio and pH and (d) t and j.

At basic pH:

$$H_2O_2 + OH^- \longrightarrow HO_2^- + H_2O \quad (12)$$

$$HO_2^{\bullet} + OH^- \longrightarrow O_2^{\bullet -} + H_2O \quad (13)$$

$$ClO^- + OH^- \longrightarrow ClO_2^- + H^+ + e^- \quad (14)$$

3.1.3. Effect of j, pH, n, and t on SEC, Z_2

Fig. 3C shows the interaction between pH and N/Cl ratio as well as their effect on SEC, Z_2. The results depict that Z_2 was found decreasing with increasing N/Cl ratio up to 1.0, for all values of pH. Further increase in N/Cl ratio from 1.0 to 1.7, led to an increase in values of Z_2 for all values of pH. However, the values of Z_2 was found maximum at higher values of pH from 7.5 to 9.0 at N/Cl ratio ≈1.7. At lower values of N/Cl ratio up to 0.3, Z_2 was found constant for all values of pH. It depicts that at lower values of the N/Cl ratio, there was no effect of pH was observed on Z_2. While at higher values of N/Cl ratio ≈1.7, Z_2 was found increasing with increasing values of pH. Fig. 3D shows the interaction between j and t as well as their effect on Z_2. The results showed that at lower values of t to 7.5 h and j to 26.18 mA/cm^2, Z_2 was found to be minimum. However, a further increase in j and t values i.e. 47.61 mA/cm^2 and 12 h respectively showed a gradual increase in values of Z_2. Furthermore, at higher values of pH Z_2 was found maximum while minimum (Z_2) at lower values of pH. This was due to the production of strong oxidant species at lower pH lead to maximum oxidation and requires less energy (Singla et al., 2017).

Optimization of operating parameters for the EO treatment of SU with MMO anode was done for maximizing the Z_1 and minimizing the Z_2. One-sided desirabilities (di) and overall desirability (D) were calculated by using maximum (Z_1) and minimum (Z_2) acceptable values of both responses as shown in Eqs. (15) and (16).

The desirability for response Z_1 for SU was calculated by Eq. (5) with acceptable values of $Z_{1\text{-}min}$ as 22.0% and $Z_{1\text{-}max}$ as 88.5%. Similarly, for the response, Z_2 was calculated by taking $Z_{2\text{-}min}$ as 11.19 and $Z_{2\text{-}max}$ as 140.00 kWh/kg of COD removed respectively.

$$d_{1(SU)} = \begin{cases} 0 & \\ \left[\dfrac{Z_1 - 22.0}{88.5\text{–}22.0}\right] & \begin{array}{l} if\ Z_1 \le 22.0 \\ if\ 22.0 < Z_1 < 88.5 \end{array} \\ 1 & if\ Z_1 \ge 88.5 \end{cases} \quad (15)$$

$$d_{2(SU)} = \begin{cases} 0 & \\ \left[\dfrac{Z_2 - 11.19}{140.00\text{–}11.19}\right] & \begin{array}{l} if\ Z_2 \le 11.19 \\ if\ 11.19 < Z_2 < 140.00 \end{array} \\ 1 & if\ Z_2 \ge 140.00 \end{cases} \quad (16)$$

In above all equations value of r was taken as 1. Therefore, overall desirability (D) for SU was calculated using Eq. (4). The best optimized conditions of process parameters for SU were obtained at pH = 3.42, N/Cl ratio = 0.42, j = 30.33 mA/cm^2, t = 8.8 h and showed highest overall desirability, D = 0.985 as shown in Table 3. At this optimum condition, the value for responses Z_1 and Z_2 suggested by BBD were found out to be 86.056% and 11.88 kWh/kg of COD removed. In order to confirm the values of responses, further experiments were conducted in triplicate at the optimized condition. The average experimental value of both responses Z_1 and Z_2 for SU were found close to the predicted values i.e. 85.25% and 11.75 kWh/kg of COD removed respectively as shown in Table 4.

During the EO treatment process, it has been observed that conductivity and pH of SU changes (Fig. 4A and B). It was observed the change in conductivity is insignificant, while pH was found to be increased during the treatment process. The increase in pH at the beginning of the treatment test was observed and kept constant at pH 8.0 until the end of the process. This shift of pH from acidic towards neutral was due to the production of hydroxyl ion (OH^-) by water reduction at the surface of the cathode. Furthermore, pH during electrolysis between 7.5 h and 9 h was found stabilized due to the formation of the HCO_3^- buffer from the produced CO_2 while degrading the organic pollutants present in SU (Dbira et al., 2015).

Table 3
Individual and multi-response optimization results for desirability calculations.

Response	Current density (mA cm^{-2})	N/Cl ratio	Time (h)	pH	Desirability
Individual Response optimization					
% COD removed = 91.234%	43.06	0.46	10.26	4.42	1
Specific energy consumption = 2.400 kWh/kg of COD removed	21.82	0.35	7.00	5.51	1
Simultaneously optimization of responses					
% COD removed = 86.056%	30.33	0.42	8.79	3.42	0.985
Specific energy consumption = 11.78 kWh/kg of COD removed					

Table 4
Comparison between predicted and actual value at optimized conditions.

Responses	Predicted	Actual
% COD removed	86.056%	85.25%
Specific energy consumption (kWh/kg of COD removed)	11.88	11.75

3.2. Synergistic studies

In order to investigate the photoactivity of MMO anode, studies were performed by three different techniques which include PC (interaction of light with anode surface), EO (constant applied current only) and PEC (constant applied current and light) at optimized conditions. The synergistic studies were performed in order to check the degradation efficiency of dual-process over single processes. The effect was calculated and quantified using kinetic rate constant obtained through pseudo-first-order reactions as discussed in Section 2.8. The oxidation experiments for SU were performed with MMO in a batch reactor under UV light. Fig. 5A shows the results for % COD removal of SU treated with different processes i.e. PC, EO, and PEC. Among all the processes, % COD of SU was found maximum in the dual process i.e. PEC over individual processes. Furthermore, treatment time for SU through PEC was also found to be reduced from 8.8 h to 6 h. PC treatment was found less efficient for the % COD removal as compared to the other two processes. A similar kind of results was also observed when the plot between COD_t/COD_o and electrolysis time was studied (Fig. 5B). Fig. 5C shows the plot of the rate constant versus different treatment processes. From the results, it was depicted that an immense increase in the first-order rate constant in case of the integrated process (0.2991 h^{-1}) which was 10.2 times of PC (0.0294 h^{-1}) and 1.25 times to EO (0.2334 h^{-1}). Proving the viability of the dual-process over a single treatment process. To further confirm, experimental studies were carried out using fluorescence spectroscopy for the estimation of $OH^{\bullet}$ production at MMO under different light sources, at different pH and time intervals. The detailed information has been discussed in File S6.

3.3. Mineralization

Mineralization studies were performed at optimized conditions in terms of in-situ chemical analysis, CV, FT-IR, LC-MS analysis.

Chemical analysis: The quality of treated and untreated samples were checked by performing in-situ analysis, which depicts the results of

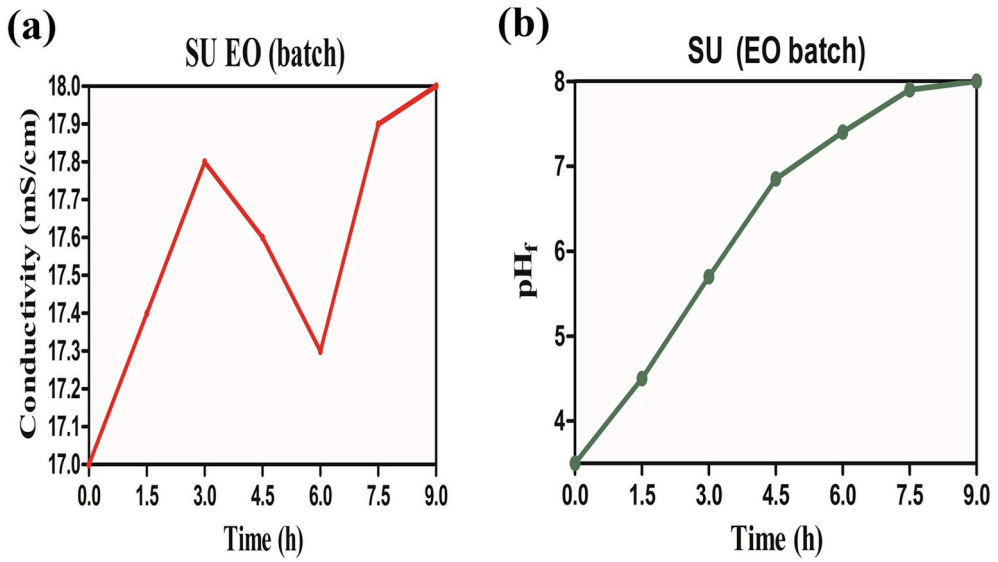

Fig. 4. Changes in the (a) conductivity and (b) pH during electrolysis of SU with MMO anode at optimized conditions.

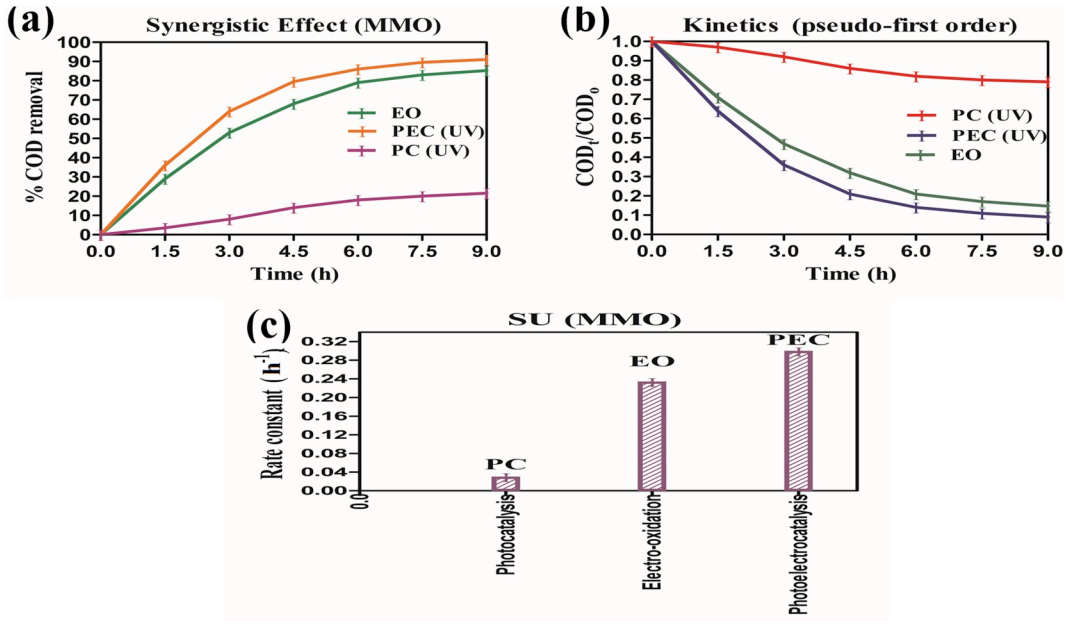

Fig. 5. Plot of synergistic effect for SU through different processes (a) % COD removal vs time, (b) plot of C_t/C_o vs time and (c) pseudo-first-order rate constant versus different processes.

the transformation of micro-pollutants into carbon dioxide, water and inorganic salts; confirmed through a reduction in COD (87.25%) and TOC (85.88%) at optimized conditions, which reached up to 89.0% and 86.9% when the reaction was extended to 12 h (Fig. 6A). The reduction in COD confirms the degradation of initial pollutants and the formation of intermediates chemical species during the treatment and decay in TOC value corresponds to the conversion of organic carbon into carbon dioxide (CO_2) (Dbira et al., 2019).

The oxidation of nitrogen-based organic matter (present in SU i.e. uric acid, creatinine and urea) into inorganic ions such as NO_2^-, NO_3^- and NH_4^+ was checked by ion testing analysis along with the estimation of reduction in total nitrogen. The total nitrogen present in SU was around 6300 mg/L. The most of the nitrogen (≈95%) associated with urea present in raw SU, rest is being free ammonium ion and organic nitrogen associated with creatinine and uric acid respectively. A continuous generation of nitrite and ammonium ions was observed, while the concentration of nitrate increases slowly (Fig. 6B). The concentration of nitrite and ammonium ions were found depleting after 3.0 h and 4.5 h indicating the conversion of NO_2^- into NO_3^-. While in the case of NO_3^-, a continuous increase in concentration was observed. This might be due to the reaction between ammonium ion and hypochlorous acid.

From Fig. 6C it can be observed that chloride level was continuously decreasing due to oxidation of chloride on the anode to produce strong oxidant species like HOCl/OCl^- for the destruction of organic matter present in SU. The level of TAC increased gradually during the electro-oxidation treatment of urea and then increased sharply to higher values when urea was depleted to the maximum. During the treatment process TAC, an aggregate part of reactive intermediates does not remain constant. This might be due to the balance between the oxidation of nitrogen-based components and the generation of chlorine species along with their bond forms during the treatment process as reported in the literature (Hernlem, 2005).

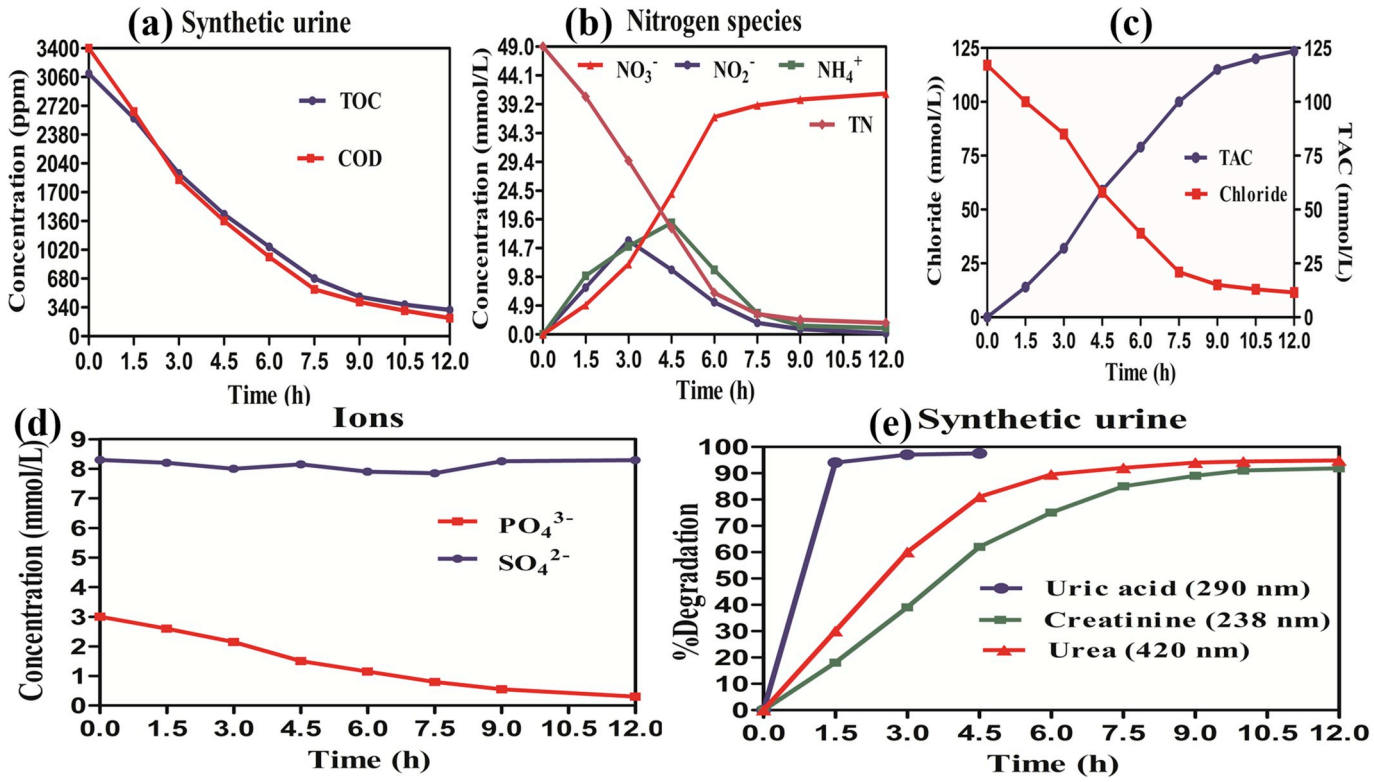

Fig. 6. Plot of mineralization at optimized conditions at different time intervals (a) concentration (COD &TOC), (b) generation of different nitrogen species, (c) chloride and total available chlorine (d) concentration of ions and (e) % degradation of organic pollutants present in SU.

Fig. 6D represents changes in the concentration of sulfates and phosphates with time during the EO treatment of SU wastewater. From the plot, it can be observed that the concentration of phosphate was found decreasing with increasing time. This might be happening due to the acid-base distribution and solubility dependence of inorganic ions (phosphates). However, in the case of sulfates, negligible change in concentration was found during the 8.8 h of electrolysis, depicting the non-dependency on values of pH due to the higher solubility of sulfates in water (Dbira et al., 2015).

Cyclic Voltammetry (CV): Fig. 7A shows the continuous CV for untreated and treated samples of SU at platinum rod with a potential range of −1.2 to 0.0 V. The treated and untreated samples of SU has also shown a few visible peaks in the potential range window. As it can be seen that in 0 h samples one oxidation peak at ≈ 0.0001 A in a first cycle and one reduction peak at ≈ 0.0001 A was observed. However, in the case of the treated sample, cycle 1 showed the disappearance of the oxidation peak while cycle 2 exhibit a remarkable decrease in reduction peak (<−0.0001 A). The shifting of the peaks depicts the generation of

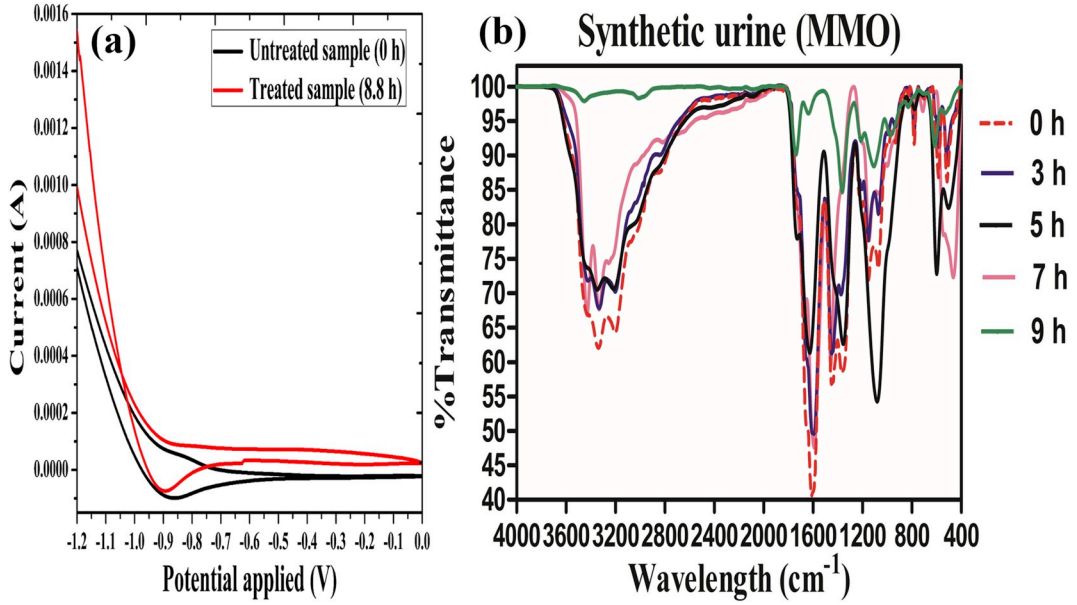

Fig. 7. Plot of (a) cyclic voltammeter and (b) FTIR for untreated and treated SU samples.

simpler oxidative and reductive species during the oxidation of SU with MMO anode. Moreover, an increase in oxidation peak current and a decrease in oxidation peak potential indicates the great electrocatalytic activity (Zhang and Yin, 2014).

FT-IR (Fourier transformed infrared spectroscopy) analysis: To examine the removal phenomenon of pollutants present in SU during electrolysis, FT-IR of untreated and treated samples were performed under optimal conditions. Fig. 7B represents the FT-IR spectra of SU and results show the characteristic absorption broad peaks with wavenumber (cm^{-1}) at 3254.8, 3388.64, 3455.08, 612.10, 698.80 and 781.84, respectively were formed due to the $OH^{\bullet}$ and chloro-oxidant species generated during EO of SU. The sharp peaks at 1600.69, 1738.41, 3356.12 and 3455.08, respectively were due to the presence of characteristic absorption of C═O, C–H and N–H groups. The vibrational frequency of C≡N, C═N, C–N, C═C stretching linked with the heterocyclic structure was around at 1101.36, 1215.1, 1349.93, 1581.68, 1656.12 and 1738.40, respectively (Hiwarkar et al., 2017). The results show that most of the peaks were got shifted at distinct wavenumber, might be due to the structural changes occurred during the EO process.

LC-MS analysis: The organic and inorganic components present in untreated and treated samples of SU were identified through LCMS (Fig. S3). The results of the untreated sample (0 h) have shown the sharp peaks of metabolites like urea, uric acid, and creatinine. However, it was observed that after electrolysis most of the diagnosed organic components got erased and converted into intermediates like oxalic acid, 1-methylurea, guanidine, etc. while some new components were also diagnosed in trivial proportions. Based on the above discussion, a provisional mechanism has been proposed for the treated SU (Fig. 8). Moreover, most of the intermediates generated during the electrolytes of SU were found almost similar to the intermediates generated during electrolysis of urine metabolites alone (Singla et al., 2017, 2018). Further to confirm the oxidation of organic components a spectrophotometric analysis was done. Fig. 6E shows that 97.5% of uric acid remove in 1.0 h only while urea (91%) and creatinine (87.5%) took 7.5 h. In addition, the non-toxicity of diagnosed components in the final samples was confirmed through the toxicity analysis test discussed in detailed in File S7.

3.4. Treatment of SU spiked with E. coli

The efficacy of EO and PEC processes were checked for the disinfection of SU containing pathogenic microorganisms (Fig. 9). The experimental study was carried out at optimized conditions using MMO anodes. Besides its efficacy towards oxidation of organic components, the disinfection efficiency of EO and PEC was studied using *E. coli* as (pathogenic microorganism) spiked SU. The untreated and treated samples of volume 1 mL was poured in plates containing media called MacConkey agar. After that, media plates were then placed at 37 °C for getting discreet colonies of *E. coli*. The concentration of coliform in SU samples was estimated in terms of CFU 100 mL^{-1}. Fig. 9A showed that the total removal of *E. coli* from SU was achieved within 30 min through PEC and 45 min via EO as compared to the untreated sample. Based on these observations a plot was made between CFU 100 mL^{-1} vs treatment time. Fig. 9B represents the changes in the concentration of *E. coli* during electrolysis of SU at different time intervals at optimized conditions. As it can be seen that the concentration of *E. coli* was found decreasing rapidly with time. However, it was observed that the time required to disinfect SU wastewater was very less as compared to complete/partial oxidation of organic matter present in SU. The complete disinfection of wastewater was seemed dependent directly on the production of disinfectants which further depends on the concentration of chlorides added and the concentration of reduced nitrogen species present in solution. Additionally, the treatment processes convert the organic matter into inorganic ions such as nitrates, sulfates, phosphates, chlorides, etc., water and carbon dioxide (Cotillas et al., 2018).

3.5. Economic evaluation

To visualize the successful commercialization of the proposed method, treatment technology must provide viable solution economically. In the case of the EO treatment unit, the overall economy for removal of per kg of COD removal came out to be 0.85 $/kg of COD removed as shown in Table S2.

3.6. Continuous recirculation EO treatment of SU along with simultaneous production of molecular hydrogen

In order to promote the field scale applications, scale-up trials are required with continuous recirculation treatment of human urine. Besides this, there is a strong possibility of harnessing molecular H_2 production as commercial fuel during EO treatment of urine. In this context, lab-scale trials have been used to execute the scaled-up version of EO

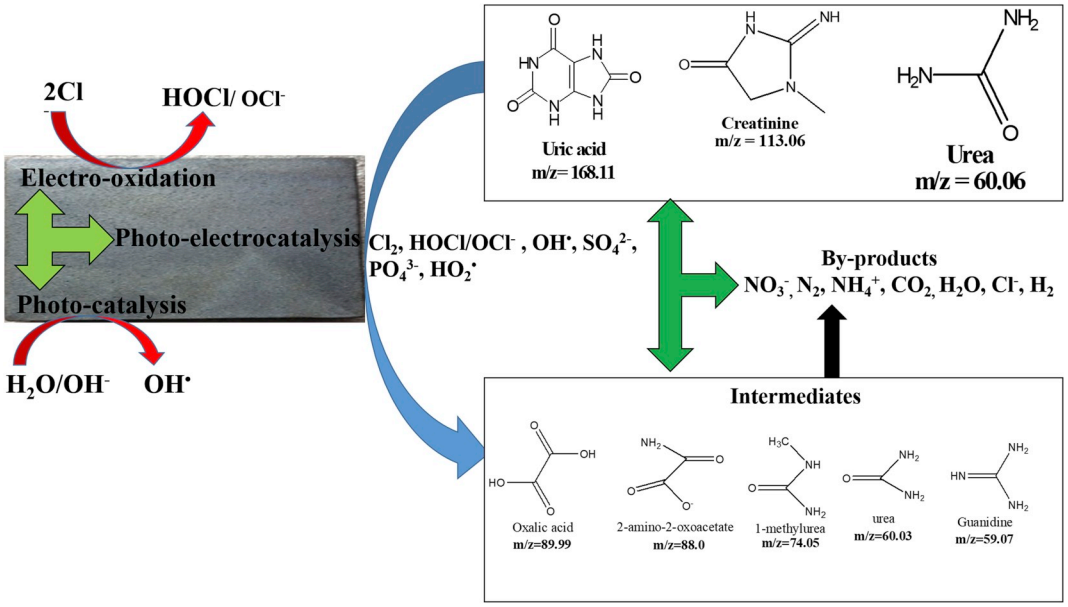

Fig. 8. The tentative proposed degradation pathway for electrochemically treated SU.

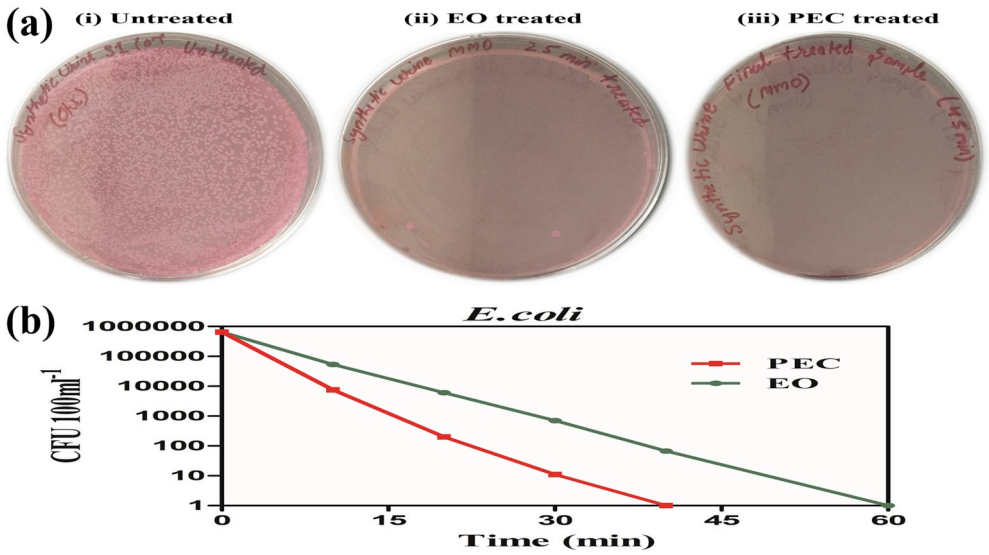

Fig. 9. (a) Total coliform (*E.coli*) count images of treated and untreated samples of SU and (b) plot of CFU 100 mL^{-1} versus treatment time.

treatment of SU under continuous recirculation mode in a PV driven wastewater electrolytic reactor. The EO experiments were conducted at optimized conditions. Fig. 10A shows the plot of % removal (COD, urea, creatinine and uric acid) versus treatment time. As it can be seen that 80.85% removal in COD was achieved in 6 h of electrolysis. The volumetric fraction of molecular hydrogen (XH_2) during 6 h electrolysis was generated in the range of 69.740%–1.7190%. Other gases as a byproduct such as N_2, CO_2, CH_4, and CO has also been generated during electrolysis, the volumetric molecular fraction of these gaseous byproducts was found increasing with treatment time due to the oxidation of micropollutants into molecular N_2 and CO_2 (Fig. 10B).

3.7. Durability studies, SEM/EDS and XRD analysis

The practical applicability and economy of the EO process towards pilot scale application were also studied in terms of the durability and stability of MMO anodes. Evaluation of the stability and durability in terms number of recycles and % COD removal of SU (Fig. 11A). Along with surface morphology and structural properties of freshly coated and recycled MMO anodes were checked through SEM while EDS was used for elemental composition of the different metal oxides layer coated on anode surface (Fig. 11B). To know the structure of MMO anodes, X-ray diffractogram analysis of the Ti sheet, freshly coated MMO and recycled MMO was done (Fig. 11C). Further information has been discussed in File S8, along with SEM/EDS and XRD analysis.

4. Conclusion

The electrochemical oxidation treatment with MMO leads to the complete deactivation of *E. coli* present in SU wastewater with 85.25% removal in COD at low current densities of 30.33 mA/cm^2. It was found that most of the nitrogen-based organic components got mineralized into inorganic ions in a few hours. The final products generated were confirmed non-toxic as checked by toxicity analysis. The combination of EO with UV photolysis significantly reduced the treatment by 2.8 h. During the electrolysis, a significant amount of RCS and $OH^{\bullet}$ species were generated during electrolysis resulting in the destruction of micropollutants and disinfection of urinal wastewater. Characterization techniques like SEM-EDS and XRD have proved the durability and stability of MMO in terms of significant % COD removal even after 100 recycles. From the scale-up studies, the appropriate amount of molecular hydrogen and nitrogen was produced. Future investigations would

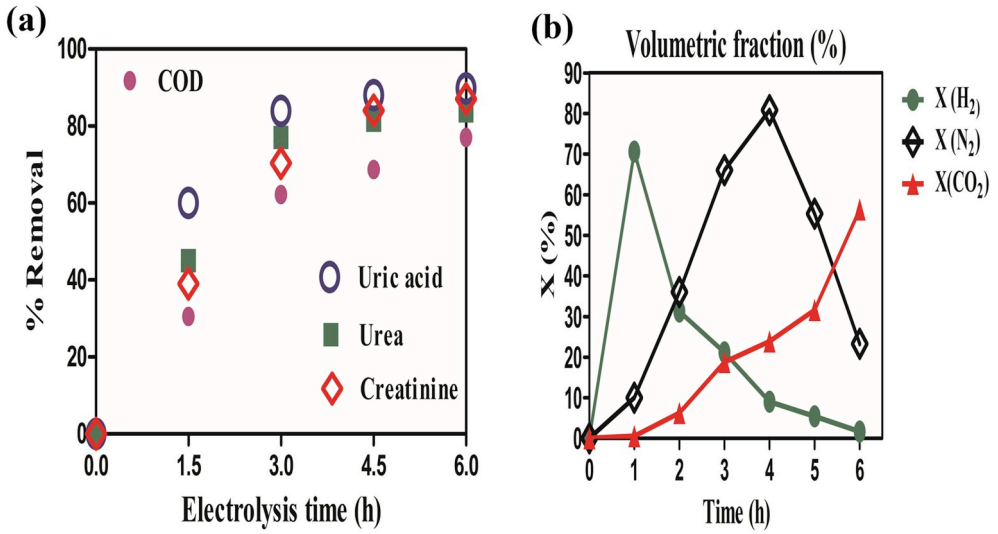

Fig. 10. (a) Percentage removal versus time and (b) volumetric fraction (X%) of gases versus treatment time during continuous EO treatment of SU.

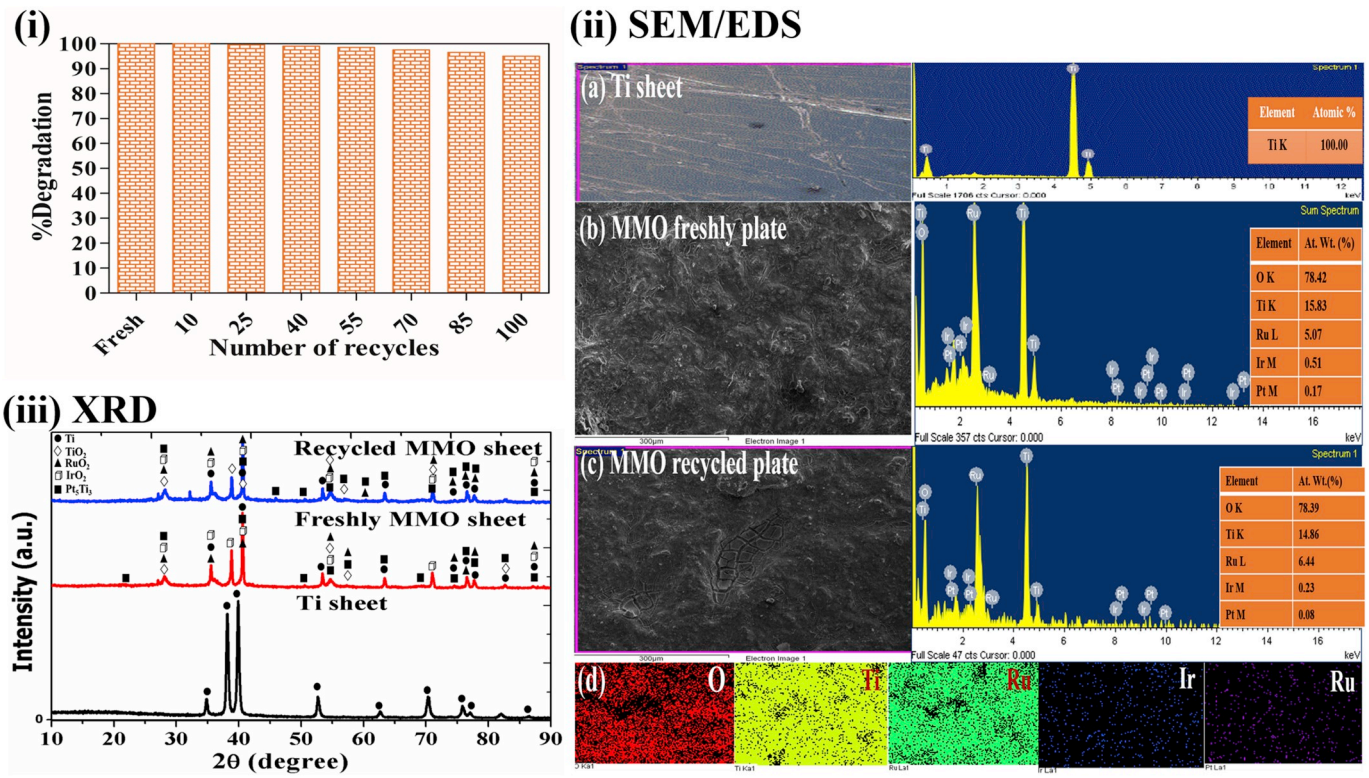

Fig. 11. (i) Recyclability studies of MMO anode for the oxidation of SU for 100 recycles, (ii) SEM/EDS images along with elemental mapping and (iii) XRD pattern of MMO anodes (Ti sheet, freshly coated and recycled plate).

emphasize on more techno-economic analysis of field-scale applications such as on-site treatment of urinal wastewater and reuse as flush water using these anodes along with harnessing the molecular H_2.

Appendix A. Supplementary data

Supplementary data to this article can be found online at https://doi.org/10.1016/j.jenvman.2019.109847.

References

Baddouh, A., Bessegato, G.G., Rguiti, M.M., El Ibrahimi, B., Bazzi, L., Hilali, M., Zanoni, M.V.B., 2018. Electrochemical decolorization of Rhodamine B dye: influence of anode material, chloride concentration and current density. J. Environ. Chem. Eng 6, 2041–2047. https://doi.org/10.1016/j.jece.2018.03.007.

Bansal, P., Verma, A., 2018. In-situ dual effect studies using novel Fe-TiO_2 composite for the pilot-plant degradation of pentoxifylline. Chem. Eng. J. 332, 682–694. https://doi.org/10.1016/j.cej.2017.09.121.

Barrera-Díaz, C., Cañizares, P., Fernández, F.J., Natividad, R., Rodrigo, M.A., 2017. Electrochemical advanced oxidation processes: an overview of the current applications to actual industrial effluents. J. Mex. Chem. Soc. 58, 256–275. https://doi.org/10.29356/jmcs.v58i3.133.

Bergmann, M.E.H., Rollin, J., Iourtchouk, T., 2009. The occurrence of perchlorate during drinking water electrolysis using BDD anodes. Electrochim. Acta 54, 2102–2107. https://doi.org/10.1016/j.electacta.2008.09.040.

Cho, K., Kwon, D., Hoffmann, M.R., 2014. Electrochemical treatment of human waste coupled with molecular hydrogen production. RSC Adv. 4, 4596–4608. https://doi.org/10.1039/C3RA46699J.

Cotillas, S., Lacasa, E., Sáez, C., Cañizares, P., Rodrigo, M.A., 2018. Disinfection of urine by conductive-diamond electrochemical oxidation. Appl. Catal. B Environ. 229, 63–70. https://doi.org/10.1016/j.apcatb.2018.02.013.

Cruz-Díaz, M.R., Rivero, E.P., Rodríguez, F.A., Domínguez-Bautista, R., 2018. Experimental study and mathematical modeling of the electrochemical degradation of dyeing wastewaters in presence of chloride ion with dimensional stable anodes (DSA) of expanded meshes in an FM01-LC reactor. Electrochim. Acta 260, 726–737. https://doi.org/10.1016/j.electacta.2017.12.025.

Daudey, L., 2018. The cost of urban sanitation solutions: a literature review. J. Water Sanit. Hyg. De 8, 176–195. https://doi.org/10.2166/washdev.2017.058.

Dbira, S., Bensalah, N., Ahmad, M.I., Bedoui, A., 2019. Electrochemical oxidation/disinfection of urine wastewaters with different anode materials. Materials 12 (1254). https://doi.org/10.3390/ma12081254.

Dbira, S., Bensalah, N., Cañizares, P., Rodrigo, M.A., Bedoui, A., 2015. The electrolytic treatment of synthetic urine using DSA electrodes. J. Electroanal. Chem. 744, 62–68. https://doi.org/10.1016/j.jelechem.2015.02.026.

Ganesapillai, M., Simha, P., Gupta, K., Jayan, M., 2016. Nutrient recovery and recycling from human urine: a circular perspective on sanitation and food security. Procedia Eng 148, 346–353. https://doi.org/10.1016/j.proeng.2016.06.461.

Gurung, K., Ncibi, M.C., Shestakova, M., Sillanpää, M., 2018. Removal of carbamazepine from MBR effluent by electrochemical oxidation (EO) using a Ti/Ta_2O_5-SnO_2 electrode. Appl. Catal. B Environ. 221, 329–338. https://doi.org/10.1016/j.apcatb.2017.09.017.

Hernlem, B.J., 2005. Electrolytic destruction of urea in dilute chloride solution using DSA electrodes in a recycled batch cell. Water Res. 39, 2245–2252. https://doi.org/10.1016/j.watres.2005.04.018.

Hiwarkar, A.D., Singh, S., Srivastava, V.C., Mall, I.D., 2017. Mineralization of pyrrole, a recalcitrant heterocyclic compound, by electrochemical method: multi-response optimization and degradation mechanism. J. Environ. Manag. 198, 144–152. https://doi.org/10.1016/j.jenvman.2017.04.051.

Ikematsu, M., Kaneda, K., Iseki, M., Yasuda, M., 2007. Electrochemical treatment of human urine for its storage and reuse as flush water. Sci. Total Environ. 382, 159–164. https://doi.org/10.1016/j.scitotenv.2007.03.028.

Isarain-Chávez, E., Baró, M.D., Rossinyol, E., Morales-Ortiz, U., Sort, J., Brillas, E., Pellicer, E., 2017. Comparative electrochemical oxidation of methyl orange azo dye using Ti/Ir-Pb, Ti/Ir-Sn, Ti/Ru-Pb, Ti/Pt-Pd, and Ti/RuO_2 anodes. Electrochim. Acta 244, 199–208. https://doi.org/10.1016/j.electacta.2017.05.101.

Kaur, P., Kushwaha, J.P., Sangal, V.K., 2017. Evaluation and disposability study of actual textile wastewater treatment by an electro-oxidation method using Ti/RuO_2 anode. Process Saf. Environ 111, 13–22. https://doi.org/10.1016/j.psep.2017.06.004.

Mondal, B., Srivastava, V.C., Kushwaha, J.P., Bhatnagar, R., Singh, S., Mall, I.D., 2013. Parametric and multiple response optimization for the electrochemical treatment of textile printing dye-bath effluent. Separ. Purif. Technol. 109, 135–143. https://doi.org/10.1016/j.seppur.2013.02.026.

Moreira, F.C., Boaventura, R.A.R., Brillas, E., Vilar, V.J.P., 2017. Electrochemical advanced oxidation processes: a review on their application to synthetic and real wastewaters. Appl. Catal. B Environ. 202, 217–261. https://doi.org/10.1016/j.apcatb.2016.08.037.

Simha, P., Ganesapillai, M., 2017. Ecological Sanitation and nutrient recovery from human urine: how far have we come? A review. Sustain. Environ. Res. 27, 107–116. https://doi.org/10.1016/j.serj.2016.12.001.

Singh, S., Cheema, P.P.S., 2016. Use of eco-sanitation process in rural areas of Punjab (India). J. Environ. Sci. Toxicol. Food Technol 10, 29–33. https://doi.org/10.9790/2402-1011032933.

Singla, J., Verma, A., Sangal, V.K., 2017. Performance and evaluation of electro-oxidation treatment of human urine metabolite uric acid using response surface methodology. J. Electrochem. Soc. 164, E312–E320. https://doi.org/10.1149/2.0681712jes.

Singla, J., Verma, A., Sangal, V.K., 2018. Parametric optimization for the treatment of human urine metabolite, creatinine using electro-oxidation. J. Electroanal. Chem. 809, 136–146. https://doi.org/10.1016/j.jelechem.2017.12.061.

Spångberg, J., Tidåker, P., Jönsson, H., 2014. Environmental impact of recycling nutrients in human excreta to agriculture compared with enhanced wastewater treatment. Sci. Total Environ. 493, 209–219. https://doi.org/10.1016/j.scitotenv.2014.05.123.

Zahedi, M., Jafarzadeh, K., Mirjani, M., Abbasi, H.M., 2018. The effect of anodizing time on the electrochemical behavior of the Ti/TiO_2 NTs/IrO_2-RuO_2-Ta_2O_5 anode. Ionics 24, 451–458. https://doi.org/10.1007/s11581-017-2210-y.

Zhang, Z., Yin, J., 2014. Sensitive detection of uric acid on partially electro-reduced graphene oxide modified electrodes. Electrochim. Acta 119, 32–37. https://doi.org/10.1016/j.electacta.2013.12.033.

Zhuo, Q., Deng, S., Yang, B., Huang, J., Yu, G., 2011. Efficient electrochemical oxidation of perfluorooctanoate using a Ti/SnO_2-Sb-Bi anode. Environ. Sci. Technol. 45, 2973–2979. https://doi.org/10.1021/es1024542.